The role of GLI2 in human basal cell carcinoma tumourigenesis

Pantazi, Eleni

The role of GLI2 in Human Basal Cell Carcinoma tumourigenesis

A thesis submitted in accordance with regulations for the degree of Doctorate of Philosophy.

June 2010

Eleni Pantazi

Centre for Cutaneous Research

Institute of Cell and Molecular Science

Barts and the London School of Medicine and Dentistry

University of London

Declaration

I hereby declare that all the work contained in this thesis is the result of my own independent investigation unless otherwise stated.

No portion of the work referred to in this thesis has been submitted in support of an application for another degree or qualification of this, or any other, university or other institute of learning.

Eleni Pantazi

_____

Acknowledgements

I would like to thank most importantly my supervisor Prof. Mike Philpott for the opportunity of partaking in such an interesting project and for his invaluable support and cheerful help and guidance over the last years, that he provided throughout even in times of hardship, supporting me with patience and encouragement.

I would also like to extend my absolute gratitude to Dr Giuseppe Trigiante for his continuous assistance and advice. I am deeply grateful to Dr Muy-Teck Teh for being always available to offer advice and help and also to Dr Gary Warnes for his constant enthusiasm to provide scientific and technical assistance in flow cytometry whenever I needed it.

I would like also to thank everyone in the laboratory, who were able to provide me with help and advice when I needed it absolutely willingly, and for the friendly atmosphere which made me feel welcome.

I could not have been more grateful to my partner, Emilios Gemenetzidis, for his deep understanding, support and patience, not only during this thesis' writing period, but since the first day of my PhD.

Last, but not least, I am indebted to my mother, to whom this thesis is dedicated, who showed me the deepest love, support and encouragement during this period without which this thesis would not have materialised.

In remembrance of my father, Ioannis Pantazis

Abstract

Abnormal Sonic Hedgehog (SHH) signalling leads to increased transcriptional activation of its downstream effector, GLI2, which is implicated in the pathogenesis of a variety of human tumours, including human basal cell carcinoma (BCC). However, little is known about the molecular mechanisms underlying the tumourigenic role of GLI2 in human skin keratinocytes. This study examines the effects of inducible and stable expression of constitutively active GLI2 (GLI2ΔN) oncogenic transcription factor, on immortalised human epidermal keratinocytes. It is shown here that GLI2ΔN overexpressing N/TERT keratinocytes display gene expression patterns and phenotypic characteristics reminiscent of those observed in human BCC *in vivo*. It is also shown for first time, that expression of GLI2ΔN in N/TERT keratinocytes is sufficient to induce accumulation of binucleated/tetraploid cells as evidenced by an increase in G2/M phase of the cell cycle and binucleate cell counting, and to promote polyploidy and aneuploidy, in the absence of increased cell death or apoptosis. This cell cycle deregulation is accompanied by strong activation of anti-apoptotic protein BCL-2 and simultaneous suppression of important cell-cycle regulators such as 14-3-3σ and CDK inhibitor $p21^{WAF1/CIP1}$, with no change in p53 protein levels, indicating uncontrolled proliferation of cells with ploidy abnormalities and/or DNA damage. Consistently, it is shown that $p21^{WAF1/CIP1}$ protein is also absent in human BCC tumours and that forced overexpression of GLI2ΔN renders human keratinocytes resistant to apoptosis mediated by ultraviolet B (UVB, 290-320 nm), one of the most important etiological factors in BCC formation. Karyotype analysis of GLI2ΔN N/TERT keratinocytes further demonstrates that overexpression of GLI2ΔN induces numerical (tetraploidy, polyploidy, aneuploidy) and structural instability in N/TERT keratinocytes including chromosomal translocations and double minute chromosomes. Furthermore, β-catenin activation is the most common alteration observed during aberrant WNT signalling, and is often implicated in the development of human carcinogenesis and metastasis. In this study it is shown that GLI2ΔN induction induces nuclear accumulation of β-catenin in keratinocyte cell culture and in the basal layer of organotypic skin rafts, similar to human BCCs. In addition, several WNT genes were found to be upregulated upon GLI2ΔN induction, while β-catenin transcriptional activity is increased upon stable and conditional expression of GLI2ΔN. Overall these data give new insights for the possible mechanisms that mediate the tumourigenic potential of GLI2.

Contents

List of Figures

CHAPTER 1

CHAPTER 2

CHAPTER 3

CHAPTER 4

CHAPTER 5

List of Tables

CHAPTER 1

CHAPTER 2

Abbreviations

2D	two-dimensional
^{3}H-TdR	tritiated thymidine
5-FU	fluorouracil, 5-fluoro-dUMP
A	area
AML	acute myeloid leukaemia
AMV	avian myeloblastosis virus
AMVRT	avian myeloblastosis virus reverse transcriptase
APC (fluorophore)	allophycocyanin
APC	adenomatous polyposis coli
ATP	adenosine triphosphate
BCC	basal cell carcinoma
BCL-2/Bcl-2	B-cell lymphoma 2
BMP	bone morphogenetic protein
BMZ	basement membrane zone
bp	base pair
BPB	bromophenol blue
BrdU	bromodeoxyuridine
bri	bright
BSA	bovine serum albumin
C	cytosine
Ca^{2+}	calcium ions
CCNB1	cyclin B1
CCND1	cyclin D1
CDK	cyclin dependent kinase
CDKI	cyclin dependent kinase inhibitor
cDNA	complementary DNA
c-FLIP	(c (cellular)-FAS-associated death domain-like IL (interleukin)-1-converting enzyme-like inhibitory protein
ChIP	chromatin immunoprecipitation
Ci	cubitus interruptus
CK1	casein kinase 1
cm	centimetre

CMV	cytomegalovirus
c-MYC	v-myelocytomatosis viral oncogene homolog
col	collagen
Cos2	costal 2
CpG	Cytosine-phosphate-Guanine sites
Ct	crossing point
C-terminal	carboxyl-terminal
Cy	cyanine
d	days
DAB	3,3'-diaminobenzidine
DAPI	4',6-diamidino-2-phenylindole
DED	de-epidermalised dermis
DHH	desert hedgehog
DKK	dickkopf
DKK-1	dickkopf-1
DMBA	7-8-dimethylbenz(a)anthracene
DMSO	dimethyl sulphoxide
DNA	deoxyribonucleic acid
DNMT	methyltransferases
dNTP	deoxyribonucleotide triphosphate
Dox	doxycycline
DP	dermal papilla cells
Dpp	decapentaplegic
dsDNA	double stranded DNA
DTT	dithiothreitol
dTTP	thymidine triphosphate
dUMP	deoxyuridine monophosphate
dUTP	deoxyuridine triphosphate
DW	distilled water
E-cadherin	epithelial-cadherin
ECL	enhanced chemilluminescence
ECM	extracellular matrix
EDTA	ethylediamine-tetra-acetic acid
EGFP	enhanced green fluorescent protein

EMT	epithelial-mesenchymal transition
EPU	epidermal proliferative unit
ER	estrogen responsive
etc	*et cetera*; and so on
FACS	fluorescence activated cell sorting
FADH2	1,5 - dihydro flavine adenine dinucleotide
FBS	foetal bovine serum
FCM	flow cytometry
FCS	foetal calf serum
FITC	fluorescein isothiocyanate
FMNH2	flavin mononucleotide reduced
FOXE1	forkhead box E1
FOXM1	forkhead box M1
FSC	forward scatter channel
Fu	fused
FZD	frizzled
g	gram
G	guanine
GAPDH	glyceraldehyde-3-phosphate dehydrogenase
GFP	green fluorescent protein
GLI1/Gli1	glioma 1
GLI2/Gli2	glioma 2
GLI2ΔN	GLI2-β isoform, which lacks the N-terminal repressor domain
GLI3/Gli3	glioma 3
GSK3β	glycogen synthase kinase 3 beta
h/TERT	human telomerase reverse transcriptase
HF	hair follicle
hFu	human fused
HH	hedgehog
HMG	high mobility group
Hoechst-33342	bisbenzimide H33342 trihydrochloride
HPV	human papillomavirus
hr, h, hrs	hour/hours

HRP	horseradish peroxidase
hSuFu	human suppressor of fused
Hygro B	hygromycin B
i.e.	*id est*; that is; for example
IdU	iododeoxyuridine
IFE	interfollicular epidermis
IHH	Indian Hedghehog
IR	infra red
IRS	inner root sheath
ITGB1	integrin beta 1
IVL	involucrin
K/k	thousand
K1-K20	keratins1 to 20
kb	kilobases
kDa	kilodalton
L	litre
Lef	lymphoid enhancer factor
LOH	loss of heterozygosity
LRC	label retaining cell
LRP	low density lipoprotein receptor related protein
LTR	long terminal repeat
Luc	luciferase
M	molar, molarity
MCS	multiple cloning site
MEFs	mouse embryonic fibroblasts
M-FISH	multiplex fluorescent *in situ* hybridisation
mg	milligram
min	minute/minutes
ml	millilitre
mm	milimetre
mM	millimolar
MMP	matrix metalloproteinase
mo	months
MPMVE	Mason-Pfizer monkey virus-exosome-like form

mRNA	messenger RNA
MTT	3-(4,5-dimethylthiazol-2-yl)-2,5-diphenyl tetrazolium bromide
N	haploid number
NADH	nicotinamide adenine dinuleotide
NADPH	nicotinamide adenine dinuleotide phosphate
NBCC	nevoid basal cell carcinoma
ng	nanogram
nm	nanometre
nM	nanomolar
NMSCs	non-melanoma skin cancers
NOD	non obese diabetic
N-terminal	amino-terminal
OD	optical density
OHT	hydroxy tamoxifen
ORS	outer root sheath
OTC	organotypic culture
PBS	phosphate buffered saline
PBS/T	phosphate buffered saline/Tween-20
PCNA	proliferating cell nuclear antigen
PCR	polymerase chain reaction
PD	population doublings
PE	phycoerythrin
PI	propidium iodide
PKA	protein kinase A
PLC	phospholipase C
pM	picomolar
PMA	12-0-tetradecanoyl phorbol-13-acetate
PMSF	phenylmethanesulfonylfluoride
POLR2A	RNA II (DNA directed) polypeptide A
PS	phosphatidylserine
pSIN	self-inactivating retroviral vector
PTCH	patched
qPCR	quantitative polymerase chain reaction

qRT-PCR	quantitative real time PCR
REDOX	reduction - oxidation reaction
RFU	relative fluorescence unit
RLU	relative luminescence unit
RNA	ribonucleic acid
RNAi	RNA interference
RNase	ribonuclease
rpm	revolution per minute
RT	room temperature
s.e.m	standard error mean
SC	stem cell
sca	scaffold
SCC	squamous cell carcinoma
SCID	severe combined immunodeficient
SDS	sodium dodecyl sulfate
sec	second/seconds
SG	sebaceous glands
SHH	sonic hedgehog
shRNA	short hairpin RNA
siRNA	small interfering RNA
SMO	smoothened
SNP	single nucleotide polymorphism
SOX2	SRY (sex determining region Y)-box 2
SPRR2A	small proline-rich protein 2A
SSC	side scatter channel
ssDNA	single stranded DNA
SuFu	suppressor of fused
SV-40	Simian virus 40
SYBR	syber
T	thymine
TA	transit-amplifying
TBS	tris buffered saline
TBS/T	tris buffered saline/Tween-20
Tcf	T-cell factor

Tcf/Lef	T-cell factor/lymphoid enhancer factor
TG	trans-glutaminase
TLE	transducing-like enhancer
TNC	Tenascin C
TPA	12-0-tetradecanoyl phorbol-13-acetate
tRNA	transfer RNA
U	uracil
UV	ultraviolet
UVB	ultraviolet B
V	volts
v/v	volume/volume
vol	volume
W	width
w/v	weight/volume
WCP	whole chromosome paint
Wg	wingless
WNT	wingless-type MMTV (mouse mammary tumour virus) integration site family (Wingless (Wg) and the related mammalian oncogene integration 1 (Int-1))
WRE	WNT responsive element
XP	xeroderma pigmentosum
YAP1	Yes-associated protein 1
α	alpha
β	beta
β-actin	beta-actin
β-cat	beta-catenin
β-catenin	beta-catenin
β-gal	beta-galactosidase
β-TrCP	beta transducin repeat containing
γ	gamma
δ	delta
µg	microgram
µl	microlitre
µm	micrometer

µM	micromolar
σ	sigma

CHAPTER ONE

1 INTRODUCTION

1.1 Human skin

The skin is a vital organ that covers the entire outside of the body and guards the underlying muscles, bones, ligaments and internal organs, forming a protective barrier against pathogens and injuries from the environment. The skin is the largest organ of the body in surface area and weight and it consists of two main layers, the epidermis and dermis, which are the superficial thinner portion, and the deeper connective tissue respectively (anatomical representation of skin is given in **Figure 1.1**). During embryogenesis epidermis is derived from the ectoderm and the dermis from the mesoderm. Below the dermis, but not strictly part of the skin is the subcutaneous layer (hypodermis). The skin and its appendages including hair follicles, sebaceous and sweat glands and nails, ensure a number of critical functions necessary for animal survival. Skin, apart from protecting mammals from pathogen and injuries, also protects from water loss and temperature change. Other functions include sensory roles, vitamin D synthesis, immune surveillance, excretion of wastes through sweat glands, sociosexual communication and reproduction by virtue of its appearance and smell (i.e. hormones and pherormones) (Freinkel & Woodley, 2001; Tortora & Grabowski, 2003; Goldsmith, 2005a; Blanpain & Fuchs, 2006).

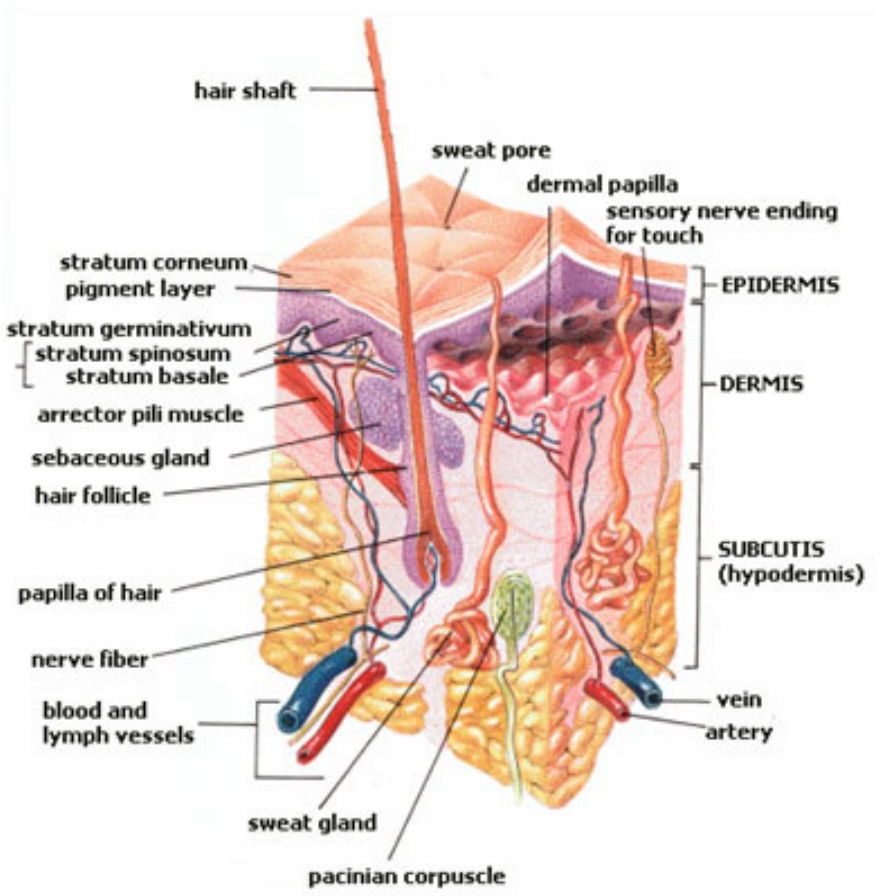

Figure 1.1: Skin structure.

Diagram showing the multi layered structure of human skin.

http://www.essentialdayspa.com/Skin_Anathomy_and_Physiology.htm

1.1.1 Epidermis

Human epithelia are tissues composed of cells lining the cavities and surfaces of the body. They are classified into different groups, according to their structure and the amount of layers of which they are composed. Mature epidermis is a stratified squamous epithelium whose outermost layer is the skin surface. The outer covering of the skin, is comprised of a stratified multilayered squamous epithelium - known as the interfollicular epidermis (IFE) - and associated hair follicles, sebaceous glands and

sweat glands which are mainly parts of the dermis. Its main function is to act as a waterproof protective barrier and it contains four main types of cells: keratinocytes, about 90% of epidermal cells, melanocytes, Langerhans cells, and Merkel cells (Freinkel & Woodley, 2001; Tortora & Grabowski, 2003; Goldsmith, 2005a).

Keratinocytes, the most abundant cell type in the epidermis are epithelial cells and produce hair follicles, sweat and sebaceous glands, and the outer covering of the skin. Keratinocytes are named after the filamentous keratin family of proteins that make up a major part of its distinctive cytoskeleton (network of keratin intermediate filaments - IFs). Along with microtubules and microfilaments, keratins giving rise to the keratinized layer of the epidermis can be used as markers for the epidermis layers, since the proportion of different keratins changes as the keratinocytes differentiate. The basal layer of the stratified epithelium is typified by the expression of keratins K5 and K14 as well as keratin K15 (in the embryo), whereas the intermediate suprabasal layers express K1 and K10 (Fuchs, 1993; Freinkel & Woodley, 2001; Tortora & Grabowski, 2003; Goldsmith, 2005a; Blanpain & Fuchs, 2006).

The epidermis is divided into many layers where cells are formed through mitosis at the innermost layers. They move up the strata changing shape and composition as they differentiate and become filled with keratin. They eventually reach the top layer and become sloughed off or desquamated, being replaced by inner cells moving outward. This process is called keratinization and takes place within weeks (~ 14 days for mice and 28-30 days for human) (Potten & Morris, 1988; Potten & Booth, 2002). The outermost layer of epidermis consists of 25 to 30 layers of dead cells.

The five layers of the epidermis are the stratum basale or stratum germinativum (basal layer), and the suprabasal layers including stratum spinosum (spinal layer), stratum granulosum (granular layer), stratum lucidum (clear layer), and the outermost layer stratum corneum (cornified layer), which represent the progressing stages of keratinocytes differentiation (maturation of keratinocytes) **(Figure 1.2)**. All the four layers (basal layer, spinal layer, granular layer and cornified layer) are found both in thick and thin skin, which is defined according to the thickness of the epidermis, while the clear layer is only found in thick skin which lacks hair follicles, and as such is only observed in the palms of the hands and the soles of the feet. Thin skin covers most of

the body and contains hair follicles as well (Freinkel & Woodley, 2001; Tortora & Grabowski, 2003; Goldsmith, 2005a).

Differentiation of human epidermis is associated with a series of morphological and biochemical changes as cells migrate from the proliferative and mitotic basal cell layer through the non proliferative, post mitotic but metabolically active suprabasal layers where the terminal phase of maturation is completed (Fuchs, 1990). Keratinocytes in each of these layers are expressing different molecular markers such as keratins, involucrin, filaggrin, and loricrin (Fuchs, 1990; Fuchs, 1993; Candi et al., 2005; Fuchs, 2008).

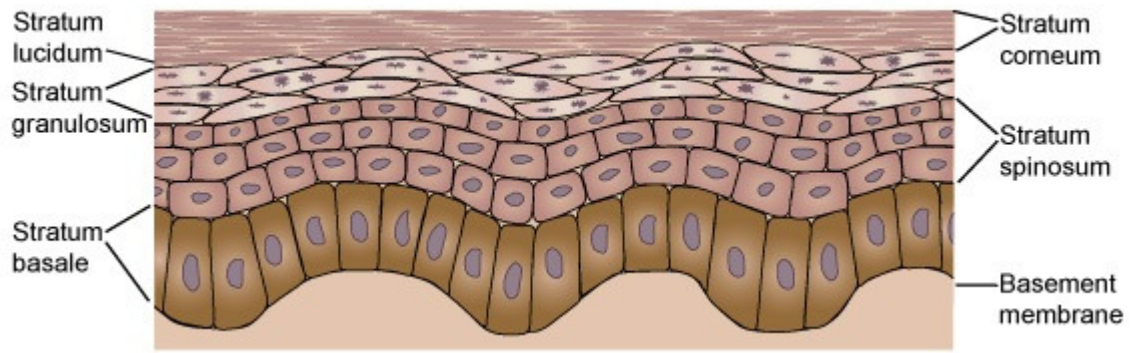

Figure 1.2: Layers of the epidermis.

The epidermis consists of five different layers of keratinocytes: the stratum basale, the stratum spinosum, the stratum granulosum, the stratum lucidum and the stratum corneum (http://dermatology.about.com/od/anatomy/ss/epidermis.htm).

The stratum germinativum (stratum basale or basal cell layer) is the layer of keratinocytes that lies at the base of the epidermis immediately above the dermis and is responsible for constantly renewing epidermal cells. It consists of a single layer of tall, simple columnar epithelial cells lying on a basement membrane. These undifferentiated, proliferative cells are mitotically active and differentiate outward to form the distinctive suprabasal layers of the differentiated tissue. About 25% of the basal cells are also melanocytes, which produce melanin that provides pigmentation for skin and hair. Keratinocytes of the basal layer synthesize K5 and K14 forming cytoskeletal filaments

(keratin intermediated filaments) that aggregate into thin bundles (tonofilaments) (Fuchs, 1990; Fuchs, 1993; Freinkel & Woodley, 2001; Tortora & Grabowski, 2003; Goldsmith, 2005a).

The basement membrane zone (BMZ) which provides the support of basal keratinocytes is an extracellular network, rich in extracellular matrix (ECM) and growth factors that are produced and deposited at the interface of the epidermis and separate the epidermis from the dermis **(Figure 1.3A)**. The ECM, also known as connective tissue (fibrous tissue) or mesenchyme, which includes the interstitial matrix (present between various animal cells - dermal fibroblasts - (i.e. in the intercellular spaces)) and the basement membrane is composed of a mixture of proteins and polysaccharides, including laminin, fibronectin, and collagen and elastin which give structural support to the resident cells and elasticity to tissues respectively **(Figure 1.3A)** (Stanley et al., 1982; Alonso & Fuchs, 2003b; Blanpain & Fuchs, 2006; Blanpain et al., 2007; Fuchs, 2008). In culture, keratinocytes synthesize and deposit the major basement membrane components (i.e. fibronectin, laminin, collagen IV), even though the proteins are not organized into a recognizable basement membrane (Alitalo et al., 1982; Brown & Parkinson, 1983; Kubo et al., 1984; O'Keefe et al., 1984; Oguchi et al., 1985; Bohnert et al., 1986), supporting the idea that epidermal keratinocytes are responsible for the synthesis of at least some of the components of the basement membrane in human skin (Brown & Parkinson, 1983). Fibroblasts (dermal cells) are also capable of synthesising many of the components of the basement membrane (Bohnert et al., 1986; Okamoto & Kitano, 1993). Different layers have been identified within the basement membrane zone including (i) the plasma membrane of the basal keratinocytes, (ii) the lamina lucida that contains mainly laminin, integrins and anchoring filaments, (iii) the lamina densa that contains mainly type IV collagen, and which fuses with lamina lucida and forms the basal lamina, and (iv) the lamina reticularis that contains mainly type VII collagen and is attached to the basal lamina with type VII anchoring fibrils and microfibrils **(Figure 1.3B)** (Stanley et al., 1982). Anchoring of keratinocytes to the basement membrane is mediated through hemidesmosomes, which are protein complexes in the inner basal surface of keratinocytes in the epidermis (integrin β4 participates in the formation of hemidesmosomes (Dowling et al., 1996)), and are anchoring the cell to the underlying basement membrane, by connecting the intermediate keratin filaments with the extracellular matrix (Borradori & Sonnenberg, 1999; Nievers et al., 1999; van der Flier

& Sonnenberg, 2001), as well as through focal adhesions which are formed by clustering of integrins interspersed on the basal surface of the basal keratinocytes in the epidermis and connects the actin cytoskeleton with the extracellular matrix **(see Chapter 3, Section 3.3.5)** (De Strooper et al., 1989; Peltonen et al., 1989; Hynes, 1992; Jensen et al., 1999; van der Flier & Sonnenberg, 2001; Blanpain & Fuchs, 2006; Blanpain et al., 2007; Fuchs, 2008). The cells of the basal (expressing keratin filaments K5 and K14) and spinous layers (expressing keratin filaments K1 and K10) are attached to each other by means of cadherin (calcium dependent adhesion molecules)-based adherens junctions **(see Section 1.4.1)** and desmosomes using cadherin proteins, respectively, whereas cells in the granular layer are attached to each other by means of tight junctions (Fuchs, 1990; Fuchs, 1993; Garrod, 1993; Nievers et al., 1999; Cereijido & Anderson, 2001; van der Flier & Sonnenberg, 2001; Blanpain & Fuchs, 2006; Blanpain et al., 2007; Fuchs, 2008). Desmosomes are membrane junctions that interconnect cells into three-dimensional lattices by connecting the keratin filament cytoskeletons of adjacent cells using different cadherin proteins (i.e. desmoglein), whereas adherens junctions are membrane junctions that connect the actin filament cytoskeletons of adjacent cells, using different cadherin proteins (i.e. E-cadherin) **(see Section 1.4.1)**. Tight junctions are membrane junctions that join the actin cytoskeletons of adjacent cells using claudin and occludin proteins which establish a paracellular barrier that controls the flow of molecules and water in the intercellular space between the cells (sealing of the intercellular space).

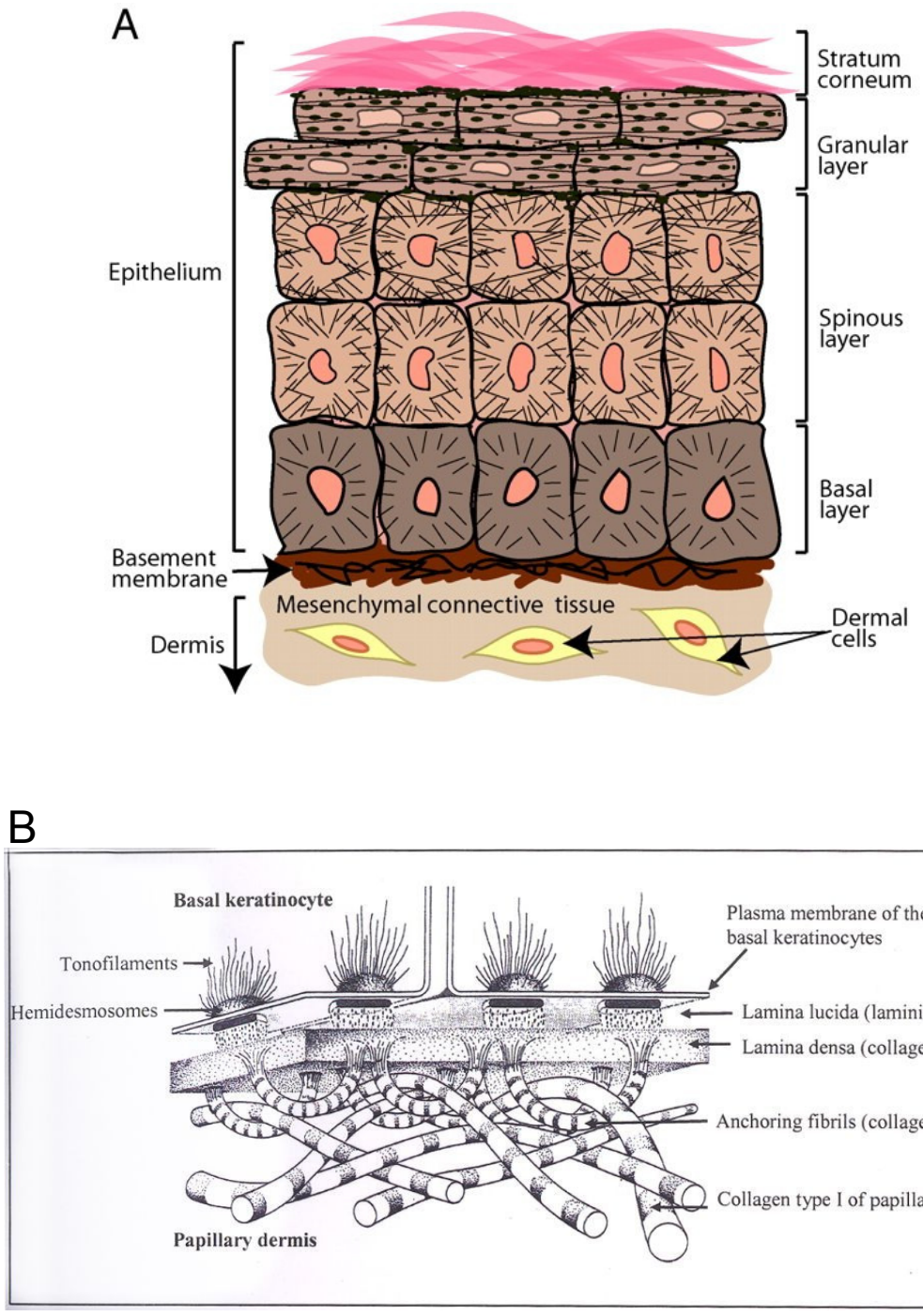

Figure 1.3: Basement membrane zone.

(A) The basement membrane supports the basal keratinocytes and separates the epidermis from the dermis (Alonso & Fuchs, 2003b). **(B)** The different layers of the basement membrane zone at dermal-epidermal junction (IBC Ltd, USA 'Bioengineering of Skin Substitutes' handbook September 1997).

Keratinocytes originate in the basal layer from the division of keratinocyte stem cells known as epidermal stem cells which are undifferentiated and have an unlimited self-renewal capacity. Epidermal basal stem cells strongly adhere to their underlying basement membrane and maintain the homeostasis of the interfollicular epidermis by replenishing the suprabasal terminally differentiated cells (Blanpain & Fuchs, 2006). Undifferentiated basal keratinocyte stem cells, compared to differentiated keratinocytes, have greater life span, are slow cycling and divide to rise to a cell that will remain in the basal layer as a stem cell and to a daughter cell, known as transit-amplifying cell (TA). Transit-amplifying cells, initially will undergo a few rounds of division and then following an irreversible withdrawal from the cell cycle (Potten & Morris, 1988), along with loss of integrins expression from the cell surface (De Strooper et al., 1989; Peltonen et al., 1989) and loss of adhesiveness to a range of extracellular matrix proteins, they will be pushed up through the layers of the epidermis, undergoing gradual differentiation until they will reach the stratum corneum where they form a layer of enucleated, flattened, highly keratinized cells called squamous **(Figure 1.4)** (Adams & Watt, 1990; Lavker & Sun, 2000; Watt et al., 2006; Fuchs, 2008). This layer forms an effective barrier to the entry of foreign matter and infectious agents into the body and minimises moisture loss.

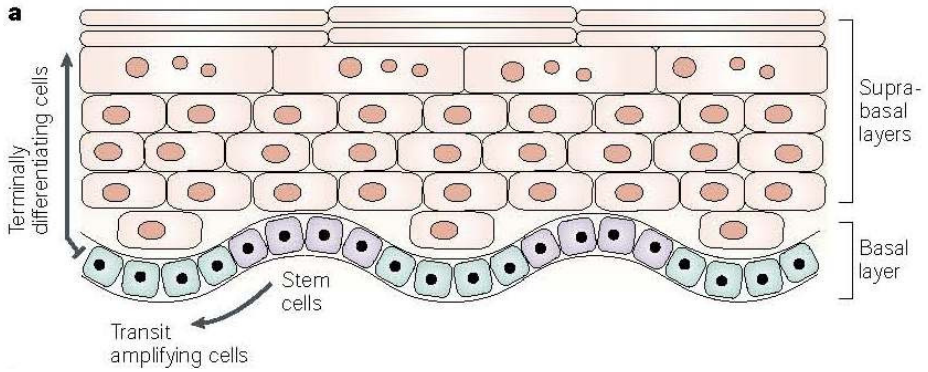

Figure 1.4: Stages of keratinocyte differentiation in the epidermis.

Homeostasis of the epidermis is maintained by a subpopulation of basal stem cells (stem cell keratinocytes) which adhere to their underlying membrane and are mitotically active cells. Their daughter cells known as transit-amplifying cells have a limited proliferative potential, withdraw irreversibly from the cell cycle and are destined to undergo terminal differentiation as they move upward to the suprabasal layers of the epidermis. Stem cells (purple), Transit-amplifying cells (green), Terminally differentiated cells (pink) (Owens & Watt, 2003).

The stratum spinosum or spinal layer is a multi-layered (4-8 layers) arrangement of cuboidal cells and is the first layer of the differentiation compartment formed by the migration of cells from the basal layer (Fuchs, 1990; Freinkel & Woodley, 2001; Tortora & Grabowski, 2003; Goldsmith, 2005a). Although, cells of the stratum spinosum are normally post-mitotic, they are still metabolically active and synthesize K1 and K10 forming cytoskeletal filaments that aggregate to form tonofibrillar bundles which are thicker than tonofilament bundles in basal cells (Fuchs, 1993). These keratin intermediate filaments are anchored to the desmosomes, which are more abundant in spinous cells than in basal cells, joining adjacent cells to provide extra structural support, helping the skin resist abrasion (Fuchs, 1993; Blanpain & Fuchs, 2006; Fuchs, 2008). As cells move upwards within the spinal layer they synthesize lamellar granules which contain lipids that are going to be released into the intercellular spaces of granular and stratum corneum cells, and they are responsible for the barrier properties of these cells (avoidance of transepidermal water loss) (Fuchs, 1990; Fuchs, 1993). In addition, spinous cells at this time also make glutamine and lysine-rich envelope proteins, such as involucrin, which is the major soluble cytoplasmic protein precursor of the cornified envelope (stratum corneum) in human stratified squamous epithelia, and provides a scaffold to which other proteins subsequently become cross-linked and form the cornified envelop (Rice & Green, 1977; Murphy et al., 1984; Fuchs, 1990; Fuchs, 1993; Candi et al., 2005; Fuchs, 2008).

The stratum granulosum or granular layer typically contains 3 to 5 of layers of squamous cells with many small basophilic granules (keratohyalin granules - made from free ribosomes) in their cytoplasm. Keratohyalin protein forms dense cytoplasmic granules that contain profilaggrin - the precursor of the interfilamentous protein filaggrin. Additional structural proteins of the cornified envelope including loricrin and involucrin are further synthesised by granular cells to reinforce the cornified envelope just beneath the plasma membrane. The cells in the stratum granulosum have lost their nuclei and are characterised by dark clumps of cytoplasmic material (lamellar granules - produced by Golgi apparatus). Lamellar granules that have been made earlier in the upper spinous layers, fuse with the plasma membrane and release lipids in into intercellular spaces of granular and stratum corneum cells, whereas some of the lipids become covalently attached to proteins of the cornified envelope. The envelope proteins are vital for the formation of the cornified envelope, which is an insoluble protein

structure that is assembled by the cross-linking of the envelope proteins through the activation of several enzymes known as transglutaminases (TGs). Transglutaminases are calcium dependent enzymes which mediate the formation of a covalently linked network of proteins, to finally replace the plasma membrane of terminally differentiated keratinocytes in the stratum corneum, and to also act as a scaffold for lipid attachment (Fuchs, 1990; Fuchs, 1993; Steven & Steinert, 1994; Candi et al., 2005; Fuchs, 2008). Granular layer is the highest layer in the epidermis where living cells are found (Freinkel & Woodley, 2001; Tortora & Grabowski, 2003; Goldsmith, 2005a).

The stratum lucidum or clear layer is a thin, clear layer of dead skin cells in the epidermis and it helps reduce friction and shear forces between the stratum corneum and stratum granulosum. It is named for its translucent appearance under a microscope and its keratinocytes are flattened and contain a clear substance called eleidin (intermediate form of keratin), which eventually is transformed to keratin that gives the stratum lucidum its waterproof properties. This layer is found beneath the stratum corneum of thick skin, and as such is only found on the palms of the hands and the soles of the feet (Freinkel & Woodley, 2001; Tortora & Grabowski, 2003; Goldsmith, 2005a).

The stratum corneum or cornified layer is the outermost layer of the epidermis (the outermost layer of the skin) that constitutes a barrier for the organism against the external environment, keeping microorganisms out and essential body fluids in (Fuchs, 1990; Fuchs, 1993; Freinkel & Woodley, 2001; Tortora & Grabowski, 2003; Goldsmith, 2005a; Fuchs, 2008). It is composed mainly of dead, terminally differentiated, cornified, flattened cells that lack nuclei and are known as corneocytes (cornified keratinocytes). As these dead cells slough off, they are continuously replaced by new cells from the stratum germinativum (basale). During the transition of granular cells to cornified keratinocytes profilaggrin is converted to filaggrin which aggregates the keratin filaments into tight bundles (conversion of bundling tonofibrils into macrofirillar cables). This promotes the collapse of the cell into a flattened shape which is characteristic of the corneocytes of the cornified layer (Fuchs, 1990; Fuchs, 1993; Steven & Steinert, 1994; Candi et al., 2005; Fuchs, 2008). Therefore, corneocytes mostly consist of keratin intermediate filaments embedded in a filaggrin matrix and surrounded by insoluble lipids (Steven & Steinert, 1994; Candi et al., 2005; Fuchs, 2008). Corneocytes are tightly attached to each other by corneodesmosomes (modified

desmosomal structures), which are proteolytically degraded in the uppermost layers of the cornified layer to allow desquamation (Serre et al., 1991; Candi et al., 2005).

1.1.2 Dermis

The dermis is the thickest of the three layers of the skin. It is a layer of skin beneath the epidermis that consists of connective tissue **(see Section 1.1.1)**, and cushions the body from stress and strain. The main function of the dermis is to regulate the temperature, to supply the epidermis with nutrient-saturated blood and to store much of the body's water supply. The dermis is tightly connected to the epidermis by a basement membrane **(see Section 1.1.1)**, and harbours many nerve endings that provide the sense of touch and heat. It provides skin's pliability, elasticity, and tensile strength, and thus protecting the body from mechanical injury.

The dermis is composed of two layers the papillary layer, a superficial area adjacent to the epidermis and a deep thicker one, known as the reticular layer **(Figure 1.1)**. The papillary region is composed of loose areolar connective tissue with elastic fibres and it contains dermal papillae that house capillaries and free nerve endings. The papillae provide the dermis with a "bumpy" surface that interdigitates with the epidermis, strengthening the connection between the two layers of skin. The reticular region lies deep to the papillary region and is usually much thicker. It is composed of dense irregular connective tissue with bundles of collagen, some elastic fibers and adipose tissue may be present, and receives its name from the dense concentration of collagenous, elastic, and reticular fibers that weave throughout it. These protein fibers give the dermis its properties of strength, extensibility, and elasticity. Type I collagen - the main component of the dermis - is the major dermal collagen with 15% of type III and lesser amounts of type IV and V. Dermis contains most of the skin's specialized cells such as adipose cells, mast cells, schwan cells, neurons, with fibroblasts being its principal cells. Located in the dermis are also the hair follicles, sebaceous glands, lymph vessels, blood vessels, sweat glands and nerve endings **(Figure 1.1)** (Freinkel & Woodley, 2001; Tortora & Grabowski, 2003; Goldsmith, 2005a).

1.1.3 Hair follicle

Hair follicle is a complex 'mini-organ'. A hair follicle is part of the skin that grows hair by packing cells together (Schmidt-Ullrich & Paus, 2005). Hair like sebaceous glands, have evolved in skin to form a thermoregulatory system common in mammals.

1.1.3.1 Hair follicle morphogenesis

Hair follicle is formed during embryogenesis as an appendage of the epidermis and involves a temporal series of epithelial-mesenchymal interactions **(Figure 1.5)** (Millar, 2002; Schmidt-Ullrich & Paus, 2005; Alonso & Fuchs, 2006; Blanpain & Fuchs, 2006). In the embryo, the skin begins as a single layer of epidermal stem cells. Soon after, as mesenchymal cells populate the skin to form the underlying collagenous dermis, morphogenesis of the hair follicle begins (Schmidt-Ullrich & Paus, 2005; Alonso & Fuchs, 2006). Initially, some of the undifferentiated basal cells receive a signal from the overlaying epidermis to make an appendage and to adopt a hair follicular fate. In response, the epidermis transmits a signal to the underlying dermal cells, in order to condense and form the dermal papilla cells (DP). The condensation of these specialized cells (DP) in the dermis, stimulates the epithelial stem cells within the overlying epidermal basal layer and these start to respond to this DP signal by changing their shape (elongate) to develop a bud or "placode", of hair progenitor cells that subsequently proliferate and grow downward, elaborating differentiation required to form the epidermal appendage (discrete lineages of the hair follicle and its hair). As the developing follicle extends downward and enwraps the DP, the cells at the base maintain a highly proliferative state. During follicle maturation, these rapidly proliferating cells, called matrix cells, after several rounds of cell division, differentiate upward to form the hair shaft (the structure composed of terminally differentiated keratinocytes that emerges from the skin surface as hair), its channel the inner root sheath (IRS) and the companion layer. Enclosed by the basement membrane, the basal layer of the follicle is referred to as the outer root sheath (ORS) and similar to the interfollicular epidermis it also expresses K5 and K14 keratins. Hair follicles also contain sebaceous glands to ensure the water impermeability of the hair. Also attached to the follicle is a tiny bundle of muscle fiber called the arrector pili, that is responsible for causing the follicle lissis to become more perpendicular to the surface of the skin,

and causing the follicle to protrude slightly above the surrounding skin (Blanpain & Fuchs, 2006).

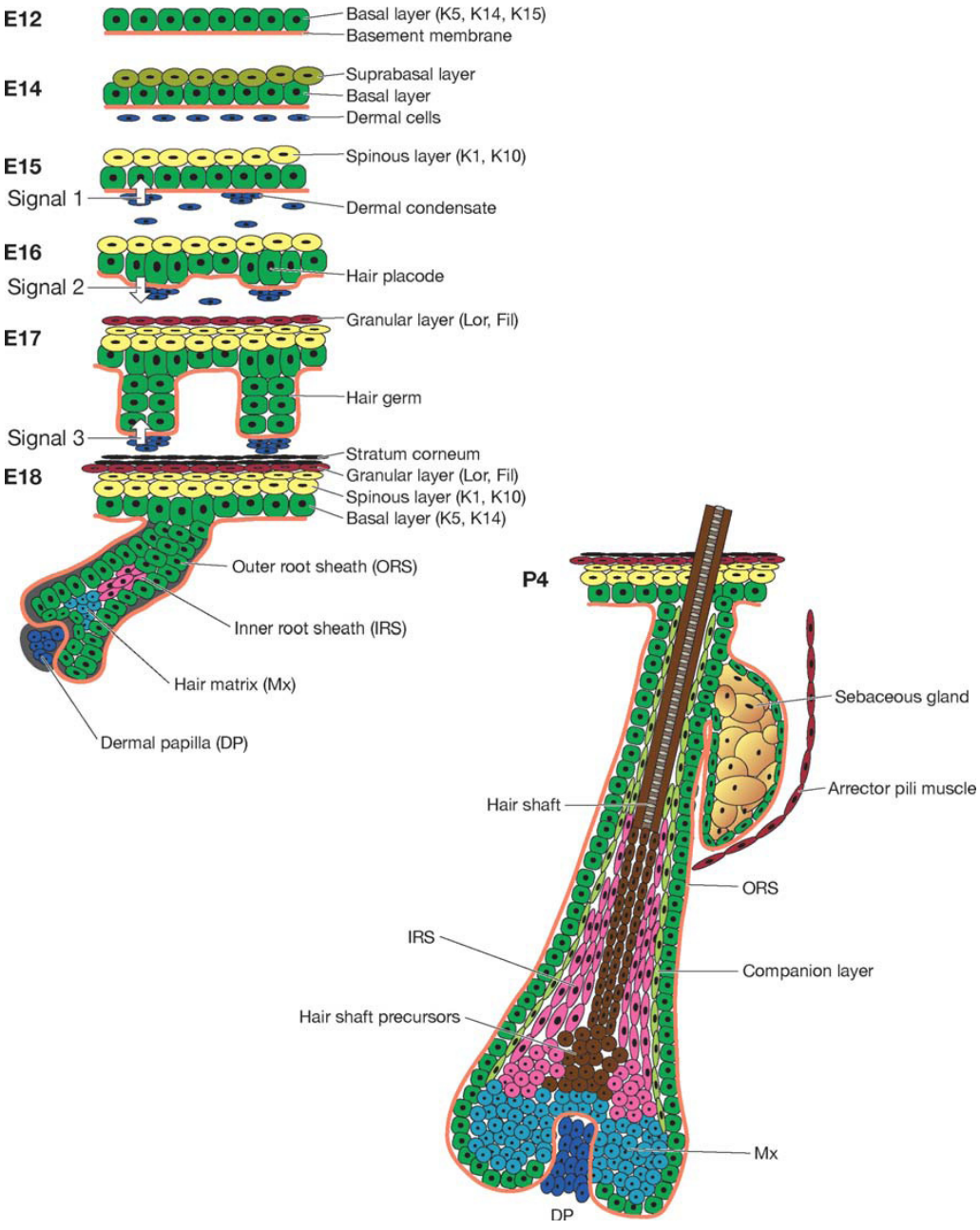

Figure 1.5: Hair follicle formation.

Hair follicle development during embryogenesis involves a series of epithelial-mesenchymal interactions. Mesenchymal cells (dermal papilla) initially stimulate the single layer of epidermal stem cells to adopt a hair follicular fate, which in turn stimulates the dermal papilla (DP) cells to condense. Then, the dermis by the condensation of DP sends a signal to the epidermis, stimulating the overlying epithelial stem cells to grow downward and produce a hair follicle. The hair follicle consists of the outer root sheath (ORS), the inner root sheath (IRS), the companion layer, the hair shaft, the arrector pili muscle and the sebaceous gland (Blanpain & Fuchs, 2006).

1.1.3.2 Hair follicle cycle

The hair coat requires a constant supply of new hairs throughout the lifetime. To produce new hairs, existing follicles undergo cycles of growth (anagen), regression (catagen) and rest (telogen) **(Figure 1.6)**. During each anagen phase, follicles produce an entire hair shaft, while, during catagen and telogen, follicles reset and prepare their stem cells so that they can receive the signal to start the next growth phase and make the new hair shaft (Alonso & Fuchs, 2006).

After hair follicle formation, and when matrix cells exhaust their proliferative capacity or the stimulus required for it, hair growth stops and the follicle regresses and draws the dermal papilla upward. At this time, the follicle enters a destructive phase - catagen- in which the lower two-thirds of the hair follicle rapidly degenerates by a process involving apoptosis. The upper third of the follicle remains intact as a pocket of cells surrounding the old hair shaft. The base of this pocket of cells is known as the "bulge", which is the natural reservoir of hair follicle stem cells necessary to form a new hair follicle. After catagen, the bulge stem cells enter a resting stage, known as telogen, in which the DP cells are in close contact with the bulge stem cells. At the start of the next hair cycle, quiescent stem cells residing at the base of the bulge are stimulated to migrate and proliferate to supply the cells needed for hair-follicle regeneration and hair growth (anagen), in a process that significantly resembles to that of embryonic folliculogenesis (Blanpain & Fuchs, 2006; Blanpain et al., 2007).

The three main signalling pathways which are involved in hair follicle morphogenesis and adult hair cycle are the Wnt/β-catenin (WNT), the sonic hedgehog (SHH) and the bone morphogenetic protein (BMP) (Millar, 2002; Schmidt-Ullrich & Paus, 2005; Blanpain & Fuchs, 2006). Bone morphogenetic proteins are secreted proteins that activate signal transduction by binding to a transmembrane receptor complex composed of Bmpr1 (Bone morphogenetic protein receptor 1) and Bmpr2 (Bone morphogenetic protein receptor 2) receptors (Blanpain & Fuchs, 2006). The role of BMPs in skin development begins in the neuroectothelium, when BMP signalling specifies uncommitted ectodermal cells to become epidermis (Nikaido et al., 1999; Blanpain & Fuchs, 2006). Later, during early hair follicle morphogenesis, BMP signalling is inhibited by a soluble inhibitor named Noggin, which is expressed by the dermal

condensates in order for the placode formation and hair follicle induction to occur (by promoting expression of LEF-1) (Botchkarev et al., 1999; Jamora et al., 2003; Blanpain & Fuchs, 2006). After placode formation through WNT signalling activation and as follicle maturation has progressed through SHH signalling activation, the activation of BMP signalling is essential for the matrix cell to differentiate to form the hair shaft and the inner root sheath (IRS) (Blanpain & Fuchs, 2006). Noggin is not only necessary in early stages of hair follicle morphogenesis, but it has also been reported to be required in the hair growth propagation (telogen to anagen transition) in the postnatal skin, via inhibition of BMP4 (Bone Morphogenetic Protein 4) and activation of SHH signalling (Botchkarev et al., 2001). The other two signalling pathways and their role to hair follicle morphogenesis and adult hair cycle are described in the following sections **(Section 1.3.1 and Section 1.3.3, and Section 1.4.2 and Section 1.5.1)**.

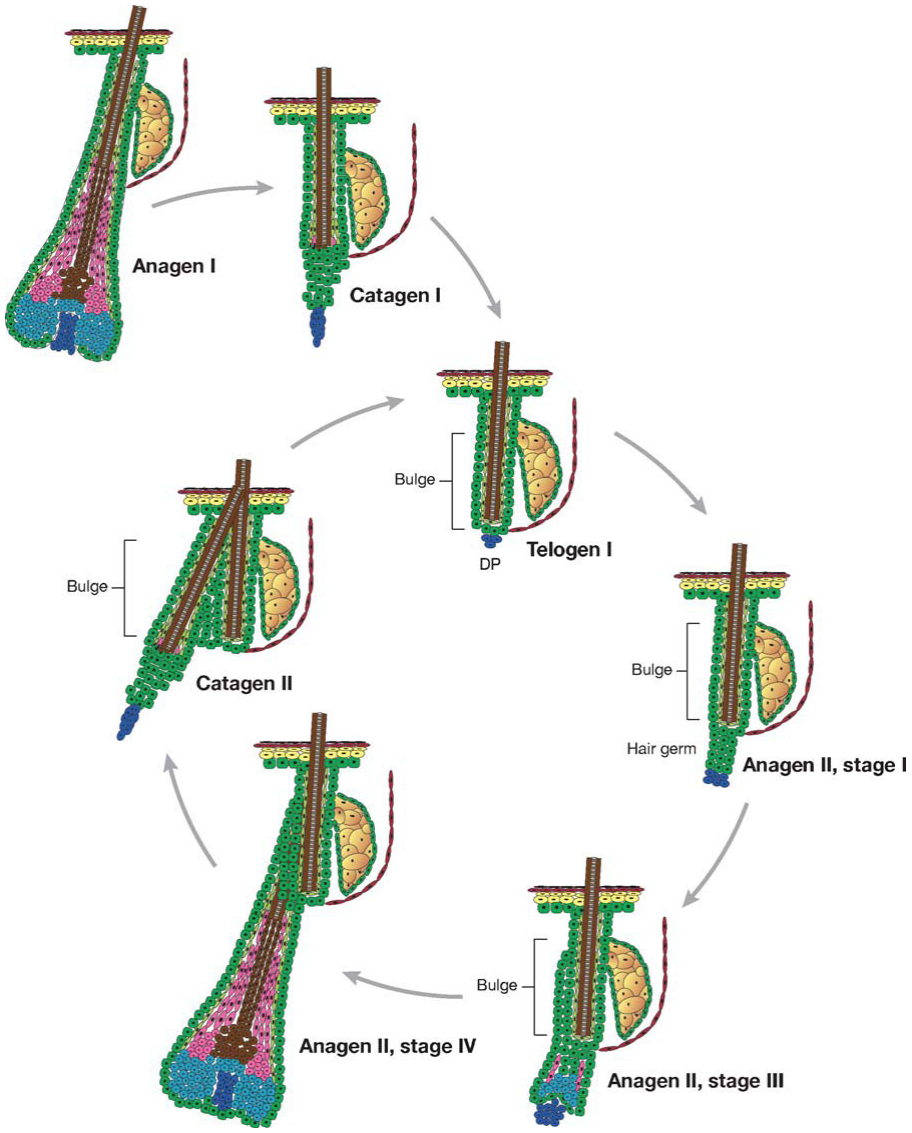

Figure 1.6: Hair follicle cycle.

Existing follicles undergo cycles of growth (anagen), regression (catagen), and rest (telogen) (Blanpain & Fuchs, 2006).

1.1.4 Hypodermis

The hypodermis or subcutaneous skin, consists of areolar and adipose tissue that insulates the body, and serves as a reserve energy supply **(Figure 1.1)** (Freinkel & Woodley, 2001; Tortora & Grabowski, 2003; Goldsmith, 2005a).

1.1.5 Epidermal stem cells

Stem cells are cell types capable of extensive self-renewal and unlimited replicative potential throughout adult life, which also have the ability to produce daughters that undergo terminal differentiation and thus differentiate into a diverse range of specialized cell types (Lajtha, 1979). Most epithelial tissues, including skin, self-renew throughout adult life due to the presence of multipotent stem cells and/or unipotent progenitor cells. This renewal capacity of the skin is dependent on proliferation of a subpopulation of keratinocytes, known as epidermal stem cells (Lavker & Sun, 2000; Blanpain & Fuchs, 2006; Watt et al., 2006; Blanpain et al., 2007). Thus, epidermal stem cells (SC) are responsible for renewing the epidermis throughout adult life giving rise to the differentiating cells of the interfollicular epidermis (IFE), hair follicles (HF) and sebaceous glands (SG) (Watt, 2001; Watt, 2002; Blanpain et al., 2007). Therefore, it appears to be at least three distinct niches of skin epidermal stem cells, the follicle bulge, the base of the sebaceous glands and the basal layer of the epidermis **(Figure 1.7)** and it also seems that these three progenitor populations share a few common expression markers such as K5, K14, p63, E-cadherin, $\alpha_3\beta_1$ and $\alpha_6\beta_4$ integrins as well as reduced levels of desmosomes and increased levels of adherens junctions (Fuchs, 2008).

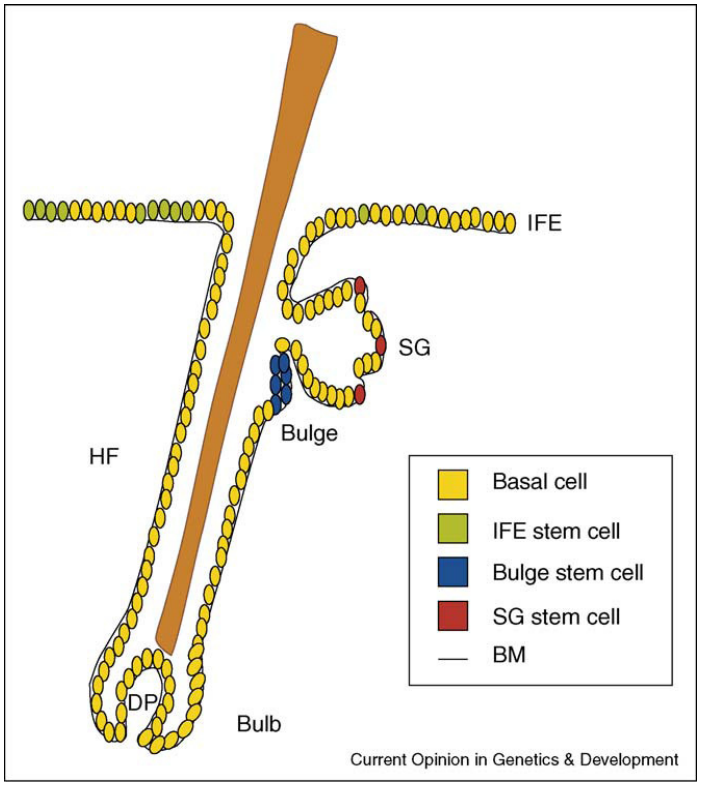

Figure 1.7: Location of epidermal stem cells.

Epidermal stem cells is believed to reside in three locations: in the hair follicle bulge, in the basal layer of the interfollicular epidermis (IFE) either as clusters (left of the IFE) or singly distributed (right of the IFE) (it is still unclear), and in the sebaceous gland (SG) (Watt et al., 2006).

The best characterised of these three reservoirs of stem cells, is the bulge of the hair follicle which consists of multipotent stem cells that can give rise to all lineages of skin epithelia including interfollicular epidermis **(Figure 1.8)**, when the skin is wounded in order to help the repair of the epidermis leading to the complete regeneration of the damaged epidermis (Cotsarelis et al., 1990; Taylor et al., 2000; Oshima et al., 2001; Blanpain & Fuchs, 2006; Levy et al., 2007). However, unless the skin is wounded, bulge cells only function in hair follicle homeostasis and are not essential for maintenance of the interfollicular epidermis, which instead depends on its own resident

stem cell population (Claudinot et al., 2005; Ito et al., 2005; Levy et al., 2005; Watt et al., 2006).

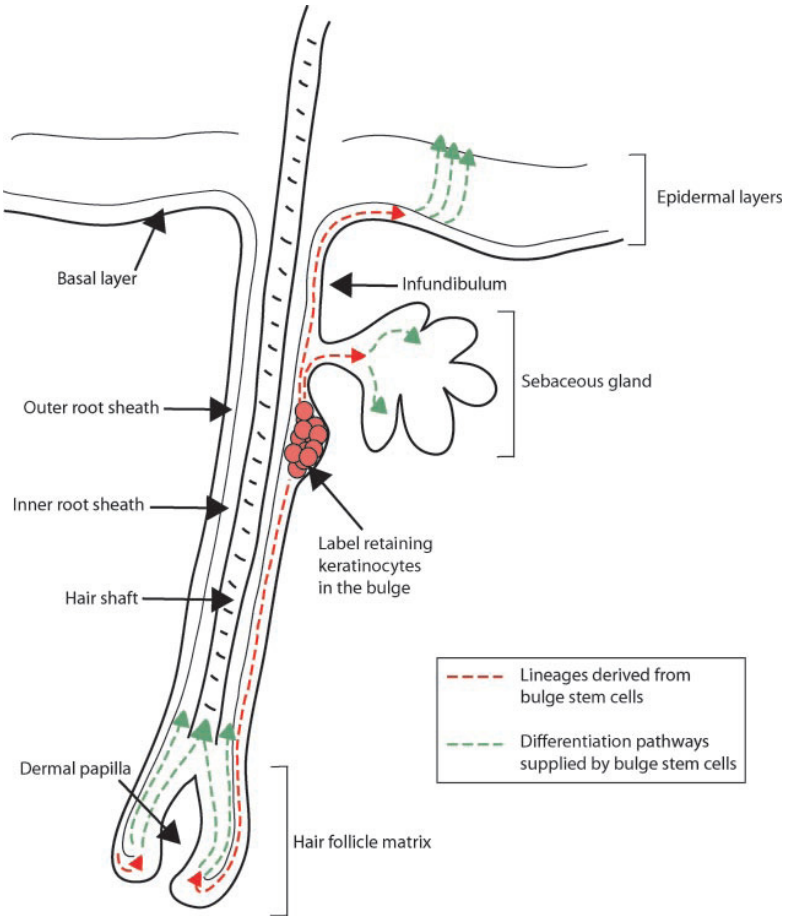

Figure 1.8: Bulge stem cells.

The bulge dominance model. Epidermal stem cells of the bulge are multipotent stem cells which are thought to contribute to the lineages of the hair follicle, the sebaceous gland and the epidermis and are the only reservoir of stem cells in the skin. Transit-amplifying cells from bulge stem cells differentiate in order to form the respective tissues (Alonso & Fuchs, 2003b).

However, more recently it was shown by Jaks et al. (Jaks et al., 2008) that there is another 'primitive' stem cell population which is able to give rise to all cell types in the mouse hair follicle including the bulge cells and is marked by high expression of Lgr5. These Lgr5-expressing cells are located in the lower bulge and secondary germ area of mouse telogen hair follicles and in the lower outer root sheath of anagen hair follicles (Jaks et al., 2008). Surprisingly, in contrast with the notion thet hair follicle stem cells

are relatively quiescent and located in the bulge of telogen hair follicles, the Lgr5-expressing cells are actively-cycling and showed potent self-renewal and hair follicle reconstitution ability (Jaks et al., 2008). In addition, Lgr6, a close relative of Lgr5 stem cell gene, marks a distinct population of stem cells giving rise to all lineages of the skin (Snippert et al., 2010). Lgr6 is expressed in the earliest embryonic hair placodes and resides in a previously uncharacterised region directly above the mouse follicle bulge. Therefore, Lgr6 marks the most primitive epidermal stem cells which are located directly above the CD34 and keratin 15-positive bulge and replace the whole epidermis and its appendages under normal conditions and upon wounding (Snippert et al., 2010).

Even though it is known for many years that stem cells exist within the basal layer, it is not yet resolved whether all cells of the basal compartment are stem cells, and thus a single progenitor population through asymmetric division can give rise to committed cells by differentially partitioning proteins to the daughters (asymmetric division model) as very recently proposed by Clayton et al. (Clayton et al., 2007; Jones et al., 2007; Fuchs, 2008), or only a small number of stem cells exist within the basal layer as originally proposed by Potten et al. (Epidermal Proliferative Unit - EPU model) (Potten, 1974; Fuchs, 2008).

According to the EPU model **(Figure 1.9)**, the mouse epidermis is divided into a number of units each of which is known as epidermal proliferative unit that consists of ~ 10 tightly packed basal cells, which yield a stack of increasingly larger and flatter intermediate keratinized cells ('columnar unit'), finally giving rise to a single hexagonal surface cell (Mackenzie, 1970; Potten, 1974; Mackenzie, 1997). Although, this model is extensively studied in mice, a similar columnar (stacking) organization is also present in the human epidermis and in that of other mammalians, suggesting some compartmentalization comparable to the EPU of the mouse (Mackenzie, 1969; Mackenzie et al., 1981). This notion was further supported by experiments where either mice or human keratinocytes were retrovirally transduced with the Lac-Z gene, which coded for the β-gal, and grafted into athymic mice (Mackenzie, 1997; Kolodka et al., 1998). β-gal expression in the reconstituted epidermis occurred in columnar clusters, consistent with the concept of the EPU model. In addition, due to the columnar organization, and the highly mitotic activity of the basal cells in the periphery of the units compared to the mitotically quiescent cells beneath the central regions of the units,

it is suggested that each EPU contains a single slow-cycling, self-renewing stem cell. The remaining basal cells of the unit, are stem cell daughters that have left the stem cell compartment, are able to divide a small number of times prior to terminal differentiation, and are known as transit-amplifying cells or committed progenitors for the hemopoietic system (Mackenzie, 1970; Potten, 1974; Mackenzie, 1997; Kolodka et al., 1998; Watt, 2002).

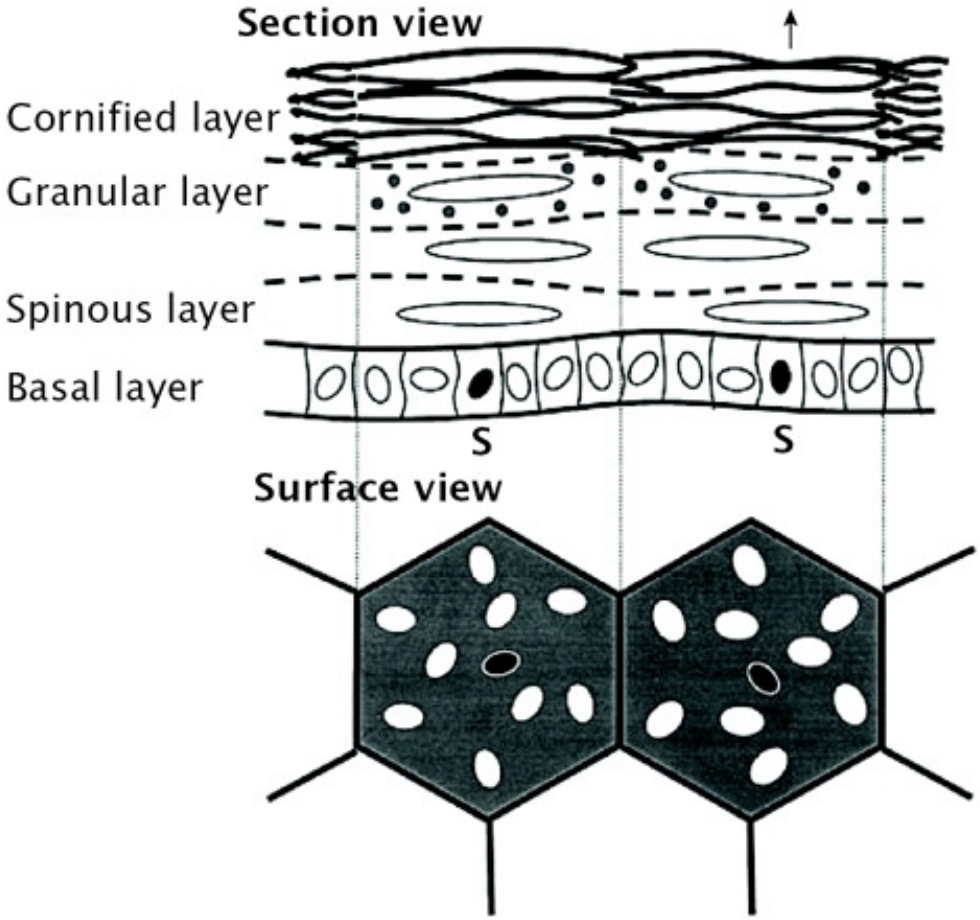

Figure 1.9: Epidermal Proliferative Unit (EPU) model.

Potten's model of the epidermal proliferation unit for mice. Each approximately hexagonal unit of surface skin renews from a basal layer comprising about ten cells, of which only one basal stem cell **(S)** renews the unit (Steven, 2007).

1.1.5.1 Heterogeneity in the epidermal basal layer

1.1.5.1.1 Heterogeneity *in vitro* and *in vivo*

The existence of a progenitor cell compartment (hemopoietic system) equivalent to transit-amplifying cells in the basal membrane that are still cycling (Potten & Morris, 1988), amplifies the effect of each stem cell division so that a relatively small number of slow rounds of stem cell division-probably a requirement for stem cell 'safety' ('error free' stem cell genome) and conservation of cell's proliferative potential - results in the production of a large number of terminally differentiated cells (Lajtha, 1979; Jones & Watt, 1993; Lavker & Sun, 2000; Potten & Booth, 2002). Thus, under steady-state conditions *in vivo*, epidermal stem cells in mouse epidermis are believed to divide infrequently, and to have a long cell cycle time, estimated to be about twice (200 hr or 8 days) that of the transit-amplifying cells, unless there is need for regeneration of the tissue due to tissue damage or due to *in vitro* culture conditions, in which cases they are capable of sustained self-renewal (more frequent divisions) (Potten, 1974; Potten et al., 1982; Clausen et al., 1986; Loeffler et al., 1987; Potten & Morris, 1988; Kirkhus & Clausen, 1990; Potten & Booth, 2002). Information for the human epidermis is largely lacking, but the stem cell cycle time is likely to be greater than 500 hr (about 21 days) (Potten & Booth, 2002). *In vivo*, the mouse stem cell cycle times are capable of reductions from 200 hr to significantly less than 12 hr under wounding conditions (Potten & Booth, 2002). *In vitro*, although epidermal stem cells are capable of sustained self-renewal (frequent divisions - clonal growth), transit-amplifying cells will undergo differentiation within a few rounds of division (no clonal growth) (Watt et al., 2006). On the other hand, adult tissue stem cells have a long cell cycle time *in vivo*, or may spend much of their time out of cycling in G_0 or quiescence (rarely cycling), one of the most universally accepted criterion of stem cells (Lajtha, 1963; Lajtha, 1979; Potten et al., 1982; Clausen et al., 1986; Potten & Morris, 1988; Clausen & Potten, 1990; Potten & Booth, 2002).

During *in vitro* culture conditions, even if stem cells have sustained self-renewal and their overall cell cycle length might be shorter from their *in vivo* one, still there is heterogeneity in the cell cycle times between human cells in culture (Potten & Morris, 1988; Clausen & Potten, 1990). Cell kinetic analysis in human keratinocytes *in vitro*, revealed two discrete subpopulations, one fast and one more slowly cycling population

(Dover & Potten, 1983). Results based on multiparameter RNA/DNA analysis of cells stained with the metachromatic dye acridine orange, also revealed two distinct subpopulations of human epidermal cells, markedly differing in RNA content, growing *in vitro* (Eisinger et al., 1979). Usage of the acridine orange dye allows differential staining of DNA and RNA due to the fact that when the dye binds the double-stranded DNA fluoresces green, while when it binds the single-stranded RNA fluoresces red. Thus, flow cytometry analysis showed that the majority of the epidermal cells had high-RNA content and were rapidly cycling, while a minority population had lower RNA values and were cycling much slower (Eisinger et al., 1979). Given that in other cell systems the non-cycling quiescent cells are characterised by a low RNA content compared to their cycling counterparts (Darzynkiewicz et al., 1977; Darzynkiewicz et al., 1979), a proportion of these low RNA content epidermal cells might represent a non-cycling quiescent subpopulation.

It has also further been shown that in human epidermal cultures grown *in vitro*, the low-RNA content and long cell-cycle time epidermal cells were small, while the high-RNA content and short cell-cycle time epidermal cells were significantly larger (two to three times) (Staiano-Coico et al., 1986). Both of these subpopulations were proliferating, albeit at different rates, but there was also a third subpopulation of cells consisting of large, non-dividing cells with the highest RNA content. Therefore, it is suggested that the small basal cells (low RNA, long cell cycle time) have stem cell properties, while the larger cells (high RNA, short cell cycle time) resemble the transit-amplifying cells and terminally differentiating keratinocytes (Barrandon & Green, 1985; Staiano-Coico et al., 1986).

The evidence of this heterogeneity within the proliferative compartment in the epidermis (Clausen & Potten, 1990) is supported not only from *in vitro* studies of cultured human keratinocytes (holoclones, paraclones, meroclones) **(see Chapter 3, Section 3.3.4)** (Barrandon & Green, 1987), but also by further *in vivo* functional studies which show that even though a 60% of basal cells are known to be cycling, only 10% of the basal keratinocytes are able to form new epidermis when mouse skin is damaged by radiation (Withers, 1967; Potten & Hendry, 1973; Potten & Morris, 1988). Thus, this 10% of dividing cells with a high proliferative capacity are believed to correspond to stem cells, while the rest 50% of dividing cells are the transit-amplifying cells which are

able to divide for a small number of times, before they will give rise to the remaining 40% of the basal layer cells. This 40% seems to be the cells that have withdraw irreversibly from the cell cycle (post-mitotic) and are committed to terminal differentiation (Potten et al., 1982; Potten & Morris, 1988).

1.1.5.1.2 Heterogeneity of basal keratinocytes on their ability to respond to tumour promoter treatment

The functional heterogeneity of basal keratinocytes can also be reflected in their differential ability to respond to tumour promoter treatment *in vitro*. Phorbol esters such as TPA (12-0-tetradecanoyl phorbol-13-acetate), also known as PMA (phorbol 12-myristate 13 acetate), are strong tumour promoters for carcinogen-initiated mouse skin, due to their ability to modulate the balance between keratinocyte proliferation and differentiation (Boutwell, 1974; Yuspa et al., 1976; Scribner & Suss, 1978). Single application of TPA in mouse skin causes differentiation/cell death and regenerative epidermal hyperplasia which is thought to be essential for tumour promotion (Argyris, 1980a; Argyris, 1980b). Induction of sustained hyperplasia by TPA treatment has also been reported in human foreskin epidermis maintained as a xenograft in nude mice (Yuspa et al., 1979). *In vitro*, TPA induces terminal differentiation in cultures of normal (Hawley-Nelson et al., 1982; Parkinson & Emmerson, 1982) and SV-40-transformed (Mufson et al., 1982) human epidermal keratinocytes, while keratinocytes derived from human squamous cell carcinoma oppose suspension induced differentiation *in vitro* (Rheinwald & Beckett, 1980) suggesting that transformed cells might be less sensitive to TPA-induced terminal differentiation compared to their normal counterparts (Parkinson et al., 1983).

Treatment of mouse basal keratinocytes cultured in low calcium, with TPA, can induce both terminal differentiation by induction of the enzyme epidermal transglutaminase in a subpopulation of cells, and cell growth and proliferation in another (resistant to differentiation), a response that depends upon the nature of the target cell (Yuspa et al., 1980; Yuspa et al., 1982). The resistant in TPA-induced differentiation basal cells kept also their resistance to subsequent extracellular calcium-induced differentiation, while upon a second exposure to TPA (applied in a short term after the first one - 4 days), instead of these cells to differentiate like the control cells did, they were stimulated to

proliferate (Yuspa et al., 1982). Further work has shown that a similar functional heterogeneity is also present in normal human epidermal keratinocytes *in vitro* with transformed human keratinocyte lines containing far more TPA-differentiation resistant cells than their normal counterparts (Parkinson et al., 1983). It was estimated that a sub-population comprising approximately 10% of cultured normal human epidermal keratinocytes, is refractory to TPA-induced differentiation, and does not loose its cloning efficiency (colony formation capacity) upon exposure to TPA (Parkinson et al., 1983). Interestingly, the estimate of TPA resistant keratinocytes was roughly equivalent to the estimated proportion of stem cells occupying the mouse basal layer of the epidermis *in vivo* (Parkinson et al., 1983; Parkinson et al., 1987; Potten & Morris, 1988; Clausen & Potten, 1990). It was thus postulated that TPA resistant cells may represent a population of immature keratinocytes that are defective in their commitment to terminal differentiation, and are thus likely to be stem cells.

It was later established that the growth inhibitory effect of TPA was indeed targeted to keratinocytes that were more committed to terminal differentiation rather than immature basal cells (Parkinson et al., 1987). TPA treatment was able to induce a strong proliferative effect in human keratinocytes derived from the more immature foetal skin, but had the opposite effect when it was used to treat juvenile human keratinocytes (Parkinson et al., 1987). Furthermore, the proportion of TPA resistant keratinocytes was shown to be inversely correlated with donor age of either human or mouse skin, and can reach up to 30% in newborn mice (Parkinson et al., 1987). This further supported the evidence of a functional heterogeneity among basal epidermal keratinocytes *in vitro* and further suggested that the more immature basal epidermal keratinocytes comprise the proliferating keratinocyte population in response to phorbol ester treatment.

1.1.5.1.3 Heterogeneity of basal keratinocytes revealed from studies of label-retaining cells (LRC)

More evidence for the cellular heterogeneity in the basal layer is also provided by studies of label-retaining cells (LRC). Due to the infrequent and slow-cycling nature of stem cell, a single pulse with tritiated thymidine (^{3}H-TdR), a DNA precursor typically used to label cells in S phase, will not be enough to label all stem cells. Therefore, continuous administration of ^{3}H-TdR for a prolonged period to neonatal or young adult

mice will be required, in order for the majority of stem cells to be labelled. Hence, once epidermal stem cells are labelled, due to their slow cycling status they will retain the isotope for an extended period of time in contrast to rapidly dividing cells (transit-amplifying cells) and thus can be identified as "label-retaining cells" (Bickenbach, 1981; Potten & Morris, 1988; Clausen & Potten, 1990). Studies on these cells show that label-retaining cells have a non-random distribution in the epidermis, found scattered and located towards the centre of columns of keratinocytes in the interfollicular epidermis (~ 1 - 4% - 30 d chase period) (EPU-epidermal proliferation unit), the site suggested for basal stem cells (Potten, 1974; Bickenbach, 1981; Potten & Morris, 1988; Mackenzie, 1997; Potten & Booth, 2002), or being concentrated in a region of the hair follicle known as the 'bulge' (~ 60% LRCs - 20 d chase period), the site suggested for the hair follicle stem cells (Cotsarelis et al., 1990; Morris & Potten, 1994; Morris & Potten, 1999).

Even though, label-retaining cells are slow cycling, they can be stimulated to proliferate by mitotic activation accompanied by an undifferentiated phenotype, following application of the tumour promoter TPA, known to stimulate DNA synthesis in both the epidermis and hair follicle (Bickenbach, 1981; Morris et al., 1986; Cotsarelis et al., 1990). In contrast, most of the mature pulse-labelled cells were rarely found in mitosis in response to TPA treatment but were instead displaced from the basal layer and ultimately lost from the epidermis (Morris et al., 1986). Thus, label-retaining cells proliferate, whereas most pulse-labelled cells differentiate in early response to TPA, in agreement with the *in vitro* study (Parkinson et al., 1983) that reported the existence of a subpopulation of normal cultured human keratinocytes which are resistant to TPA induced differentiation, and thus may represent stem cells which have been selected by TPA, due to their defective commitment to terminal differentiation.

Although, at least some of the labelled cells might be arrested in S phase as a consequence of radiation-induced DNA damage, Morris and Potten (Morris & Potten, 1994) ruled out this possibility by correlating label retention with proliferative potential *in vitro*. They showed that label retaining basal cells cultured from mouse epidermis, divide to form colonies (more clonogenic) and appear to possess greater proliferative potential than do pulse-labelled cells (mature basal cells), which form colonies only rarely (Morris & Potten, 1994). Another study by Bickenbach et al. (Bickenbach &

Chism, 1998) further supported the clonogenic capacity and extended growth of mice ^{3}H-TdR and bromodeoxyuridine - BrdU (thymidine analog incorporated into proliferating cells - S phase) LRCs, consisting of clones of small and slow growing cells, which are also accompanied by another keratinocyte stem cell characteristic (Li et al., 1998), the rapid attachment to different extracellular matrix proteins of the basal membrane. This *in vitro* clonogenic capacity of the ^{3}H-TdR LRC and BrdU LRC along with their capability of rapid attachment to different substrates, further support the view that LRC may be representative of slow cycling epidermal stem cells. In addition, this further supports previous studies that have demonstrated that the clonogenic keratinocytes *in vitro* of the rat and human hair follicles reside primarily in the bulge region of the hair follicle, where LRC have been found to be located (Cotsarelis et al., 1990), with the only difference that in human, the zone of clonogenic cells was broader extending from the bulge to the lower outer-root-sheath (ORS) (Kobayashi et al., 1993; Rochat et al., 1994).

More recent studies have also demonstrated that LRC, apart from being clonogenic *in vitro*, have also the capacity of self-renewal, another stem cell characteristic. Both Taylor et al. (Taylor et al., 2000) and Tumbar et al. (Tumbar et al., 2004) showed that bulge LRC have the capacity to regenerate epidermis in response to injury. Tumbar et al. (Tumbar et al., 2004) also showed that bulge LRC are able to regenerate hair follicle during the normal hair cycle, which supports the studies of Oshima et al. (Oshima et al., 2001) demonstrating the ability of bulge cells to contribute to all the differentiation lineages involved in the formation of hair follicle as well as in the differentiation into sebocytes and interfollicular epidermis.

Label-retaining basal cells also resemble morphological stem cell characteristics. *In vitro* density gradient sedimentation methods, which allow the separation of cells on the basis of size and density, were used in order to separate epidermal cells harvested from mice adult skin (Morris et al., 1990). It is well established that decreasing density and increasing size are correlated with maturity (differentiation) of keratinocytes and therefore differences in density might permit enrichment for a subpopulation of basal cells having *in vivo* and *in vitro* properties of immature undifferentiated epidermal cells (Morris et al., 1990). Thus, suprabasal keratinocytes remained primarily at the top of the gradient (less dense, large size), while basal keratinocytes sedimented throughout, but

were enriched at the lower part of the gradient (more dense, small size), following further continuous sedimentation in order for the basal cells to become separated according to different density. Interestingly, sedimentation of subpopulations of epidermal basal cells from adult mice labelled *in vivo* with ^{3}H-TdR or with a carcinogen, showed that the densest fraction which is morphologically characterised by small cells with high nuclear to cytoplasmic ratio is enriched for LRCs, or carcinogen retaining cells, while maturing pulse labelled cells were enriched in lighter fractions (larger cells) (Morris et al., 1990). Moreover, dense basal cells from normal epidermal cells were enriched about two fold for cells that can form colonies *in vitro* (Morris et al., 1990). Therefore, overall LRC are small, dense cells with high ratio of nuclear to cytoplasmic volume, with self-renewal capacity and high clonogenic *in vitro* potential, all of which are known epidermal stem cell characteristics (Barrandon & Green, 1987; Morris et al., 1990; Jensen et al., 1999; Morris, 2000; Tani et al., 2000; Zhou et al., 2004).

1.1.5.1.4 Functional validity of LRCs

The functional validity of LRCs was further supported by the first study that linked specific cell surface markers (potentially epidermal stem cell markers) with both *in vitro* growth potential and *in vivo* cell kinetic analysis (Li et al., 1998; Tani et al., 2000). Tani et al. (Tani et al., 2000) isolated mice keratinocytes through FACS and demonstrated that the subpopulation of mice keratinocytes characterised by high levels of integrin α_6 (adhesion molecule) and low levels of trasferrin-receptor CD71 (proliferation associated surface marker), termed α_6^{bri} $CD71^{dim}$ cells, are enriched for epithelial stem cells due to their small, blast like with high nuclear to cytoplasmic ratio morphology and due to the fact that are comprising only a minor population (~ 8%) of quiescent cells at the time of the isolation from the epidermis, exhibiting a great long-term proliferative capacity *in vitro*, as it has been previously shown for α_6^{bri} $CD71^{dim}$ human keratinocytes (Li et al., 1998). Interestingly, this cell fraction (α_6^{bri} $CD71^{dim}$) was enriched in label-retaining cells (~ 70%), rendering slow-cycling ^{3}H-TdR LRCs, a valid term for murine keratinocyte stem cells. Conversely, the other subpopulation of murine keratinocytes expressing both high levels of α_6 and CD71 markers, termed as α_6^{bri} $CD71^{bri}$ cells, represent the majority of keratinocytes (~ 60%), which are larger and exhibit only short-term proliferative potential *in vitro*, as it has also been shown for α_6^{bri} $CD71^{bri}$

human keratinocytes (Li et al., 1998), and thus thought to represent the transit-amplifying cells (Tani et al., 2000). Importantly, this fraction is enriched (~ 70%) in ^{3}H-TdR pulse-labelled cells (PLCs) labelled after a single injection of ^{3}H-TdR. In addition, immunostaining of skin mouse revealed the presence of CD71^{dim} cells in the bulge of the hair follicle, a well documented location of keratinocyte stem cells (Cotsarelis et al., 1990).

1.1.5.1.5 LRCs in human

The evidence for the presence of LRCs *in vivo* is restricted to mice, due to the unfeasible application of labelling protocols to humans. However, LRCs have been observed in human embryonic and fetal epidermis growing *in vitro* (organ cultures) (Bickenbach & Holbrook, 1987). Approximately 4% and 2% of the embryonic and the fetal epidermal cells respectively, retained ^{3}H-TdR label after a chase period of 21 days in organ culture. In addition, a recent study demonstrated the presence of human LRCs in reconstructed human epidermis. Human epidermal keratinocytes were grown on top of either collagen matrix (maximum 4 weeks - one complete epidermal regeneration cycle), or on modified dermal equivalents (human fibroblasts scaffolds), the latter of which are able to support tissue regeneration for a minimum period of 12 weeks (Muffler et al., 2008). Keratinocytes were repeatedly pulsed with iododeoxyuridine - IdU (thymidine analog incorporated into proliferating cells - S phase) for either 2 days or for 2 weeks for collagen (col-OTC) and scaffold (sca-OTC) organotypic cultures respectively, and basal LRCs unevenly and randomly dispersed throughout the basal layer, were identified in both types of reconstructed epidermis after a chase period of 2 weeks for collagen and 2-10 weeks for scaffold supported reconstructs, but only the scaffold organotypic cultures supported the maintenance of human epidermal stem cells and long-term epidermal regeneration. Even though, initially all cells were labelled (100%) in sca-OTS, LRC percentages decreased down to ~ 1% of basal cells, and remained constant for the 8 and 10 week chase period, suggesting reestablishment of the homeostasis of the epidermis. Interestingly, longer chase periods of 10 weeks in scaffold supported epithelium, revealed the presence of quiescent basal LRCs, which were frequently close to mitotically active non-labelled basal keratinocytes. However, some Ki-67 positive LRCs were seen at all time points (including 10 week chase period)

indicating that while in long term OTCs and presumably in homeostatic conditions, LRCs are largely quiescent, they are still capable of proliferation. Although organotypic reconstruction of human epithelium is not an exact representation of the *in vivo* situation, this study, based on the demonstration of LRCs in an optimised tissue organization, and the finding that LRCs appear at a frequency (<1%) (after a 6 week chase period in the interfollicular epidermis), similar to the percentage estimated of cells which are able to reconstitute the mouse epidermis (stem cells) observed in another *in vivo* study in mice (Schneider et al., 2003), and very close to the number of LRCs found in mouse epidermis (2% 30 d after labelling - 0.2% 8 mo after labelling) (Bickenbach, 1981), suggests that a similar LRC-based stem cell hierarchy may exist in human epithelium.

However, previous studies in mice had shown that the percentage of cells which are able to reconstitute the mouse epidermis after irradiation, are ~ 10% as I have previously mentioned (Withers, 1967; Potten & Hendry, 1973). The discrepancies regarding the estimated percentages (0.01-10%) of stem cells occupying the basal layer of the epidermis could potentially be attributed to the differences in the techniques that were employed to detect such populations (Potten & Morris, 1988; Clausen & Potten, 1990; Bickenbach & Chism, 1998; Schneider et al., 2003). Notably, the percentage of cells that could reconstitute mouse epidermis after transplantation in the fascia (soft tissue component of the connective tissue system) of immune deficient mice was only 0.01%, which is 1000 times smaller than the estimated percentage of cells that reconstituted mouse epidermis following irradiation (~ 10%). One limitation of the former observation could be the possibly reduced transplantation efficiency of mouse keratinocytes, taking into account that fascia might be a suboptimal environment for epidermal stem cell growth compared to the observations made in intact mouse epidermis during irradiation experiments. On the other hand, the estimate of 0.2 - 2% of LRCs in mouse epidermis, reported by Bickenbach et al. (Bickenbach, 1981) and other label retaining studies (Clausen & Potten, 1990; Bickenbach & Chism, 1998) is in good approximation to the percentage of LRCs found in human embryonic and fetal epidermis *in vitro* (Bickenbach & Holbrook, 1987) and in human sca-OCTs (Muffler et al., 2008), if one takes into account the intrinsic differences between mouse and human keratinocytes, and the differences between an *in vivo* situation and an *in vitro*

reconstituted epidermis or *in vitro* culture. Thus the exact number of epidermal stem cells still remains elusive.

1.1.5.1.6 LRCs and immortal strand hypothesis

Even if the slow cell cycle of stem cells seems to be the reason for the presence of LRCs, it is unlikely to be the sole explanation. The retention of label in bulge stem cells is not surprising, taking into account that these cells rarely undergo cell cycle progression and division once the follicle is formed. On the other hand, it is surprising that label retention persists in the interfollicular epidermis for many weeks and over a time course when stem cells would have been expected to have divided many times, according to cell kinetic analysis, and hence to have diluted their incorporated label (Potten & Morris, 1988; Potten & Booth, 2002; Potten et al., 2002). Thus, either stem cells divide even less frequent and much slower than the initial kinetic studies have predicted, or other explanations for the label retention must apply. One such explanation could be the selective DNA strand segregation in which case stem cells do not randomly segregate their DNA but selectively retain some radiolabelled DNA strands. This hypothesis (immortal DNA strand hypothesis) was first proposed for stem cells self-renewal by John Cairns in 1975 **(Figure 1.10)** (Cairns, 1975). During replication, the double helix of each chromosome is pulled apart and each strand serves as the template for creating the new opposite strand. After replication, due to fact that DNA is duplicated semi-conservatively, the two copies called sister chromatids are each half old and half brand new. During mitosis, the chromatid pairs are separated from each other and are randomly segregated into the daughter cells (one pair per daughter cell). According to Cairns' hypothesis, adult stem cells during mitosis, sort the old (templates) from the new DNA strands (non-random template segregation) and divide their DNA asymmetrically in a way that one daughter cell will always contain the older ('grandparent') template strands (stem cell), while the other daughter cell will contain the newly ('parent') synthesised strands (transit-amplifying cells) **(Figure 1.10)** (Cairns, 1975; Rando, 2007). According to Cairns (Cairns, 1975) this is a protective mechanism, by which adult stem cells avoid acquiring mutations arising from errors in DNA replication that could lead to cancer. Thus, stem cell would retain, throughout the life of the organism, its original ('immortal') error-free DNA strands, that were generated when the cell population first arose during development, and these immortal strands

would continue to serve as error-free templates indefinitely. At the same time the newly synthesised strands (with any replication-associated errors) would pass to the daughters destined for terminally differentiation and subsequent loss (transit-amplifying cells) (Cairns, 1975; Rando, 2007). This phenomenon would suggest that label given at a time when new stem cells are being made either during development or tissue regeneration after injury (label-retention assay), would be incorporated into the permanent (immortal) template DNA strands in the stem cells and thus become permanently labelled - become LRCs of which label retention will not be necessarily related to the length of the cell cycle (Cairns, 1975; Potten & Booth, 2002; Rando, 2007). On the other hand, if the label is given under homeostatic conditions, where only the newly synthesised strands will be labelled, and if the segregation is not random and the stem cell retains the older unlabelled template strands, it will lose all label by the second division after administration of the label (label-release assay) (Rando, 2007).

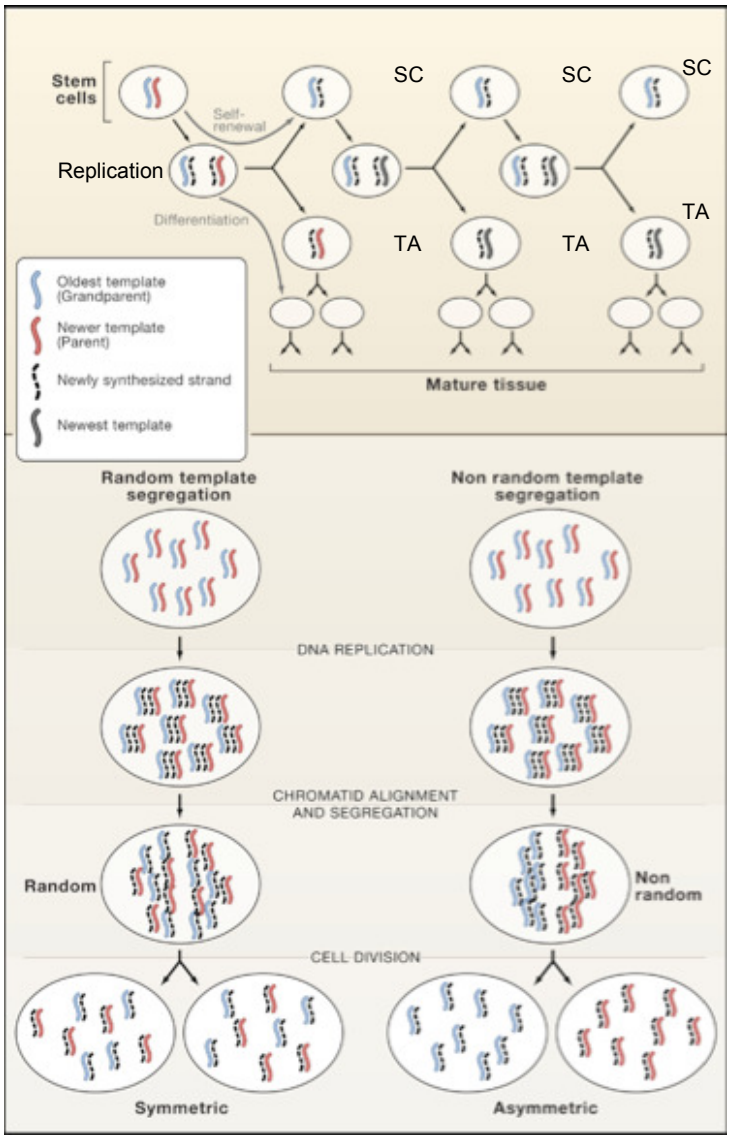

Figure 1.10: Immortal strand hypothesis.

Retention of an immortal strand during self-renewal **(Top panel)**. Adult stem cell, containing a single chromosome consisting of an older ('grandparent') template (blue) and a younger ('parent') template (red). Following DNA replication and due to an asymmetric division it gives rise to a new stem cell **(SC)** through self-renewal and to the transit-amplifying cell **(TA)** which will give rise to the differentiated mature cells. According to the immortal strand hypothesis the sister chromatid containing the older 'immortal' strand (blue) remains with the continually renewing stem cell through repeated asymmetric divisions for the life of the organism. Random and non-random template strand segregation **(Bottom panel)**. Differences in distribution of multiple chromatids (in this example, in a theoretical cell with 4 pairs of chromosomes giving rise to 16 sister chromatids following DNA replication) if the segregation is either random or non-random. According to Cairns (Cairns, 1975), following DNA replication adults stem cells sort the old (templates) from the new DNA strands (non-random template segregation) and divide their DNA asymmetrically in a way that one daughter cell will always contain the older ('grandparent') template strands, while the other daughter cell will contain the newly ('parent') synthesised strand (Rando, 2007).

The immortal strand hypothesis proposed by Cairns was not purely theoretical. Studies since 1960 had shown that there was non-random template strand segregation based in DNA template age in bacteria (Cuzin & Jacob, 1965), in mouse embryonic fibroblasts (Lark et al., 1966) and in the growing root tips of plants (Lark, 1967). Further, *in vitro* and *in vivo* studies using either label-retention or label-release assays in stem cells of the mouse small intestine (Potten et al., 1978; Potten et al., 2002), breast (Smith, 2005), brain (Karpowicz et al., 2005) and muscle (Shinin et al., 2006) have shown that stem cells segregate their chromosomes non randomly and asymmetrically, and tend to keep the same old template DNA strand through successive divisions, highly supporting the immortal strand hypothesis. In another noteworthy study by Merok et al. (Merok et al., 2002), *in vitro* cultured cells (immortal non-tumourigenic mouse mammary epithelial cells), that model the *in vivo* asymmetric cell kinetics of adult stem cells (renewal growth) upon p53 inducible activation, were used (Sherley et al., 1995). They used this *in vitro* model in order to show that when p53 is continuously overexpressed in non-stem cells, the cells are induced to divide asymmetrically like adult stem cells (one dividing self-renew stem cell and one daughter cell destined for differentiation), and they also keep their old template strands together (non-random co-segregation of chromosomes containing immortal DNA strands) compared to the non-continuously overexpressing p53 cells (Merok et al., 2002).

One of the main restrictions in order for the immortal strand hypothesis to become broadly accepted is the fact that all *in vivo* stem cell examples of non random strand segregation have been limited to, at most, a few percent of the cells. However, recently Conboy et al. (Conboy et al., 2007) showed that in muscle stem cells (satellite cells), during tissue regeneration, the frequency of asymmetric divisions associated with template strand segregation is not as rare as in the other stem cell self-renewal *in vivo* studies, but it is approaching the 50% of the proliferating (dividing) stem cells labelled *in vivo*. This difference in frequency, is probably due to the fact that previous *in vivo* studies have sought evidence of the non-random segregation during normal homeostatic turnover, while in Conboy et al. (Conboy et al., 2007) study, the experiments were carried out during tissue repair, where there is tremendous cell division and thus high rate of stem cell expansion. Interestingly, satellite cells not only segregate their DNA non-randomly by separating all the chromatids with the older templates from those containing the newer templates during multiple and subsequent divisions, but also the

daughter cells adopt different fates according to the age of the DNA that they inherited (Conboy et al., 2007). The daughter cells that inherit the older strands retain the more undifferentiated phenotype while the daughter cells that inherit the new strands are more prone to differentiation as revealed by Desmin expression, a marker for muscle differentiation (Conboy et al., 2007).

While it is obvious from all these studies that chromosomes are segregated asymmetrically in certain cells, it is not yet clear what is the mechanism behind this segregation process, whether the fate of the daughter cells is determined by chromosome segregation or vice versa, and if the only reason of this non-random segregation is the protection of the genome from acquiring mutations. Thus, one other possibility for the latter, which is proposed by Lansdorp (Lansdorp, 2007) is that asymmetric cell division and cell fate are co directed by epigenetic differences between sister chromatids ('silent sister hypothesis'). According to this hypothesis, epigenetic signatures that are present in centromeric DNA regions as well as in certain stem cell-associated gene regions in the chromatids, can direct chromatid specific non-random segregation during mitosis. Non-random segregation of sister chromatids will therefore result in one daughter cell retaining the sister chromatid with an 'active' stem cell gene pattern (stem cell), and another daughter where stem cells related genes are 'silenced' (transit-amplifying cell). This supports a mechanism whereby the fate of each cell is decided, based upon the epigenetic signatures present on the inherited chromatid, and proposes that non-random chromatid segregation serves not to avoid DNA replication errors, but instead to regulate cell fate (Lansdorp, 2007).

1.1.5.2 Epidermal stem cells and cancer

The latent period between exposure to known carcinogens and the development of tumours is long, generally months in mice or decades in humans, and involves several steps the first of which is tumour initiation. Thus, initiated cells or their progeny must persist in epithelial tissues at least for these lengths of time (Potten & Morris, 1988). According to this, in two-stage carcinogenesis (benign and malignant cutaneous neoplasma) in mice the tumour responses are evoked whether promotion (exposure to a non carcinogenic promoter - i.e. TPA) is begun one week or one year after the exposure to the carcinogen (tumour initiation i.e. DMBA - 7,12-dimenthylbenz(a)anthracene

mutagen) (Potten & Morris, 1988). The initiation event is commonly through a mutational event presumably one associated with genes controlling cell proliferation and/or self-maintenance, and which is able to make an epidermal cell a neoplastic cell, while promotion is the expression of the neoplastic cells (Scribner & Suss, 1978). Although such initiation mutational events could in principle occur in any cell within the tissue, the high and rapid cell migration, would mean that most of these cells that have acquired the mutations, are lost through the normal process of terminal differentiation within a few days of being mutated (Potten & Morris, 1988) (unless of course the mutation's effect is expressed very quickly and serves to prevent cell from being discarded (Cairns, 1975)). Moreover, most tumours are clonal in origin and it has been estimated that five events in humans, and two or three in mice are required to transform a normal cell into a cancer cell (Hahn et al., 1999; Hahn & Weinberg, 2002).

The process of skin carcinogenesis in mice, also involves a series of biological transitions through different stages including hyperplasia, dysplasia, benign papilloma, keratoacanthoma, squamous invasive carcinoma, which are induced by or associated with the accumulation of multiple genetic alterations in the target-cell population (Perez-Losada & Balmain, 2003). Therefore, immortalization of the cancer cells is a necessary prerequisite to allow the accumulation of these genetic alterations. According to all these notions, only long-term residents of the epidermis, and presumably stem cells, have the ability to accumulate the multiple additional mutations that can lead to aberrant activation of signalling pathways that normally control proliferation, differentiation, and eventually resulting in tumour formation (Owens & Watt, 2003).

In agreement with this and similar to LRC studies, radioactively labelled carcinogens are also retained in a few cells in the basal layer predominantly located towards the centre of the EPU, as well as in hair follicles (Morris et al., 1986). These carcinogen label retaining cells resembled the slow cycling ^{3}H-TdR LRC characteristics including mitotic activation by TPA, rather than the rapid dividing basal cells ones (mature basal cells). Double labelling experiments with ^{3}H-TdR and carbon-14-labelled benzo(a)pyrene (BP) carcinogen, showed that both molecules are detecting the same slow cycling sub-population of epidermal basal cells suggesting that LRCs, and presumably epidermal stem cells, are the cells that retain carcinogens for long periods of time (Morris et al., 1986; Potten & Morris, 1988).

This suggestion was further supported by the later finding, that cells within the basal layer of mouse epidermis that are predominantly responsible for tumour formation, in a modified application of the classic two-stage carcinogenesis model, are not only persistent but are also quiescent, another known stem cell characteristic (Morris et al., 1997). By the use of fluorouracil 5-fluoro-dUMP (5-FU) which blocks DNA synthesis, Morris et al. (Morris et al., 1997) were able to selectively kill all rapidly dividing cells, sparing all quiescent populations of the mouse epidermis. Despite the extensive damage to the epidermis and hair follicles (reduction in the number of basal cells in the interfollicular epidermis, reduction and completely slough off of the epidermis, death of the cells of anagen hair germ and thus blockade of the hair growth) inflicted by 5-FU treatments, complete hair follicle and epidermal regeneration was achieved after 30 days and 6 weeks respectively, suggesting the persistence of quiescent stem cell populations in mouse epidermis responsible for the regeneration (Morris et al., 1997). 5-FU drug is neither an initiator (5-FU + TPA), nor a promoter (DMBA + 5-FU) of carcinogenesis, since its application does not cause any tumour formation. Surprisingly, 5-FU treatment before (5-FU + DMBA + TPA) or after (DMBA + 5-FU + TPA) initiation of mouse skin with DMBA, did not affect the rate of neither papilloma nor carcinoma formation, following tumour promotion with TPA (Morris et al., 1997). This suggests that initiated cells by DMBA are resistant to 5-FU and thus are not actively cycling, but quiescent cells, residing mainly in the bulge of the hair follicle. Therefore, the fact that mice developed epidermal tumours after selective killing of rapidly dividing cells, further strengthened the idea that the targets of tumour initiation are indeed quiescent, and probably stem cells, which after application of a tumour promoter undergo multiple rounds of division, fix the damage within the genome and thus express the transforming mutation, caused by initiation (Morris, 2000).

Finally, due to all these studies, it is not surprising that these quiescent target cells of carcinogenic action are residing in places where stem cells are thought to be located. Initiated mouse skin (DMBA-initiated) can also be promoted to form tumours, by repeated induction of full thickness epidermal wounding (repeated abrasion), possibly as a consequence of the regenerative hyper-proliferative response of the epidermis (Argyris, 1980b). Importantly, the technique used to cause such epidermal abrasions allows complete removal of the interfollicular epidermis, while preserving hair follicles intact. Therefore, tumours that formed after this continuous epidermal abrasion, have

arised from hair follicles suggesting that follicular stem cells are strong candidates for tumour initiation (Argyris, 1980b). Following up on this possibility, and using the same skin abrasion technique, Morris et al. (Morris et al., 2000) aimed to define the location of epidermal tumour initiating cells, again by making use of the two-stage carcinogenesis model on either abraded or unabraded skin. Although removal of interfollicular epidermis by single abrasion in DMBA initiated mice following by TPA treatment, resulted in reduced incidence of papillomas, the number of carcinomas was essentially the same for either abraded or unabraded mouse skin (Morris et al., 2000). This also supports the previous observations, and suggests that targets of tumour initiation in two-stage carcinogenesis models, are stem cells found in the hair follicles and to a lesser degree in the interfollicular epidermis (Morris et al., 2000).

The principal that epidermal stem cells already possess the features (self renewal and unlimited replicative potential), which are required for cell transformation, and thus are strong candidates for the origin of epidermal tumours, is well illustrated in the case of p53 mutations with the typical UVB-signature, that have been found in clones of phenotypically normal, human sun-exposed skin (Brash & Haseltine, 1982; Jonason et al., 1996; Brash & Ponten, 1998; Jensen et al., 1999; Owens & Watt, 2003). Although single mutated cells were predominantly suprabasal, terminally differentiated cells, patches of p53 mutant cells possess characteristics such as size, distribution, and location that are indicative of stem and transit-amplifying cells (Jensen et al., 1999; Owens & Watt, 2003). This sets an example for the clonal expansion of mutant stem cells that are increasingly susceptible to the acquisition of further genetic hits and thus oncogenic transformation.

On the other hand, the possibility that tumours arise from de-differentiated transit-amplifying cells cannot be excluded but in that case, immortalization does not exist like in the primitive target stem-cell population. Thus, more genetic events are required to these committed, with limited self-renewal capacity cells, in order first to acquire self-renewal and unlimited replicative capacity, followed by further mutations that will be necessary to result in tumour formation. According to this notion, both *in vitro* and *in vivo* studies have shown that committed to differentiation (transit-amplifying cells) or even post-mitotic terminally differentiated epidermal cells, can re-acquire the ability of sustained proliferation in response to retroviral (*in vitro*) or to forced targeted (under the

control of keratin or involucrin promoter) expression (*in vivo*) of several oncogenes such as Ras and c-myc (Barrandon et al., 1989; Bailleul et al., 1990; Greenhalgh et al., 1993; Brown et al., 1998; Pelengaris et al., 1999). However, in all these cases either the lesions that formed did not progress to malignancy, or the only tumours that formed were benign papillomas that tend to regress (Bailleul et al., 1990; Greenhalgh et al., 1993; Brown et al., 1998; Pelengaris et al., 1999), compared to the non-regressed malignant carcinomas that mice developed upon targeted Ras expression in the putative epidermal stem cells of the hair follicles (Brown et al., 1998). Thus, even though some aspects of transformation might be reactivated in the differentiated cells (i.e. hyperplasia), and can contribute to skin cancer development, fully malignant cells, maintenance of benign tumours or progression of benign tumours to carcinomas, might require many more genetic events (Owens & Watt, 2003; Perez-Losada & Balmain, 2003).

1.2 Skin cancer

Skin cancer is the most common human malignancy partly due to the fact that the skin is vulnerable to the effects of carcinogens such as UV radiation. Skin cancer can be subdivided generally into melanoma skin cancers which consist of malignant melanoma derived from melanocytes, and non-melanoma skin cancers (NMSCs) which consist of Basal Cell Carcinoma (BCC) and Squamous Cell Carcinoma (SCC), derived from keratinocytes of the skin (Brash & Ponten, 1998). Other types of epidermal tumours mainly arising from the hair follicle include the trichofolliculoma, cylindroma, pilomatrichoma and sebaceous adenoma (Toftgard, 2000; Owens & Watt, 2003).

1.2.1 Basal Cell Carcinoma (BCC)

Basal cell carcinoma (BCC), first described by Jacob in 1827 (Jacob, 1827), is the most common malignant neoplasm of humans (Miller, 1991a; Miller, 1991b; Miller & Weinstock, 1994; Dicker et al., 2002; Lacour, 2002; Wong et al., 2003; Rubin et al., 2005; Crowson, 2006; Epstein, 2008). Accounting for about half of all cancers in the United States and approximately for 80% of all non-melanoma skin cancers (NMSCs), with almost 1,000,000 new occurrences per year in the United States (US) alone, BCC is the most common cancer in the Western world (Miller, 1991a; Miller & Weinstock, 1994; Wong et al., 2003; Rubin et al., 2005; Crowson, 2006; Rubin & de Sauvage, 2006; Epstein, 2008; Ramsey, 2009). BCC is generally a disorder of white individuals (especially those with fair skin) and more commonly of those of European ancestry, which occurs more frequently in men than in women, mainly on the sun-exposed skin, and that tends to occur after the age of 50 (Wong et al., 2003; Crowson, 2006; Epstein, 2008; Jiang & Szyfelbein, 2009; Ramsey, 2009). However, recent literature reports an increase in the incidence of BCC in the 30-39 age group, perhaps correlated with the use of ultraviolet (UV) light sunbeds for cosmetic tanning purposes, especially among younger women (Karagas et al., 2002; de Vries et al., 2004; Christenson et al., 2005; Rubin et al., 2005; Delfino et al., 2006; Bath-Hextall et al., 2007; Epstein, 2008; Jiang & Szyfelbein, 2009). In addition, the incidence of BCC also varies geographically and globally. States that are close to the equator, such as Hawaii, have an incidence of almost 3 times that of states in the Midwest, such as Minnesota, while Australia has the highest rate of basal cell carcinoma in the world, with certain regions reporting an

incidence of up to 2% per year (Marks et al., 1993; Diepgen & Mahler, 2002; Daya-Grosjean & Couve-Privat, 2005; Rubin et al., 2005; Epstein, 2008; Jiang & Szyfelbein, 2009).

Basal cell carcinomas (BCCs) are keratinocyte tumours that are so named because of their histological resemblance to the cells along the basement membrane - the 'basal' layer of the epidermis of the skin (Epstein, 2008). The majority of BCCs are slow growing, locally invading, rarely metastasizing, with no precursor lesions and are negative for markers of differentiation (undifferentiated tumours) **(see Section 1.3.6)**, in contrast to squamous cell carcinomas (SCCs), which are positive for differentiation markers (differentiated tumours), and which unlike BCCs, have detectable precursor lesions and are more aggressive (Miller, 1991a; Miller, 1991b; Brash & Ponten, 1998; Lacour, 2002; Owens & Watt, 2003; Wong et al., 2003; Daya-Grosjean & Couve-Privat, 2005; Rubin et al., 2005; Crowson, 2006; Epstein, 2008; Telfer et al., 2008; Ramsey, 2009).

Despite the high frequency of BCCs, the death rate is extraordinarily low, reflecting the effective treatment of BCCs, including surgical and non-surgical (i.e. radiotherapy, topical therapy, photodynamic therapy) methods, and the fact the these tumours rarely metastasize (metastatic rates ranging from 0.0028 - 0.55% and BCC most often metastasize to the regional lymph nodes, followed by bone, lung and liver) (Miller, 1991a; Miller, 1991b; Wong et al., 2003; Walling et al., 2004; Rubin et al., 2005; Epstein, 2008; Telfer et al., 2008; Jiang & Szyfelbein, 2009; Ramsey, 2009). It is not entirely clear why BCC usually does not metastasize, but a possibility might be that specialised abnormal stroma is required for its growth, which might be absent or of different composition at the new site that BCC cells translocate to, and thus does not favour their growth (Blewitt, 1980; Miller, 1991b; Epstein, 2008). This could also explain why attempts to transplant (Van Scott & Reinertson, 1961; Cooper & Pinkus, 1977) or culture (Flaxman & Van Scott, 1968; Flaxman, 1972) BCC cells often result in limited growth with frequent terminal differentiation (Miller, 1991b). Indeed there is some evidence that BCCs are especially dependent on stroma (stroma-dependent tumours), at least for their experimental transplantation to other sites in humans (Van Scott & Reinertson, 1961; Epstein, 2008). However, BCC can cause significant tissue destruction by local invasion and because BCC most commonly affects the head and

neck, surgery is often complicated with unsightly scarring and cosmetic disfigurement is frequent (Epstein, 2008; Ramsey, 2009). In addition, recurrence of BCC after local excision is common because of non-contiguous growth and difficulty in defining surgical margins (Miller, 1991a; Gailani & Bale, 1997). Furthermore, loss of vision or the eye may occur with orbital involvement, while perineural invasion and spread of BCC can result in loss of nerve function (Ramsey, 2009). Moreover, because BCCs are prone to ulceration, they provide a focus of infection (Ramsey, 2009). Therefore, enlightening and understanding the molecular pathogenesis and the events contributing to BCC development, might be translated into more effective prevention and treatment (Dicker et al., 2002; Rubin et al., 2005; Epstein, 2008).

1.2.2 Clinical and Histological features of Basal Cell Carcinoma

Basal cell carcinoma (BCC) characteristically arises in body areas exposed to the sun and is most common on the head (face, ears, scalp) and neck, followed by the trunk and arms and legs (Miller, 1991a; Rubin et al., 2005; Jiang & Szyfelbein, 2009; Ramsey, 2009). They have also been reported in unusual sites such as breasts, perianal area, genitalia, palms and soles, whereas the natural history of basal cell carcinoma is that of a slowly growing lesion, increasing in size and depth over months and years (Rubin et al., 2005; Nahabedian, 2008). Several clinical and histologic subtypes of basal cell carcinoma have been described, exhibiting different patterns of behaviour (Ramsey, 2009). Clinically and histologically, basal cell carcinomas (BCCs) are divided into five major types including nodular (solid), superficial, micronodular, infiltrating and morpheaform (sclerosing), which are all undifferentiated tumours and from which the aggressive growth tumours are the micronodular (intermediate between least and most aggressive), infiltrating (most aggressive) and morpheaform (most aggressive) (Sexton et al., 1990; Brown & Perry, 2000; Wong et al., 2003; Walling et al., 2004; Rubin et al., 2005; Crowson, 2006; Nahabedian, 2008; Jiang & Szyfelbein, 2009; Ramsey, 2009). Tumours with mixed patterns can be common, and other rare morphologic subtypes have also been described (Sexton et al., 1990; Wong et al., 2003; Walling et al., 2004; Rubin et al., 2005; Jiang & Szyfelbein, 2009).

Nodular BCC **(Figure 1.11)** represents the most common variant of this neoplasm and frequently occurs on the head, neck and upper back (Ramsey, 2009). This is the type of BCC that shows a translucent pearly papule with a rolled (raised) border and telangiectasia, whereas the lesions may be crusted or ulcerated and they may be associated with intermittent bleeding **(Figure 1.11A, B)** (Wong et al., 2003; Rubin et al., 2005; Crowson, 2006; Jiang & Szyfelbein, 2009; Ramsey, 2009). The nodular form of BCC is characterised by discrete large or small nests of basaloid cells in either the papillary or reticular dermis, accompanied by slit-like retractions from the stroma **(Figure 1.11C, D)** (Crowson, 2006). Regardless of the overall size of these nodular nests, tumour cells tend to align more densely in a palisade pattern in the periphery of these nests and typically have large, hyperchromatic, oval nuclei and little cytoplasm **(Figure 1.11D ii)** (Ramsey, 2009). Mitoses are infrequent and apoptotic cells are rare (Crowson, 2006).

Superficial BCC **(Figure 1.12A, B)** is characterised by scaly patches that are pink to red-brown, often with central clearing and with slightly raised border (Wong et al., 2003; Rubin et al., 2005; Jiang & Szyfelbein, 2009; Ramsey, 2009). A threadlike border is frequent and superficial BCC is commonly observed on the trunk and has little tendency to become invasive (Ramsey, 2009). Superficial BCC **(Figure 1.12C)** appears as buds of basaloid cells attached to the undersurface of the epidermis. Nests of various sizes are often seen in the upper dermis and tumour cell aggregates typically show peripheral palisading (Ramsey, 2009). Commonly, superficial BCC is characterised by a proliferation of basaloid cells that form an axis parallel to the epidermal surface and demonstrate slit-like retraction of the palisaded basal cells from the subjacent stroma **(Figure 1.12D)** (Crowson, 2006). Mitoses and individual cell necrosis are uncommon (Crowson, 2006).

Micronodular BCC **(Figure 1.13)** manifests a plaque-like indurated lesion with a poorly marked contour (Crowson, 2006). It is not prone to ulceration while it may appear yellow-white when stretched and it is firm to the touch (Ramsey, 2009). Histologically, the micronodular type **(Figure 1.13 i)** is similar to nodular, manifesting tumour nests of basaloid cells with roughly the same round shape and contour as nodular BCC, but are smaller and widely dispersed in an often asymmetric distribution extending deeper into the dermis and/or subcutis (Crowson, 2006; Jiang & Szyfelbein, 2009; Ramsey, 2009).

The retraction spaces are less pronounced than in the nodular form of BCC, and the surrounding stroma shows a collagenised morphology **(Figure 1.13 ii)**, suggesting that micronodular lesions may be an intermediate step between nodular and aggressive growth subtypes, such as infiltrating and morpheaform (Crowson, 2006; Nahabedian, 2008; Ramsey, 2009). Micronodular BCC has been also reported to have a higher incidence of local recurrence that nodular BCC (Crowson, 2006; Jiang & Szyfelbein, 2009).

Infiltrating BCC **(Figure 1.14A)** and morpheaform (sclerosing) BCC **(Figure 1.15A)** clinically both appear as an indurated white-to-waxy sclerotin (scarlike) plaque with ill-defined margins (indistinct borders which are often extend well beyond clinical margins), resembling a scar and is most commonly observed in the head and neck area. Ulceration, bleeding and crusting are uncommon in infiltrating BCC, as well as in morpheaform BCC (Wong et al., 2003; Rubin et al., 2005; Crowson, 2006; Nahabedian, 2008; Jiang & Szyfelbein, 2009; Ramsey, 2009). Histologically, both infiltrating **(Figure 1.14B)** and morpheaform **(Figure 1.15B)** BCCs have growth patterns resulting in elongated strands of basaloid cells that are extending into the tissue, rather than round nests (Walling et al., 2004; Crowson, 2006; Ramsey, 2009). Infiltrating BCC **(Figure 1.14B)** arises as strands of basaloid tumour cells, 4-8 cells thick, with spiky, irregular appearance, embedded in a dense fibrous stroma (the stroma is frequently fibrotic with proplastic stromal fibroblasts), whereas an admixed nodular component is often observed in this BCC subtype (Crowson, 2006; Jiang & Szyfelbein, 2009; Ramsey, 2009). Similarly, morpheaform BCC **(Figure 1.15B)** arises as thinner, narrow strands of basaloid tumour cells, 1-2 cells thick and cords up to five cells may be present (tumour tongues), with no basal lamina and embedded in a densely collagenised stroma containing proplastic fibroblasts (Crowson, 2006; Jiang & Szyfelbein, 2009; Ramsey, 2009). Slit-like retraction from the stroma is less pronounced in infiltrating and morpheaform BCC, compared to nodular and superficial ones, but is still often demonstratable (Crowson, 2006; Ramsey, 2009). In addition, both infiltrating and morpheaform BCC show individual cell necrosis and mitotic activity of the neoplastic cells (Crowson, 2006). Infiltrating and morpheaform subtypes which are classified as aggressive BCCs, in contrast to non-aggressive nodular and superficial BCCs, apart from showing deep invasion of the dermis and at some times invasion of the subcutis, they may exhibit perineural invasion as well, making difficult their removal and

increasing the incidence of recurrence (Brown & Perry, 2000; Walling et al., 2004; Crowson, 2006; Nahabedian, 2008).

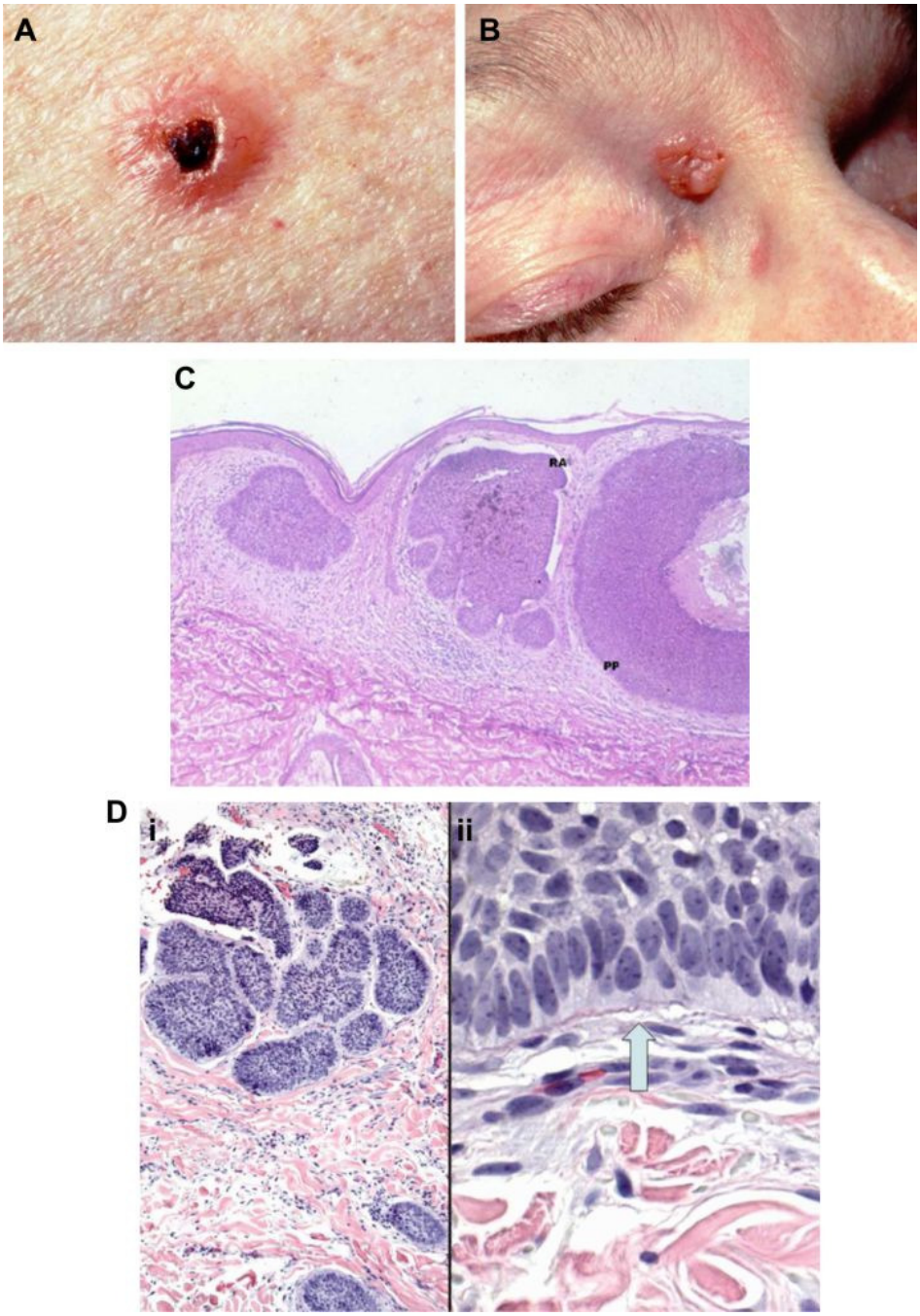

Figure 1.11: Nodular BCC.

Clinical morphology: **(A)** This translucent pink papule has telangiectases and a crusted erosion, characteristic of nodular basal cell carcinoma. **(B)** Nodular basal cell carcinoma appearing as a waxy, translucent papule with central depression and a few small erosions. Histomorphology: **(C)**, **(D), (i)** Rounded nodular aggregates of basalioma cells and of variable size are present in the dermis and exhibit peripheral palisading (PP) and retraction artefact (RA) (cleft formation). **(D), (ii)** The nodules of tumour show a peripheral palisade of basaloid cells, and at the interface with the stroma, slit-like retraction is seen (arrow) whereas stromas so no significant fibroplasias. Modified from (Crowson, 2006; Ramsey, 2009).

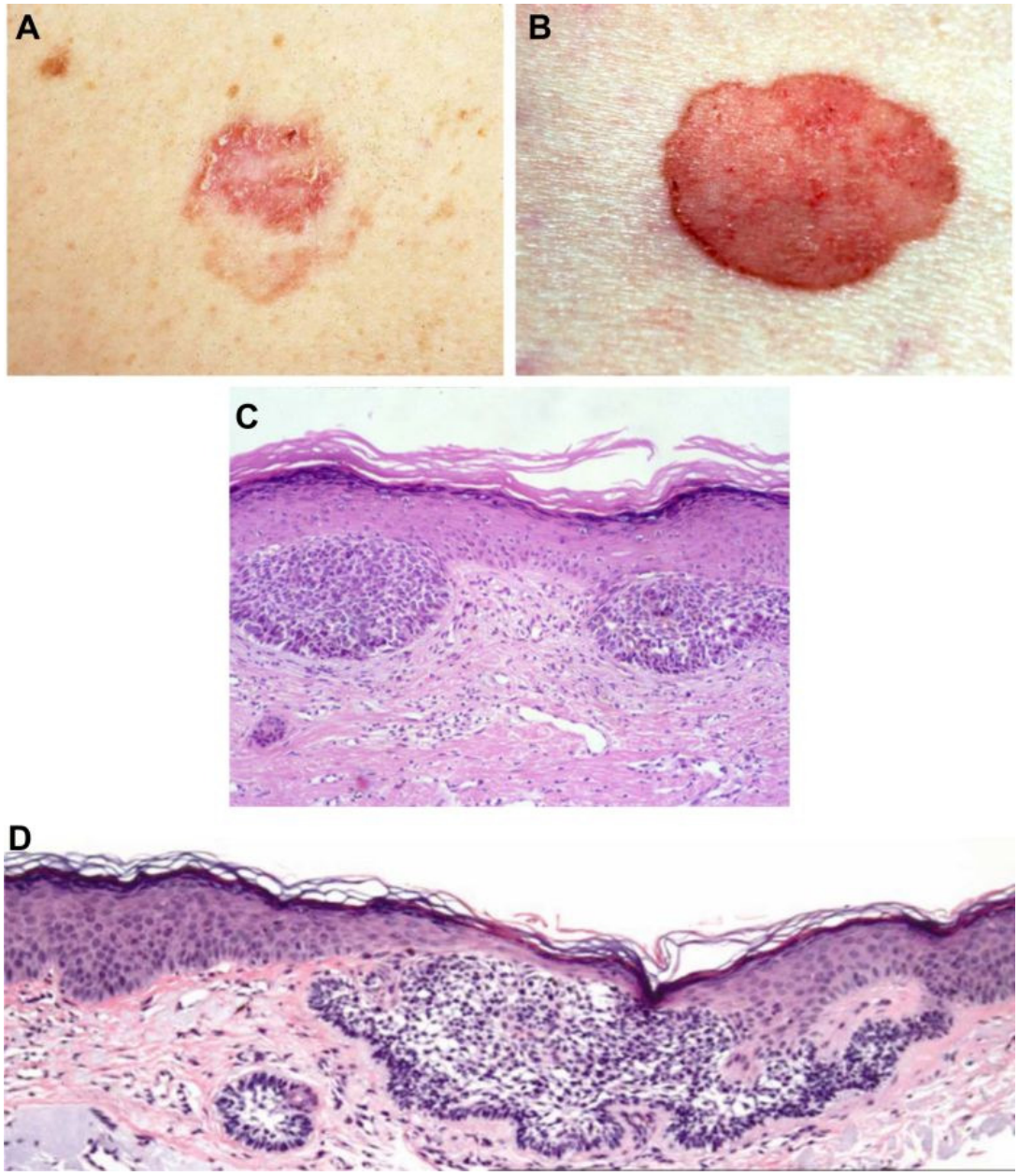

Figure 1.12: Superficial BCC.

Clinical morphology: **(A)** Scale, erythema (redness of the skin caused by hyperemia of the capillaries in the lower layers of the skin), and a threadlike raised border are present in this superficial basal cell carcinoma on the trunk. **(B)** Larger, superficial basal cell carcinoma. Histomorphology: **(C)** Nests of basaloid cells are seen budding from the undersurface of the epidermis. **(D)** A proliferation of basaloid cells parallel to the long axis of the epidermis. Serial sectioning showed the small nest at left to connect to the remainder of the tumour, which is in continuity with the undersurface of the epidermis. Modified from (Crowson, 2006; Ramsey, 2009).

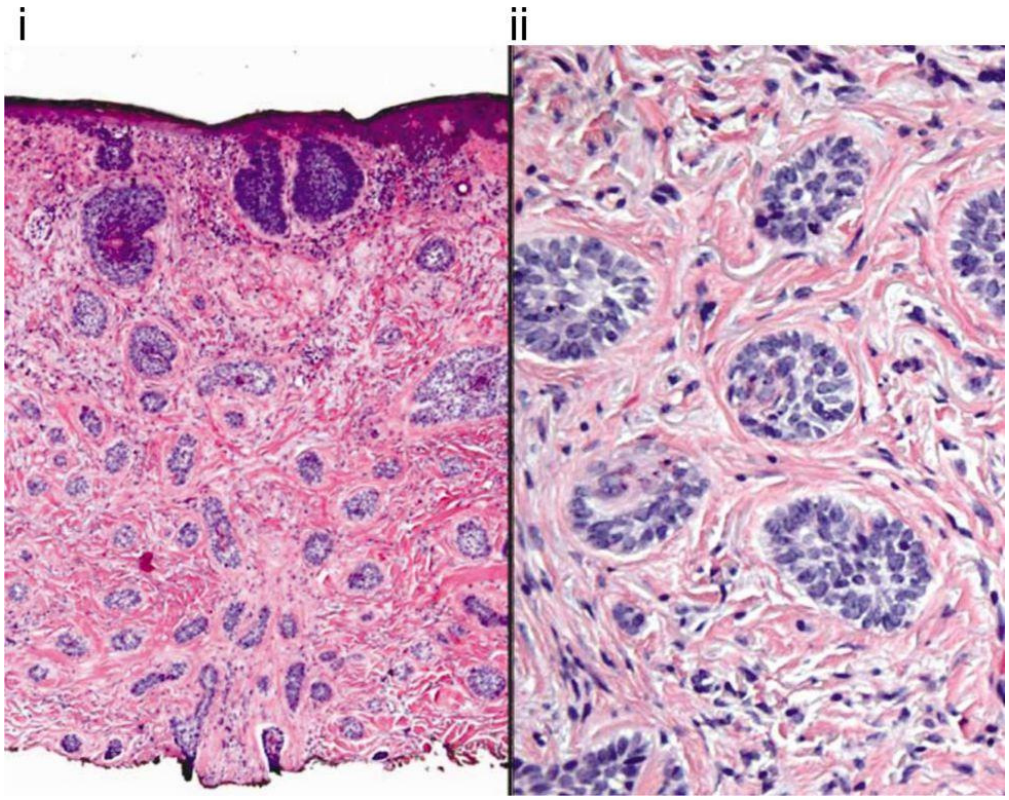

Figure 1.13: Micronodular BCC.

Histomorphology: **(i), (ii)** Micronodular BCC manifests uniformly small nests of neoplastic basal cells with rounded peripheral contours extending widely throughout the sampled dermis. **(ii)** The adjacent stroma shows fibroplasia, indicating a transition step in evolution from nodular to aggressive growth BCC. Modified from (Crowson, 2006).

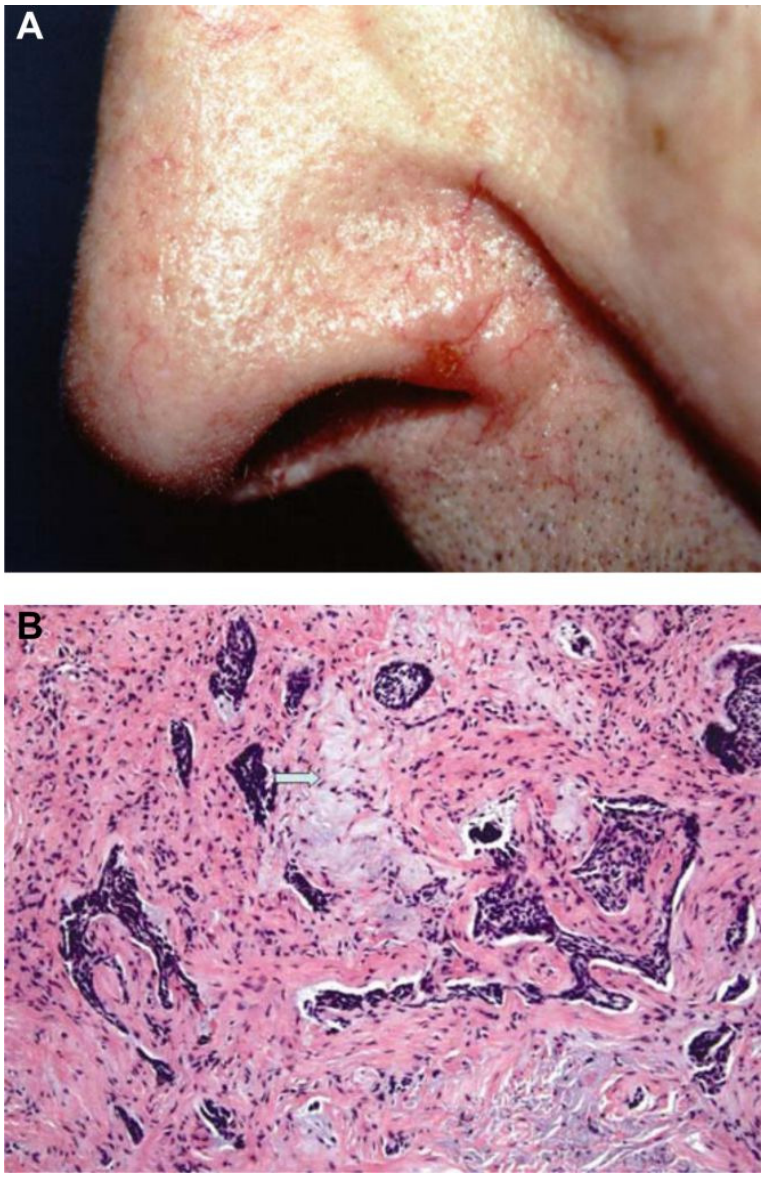

Figure 1.14: Infiltrating BCC.

Clinical morphology: **(A)** This infiltrating basal cell cancer has ill-defined borders and telangiectases. Histomorphology: **(B)** In a densely proplastic and heavily collagenised stroma, small irregular tongues of neoplastic basaloid cells often 5-8 cells thick are embedded in the collagen table. However the tumour tongues manifest an admixture of rounded nodules, large nodules with irregular contours and small irregular tongues of tumour cells embedded in the fibrous stroma. These lesions almost invariably arise in sun-damaged skin, the morphologic evidence of which is solar elastosis (arrow). Modified from (Crowson, 2006; Ramsey, 2009).

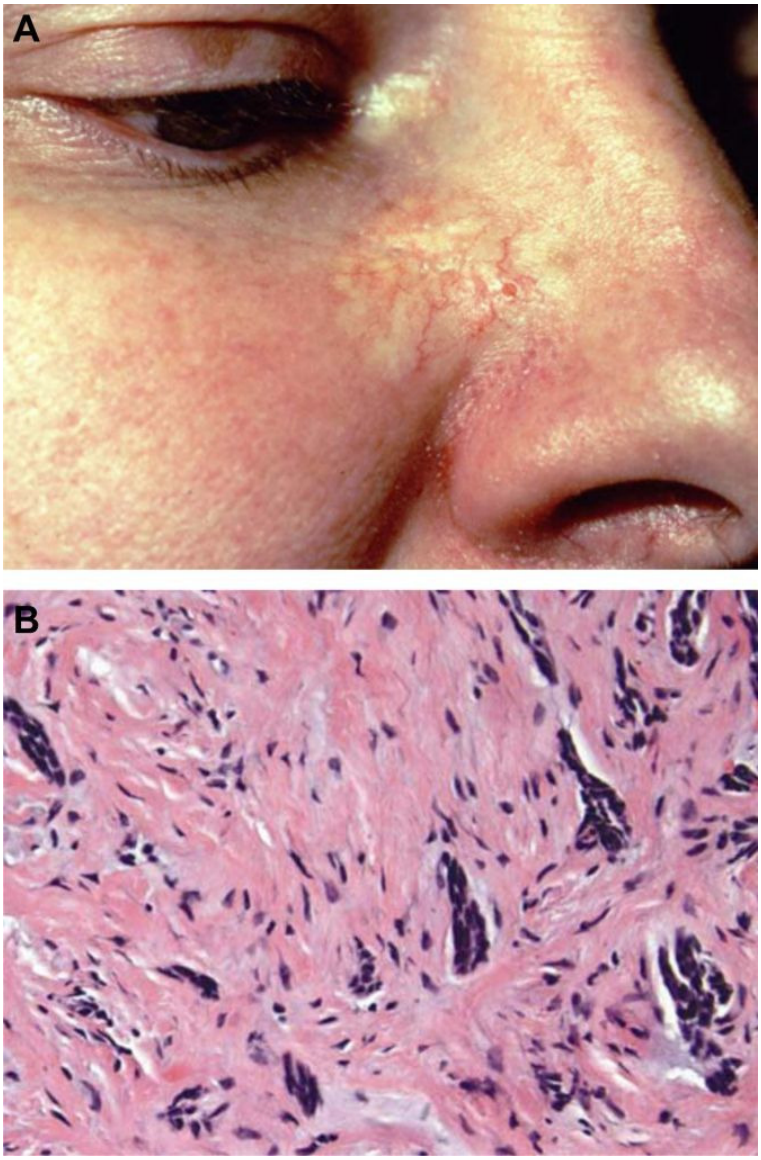

Figure 1.15: Morpheaform BCC.

Clinical morphology: **(A)** Large, scarlike morpheaform basal cell cancer. Histomorphology: **(B)** Like infiltrating BCC, the morpheaform BCC shows heavy stromal collagenisation and proplasia of stromal fibroblasts. Small irregular (sharply angulated) tongues of neoplastic basaloid cells, often 1-4 cells thick are embedded in this fibrous stroma. Modified from (Crowson, 2006; Ramsey, 2009).

1.2.3 Risk factors and Molecular genetics of Basal Cell Carcinoma

Ultraviolet (UV) radiation which is the carcinogenic factor in sunlight (Soehnge et al., 1997) is known to be one of the main risk and etiological factors in human skin BCC formation (Miller, 1991b; Gailani & Bale, 1997; Lacour, 2002; Wong et al., 2003; Daya-Grosjean & Couve-Privat, 2005; Rubin et al., 2005; Crowson, 2006; Epstein, 2008; Jiang & Szyfelbein, 2009; Ramsey, 2009), since the most frequent mutations found in particular genes (tumour suppressor genes) in human BCCs, have the 'UV signature' of UV-light mediated mutations (Grossman & Leffell, 1997; Soehnge et al., 1997; Brash & Ponten, 1998; Armstrong & Kricker, 2001; de Gruijl et al., 2001; Ehrhart et al., 2003; Epstein, 2008). These specific mutations in DNA, are consistently associated with UV radiation, and are characterised by C (cytidine) to T (thymidine) or CC to TT transitions at dipyrimidine sites, induced by UVB (solar ultraviolet B, 280-320 nm) radiation **(see Chapter 4, Section 4.2.5)** (Brash & Haseltine, 1982; Grossman & Leffell, 1997).

In addition, physical factors such as skin type, hair and eye colour are also an important consideration for BCC tumour formation, since very fair skinned individuals (skin type 1) with red or blonde hair and light coloured eyes are at high risk of developing BCCs, a risk which increases with childhood freckling and severe sunburn (Wong et al., 2003; Daya-Grosjean & Couve-Privat, 2005; Rubin et al., 2005; Crowson, 2006; Ramsey, 2009). Other risk factors that have been linked to the development of BCC are environmental insults such as ionizing radiation and arsenic exposure, family history of BCC, low intake of vitamins and high intake of fats (Miller, 1991b; Wong et al., 2003; Daya-Grosjean & Couve-Privat, 2005; Rubin et al., 2005; Crowson, 2006; Epstein, 2008; Ramsey, 2009). Moreover, patients on immunosuppressive treatment (organ-transplant recipients) such as renal and heart transplant recipients, also have an increased risk of basal cell carcinoma (Miller, 1991b; Wong et al., 2003; Daya-Grosjean & Couve-Privat, 2005; Rubin et al., 2005; Crowson, 2006; Jiang & Szyfelbein, 2009; Ramsey, 2009).

Interestingly, several genetic conditions are associated with the predisposition to basal cell carcinoma, including albinism (defect of melanin production), Bazex's syndrome (X-linked dominant condition with features of follicular atrophoderma, hypotrichosis,

hypophidrosis and multiple BCCs), xeroderma pigmentosum and nevoid basal cell carcinoma syndrome (Gorlin syndrome) (Miller, 1991b; Wong et al., 2003; Daya-Grosjean & Couve-Privat, 2005; Crowson, 2006; Jiang & Szyfelbein, 2009; Ramsey, 2009). Xeroderma pigmentosum (XP) is an autosomal recessive genetic disorder of DNA repair in which the ability to repair damage caused by ultraviolet (UV) light is deficient and is associated with an acute photosensitivity manifested by sunlight induced abnormal pigmentation, a dry prematurely aged skin and a predisposition to develop multiple skin cancers at a very early age, including BCCs (Stary & Sarasin, 2002; Lehmann, 2003; Daya-Grosjean & Couve-Privat, 2005; Crowson, 2006; Ramsey, 2009). Gorlin or nevoid basal cell carcinoma (NBCC) syndrome is an autosomal dominant hereditary disease which predisposes patients to the early development of multiple BCCs, medulloblastomas and ovarian fibromas and is characterised by a range of developmental anomalies, including skeletal abnormalities, dental malformations, facial dysmorphism, hyperkeratosis of the palms and soles and basal cell nevi (Gorlin, 1987; Gorlin, 1995; Chiang et al., 1996; Gailani & Bale, 1997; Kimonis et al., 1997; Ming et al., 1998; Booth, 1999; Wicking et al., 1999; Villavicencio et al., 2000; Bale & Yu, 2001; Mullor et al., 2002; Wong et al., 2003; Daya-Grosjean & Couve-Privat, 2005; Athar et al., 2006; Crowson, 2006; Ramsey, 2009).

The genetic analysis of Gorlin or nevoid basal cell carcinoma (NBCC) syndrome has been shown to be caused by patched (PTCH) gene germline inactivation mutations, a tumour suppressor gene which is located to chromosome 9q22.3, while frequent loss of heterozygosity at 9q22.3 (loss of the remaining wild-type allele at 9q22.3) is observed in BCCs and other tumours from these patients (Gailani et al., 1992; Hahn et al., 1996b; Johnson et al., 1996; Unden et al., 1996; Gailani & Bale, 1997; Unden et al., 1997; Brash & Ponten, 1998; Happle, 1999; Ling et al., 2001; Dicker et al., 2002; Daya-Grosjean & Couve-Privat, 2005). Loss of heterozygosity is a genetic mechanism by which a cell heterozygous for a gene – i.e. tumour suppressor gene – (due to mutation of the gene in one allele) becomes either homozygous or hemizygous for the mutant allele, because the corresponding wild-type allele is lost due to a somatic mutational event (Happle, 1999). Mutation of the inherited wild-type copy in Gorlin patients has been shown to occur by both loss of heterozygosity (germline mutation of one PTCH allele and loss of the normal copy of PTCH) and point mutation (germline mutation of one PTCH allele and point mutation in the remaining non-deleted wild-type PTCH allele)

(Unden et al., 1996; Gailani & Bale, 1997; Booth, 1999). Similarly, PTCH inactivated mutations occur frequently in sporadic BCCs (60-70%) and in BCCs associated with xeroderma pigmentosum (80-90%), as well as allelic loss of the remaining wild-type patched gene (53%) (loss of heterozygosity of PTCH) (Gailani et al., 1996; Gailani & Bale, 1997; Soehnge et al., 1997; Unden et al., 1997; Brash & Ponten, 1998; Bodak et al., 1999; Booth, 1999; D'Errico et al., 2000; Ling et al., 2001; Dicker et al., 2002; Lacour, 2002; Daya-Grosjean & Couve-Privat, 2005; Reifenberger et al., 2005; Teh et al., 2005). UVB irradiation has been shown to be responsible for a 40-50% of PTCH mutations in sporadic human BCCs and for an 80% of PTCH mutations in BCCs associated with xeroderma pigmentosum (Bodak et al., 1999; D'Errico et al., 2000; Lacour, 2002; Daya-Grosjean & Couve-Privat, 2005; Reifenberger et al., 2005). Interestingly, a study by Teh et al. (Teh et al., 2005) using genomewide single nucleotide polymorphism microarray in sporadic human basal cell carcinoma, followed by DNA sequencing, showed that 93% of BCCs had loss of heterozygosity (LOH) at 9q, of which 69% had mutations in the Patched gene, while 62% of the 9q LOH were a result of allelic loss and 38% of the 9q LOH, with no change in copy number, were a result of uniparental disomy. Uniparental disomy during meiosis (division of sperm and egg cells) is when a person receives two copies of a chromosome or part of a chromosome from one parent and no copies from the other parent. Uniparental disomy occurs also as a somatic event either due to chromosome non-disjunction, where one daughter cell acquires three copies of a chromosome and the other daughter cell one copy of the chromosome (one daughter cell acquires both copies of the wild-type gene and one copy of the mutant gene whereas the other daughter cell acquires one copy of the mutant gene and no copy of the wild-type gene followed by subsequent chromosomal duplication) or due to mitotic recombination (mitotic cross-over) where there is exchange of segments between chromatids of homologous chromosomes (Happle, 1999).

Importantly, the protein encoded by PTCH gene, the gene affected in Gorlin patients and in sporadic BCCs, is the Hedgehog (HH) ligand receptor and the HH signalling pathway repressor, a pathway which is critical in embryonic development **(see Section 1.3)** (Chen & Struhl, 1996; Marigo & Tabin, 1996; Stone et al., 1996; Brash & Ponten, 1998; Athar et al., 2006; Kasper et al., 2006a; Epstein, 2008). Thus patched inactivation (i.e. by mutations) is linked to constitutive activation of the HH pathway and gives the

first evidence for an involvement of HH signalling pathway in tumourigenesis **(see Section 1.3)** (Brash & Ponten, 1998; Booth, 1999; Bale & Yu, 2001; Daya-Grosjean & Couve-Privat, 2005; Kasper et al., 2006a; Epstein, 2008).

Another gene which is frequently mutated (40-60%) in sporadic human BCCs and in BCCs associated with xeroderma pigmentosum is the p53 tumour suppressor gene, which encodes for a protein that regulates the cell cycle and induces apoptosis in the cells (Barbareschi et al., 1992; Shea et al., 1992; Grossman & Leffell, 1997; Ponten et al., 1997; Soehnge et al., 1997; Bodak et al., 1999; D'Errico et al., 2000; de Gruijl et al., 2001; Ling et al., 2001; Dicker et al., 2002; Lacour, 2002; Daya-Grosjean & Couve-Privat, 2005; Reifenberger et al., 2005; Epstein, 2008). UVB irradiation is known to be responsible for a high number (65-75%) of p53 mutations in human sporadic and XP-related BCCs (Bodak et al., 1999; D'Errico et al., 2000; Demirkan et al., 2000; Dicker et al., 2002; Lacour, 2002; Bolshakov et al., 2003; Daya-Grosjean & Couve-Privat, 2005; Reifenberger et al., 2005).

1.3 Hedgehog (HH) signalling pathway

1.3.1 HH signalling network

The hedgehog (HH) signal transduction pathway was originally discovered by genetic analysis in *Drosophila melanogaster* embryos (Nusslein-Volhard & Wieschaus, 1980), containing a single hedgehog gene (hh), but subsequent studies showed that it is more complex in vertebrates, and three hedgehog homologue proteins have been identified in mammals (Echelard et al., 1993; Goodrich et al., 1996; Wicking et al., 1999; Bale & Yu, 2001; Ingham & McMahon, 2001; Hooper & Scott, 2005). These include the Sonic hedgehog (Shh (mouse) /SHH (human)), Indian hedgehog (Ihh (mouse) /IHH (human)) and the Desert hedgehog (Dhh (mouse) / DHH (human)) (Echelard et al., 1993), of which the Shh/SHH is the best-characterised since it is the most potent and most broadly expressed in embryonic and adult tissues (Chiang et al., 1996; Ming et al., 1998; Wicking et al., 1999; Bale & Yu, 2001; Pathi et al., 2001; Ruiz i Altaba et al., 2002b; Daya-Grosjean & Couve-Privat, 2005; Athar et al., 2006).

Although some crucial differences exist, the HH signalling mechanisms are generally conserved between *Drosophila* and higher organisms (Goodrich et al., 1996; Hahn et al., 1996a; Booth, 1999; Ingham & McMahon, 2001; Ruiz i Altaba et al., 2002a; Cohen, 2003; Pasca di Magliano & Hebrok, 2003; Wetmore, 2003; Beachy et al., 2004; Lum & Beachy, 2004; Daya-Grosjean & Couve-Privat, 2005; Hooper & Scott, 2005; Rubin & de Sauvage, 2006; Rohatgi & Scott, 2007; Varjosalo & Taipale, 2007). In the absence of hh/HH signal (i.e. SHH) **(Figure 1.16a)**, a 12-transmembrane receptor protein Patched (Ptc in *Drosophila* and PTCH or PTCH1 in humans, Ptch or Ptch1 in mouse, since a second patched gene PTCH2/Ptch2 was identified in vertebrates (Carpenter et al., 1998; Motoyama et al., 1998a; Booth, 1999; Smyth et al., 1999; Wicking et al., 1999; Zaphiropoulos et al., 1999; Toftgard, 2000; Pasca di Magliano & Hebrok, 2003)) (Hooper & Scott, 1989; Nakano et al., 1989; Goodrich et al., 1996; Hahn et al., 1996a), inhibits the activity of a 7-transmembrane protein Smoothened (SMO in humans, Smo in mouse and *Drosophila*) (Alcedo et al., 1996; van den Heuvel & Ingham, 1996; Xie et al., 1998; Ingham & McMahon, 2001; Cohen, 2003; Ruiz-Gomez et al., 2007), possibly catalytically and not through protein-protein interaction (Stone et al., 1996; Denef et al., 2000; Kalderon, 2000; Taipale et al., 2002; Rohatgi & Scott, 2007; Varjosalo & Taipale,

2007), thereby inhibiting the downstream transduction cascade. In *Drosophila* the cytoplasmic tail of Smo interacts with a multimolecular complex in the cytoplasm, consisting of (i) microtubule-associated kinesin-like protein Costal2 (Cos2) - a key negative regulator of the Hh pathway downstream of Smo that promotes phosphorylation of Ci transcription factor, (ii) serine-threonine protein kinase Suppressor of Fused (Sufu) - a negative regulator (minor role) of the Hh pathway downstream of Smo, (iii) serine-threonine protein kinase Fused (Fu) - a protein that acts positively on the Hh pathway downstream of Smo by inducing the nuclear accumulation of Ci and enhancing its transcriptional activity, and (iv) the zinc-finger transcription factor cubitus interruptus (Ci) **(see Section 1.3.2)** (Preat et al., 1990; Limbourg-Bouchon et al., 1991; Preat, 1992; Chen & Struhl, 1996; Robbins et al., 1997; Sisson et al., 1997; Monnier et al., 1998; Chuang & McMahon, 1999; Methot & Basler, 2000; Fukumoto et al., 2001; Methot & Basler, 2001; Cohen, 2003; Jia et al., 2003; Lum et al., 2003; Lum & Beachy, 2004; Hooper & Scott, 2005; Rubin & de Sauvage, 2006; Varjosalo & Taipale, 2007); whereas in vertebrates the cytoplasmic tail of smoothened containing the domain that binds to Cos2 and Cos2 are not involved (Varjosalo et al., 2006) and the multimolecular complex consists of (i) SUFU/Sufu - a key negative regulator (major role) of the Hh pathway downstream of Smo, with an important role also in the shuttling of the GLI proteins between the cytoplasm and the nucleus, (ii) FU/Fu (?) - a protein that acts positively on the Hh pathway downstream of Smo and (iii) GLI1/Gli1, GLI2/Gli2, GLI3/Gli3 (*Ci* homologues in *Drosophila* **(see Section 1.3.2)**), which in both cases (*Drosophila* and vertebrates) the protein complexes are bound to microtubules/cytoskeleton and serve to retain the Ci/Gli transcription factors in the cytoplasm without activating transcription (Ding et al., 1999; Kogerman et al., 1999; Pearse et al., 1999; Stone et al., 1999; Murone et al., 2000; Ruiz i Altaba et al., 2002a; Pasca di Magliano & Hebrok, 2003; Wetmore, 2003; Beachy et al., 2004; Lum & Beachy, 2004; Merchant et al., 2004; Barnfield et al., 2005; Chen et al., 2005; Daya-Grosjean & Couve-Privat, 2005; Merchant et al., 2005; Rubin & de Sauvage, 2006; Svard et al., 2006; Varjosalo et al., 2006; Rohatgi & Scott, 2007; Varjosalo & Taipale, 2007). The Ci/Gli transcription factors which are bound to these protein complexes are phosphorylated by several kinases, followed by binding of the phosphorylated Ci/Gli proteins to Slimb/β-TrCP protein which directs the (i) ubiquitin proteasome processing of Ci/Gli proteins into carboxy-terminus-truncated repressors that move to the nucleus and repress the Ci/Gli-dependent transcription of target genes, and/or (ii) the ubiquitin

proteasome degradation of full-length Gli transcription factors **(see Section 1.3.2)** **(Figure 1.16a)** (Ruiz i Altaba et al., 2002a; Wetmore, 2003; Daya-Grosjean & Couve-Privat, 2005; Hooper & Scott, 2005; Zhang et al., 2005; Rubin & de Sauvage, 2006; Varjosalo & Taipale, 2007; Wang et al., 2007).

In the presence of hh/HH ligand (i.e. SHH) **(Figure 1.16b)**, activation of the pathway, either in *Drosophila* or in vertebrates, is initiated through binding of any of the three secreted hh/HH (i.e. SHH) ligands to patched receptor (Chen & Struhl, 1996; Marigo & Tabin, 1996; Stone et al., 1996) which results in loss of patched activity, and possibly inhibition of the catalytic activity that activated patched exerted to smoothened and rendered it inactive, leading to consequent activation of smoothened which transduces the signal from plasma membrane to the cytoplasm (Chen & Struhl, 1996; Stone et al., 1996; Denef et al., 2000; Kalderon, 2000; Ruiz i Altaba et al., 2002a; Taipale et al., 2002; Pasca di Magliano & Hebrok, 2003; Wetmore, 2003; Lum & Beachy, 2004; Zhu & Scott, 2004; Daya-Grosjean & Couve-Privat, 2005; Hooper & Scott, 2005; Rubin & de Sauvage, 2006; Rohatgi & Scott, 2007; Varjosalo & Taipale, 2007; Wang et al., 2007). After HH binding in patched, followed by smoothened activation, in *Drosophila* smoothened is phosphorylated in the serine/threonine residues of its C-terminal cytoplasmic tail - the region responsible for binding to Cos2 that forms a complex with Fu, SuFu and Ci - and becomes stabilised and transduces the signal to Ci through the Cos2-Fu-SuFu complex. Hence, through inactivation of Cos2 and SuFu and activation of Fu, the protein complex dissociates from the microtubules, Ci is released from the complex and thus its phosphorylation and cleavage ceases, leading to its translocation to the nucleus, subsequent binding to DNA and transcriptional activation of downstream genes **(see Section 1.3.2)** (Ohlmeyer & Kalderon, 1998; Matise & Joyner, 1999; Denef et al., 2000; Methot & Basler, 2001; Cohen, 2003; Jia et al., 2003; Lum et al., 2003; Wetmore, 2003; Lum & Beachy, 2004; Hooper & Scott, 2005; Zhang et al., 2005; Kasper et al., 2006a; Rubin & de Sauvage, 2006; Wang et al., 2007). In vertebrates, where phosphorylation and stabilisation of the cytoplasmic tail of smoothened that binds to Cos2 as well as Cos2 protein and possibly Fu protein are not involved to the transduction of the HH signal from the plasma membrane to the cytoplasm (Murone et al., 2000; Chen et al., 2005; Merchant et al., 2005; Varjosalo et al., 2006; Varjosalo & Taipale, 2007; Wang et al., 2007), activated smoothened somehow inhibits SuFu - a major negative regulator of the hedgehog signalling in vertebrates that directly binds to

Gli/GLI proteins and which also serves as an adaptor protein that links GLI to the Slimb/β-TrCP-dependent proteasomal degradation/processing pathway (Stone et al., 1999; Cheng & Bishop, 2002; Cohen, 2003; Merchant et al., 2004; Kasper et al., 2006a; Svard et al., 2006; Varjosalo & Taipale, 2007) - and thus through an unknown mechanism triggers the dissociation of Gli/GLI transcription factors from the SuFu-Fu(?) protein complex, resulting to the inhibition of their phosphorylation and processing and/or degradation, leading to their translocation to the nucleus and hence subsequent DNA binding and transcriptional activation of HH-target genes **(see Section 1.3.2)** (Matise & Joyner, 1999; Toftgard, 2000; Ruiz i Altaba et al., 2002a; Cohen, 2003; Pasca di Magliano & Hebrok, 2003; Wetmore, 2003; Beachy et al., 2004; Lum & Beachy, 2004; Daya-Grosjean & Couve-Privat, 2005; Hooper & Scott, 2005; Kasper et al., 2006a; Rubin & de Sauvage, 2006; Rohatgi & Scott, 2007; Varjosalo & Taipale, 2007; Wang et al., 2007; Epstein, 2008).

Target genes of hh/Ci signalling in *Drosophila* include Wingless (Wg) and Decapentaplegic (Dpp) which are essential for normal embryonic development and differentiation of many adult tissues. These genes are the orthologues of the vertebrate target genes: the Wnt (WNT family) **(see Section 1.4, Section 1.5.1 and Section 1.5.3)** and the bone morphogenetic proteins (BMPs) **(see Section 1.1.3.2)** (Matise & Joyner, 1999; Methot & Basler, 1999; Wicking et al., 1999; Ruiz i Altaba et al., 2002b; Cohen, 2003; Ruiz i Altaba et al., 2003; Daya-Grosjean & Couve-Privat, 2005). Interestingly, both in *Drosophila* and in vertebrates Ptc/Ptch which is an inhibitor of the HH/Gli pathway, is a transcriptional target gene, suggesting a negative-feedback loop that restricts the extent of HH signalling (Chen & Struhl, 1996; Matise & Joyner, 1999; Ruiz i Altaba et al., 2002a; Cohen, 2003; Pasca di Magliano & Hebrok, 2003; Wetmore, 2003; Beachy et al., 2004; Zhu & Scott, 2004; Daya-Grosjean & Couve-Privat, 2005; Athar et al., 2006; Eichberger et al., 2006; Varjosalo & Taipale, 2007). Similarly, in vertebrates an additional transmembrane protein, like patched, the Hh-interacting protein (Hip) which binds to HH proteins and reduces their range of movement by attenuating ligand diffusion, thereby possibly acting as a negative regulator of HH signalling pathway, has also been reported to be a transcriptional target of HH/Gli signalling (Chen & Struhl, 1996; Chuang & McMahon, 1999; Wicking et al., 1999; Ruiz i Altaba et al., 2002a; Pasca di Magliano & Hebrok, 2003; Beachy et al., 2004;

Zhu & Scott, 2004; Daya-Grosjean & Couve-Privat, 2005; Athar et al., 2006; Varjosalo & Taipale, 2007).

Furthermore, other target genes of HH/Gli signalling are not only Gli genes themselves, but also genes that are involved in proliferation **(see Section 1.3.7)** (i.e. PDGFRα (platelet-derived growth factor receptor), cyclin D, cyclin E, FOXM1 (forkhead box M1), apoptosis (i.e. BCL-2 (B-cell lymphoma 2), c-FLIP (c (cellular)-FAS-associated death domain-like IL (interleukin)-1-converting enzyme-like inhibitory protein), invasion and metastasis (i.e. SNAIL transcription factor **(see Chapter 5, Section 5.2.1.5)**), as well as stem cell genes (i.e. SOX9 transcription factor (SRY (sex determining region Y)-box 9), and transcription factors which have been shown to have a repressor function such as FOXE1 (winged helix domain transcription factor) **(overall see Section 1.3.6.1)** (Matise & Joyner, 1999; Ruiz i Altaba et al., 2002a; Ruiz i Altaba et al., 2002b; Pasca di Magliano & Hebrok, 2003; Ruiz i Altaba et al., 2003; Wetmore, 2003; Beachy et al., 2004; Daya-Grosjean & Couve-Privat, 2005; Aberger & Frischauf, 2006; Athar et al., 2006; Kasper et al., 2006a).

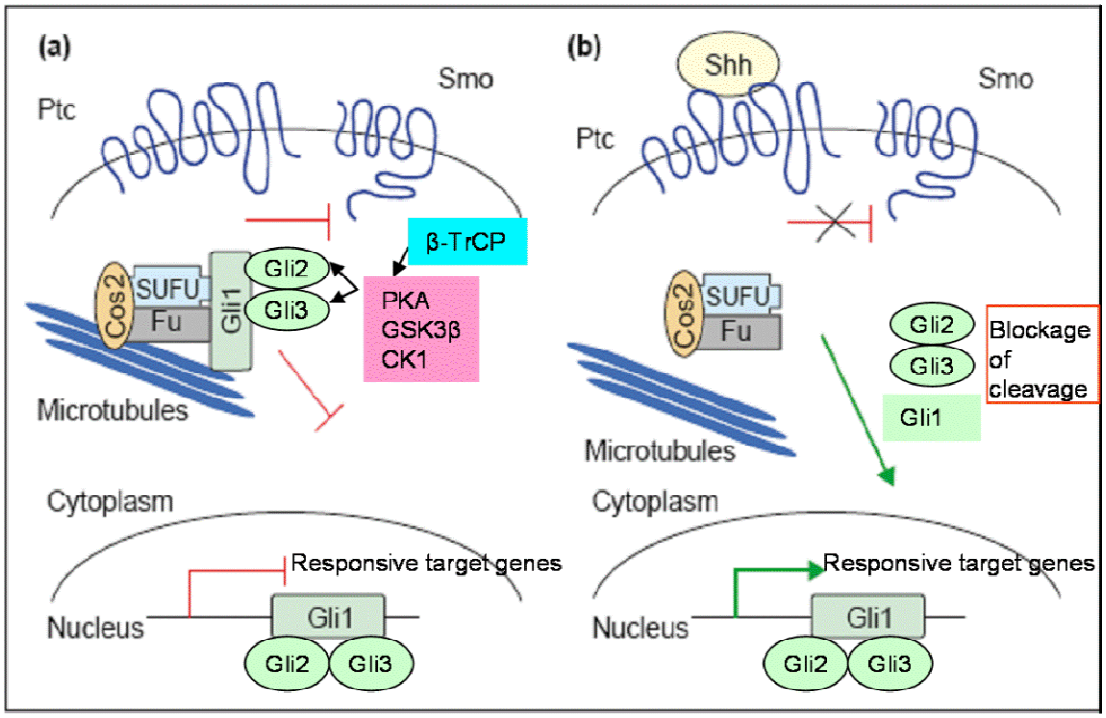

Figure 1.16: **The Shh/Gli signalling pathway.**

(a) In the absence of the Shh ligand, Ptch is unstimulated and inhibits Smo and Gli activity, as Gli transcription factors are retained as a complex associated with other proteins and microtubules in the cytoplasm and thus unable to activate transcription. Gli transcription factors are phosphorylated by PKA, GSK3β and CK1 proteins and then targeted for proteasomal degradation and/or processing through β-TrCP ubiquitin ligase. **(b)** Shh ligand binding stimulates Smo and allows Gli nuclear translocation, and thereby activating transcription. **Ptc**, Patched; **Smo**, Smoothened; **Cos2**, Cotal2; **SUFU**, Suppressor of Fused; **Gli1**, **Gli2**, **Gli3**, Gli zinc-finger trasncription factors; **Fu**, Fused; **PKA**, protein kinase A; **GSK3β**, glycogen synthase kinase 3β; **CK1**, casein kinase 1; **β-TrCP**, beta-transducin repeat containing protein. Modified from (Wetmore, 2003).

1.3.2 Gli/GLI transcription factors

In contrast to *Drosophila* where all transcriptional responses to HH signalling are controlled by the Gli homologue Ci segment polarity gene (Cubitis interruptus) (Orenic et al., 1990), which can both activate and repress HH-target genes, vertebrates (mouse and human) have at least three distinct Gli (mouse) / GLI (human) genes, Gli1/GLI1, Gli2/GLI2 and Gli3/GLI3, and the proteins encoded by these Gli/GLI genes are transcription factors (Ruppert et al., 1988; Ruppert et al., 1990; Hui et al., 1994; Villavicencio et al., 2000; Ingham & McMahon, 2001; Kasper et al., 2006a).

Human GLI1 (also known as GLI) is the first vertebrate GLI gene that was discovered and thus is the founder member of the GLI gene family (GL1, GLI2, GLI3 in humans, Gli1, Gli2, Gli3 in mice and Ci *in Drosophila*), which was originally identified as an amplified gene in a human glioblastoma (Kinzler et al., 1987; Kinzler et al., 1988; Matise & Joyner, 1999; Villavicencio et al., 2000; Cohen, 2003; Epstein, 2008). GLI1 was also detected as an amplified gene in other cancers such as osteosarcomas, rhabdomyosarcomas and B cell lymphomas, while it has been classified as an oncogene due to its ability to transform mouse cells in cooperation with adenovirus E1A *in vitro*, and also to be tumourigenic in nude mice that have been subcutaneously injected with these cells (Roberts et al., 1989; Ruppert et al., 1991; Werner et al., 1997; Matise & Joyner, 1999; Villavicencio et al., 2000; Kasper et al., 2006a). GLI1 maps to chromosome 12q13, GLI2 maps to chromosome 2q14 and GLI3 maps to chromosome 7p13 (Ruppert et al., 1990; Matsumoto et al., 1996; Reifenberger et al., 1996; Villavicencio et al., 2000; Cohen, 2003).

All three vertebrate Gli/GLI proteins have high homology to Ci in the zinc-finger domain, and limited homology in a number of domains outside this region (Matise & Joyner, 1999). The common, highly conserved DNA binding domain (zinc-finger domain) of GLI1, GLI2 and GLI3 transcription factors, comprises of five conserved tandem C2-H2 zinc-fingers and a conservative histidine (H) - cysteine (C) linker sequence between zinc fingers (Ruppert et al., 1988; Pavletich & Pabo, 1993; Matise & Joyner, 1999; Villavicencio et al., 2000; Cohen, 2003; Kasper et al., 2006a). GLI1 and GLI3 proteins were shown to recognize and bind to a conserved **GACCACCCA** nucleotide sequence in the promoters of target genes (Kinzler & Vogelstein, 1990;

Ruppert et al., 1990; Pavletich & Pabo, 1993; Vortkamp et al., 1995), and GLI2 recognizes and bind to a nearly identical **GAACCACCCA** motif (Tanimura et al., 1998; Villavicencio et al., 2000).

Gli1 and Gli2 appear to act primarily as transcriptional activators, whereas Gli3 (and at times Gli2) functions as a repressor (Matise & Joyner, 1999; Ruiz i Altaba, 1999b; Ingham & McMahon, 2001; Ruiz i Altaba et al., 2002b; Daya-Grosjean & Couve-Privat, 2005; Kasper et al., 2006a; Wang et al., 2007; Epstein, 2008). Gli3 has also been reported to act to a much lesser extent as an activator (Sasaki et al., 1999; Shin et al., 1999; Buttitta et al., 2003; Kasper et al., 2006a). In addition, in the absence of SHH signalling, the biological activity of Gli2 is suppressed by its N-terminal repressor domain since deletion of N-terminus of Gli2 converts the protein into a strong activator in cultured cells and *in vivo*, compared to full-length Gli2 protein (weaker activator), suggesting that both Gli2 and Gli3 have additional regulatory domains in their N-terminal, which either through proteolytic removal or their functional inactivation via an unknown mechanism, might allow the full activation of Gli2 or Gli3 and their transcriptional activity (Sasaki et al., 1999; Kasper et al., 2006a). In addition to proteolytic processing, recently Speek et al. (Speek et al., 2006) showed that alternative splicing may be another important regulatory mechanism which causes deletion of the major part of repressor domain and thus is responsible for the enhanced activation of human GLI2 and its transcriptional activity. Speek et al. (Speek et al., 2006) identified a GLI2 splice variant missing the N-terminal repressor domain, encoding a protein isoform with activator properties only, in human gonadal tissue and several cell lines with comparable transcriptional activity *in vitro* (Speek et al., 2006; Laner-Plamberger et al., 2009). Although initially it was thought that human GLI2, in contrast to mouse Gli2, does not contain an amino-terminal repressor domain (N-terminal repressor domain), recently, human GLI2 was shown to include a longer variant comprising 328 extra N-terminal amino acids (containing an N-terminal repressor domain), for which the name "full length GLI2" has been suggested, while denominating all previous forms GLI2* or GLI2ΔN with reduced N-terminus **(Figure 1.17A, bottom panel)** (Roessler et al., 2005). Gli1 protein has not been found to contain any repressor domain, consistent with its role as a strong transcriptional activator (Dai et al., 1999; Sasaki et al., 1999). Therefore both full-length Gli2 (mouse and human) and Gli3 (mouse and human) proteins contain carboxy- and amino-terminal domains, whereas full-length Gli1 (mouse

and human) contains only a carboxy-terminal activator domain **(Figure 1.17A, top and bottom panel)** (Matise & Joyner, 1999; Kasper et al., 2006a).

In *Drosophila* the single Gli orthologue Ci protein (Ci-155, full-length form) contains amino- and carboxy-terminal domains and functions either as a transcriptional repressor or Hh-dependent transcriptional activator (Aza-Blanc & Kornberg, 1999; Matise & Joyner, 1999; Methot & Basler, 1999; Ruiz i Altaba, 1999b; Methot & Basler, 2001; Lum & Beachy, 2004; Jiang, 2006). In the absence of Hh **(Figure 1.16a)**, Ci protein functions as a potent transcriptional repressor of Hh target genes, due to proteolytic cleavage by phosphorylation of several serine residues at their C-terminal regions, in the cytoplasm, by protein kinase A (PKA), glycogen synthase kinase 3β (GSK3β), casein kinase 1 (CK1) and subsequent ubiquitination by supernumery limbs (Slimb) (homologous to β-TrCP in human), resulting in accumulation of nuclear protein with intact DNA-binding zinc fingers and amino-terminus, but missing the carboxy-terminal transactivation domain (Ci-75, C-terminal truncated form through proteolysis) (Aza-Blanc et al., 1997; Jiang & Struhl, 1998; Tanimura et al., 1998; Chen et al., 1999a; Matise & Joyner, 1999; Methot & Basler, 1999; Lum & Beachy, 2004; Zhang et al., 2005; Jiang, 2006). In the presence of Hh, Ci repressor (Ci-75) formation is inhibited and full-length (Ci-155) nuclear activators of transcription are made instead (Ohlmeyer & Kalderon, 1998; Chen et al., 1999a; Matise & Joyner, 1999; Methot & Basler, 1999; Ruiz i Altaba, 1999b; Ingham & McMahon, 2001; Methot & Basler, 2001; Ruiz i Altaba et al., 2002b; Lum & Beachy, 2004; Zhang et al., 2005). Ci-155 and Ci-75 have both unique and common targets: hh appears to be primarily repressed by Ci-75 and ptch activated by Ci-155, while dpp (decapentaplegic) responds to both forms (Matise & Joyner, 1999; Methot & Basler, 1999).

Similarly, in vertebrates **(Figure 1.16a)**, Gli3 becomes proteolytically cleaved in numerous serine residues at their C-terminal regions by protein kinase A (PKA), casein kinase 1 (CK1), and glycogen synthase kinase 3β (GSK3β) and targeted for ubiquitination by beta-transducin repeat containing protein (β-TrCP) ubiquitin ligase, in order to produce truncated transcriptional N-terminal repressors (processing) (Dai et al., 1999; Ruiz i Altaba, 1999a; Sasaki et al., 1999; Wang et al., 2000a; Pan et al., 2006; Wang & Li, 2006; Pan & Wang, 2007; Wang et al., 2007). Gli2 on the other hand, shares with Gli3 a 44% sequence identity and conserved PKA and GSK3β

phosphorylation sites, but the protein is inefficiently processed *in vivo* (Pan et al., 2006) and its processing is undetectable or very low in cell culture resulting in the presence of the vast majority of mouse Gli2 in the full-length form and the existence of only a small fraction in the processed form (Matise & Joyner, 1999; Wang et al., 2000a; Pan et al., 2006; Pan & Wang, 2007; Wang et al., 2007). However, in different cell contexts (i.e. frog), several protein fragments smaller than full-length Gli2 have been observed (Matise & Joyner, 1999; Ruiz i Altaba, 1999a; Aza-Blanc et al., 2000). In contrast, Gli1 protein has not been found to be proteolytically processed (Dai et al., 1999; Ruiz i Altaba, 1999a; Sasaki et al., 1999). Importantly, Gli2, has also been shown to be phosphorylated by PKA, CK1 and GSK3β in its C-terminal activation domain (Pan et al., 2006; Riobo et al., 2006) and targeted for ubiquitination and proteasome mediated full protein degradation by β-TrCP ubiquitin ligase (Bhatia et al., 2006; Pan et al., 2006; Wang et al., 2007), as well as Gli1 (Huntzicker et al., 2006; Wang et al., 2007). Both Ci, Gli2 and Gli3 processing and Gli2 degradation, are inhibited by SHH signalling *in vivo* and *in vitro* (Ruiz i Altaba et al., 2002a; Zhang et al., 2005; Huntzicker et al., 2006; Pan et al., 2006; Riobo et al., 2006; Wang & Li, 2006; Wang et al., 2007).

All three Gli transcription factors are known to be mediators of the SHH signalling, with GLI2 being the key transcriptional effector of the HH pathway in skin and other organs both in mice and human **(see Section 1.3.3 and Section 1.3.6.2)** (Sasaki et al., 1999; Ingham & McMahon, 2001; Kasper et al., 2006a). In turn, human GLI2, has been shown to be present in several splice variants, α (alpha), β (beta), γ (gamma) and δ (delta) isoforms **(Figure 1.17B)**, and these four isoforms encode 133-, 131-, 88-, and 86 kDa proteins, respectively (Tanimura et al., 1998). All these isoforms are larger by ~ 30 kDa according to the full length of human GLI2 discovered by Roessler et al. **(Figure 1.17A, bottom panel)** (Roessler et al., 2005). Furthermore, GLI2 which is the gene of interest in my study has been reported to be implicated in many cancers including human BCCs, prostate and breast cancers, oral squamous cell carcinomas and osteosarcomas (Mullor et al., 2001; Regl et al., 2002; Ruiz i Altaba et al., 2002b; Tojo et al., 2003; Beachy et al., 2004; Rajagopalan & Lengauer, 2004; Regl et al., 2004b; Sanchez et al., 2004; Bhatia et al., 2006; O'Driscoll et al., 2006; Sterling et al., 2006; Thiyagarajan et al., 2007; Snijders et al., 2008; Yu et al., 2008; Hirotsu et al., 2010).

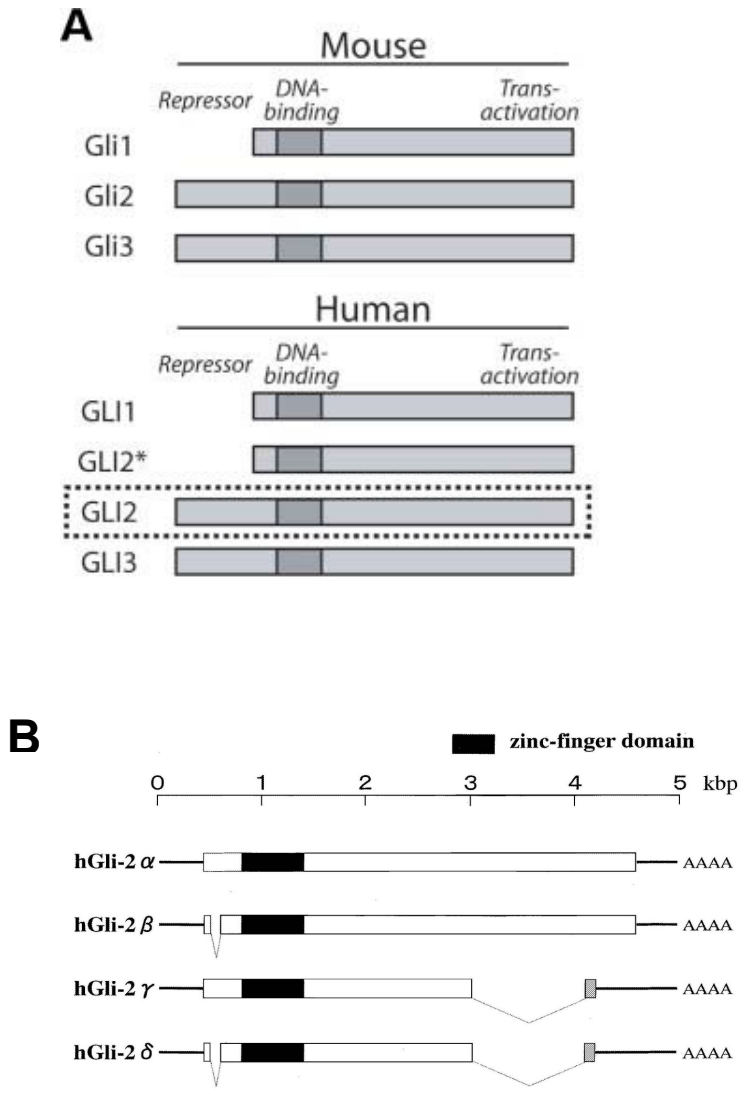

Figure 1.17: **Mouse and human Gli/GLI transcription factors and human GLI2 isoforms.**

(A) All full length Gli/GLI proteins contain a carboxy-terminal (C-terminal) domain required for transcriptional activity (*Transactivation*) and a zinc finger domain (*DNA binding* domain) which binds DNA in a sequence-specific manner. Mouse (top panel) and human (bottom panel) Gli3/GLI3 and mouse Gli2 proteins contain an amino-terminal (N-terminal) domain not present in Gli1/GLI1 which is involved in transcriptional repression (*Repressor*). Although initially it was thought that human GLI2 protein does not contain an amino-terminal domain (GLI2* or GLI2ΔN), it is now clear that human GLI2 contains an amino-terminal repressor domain (dashed box) functionally homologous to that in mouse Gli2 (Roessler et al., 2005). **(B)** Variation in human Gli2 (hGli2) mRNA. Four isoforms hGli2 α, β, γ, δ, result from combinations of two independent alternative splicing processes of the GLI2 gene, forming four different proteins of different molecular size (Tanimura et al., 1998; Tojo et al., 2003).

1.3.3 Hedgehog signalling pathway in development and skin

The Hedgehog (HH) signalling pathway is one of the most fundamental and highly conserved pathways in embryonic development, being responsible for pattern formation, proliferation and differentiation of a number of different cell types and organs including brain, bone, skin, hair, teeth and lungs (Marigo & Tabin, 1996; Bellusci et al., 1997; Mo et al., 1997; Hardcastle et al., 1998; Motoyama et al., 1998b; St-Jacques et al., 1998; Wicking et al., 1999; Litingtung & Chiang, 2000; Park et al., 2000; Ingham & McMahon, 2001; Ruiz i Altaba et al., 2002a; Wetmore, 2003; Daya-Grosjean & Couve-Privat, 2005; Athar et al., 2006).

As I mentioned earlier **(Section 1.3.1)**, three hedgehog homologue proteins have been identified in mammals (Echelard et al., 1993; Goodrich et al., 1996; Wicking et al., 1999; Bale & Yu, 2001; Ingham & McMahon, 2001; Hooper & Scott, 2005), of which the Shh is the best-characterised since it is the most potent and most broadly expressed in embryonic and adult tissues (Chiang et al., 1996; Ming et al., 1998; Wicking et al., 1999; Bale & Yu, 2001; Pathi et al., 2001; Ruiz i Altaba et al., 2002b; Daya-Grosjean & Couve-Privat, 2005; Athar et al., 2006).

In skin, the SHH pathway plays a pivotal role in maintaining the stem cell population, and regulating the development of hair follicles, hair cycle and sebaceous glands (Parisi & Lin, 1998; St-Jacques et al., 1998; Chiang et al., 1999; Wang et al., 2000b; Callahan & Oro, 2001; Allen et al., 2003; Ellis et al., 2003; Mill et al., 2003; Oro & Higgins, 2003; Schmidt-Ullrich & Paus, 2005; Silva-Vargas et al., 2005; Athar et al., 2006; Blanpain & Fuchs, 2006; Zhou et al., 2006). In skin, SHH/GLI pathway is implicated in the maintenance and regulation of the epidermal stem cell population residing in the epidermal basal layer (interfollicular epidermis) and the hair follicle bulge (Callahan & Oro, 2001; Adolphe et al., 2004; Blanpain & Fuchs, 2006; Zhou et al., 2006), while *in vitro* it is also suggested that SHH/GLI signalling has a potential role in the maintenance and proliferation of human putative epidermal stem cells (Fan & Khavari, 1999; Kameda et al., 2001; Zhang & Kalderon, 2001; Zhou et al., 2006). In addition, Shh is also involved in the proliferation and cell-fate specification of several stem cells such as neural and mesenchymal stem cells (Palma & Ruiz i Altaba, 2004; Kondo et al., 2005).

The role of SHH/GLI pathway is well established in hair follicle morphogenesis and in adult hair cycle (St-Jacques et al., 1998; Botchkarev et al., 1999; Chiang et al., 1999; Wang et al., 2000b; Millar, 2002; Oro & Higgins, 2003; Schmidt-Ullrich & Paus, 2005; Athar et al., 2006; Blanpain & Fuchs, 2006), and its constitutive activation leads to hair follicle derived tumours and BCC (Dahmane et al., 1997; Oro et al., 1997; Grachtchouk et al., 2000; Nilsson et al., 2000; Sheng et al., 2002; Daya-Grosjean & Couve-Privat, 2005; Hutchin et al., 2005; Huntzicker et al., 2006). Studies in normal skin of transgenic mice, have shown that Wnt/β-catenin is required upstream of the Bmp and Shh in placode formation during hair follicle morphogenesis **(see Section 1.5.1)**, and thus specifying the hair follicle fate in the undifferentiated basal epidermis and initiate hair bud formation (Gat et al., 1998; Huelsken et al., 2001; Andl et al., 2002; Lo Celso et al., 2004; Silva-Vargas et al., 2005; Blanpain & Fuchs, 2006). Then, it subsequently activates Shh signalling, which is required for the proliferation and expansion of follicle epithelium in order to assemble a mature follicle (St-Jacques et al., 1998; Chiang et al., 1999; Mill et al., 2003; Lo Celso et al., 2004; Silva-Vargas et al., 2005; Blanpain & Fuchs, 2006). The crucial role of SHH/GLI pathway in hair follicle morphogenesis is underscored by the fact that loss-of-function mutations in SHH in transgenic mice are still permissive for hair placode and hair germ formation but are not permissive for the further development of the hair placodes and thus for the formation of a mature follicle (lack of hairs) (St-Jacques et al., 1998; Chiang et al., 1999; Wang et al., 2000b; Blanpain & Fuchs, 2006). In addition, mice deficient either in Shh ($Shh^{-/-}$ mutants) or in Gli2 ($Gli2^{-/-}$ mutants) exhibit an arrest in hair follicle development with reduced cell proliferation and Shh-responsive gene expression (Ptch1 and Gli1) (Mill et al., 2003). The fact that Gli2 deficient mice ($Gli2^{-/-}$ mutants) present a phenotype similar to Shh-null mice ($Shh^{-/-}$ mutants), suggests that Shh is essential for embryonic hair follicle development and acts mainly through Gli2 (Mill et al., 2003; Blanpain & Fuchs, 2006).

Therefore, SHH is expressed in the hair placode of embryonic skin (St-Jacques et al., 1998), but is also expressed in the matrix and the developing hair germ and thus it is also important for follicle regeneration during the adult hair cycle (Wang et al., 2000b; Oro & Higgins, 2003; Silva-Vargas et al., 2005; Blanpain & Fuchs, 2006). Conditional disruption of SHH/GLI pathway in postnatal mice (anti-hedgehog monoclonal antibody treatment) during the growing (anagen) phase of the hair cycle, resulted in blockage of anagen progression and thus in a hairless phenotype further supporting the notion that

SHH/GLI pathway is required for hair growth phases of the hair cycle in adult mice (Wang et al., 2000b). Similarly, treatment of postnatal transgenic mice with the SHH inhibitor, cyclopamine, a specific HH pathway antagonist (Taipale et al., 2000), resulted in the blockage of anagen and hair regeneration (Silva-Vargas et al., 2005).

1.3.4 SHH signalling and disease

The importance of SHH/GLI signalling in human development can be demonstrated by the fact that mutations in the key components of SHH/GLI signalling pathway, can result in severe developmental disorders such as Holoprosencephaly (HPE) (incomplete separation of cerebral hemispheres, craniofacial anomalies (i.e. cyclopia)), which is caused by loss-of-function mutations in SHH gene (Belloni et al., 1996; Roessler et al., 1996; Roessler et al., 2003), Greig cephalopolysyndactyly syndrome (GCPS) (a disorder that affects development of the limbs, head, and face), which is caused by inactivation mutations in GLI3 gene (Vortkamp et al., 1991), and tumour formation such as Nevoid Basal Cell Carcinoma (Gorlin syndrome), which is caused by PTCH germline inactivation mutations (Hahn et al., 1996b; Johnson et al., 1996; Gailani & Bale, 1997), and is associated with developmental abnormalities **(see Section 1.2.3)** and familial multiple basal cell carcinomas (BCCs), medulloblastomas and ovarian fibromas (Gorlin, 1987; Gorlin, 1995; Chiang et al., 1996; Ming et al., 1998; Wicking et al., 1999; Villavicencio et al., 2000; Bale & Yu, 2001; Mullor et al., 2002; Daya-Grosjean & Couve-Privat, 2005; Athar et al., 2006). A recent report indicated, that loss-of-function mutations in the human GLI2 gene, are associated with holoprosencephaly-like features (Roessler et al., 2003).

1.3.5 SHH signalling and cancer

Uncontrolled Sonic Hedgehog (SHH) signalling is implicated in tumour development in many tissues (Ming et al., 1998; Toftgard, 2000; Villavicencio et al., 2000; Taipale & Beachy, 2001; Ruiz i Altaba et al., 2002b; Pasca di Magliano & Hebrok, 2003; Wetmore, 2003; Beachy et al., 2004; Kasper et al., 2006a; Rubin & de Sauvage, 2006), predominantly BCCs in skin (Gailani et al., 1996; Hahn et al., 1996b; Johnson et al., 1996; Gailani & Bale, 1997; Daya-Grosjean & Couve-Privat, 2005; Epstein, 2008),

medulloblastomas (Goodrich et al., 1997; Raffel et al., 1997; Berman et al., 2002; Taylor et al., 2002) and gliomas in brain (Kinzler et al., 1987; Dahmane et al., 2001), and rhabdosarcomas in muscle (Hahn et al., 1998; Tostar et al., 2006).

It has also recently been found to be inappropriately activated in highly aggressive cancers in the absence of mutations in the pathway components, suggesting that activation of the HH pathway may occur through mechanisms other than by mutations of pathway components (Ruiz i Altaba et al., 2002b; Pasca di Magliano & Hebrok, 2003; Beachy et al., 2004; Kasper et al., 2006a; Rubin & de Sauvage, 2006). These cancers include the digestive tract (oesophagus, stomach, biliary tract) (Berman et al., 2003), pancreatic (Thayer et al., 2003; Hidalgo & Maitra, 2009), small-cell lung (Watkins et al., 2003), breast (Kubo et al., 2004; Sterling et al., 2006; Kameda et al., 2009), ovarian (Bhattacharya et al., 2008) and prostate caners (Karhadkar et al., 2004; Sanchez et al., 2004; Sheng et al., 2004; Bhatia et al., 2006; Thiyagarajan et al., 2007), colon (Oniscu et al., 2004; Qualtrough et al., 2004; Monzo et al., 2006), liver (Huang et al., 2006; Eichenmuller et al., 2009) cancers, as well as the oral squamous cell carcinoma (Snijders et al., 2008) and osteosarcomas (Hirotsu et al., 2010).

Furthermore, HH pathway in some of these cancers, not only has a pivotal role in tumour formation, but also in its maintenance by enhancing the survival of transformed cells, as has been judged by studies using cyclopamine, a specific HH pathway antagonist (Taipale et al., 2000), and resulting in inhibition of growth of several tumours, suggesting an ongoing requirement for pathway activity in the growth of a series of cancers (Ruiz i Altaba et al., 2002b; Pasca di Magliano & Hebrok, 2003; Beachy et al., 2004; Rubin & de Sauvage, 2006). Recent evidence, also suggests that SHH/GLI signalling pathway is also implicated in metastasis, at least in some types of cancer (Beachy et al., 2004; Karhadkar et al., 2004; Sheng et al., 2004; Rubin & de Sauvage, 2006; Sterling et al., 2006). Accordingly, human prostate cancer metastases have higher HH/GLI signalling activity than do the primary tumours from which they arose, while augmented Hh pathway activity (GLI1 overexpression) in mice prostate cancer cell lines resulted in increased levels of Snail, reduced levels of E-cadherin, and to a metastatic phenotype in mice inoculated subcutaneously with these cells (Karhadkar et al., 2004). In addition, treatment with cyclopamine, of mice inoculated subcutaneously with highly metastatic rat prostate cancer cell lines (i.e. AT6.3), resulted

in complete abrogation of their capacity to metastasize to the lung (Karhadkar et al., 2004). Similarly, SHH/GLI signalling has been reported to be involved in bone metastasis (Sterling et al., 2006). Overexpression of GLI2 in human breast cancer cell lines enhances their metastatic potential to bone, through the upregulation of parathyroid hormone-related peptide (PTHrP) and subsequent osteolysis, as observed *in vitro* and in mice inoculated subcutaneously with these cells (Sterling et al., 2006).

1.3.6 SHH signalling and Basal cell carcinoma (BCC)

Deregulation of the SHH pathway by mutations in the components of the pathway leads to constitutive activation of the SHH signalling and to development of basal cell carcinomas (BCCs) **(Figure 1.18)** (Bale & Yu, 2001; Pasca di Magliano & Hebrok, 2003; Daya-Grosjean & Couve-Privat, 2005; Rubin & de Sauvage, 2006; Epstein, 2008). PTCH germline inactivated mutations are present in Nevoid Basal Cell Carcinoma (NBCC) patients and frequent loss of heterozygosity at 9q locus (loss of the remaining wild-type allele of patched gene) is observed in BCCs from these patients (Hahn et al., 1996b; Johnson et al., 1996; Unden et al., 1996; Gailani & Bale, 1997; Booth, 1999; Happle, 1999; Daya-Grosjean & Couve-Privat, 2005). PTCH inactivated and SMO activated mutations occur frequently in sporadic BCCs and in BCCs associated with xeroderma pigmentosum (Gailani et al., 1996; Unden et al., 1996; Gailani & Bale, 1997; Soehnge et al., 1997; Unden et al., 1997; Reifenberger et al., 1998; Xie et al., 1998; Bodak et al., 1999; Ling et al., 2001; Couve-Privat et al., 2002; Dicker et al., 2002; Lacour, 2002; Daya-Grosjean & Couve-Privat, 2005; Reifenberger et al., 2005; Teh et al., 2005), whereas SHH activated mutations are extremely rare in sporadic BCCs, but are present in BCCs associated with xeroderma pigmentosum (Reifenberger et al., 1998; Couve-Privat et al., 2004; Daya-Grosjean & Couve-Privat, 2005).

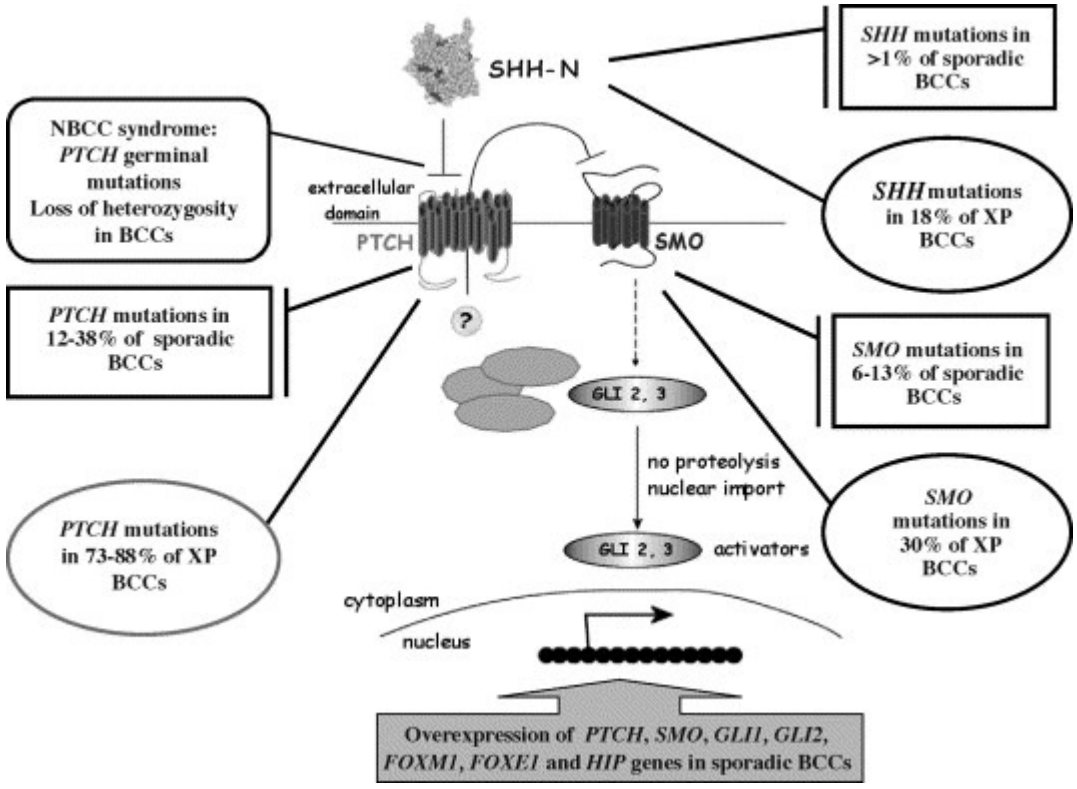

Figure 1.18: Modifications of SHH pathway genes in Basal Cell Carcinomas.

Germline mutations of the tumour suppressor gene PTCH gene are found in the nevoid basal cell carcinoma (NBCC) patients. Sporadic and Xeroderma Pigmentosum (XP) BCCs present mutations of PTCH as well as the proto-oncogenes SHH and SMO. Overexpression of downstream target genes is also implicated in BCC development (Daya-Grosjean & Couve-Privat, 2005).

The majority of BCCs are thought to be derived from keratinocytes of the basal stem cell layer of the epidermis (interfollicular epidermis) which are negative for markers of differentiation (Miller, 1991a; Miller, 1991b; Lacour, 2002; Owens & Watt, 2003; Wong et al., 2003; Daya-Grosjean & Couve-Privat, 2005; Crowson, 2006; Fuchs, 2008), such as involucrin (Murphy et al., 1984; Said et al., 1984; Sumitomo et al., 1986; Miller, 1991a; Fuchs, 2008), and positive for keratin 5 and keratin 14 (Miller, 1991a; Crowson, 2006) which are mainly expressed by cells of the basal layer of the epidermis (Stoler et al., 1988; Coulombe et al., 1989; Fuchs, 2008). Consistent with this notion, human BCCs exhibit continuous proliferation and slow growth and they also manifest a

stem cell gene expression profile similar to that expressed by the cells of the interfollicular epidermis and hair follicle bulge region, such as keratins 15 and 19, and α2 and β1 integrins **(see Chapter 3, Section 3.3.6)** (Lane et al., 1991; Miller, 1991a; Jones & Watt, 1993; Jones et al., 1995; Pentel et al., 1995; Kruger et al., 1999; Lyle et al., 1999; Morris et al., 2004; Tumbar et al., 2004; Crowson, 2006). These observations are consistent with the role of SHH/GLI pathway in skin, which has been shown to be implicated in the maintenance and regulation of the epidermal stem cell population residing in the epidermal basal layer (interfollicular epidermis) and the hair follicle bulge (Parisi & Lin, 1998; Callahan & Oro, 2001; Adolphe et al., 2004; Blanpain & Fuchs, 2006; Zhou et al., 2006), while *in vitro* it is also suggested that SHH/GLI signalling has a potential role in the maintenance and proliferation of human putative epidermal stem cells **(Section 1.3.3)** (Fan & Khavari, 1999; Kameda et al., 2001; Zhang & Kalderon, 2001; Zhou et al., 2006).

In addition, due to (i) the very well established role of SHH/GLI in hair follicle morphogenesis and in adult hair cycle **(Section 1.3.3)** (St-Jacques et al., 1998; Botchkarev et al., 1999; Chiang et al., 1999; Wang et al., 2000b; Millar, 2002; Mill et al., 2003; Oro & Higgins, 2003; Schmidt-Ullrich & Paus, 2005; Silva-Vargas et al., 2005; Athar et al., 2006; Blanpain & Fuchs, 2006), (ii) the striking relation between BCC development and deregulation of the SHH pathway (Dahmane et al., 1997; Oro et al., 1997; Grachtchouk et al., 2000; Nilsson et al., 2000; Sheng et al., 2002; Daya-Grosjean & Couve-Privat, 2005; Hutchin et al., 2005; Huntzicker et al., 2006), and as I mentioned earlier (iii) the expression of hair follicle bulge stem cell markers in human BCCs, basal cell carcinomas are also thought to be derived from undifferentiated cells of hair follicles (outer root sheath of hair follicles) (Miller, 1991b; Kruger et al., 1999; Lacour, 2002; Owens & Watt, 2003; Hutchin et al., 2005; Blanpain & Fuchs, 2006; Crowson, 2006; Huntzicker et al., 2006; Mancuso et al., 2006).

However, a very recent study by Youssef et al. (Youssef et al., 2010), using conditional (tamoxifen administration) overexpression of a constitutively active form of mouse smoothened gene (SmoM2) in different cellular compartments of the skin epidermis of transgenic mice, under the control of specific promoters such as Keratin 14, Keratin 15, Keratin 19 and Shh, favours the notion that BCCs arise from the undifferentiated stem cells of the basal layer of the epidermis (interfollicular epidermis) and not from hair

follicle bulge stem cells or transit-amplifying matrix cells that reside at the base of hair follicle. By achieving a low level transgene induction through administration of low dose of tamoxifen, Youssef et al. (Youssef et al., 2010) were able to efficiently induce the expression of either K14-SmoM2 or K14-YFP (Yellow Fluorescent Protein) control in individual basal cells of the interfollicular epidermis (IFE) in transgenic mice at a very low frequency (4-5 cells/IFE) and to investigate the cell of origin of the arising BCCs from the IFE. Due to continuous epithelial renewal, several marked clones expressing the transgenes were progressively lost from the epidermis. By tracking their fate during several weeks, it was shown that the rate of decline in the abundance of clones in the IFE, was almost the same whether the cells expressed K14-SmoM2 or K14-YFP. Since K14-SmoM2 expressing clones did not persist in the epidermis longer than their K14-YFP expressing counterparts, it was suggested that SmoM2 expression is unable to oppose differentiation and/or to re-induce long-term renewing potential to more committed (TA) or differentiated keratinocytes. Yet, all long-term expressing K14-SmoM2 clones that remained in the mouse epidermis had stopped differentiation, adopting a placode-like shape with subsequent expression of follicular progenitor markers like K17, K15, and P-cadherin, and concomitant formation of BCCs, contrarily to K14-YFP expressing clones which either remained as columns of marked cells expanding from the basal to the top cornified layers or progressively differentiate and lost from the epidermis. This strongly suggested that the cell of origin of these BCCs is a long-lived resident of the interfollicular epidermis (SC), rather than a more committed progenitor (TA) that has re-acquired the potential to oppose differentiation and to self-renew as a result of K14-SmoM2 overexpression. The model of BCC initiation that was deduced from these observations suggests that Hh activation in IFE stem cells can block the normal process of epidermal differentiation (affecting/increasing the self-renewal capacity of stem cells) whereby a stem cell would normally give rise to one stem cell and one committed TA daughter cell. Instead, its activation leads to the expansion of stem cells, with concomitant expression of follicular progenitor markers, and finally generation of locally invasive BCC tumours (Youssef et al., 2010).

Therefore, constitutive activation of the SHH/GLI pathway in skin, could disrupt the epidermal homeostasis and lead to tumourigenesis with a phenotype that resembles stem cell characteristics (stem-like tumour phenotype), such as human BCCs (Miller, 1991a; Miller, 1991b; Taipale & Beachy, 2001; Ruiz i Altaba et al., 2002b; Owens & Watt,

2003; Pasca di Magliano & Hebrok, 2003; Perez-Losada & Balmain, 2003; Beachy et al., 2004; Crowson, 2006). However, whether HH/GLI signalling is inappropriately activated in epidermal stem cells or in commited to differentiation transit-amplifying cells (TA) is not yet completely resolved. Taking into account that human BCCs have inactivating or activating mutations of PTCH and SMO respectively (Daya-Grosjean & Couve-Privat, 2005; Epstein, 2008), if the oncogenic events occur in TAs, then loss of PTCH or gain of SMO function in TA cells resulting in ligand-independent constitutive activation of GLI1 and GLI2 oncogenes, and presumably activation of other oncogenic pathways and repression of differentiation signals, might be the initiation step in BCC development (Aberger & Frischauf, 2006). Further mutations such as loss of TP53 function may promote BCC development (Ling et al., 2001; Reifenberger et al., 2005; Aberger & Frischauf, 2006). This scenario of course, presupposes that the effect of the activated GLI1 and GLI2 oncogenes is expressed immediately or very quickly, so as for the TA cell to acquire the long self-renewal capacity of the stem cell, and to avoid becoming terminally differentiated and discarded from the epidermis.

However, unlike the classical step-wise model of carcinogenesis requiring multiple genetic lesions, SHH/GLI pathway activation alone in human keratinocytes appears to be sufficient to induce basal cell carcinoma features in transgenic human skin (4 weeks postoperatively), when grafted onto the back of nude mice (Fan et al., 1997). Moreover, targeted overexpression of the oncogenic forms of Smo, Gli1, Gli2 and Shh in epidermal cells of transgenic mice can induce the formation of BCC or BCC-like tumours (Fan et al., 1997; Oro et al., 1997; Grachtchouk et al., 2000; Nilsson et al., 2000; Sheng et al., 2002; Hutchin et al., 2005; Huntzicker et al., 2006; Youssef et al., 2010). Thus, collectively these studies suggest that a single genetic alteration is sufficient to induce experimentally human neoplasia *in vivo*. This one-hit induction of BCC tumourigenesis by SHH/GLI may partially explain the biologically mild behavioural characteristics (slow growing, locally invade, rarely metastasize), the absence of precursor lesions and the lack of the aggressiveness of BCCs compared to other malignancies characterised by multiple genetic lesions necessary for more aggressive behaviour (Miller, 1991a; Crowson, 2006; Khavari, 2006).

Therefore, in a tumour such as BCC which might be considered as an one-hit tumour due to the lack of multiple genetic alterations, arguments are in favour of stem cells

being the appealing candidates as the 'cell of origin' of BCC, because of their pre-existing capacity of self-renewal and unlimited proliferative capacity which are prerequisites for the extra genetic hit (one-hit) that will transform the normal cell into a cancer cell **(see Section 1.1.5 and Section 1.1.5.2)** (Miller, 1991a; Owens & Watt, 2003; Perez-Losada & Balmain, 2003; Beachy et al., 2004; Crowson, 2006; Khavari, 2006; Youssef et al., 2010). On the other hand there is always the case that this 'one hit' is so strong that can target a TA cell, become expressed rapidly by the TA cell and concomitantly influence differentiation signals, promote long self-renewal capacity, transformation, expansion and finally cause BCC tumour formation, which although possible is quite unlikely to happen.

1.3.6.1 SHH/GLI2 and human BCCs

It is clear that altered activity of one or more members of the SHH pathway can lead to constitutive activation of the pathway and subsequently to BCC formation (Pasca di Magliano & Hebrok, 2003; Beachy et al., 2004; Daya-Grosjean & Couve-Privat, 2005; Rubin & de Sauvage, 2006; Epstein, 2008). Indeed upregulation of mRNA and protein levels of GLI2 transcription factor is frequently observed in human BCCs, as well as upregulation of GLI1 transcription factor, SMO and PTCH genes (Dahmane et al., 1997; Kallassy et al., 1997; Unden et al., 1997; Ghali et al., 1999; Tojo et al., 1999; Zaphiropoulos et al., 1999; Bonifas et al., 2001; Mullor et al., 2001; Regl et al., 2002; Tojo et al., 2003; Ikram et al., 2004; Regl et al., 2004b; Daya-Grosjean & Couve-Privat, 2005; O'Driscoll et al., 2006; Asplund et al., 2008; Epstein, 2008; Yu et al., 2008). In addition, Ikram et al. (Ikram et al., 2004), using in situ-hybridization, further demonstrated the importance of GLI2 in BCC, by showing that GLI2 is expressed not only in human BCC tumour islands, but also in the interfollicular epidermis and the outer root sheath of hair follicles in normal human skin. This observation is consistent since Shh/Gli2 is known to regulate hair follicle morphogenesis and growth **(see Section 1.3.3)** (St-Jacques et al., 1998; Botchkarev et al., 1999; Chiang et al., 1999; Wang et al., 2000b; Millar, 2002; Mill et al., 2003; Oro & Higgins, 2003; Schmidt-Ullrich & Paus, 2005; Silva-Vargas et al., 2005; Athar et al., 2006; Blanpain & Fuchs, 2006), and its constitutive activation leads to hair follicle derived tumours and BCC-like tumours (Dahmane et al., 1997; Oro et al., 1997; Grachtchouk et al., 2000; Nilsson et al., 2000; Sheng et al., 2002; Daya-Grosjean & Couve-Privat, 2005; Hutchin et al.,

2005; Huntzicker et al., 2006) which are thought to arise from epidermal basal layer or hair follicle stem cells (Miller, 1991a; Kruger et al., 1999; Owens & Watt, 2003; Daya-Grosjean & Couve-Privat, 2005; Hutchin et al., 2005; Blanpain & Fuchs, 2006; Crowson, 2006; Huntzicker et al., 2006; Mancuso et al., 2006; Youssef et al., 2010). Furthermore, targeted overexpression of Gli2 in epidermal cells of transgenic mice can induce the formation of BCC or BCC-like tumours (Grachtchouk et al., 2000; Sheng et al., 2002; Hutchin et al., 2005; Huntzicker et al., 2006).

Further studies have also shown that constitutively active GLI2 (GLI2ΔN) can regulate a large number of genes and plays a dual role as activator of keratinocyte proliferation and repressor of epidermal differentiation in HaCaT human keratinocytes, therefore its continuous expression by sustained HH/GLI signalling could disrupt the epidermal homeostasis and lead to tumourigenesis (Regl et al., 2004a; Eichberger et al., 2006). Moreover, the anti-apoptotic protein BCL-2 (B-cell lymphoma 2, an antagonist of the cell intrinsic pathway of apoptosis) **(see Chapter 4, Section 4.2.5.3)** is directly controlled by GLI1 in primary human keratinocytes (Bigelow et al., 2004) and it has also been identified in HaCaT human keratinocyte cell line, as a direct transcriptional target of GLI2 transcription factor (Regl et al., 2004b). Similarly, the apoptotic inhibitor c-FLIP (c (cellular)-FAS-associated death domain-like IL (interleukin)-1-converting enzyme-like inhibitory protein, an antagonist of the cell extrinsic pathway of apoptosis) **(see Chapter 4, Section 4.2.5.3)** has been found in HaCaT human keratinocytes to be a direct target of GLI2 (Kump et al., 2008), suggesting that both of them might play a role in BCC tumourigenesis and maintenance, since human BCCs highly express both BCL-2 and c-FLIP protein, as well as GLI2 protein (Regl et al., 2004b; Kump et al., 2008). Lastly, several genes, other than BCL-2 and c-FLIP, that have been found to be downstream targets of GLI1 and constitutively active GLI2 (GLI2ΔN) transcription factors, have also been reported to be upregulated in human BCCs, including PDGFRα (platelet-derived growth factor receptor) (target of GLI1), FOXM1 (forkhead box M1) (target of GLI1), Basonuclin (target of GLI2 and GLI1), HIP gene (Hh-interacting protein) (target of GLI2 and GLI1), SOX9 (SRY (sex determining region Y)-box 9) (target of GLI2) **(see Chapter 3, Section 3.3.6.2)** and FOXE1 (winged helix domain transcription factor) (target of GLI2) (Chuang & McMahon, 1999; Xie et al., 2001; Dicker et al., 2002; Teh et al., 2002; Tojo et al., 2002; Cui et al., 2004; Eichberger et al.,

2004; Daya-Grosjean & Couve-Privat, 2005; Vidal et al., 2005; Crowson, 2006; Eichberger et al., 2006; Kasper et al., 2006a; Epstein, 2008; Vidal et al., 2008).

1.3.6.2 Shh/Gli transgenic studies and BCC carcinogenesis

Previous work from mice models further highlights the significance of Hh/Gli-signalling activation in BCC tumourigenesis (Wicking et al., 1999; Toftgard, 2000; Wetmore, 2003; Daya-Grosjean & Couve-Privat, 2005; Athar et al., 2006; Kasper et al., 2006a; Epstein, 2008).

$Ptch^{+/-}$ heterozygous knockout mice show an increased susceptibility to BCC-like tumour formation (trichoblastomas and BCC) in response to chronic UV radiation or to single dose of ionizing radiation, and those BCCs often have deletion of the wild-type copy of Ptch1 (Ptch loss of heterozygosity), activation of hedgehog target gene transcription, loss of normal hemidesmosomal components, as well as p53 inactivated mutations (40% of BCC-like tumours had p53 gene mutations) (Aszterbaum et al., 1999). The importance of p53 inactivation in skin carcinogenesis, is highlighted by the fact that homozygous or heterozygous p53 knockout mice develop skin tumours much earlier than wild-type mice upon UV radiation (Jiang et al., 1999; Erb et al., 2005), while human BCCs exhibit a high incidence of p53 gene mutations (Barbareschi et al., 1992; Shea et al., 1992; Grossman & Leffell, 1997; Ponten et al., 1997; Soehnge et al., 1997; de Gruijl et al., 2001; Ling et al., 2001; Dicker et al., 2002; Lacour, 2002; Daya-Grosjean & Couve-Privat, 2005; Reifenberger et al., 2005; Epstein, 2008). The notion that p53 loss markedly enhances HH-driven tumourigenesis, and thus possibly contributing to the development of cancers including BCCs and thus is not just a result of the fact that BCCs usually arise in sun-exposed skin, was first shown by the development of medulloblastomas in almost 100% of $Ptch1^{+/-}$; $Trp53^{-/-}$ mice, compared to an incidence of less than 10% in $Ptch1^{+/-}$ mice with wild-type p53 (Wetmore et al., 2001; Epstein, 2008). In addition, another study by Adolphe et al. (Adolphe et al., 2006) further demonstrated that conditional loss of Ptch1, upon the control of keratin 6 promoter and topical retinoic acid treatment, in the basal cell population of mouse skin, induces the formation of human BCC-like tumours (Adolphe et al., 2006). Similarly, $Sufu^{+/-}$ mice, mice carrying one inactivated, mutant allele of the SHH suppressor SuFu, are also susceptible to BCC-like tumour development (Svard et al., 2006).

Furthermore, human keratinocytes over-expressing SHH, followed by seeding in human dermal tissue, regeneration of human skin epidermis and subsequent grafting onto the back of immune-deficient mice, have the power to induce BCC-like structures (Fan et al., 1997; Khavari, 2006), while targeted overexpression of the oncogenic forms of Smo, Shh, Gli1, and Gli2 in epidermal cells of transgenic mice under the control of specific promoters (i.e. Keratin 5 promoter), can induce the formation of BCC and BCC-like tumours (Fan et al., 1997; Oro et al., 1997; Xie et al., 1998; Grachtchouk et al., 2000; Nilsson et al., 2000; Sheng et al., 2002; Hutchin et al., 2005; Huntzicker et al., 2006; Youssef et al., 2010).

Importantly, it seems that the degree of activation of HH signalling is correlated with the tumour phenotype as Grachtchouk et al. (Grachtchouk et al., 2003) showed that different levels of SHH/GLI signalling activity can result in distinct tumour types in skin. High levels of HH activation and target genes (transgenic mice overexpressing Gli2 under the control of keratin 5 promoter) lead to the formation of BCC-like tumours, whereas low levels of HH activation and target genes (transgenic mice overexpressing human M2SMO - mutant SMO under the control of keratin 5 promoter) result to the formation of hair-follicle-like tumours such as basaloid follicular hamartomas (Grachtchouk et al., 2003).

Studies by Hutchin et al. (Hutchin et al., 2005), using a conditional Gli2 mouse model under the control of keratin 5 promoter to examine the role of Gli2 in established BCCs, showed that continuous expression of Gli2 due to sustained and uncontrolled HH signalling pathway, is required for BCC-like tumour proliferation and survival. Inactivation of the transgene upon doxycycline treatment led to reduced HH target gene expression and BCC regression accompanied by reduced tumour cell proliferation and increased apoptosis, leaving behind a small subset of non-proliferative cells which upon transgene reactivation could form BCC-like tumours (regressed tumours resume growth) (Hutchin et al., 2005).

Accordingly, Gli2 knockdown via RNA interference (RNAi) inhibits BCC-like tumour growth *in vivo* (Ji et al., 2008). In this study (Ji et al., 2008), mouse Gli2 gene was silenced in a mouse BCC-like tumour cell line (K5-Gli2ΔN2) that constitutively express high levels Gli2ΔN2, is originated from a K5-Gli2ΔN2-induced trichoblastoma and is

tumourigenic (Sheng et al., 2002). When the Gli2 knock down cells were injected subcutaneously into nude mice, they gave rise to tumours of a much slower growth rate (smaller size) and with disruption of the BCC-like structure characterised by lots of typical tumour nodules surrounded by stroma cells, possibly due to the increased susceptibility to apoptosis (increases cell death) and decreased vascularisation (decreased microvasulogenesis - formation of new blood vessels, by vascular endothelial cells that migrate into tissue, which are required to provide blood supply in tumours, a requirement for their growth) of tumour cells, compared to the tumours arising from control cells (K5-Gli2ΔN2 cells) (Ji et al., 2008).

Importantly, removal of Gli2 but not Gli1, can partially reduce the severity of the phenotype, mediated by HH signalling hyperactivation, in Patched knockout mice (Bai et al., 2002), while loss of Gli2 alone, but not of Gli1, is sufficient to cause severe developmental abnormalities resembling those seen in Shh knockout mice (Ding et al., 1998; Matise et al., 1998; Park et al., 2000; Mill et al., 2003). Furthermore, Gli1 has been found to be dispensable for SHH-induced medulloblastoma in transgenic mice (overexpression of Shh (injection of the Shh-expressing retrovirus) in $Gli1^{-/-}$ homozygous null mutant mouse embryos resulting in tumour formation), suggesting that SHH signalling activation leads to Gli2 upregulation which in turns activate Gli1 (Weiner et al., 2002).

Taken together, all these mouse model studies highlight the role of Gli2 as the primary effector of HH signalling during development and carcinogenesis. Further support to this statement is provided by the fact that Gli2 has been shown to act as an upstream regulator of Gli1, since the absence of Gli2 function decreases the mRNA levels of Gli1 (Ding et al., 1998; Bai et al., 2002; Mill et al., 2003). Also, overexpression of GLI2 in human epidermal cells induces GLI1 protein expression, whereas GLI2 is likely to be an indirect target of GLI1 (Regl et al., 2002). It has also been shown that GLI2 specifically binds to the GLI1 promoter, suggesting that GLI1 is a direct target of GLI2 (Ikram et al., 2004).

1.3.7 SHH/GLI and cell cycle regulation

Little is known about the molecular mechanisms involved in the transformation of epidermal keratinocytes in response to HH/GLI signalling, despite the identification of the genetic hits involved in BCC development. However, several mechanisms have been proposed for the interactions of SHH/GLI signalling with important cell cycle mediators that promote cell proliferation (Ruiz i Altaba et al., 2002a; Pasca di Magliano & Hebrok, 2003; Wetmore, 2003; Daya-Grosjean & Couve-Privat, 2005; Aberger & Frischauf, 2006; Athar et al., 2006; Kasper et al., 2006a).

In various cell types activation of HH pathway activity increases the expression of key regulators of G1/S and G2/M phase progression of the cell cycle (Kasper et al., 2006a). In *Drosophila*, Hh/Ci signalling can regulate cell proliferation in the developing eye, by the induction of cyclin D expression, and of the cyclin E expression which has been identified as a direct transcriptional target of Ci (Cubitus interruptus) (the *Drosophila* homologue of vertebrate GLI genes) (Duman-Scheel et al., 2002), and which both cyclin D and cyclin E are involved in G1-S transition (Knoblich et al., 1994; Weinberg, 1995). In vertebrates (mice), Shh protein can also stimulate and maintain the proliferation of cerebellar neuronal precursor cells via the regulation of D-type cyclins (increased mRNA and protein levels of cyclin-D1 and cyclin-D2) (Kenney & Rowitch, 2000), while in chicken embryos Shh regulates cyclin-D1 in neural groove, during early steps of spinal cord development (Lobjois et al., 2004). In addition, induction of cyclin-D2 transcription is likely to be directly controlled by Shh/Gli signalling pathway, as revealed by analysis in GLI1-expressing rat kidney epithelial cells and in Shh-protein treated murine mesodermal cells (Yoon et al., 2002; Buttitta et al., 2003). Human GLI1 upregulates cyclin-D2 based on microarray analysis of GLI1-expressing rat kidney epithelial cells, and the human cyclin D2 promoter contains a GLI1-binding site (Yoon et al., 2002). Cyclin-D2 is upregulated both in Gli2-expressing and Shh-expressing murine mesodermal cells, while cyclin-D2 mRNA expression is induced in Shh-protein treated murine mesodermal cells even in the absence of protein synthesis (treatment with cyclohexamide to block protein synthesis), supporting the notion that cyclin-D2 is a direct target of Shh/Gli signalling pathway (Buttitta et al., 2003). Moreover, Mill et al. (Mill et al., 2003) showed that the transcription of Cyclin-D1 and Cyclin-D2 in developing mouse hair follicles, is regulated by the Shh-dependent activator function of

Gli2, since only ΔNGli2 (activated form of Gli2), and not full-length Gli2, can induce cyclin-D1 and cyclin-D2 expression in the absence of Shh.

SHH expression has also been shown to increase the life-span of primary human keratinocytes by promoting cell proliferation, and to oppose the normal growth arrest (G1 cell cycle arrest) of primary epidermal keratinocytes in response to extracellular calcium, as well as to ectopic expression of CDKI $p21^{WAF1/CIP1}$ (Fan & Khavari, 1999). On the other hand, loss of Shh or Gli2 function in mice, leads to a significant decrease in the rate of cell proliferation in the developing hair follicle (arrest in hair follicle development) (Mill et al., 2003). Accordingly, Gli2 knockdown in a mouse BCC-like tumour cell line slightly reduced the cell proliferation rate (Ji et al., 2008), while GLI1 knockdown in human gastric carcinoma cells, markedly repress cell proliferation, followed by a significant increase in the proportion of cells in G1 cell cycle phase and in the mRNA and protein levels of $p21^{WAF1/CIP1}$ (Ohta et al., 2005).

In a different context, GLI1 and GLI2 inducible expression has been shown to stimulate entry into the S phase of confluent growth arrested HaCaT human keratinocytes, whereas no difference in DNA synthesis between GLI1/or/GLI2-expressing HaCaT cells and control cells was detected at sub-confluent cultures (Regl et al., 2002). Further, inducible expression of GLI2ΔN in contact inhibited (confluent) cultures of HaCaT and primary human keratinocytes is sufficient to stimulate DNA synthesis (G1-S progression), re-entry to the cell cycle, and to regulate the mRNA levels of specific cell cycle genes involved in G1-S and G2-M phase progression, such as cyclin D1 (CCND1), E2F transcription factor 1 (E2F1) and cyclin B1 (CCNB1) respectively (Regl et al., 2004a). Moreover, a larger scale expression microarray analysis, that was performed using the same cell line GLI2ΔN HaCaT and GLI1 HaCaT cell line, further showed that some proliferation associated genes, including E2F1 and cyclin B1, are upregulated in response to inducible expression of both GLI1 and GLI2ΔN (Eichberger et al., 2006).

In addition, a novel link between the SHH/GLI signalling and the G2-M transition has been observed. PTCH1 expression in human embryonic kidney cells inhibits cell proliferation (G2-M transition), by interacting with, and determining the subcellular localisation of the phosphorylated (non-active) cyclin B1 (Barnes et al., 2001). Thus,

PTCH1 maintains the phosphorylated cyclin B1 in the cytoplasm and prevents its relocalisation to the nucleus. Addition of the SHH ligand disrupts this interaction, and allows cyclin B1 to translocate to the nucleus, required for mitotic progression (Barnes et al., 2001). In the absence of Ptch1 from the basal cells in mouse skin, a large proportion of them exhibit nuclear accumulation not only of cyclin B1, but also of cyclin D1, suggesting that Ptch1 inhibits not only the G2-M transition, but also the G1-S phase cell cycle progression (Adolphe et al., 2006). Recently, it was also shown that the phosphatase CDC25B, a regulator of G2-M transition (controls the entry into mitosis), is transcriptionally upregulated by the Shh/Gli signalling during embryonic development, both in chick and mice (Benazeraf et al., 2006). Additionally, Hh/Gli1 signalling mediates regulation of the G2/M phase in neural precursors of the developing retina in *Xenopus* embryos, by transcriptionally activating important G2 phase regulators, such as cyclin B1 and CDC25C (Locker et al., 2006).

Therefore, all these studies provide evidence for the interactions of the HH/GLI pathway, with components of the cell-cycle machinery which are involved in the progression of the cell cycle and promote cell proliferation, giving a possible explanation for the role of HH/GLI signalling in tumourigenesis. Increased cell proliferation is a hallmark of tumour formation (Hanahan & Weinberg, 2000), and thus cell cycle regulation is important for the maintenance of genomic integrity and is necessary to impose the appropriate limitations to uncontrolled proliferation (Sherr, 1996).

1.3.7.1 Checkpoint cell-cycle control mechanisms

Checkpoints are the control mechanisms that enhance genetic fidelity by controlling the order and timing of cell cycle transitions and by successful completion of critical events such as DNA replication and chromosome segregation (Hartwell & Weinert, 1989; Murray, 1992; Elledge, 1996). Thus, cell cycle checkpoints monitor the structural integrity of chromosomes before progression through crucial cell cycle stages (Hartwell & Weinert, 1989; Lobrich & Jeggo, 2007). There are at least two checkpoints that monitor DNA damage, one at the G1/S transition and the other at the G2/M transition, preventing replication of damaged DNA or entry of damaged or incompletely replicated DNA into mitosis respectively (Kastan et al., 1992; Elledge, 1996; Bartek & Lukas,

2001; Taylor & Stark, 2001; Lobrich & Jeggo, 2007). There is also the mitotic checkpoint, that monitors the successful assembly of the spindle and prevents chromosome missegregation, by controlling the initiation of metaphase (Elledge, 1996; Rudner & Murray, 1996; Gorbsky, 1997; Musacchio & Hardwick, 2002).

The tumour suppressor p53 and its direct transcriptional target $p21^{WAF1/CIP1}$ (el-Deiry et al., 1994), have been found to be primarily associated with both DNA damage checkpoints and to act as a backup mechanism in the mitotic checkpoint control, either by inducing cell cycle arrest and/or apoptosis (Kuerbitz et al., 1992; el-Deiry et al., 1994; Brugarolas et al., 1995; Cross et al., 1995; Minn et al., 1996; Bunz et al., 1998; Khan & Wahl, 1998; Lanni & Jacks, 1998; Wang et al., 1998; Chehab et al., 1999; Andreassen et al., 2001a; Andreassen et al., 2001b; Taylor & Stark, 2001; Borel et al., 2002; Margolis et al., 2003; Sherr, 2004; Castedo et al., 2006). The inactivation of checkpoint genes can result in gene mutations, chromosome damage, ploidy abnormalities (tetraploidy, polyploidy, aneuploidy), defective apoptosis, all of which can contribute to genomic instability (structural and/or numerical) and carcinogenesis **(Figure 1.19)** (Solomon et al., 1991; Paulovich et al., 1997; Lengauer et al., 1998; Stewart et al., 1999; Nowak et al., 2002; Albertson et al., 2003; Liu et al., 2004a; Nelson et al., 2004; Zhivotovsky & Kroemer, 2004; Jefford & Irminger-Finger, 2006; Lobrich & Jeggo, 2007).

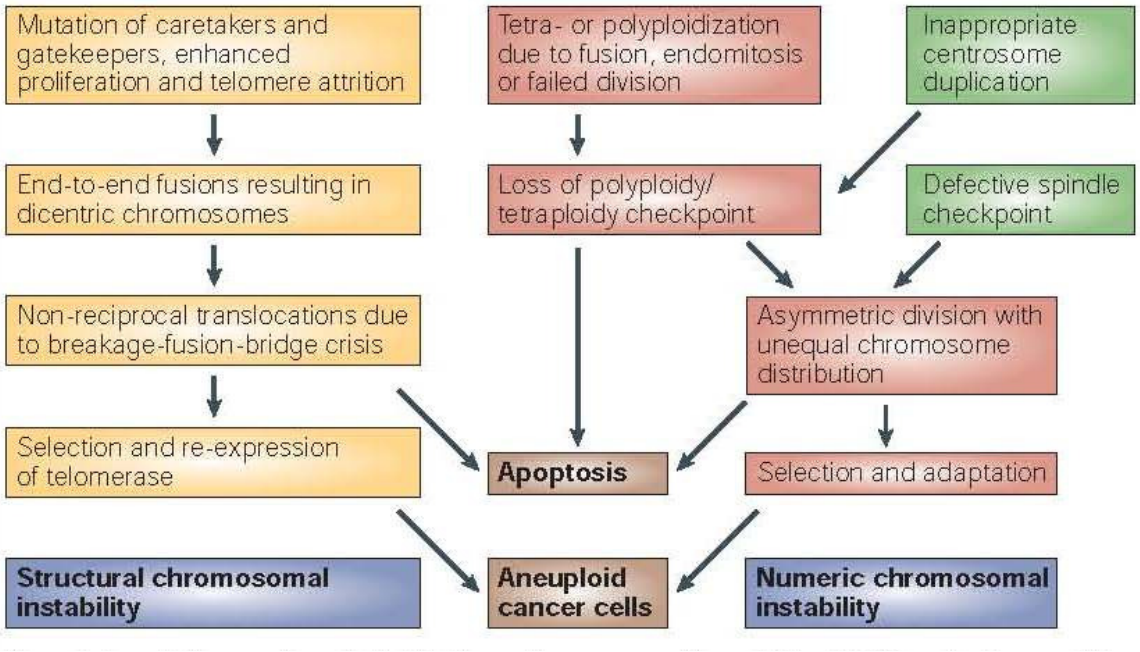

Figure 1.19: Types of genomic instability.

Genomic instability can be divided into chromosomal instability (CIN), and microsatellite instability (MSI) (due to mutated or silenced DNA-mismatch-repair genes). Chromosomal instability can be classified into structural and numeric. Structural chromosomal instability can result from mutations of the elements of the DNA-damage checkpoint ("gatekeepers"), of the elements of the two (non-homologous end joining and homologous recombination) DNA double-strand break repair mechanisms ("caretakers"), and also from telomere attrition (telomere shortening). Numeric chromosomal instability can result from aberrant tetra/polyploidisation (cells that have acquired more than two homologous sets of chromosomes), inappropriate centrosome duplication, or by defects in the spindle checkpoint. Both structural and numeric CIN tend to induce apoptosis as a default pathway that aborts damaged cells after DNA damage, polyploidisation, or asymmetric cell division (aneuploid cells, cells with chromosome complements that are not a simple multiple of the haploid set). Defective apoptosis increases the probability to these cells to survive, become selected and generate cancers (Zhivotovsky & Kroemer, 2004).

1.4 WNT signalling pathway

Human BCCs show, (a) increased levels of SHH effector genes such as GLI1 and GLI2 (Dahmane et al., 1997; Ghali et al., 1999; Mullor et al., 2001; Regl et al., 2002; Tojo et al., 2003; Ikram et al., 2004; Regl et al., 2004b; O'Driscoll et al., 2006; Asplund et al., 2008; Yu et al., 2008), (b) increased levels of WNT genes such as WNT2β, WNT5a and WNT7β (Bonifas et al., 2001; Mullor et al., 2001; Saldanha et al., 2004; O'Driscoll et al., 2006; Yu et al., 2008), as well as (c) accumulation of nuclear β-catenin (Yamazaki et al., 2001; El-Bahrawy et al., 2003; Saldanha et al., 2004; Yang et al., 2008a), (d) increased protein and mRNA levels of the β-catenin nuclear binding partner, LEF-1 (O'Driscoll et al., 2006; Asplund et al., 2008; Kriegl et al., 2009), and (e) increased mRNA levels of the matrix metalloproteinases (MMP), which are known targets of β-catenin-TCF/LEF-1 signalling and are involved in cell invasion (O'Driscoll et al., 2006; Yu et al., 2008).

WNTs are secreted glycoproteins, lipid-modified signalling proteins, which although their primary amino-acid sequence suggests that they should be quite soluble, secreted Wnts have been shown to be hydrophobic and thus difficult to manipulate, which was also further supported by the purification of active Wnts (Willert et al., 2003; Mikels & Nusse, 2006b; Hausmann et al., 2007). Wnts act in a wide range of developmental processes during embryogenesis, such as gastrulation, early pattern formation, organogenesis and adult tissue homeostasis (bone, gut, hair follicle), while gain-or-loss-of-function mutations in WNT genes or Wnt pathway, lead to developmental abnormalities such as kidney and reproductive tract defects, as well as stem cell loss and cancer (Cadigan & Nusse, 1997; Wodarz & Nusse, 1998; Logan & Nusse, 2004; Nelson & Nusse, 2004; Nusse, 2005; Clevers, 2006; Klaus & Birchmeier, 2008; Nusse et al., 2008; MacDonald et al., 2009). There are nineteen Wnt genes in the human genome and their name was derived from the *Drosophila* gene Wingless (Wg) and the related mammalian oncogene integration 1 (Int-1) (Nusse & Varmus, 1982; van Ooyen & Nusse, 1984; Cabrera et al., 1987; Rijsewijk et al., 1987; Cadigan & Nusse, 1997; Klaus & Birchmeier, 2008). Secreted Wnt proteins (ligands), bind to frizzled seven-transmembrane span receptors (Frz) in the plasma membrane (Bhanot et al., 1996), and depending on the specific Wnt/Frz binding, initiate the signalling of three different pathways: (1) the Wnt/Ca^{2+} pathway, (2) the planar cell polarity pathway (PCP), and (3)

the canonical Wnt pathway **(Figure 1.23)** (Huelsken & Behrens, 2002; van Es et al., 2003; Nelson & Nusse, 2004; Cadigan, 2008; Klaus & Birchmeier, 2008).

β-catenin (the *Drosophila* version of which is Armadillo) (Nusslein-Volhard & Wieschaus, 1980; Wieschaus & Riggleman, 1987; Perrimon et al., 1989; Riggleman et al., 1990; Klaus & Birchmeier, 2008) is a protein that plays essential roles in two different cellular processes: calcium-dependent intercellular adhesion (McCrea & Gumbiner, 1991; McCrea et al., 1991; Peifer et al., 1992; Kemler, 1993; Gumbiner, 2000; Jamora & Fuchs, 2002; Bienz, 2005; Brembeck et al., 2006) and WNT-mediated transcriptional activation. WNT/β-catenin signalling pathway (canonical WNT pathway) (Riggleman et al., 1990; Rubinfeld et al., 1993; Noordermeer et al., 1994; Siegfried et al., 1994; Behrens et al., 1996) is involved in a wide range of embryonic patterning events and adult tissue homeostasis (Cadigan & Nusse, 1997; Wodarz & Nusse, 1998; Clevers, 2006; Klaus & Birchmeier, 2008), and also found to contain cancer-causing genes (Polakis, 2000; Taipale & Beachy, 2001; Giles et al., 2003; Sherr, 2004; Vogelstein & Kinzler, 2004). Still it is not clear if the roles of β-catenin in cell-cell adhesion and Wnt signalling, both in development and tumourigenesis, are either largely independent from each other, or interrelated, since evidence occurs for both possibilities in different cell contexts (Cavallaro & Christofori, 2004; Gottardi & Gumbiner, 2004; Nelson & Nusse, 2004; Bienz, 2005; Brembeck et al., 2006).

1.4.1 The role of β-catenin in calcium-dependent intercellular adhesion

β-catenin protein was initially discovered for its role in cell-cell adhesion, as a component of the E-cadherin-catenin complex in the epithelial cell membrane (McCrea & Gumbiner, 1991; McCrea et al., 1991; Peifer et al., 1992; Kemler, 1993; Bienz, 2005). E-cadherin (epithelial cadherin), is a calcium (Ca^{2+}) - dependent, type I integral membrane protein, which is required to hold epithelial cells together and thus contribute to the formation and maintenance of a variety of solid epithelial tissues, such as skin, gut and lung (Gumbiner, 1996; Gumbiner, 2005).

E-cadherin protein consists of a large extracellular domain, a single transmembrane segment and a short cytoplasmic domain (highly conserved cytoplasmic tail) **(Figure**

1.20) (Pecina-Slaus, 2003). The extracellular domain consists of five cadherin-type repeats (extracellular domains), that are bound together by Ca^{2+} ions to form stiff rod-like proteins, and mediates the calcium-dependent adhesive binding function between adjacent cells, through homophilic protein-protein interactions of the extracellular domains in a process of lateral dimerization, forming the known as adherens junctions **(Figure 1.20 and Figure 1.21)** (Pokutta et al., 1994; Pecina-Slaus, 2003; Cavallaro & Christofori, 2004; Gumbiner, 2005). In the proximal region (juxtamembrane region) of its intracellular cytoplasmic domain, E-cadherin, has p120 catenin bound, of which the exact role is unclear but it has been suggested to regulate the structural integrity and the E-cadherin stability (Davis et al., 2003). In the distal part of its intracellular cytoplasmic domain, E-cadherin has β-catenin bound, which in turns binds to the actin binding protein α-catenin (adaptor protein) to bridge the extracellular adhesive activity of cadherins with the underlying actin cytoskeleton **(Figure 1.20)**. α-catenin is able to mediate physical links to the actin cytoskeleton either by directly binding actin filaments or indirectly through other actin-binding proteins such as vinculin, α-actinin or formin-1 **(Figure 1.20)**. Therefore, the E-cadherin-β-catenin complex serves to link the cytoskeletal networks of adjacent cells and thus mediates the Ca^{2+}- dependent cell-cell adhesion, which is essential for normal tissue architecture and morphogenesis **(Figure 1.21)** (Gumbiner, 1996; Gumbiner, 2000; Jamora & Fuchs, 2002; Cavallaro & Christofori, 2004; Nelson & Nusse, 2004; Gumbiner, 2005; Brembeck et al., 2006).

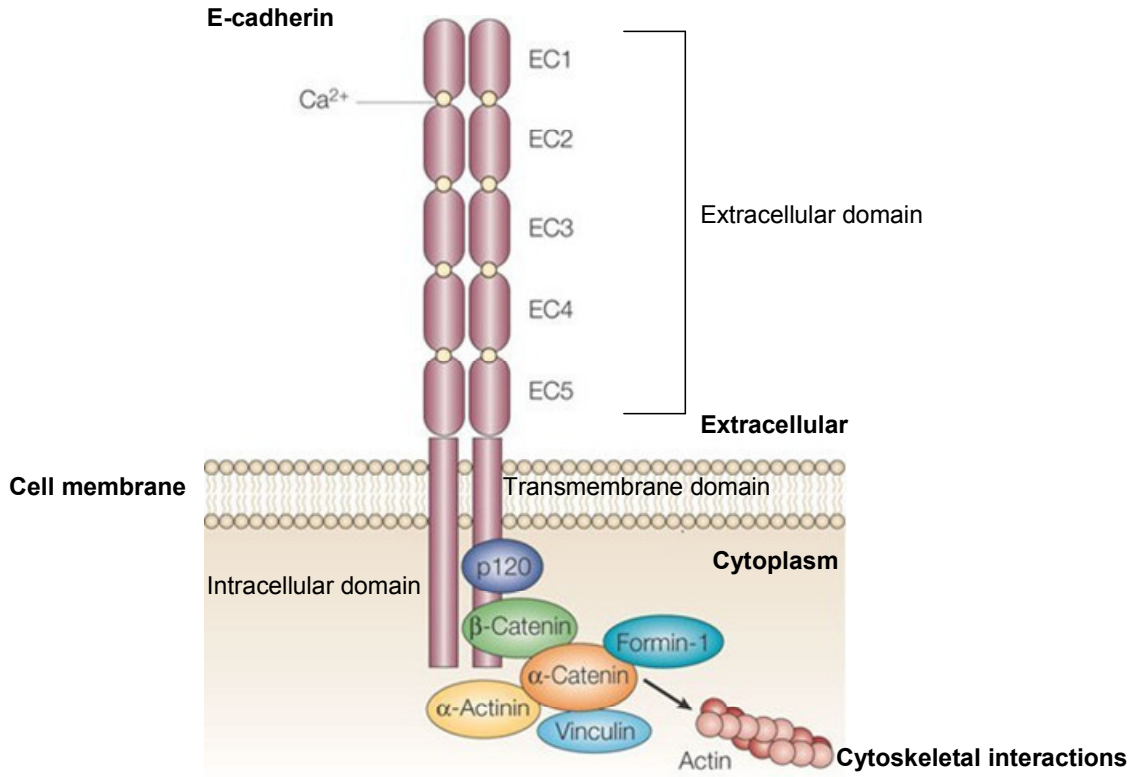

Figure 1.20: The cadherin-catenin protein complex.

E-cadherin is a parallel or cis homodimer (parallel (cis) cadherin dimer) that consists of a large extracellular domain, a single transmembrane segment, and a short cytoplasmic domain. The extracellular region (extracellular domain), consists of five cadherin-type repeats (EC domains: extracellular cadherin domains), that are bound together by calcium ions (Ca^{2+}) in a rod-like structure. The core-universal complex, consists of p120 catenin, which is bound to the juxtamembrane region of the intracellular cytoplasmic domain and β-catenin, which is bound to the distal part of the intracellular cytoplasmic domain, which in turns bind α-catenin. α-catenin bind to actin or to other actin-binding proteins such as vinculin, α-actinin and formin-1, in order to mediate physical links to the actin cytoskeleton (Gumbiner, 2005).

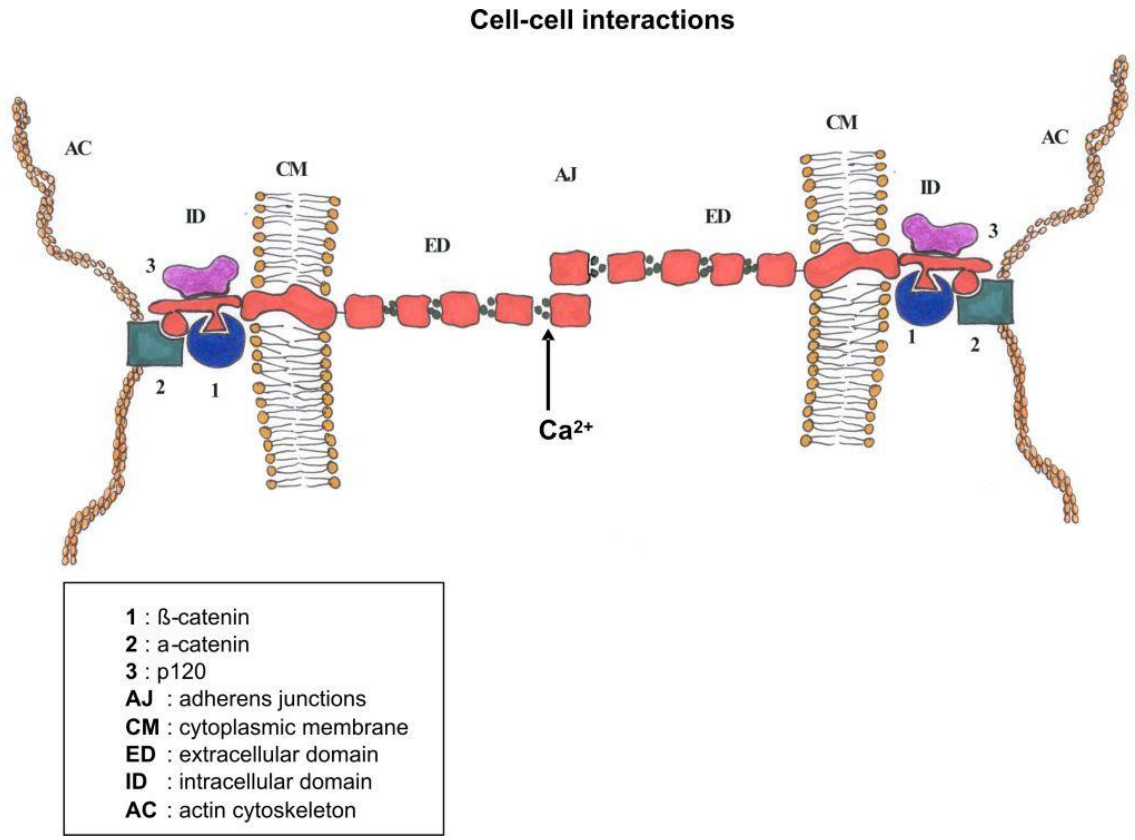

Figure 1.21: Schematic illustration of E-cadherin in adherens junction of adjacent cells.

E-cadherin-β-catenin complex links the cytoskeletal networks of adjacent cells and thus mediates calcium-dependent adhesive binding function, through homophilic protein-protein interactions of the extracellular domains in a process of lateral dimerization, forming the known as adherens junctions (Pokutta et al., 1994; Pecina-Slaus, 2003; Gumbiner, 2005).

Serine/threonine phosphorylation of β-catenin (CTNNB1 gene) or E-cadherin (CDH1 gene) results in increased stabilisation of the cadherin-catenin complex (Lickert et al., 2000; Bek & Kemler, 2002), while tyrosine phosphorylation of E-cadherin or β-catenin is correlated with loss of cadherin mediated cell-cell adhesion, and an increase in the level of cytoplasmic β-catenin for the latter (Roura et al., 1999; Fujita et al., 2002; Lilien et al., 2002; Cavallaro & Christofori, 2004; Nelson & Nusse, 2004). Loss of e-

cadherin expression, and subsequent loss of cell-cell adhesion often occurs both (a) during normal developmental epithelial-mesenchymal transitions (EMTs), where polarized epithelial cells from a primitive epithelium are converted into motile mesenchymal cells (loss of the epithelial phenotype) that migrate to an extracellular environment and subsequently settle to other areas, a process essential for organ formation during embryonic development (i.e. mesoderm formation and many histogenic processes), as well as (b) during tumour progression (Birchmeier & Behrens, 1994; Gumbiner, 1996; Thiery, 2002; Pecina-Slaus, 2003; Cavallaro & Christofori, 2004; Nelson & Nusse, 2004; Gumbiner, 2005; Hugo et al., 2007). Loss of E-cadherin-mediated cell-cell adhesion is a prerequisite for tumour cell invasion and metastasis formation (Birchmeier & Behrens, 1994; Cavallaro & Christofori, 2004) and loss of E-cadherin in cancers of epithelial origin is concomitant with the progression towards malignancy, since there is an inverse correlation between E-cadherin levels and tumour grade (Birchmeier & Behrens, 1994; Hirohashi, 1998; Hirohashi & Kanai, 2003). Various genetic or epigenetic mechanisms, such as loss-of-function mutations of the E-cadherin gene (Risinger et al., 1994; Berx et al., 1995), or transcriptional repression by transcription factors such as Snail, Slug (Batlle et al., 2000; Cano et al., 2000; Hajra et al., 2002) and promoter hypermethylation of the E-cadherin gene (Yoshiura et al., 1995; Tamura et al., 2000; Di Croce & Pelicci, 2003), respectively, have been found to cause downregulation/loss of E-cadherin during carcinoma progression (Strathdee, 2002; Thiery, 2002; Cavallaro & Christofori, 2004; Hugo et al., 2007).

1.4.2 Canonical WNT/β-catenin signalling pathway

β-catenin is the key component of the canonical Wnt signalling pathway, that functions by regulating the amount/stability of the co-activator β-catenin, which controls key developmental and tissue homeostasis gene expression programs (Huelsken & Behrens, 2002; Logan & Nusse, 2004; Nusse, 2005; Cadigan, 2008; Klaus & Birchmeier, 2008; MacDonald et al., 2009).

In the absence of WNT signal **(Figure 1.22a)**, cytoplasmic β-catenin - non E-cadherin bound, is kept low as it is recruited in and is constantly degraded by the action of, a destruction complex, which is composed of the Axin, adenomatous polyposis coli

(APC), casein kinase 1 (CK1) and glycogen synthase kinase 3β (GSK3β) proteins (Behrens et al., 1998; Amit et al., 2002; Liu et al., 2002; Logan & Nusse, 2004). Both the scaffolding protein axin and the tumour suppressor APC protein, seem to act as scaffolds, positioning β-catenin and the kinases to allow efficient phosphorylation. Serine/threonine kinases CK1α and GSK3β sequentially phosphorylate the amino terminal regions (N-terminus) of β-catenin. Following phosphorylation, β-catenin is recognized and targeted by β-TrCP (β-transducin repeat-containing protein), a component of the E3 ubiquitin ligase complex, which triggers poly-ubiquitination and subsequent proteasomal degradation of β-catenin (Aberle et al., 1997; Jiang & Struhl, 1998; Latres et al., 1999; Liu et al., 1999; He et al., 2004; MacDonald et al., 2009). Thus, free cytoplasmic β-catenin has an average half-life of ~ 30 minutes in the cell (Cadigan, 2008). This continual elimination of β-catenin prevents its translocation to the nucleus and ensures repression of Wnt target genes by recruitment of the co-repressor Groucho (TLE1 in human) to TCF/LEF (T-cell factor / lymphoid enhancer factor) transcription factors, of which repressing effect is mediated by interactions with Histone Deacetylases (HDAC) that are thought to make DNA refractive to transcriptional activation (Cavallo et al., 1998; Levanon et al., 1998; Chen et al., 1999b; Nusse, 2005; Klaus & Birchmeier, 2008; MacDonald et al., 2009).

In the presence of WNT signal **(Figure 1.22b)**, the Wnt/β-catenin pathway is activated. WNT ligands bind to the cell surface receptors in the plasma membrane, which are the seven-pass transmembrane Frizzled (FZD) receptor (Bhanot et al., 1996) and its co-receptor LRP6 or its close relative LRP5 (low-density lipoprotein receptor-related protein 6 or 5), known as Arrow in *Drosophila* (Tamai et al., 2000; Wehrli et al., 2000; He et al., 2004). Several inhibitors of this interaction have been identified (Klaus & Birchmeier, 2008), including secreted Frizzled-related proteins (SFRPs) and Wnt inhibitory factor 1 (WIF1) that both bind to WNTs and inhibit their activities (Finch et al., 1997; Rattner et al., 1997; Wang et al., 1997; Hsieh et al., 1999), secreted Dickkopfs (DKKs) which bind and antagonizing LRP5/LRP6 (Glinka et al., 1998), and an additional DKK-receptor Kremen, which inhibits the Wnt signalling pathway by internalization of LRP6 (endocytosis and removal from the plasma membrane) (Mao et al., 2002) **(Figure 1.22a)**. In the absence of these antagonists, and upon binding of Wnt ligands to both FZD and LRP5/LRP6 (FZD-LRP5/6 complex) **(Figure 1.22b)**, there is subsequent LRP5/LRP6 phosphorylation in its cytoplasmic tail by CK1γ and GSK3β, as

well as recruitment of the scaffolding protein Dishevelled (DVL) (Noordermeer et al., 1994) to the plasma membrane, where it associates with FZD receptors, polymerises with other Dishevelled molecules and promotes LRP5/LRP6 phosphorylation along with Axin recruitment to the receptors (FZD and LRP5/LRP6) in the plasma membrane (Cadigan, 2008; Klaus & Birchmeier, 2008; Zeng et al., 2008; MacDonald et al., 2009). Interaction of Axin with phosphorylated LRP5/LRP6 and the Dishevelled polymer, leads to the inactivation of the destruction complex, and subsequently to the stabilisation of β-catenin due to the inhibition of axin-mediated β-catenin phosphorylation, and its translocation to the nucleus (He et al., 2004; Cadigan, 2008; Klaus & Birchmeier, 2008; MacDonald et al., 2009). In the nucleus, β-catenin acts as a transcriptional co-regulator that binds to the TCF/LEF-1 DNA-binding proteins (Behrens et al., 1996; Molenaar et al., 1996; Arce et al., 2006), and thereby converting the TCF/LEF-1 repressor complex into a transcriptional activator complex critical for activation of WNT target genes, by displacing Groucho/TLE (Daniels & Weis, 2005) and interacting with other co-activators (Klaus & Birchmeier, 2008). These co-activators include pygopus *(Drosophila)* (Thompson et al., 2002), which binds to the amino-terminal half of β-catenin, and histone acetylase CBP (vertebrates) (CREB-binding protein) (Hecht et al., 2000), which binds to the carboxy-terminal and is thought to induce chromatin remodelling that favours target gene transcription (Barker et al., 2001; Wolf et al., 2002; Logan & Nusse, 2004; Nusse, 2005; MacDonald et al., 2009). However, many of these factors are likely to be gene specific, cell-type or species specific (Cadigan, 2008; Klaus & Birchmeier, 2008).

The TCF/LEF family of DNA-bound transcription factors, which is the main partner for β-catenin in gene regulation, belongs to the high mobility group (HMG) DNA binding factors with only a single HMG box (a single homologous sequence) (Travis et al., 1991; van de Wetering et al., 1991; Roose & Clevers, 1999; Arce et al., 2006), similar to SOX factors **(Chapter 3, Section 3.3.6.2.)** (Pevny & Lovell-Badge, 1997; Werner & Burley, 1997; Wegner, 1999; Kamachi et al., 2000; Wilson & Koopman, 2002). The HMG box is a DNA binding domain, which binds DNA in the promoter or the enhancer regions of other genes in a sequence-specific manner, and thus it is implicated in the regulation of transcription and chromatin architecture (Grosschedl et al., 1994), by rendering TCF/LEF or other proteins that belong to this family (SOX proteins), as transcription factors which either activate or repress target genes (Roose & Clevers,

1999; Wegner, 1999; Kamachi et al., 2000; Arce et al., 2006). Therefore, upon binding of the TCF/LEF factors to the specific DNA consensus sequence of other genes (CCTTTGWW - W represents either T or A), referred to as the WNT responsive element (WRE), a significant DNA bending is caused, which is thought to alter the chromatin structure and thus recruiting β-catenin and its co-activators to WNT target genes (Arce et al., 2006; MacDonald et al., 2009). In *Drosophila*, there is only a single TCF/LEF gene (*dTCF* or *pangolin*), while in mammals four TCF/LEF genes, TCF1, LEF-1, TCF3 and TCF4 do exist (Roose & Clevers, 1999; Arce et al., 2006). Evidence for diverse actions of TCF/LEF genes during development, comes from studies in different organisms, which have shown, in general, that LEF-1 is mainly an activator, TCF1 and TCF4 can act both as repressors and activators, while TCF3 is mainly a repressor (Arce et al., 2006; Cadigan, 2008; MacDonald et al., 2009).

The recognition of target genes from TCF/LEF factors appears to be context-dependent, as well as co-factor-dependent (Arce et al., 2006). Due to the weak ability of TCF/LEF factors for target gene recognition and the ability only for loose binding to the DNA of target genes, TCF/LEF factors require the recruitment of other co-factors (partners) including β-catenin, in order to bind and activate/suppress the correct set of target genes (Roose & Clevers, 1999; Arce et al., 2006). Therefore, since Wnt/β-catenin signalling regulates proliferation, fate specification, stem cell maintenance and differentiation in numerous developmental stages and adult tissue homeostasis, it is plausible that Wnt target genes are diverse and cell and context specific (Logan & Nusse, 2004; Vlad et al., 2008; MacDonald et al., 2009). This means that Wnt/β-catenin signalling has distinct transcriptional outputs which are only expressed in certain cells, whereas in many cases the cell rather than the signal determines the nature of the response and the up-or-downregulation of Wnt target genes is cell-type specific as well (Logan & Nusse, 2004; Nusse, 2005). However, Wnt/β-catenin signalling can also control genes that are more widely induced (induction of same target genes in multiple cell and tissue types), such as genes that are components of the Wnt/β-catenin pathway including Axin2, Frizzleds, β-TrCP and TCF/LEF, indicating a feedback control mechanism (Logan & Nusse, 2004; Klaus & Birchmeier, 2008; MacDonald et al., 2009). In addition Wnt/β-catenin signalling has been shown to induce expression of target genes which have been linked to increased cell proliferation, invasion and tumour metastasis, including cyclin D1, c-

Myc, MMP26, MMP7, PPAP-δ and AF17 (He et al., 1998; Brabletz et al., 1999; He et al., 1999; Shtutman et al., 1999; Lin et al., 2001; Marchenko et al., 2002).

Interestingly, studies both in *Drosophila* and in mammals have shown that many genes are downregulated in response to Wnt signalling (Logan & Nusse, 2004; Vlad et al., 2008), suggesting that even if β-catenin typically converts the TCF/LEF factors from repressors to activators, the TCF/LEF-β-catenin complex is also able to repress transcription of certain genes, which is a distinct process from TCF/LEF-mediated repression in the absence of β-catenin (Cadigan, 2008; MacDonald et al., 2009). Although, it is not clear which of these downregulated genes are directly or indirectly (through a Wnt-activated repressor protein) repressed by Wnt/β-catenin signalling, at least in some cases it has been confirmed that TCF/LEF-β-catenin complex directly mediates this repression (Piepenburg et al., 2000; Blauwkamp et al., 2008), and that in some of these target genes, repression required the traditional TCF/LEF-binding sites (Jamora et al., 2003; Theisen et al., 2007). However, the mechanism by which TCF/LEF-β-catenin complex exhibits repression rather than activation in certain genes remains unclear, and it appears to be different among the few genes studied in detail (Cadigan, 2008; MacDonald et al., 2009). For example, dpp (decapentaplegic - homolog of the vertebrate bone morphogenetic proteins/BMPs) gene in *Drosophila*, which is a morphogen necessary for the development of the leg imaginal discs of the fruit fly, is directly repressed via TCF/LEF-β-catenin binding to the canonical WREs on the dpp enhancer region by recruiting the co-repressor Brinker (BRK) (Theisen et al., 2007); while Ugt36Bc gene in *Drosophila*, an enzyme that belongs to the UDP-glycosyltransferase superfamily and is thought to exert an effect in detoxification, is directly repressed via TCF/LEF-β-catenin binding to a novel TCF/LEF binding site to the enhancer of the Ugt36Bc gene, which mediates TCF/LEF-β-catenin repression instead of activation (Blauwkamp et al., 2008).

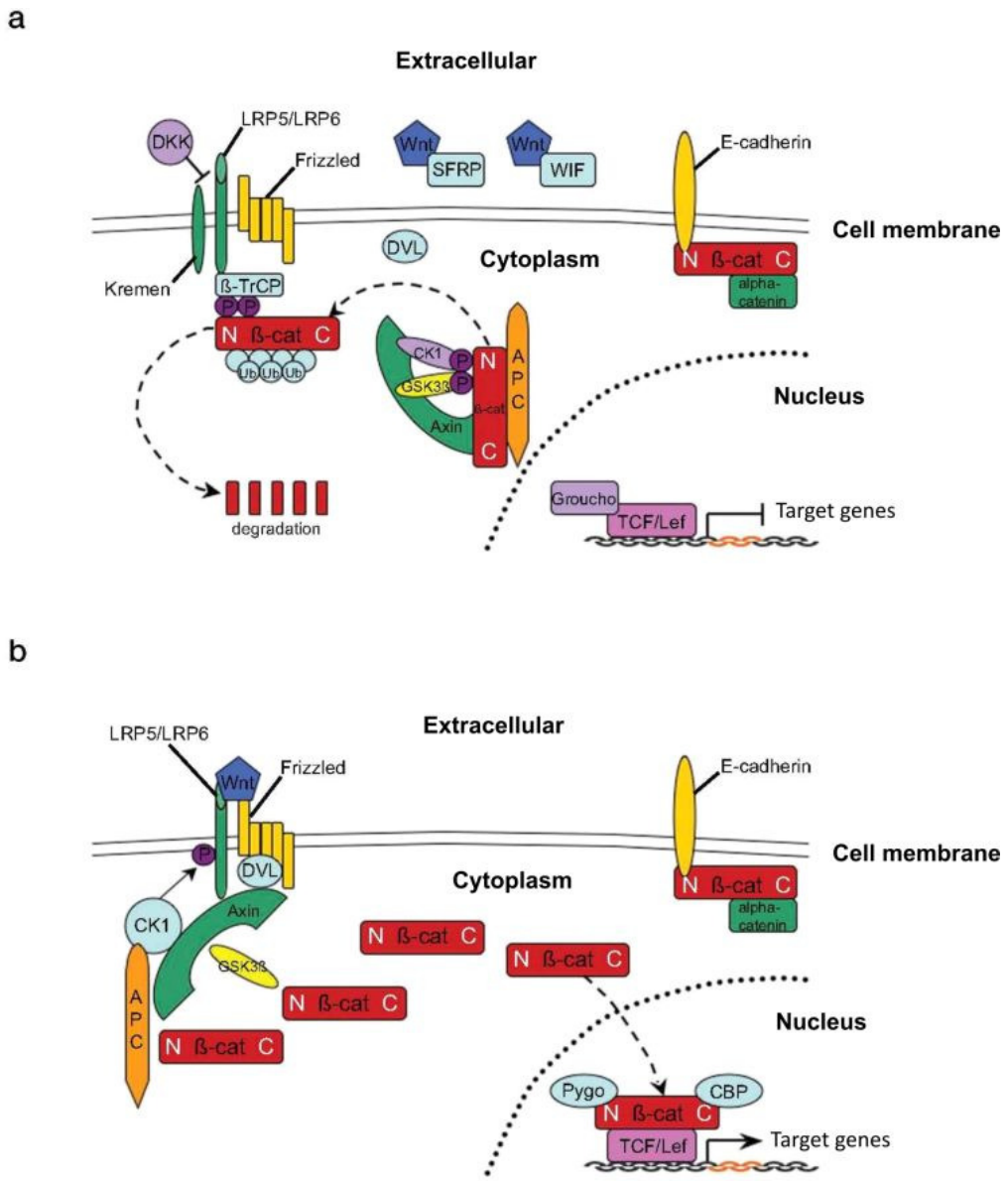

Figure 1.22: Canonical WNT/β-catenin pathway.

(a) In the absence of WNT signal, cytoplasmic β-catenin **(β-cat)** - non E-cadherin bound, is phosphorylated and targeted for degradation by a complex of proteins, including Axin, APC, GSK3β and β-TrCP. **(b)** In the presence of WNT signal the degradation machinery is inhibited, β-catenin accumulates in the cytoplasm and translocates to the nucleus, where it interacts with TCF/LEF-1 transcription factor and activates transcription of targeted genes. **DKK**, Dickkopf; **LRP**, LDL-related receptor protein; **SFRP**, secreted Frizzled-related protein; **WIF**, Wnt inhibitory factor 1; **DVL**, Dishevelled; **β-TrCP**, β-transducin repeat-containing protein; **CK1**, casein kinase 1; **GSK3β**, glycogen synthase kinase 3β; **APC**, adenomatous polyposis coli; **TCF**, T-cell factor; **Lef**, lymphoid enhancer factor; **Pygo**, Pygopus; **CBP**, CREB-binding protein; **P**, phosphorylation; **Ub**, ubiquitylation; **N**, amino terminus; **C**, carboxyl terminus; (Klaus & Birchmeier, 2008; Watt & Collins, 2008).

1.4.3 The planar cell polarity and the Wnt/Ca^{2+} pathway

The specific Wnt/Frz binding, does not only initiate the signalling of the canonical Wnt pathway described in **Section 1.4.2**, but is also capable of activating a β-catenin-independent, non-canonical Wnt signalling cascade, which is not as well characterised as the canonical Wnt/β-catenin pathway **(Figure 1.23)** (Huelsken & Behrens, 2002; Strutt, 2003; Veeman et al., 2003; Gordon & Nusse, 2006; van Amerongen et al., 2008). These non-canonical Wnt pathways regulate crucial cell-fate decisions and include the planar cell polarity pathway, which was first identified in *Drosophila* (McEwen & Peifer, 2000; Sokol, 2000; Seifert & Mlodzik, 2007), and the Wnt/Ca^{2+} pathway, which was first described in vertebrates (Kuhl et al., 2000a; Kuhl et al., 2000b; Saneyoshi et al., 2002).

All epithelial cells have distinct Apical/Basal polarity. That is some proteins are exclusively localised to the top or the bottom of the cell and are separated from each other with cell junctions in order to avoid the mixing of the proteins from the two regions and to maintain a rigid epithelial structure (Dollar & Sokol, 2007). Thus, in epithelia, cells are uniformly polarized along the apical-basal axis. However, in addition to apical-basal polarity, cells in most tissues require positional information in the plane to generate polarized structures or to move or orient themselves in a directed fashion, like for example hairs or feathers that must point the right way on animal skin (Strutt, 2003; Seifert & Mlodzik, 2007). This type of polarization of fields of cells that orient themselves relative to the plane of the tissue in which they reside, is referred to as planar cell polarity (PCP) and is essential for tissue functioning (Strutt, 2003; Seifert & Mlodzik, 2007). Therefore, Wnt/planar cell polarity pathway regulates planar cell polarity and morphogenetic movements (Sokol, 2000; Strutt, 2003; Seifert & Mlodzik, 2007; Wang & Nathans, 2007). In the planar cell polarity pathway **(Figure 1.23)**, activated Frizzled by WNT signal, activates Dishevelled which in turns signals to small GTPases Rho and Rac (members of the Ras superfamily of small guanosine triphosphatases - GTPases) and activates Jun N-terminal kinase (JNK), which are both (Rho/Rac and JNK) known to regulate cytoskeleton and specify planar cell polarity (Strutt et al., 1997; Boutros et al., 1998; Hall, 1998; Noselli & Agnes, 1999; McEwen & Peifer, 2000; Peifer & McEwen, 2002). Although it has been shown that Dishevelled activates both Rho (Strutt et al., 1997) and JNK (Boutros et al., 1998; Li et al., 1999) in

planar cell polarity pathway, it is still controversial whether the Rho family GTPases and particular Rac, is also involved in JNK activation by Dishevelled (Li et al., 1999; Habas et al., 2003; Veeman et al., 2003).

The Wnt/Ca^{2+} pathway regulates cell-cell interactions and motility during development (Kuhl et al., 2000b; Kuhl et al., 2001; Winklbauer et al., 2001; Kohn & Moon, 2005). The Wnt/Ca^{2+} pathway **(Figure 1.23)** (Miller et al., 1999; Kuhl et al., 2000b; Huelsken & Behrens, 2002; Kohn & Moon, 2005), involves the binding of Wnt to the Frizzled receptor, which promotes Frizzled-mediated activation of pertussis toxin-sensitive heterotrimeric (α, β, γ) guanine nucleotide-binding proteins (G proteins) (Slusarski et al., 1997; Sheldahl et al., 1999; Kuhl et al., 2000a) and / or Dishevelled (Sheldahl et al., 2003). G proteins have also been thought to transmit/mediate signals from the Frizzled receptors to the downstream effectors, in both the canonical Wnt and planar cell polarity pathways (Malbon et al., 2001; Huelsken & Behrens, 2002; Nusse, 2005; Mikels & Nusse, 2006b), because Frizzled receptors have seven transmembrane domains (serpentine receptors) like other heterotrimeric G protein-coupled receptors, and an heptithelical structure that is conserved among all members of the superfamily of G protein-coupled receptors (Slusarski et al., 1997; Dale, 1998; Kohn & Moon, 2005). Although, there are biochemical studies, that support this notion, of which the evidence is largely based on overexpression or usage of inhibitors (Slusarski et al., 1997; Sheldahl et al., 1999; Kuhl et al., 2000a; Wang & Malbon, 2004), there is no study to show natural and direct interaction of G proteins with Frizzleds. Only recently, Katanaev et al. (Katanaev et al., 2005) showed by genetic analysis, that G proteins are indeed required for Frizzled signalling (are activated in response to Fzd signalling) in *Drosophila* both in canonical Wnt and cell polarity pathway. Thus, genetic analysis in vertebrates is required in order to provide further support to this notion (Kohn & Moon, 2005). Therefore, upon Dishevelled and G proteins stimulation in the Wnt/Ca^{2+} pathway **(Figure 1.23)**, there is activation of the phospholipase C (PLC) (Kuhl et al., 2000b; Kohn & Moon, 2005), which leads to elevated Ca^{2+} levels (release of intracellular calcium) (Slusarski et al., 1997) and the activation of calcium sensitive enzymes such as protein kinase C (PKC) (Sheldahl et al., 1999) and calmodulin-dependent protein kinase II (CaMKII) (Kuhl et al., 2000a). The elevated levels of Ca^{2+} can activate the calcium/calmodulin-dependent serine/threonine phosphatase, calcineurin which leads to dephosphorylation of the transcription factor NF-AT (nuclear factor of activated T cells)

(Crabtree & Olson, 2002). This leads to the nuclear accumulation of NF-AT, which activates target genes that are mainly implicated in developmental cell-cell interactions (Crabtree & Olson, 2002; Huelsken & Behrens, 2002; Saneyoshi et al., 2002). The function of calcineurin has been elucidated in great detail in the immune system, where it activates the T-cells through the activation of NF-AT, which translocates to the nucleus and upregulates the expression of proteins such as interleukin 2 which in turn stimulates the growth and differentiation of T-cells, but it has also been shown to be implicated in other systems including hematopoietic, neuronal and myogenic (Crabtree & Olson, 2002). Interestingly the calcineurin/NF-AT activity has also been implicated in primary mouse keratinocyte growth/differentiation control (Santini et al., 2001) and in the regulation of the hair keratinocyte differentiation and hair cycle *in vivo* (Gafter-Gvili et al., 2003), while calcineurin/NF-AT have also been found to be expressed in human skin (predominantly in epidermal keratinocytes) and in human keratinocytes in culture (Al-Daraji et al., 2002).

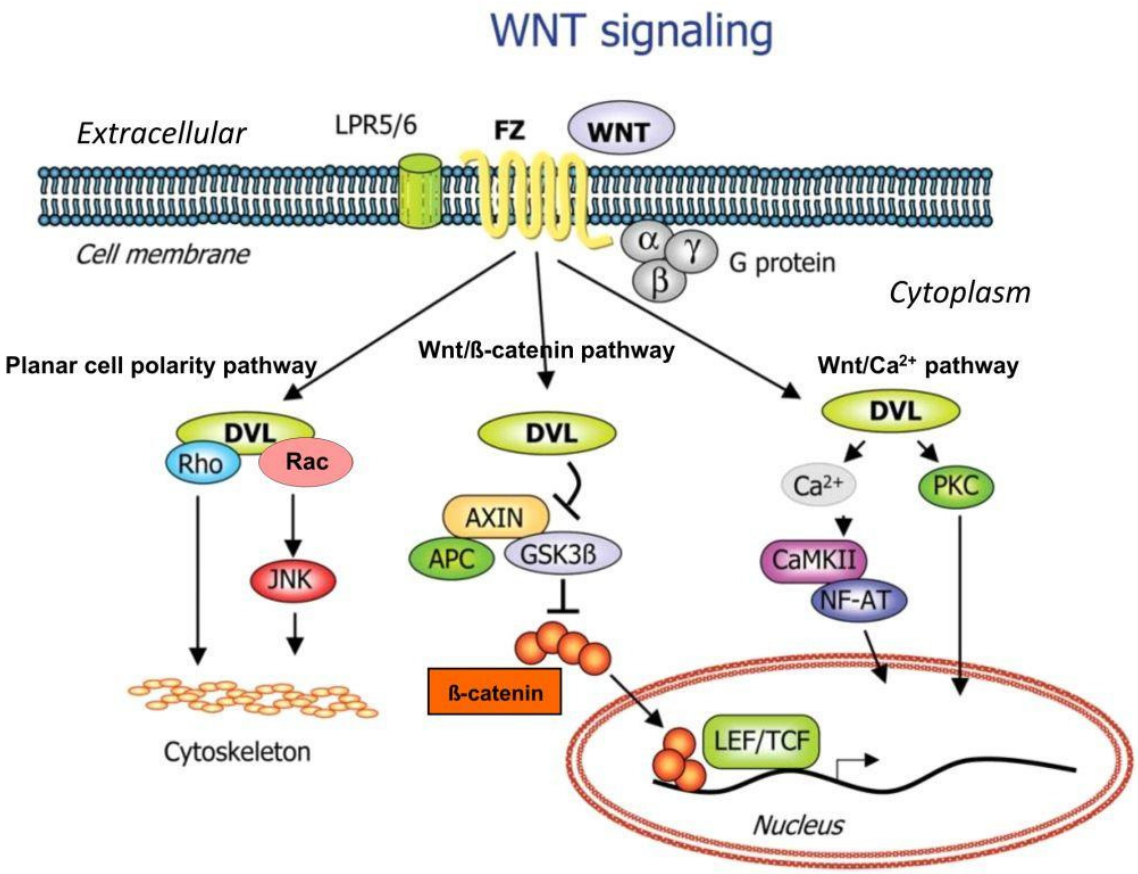

Figure 1.23: WNT signalling pathways.

The extracellular signalling molecule WNT activates three pathways: (1) The canonical Wnt/β-catenin pathway **(middle)**, (2) the planar cell polarity pathway **(left)**, and the (3) the Wnt/Ca^{2+} pathway **(right)**. **FZ**, Frizzled; **LRP**, LDL-related receptor protein; **DVL**, Dishevelled; **GSK3β**, glycogen synthase kinase 3β; **APC**, adenomatous polyposis coli; **TCF**, T-cell factor; **LEF**, lymphoid enhancer factor; **Rho**, Ras family-like protein; **Rac**, Ras family-like protein; **JNK**, Jun N-terminal kinase; **G protein**, pertussis toxin-sensitive heterotrimeric (**α, β, γ**) guanine nucleotide-binding proteins; **Ca^{2+}**, calcium; **PKC**, protein kinase C; **CaMKII**, calmodulin-dependent protein kinase II; **NF-AT**, nuclear factor of activated T-cells; (Klipp & Liebermeister, 2006).

1.5 WNT/β-catenin signalling pathway in skin development and cancer

1.5.1 Wnt/β-catenin signalling in hair follicle formation and stem cell regulation

In skin, Wnt/β-catenin signalling pathway plays a crucial role in hair follicle morphogenesis, hair follicle stem cell maintenance and/or activation, and hair shaft differentiation, as well as in skin epithelial stem cell lineage selection (Gat et al., 1998; DasGupta & Fuchs, 1999; Huelsken et al., 2001; Millar, 2002; Alonso & Fuchs, 2003a; Lowry et al., 2005; Schmidt-Ullrich & Paus, 2005; Blanpain & Fuchs, 2006; Blanpain et al., 2007; Watt & Collins, 2008). Previous studies in normal skin of transgenic mice, have shown that Wnt/β-catenin is required upstream of the Bmp and Shh in placode formation during hair follicle morphogenesis, and thus specifying the hair follicle fate in the undifferentiated basal epidermis and initiate hair bud formation (Gat et al., 1998; Huelsken et al., 2001; Andl et al., 2002; Lo Celso et al., 2004; Silva-Vargas et al., 2005; Blanpain & Fuchs, 2006). Then, it subsequently activates Shh signalling, which is required for the proliferation and expansion of follicle epithelium in order to assemble a mature follicle (St-Jacques et al., 1998; Chiang et al., 1999; Mill et al., 2003; Lo Celso et al., 2004; Silva-Vargas et al., 2005; Blanpain & Fuchs, 2006).

The importance of Wnt/β-catenin signalling pathway in skin, during embryogenesis is underscored by the absence of placode formation (first stage of hair follicle morphogenesis-early embryonic stage) in neonate mice, upon conditional loss (conditional mutation under the control of K14) of β-catenin in transgenic mice (Huelsken et al., 2001), or upon inhibition of the Wnt/β-catenin signalling pathway by overexpressing Dkk1 inhibitor (Andl et al., 2002). Transgenic mice lacking the β-catenin after hair follicle formation, exhibit complete hair loss after the first hair cycle and also failure of stem cell differentiation into follicular keratinocytes, but instead adopt an epidermal fate (Huelsken et al., 2001), while transgenic mice overexpressing a constitutively active form of β-catenin (N-terminal truncated) under the control of K14 promoter in the basal layer of skin epidermis and hair follicles, display *de novo* hair follicle formation, including development of dermal papilla and sebaceous glands normally established only in embryogenesis and are permanent in postnatal life (Gat et al., 1998). Similarly, overexpression of a dominant negative form of Lef-1 (unable to

bind to β-catenin), under the control of K14 promoter in skin of transgenic mice, resulted in conversion of hair follicles into cysts of interfollicular epidermis with ectopic sebocytes (Niemann et al., 2002). Recently, Silva-Vargas et al. (Silva-Vargas et al., 2005), showed that inducible stabilisation of β-catenin in the adult skin of transgenic mice leads to ectopic hair follicle formation from the interfollicular epidermis. In line with this study, Ito et al. (Ito et al., 2007), showed that upon severe wounding of the skin in mice, Wnt/β-catenin signalling is elevated, leading to the induction of hair follicle formation from the epidermal stem cells. Taken together, these studies suggest that fate decisions of stem cells in the skin depend on β-catenin activation/stabilisation, which directs lineage selection in *vivo* and thus specification of either interfollicular epidermis or hair follicle development, both in embryonic and adult epidermis (β-catenin promotes hair follicle lineages) (Blanpain et al., 2007; Fuchs, 2008; Watt & Collins, 2008).

Interestingly, Wnt/β-catenin is not only activated during the placode formation, but is also required during the adult hair cycle both for HF stem cell maintenance (Lowry et al., 2005), and for stem cell activation, in order to initiate the growth of a new hair during the telogen-to-anagen transition (transition from the quiescent to the growing phase of the hair cycle) (DasGupta & Fuchs, 1999; Van Mater et al., 2003; Lo Celso et al., 2004; Lowry et al., 2005; Blanpain & Fuchs, 2006). The role of Wnt/β-catenin signalling and Wnt proteins in the specification and maintenance of stem cells and stem cell lineages is well established in various tissues and organs (Klaus & Birchmeier, 2008; Nusse et al., 2008). In the small intestine of transgenic mice, Tcf4 - a nuclear binding partner of β-catenin, was found to maintain the crypt stem cells, since loss-of-function mutations of the Tcf4 resulted in the complete absence of the stem cell compartment (Korinek et al., 1998). In addition, Wnt/β-catenin signalling has also been implicated in the increase of the haematopoietic stem cell renewal (Reya et al., 2003; Willert et al., 2003), as well as in the regulation of precursor cell maintenance in the central and peripheral nervous system (Lee et al., 2004; Zechner et al., 2007). In cultured human keratinocytes, the putative epidermal stem cells (keratinocytes with high proliferative potential) (Jones & Watt, 1993), express higher level of non-E-cadherin-associated β-catenin than transit-amplifying cells (Zhu & Watt, 1999). In addition, expression of stabilised β-catenin in cultured human keratinocytes, induces the expansion of putative epidermal stem cells, while the expression of an inactive form of

β-catenin induces exit from the stem cell compartment (Zhu & Watt, 1999). In contrast to the *in vitro* results, the loss of β-catenin does not seem to affect the maintenance of epidermal basal layer stem cells *in vivo* (no depletion of the interfollicular epidermal stem cells in skin) (Huelsken et al., 2001; Niemann et al., 2002), while, when β-catenin is stabilised through either genetic manipulation or wounding, epidermal basal layer stem cells adopt a hair follicle cell fate (Gat et al., 1998; Lo Celso et al., 2004; Silva-Vargas et al., 2005; Ito et al., 2007). The difference between the *in vitro* and *in vivo* results can be attributed to the fact that *in vitro*, hair follicle morphogenesis is not permissive and thus the epidermal stem cell compartment expands upon β-catenin stabilisation. Another possible explanation could be that *in vivo*, the response of epidermal stem cells to β-catenin is largely dependent on the interactions with the underlying mesenchyme, which is absent in culture (Watt & Collins, 2008).

However, postnatally, conditional targeted inducible ablation of β-catenin in adult mice skin, when backskin follicles are in telogen, results in the loss of the follicle stem cell niche (inability of β-catenin-null skin to preserve the quiescence and the expression of stem cell markers in the bulge niche) and failure of bulge stem cells to undergo proper activation in the onset of anagen (no reinitiation of the hair cycle) (Lowry et al., 2005). The role of Wnt/β-catenin in anagen induction and thus in bulge stem cell activation in transgenic mice, is also strengthened by the fact that although, most bulge cells in the hair follicle appear to be in a state of Wnt inhibition during telogen (resting phase), as judged by the inactivation of a Wnt reporter transgene TOPGAL and the lack of detectable nuclear β-catenin, at the onset of anagen in TOPGAL transgenic mice, there is an increase in OT-promoter in the bulge region of the hair follicle (DasGupta & Fuchs, 1999). Therefore, stabilised β-catenin is a feature of activated stem cells that drive the resting follicle into active growth. Accordingly, transgenic mice expressing constitutive elevated levels of stabilised β-catenin in their skin, exhibit *de novo* formation of hair follicles (Gat et al., 1998), as well as, by inducing expression of stabilised β-catenin in telogen-phase follicles in adult epidermis of transgenic mice, first, precocious re-entry into the anagen phase of hair growth occurs (Van Mater et al., 2003; Lo Celso et al., 2004; Lowry et al., 2005), and then *de novo* hair follicle formation from existing follicles, interfollicular epidermis and sebaceous glands (Lo Celso et al., 2004). Finally, the strongest Wnt/β-catenin signal, which is required postnatally in normal follicles, is for the terminal differentiation of cortical cells

(differentiated matrix cells) of the hair shaft (DasGupta & Fuchs, 1999), which is further supported by the fact that overexpression of stabilised β-catenin in transgenic mice develop pilomatricomas, which are pure masses of cortical cells (Gat et al., 1998), and also that (stabilising) mutations of β-catenin (CTNNB1), have been identified in human pilomatricomas (Chan et al., 1999a; Kajino et al., 2001; Moreno-Bueno et al., 2001; Xia et al., 2006).

Collectively, these findings underscore the sequential roles of Wnt/β-catenin in regulating epidermal and follicle stem cell lineage commitment and adult hair cycle, perhaps in a way that depends on the level of the signal (Niemann & Watt, 2002; Blanpain & Fuchs, 2006), as judged by gain-and-loss of function studies, using K14ΔN-β-cateninER adult mice in which the onset and duration of β-catenin activation are controlled by topical application of the drug 4-hydroxytamoxifen (4OHT) (Van Mater et al., 2003; Lo Celso et al., 2004; Silva-Vargas et al., 2005), or K14ΔN-β-catenin hemizygous (ΔN) and homozygous (ΔNΔN) mice, expressing low and high doses of active β-catenin respectively (Lowry et al., 2005). High levels of Wnt/β-catenin signalling stimulate hair follicle formation, intermediate levels favour sebocyte differentiation and low levels convert hair follicle into interfollicular epidermis (Gat et al., 1998; Huelsken et al., 2001; Niemann et al., 2002; Lo Celso et al., 2004). A study using whole-mounts of epidermal skin of transgenic mice, showed that while low levels of ectopic stabilised β-catenin are required for *de novo* hair follicle formation from sebaceous glands and interfollicular epidermis, only sustained high level activation of ectopic stabilised β-catenin is able to induce *de novo* hair follicles from pre-existing ones (Silva-Vargas et al., 2005). Furthermore, low levels of β-catenin stabilisation are required for hair follicle SC maintenance, followed by higher levels of β-catenin stabilisation that promote hair follicle SC activation, proliferation (re-entry hair cycle) and follicle regeneration (Van Mater et al., 2003; Lo Celso et al., 2004; Lowry et al., 2005). Much higher levels of β-catenin stabilisation are required for the transition from proliferation to differentiation of cortical cells of the hair shaft, while uncontrolled, constitutive β-catenin stabilisation results in pilomatricoma hair tumours (Gat et al., 1998; DasGupta & Fuchs, 1999; Huelsken et al., 2001; Blanpain & Fuchs, 2006).

1.5.2 Wnt/β-catenin and cancer

β-catenin cytoplasmic stabilisation/accumulation and subsequent nuclear translocation is the most common alteration observed during aberrant WNT signalling (constitutive activation of WNT signalling pathway), and is often implicated in the development of human carcinogenesis, invasion and later stages of tumour progression such as metastasis (Hugh et al., 1999; Polakis, 1999; Polakis, 2000; Fodde et al., 2001; Taipale & Beachy, 2001; Giles et al., 2003; Beachy et al., 2004; Nusse, 2005; Reya & Clevers, 2005; Stein et al., 2006; Fuerer et al., 2008; Klaus & Birchmeier, 2008). In humans, CTNNB1 (β-catenin gene) **(Table 1.1)**, APC, and in a less extent AXIN1 and AXIN2 mutations, that generally lead to inappropriate cytoplasmic stabilisation of β-catenin, subsequent translocation to the nucleus and constitutive activation of target genes, are being involved in many cancers including colon cancer, melanoma, pilomatricoma, hepatocellular carcinoma, gastrointestinal tumours, ovarian carcinomas and kidney Wilms tumours (Polakis, 2000; Giles et al., 2003; Polakis, 2007).

tissue	freq.	S29	Y30	L31	D32	S33	G34	I35	H36	S37	G38	A39	T40	T41	T42	A43	P44	S45	L46	S47	G48	K49	Δ	reference
colorectal	9/202						1							3				5					0	Samowitz 1999
colorectal	2/92													1				1						Kitaeva 1997
colorectal-w/o APC mutation	7/58																						7	Iwao 1998
colorectal-w/o APC mutation	13/27					2	1							3				5					1	Sparks 1998
colorectal HNPCC	12/28				2		2			1				2				5						Miyaki 1999
colorectal w/ MSI	13/53																	6						Mirabelli-primdahl 1999
colorectal w/o MSI	0/27																							Mirabelli-primdahl 1999
desmoid, sporadic	1/1													1									0	Shitoh 1999
desmoid, sporadic	22/42													10				12						Tejpar 1999
endometrial w/ MSI	3/9				2	1																		Mirabelli-primdahl 1999
endometrial w/o MSI	10/20				3	1	2			3				1										Mirabelli-primdahl 1999
gastric, Intestinal-type	7/26	2			5																			Park 1999
gastric, diffuse-type	0/17																							Park 1999
hepatocellular w/HCV	9/22				3	1				3				1				2						Huang 1999
hepatocellular	12/35				1	1	2	1	1				1	2				2		1			2	Van Nhieu 1999
hepatocellular	6/26				2		1			1								1					1	de la Coste 1998
hepatocellular	14/75				5	1	1							1				4					2	Miyoshi 1998
hepatocellular	21/119				3	3	1	1		2				4				8					2	Legoix 1999
hepatoblastoma, sporadic	8/9						2			1								1					4	Jeng 2000
hepatoblastoma, sporadic	27/52				2		3			1				5									16	Koch 1999
hepatoblastoma	12/18				2		1							1				1					7	Wei 2000
kidney, Wilm's tumor	6/40													1				2					3	Koesters 1999
medulloblastoma, sporaic	3/67					2				1														Zurawel 1998
melanoma	1/65																	1						Garcia-Rostan 1999
ovarian, endometriod	7/13				3	1				2				1									0	Gamallo 1999
ovarian, endometriod	3/11									2				1										Palacios 1998
ovarian, endometriod	10/63					2	2			6														Wright 1999
pancreatic tumors	0/111																							Gerdes 1999
pilomatricoma	12/16				2	4	3			2				1										Chan 1999
prostate cancer	5/104				1	2								1				1						Voeller 1998
thyroid, anaplastic	19/31					1			1	3	1		8	2	1	1	4	2	1	2		9	0	Garcia-rostan 1999
uterine endometrium	10/76					1				2				4				3						Fukuchi 1998

Table 1.1: β-catenin mutations in human cancers.

Amino acids affected by mutations in CTNNB1 gene are indicated for sequence located between serine-29 (S29) and lysine-49 (K49). The overall frequency (freq.) of mutations in each tumour type is represented as the number of tumours with mutations/total number of tumours analysed (Polakis, 2000).

Truncating mutations in APC, that promote aberrant activation of WNT/β-catenin signalling and consequently increased cell proliferation, have been found in both patients with Familial Adenomatous Polyposis (FAP - an autosomal, dominantly inherited disease in which patients develop polyps in the colon and rectum) (Bodmer et al., 1987; Groden et al., 1991; Kinzler et al., 1991; Nishisho et al., 1991) and in sporadic colorectal cancers (Ashton-Rickardt et al., 1989; Morin et al., 1997). Also, gain-of-function mutations of CTNNB1, that prevent phosphorylation, subsequent ubiquitylation and proteasomal degradation of β-catenin, are characterizing a fraction of sporadic colorectal human cancers (Morin et al., 1997). Similarly, loss-of-function mutations of AXIN1 and AXIN2 have also been detected in rare cases of colon cancer (Liu et al., 2000), as well as in ovarian (Wu et al., 2001) and hepatocellular cancer (Satoh et al., 2000).

In addition, APC mutations have been found in human sporadic medulloblastomas (brain tumours) (Huang et al., 2000) and germ-line APC mutations have been found in patients with Turcot's syndrome, a tumour-predisposition syndrome characterised by the development of multiple colorectal adenomas and medulloblastomas (Hamilton et al., 1995). At the same time, mutations in target residues S33 and S37 of β-catenin, that block the degradation of β-catenin, have also been reported in human sporadic medulloblastomas (Zurawel et al., 1998; Gilbertson, 2004).

Interestingly, activating (stabilising) mutations of β-catenin (CTNNB1), that prevent the phosphorylation-dependent, ubiquitin-mediated degradation of the protein, have been identified in human pilomatricomas (hair matrix cell tumourigenesis) (Chan et al., 1999a; Kajino et al., 2001; Moreno-Bueno et al., 2001; Xia et al., 2006), while transgenic mice that over-express a stabilised form of β-catenin in the epidermal basal layer and follicle outer root sheath of the skin, develop trichofolliculomas and pilomatricomas (Gat et al., 1998; Lo Celso et al., 2004).

Therefore, it is obvious, from all these studies, that uncontrolled WNT/β-catenin signalling, due to mutations of the pathway components or due to interactions with other inappropriate activated signalling cascades, which might cause its constitutive activation (cytoplasmic accumulation / nuclear relocalisation), is an important event in the genesis of many cancers.

1.5.3 HH and WNT interaction

Studies in different organisms, have shown that parallels and crosstalk between HH and WNT signalling occur both during development and tumourigenesis (Taipale & Beachy, 2001; Alonso & Fuchs, 2003a; Beachy et al., 2004; Hooper & Scott, 2005; Blanpain & Fuchs, 2006; Watt & Collins, 2008). In skin, both Hh and Wnt pathways are implicated in hair follicle morphogenesis and adult hair cell cycle (Millar, 2002; Schmidt-Ullrich & Paus, 2005; Blanpain & Fuchs, 2006). Wnt/β-catenin is required upstream of Shh in placode formation, during hair follicle morphogenesis (Gat et al., 1998; Huelsken et al., 2001; Andl et al., 2002; Lo Celso et al., 2004; Silva-Vargas et al., 2005; Blanpain & Fuchs, 2006), while Shh signalling is required for the proliferation and expansion of

follicle epithelium in order to assemble a mature follicle (St-Jacques et al., 1998; Chiang et al., 1999; Mill et al., 2003; Silva-Vargas et al., 2005; Blanpain & Fuchs, 2006). In response to β-catenin activation in the epidermis of transgenic mice, Shh signalling pathway is upregulated (Lo Celso et al., 2004; Silva-Vargas et al., 2005) with Shh, Ptch2, Gli1 and Gli2 being the most highly induced members of the Shh signalling cascade, as indicated by gene expression arrays (Silva-Vargas et al., 2005). In contrast, Shh expression was lost in β-catenin negative skin of transgenic mice, as confirmed by in situ hybridization, further suggesting that during hair development Shh is downstream of β-catenin (Huelsken et al., 2001).

In addition, studies in human colon cancer cells have shown that suppressor of fused (Su(fu)), which is a negative regulator of Hh/HH signalling pathway that controls the nuclear/cytoplasmic distribution of Ci/Gli transcription factors including Gli2, through direct protein-protein interactions (Ding et al., 1999; Kogerman et al., 1999; Stone et al., 1999; Murone et al., 2000; Barnfield et al., 2005; Varjosalo et al., 2006), is also a negative regulator of the WNT/β-catenin pathway (Meng et al., 2001). Therefore, Su(fu) apart from preventing accumulation of Gli2 in the nucleus, it has also been found to be in a complex with β-catenin in human colon cancer cells, and upon its overexpression to suppress the TCF/LEF - dependent transcription and to reduce the nuclear β-catenin levels by promoting its export from the nucleus (nuclear export of β-catenin) (Meng et al., 2001). Furthermore, the degradation process of both Ci/Gli transcription factors including Gli2, and β-catenin, in *Drosophila* and in mammalian cells, is mediated and regulated by Slimb/β-TrCP ubiquitin ligase (Aberle et al., 1997; Jiang & Struhl, 1998; Latres et al., 1999; Bhatia et al., 2006; Huntzicker et al., 2006; Pan et al., 2006).

However, HH signalling has also be found to be an antagonist of WNT signalling in human colon cancer cells (van den Brink et al., 2004). Indian Hedgehog (Ihh), which is required for human and rat colonic epithelial cell differentiation *in vitro* and *in vivo*, suppresses WNT/β-catenin signalling in human colorectal cancer cell lines *in vitro* (van den Brink et al., 2004). At the same time, Ihh is absent from the dysplastic epithelial cells of human adenomatous polyps *in vivo*, where β-catenin is abnormally localised, probably due to constitutive β-catenin-Tcf signalling (van den Brink et al., 2004). In addition, GLI1, a mediator of HH signalling, plays an inhibitory role in the nuclear β-catenin accumulation and the subsequent β-catenin-Tcf signalling in human colorectal

cancer cells *in vitro*, followed also by their suppression of proliferation (Akiyoshi et al., 2006). In line with these observations, a reverse association between GLI1 immunostaining and nuclear β-catenin accumulation, was found in human colorectal carcinoma tissues (Akiyoshi et al., 2006).

On the other hand, in different contexts, Wnt signalling can also be a downstream effector of Shh/Gli signalling pathway. Wingless (Wg), a Wnt family member, is directly regulated by *Ci*-the *Drosophila* Gli homologue, in *Drosophila* imaginal discs (Von Ohlen et al., 1997). In *Xenopus*, Gli2 the key transcriptional regulator of Hh signalling, affects ventro-posterior mesodermal development by regulating *Branchyruy* genes, *Xho3* genes and *Wnt* genes, such as Wnt8 and Wnt11 (Brewster et al., 2000; Mullor et al., 2001; Ruiz i Altaba et al., 2003). Most recently, it was shown by Ulloa et al. (Ulloa et al., 2007) that Gli3, the transcriptional repressor of the Hh pathway, in the absence of Shh, acts by antagonising Wnt3a ligand and the active forms of the Wnt transcriptional effector, β-catenin, in established human and monkey cell lines and in mice and frog embryos.

In mice, constitutive activation of β-catenin promotes hair follicle-like tumours such as pilomatricomas and trichofolliculomas, or BCC-like tumours (Gat et al., 1998; Nicolas et al., 2003; Lo Celso et al., 2004), similar to those induced by Gli1 and Gli2 - Shh pathway genes (Grachtchouk et al., 2000; Nilsson et al., 2000; Sheng et al., 2002; Hutchin et al., 2005; Huntzicker et al., 2006). In human pilomatricomas (hair matrix cell tumourigenesis), stabilising mutations of β-catenin have also been identified (Chan et al., 1999a; Kajino et al., 2001; Moreno-Bueno et al., 2001; Xia et al., 2006), while human BCCs show increased levels of GLI2 and GLI1 - SHH genes (Dahmane et al., 1997; Ghali et al., 1999; Mullor et al., 2001; Regl et al., 2002; Tojo et al., 2003; Ikram et al., 2004; Regl et al., 2004b; O'Driscoll et al., 2006; Asplund et al., 2008; Yu et al., 2008) and accumulation of nuclear β-catenin (Yamazaki et al., 2001; El-Bahrawy et al., 2003; Saldanha et al., 2004; Yang et al., 2008a).

In addition, analysis of gene expression in human BCCs revealed that both GLI1/GLI2/GLI3 (SHH mediators) and several WNT genes such as WNT2, WNT5A are expressed (Bonifas et al., 2001; Mullor et al., 2001; Saldanha et al., 2004), which was further confirmed by cDNA microarray analysis in human BCCs (O'Driscoll et al.,

2006; Yu et al., 2008). Recently, Li et al. (Li et al., 2007) showed that in rat kidney epithelial cells, Gli1 acts through Wnts and Snail to promote nuclear signalling of β-catenin, during epithelial transformation.

In line with these observations, human BCCs compared to normal skin, exhibit increased protein and mRNA levels of LEF-1, which belongs to the family of TCF/LEF transcription factors and is an important nuclear binding partner for β-catenin in skin (O'Driscoll et al., 2006; Asplund et al., 2008; Kriegl et al., 2009), as well as increased mRNA levels of frizzled receptors (FZD) for WNT proteins, and matrix metalloproteinases (MMP) known targets of β-catenin-TCF/LEF signalling (O'Driscoll et al., 2006; Yu et al., 2008). However, due to the complexity and context-dependency of both HH and WNT pathways during development and tumourigenesis in different organisms, still little is known about SHH and WNT interactions in human carcinogenesis.

Aim of the project

Taking into account the difficulty of culturing basal cell carcinomas *in vitro*, the molecular mechanisms involved in human BCC formation are poorly understood.

The aim of this project is to investigate the effects of the over expression of one isoform of human GLI2, the GLI2-β isoform, which also lacks the N-terminal repressor domain and is thus constitutively active (Tanimura et al., 1998), GLI2ΔN-β, (henceforth abbreviated to GLI2ΔN), on human N/TERT keratinocytes.

The GLI2-β isoform is the most prevalent in human BCCs (Tojo et al., 2003), and the truncated human GLI2-β/N-terminal deleted is a valuable tool to mimic the activated form of GLI2 (Eichberger et al., 2006). The use of the active form of GLI2, is also a way of partly mimicking sustained HH signalling, which is required for BCC-like growth, proliferation and survival in transgenic mice (Hutchin et al., 2005) and is implicated in human BCC development and in many other cancers (Ruiz i Altaba et al., 2002b; Pasca di Magliano & Hebrok, 2003; Beachy et al., 2004; Daya-Grosjean & Couve-Privat, 2005; Rubin & de Sauvage, 2006).

Therefore, GLI2ΔN will be used, in order (i) to generate and characterise GLI2ΔN-expressing stable and inducible N/TERT cell lines, (ii) to study the effects of its overexpression in the cell cycle and ploidy status of human N/TERT keratinocytes, and (iii) to identify possible interactions between HH/GLI2 and WNT/β-catenin signalling pathways.

CHAPTER TWO

2 MATERIALS AND METHODS

2.1 Cell lines and culture methods

2.1.1 Plasmids and cloning

The pCMV-EGFP-GLI2ΔN expression vector was a kind gift of Prof. Fritz Aberger (Department of Molecular Biology, University of Salzburg, Austria). The pSIN-CMV-EGFP plasmid (Deng et al., 1997), was kindly provided by Prof. Paul Khavari (Stanford University School of Medicine, CA). The pSIN-MCS vector, containing an MCS insert, was kindly cloned from pSIN-CMV-EGFP plasmid by Dr. Muy-Teck Teh (Clinical and Diagnostic Oral Sciences, Institute of Dentistry, Barts and the London School of Medicine and Dentistry, London, UK). The Tcf-4 responsive luciferase plasmid pGL3-OT (OT-β-catenin responsive promoter), an improved version of TOPFLASH (Shih et al., 2000), was kindly provided by Prof. Bert Vogelstein (The John Hopkins Oncology Centre Baltimore, MD). The retroviral regulatory tTA vector (pRevTet-Off) and the retroviral response cloning vector (pRevTRE) were purchased from Clontech (Palo Alto, CA) as part of the RevTet-Off System. The pSIN-OT-Luciferase (pSIN-OT-Luc) reporter transduction vector, the pSIN-CMV-EGFP-GLI2ΔN stable expression retroviral transduction vector and the pRevTRE-CMV-EGFP-GLI2ΔN inducible expression retroviral transduction vector were all obtained by Dr Giuseppe Trigiante (Centre for Cutaneous Research, Institute of Cell and Molecular Science, Barts and the London School of Medicine and Dentistry, London, UK).

2.1.2 General reagents and materials

Puromycin and Hexadimethrine bromide (polybrene) were supplied by Sigma-Aldrich (Dorset, UK). Mitogens, including hydrocortisone, transferrin, liothyronine and insulin were all supplied by Sigma-Aldrich (Dorset, UK), while cholera toxin was obtained by BioMol (Exeter, UK) and epidermal growth factor (EGF) was supplied by AbD Serotec (Kidlington, UK). Doxycycline (Dox), Geneticin (G418) and Hygromycin B (Hygro B) were all obtained from Clontech (Palo Alto, CA). All cell culture was performed in a laminar flow hood under aseptic conditions in accordance with standard tissue culture technique. All sterile disposable tissue culture flasks, plates and dishes were purchased from Nunc (Roskilde, Denmark).

2.1.3 Human immortalised N/TERT keratinocytes

Human telomerase (h/TERT)-immortalised N/TERT-1 (N/TERT) newborn epidermal keratinocytes are derived from clinically normal foreskin tissue and are further immortalised by the addition of ectopic telomerase, followed by spontaneous downregulation/loss of $p16^{INK4a}$ (Dickson et al., 2000). N/TERT keratinocytes were supplied by Prof. James Rheinwald (Department of Dermatology, Harvard University Medical School, Boston) and were cultured in complete RM+ medium. RM+ culture medium consists of Dulbecco's modified Eagle's medium (DMEM) supplemented with 25% (v/v) Ham's F12 medium (PAA, Somerset, UK), 10% (v/v) foetal calf serum (FCS) (Biosera, East Sussex, UK), 1% (v/v), glutamine (PAA, Somerset, UK), 1% (v/v) penicillin/streptomycin (PAA, Somerset, UK), and various mitogens (0.4 μg/ml hydrocortisone, 0.1 nM cholera toxin, 5 μg/ml transferrin, 20 pM liothyronine, 5 μg/ml insulin and 10 ng/ml EGF-epidermal growth factor **(see Appendix I)**). Cells were grown at 37°C in a humidified atmosphere of 10% (v/v) CO_2/90% (v/v) air. The culture medium was refreshed every 2-3 days and cells were passaged according to **Section 2.1.8**.

2.1.4 Phoenix amphotropic cells

Phoenix amphotropic (Phoenix A) cells (human embryonic 293T derived) were supplied by Prof. Garry Nolan (Nolan Lab, Medical Centre, Stanford University Medical School, CA). Phoenix is a retrovirus producer cell line, capable of delivering genes to dividing cells of most mammalian species including human (amphotropic), and are based on the 293T cell line (a human embryonic kidney line transformed with adenovirus E1A and carrying a temperature sensitive T antigen co-selected with neomycin). Phoenix A cells were cultured in DMEM (PAA, Somerset, UK) supplemented with 10% (v/v) FCS (Biosera, East Sussex, UK), 1% (v/v) penicillin/streptomycin (PAA, Somerset, UK), and 1% (v/v) Glutamine (PAA, Somerset, UK). Cells were grown at 37°C in a humidified atmosphere of 10% (v/v) CO_2/90% (v/v) air. The culture medium was refreshed every 2-3 days and cells were passaged according to **Section 2.1.8**.

2.1.5 Stable EGFP and EGFP-GLI2ΔN-expressing cell lines

N/TERT cells were stably transduced with retroviruses **(see Section 2.3 and Section 2.3.1)** encoding, pSIN-CMV-EGFP and pSIN-CMV-EGFP-GLI2ΔN (EGFP-GLI2ΔN fusion gene; EGFP - a marker for gene expression (Chalfie et al., 1994; Kain et al., 1995)) plasmids according to **Section 2.3.5.1**, to yield the SINCE and SINEG2 stable gene expressing cell lines respectively. Both the expression of EGFP (Enhanced Green Fluorescent Protein) and EGFP-GLI2ΔN fusion gene (GLI2ΔN - the GLI2-β isoform, which also lacks the N-terminal repressor domain and is thus constitutively active) are under the control of the CMV (cytomegalovirus gene) promoter which gives strong expression of target genes in a variety of mammalian cells (Davis & Huang, 1988; Cheng et al., 2004). SINCE and SINEG2 cells were cultured in complete RM+ medium at 37^{o}C in a humidified atmosphere of 10% (v/v) CO_2/90% (v/v) air. The culture medium was refreshed every 2-3 days and cells were passaged according to **Section 2.1.8**.

2.1.6 Inducible EGFP-GLI2ΔN-expressing cell line

The N/TERT RevTRE-CMV-EGFP-GLI2ΔN inducible cell line, referred to as NTEG2 cell line, was prepared as recommended by the kit manufacturer (RevTet-Off System, Clontech Laboratories, Palo Alto, CA), by Dr Giuseppe Trigiante at Centre for Cutaneous Research, Institute of Cell and Molecular Science, Barts and the London School of Medicine and Dentistry, London, UK **(see Section 2.3.5.2 and Chapter 3, Section 3.2.2.1, Figure 3.6)** (Chang et al., 2000; Chi et al., 2005). The retrovirus-mediated tet-regulated gene expression system (RevTet-Off) (Clontech Laboratories, Palo Alto, CA) combines the advantages of retroviral transfer with those of tet-regulation and thus allows efficient and tight quantitative and temporal control of gene expression. In the RevTet-Off system, transcription of the gene of interest (in this study EGFP-GLI2ΔN fusion gene) is turned off in the presence of doxycycline (a derivative of tetracycline), while transcription of this gene (EGFP-GLI2ΔN fusion gene) is turned on in the absence of doxycycline. NTEG2 cells were maintained in DMEM supplemented with 25% (v/v) Ham's F12 medium (PAA, Somerset, UK), 10% (v/v) FCS (Biosera, East Sussex, UK), 1% (v/v) Glutamine (PAA, Somerset, UK), 1% (v/v) penicillin/streptomycin (PAA, Somerset, UK), various mitogens (same as RM+

complete medium; **see Appendix I**), 50 μg/ml Hygromycin B **(Appendix I)** and 250 μg/ml G418 **(Appendix I)** and kept under Doxycycline (40 ng/ml) **(Appendix I)** repression for maintenance and characterisation studies. Due to the heterogeneity of the cell population, a higher concentration of Dox (10 μg/ml) **(Appendix I)** was used to maximize repression in subsequent experiments. Hygromycin B and G418 concentrations were optimised by me according to **Section 2.4** and Doxycycline concentrations were optimised by me according to **Section 2.5**. When doxycycline was removed, by aspirating culture medium and wash cells 4x with 1x sterile PBS (PAA, Somerset, UK), the inducible cell line (NTEG2 Dox-) was cultured in DMEM supplemented with 25% (v/v) Ham's F12 medium (PAA, Somerset, UK), 10% (v/v) Tet System Approved fetal bovine serum (Tet-FBS) (Clontech, Palo Alto, CA), 1% (v/v) glutamine (PAA, Somerset, UK), 1% (v/v) penicillin/streptomycin (PAA, Somerset, UK), 50 μg/ml Hygromycin B and 250 μg/ml G418 and various mitogens (same as RM+ complete medium; **see Appendix I**). All cells were grown at 37^{o}C in a humidified atmosphere of 10% (v/v) CO_2/90% (v/v) air. The culture medium was refreshed every 2-3 days and cells were passaged according to **Section 2.1.8**.

2.1.7 OT-Luciferase Reporter cell lines

NTERT, SINEG2, SINCE and NTEG2 cells were further transduced as described in **Section 2.3, Section 2.3.5.1** and **Section 2.3.5.3**, with the pSIN-OT-Luciferase (pSIN-OT-Luc) plasmid, containing the OT-β-catenin-responsive promoter (OT), an improved version of TOPFLASH, which contains the TCF-4 binding sites **(CCTTTGATC)** (Korinek et al., 1997; He et al., 1998; Shih et al., 2000), to produce reporter stable (N/TERT-OTLuc, SINEG2-OTLuc, SINCE-OTLuc respectively) or inducible cell line (NTEG2-OTLuc). The OT promoter drives the expression of a luciferase gene to facilitate the detection of promoter activity, and indirectly β-catenin protein transcriptional activity. Luciferase is used as a reporter gene to provide information about the activity of the promoter that drives its expression. In this study, luciferase was used to detect and measure the activity of the OT promoter, and indirectly the transcriptional activity of β-catenin **(see Section 2.15)**. Reporter stable cell lines were then propagated in RM+ growth medium. The reporter inducible cell line was cultured in RM+ growth medium, containing 100 μg/ml Hygromycin B, 500 μg/ml G418, and

kept under Doxycycline repression until required for experiments. All cells were grown at 37°C in a humidified atmosphere of 10% (v/v) CO_2/90% (v/v) air. The culture medium was refreshed every 2-3 days and cells were passaged according to **Section 2.1.8**.

2.1.8 Cell passaging

All cell types described above were cultured in (T25, T75 or T150/T175) flasks containing 10, 20 or 30/40 ml growth medium respectively. When cells became ~ 60-70% confluent they were passaged - i.e. the cells were lifted off the flask and re-seeded at a lower density to enable continued cell division. This was achieved by aspirating the old tissue culture media from the flask followed by a single wash with 3, 5 or 10 ml sterile PBS (phosphate buffered saline) (PAA, Somerset, UK) and once in pre-warmed 3, 5 or 10 ml 1x versene (Gibco Invitrogen, Paisley, UK) to cover the bottom of T25, T75 or T150/T175 flasks, respectively. PBS is an isotonic, water-based, buffer solution that helps to maintain a constant pH (i.e. pH 7.4). Versene is an isotonic solution containing 0.53 mM EDTA (ethylenediaminetetraacetic acid) (0.2 g/L EDTA in phosphate buffered saline) that chelates cationic ions, weakening cells adhesion to the flask, and prevents divalent cations inhibiting trypsin enzymatic activity. The versene was aspirated off and replaced by 3, 5 or 10 ml pre-warmed 1x Trypsin/EDTA (PAA, Somerset, UK) solution (0.5 mg/ml trypsin and 0.22 mg/ml EDTA in PBS without Ca and Mg). Flasks were returned to the tissue culture incubator for 5-10 min. During this time, the trypsin cleaves the extracellular cell adhesion proteins needed for cells to adhere, causing the cells to lift off the flask. The detachment process was encouraged by tapping the flasks every few minutes and was monitored under the light microscope **(see Section 2.2)**. To prevent cell death of detached keratinocytes, cells that had lifted off the flask after 5 min (i.e. 10 ml of trypsinised cells in a T75 flask) were transferred to a 50 ml falcon tube containing 10 ml complete RM+ culture medium (containing either 10% (v/v) FCS (Biosera, East Sussex, UK) or 10% (v/v) Tet-FBS (Clontech, Palo Alto, CA), depending on cell type, to stop the trypsinisation), and 3, 5 or 10 ml fresh pre-warmed 1x Trypsin/EDTA (PAA, Somerset, UK) solution was added to the remaining keratinocytes in the flask. The serum in the media blocks the protease activity of the trypsin, which would be harmful to the cells. This process was repeated several times

until all the keratinocytes were removed from the flask. The cells in the falcon tube were centrifuged at 1,000 rpm (revolutions per minute) for 5 min. The supernatant was aspirated and the cell pellet was resuspended in 10 ml fresh culture media. Resuspended cells were counted **(see Section 2.1.9)** using either a haemocytometer (Weber Scientific International Ltd, Middlesex, UK) **(see Section 2.1.9.1)** or a CAsy® Cell Counter (Innovatis, Sittingbourne, UK) **(see Section 2.1.9.2)**. Cells were then plated out for experiments, transferred to new flasks for propagation (at 10-20% of their original density) or cryopreserved for storage **(see Section 2.1.10)**.

2.1.9 Cell counting

2.1.9.1 Haemocytometer

After trypsinisation, resuspended cells (10 µl of cell suspension) were counted by pipetting under a coverslip on a gridded glass slide known as haemocytometer (Weber Scientific International Ltd, Middlesex, UK). To count viable cells only, a 10 µl aliquot of resuspended cells was diluted 1: 2 with trypan blue (Invitrogen, Paisley, UK) - 10 µl of cell suspension mixed with 10 µl trypan blue - and 10 µl of this solution was pipetted on the haemocytometer. Trypan blue is selective for membrane-damaged, non-viable cells, since it has a negatively charged chromophore which cannot penetrate an intact cell membrane. Thus viable cells appeared bright and not stained when viewed under the microscope **(Section 2.2)**, whereas non-viable cells appeared dark blue. The haemocytometer grid arrangement has four primary squares, each containing sixteen squares. Cell concentration was calculated by adding up the number of cells counted in each of the four 4x4 square sections under a microscope **(Section 2.2)**, dividing by four giving the average count and multiplying by $1x10^4$, to give cells per ml (cells/ml). If the cells had been counted in trypan blue for cell viability, then the average count was multiplied by two to allow for the 1 in 2 trypan blue to cell dilution factor.

2.1.9.2 CAsy® Cell Counter

Cell number and density of viable cells were determined using CAsy® Cell Counter (Innovatis, Sittingbourne, UK). Cell pellets obtained by centrifugation were resuspended in normal growth medium (i.e. 5, 10, 20 ml depending on the confluence

and the size of the flask) and were added in 1:100 dilution into CasyTon® (Innovatis Sittingbourne, UK) buffer (60 µl of cell suspension into 6 ml CasyTon® buffer). Each sample (cell suspension) was prepared three times in CAsyTon® (Innovatis Sittingbourne, UK) buffer, followed by triplicate measurements of 200 µl sample volume. Based on the dilution that is used, Casy® Cell Counter calculated the concentration of viable cells per ml (counts/ml, cells/ml) in the original cell suspension. Viable cells were measured by Casy® Cell Counter by excluding all counts that were of a size smaller that 10 µm (dead cells and debris).

2.1.10 Cryopreservation and recovery of cells

To maintain cell stocks for experiments, trypsinised cells were centrifuged at 1,000 rpm at room temperature and the cell pellet was resuspended in freezing medium (10% (v/v) dimethyl sulphoxide (DMSO) (Fisher, Leicestershire, UK), 90% (v/v) FCS (Biosera, East Sussex, UK)) to give a concentration of 2 million cells per ml ($2x10^6$ cells/ml). DMSO was included in the freezing medium to prevent the formation of crystals during the freezing process that would otherwise lyse the cells. The DMSO/FCS cell suspension (1 ml) was transferred into each 1.8 ml freezing cryogenic vial (Fisher, Leicestershire, UK). To ensure a constant cooling rate of 1^oC/min, the cryovials containing cells were transferred to isopropyl freezing container (NALGENE Cryo 1^oC Freezing container, BDH Laboratories Supplies, UK) and stored at -80°C for 1 to 3 days. The cryovials were then transferred to liquid nitrogen for long-term storage, until required.

Cryopreserved frozen cells were recovered, by removing the vial from liquid nitrogen storage and thawing it rapidly at 37^oC in a waterbath. As soon as the cell aliquot had thawed, the DMSO/FCS cell suspension was immediately transferred into a 15 ml falcon tube containing 10 ml complete culture medium (relevant to the cell type) and centrifuged at 1,000 rpm for 5 min to remove the DMSO (Fisher, Leicestershire, UK). The supernatant was discarded and the cell pellet was resuspended in complete culture medium. Resuspended cells were seeded in a T75 cm^2 flask at 2 million per flask.

2.2 Light and Fluorescence microscopy

Normal cultured cells, cultured cells expressing EGFP (enhanced green fluorescent protein) or EGFP-GLI2ΔN fusion protein were visualised using a light fluorescence microscope (Leica DM IRB/Nicon Eclipse TE-2000-S, Leica Microsystems, Germany) to detect cell morphology and gene/protein expression. Images were captured with a digital imaging system (Leica DC2000 camera) attached to the microscope.

2.3 Retrovirus Mediated Gene Transfer

2.3.1 Retroviruses and Retroviral vectors

Retrovirus mediated gene transfer (retroviral infection) represents one of the most efficient methods for inducing long-term, stable gene expression in human keratinocytes, since simple plasmid transfection methods are particularly ineffective in this cell type. For that purpose retroviral vectors are used to induce the expression of a specific gene in keratinocytes. Retroviral vectors allow the efficient integration of retroviral DNA into actively transcribing regions of the host genome, resulting in reliable and heritable expression of the gene of interest and subsequent expression of the protein encoded by this gene, without variability or loss of gene expression due to loss of the construct. Thus, retroviruses are utilized as a permanent gene delivery vehicle, and retroviral infection/transduction yields stable gene of interest-expressing cell lines **(Figure 2.2)**.

Viruses are small infectious agents that can only replicate inside the living cells or organisms (hosts). Although a virus may contain either DNA (DNA virus) or RNA (Retrovirus), their genomic structure varies greatly among different types of viruses. The retroviral virions consist of small enveloped particles, a capsid and the single-stranded viral RNA (3 genes are encoded in viral RNA, *gag* - encodes capsid core proteins, *pol* - encodes reverse transcriptase, integrase and protease and *env* - encodes envelope antigens), and begin their cycle by entering the host target cell **(Figure 2.1)**. While entering into the cell and migrating to the host cell's nucleus, the retroviral particle loses its envelope and its viral capsid respectively, and thus its genetic material

(viral RNA) is exposed. By using the retroviral enzyme reverse transcriptase, the retroviral RNA is then reverse-transcribed into double stranded DNA. The next crucial step in the retroviral cycle is the integration of the viral DNA into the host genome. This is accomplished by retroviral integrase, which mediates the excision of DNA bases at the host genome that is necessary for the incorporation of the viral DNA (pro-viral stage). Once viral DNA is incorporated, the long terminal repeat (LTR - Long Terminal Repeat sequence, a region that contains enhancer, promoter, transcription initiation, transcription terminator and polyadenylation signal - U3, R, U5 regions), and specifically the U3 region in the 5' LTR which normally acts as a promoter/enhancer, of the retrovirus will promote the transcription of viral DNA into single stranded retroviral RNA. The 3' LTR (U3, R, U5 regions) of the integrated pro-viral DNA functions as the terminator sequence. Once the retroviral RNA is translated, it will give rise to all the envelope and capsid proteins and retroviral enzymes (i.e. reverse transcriptase, integrase) that are required to generate new retroviral particles. Once retroviral assembly is finished, the produced retrovirus can exit the cell and re-infect new host cells where it can re-initiate its infectious cycle.

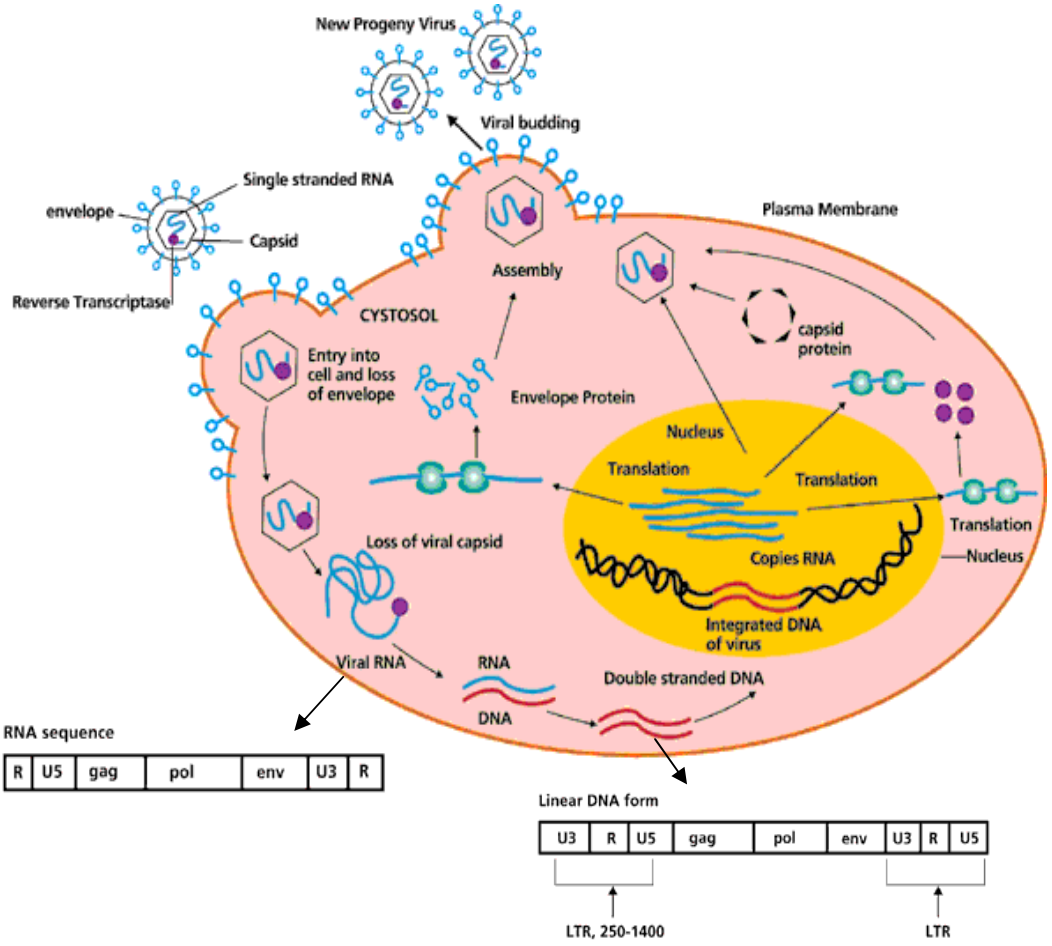

Figure 2.1: Retroviral replication.

This diagram depicts a typical life cycle of a retrovirus. Upon entry and migration into the host cell, the retrovirus looses its envelope and its viral capsid, and the exposed viral RNA is then reverse transcribed, through reverse transcriptase retroviral enzyme activation, into double stranded DNA. The latter is then integrated randomly within the host cell's genome by a process that is mediated by the retroviral integrase enzyme. Following successful integration, the viral genome is then transcribed by the LTRs (Long Terminal Repeats) into retroviral single stranded RNA. Upon RNA translation, the core retroviral proteins including reverse transcriptase, retroviral integrase, as well as several retroviral packaging proteins such as envelope and capsid proteins, are being produced, which will later help in the assembly of new virions that will be exported from the host cell's membrane in order to infect new host target cells. Modified from http://www.clontech.com/support/tools.

In this study, replication incompetent retroviral vectors **(Table 2.1)** have been used to allow a one-time infection of target cells and to minimize safety hazards that may arise from continuous spreading of replication competent retroviruses. This is achieved by removal of viral packaging genes from the retroviral backbone, therefore incapacitating the self-replication machinery of retroviral vectors. The viral packaging proteins that are needed for retrovirus production are instead provided *in trans* by retrovirus packaging cell systems (i.e. Phoenix and PT67 cells) **(Figure 2.2A)**. Once the infectious, but replication incompetent, retroviral particles are assembled they are released from the packaging cells and are ready to infect new target cells **(Figure 2.2B)**. In addition, in this study, p**SIN** (**S**elf **In**activating) vectors (Deng et al., 1997; Zufferey et al., 1998) were employed, and packaging cells were transfected with these retroviral vectors **(Figure 2.2A)**. These vectors were constructed by deleting the enhancer and the promoter sequences in the U3 region of the 3' LTR (**L**ong **T**erminal **R**epeat) (Deng et al., 1997; Zufferey et al., 1998). Therefore, upon infection of target cells with the virus particles carrying the 3' LTR U3 deletion **(Figure 2.2B)**, the retroviral RNA is reversed transcribed and the deletion is transferred to the 5' LTR of the proviral DNA, and thus abolishing any transcriptional activity driven by the LTR in transduced cells (no full-length vector RNA is produced in the transduced cells). Hence, gene (gene of interest) expression is only driven by the internal CMV promoter **(Figure 2.2B)** (Deng et al., 1997).

Table 2.1: Constructs used for transfections in packaging cell lines and retroviral transductions.

Construct	Function	Packaging Cell Line
pSIN-CMV-EGFP	Stable EGFP (Enhanced Green Fluorescent Protein) overexpression	Phoenix A
pSIN-CMV-EGFP-GLI2ΔN	Stable EGFP-GLI2ΔN fusion protein overexpression (the GLI2-β isoform, which also lacks the N-terminal repressor domain - active form of GLI2)	Phoenix A
pSIN-OT-Luciferase	Detection of β-catenin transcriptional activity by luciferase protein expression	Phoenix A
pRevTet-Off	tTA (tetracycline transactivator) vector that regulates the activity of the internal gene promoter.	PT67
pRevTRE-CMV-EGFP-GLI2ΔN	Contains the tetracycline response element which is activated in the absence of tetracycline, by the tTA (tetracycline transactivator) which is present in the pRevTet-Off plasmid and thus leads to inducible EGFP-GLI2ΔN fusion protein overexpression	PT67

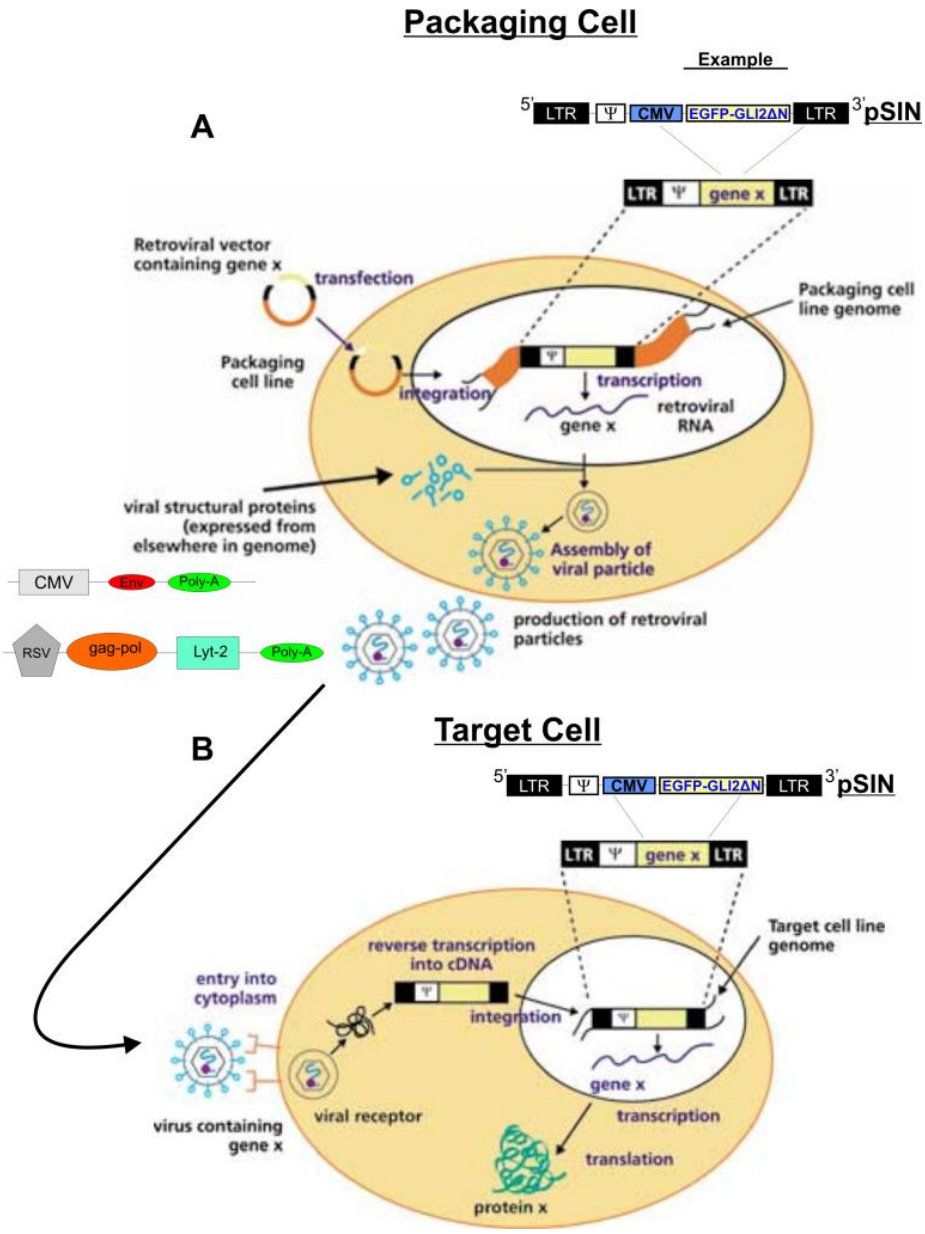

Figure 2.2: Retroviral transduction.

(A) The retroviral plasmids are transfected into packaging cell lines (i.e. Phoenix A or PT67), and following antibiotic selection, are incorporated into the host cell's genome. Following integration, the retroviral plasmid DNA will be transcribed into retroviral RNA. Since the genome of replication incompetent retroviruses lacks the genes responsible for the production of retroviral assembly proteins (i.e. gag-pol, Lyt-2, Env genes), these are provided solely from the packaging cell line which is constitutively expressing the required components for retroviral particle assembly. The retroviral assembly proteins recognise the Ψ+ packaging signal in the transcribed RNA, which is necessary for particle formation and the inclusion of retroviral RNA within the assembled virions. The retroviral RNA bearing the genes of interest is packaged into infectious particles which are released from packaging cells and are now ready to infect the target cells. **(B)** The retroviruses are now following their normal life cycle by infecting new target cells. Upon entry into the host cell, the retroviral RNA is transcribed into double stranded DNA and is later incorporated into the host genome. Since replication incompetent virus are devoid of the enhancer and promoter regions of the LTRs, the expression of the transgenes is now only under the control of the internal promoter (i.e. CMV). Therefore, the transcribed viral RNA will now be translated to the protein of interest. Modified from http://www.clontech.com.

2.3.2 DNA and RNA quantification

Isolated DNA and RNA were measured using NanoDrop™ ND-1000 Spectrophotometer (ThermoScientific, Cambridgeshire, UK) (**see Section 2.12.4.1** for spectrometry principle). A sample volume of 2 µl was used following instrument blanking with 2 µl of sterile, nuclease (enzymes that degrade DNA and RNA) free H_2O (Sigma-Aldrich, Dorset, UK). The concentration of the sample DNA or RNA content is provided in ng/µl as measured by the NanoDrop™ ND-1000 Spectrophotometer (ThermoScientific, Cambridgeshire, UK) at 260 nm absorbance, while the quality (purity of DNA or RNA) of DNA and RNA content was estimated by the nucleic acid : protein (260 nm/280 nm) ratio. Ratio values of 1.8 - 2.0 are considered of good quality and samples with this ratio were therefore used for downstream applications.

2.3.3 Stable transfection of packaging cells

All transductions using pSIN based constructs **(see Table 2.1 and Section 2.1.1, Section 2.1.5, Section 2.1.7)**, involved transfecting the plasmid into the Phoenix A packaging cell line **(Section 2.1.4)**, using FuGENE® Transfection Reagent (Roche, Burgess Hill, UK) **(see Figure 2.2A)**. All transductions using RevTet and RevTRE constructs **(see Table 2.1 and Section 2.1.6)**, involved transfecting the plasmid into the PT67 packaging cell line - cells derived from an NIH/3T3 (mouse embryonic fibroblasts)-based line expressing the 10A1 virus envelope (murine leukaemia virus) (Clontech Laboratories, Palo Alto, CA) (Miller & Chen, 1996), using FuGENE® Transfection Reagent (Roche, Burgess Hill, UK) by Dr Giuseppe Trigiante at Centre for Cutaneous Research, Institute of Cell and Molecular Science, Barts and the London School of Medicine and Dentistry, London, UK, according to manufacturer's instructions **(see Figure 2.2A and Chapter 3, Section 3.2.2.1, Figure 3.6)**. Transfection is the process of deliberately introducing nucleic acids such as plasmid DNA into cells and the term is used notably for non-viral methods. Transfection of animal cells typically involves opening transient pores or "holes" in the cell membrane, to allow the uptake of genetic material (DNA plasmid) and it can be carried out by mixing a cationic lipid with the gene material (DNA plasmid) in order to produce liposomes, which fuse with the cell membrane and deposit their cargo inside. Since the

DNA introduced in the transfection process is usually not integrated into the nuclear genome, the foreign DNA will be diluted through mitosis or degraded. Thus a marker gene (i.e. puromycin resistance gene) is co-transfected, which gives the cell some selectable advantage, such as resistance towards a certain toxin (i.e. puromycin). If the toxin (i.e. puromycin) is then added to the cell culture, only those cells with the marker gene integrated into their genomes will be able to proliferate, while other cells will die. After applying this selective stress (selection pressure) for some time, only the cells with a stable transfection remain and can be cultivated further.

The DNA concentration (ng/µl) of the retroviral plasmids used, was measured according to **Section 2.3.2**. Phoenix A cells were firstly plated at a concentration of $4x10^5$ cells per 6 cm dish covered with 5 ml growth medium **(Section 2.1.4)** to give a confluence of approximately 60-70%. Cells were allowed to attach to the culture dishes for 3 hours, and were then transfected with the retroviral plasmids mentioned at **Table 2.1** and **Section 2.1.1**, **Section 2.1.5** and **Section 2.1.7**, which also contain the puromycin resistance gene, using FuGENE® Transfection Reagent (Roche, Burgess Hill, UK). FuGENE® Transfection Reagent (Roche, Burgess Hill, UK) is a proprietary blend of lipids and other components supplied in 80% ethanol. The transfection mixture was prepared with a DNA : FuGENE® (Roche, Burgess Hill, UK) 1 µg : 2 µl ratio as follows: 10 µg of DNA, 20 µl FuGENE® (Roche, Burgess Hill, UK) and was brought up to a final volume of 70 µl with sterile PBS (PAA, Somerset, UK). The growth medium was changed to 2 ml per 6 cm dish and the transfection mixture was added to the cells, which were allowed to grow for 24 hours at 37°C in a humidified atmosphere of 10% (v/v) CO_2/90% (v/v) air. The next day, the transfection medium was replaced with normal growth medium **(Section 2.1.4)** and cells were allowed to grow to confluence.

Next, cells were passaged, according to **Section 2.1.8**, in a 1:3 ratio (i.e. cell pellet from one 6 cm dish was split into 3 x 6 cm dishes) and were plated in selection medium which consisted of complete growth medium **(Section 2.1.4)** containing 3 µg/ml puromycin selective toxin. Puromycin is an antibiotic that inhibits protein translation and therefore blocks protein synthesis. Puromycin is toxic to eukaryotic cells and it is used as selective agent in cell culture systems. Transfected Phoenix A cells were further grown for 7-10 days, in selection medium which was changed every 2-3 days, at 37°C in a humidified atmosphere of 10% (v/v) CO_2/90% (v/v) air. Then, the selection

medium was replaced with normal growth medium **(Section 2.1.4)** and cells were either cryopreserved as previously described in **Section 2.1.10** or were used for retrovirus production **(see Section 2.3.4)**.

2.3.4 Retrovirus production

Retrovirus was produced with two different approaches. First, retroviral plasmid transfected and puromycin selected Phoenix A cells **(see Section 2.3.3)**, that have reached confluence (~ 90-100% confluent) had their medium replaced with normal growth medium **(Section 2.1.4)** without puromycin (~ half of the normal medium volume - i.e. instead of 20 ml in a T75 flask 10-15 ml growth medium were added) and cells were incubated overnight at 32^{o}C in a humidified atmosphere of 10% (v/v) CO_2/90% (v/v) air, for viral collection. Retroviral supernatants from virus-containing Phoenix cells were collected in 50 ml falcon tubes the next day and thereafter collected once daily, for 2-3 days post-confluent. Upon collection, retroviral supernatants were centrifuged at high speed centrifugation at 2,000 rpm for 10 minutes to remove any non-adherent Phoenix A cells present in the medium.

Second, retroviral plasmid transfected and puromycin selected Phoenix A cells **(see Section 2.3.3)**, were splitted and cultured in normal growth medium without puromycin until they reached ~ 80-90% confluence. Then, the old medium was replaced with fresh medium (~ half of the normal medium volume - i.e. instead of 20 ml in a T75 flask 10-15 ml growth medium were added) and cells were incubated for 48 hours at 32^{o}C in a humidified atmosphere of 10% (v/v) CO_2/90% (v/v) air in complete growth medium **(Section 2.1.4)** without puromycin, for viral collection. Thus, retroviral supernatants from virus-containing Phoenix cells were collected in 50 ml falcon tubes after 48 hours and again upon collection, retroviral supernatants were centrifuged at high speed centrifugation at 2,000 rpm for 10 minutes to remove any non-adherent Phoenix A cells present in the medium.

In both cases, the retroviral supernatants were aliquoted and either directly used for transduction of N/TERT cells or frozen at -80^{o}C until required.

2.3.5 Retroviral transduction of human N/TERT keratinocytes

2.3.5.1 Retroviral transduction to yield stable gene-expressing cell lines

N/TERT cells **(Section 2.1.3)** were stably transduced with retroviruses **(see Section 2.3.1, Figure 2.2B)**, encoding pSIN-CMV-EGFP and pSIN-CMV-EGFP-GLI2ΔN plasmids, prepared as described in **Section 2.3.4**, to yield SINCE and SINEG2 stable-gene expressing cell lines, respectively **(see Section 2.1.5)**. Cells were plated $2x10^5$ cells/dish into 6 cm dishes, 24 hours before transduction. The next day, medium was aspirated and each dish was pre-incubated for 10 minutes at 37°C, in 2 ml of normal culture medium (depending on the cell type) containing 5 μg/ml polybrene (hexadimethine bromide), before replacing with 4 ml of retroviral supernatant containing the same concentration of polybrene (5 μg/ml), to facilitate infection. Polybrene is a positively charged molecule used to increase the efficiency of infection of certain cells with a retrovirus in cell culture and acts by neutralizing the charge repulsion between virions (virus particles) and sialic acid-containing molecules (sialic-acid is found on surface membranes and contributes to creating a negative charge on the cell's surface). The 6 cm dishes were then centrifuged at 350 rpm for 1 hour at 32°C. Transduced cells were then washed twice in sterile 1x PBS (PAA, Somerset, UK) and were incubated for at least 24 hours (24-72 hours) in normal growth medium (depending on the cell type) at 37°C in a humidified atmosphere of 10% (v/v) CO_2/90% (v/v) air), prior to any experiments or to cryopreservation **(Section 2.1.10)**. Because of lack of selectable markers, since the puromycin resistant gene is out of the retroviral cassette of pSIN vector, and due to the green fluorescence emitted by EGFP or EGFP-GLI2ΔN-expressing cells, the transduced cells were FACS (Fluorescent Activating Cell Sorting) sorted for green fluorescence **(see Section 2.8.2)** and collected in order to enhance the percentage of cells that have acquired the retroviral construct. FACS sorted transduced cells were either used in experiments or were cryopreserved **(Section 2.1.10)**. Expression levels of both EGFP and EGFP-GLI2ΔN proteins in stable transduced cells, which are proportional to the levels of green fluorescence, and the morphology of transduced cells expressing those proteins were detected by light and fluorescence microscopy **(Section 2.2)**. Expression levels of both EGFP and EGFP-GLI2ΔN proteins in stable transduced cells were further detected by flow cytometry **(Section 2.8)** and western blot analysis **(Section 2.12)**. Transcription mRNA levels of

full-length GLI2 and GLI2 a/β isoform in N/TERT and in stable transduced cells were detected by semi-quantitative and qRT-PCR **(Section 2.11)**, while endogenous GLI2 protein levels in N/TERT and in stable transduced cells were detected by western blot analysis **(Section 2.12)**.

2.3.5.2 Retroviral transduction to yield inducible gene-expressing cell line

N/TERT cells **(Section 2.1.3)** were stably transduced with retroviruses **(see Section 2.3.1, Figure 2.2B)**, encoding pRevTRE-CMV-EGFP-GLI2ΔN and pRevTet-Off plasmids, according to the kit manufacturer (RevTet-Off System, Clontech Laboratories, Palo Alto, CA) (Chang et al., 2000; Chi et al., 2005), by Dr Giuseppe Trigiante at Centre for Cutaneous Research, Institute of Cell and Molecular Science, Barts and the London School of Medicine and Dentistry, London, UK, to yield the N/TERT RevTRE-CMV-EGFP-GLI2ΔN (NTEG2) inducible cell line **(see Section 2.1.6 and Chapter 3, Section 3.2.2.1, Figure 3.6)**. Retroviral supernatant was obtained as described previously in **Section 2.3.4,** but using PT67 packaging cell line (Clontech Laboratories, Palo Alto, CA) **(Section 2.3.3)** (Miller & Chen, 1996), instead of Phoenix A packaging cells **(Section 2.1.4)**. Briefly, N/TERT cells were pre transduced according to **Section 2.3.5.1** with the regulatory vector pRevTet-Off (Clontech Laboratories, Palo Alto, CA), to yield the founder cell line NT-TetOff. The founder cell line was selected with G418, and then transduced according to **Section 2.3.5.1** with the expression vector pRevTRE-CMV-EGFP-GLI2ΔN (RevTRE response plasmid) and selected with Hygromycin B, to yield the NTEG2 inducible cell line. Due to the very low levels of EGFP-GLI2ΔN retroviral construct expression in human N/TERT keratinocytes, in the intitially constructed NTEG2 cell line by Dr Giuseppe Trigiante (Centre for Cutaneous Research, Institute of Cell and Molecular Science, Barts and the London School of Medicine and Dentistry, London, UK), I optimised further the Hygromycin B, G418 and Doxycycline concentrations **(see Section 2.4 and Section 2.5)**, and I have reselected the cell line. In addition, after doxycycline removal NTEG2 Dox- cells were FACS sorted **(see Section 2.8.2)** and all EGFP positive cells were collected to obtain highly EGFP-GLI2ΔN expressing population, replated and cultured under the presence of doxycycline until required for experiments or were cryopreserved **(Section 2.1.10)**. Expression levels of both EGFP and EGFP-GLI2ΔN proteins in inducible transduced

cells after doxycycline removal, which are proportional to the levels of green fluorescence, and the morphology of transduced cells expressing those proteins were detected by light and fluorescence microscopy **(Section 2.2)**. Expression levels of both EGFP and EGFFP-GLI2ΔN proteins in inducible transduced cells after doxycycline removal were further detected by flow cytometry **(Section 2.8)** and western blot analysis **(Section 2.12)**.

2.3.5.3 Retroviral transduction to yield reporter stable and inducible gene-expressing cell lines

NTERT **(Section 2.1.3)** and SINEG2, SINCE, NTEG2 cells were further transduced according to **Section 2.3.5.1** with the retrovirus **(see Section 2.3.1, Figure 2.2B)**, encoding pSIN-OT-Luciferase (pSIN-OT-Luc) plasmid, prepared as described in **Section 2.3.4**, to produce reporter stable (N/TERT-OTLuc, SINEG2-OTLuc, SINCE-OTLuc respectively) or inducible (NTEG2-OTLuc) cell lines **(see Section 2.1.7)** to either be used in experiments or to be cryopreserved **(Section 2.1.10)**.

2.4 Antibiotic selection

Antibiotics are commonly used for the selection of cells transfected or transduced with a plasmid containing a selectable marker. In this study, Geneticin (G418) and Hygromycin B (Hygro B) were the antibiotics of choice for the generation of NTEG2 inducible cell line. The former G418 is an aminoglycoside antibiotic and acts by blocking the polypeptide synthesis (protein synthesis) by inhibiting the elongation step in prokaryotic (i.e. bacteria) and eukaryotic cells. Hygromycin B is also an aminoglycoside antibiotic that kills both prokaryotic and eukaryotic cells by interfering with translocation and causing mistranslation at the 70S ribosome and thus inhibits protein synthesis. Optimal concentration for resistant clones selection in mammalian cells depends on the cell line used as well as on the plasmid carrying the resistance gene, therefore antibiotic titration should be done to find the best condition for every experimental system. The pRevTet-Off (Clontech Laboratories, Palo Alto, CA) plasmid, which was used to yield the founder cell line NT-TetOff carries the G418 resistance gene (Neomycin) **(Section 2.3.5.2)**. The founder cell line was then transduced with the

expression vector pRevTRE-CMV-EGFP-GLI2ΔN (RevTRE response plasmid) which carries the Hygromycin B resistance gene, to yield the NTEG2 inducible cell line **(Section 2.3.5.2)**.

Therefore, different concentrations of Geneticin (G418) and Hygromycin B (Hygro B) antibiotic selection were used in N/TERT keratinocytes, in order to identify the optimal concentration for selection of NTEG2 cells. N/TERT cells were seeded at $2x10^5$ cells per 10 cm dish and cultured in 10 ml RM+ normal growth medium per 10 cm dish and incubated overnight at 37°C in a humidified atmosphere of 10% (v/v) CO_2/90% (v/v) air (six 10 cm dishes for G418 selection and six 10 cm dishes for Hygromycin B selection). The next day, bright-field pictures using a light microscope **(Section 2.2)** were taken from each 10 cm dish and then different doses 0, 50, 100, 200, 400, 800 μg/ml of G418 (50 mg/ml stock solution) **(Appendix I)** or Hygro B (50 mg/ml stock solution) **(Appendix I)** were added in cells (Day 0 selection). Cells were incubated at 37°C in a humidified atmosphere of 10% (v/v) CO_2/90% (v/v) air for 8 days, replacing the selection medium every 4 days. The 10 cm dishes were examined every two days for viable cells and bright-field pictures using a light microscope **(Section 2.2)** were taken on Day 3, 5 and 8. The minimum antibiotic concentration that induced massive cell death after 3 days and total cell death after 8 days was chosen for antibiotic selection of NTEG2 inducible cell line (500 μg/ml for G418 **(Appendix I)** and 100 μg/ml for Hygromycin B **(Appendix I)**). NTEG2 cells cultured in the presence of Doxycycline were usually selected for 8-11 days and were then passaged **(Section 2.1.8)** and cultured in maintenance medium RM+ complete medium containing 250 μg/ml of G418 **(Appendix I)** and 50 μg/ml of Hygromycin B **(Appendix I)**, in presence of Doxycycline **(Section 2.1.6 and Section 2.5)**.

2.5 Doxycycline optimisation

Doxycycline (Dox) is a member of the tetracycline antibiotics, which is commonly used as a broad spectrum antibiotic to treat wide range of infections such as bacterial infections and thus it kills only prokaryotic cells. Doxycycline is part of a class of drugs called tetracyclines. It decreases bacteria's ability to make protein, necessary for their

survival. This activity does not directly kill the bacteria, but it does inhibit their growth and multiplication, which gives the immune system a chance to fight the infection. Therefore, tetracycline antibiotics are protein synthesis inhibitors, inhibiting the binding of aminoacyl-tRNA to the mRNA-ribosome complex, by binding to the 30S ribosomal subunit in the mRNA translation complex.

In this study, doxycycline was used to activate the CMV constitutive promoter and consequently, the expression of EGFP-GLI2ΔN transgene in NTEG2 keratinocytes **(Section 2.3.5.2)**. Pilot experiments were carried out, in order to optimise the concentration of doxycycline which provides the best ratio of induction/suppression of EGFP-GLI2ΔN expression, without inducing any cytotoxic effects **(see Section 2.7.1.1)** on the NTEG2 cell line.

Initially, NTEG2 cells were grown in the absence of doxycycline (Dox) for 48 or 72 hours, for transgene induction, at 37^{o}C in a humidified atmosphere of 10% (v/v) CO_2/90% (v/v) air. Next, equal densities of 1x10^5 and 2.0 x10^4 cells per 6 cm dish, were seeded in two sets respectively, each set consisting of four 6 cm dishes (two sets of four 6 cm dishes; a total of eight 6 cm dishes containing 5 ml RM+ growth medium per dish) and incubated at 37^{o}C in a humidified atmosphere of 10% (v/v) CO_2/90% (v/v) air. Each set also contained four 6 cm control dishes with two negative (N/TERT wild-type cells to acquire background fluorescence levels) and two positive (NTEG2 cells cultured in the absence of Dox for transgene induction) controls. These two sets (four samples plus four control dishes each set) were going to be used for the investigation of transgene expression/suppression in two different time points (8 dishes total were needed for the 48 hours time-point and another 8 dishes were needed for the 5 days time-point). Next, cells (except controls) were grown in the presence of different Dox **(Appendix I)** concentrations (1, 100, 1000, 10000 ng/ml) for 48 hours and 5 days. All cells had their growth medium replaced every two days. EGFP-GLI2ΔN suppression by doxycycline was investigated by detecting the EGFP-GLI2ΔN expression (green fluorescence) through flow cytometry analysis **(see Section 2.8)** after 48 hours (1st set) and 5 days (2nd set).

Initially, NTEG2 cells were grown in the absence of doxycycline (Dox) for 48 or 72 hours, for transgene induction, at 37^{o}C in a humidified atmosphere of 10% (v/v)

CO_2/90% (v/v) air. Next, equal densities of $1x10^5$ and 1.5 - 3.0 $x10^5$ cells per 10 cm dish, were seeded in two sets respectively, each set consisting of six 10 cm dishes (two sets of six 10 cm dishes; a total of twelve 10 cm dishes containing 10 ml RM+ growth medium per dish) and incubated at 37°C in a humidified atmosphere of 10% (v/v) CO_2/90% (v/v) air. These two sets were going to be used for the investigation of transgene expression/suppression in two different time points (6 dishes were needed for the 48 hours time-point and another 6 dishes were needed for the 5 days time-point). The same or the next day of plating, cells from both sets were treated with different concentrations of Dox (40 ng/ml, 1 μg/ml, 10 μg/ml) **(Appendix I)**, in duplicates for each concentration. The cells were then allowed to grow for either 24 or 48 hours in the presence of varying Dox concentrations. Following the 24 or 48 hours incubation, Dox was removed **(see Section 2.1.6)** only from one replicate for each concentration of each set, so that each set would have one series of cells cultured in different concentrations of Dox (3 dishes) and one series of cells cultured without Dox (another 3 dishes). At this point therefore, both sets are identical and have been treated similarly. Then, cells of each set were allowed to grow for another 48 hours (1^{st} set of cells; 48 hour time-point) or for another 5 days (2^{nd} set of cells; 5 day time-point). All cells had their growth medium replaced every two days. The 1^{st} set of samples, which contained one series of cells (3 dishes) cultured in varying Dox concentrations for a total of 3-4 days (depending on the time of initial incubation in Dox) and another series of cells (3 dishes) cultured in the absence of Dox for a total of 48 hours, were all harvested for total cell protein extraction **(see Section 2.12.1)** (named as 48 hour time-point), followed by western blot analysis **(see Section 2.12.5)**. The 2^{nd} set of samples, which contained one series of cells (3 dishes) cultured in varying Dox concentrations for a total of 6-7 (depending on the time of initial incubation in Dox) days and another series of cells (3 dishes) cultured in the absence of Dox for a total of 5 days, were all harvested for total cell protein extraction **(see Section 2.12.1)** (named as 5 day time-point), followed by western blot analysis **(see Section 2.12.5)**. The time points were named after the period of time that had passed after transgene induction (removal of Dox), since NTEG2 cells were otherwise normally maintained in Dox containing medium.

2.6 Rhodamine staining

Rhodamine B is a red/violet staining dye with strong orange fluorescence (emission at 625 nm) that is used as a histopathological stain for cornification and keratinisation, and is therefore a valuable marker of epidermal keratinocytes *in vitro* (Liisberg, 1968). N/TERT, SINCE, and SINEG2 keratinocytes were stained with Rhodamine B in order to visualise the colony forming ability and colony morphology of each cell line in culture (Barrandon & Green, 1987).

N/TERT, SINCE, and SINEG2 keratinocytes were seeded at $8x10^4$ cells per well of a 6-well plate in 2 ml RM+ culture medium per well and incubated at 37^oC in a humidified atmosphere of 10% (v/v) CO_2/90% (v/v) air. Cells were allowed to grow until N/TERT and SINCE controls reached confluence (6-8 days) and medium was replaced every two days. Keratinocytes were washed 1x in 1x PBS **(Appendix I)** and were immediately fixed with 1 ml of 4% (v/v) Formaldehyde/Formalin (Fisher, Leicestershire, UK) solution **(Appendix I)** per well, for 20 minutes at room temperature. The cells were then washed 2x in 1x PBS **(Appendix I)** and were stained with 2 ml Rhodamine B (Sigma-Aldrich, Dorset UK) solution (1x PBS **(Appendix I)** containing 1% (w/v) Rhodamine B (Sigma-Aldrich, Dorset UK); 1 g Rhodamine B in 100 ml 1x PBS) per well, for 30 minutes at room temperature. The cells were then thoroughly washed with dH_2O many times until all background staining was washed and only keratinocyte colonies were visible. Plates were then left at room temperature to completely dry prior to digitally capturing bright field images using Autochemi imaging system (UVP, Upland, CA). The plates were finally stored at room temperature.

2.7 Cytotoxicity and proliferation assays

2.7.1 Alamar Blue^{TM} assay

The Alamar Blue assay is very quick and sensitive method for detecting cellular viability and proliferation (Fields & Lancaster, 1993; Ahmed et al., 1994). Alamar Blue reagent gives a measure of viability and cell proliferation by detecting the level of reduction (gain of electrons) - oxidation (loss of electrons) (REDOX indicator) cycles

(chemical reactions in mitochondria - Krebs cycle) during cellular respiration, which is carried out by specific enzymes in growing metabolically active, healthy cells. Alamar Blue (electron acceptor) can be reduced by the whole range of the electron transport chain (electron donors) FMNH2, FADH2, NADH, NADPH and cytochromes, and is thus an excellent detector of reduction of all the elements of the electron transport chain. As cells being tested grow, innate metabolic activity results in a chemical reduction of Alamar Blue. Continued cell growth maintains a reduced environment, while inhibition of cell growth maintains an oxidized environment. Reduction related to cell growth causes the REDOX indicator (Alamar Blue) to change from oxidized (non-fluorescent, blue) form to reduced (fluorescent, red) form.

Alamar Blue is a safe, nontoxic aqueous dye that is used to assess both cell viability and cell proliferation. For cell viability assessment, the innate metabolic activity of cells can be monitored with Alamar Blue, since in the presence of added toxic compounds such as antimicrobial agents, this innate metabolic activity ceases. Due to the fact that Alamar Blue is soluble, stable in culture medium, non-toxic, and does not alter the viability of cells cultured for various times, the continuous monitoring of cells in culture is permitted and therefore cell proliferation assessment is allowed. Furthermore, Alamar Blue does not interfere with the reactions of the electron transport chain and cells remain unaffected by its presence.

The reduction of Alamar Blue yields a colorimetric change **(Section 2.12.4.2)** and a fluorescent signal **(Section 2.8.1.1)**, which can be detected either through measuring the optical density of the solution (absorbance at 544 nm) using a spectrophotometer or a microplate reader **(Section 2.12.4.1)**, or by detecting the fluorescent signal emitted at 590 nm, following excitation at 544 nm using a microplate reader, respectively.

2.7.1.1 Cytotoxicity

N/TERT cells were seeded in 6 cm dishes ($6.5x10^4$ cells/dish) in 1 ml RM+ culture medium per well and incubated at 37^{o}C in a humidified atmosphere of 10% (v/v) CO_2/90% (v/v) air. When the cells attached to the dishes, Alamar Blue^{TM} (Biosource^{TM}, Invitrogen, Paisley, UK) solution was prepared (RM+ medium containing 10% (v/v) Alamar Blue^{TM}) 18 ml RM+ medium + 2 ml Alamar Blue^{TM} (Biosource^{TM}, Invitrogen,

Paisley, UK) = 20 ml total). The medium was aspirated from the wells and 5 ml Alamar Blue™ solution were added in each dish. Cells were incubated for 6 h at 37°C in a humidified atmosphere of 10% (v/v) CO_2/90% (v/v) air (Day 0). Following the incubation, 100 µl of the target cell medium was obtained and added in each well of an opaque, flat bottomed 96-well microtiter white plate (Nunc, Roskilde, Denmark). Alamar Blue™ (Biosource™, Invitrogen, Paisley, UK) reduction (fluorescence) was read on a FLUOSTAR OPTIMA microplate reader (BMG LABTECH, Aylesbury, UK) at 544 excitation wavelength and at 590 nm emission wavelength. Next, medium containing the Alamar Blue™ (Biosource™, Invitrogen, Paisley, UK) was aspirated and cells were refed with fresh normal growth medium (RM+) containing different doses of Doxycycline **(Appendix I)** in each 6 cm dish (0, 1, 10, 100, 1000, 10000 ng/ml). Duplicates were prepared for each different concentration and also duplicates of medium with or without dox, without any cells, were also used as controls for background fluorescence. The measurements were repeated once after 48 h (Day 2) and once after five days (Day 5) and cytotoxicity mediated by doxycycline was measured by the rate of Alamar Blue™ (Biosource™, Invitrogen, Paisley, UK) reduction, which is quantified by fluorescence emission and directly reflects the amount of viable cells in culture. For each sample, the mean value of controls for background fluorescence was subtracted from all the values of all the different time points. In addition, for each sample, all the values for all the different time points were subtracted from the mean value of Day 0.

2.7.1.2 Proliferation

N/TERT, SINCE, SINEG2 cells were seeded in 12-well plates ($2.5x10^4$ cells/well) in 1 ml RM+ culture medium per well and incubated overnight at 37°C in a humidified atmosphere of 10% (v/v) CO_2/90% (v/v) air. The next day, the medium was aspirated from the wells and Alamar Blue™ (Invitrogen, Paisley, UK) solution was prepared (RM+ medium containing 10% (v/v) Alamar Blue™) 18 ml RM+ medium + 2 ml Alamar Blue™ (Biosource™, Invitrogen, Paisley, UK) = 20 ml total) and 1 ml was added in each well. Cells were incubated for 6 h at 37°C in a humidified atmosphere of 10% (v/v) CO_2/90% (v/v) air (Day 0). Following the incubation, 100 µl of the target cell medium was obtained and added in each well of an opaque, flat bottomed 96-well microtiter white plate (Nunc, Roskilde, Denmark). Alamar Blue™ (Biosource™,

Invitrogen, Paisley, UK) reduction (fluorescence) was read on a FLUOSTAR OPTIMA microplate reader (BMG LABTECH, Aylesbury, UK) at 544 excitation wavelength and at 590 nm emission wavelength. Next, medium containing the Alamar Blue™ (Biosource™, Invitrogen, Paisley, UK) was aspirated and cells were refed with fresh normal growth medium (RM+). Six replicate samples were prepared for each cell line and also six replicate samples of medium without cells were also used as controls for background fluorescence. The measurements were repeated once everyday for seven days. The cell growth rate was measured by the rate of Alamar Blue™ (Biosource™, Invitrogen, Paisley, UK) reduction, which is quantified by fluorescence emission and directly reflects the amount of viable cells in culture. For each cell line, the mean value of controls for background fluorescence was subtracted from all the values of all the different time points. In addition, for each cell line, the mean value of Day 0 was subtracted from all the values of all the different time points.

Samples were analysed in six replicates and statistical analysis was performed using the Microsoft Excel's software for student's *t* test analysis **(see Section 2.16)**.

2.7.2 MTT assay

The MTT (3-(4,5-dimethylthiazol-2-yl)-2,5-diphenyl tetrazolium bromide) assay is a method for detecting cellular viability and proliferation and is a rapid colorimetric analysis **(Section 2.12.4.2)** of mitochondrial reductase activity in metabolically active cells (Mosmann, 1983). The MTT is a yellow tetrazolium salt (synthetic organic heterocyclic compound) that is reduced to a purple formazan (formazans are artificially formed chromogenic products as a result of tetrazolium salt reduction) in the mitochondria of actively growing cells. MTT reagent gives a measure of viability and cell proliferation by detecting the level of reduction (gain of electrons) - oxidation (loss of electrons) (REDOX indicator) cycles (chemical reactions in mitochondria - Krebs cycle) during cellular respiration, which is carried out by specific enzymes in growing metabolic active, healthy cells. MTT (electron acceptor) can be reduced by the electron donors of the electron transport chain, FMNH2, FADH2, NADH, and NADPH but not by cytochromes. As cells being tested grow, innate metabolic activity results in a chemical reduction of MTT. Continued cell growth maintains a reduced environment,

while inhibition of cell growth maintains an oxidized environment. Reduction related to cell growth causes the REDOX indicator (MTT) to change from oxidized (yellow tetrazolium salt) form to reduced (purple formazan) form. This reduction takes place only when mitochondrial reductase enzymes are active, and therefore conversion can be directly related to the number of viable cells. The purple formazan crystals are insoluble to aqueous solutions and are therefore solubilised by the addition of isopropanol or by a mixture of isopropanol : DMSO. The absorbance of the final coloured solution is directly proportional to the percentage of actively growing cells in a given sample, and can be spectrophotometrically quantified at 500-600 nm in a spectrophotometer or a standard microplate reader **(Section 2.12.4.1)**. In contrast to Alamar Blue, MTT is highly toxic to the cells and therefore it is not possible to use the same cells throughout a time course proliferation experiment. Thus, the same number of cells needs to be plated separately for each additional time point.

N/TERT, SINCE and SINEG2 cells were seeded at $1.3x10^4$ cells per well of seven separate (one for each time point) 24-well plates in 500 µl RM+ culture medium per well and incubated overnight at 37^{o}C in a humidified atmosphere of 10% (v/v) CO_2/90% (v/v) air. Additionally, three separate 24-well plates (each of them containing six wells for each time point) containing only 500 µl RM+ culture medium per well without cells were prepared and incubated overnight at 37^{o}C in a humidified atmosphere of 10% (v/v) CO_2/90% (v/v) air. The next day, MTT (Sigma-Aldrich, Dorset, UK) solution was prepared (RM+ medium containing 10% (v/v) of MTT stock solution 5 mg/ml) **(Appendix I)** (18 ml RM+ medium + 2 ml from 5 mg/ml MTT (Sigma-Aldrich, Dorset, UK) = 20 ml total). The culture media was aspirated from the wells of one 24-well plate containing cells from each cell line and also from another 24-well plate containing six replicate samples of medium without cells and 500 µl of MTT solution **(Appendix I)** was added to each well and incubated for 2 h at 37°C in a humidified atmosphere of 10% (v/v) CO_2/90% (v/v) air (Day 0). Medium was replaced to the remaining 24-well plates, which were further incubated at 37^{o}C in a humidified atmosphere of 10% (v/v) CO_2/90% (v/v) air. The MTT solution was then aspirated and 500 µl of isopropanol (Fisher, Leicestershire, UK) was added to each well to dissolve the formazan crystals. The 24-well plate was briefly shaken and the isopropanol solution was mixed thoroughly by pipetting to ensure complete solubilisation of the crystals. 100 µl of the solution from each well was transferred to a well of a clear, flat

bottomed 96-well plate (Nunc, Roskilde, Denmark). The absorbance (optical density) was measured at 560 nm, using a 96-well microplate reader (FLUOSTAR OPTIMA microplate reader, BMG LABTECH, Aylesbury, UK). Six replicate samples were prepared for each cell line for each time-point and also six replicate samples of medium without cells were prepared for each time-point and were used as controls for background absorbance. The measurements were repeated once everyday for seven days and medium was replaced every two days in the remaining 24-well plates. The cell growth rate was measured by the rate of MTT (Sigma-Aldrich, Dorset, UK) reduction, which is quantified by absorbance (optical density) and directly reflects the amount of viable cells in culture. For each cell line, the mean value of controls for background absorbance was subtracted from all the values of all the different time points. In addition, for each cell line, the mean value of Day 0 was subtracted from all the values of all the different time points.

Samples were analysed in six replicates and statistical analysis was performed using the Microsoft Excel's software for student's *t* test analysis **(see Section 2.16)**.

2.7.3 Population Doublings

In contrast to Alamar Blue and MTT proliferation assays which give an indication of the amount of viable cells, solely depending upon of a cell's intrinsic metabolic activity and therefore its ability to reduce chemical reagents, assessing the number of population doublings (PD) allows the identification of the number of times the cell population doubles in number, during the course of culture. Therefore, the calculation of population doublings of cells in culture provides an estimation of the number of times that a cell is doubled (divides) with a specified amount of time. In cases of primary human cells, the PD is mainly used to estimate the total life-span of cells in culture since growth ceases after a limited amount of cell divisions (Rheinwald et al., 2002). However, in immortalised cells lines such as N/TERT, PD calculation provides useful information about the speed and consistency of cell division throughout a period of time (growth potential of cells).

To measure the cumulative population doublings over a period of time, N/TERT, SINCE and SINEG2 keratinocytes were initially plated at $1x10^5$ or $2x10^5$ per 6 cm dish in 5 ml RM+ growth medium and incubated at 37°C in a humidified atmosphere of 10% (v/v) CO_2/90% (v/v) air (Day 0). After 4 days (~ 60-80% confluent), cells were washed once with 1x sterile PBS (PAA, Somerset, UK) and then trypsinised until all the cells had detached **(see Section 2.1.8)**. The trypsin reaction was inhibited by transferring the trypsinised cells to 50 ml falcon tubes containing complete RM+ growth medium at a ratio of 1:1 (v/v) trypsinised cells to RM+ culture medium. Cells were then centrifuged at 1,000 rpm for 5 minutes and were counted using the CAsy® Cell Counter **(see Section 2.1.9.2)** (Day 4). Cells were then re-plated at $1x10^5$ or $2x10^5$ per 6 cm dish in 5 ml RM+ growth medium and were allowed to grow for another 4 days at 37°C in a humidified atmosphere of 10% (v/v) CO_2/90% (v/v) air (Day 4). Next cells were washed, trypsinised, counted and replated following the same procedure as described above (Day 8). The procedure of re-plating and counting was performed every 4 days for a total period of 16 days.

Keratinocyte population doublings were calculated as follows: **$PD = 3.32 \times [\log_{10}(N1) - \log_{10}(N0)]$**, where **N1** = total yield (total output) and **N0** = initial number of seeded keratinocytes. For example, if N1 = $1x10^6$ and N0 = $2x10^5$, then the population doublings that these cells have undergone is PD = 2.32. This means that each cell will have doubled on average 2.32 times during the incubation period. Therefore, all PD values were individually collected (once every 4 days) and were used cumulatively. For example, if the PD value for the first 4 days incubation (Day 4) was PD = 2.32 and then for the second incubation period (another 4 days) (Day 8) was PD = 3.3, then the cumulative PD value is PD = 2.32 + 3.3, PD = 5.62 for a total time of 8 days, that is each cell has doubled, on average, 5.62 times during a total period of 8 days.

2.8 Flow Cytometry (FCM) Analysis and Fluorescent Activated Cell Sorting (FACS)

2.8.1 Flow cytometry

Flow cytometry is a powerful technique for the analysis of multiple parameters of individual cells within heterogeneous populations. Flow cytometers are used in a range of applications from immunophenotyping, to ploidy and cell cycle analysis, to cell counting and GFP (green fluorescent protein) expression analysis and to detection of apoptosis. The flow cytometer performs this analysis by passing thousands of cells per second through a laser beam and capturing the light and colour discriminated fluorescence that emerges from each cell as it passes through. The data gathered can be analysed statistically by flow cytometry software to report cellular characteristics such as size, internal complexity, phenotype, and health. Thus, analysis and differentiation of the cells is based on size and granularity and whether the cell is carrying fluorescent molecules (fluorochromes) either in the form of antibodies or dyes (cell surface (i.e. receptors) or intracellular (i.e. DNA) epitope detection)
(http://probes.invitrogen.com/resources/education/tutorials/),
(http://www.icms.qmul.ac.uk/flowcytometry/flowcytometry/).

2.8.1.1 Fluorochromes

Fluorochromes/fluorophores (i.e. FITC - fluorescein isothiocyanate, PI - propidium iodide, Cy5 - cyanine 5, Hoechst-33342, DAPI - 4',6-diamidino-2-phenylindole, GFP - green fluorescent protein, EGFP - enhanced green fluorescent protein) are essentially dyes or proteins, which accept light energy (i.e. from a laser or lamp) at a given wavelength and re-emit it at a longer wavelength. These two processes are called excitation and emission respectively. The process of emission follows extremely rapidly, commonly in the order of nanoseconds, and is known as fluorescence. Light is a form of electromagnetic energy that travels in waves. These waves have both frequency and length, the latter of which determines the colour of light. The light that can be visualized by the human eye represents a narrow wavelength band (380-700 nm) between ultraviolet (UV) and infrared (IR) radiation. Red light is at the longer wavelength end (lower energy) and violet light at the shorter wavelength end (higher

energy). When light is absorbed by a fluorochrome (absorption), its electrons become excited and move from a resting state to a maximal energy level called the 'excited electronic singlet state'. The amount of energy required will differ for each fluorochrome and is depicted as $E_{excitation}$. This state only lasts for 1-10 nanoseconds because the fluorochrome undergoes internal conformational change and, in doing so, releases some of the absorbed energy as heat. The electrons subsequently fall to a lower, more stable, energy level called the 'relaxed electronic singlet state'. As electrons steadily move back from here to their ground state they release the remaining energy ($E_{emission}$) as fluorescence. The energy in the emitted light is dependent on the energy level to which the fluorophore is excited, and that light has a specific wavelength, and, consequently, a specific fluorescence colour (i.e. FITC fluorochrome; laser excitation at 488 nm, maximum absorbance 490 nm - blue colour, maximum emission 525 nm - green fluorescence colour)
(www.abdserotec.com/uploads/Flow-Cytometry.pdf).

2.8.1.2 Flow cytometer

The flow cytometer **(Figure 2.3)** consists of the fluidic system, a light source, collection optics (lenses, filters, mirrors), electronics and a computer to translate signals to data (www.abdserotec.com/uploads/Flow-Cytometry.pdf),
(http://probes.invitrogen.com/resources/education/tutorials/),
(http://www.icms.qmul.ac.uk/flowcytometry/flowcytometry/).

The fluidic system (flow cell, nozzle) **(Figure 2.3)**, carries and aligns the initially randomly distributed cells so that they pass single file through the light beam for sensing (through the interrogation point, where the laser and the sample intersect and the optics collect the resulting scatter and fluorescence), and takes away the waste. For accurate data collection, it is important that particles or cells are passed through the laser beam one at a time. Most flow cytometers accomplish this by injecting the sample stream containing the cells (central channel/core) into a flowing stream of sheath fluid (an outer sheath that contains faster flowing fluid). Thus, the sample stream becomes compressed to roughly one cell in diameter and this effect is called hydrodynamic focusing. When the sample leaves the flow cell the stream is in laminar flow in air. The lasers **(Figure 2.3)** are the light source for scatter and fluorescence. The light source of

choice, the laser (more than one lasers can be used simultaneously), emits coherent light at a specified wavelength (i.e. 480 nm) and as a cell passes through the laser, it will refract or scatter light at all angles. The optics (lenses, filters, mirrors) **(Figure 2.3)**, gather and direct this light. Thus, scattered light is focused through, and collected by, two lenses, one set in front of the light source (forward scatter channel (FSC)) and one set at right angles (side scatter channel (SSC)), which direct the light to the appropriate detectors (receive the light) **(Figure 2.3)**. Therefore, forward scatter, is the amount of light that's scattered in the forward direction as laser light strikes the cell, and is roughly proportional to the cell size, while light scattering at larger angles, for example to the side, depends on the granularity and the inner structural complexity inside the cell (i.e., shape of the nucleus, the amount and type of cytoplasmic granules or the membrane roughness).

Flow cytometers use separate fluorescence (FL-) channels to detect light emitted. The emitted fluorescent light, coming from labelled cells (i.e. FITC, PE) as they pass through the laser, travels along the same path as the side scatter signal and it is directed through a series of filters/mirrors (optics), which block certain wavelengths by absorption, while transmitting (passing) others, so that particular wavelength ranges are delivered to the appropriate detectors (controlled specificity of detection) **(Figure 2.3)**. When a filter is placed at a 45^{o} angle to the oncoming light it becomes a dichroic filter/mirror. This type of filter performs two functions, first, to pass specified wavelengths in the forward direction and, second, to deflect blocked light at a 90^{o} angle **(Figure 2.3)**.

Finally, through the electronics and the peripheral computer system, the signals from the detectors are converted into digital data and the necessary analysis is performed **(Figure 2.3)**. When light hits a photodetector, a small current (a few microamperes) is generated and thus is translated into a voltage pulse which is proportional to the total number of light photons received by the detector. This voltage is then amplified by a series of electronics into electrical signals large enough (5-10 volts) to be plotted graphically. The measurement from each detector is referred to as a 'parameter' i.e. forward scatter, side scatter or fluorescence and the data acquired in each parameter are known as the 'events' and refer to the number of cells displaying the physical feature or marker of

interest. The data generated by flow-cytometers can be plotted in a single dimension, to produce a histogram, or in two-dimensional (2D) dot plots.

These data can give information for the physical characteristics and the fluorescence intensity of cells. Because small cells produce a small amount of forward scatter and large cells produce a large amount of forward scatter, the magnitude of the voltage pulse recorded for each cell is roughly proportional to the cell size. Similarly, cells with low internal complexity produce a small amount of side scatter and cells with high internal complexity produce a large amount of side scatter, and therefore the magnitude of the voltage pulse recorded for each cell is roughly proportional to the internal complexity of the cell. In addition, fluorescence data is collected generally in the same way as forward and side scatter data. In a population of labelled cells, some will be brighter than others. As each cell crosses the path of the laser, a fluorescence signal is generated which is directed to the appropriate detector, where it is translated into a voltage pulse proportional to the amount of fluorescence emitted (fluorescence intensity).

Both FSC and SSC are unique for every cell, and a combination of the two (two-dimensional dot plots) may be used to differentiate different cell types in a heterogeneous sample (gate cells according to physical characteristics), such as in a typical whole blood cell analysis. The different physical properties of lymphocytes, which are small cells possessing low internal complexity; monocytes which are medium-sized cells with slightly more internal complexity, and neutrophils and other granulocytes which are large cells that have a lot of internal complexity, allow them to be distinguished from each other. Moreover, FSC and SCC data analysis may be used to eliminate results from unwanted particles (gating) i.e. dead cells, clumps and debris. For instance, subcellular debris and clumps can be distinguished from single cells by size, estimated by forward scatter, while dead cells have lower forward scatter and higher side scatter than living cells.

All Flow Cytometry analytical runs in my study were performed on a BD LSRII fitted with a Blue Argon Laser 488 nm, violet diode 405 nm, red diode 633 nm and a UV laser 325 nm (BD Biosciences, San Jose, CA), using the BD FACSDiva Software (BD Biosciences, San Jose, CA), by Gary Warnes at FACS Lab, Institute of Cell and

Molecular Science, Barts and the London Queen Mary's School of Medicine and Dentistry, Whitechapel, London, UK.

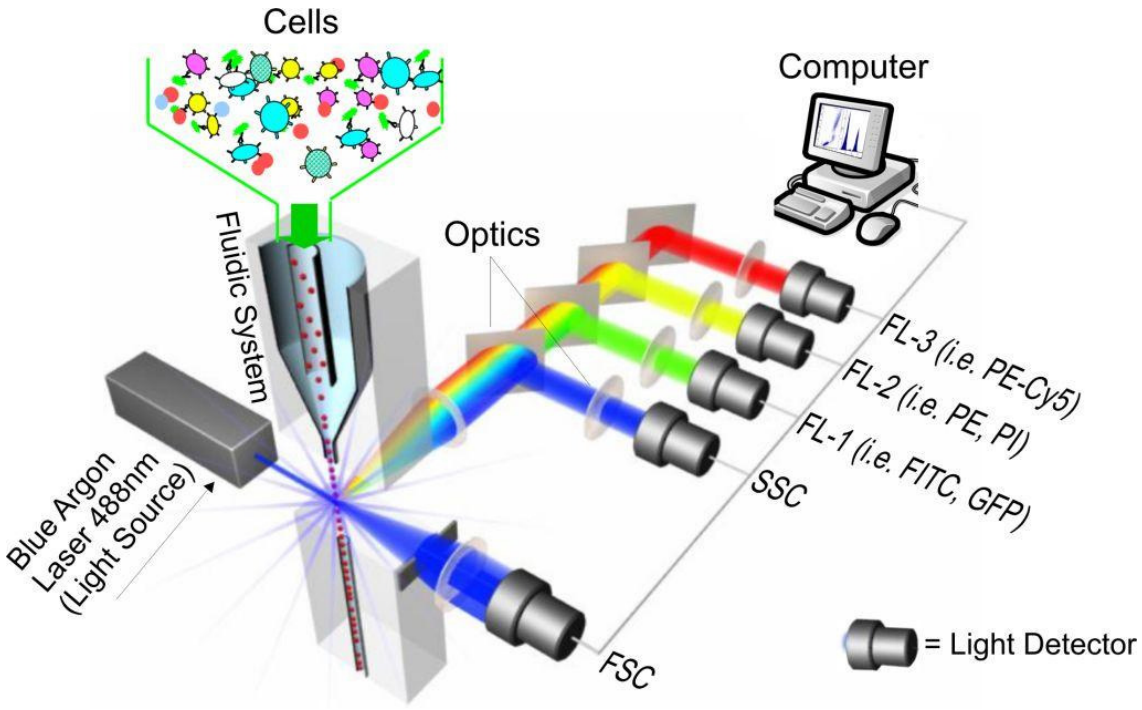

Figure 2.3: Primary systems of the flow cytometer.

The primary systems of the flow cytometer are: the fluidic system, which presents samples to the interrogation point and takes away the waste; the lasers, which are the light source for scatter and fluorescence; the optics (lenses, filters, filter/mirrors), which gather and direct the light; the detectors, which receive the light; and, the electronics and the peripheral computer system, which convert the signals from the detectors into digital data and perform the necessary analysis. **FSC**, Forward Scatter Channel; **SSC**, Side Scatter Channel; **FL-1**, Fluorescence-1 channel; **FL-2**, Fluorescence-2 channel; **FL-3**, Fluorescence-3 channel; **FITC**, fluorescein isothiocyanate; **GFP**, Green Fluorescent Protein; **PE**, phycoerythrin; **PI**, propidium iodide; **PE-Cy5**, phycoerythrin Cy (cyanine) 5). Modified from

http://probes.invitrogen.com/resources/education/tutorials/

www.abdserotec.com/uploads/Flow-Cytometry.pdf

https://www1.imperial.ac.uk/.../flow/flowcytometrycourse/lectures/

www1.ic.ac.uk/resources/A9F73252-D531-4631-A768-F14356B9E9E1/

2.8.1.3 Hoechst-33342 staining and flow cytometry

Hoechst-33342 (Sigma-Aldrich, Dorset, UK) is a fluorescent DNA (nucleic-acid) dye, that intercalates into the minor groove of double-stranded DNA and binds preferentially to A (Adenine) - T (Thymine) base pairs (Shapiro, 1981a; Shapiro, 1981b). In contrast to DAPI and to PI, Hoechst-33342 (Sigma-Aldrich, Dorset, UK) has an additional ethyl group which renders it more lipophilic and thus more able to cross intact cell membranes. Therefore, cells do not require permeabilisation for Hoechst-33342 (Sigma-Aldrich, Dorset, UK) staining/labelling and this allows live cell cycle analysis and detection of EGFP fluorescence at the same time (cells expressing EGFP protein or EGFP-GLI2ΔN fused protein). Hoechst-33342 (Sigma-Aldrich, Dorset, UK) fluorescent DNA dye is suitable for flow cytometric analysis because it binds to DNA in a linear manner and thus as DNA content of a cell increases, the fluorescent signal from the DNA dye increases proportionally in a linear manner (Shapiro, 1981a; Shapiro, 1981b). Hoechst-33342 (Sigma-Aldrich, Dorset, UK) is excited at 350 nm and emitted at 461 nm giving a blue fluorescent colour. For that reason a UV laser 325 nm was used for flow cytometry analysis and fluorescence was detected at 440 nm using the UV 440/40 nm channel on the BD LSRII (BD Biosciences, San Jose, CA). EGFP (enhanced green fluorescent protein, a mutant derivative of green fluorescent protein (GFP)) is a protein which exhibits bright green fluorescence when exposed to blue light. EGFP is excited at 488 nm and emitted at 509 nm giving a green fluorescent colour, similar to FITC (fluorescein isothiocyanate) which is excited at 490 nm and emitted at 525 nm. For that reason, a Blue Argon laser 488 nm was used for flow cytometry analysis and fluorescence was detected at 530 nm, using the FITC 440/40 nm channel on the BD LSRII (BD Biosciences, San Jose, CA).

For Hoechst-33342 (Sigma-Aldrich, Dorset, UK) staining, equal number $1x10^6$ or $6x10^5$ of N/TERT, SINCE, and SINEG2 cells were seeded in 10 cm dishes, and harvested either 24 or 48 hr after plating, respectively (~ 60% confluent). Similarly, equal number $3x10^5$ or $1x10^5$ of N/TERT and NTEG2 cells were seeded in 10 cm dishes, and harvested either 72 hr or 6 days after plating, respectively (~ 60% confluent) (48 hr or 5 days after doxycycline removal respectively). Doxycycline was removed in NTEG2 cells 24 hr after plating (NTEG2 Dox-).

Cells were washed once with 1x sterile PBS (PAA, Somerset, UK) and then trypsinised until all the cells had detached **(see Section 2.1.8)**. The trypsin reaction was inhibited by transferring the trypsinised cells to 50 ml falcon tubes containing complete RM+ growth medium at a ratio of 1:1 (v/v) trypsinised cells to RM+ culture medium. Cells were then centrifuged at 1,000 rpm for 5 minutes. After washing each pellet with 10 ml 1x sterile PBS (PAA, Somerset, UK), and centrifuging at 1,000 rpm for 5 minutes, each cell pellet was resuspended in 2 ml 1x sterile PBS (PAA, Somerset, UK) containing 10 μg/ml Hoechst-33342 (Sigma-Aldrich, Dorset, UK) (2 ml 1x sterile PBS + 2 μl 10 mg/ml Hoechst-33342; 1:1000 dilution) **(see Appendix I)**. Resuspended cells were incubated for 1 hr at 37^{o}C in a humidified atmosphere of 10% (v/v) CO_2/90% (v/v) air, and were shaken every 10 minutes. Then, cells were filtered through a 70 μm strainer (BD Falcon Cell strainers, BD Biosciences, San Jose, CA) (minimise doublets and clumps) and were transferred in sterile 5 ml polystyrene round bottom FACS tubes (BD Falcon tubes, BD Biosciences, San Jose, CA), which were kept on ice and were given for flow cytometry analysis, where the same number of events was acquired for each sample (25,000-50,000 events).

Cells stained with Hoechst-33342 (Sigma-Aldrich, Dorset, UK), were analysed both for DNA content and green fluorescence (EGFP) that corresponds to exogenous EGFP protein and EGFP-GLI2ΔN fusion protein. First, a 2D dot plot representing cell size and granularity was created for each sample **(Figure 2.4A)**. This is derived from the Forward (cell size) and Side scatter (granularity) values (FSC versus SSC) and is useful for cell population gating according to physical characteristics of cells (P1) and thus for the exclusion of cell debris as well as of dead cells, which have lower forward scatter and higher side scatter than living cells **(see Section 2.8.1.2)**. Next, a 2D doublet exclusion plot was made for the gated (P1) cells, to distinguish cell clumps, aggregates of G1 cells and G1 cell doublets from G2/M cells for each sample **(Figure 2.4B)**. Doublets of G1 cells have the same DNA content as G2/M cells and in order to distinguish them, the instrument can separate these by measuring the time it takes for the two types of cells to pass through the laser beam by a fluorescent parameter Width (W) measurement. Doublets and aggregates of cells take longer to pass through the laser of the flow cytometer and thus appear higher up on the fluorescent width scale (W) **(Figure 2.4B)**. Therefore the 2D doublet exclusion plot represents the fluorescent Area (A) scale (440/40 nm Ho33342 UV-A(rea)) which is the DNA content according to the

blue fluorescence emitted by Hoechst-33342 dye and the fluorescent Width (W) scale (440/40 nm Ho33342 UV-W(idth)) which is the time it takes for a cell to pass through the laser beam **(Figure 2.4B)**. Thus, cells were gated (P2) using specific values, which correspond to DNA content from 2N up to 16N and only to single cells so that the G2/M population contains only single mitotic cells **(Figure 2.4B)**.

This single cell gate (P2) population of cells was next examined and gated for levels of green fluorescence (EGFP fluorescence) in a 2D (440/40 nm Ho33342 UV-A(rea) - DNA content versus FITC 530/30 nm-A(rea) - EGFP fluorescence) dot plot **(Figure 2.4D)**. Cells are gated as EGFP positive (Q2) or EGFP negative (Q4) depending on the levels of background auto-fluorescence acquired from the analysis of a reference wild-type cell line, in this case N/TERT **(Figure 2.4C)**. Last, for each sample, one-dimensional histograms, representing the relative DNA content of cells (440/40 nm Ho33342 UV-A(rea) - blue fluorescence emitted by Hoechst-33342) and thus the cell cycle profile, were drawn for EGFP positive (Q2) **(Figure 2.4E i)**, EGFP negative (Q4) **(Figure 2.4E ii)**, and for the overall population (P2) **(Figure 2.4E iii)** with gates P3, P4, P5, P6 and P7 gating on G1 (2N), S, G2/M (4N), >4N, 8N respectively. The gating of cells (FSC, SSC, DNA content, doublet exclusion, green fluorescence) were initially acquired using the reference wild-type cell line (N/TERT) and remained constant in subsequent sample analysis.

Samples were analysed either in duplicates or triplicates and statistical analysis was performed using the Microsoft Excel's software for student's *t* test analysis **(see Section 2.16)**.

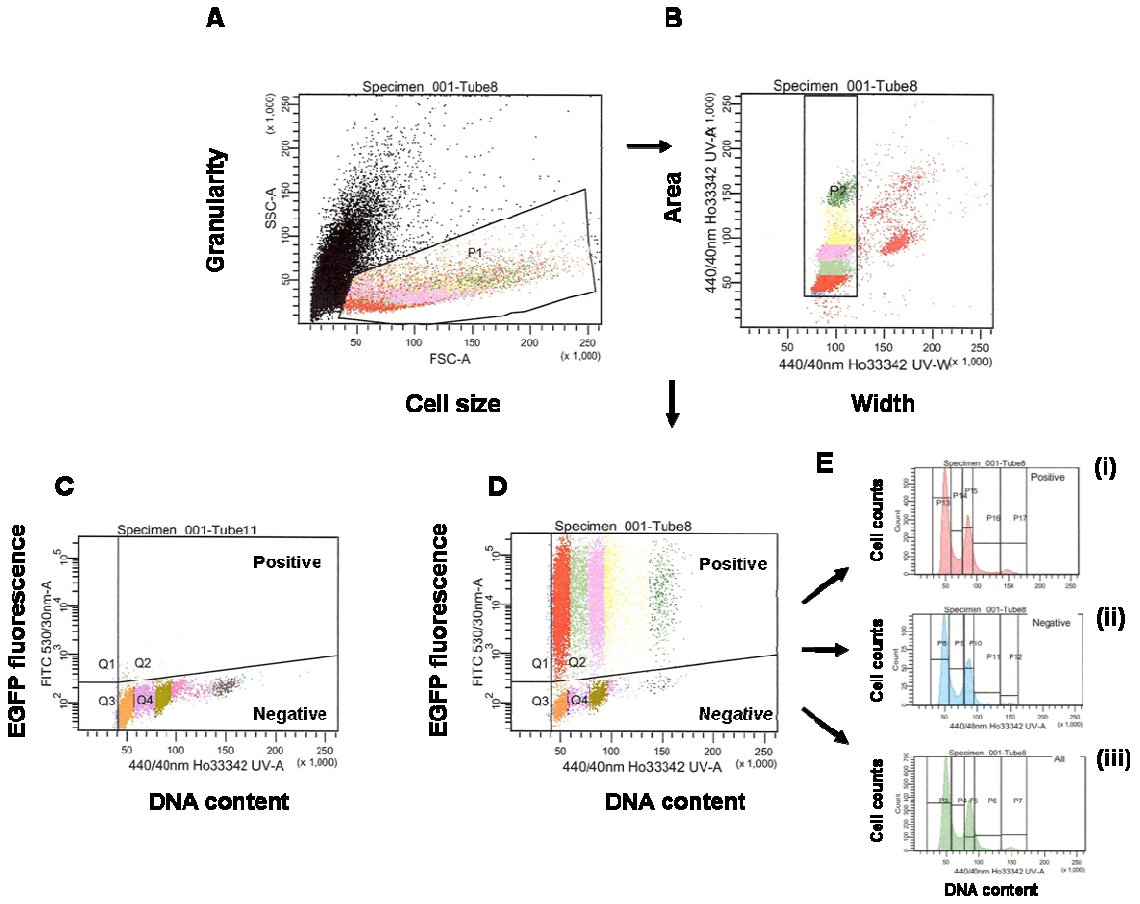

Figure 2.4: Hoechst-33342 live cell cycle analysis and EGFP fluorescence detection.

(A) Initial cell population gating (P1) for each sample is placed on FSC versus SSC (cell size versus granularity) 2D dot plot. Debris and dead cells appear to the left and upwards of healthy cell analysis gate (P1). **(B)** This cell population gate (P1) is then placed on 440/40 nm Ho33342 UV-W(idth) versus 440/40 nm Ho33342 UV-A(rea) (blue fluorescence emitted by Hoechst-33342 representing DNA content versus the time it takes for a cell to pass through the laser beam) 2D dot plot. Doublets and clumps appear to the right of single cell analysis gate (P2). **(D)** This single cell gate (P2) population of cells is then placed on 440/40 nm Ho33342 UV-A(rea) versus FITC 530/30 nm-A(rea) (blue fluorescence emitted by Hoechst-33342 representing DNA content versus EGFP fluorescence) 2D dot plot. EGFP positive (Q2) and EGFP negative (Q4) cells are gated depending on the levels of background auto-fluorescence acquired from the analysis of a reference wild-type cell line, N/TERT **(C)**. **(E)** Finally, single cell EGFP positive gate (Q2) **(i)**, single cell EGFP negative gate (Q4) **(ii)**, and single cell overall gate (P2) **(iii)** are separately displayed as histograms, using the 440/40 nm Ho33342 UV-A(rea) (blue fluorescence emitted by Hoechst-33342), representing the DNA content and thus the cell cycle profile with gates such as P3, P4, P5, P6 and P7 for the overall cell cycle profile **(iii)** gating on G1 (2N), S, G2/M (4N), >4N, 8N respectively. **N**, haploid number.

2.8.1.4 PI staining and flow cytometry

Propidium iodide (PI) (Sigma-Aldrich, Dorset, UK) is a fluorescent DNA (nucleic-acid) dye, that intercalates into the major groove of double-stranded DNA and thus allows cell cycle analysis in fixed cells (since cell membrane integrity excludes propidium iodide from staining viable and early apoptotic cells) and detection of the sub-diploid population of cells. PI (Sigma-Aldrich, Dorset, UK) fluorescent DNA dye is suitable for flow cytometric analysis because it binds to DNA in a linear manner and thus as DNA content of a cell increases, the fluorescent signal from the DNA dye increases proportionally in a linear manner (Krishan, 1990). In addition, propidium iodide (Sigma-Aldrich, Dorset, UK) staining in permeabilised cells facilitates the discrimination of cells with reduced DNA content, due to DNA fragmentation (sub-G1/sub-diploid populations). When cells are permeabilised, the apoptosis-mediated fragmented DNA multimers leak out of the cell, and therefore the resulting stained by propidium iodide (Sigma-Aldrich, Dorset, UK) sub-G1 populations, represent late apoptotic/dead cells (cells with fragmented DNA), and thus used for detection of later stages of apoptosis (Riccardi & Nicoletti, 2006). However, in order to be seen in the SubG1 area, a cell must have lost enough DNA to appear there; so if cells enter apoptosis from the S or G2/M phase of the cell cycle or if there is an aneuploid population undergoing apoptosis, they may not appear in the sub-G1 peak, since although they loose DNA due to fragmentation, their overall DNA content will still be ≥2N (http://www.icms.qmul.ac.uk/flowcytometry/flowcytometry/). In addition, DNA fragmentation is not only a characteristic of cells undergoing late stage of apoptosis but also of cells undergoing cell death due to necrosis, rendering difficult the discrimination between the apoptotic and necrotic cells in sub-G1 population. Necrosis is premature death of cells due to infection, toxins, trauma and cancer and it typically begins with swelling, chromatin digestion, and disruption of plasma membrane, while late necrosis is characterised by extensive DNA hydrolysis, vacuolation of the endoplasmic reticulum, organelle breakdown and thus cell lysis (Brown & Attardi, 2005). For those reasons, and in order to further confirm the results obtained by propidium iodide staining and flow cytometry analysis, cellular apoptosis was also measured using Cy^{TM}5 Annexin V antibody (BD Pharmingen^{TM}, BD Biosciences, San Jose, CA) staining and flow cytometry analysis **(see Section 2.8.1.5)**.

PI (Sigma-Aldrich, Dorset, UK) is excited at 488 nm and emitted at 619 nm giving a yellow fluorescent colour, similar to PE (phycoerythrin) which is excited at 490 nm and emitted at 578 nm. For that reason a Blue Argon laser 488 nm was used for flow cytometry analysis and fluorescence was detected at 575 nm using the PE 575/26 nm channel on the BD LSRII (BD Biosciences, San Jose, CA).

For PI (Sigma-Aldrich, Dorset, UK) staining and cell cycle analysis, equal number $3x10^5$ or $1.5x10^5$ of N/TERT, SINCE, and SINEG2 cells were seeded in 6 cm dishes, and harvested either 24 hr or 4 days after plating, respectively (~ 50-70% confluent) and fixed. Similarly, equal number $1.5x10^5$ of N/TERT, SINCE, and SINEG2 cells were seeded in 6 cm dishes, and were either mock treated or UVB treated 72 hr after plating (~ 50-60% confluent) **(see Section 2.13)**. 24 hr after UVB treatment, mock and UVB treated cells were harvested and fixed.

Culture media from each of the 6 cm petri dishes (either UVB or non-UVB treated) were collected to include any detached dead or apoptotic cells that may be floating in the medium. Therefore, supernatants (culture media) from each 6 cm dish were collected in 50 ml falcon tubes and adherent cells were washed once with 1x sterile PBS (PAA, Somerset, UK) and then trypsinised until all the cells had detached **(see Section 2.1.8)**. Trypsinised cells were transferred in the 50 ml falcon tubes containing the corresponding supernatant (RM+ growth medium) that included any floating cells at a ratio of 1:1 (v/v) trypsinised cells to RM+ culture medium supernatant including floating cells. Thus the trypsin reaction was inhibited and cells were centrifuged at 1,500 rpm for 5 minutes. Once the centrifugation was finished, the supernatant was aspirated and each pellet was resuspended in 5 ml 1x sterile PBS (PAA, Somerset, UK) and spun again at 1,500 rpm for 5 minutes. After centrifugation the supernatant was discarded and each cell pellet was resuspended in 1 ml of ice-cold 70% (v/v) ethanol (Fisher, Leicestershire, UK) **(see Appendix I)** (added dropwise) while vortexing to ensure fixation of all cells and minimise clumping, and incubated for 2 h at 4^oC or for up to 1 week most at 4^oC.

After 2 h incubation at 4^oC cells in the 15 ml falcon tubes were vortexed and then were transferred in 1.5 ml microcentrifuge tubes (Eppendorf, Cambridge, UK) and were centrifuged at 6,000 rpm for 2 minutes. Supernatant was aspirated and each pellet was

washed in 1 ml 1x sterile PBS (PAA, Somerset, UK) and centrifuged at 6,000 rpm for 2 minutes. Cell pellets were then resuspended in 1 ml 100 mM NaCitrate (Sigma-Aldrich, Dorset, UK) **(see Appendix I)** each, and centrifuged at 6,000 rpm for 2 minutes. Hence, supernatant was aspirated and each pellet was resuspended in 300-500 µl PI/RNaseA mixture (50 µg/ml Propidium Iodide, 125 µg/ml RNase A, 38 mM NaCitrate, 1x sterile PBS; all supplied by Sigma-Aldrich, Dorset, UK whereas 1x sterile PBS was supplied by PAA, Somerset, UK) **(see Appendix I)**. PI (Sigma-Aldrich, Dorset, UK) can also bind to RNA and thus it is necessary to treat cells with RNase A (Sigma-Aldrich, Dorset, UK) **(see Appendix I)** for optimal DNA resolution. Resuspended cells were incubated for 10-20 minutes in the dark at room temperature. Cells were then vortexed and transferred in sterile 5 ml polystyrene round bottom FACS tubes (BD Falcon tubes, BD Biosciences, San Jose, CA), which were kept on ice and were given for flow cytometry analysis, where the same number of events was acquired for each sample (25,000-50,000 events).

Cells stained with PI (Sigma-Aldrich, Dorset, UK), were analysed for DNA content. First, a 2D dot plot representing cell size and granularity was created for each sample **(Figure 2.5A)**. This is derived from the Forward (cell size) and Side scatter (granularity) values (FSC versus SSC) and is useful for cell population gating according to physical characteristics of cells (P1) and thus for the exclusion of cell debris which have lower forward scatter than living cells **(see Section 2.8.1.2)**. Next, a 2D doublet exclusion plot was made for the gated (P1) cells, to distinguish cell clumps, aggregates of G1 cells and G1 cell doublets from G2/M cells for each sample **(Figure 2.5B)**. Doublets of G1 cells have the same DNA content as G2/M cells and in order to distinguish them, the instrument can separate these by measuring the time it takes for the two types of cells to pass through the laser beam by a fluorescent parameter Width (W) measurement. Doublets and aggregates of cells take longer to pass through the laser of the flow cytometer and thus appear higher up on the fluorescent width scale (W) **(Figure 2.5B)**. Therefore the 2D doublet exclusion plot represents the fluorescent Area (A) scale (PE 575/26 nm-A(rea)) which is the DNA content according to the yellow fluorescence emitted by propidium iodide (PI) dye and the fluorescent Width (W) scale (PE 575/26 nm-W(idth)) which is the time it takes for a cell to pass through the laser beam **(Figure 2.5B)**. Thus, cells were gated (P2) using specific values, which

correspond to DNA content from 2N up to 16N and only to single cells so that the G2/M population contains only single mitotic cells **(Figure 2.5B)**.

This single cell gate (P2) population of cells was displayed as a one-dimensional histogram, representing the relative DNA content of cells (PE 575/26 nm-A(rea) - yellow fluorescence emitted by PI) and thus the cell cycle profile, with gates P3, P4, P5, P6, P7, P8 and P9 gating on sub-G1, G1 (2N), S, G2/M (4N), >4N, 8N, >8N with 0.2%, 45.7%, 20.9%, 21.5%, 8.6%, 2.0% and 0.9% respectively. The gating of cells (FSC, SSC, DNA content, doublet exclusion) were initially acquired using the reference wild-type cell line (N/TERT) and remained constant in subsequent sample analysis.

Samples were analysed either in duplicates or triplicates and statistical analysis was performed using the Microsoft Excel's software for student's *t* test analysis **(see Section 2.16)**.

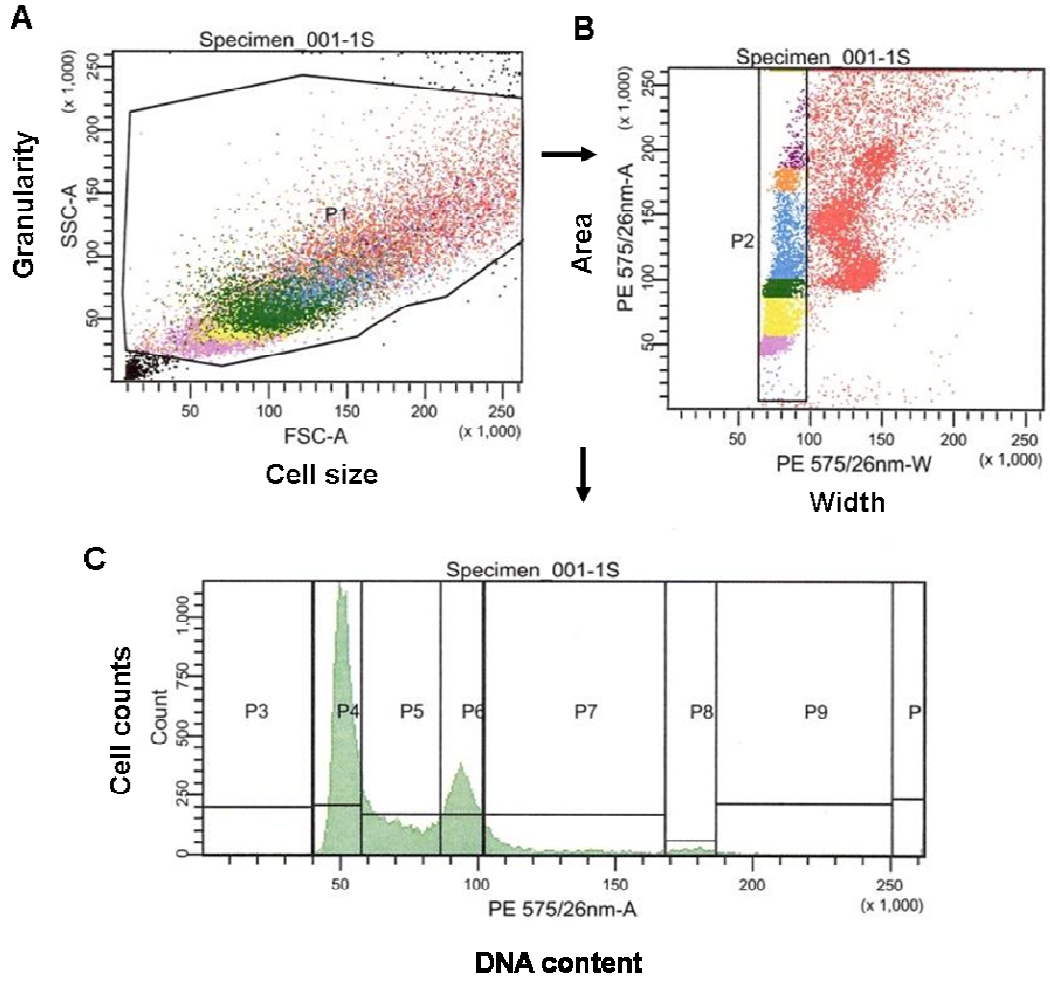

Figure 2.5: PI (propidium iodide) cell cycle analysis.

(A) Initial cell population gating (P1) for each sample is placed on FSC versus SSC (cell size versus granularity) 2D dot plot. Debris appear to the left of cell analysis gate (P1). **(B)** This cell population gate (P1) is then placed on PE 575/26 nm-W(idth) versus PE 575/26 nm-A(rea) (yellow fluorescence emitted by propidium iodide (PI) representing DNA content versus the time it takes for a cell to pass through the laser beam) 2D dot plot. Doublets and clumps appear to the right of single cell analysis gate (P2). **(C)** This single cell gate (P2) population of cells is then displayed as histogram, using the PE 575/26 nm-A(rea) (yellow fluorescence emitted by propidium iodide (PI), representing the DNA content and thus the cell cycle profile with gates such as P3, P4, P5, P6, P7, P8 and P9 gating on sub-G1, G1 (2N), S, G2/M (4N), >4N, 8N, >8N with 0.2%, 45.7%, 20.9%, 21.5%, 8.6%, 2.0% and 0.9% respectively. **N**, haploid number.

2.8.1.5 Cy™5 Annexin V staining and flow cytometry

Annexin V, is a Ca^{2+} dependent phospholipid-binding protein that has a high affinity for membrane phosholipid phosphatidylserine (PS), and binds to cells with exposed PS (Raynal & Pollard, 1994). In apoptotic cells, the membrane phosholipid phosphatidylserine (PS) is translocated from the inner to the outer leaflet of the plasma membrane, thereby exposing PS to the external cellular environment and thus enabling the binding of Annexin V to it (Koopman et al., 1994; Martin et al., 1995). Due to the fact that externalization of PS occurs in the earlier stages of apoptosis (Martin et al., 1995), Annexin V staining is used to identify apoptosis at an earlier stage, compared to assays based on nuclear changes (DNA fragmentation), such as propidium iodide staining.

In my study, the fluorophore-labelled antibody, Cy™5 Annexin V antibody (BD Pharmingen™, BD Biosciences, San Jose, CA) was used. Annexin V is conjugated with Cy™5 (Cyanine™5) fluorochrome **(see Section 2.8.1.1)** and this format retains its high affinity for PS and thus serves as a sensitive probe for flow cytometric analysis of cells that undergoing apoptosis. Therefore, the labelled antibody is added to the cell sample and binds to a specific molecule on the cell surface (i.e. PS) or in other cases inside the cell. When laser light of the right wavelength strikes the fluorophore (i.e. Cy™5), a fluorescent signal is emitted and detected by the flow cytometer.

Cy™5 Annexin V (BD Pharmingen™, BD Biosciences, San Jose, CA) staining precedes the loss of membrane integrity which accompanies the latest stages of cell death resulting from either apoptotic **(see Chapter 4, Section 4.2.1.2)** or necrotic processes **(see Section 2.8.1.4)**. For that reason, DAPI (- 4',6-diamidino-2-phenylindole) (Sigma-Aldrich, Dorset, UK) was also used for staining along with Cy™5 Annexin V (BD Pharmingen™, BD Biosciences, San Jose, CA) in order to discriminate late apoptotic or dead/necrotic cells which have lost membrane integrity, from early apoptotic cells which still have intact membranes, by dye exclusion. DAPI (Sigma-Aldrich, Dorset, UK) is a fluorescent DNA (nucleic-acid) dye, that intercalates into the minor groove of double-stranded DNA and binds preferentially to A (Adenine) - T (Thymine) base pairs of dead, damaged or fixed/permeabilised cells since it is unable to cross intact cell membranes of viable healthy cells (Kubista et al., 1987; Barcellona et al., 1990).

Cy™5 (BD Pharmingen™, BD Biosciences, San Jose, CA) is excited at 649 nm and emitted at 670 nm giving a red fluorescent colour, similar to APC (allophycocyanin) which is excited at 650 nm and emitted at 661 nm. For that reason a red diode 633 nm was used for flow cytometry analysis and fluorescence was detected at 660 nm using the APC 660/20 nm channel on the BD LSRII (BD Biosciences, San Jose, CA). DAPI (Sigma-Aldrich, Dorset, UK) is excited at 350 nm and emitted at 461 nm giving a blue fluorescent colour. For that reason a UV laser 325 nm was used for flow cytometry analysis and fluorescence was detected at 440 nm using the UV 440/40 nm channel on the BD LSRII (BD Biosciences, San Jose, CA).

For Cy™5 Annexin V (BD Pharmingen™, BD Biosciences, San Jose, CA) and DAPI staining followed by flow cytometry analysis, equal number $3x10^5$ - $5x10^5$ of N/TERT, SINCE, and SINEG2 cells were seeded in 6 cm dishes, and harvested either 24 or 48 hours after plating, in order to detect any GLI2ΔN oncogene-induced apoptosis or cell death. Similarly, equal number $3x10^5$ - $5x10^5$ of N/TERT, SINCE, and SINEG2 cells were seeded in 6 cm dishes, and were either mock treated or UVB treated 24 hr after plating (~ 50-60% confluent) **(see Section 2.13)**, in order to detect UVB-induced apoptosis. 24hr after UVB treatment, mock and UVB treated cells were harvested. In addition, 5 extra 6 cm dishes of each cell line were seeded and harvested in order to be used as controls to set up flow cytometry **(Figure 2.6)**. These controls include (1) unstained cells, (2) cells stained with Cy™5 Annexin V antibody alone (BD Pharmingen™, BD Biosciences, San Jose, CA), (3) cells stained with DAPI alone (Sigma-Aldrich, Dorset, UK), (4) untreated (wild-type) populations stained both with Cy™5 Annexin V antibody (BD Pharmingen™, BD Biosciences, San Jose, CA) and DAPI (Sigma-Aldrich, Dorset, UK), used to define the basal level of apoptotic and dead cells for each cell line and (5) positive control staining with Cy™5 Annexin V antibody (BD Pharmingen™, BD Biosciences, San Jose, CA) and DAPI (Sigma-Aldrich, Dorset, UK), on a cell line which is induced to undergo apoptosis, that is UVB-treated N/TERT cells.

Culture media from each of the 6 cm petri dishes (either UVB or non-UVB treated) were collected to include any detached dead or apoptotic cells that may be floating in the medium. Therefore, supernatants (culture media) from each 6 cm dish were

collected in 50 ml falcon tubes and adherent cells were washed once with 1x sterile PBS (PAA, Somerset, UK) and then trypsinised until all the cells had detached **(see Section 2.1.8)**. Trypsinised cells were transferred in the 50 ml falcon tubes containing the corresponding supernatant (RM+ growth medium) that included any floating cells at a ratio of 1:1 (v/v) trypsinised cells to RM+ culture medium supernatant including floating cells. Thus, the trypsin reaction was inhibited and cells were centrifuged at 2,000 rpm for 5 minutes. Once the centrifugation was finished, the supernatant was aspirated and each pellet was resuspended in 5 ml of 1x sterile iced-cold PBS (PAA, Somerset, UK) and spun again at 2,000 rpm for 5 minutes.

After centrifugation, each cell pellet was resuspended in 100 µl of 1x Annexin V Binding Buffer solution (BD Pharmingen™, BD Biosciences, San Jose, CA) (1x Binding Buffer solution; 1 ml of 10x Annexin V Binding Buffer solution (BD Pharmingen™, BD Biosciences, San Jose, CA) in 9 ml dH_2O, kept on ice) and 5 µl Cy™5 Annexin V antibody (BD Pharmingen™, BD Biosciences, San Jose, CA) (1:20 dilution) (except (1) and (3) controls where only 100 µl of 1x Annexin V Binding Buffer solution, BD Pharmingen™, BD Biosciences, San Jose, CA, were added). Resuspended cells were transferred in sterile 5 ml polystyrene round bottom FACS tubes (BD Falcon tubes, BD Biosciences, San Jose, CA), were gently vortexed and were incubated for 15 min at room temperature in the dark. Then, 400 µl of 1x Annexin V Binding Buffer solution (BD Pharmingen™, BD Biosciences, San Jose, CA) was added per sample and samples were kept on ice. Finally, DAPI (Sigma-Aldrich, Dorset, UK) was added at a final concentration of 200 ng/ml per sample (5 µl of 20 µg/ml DAPI per 500 µl sample) **(see Appendix I)** (except (1) and (2) controls) 1 - 2 minutes before the cells were given for flow cytometry analysis, where the same number of events was acquired for each sample (20,000-30,000 events).

Cells stained with Cy™5 Annexin V antibody (BD Pharmingen™, BD Biosciences, San Jose, CA) and DAPI (Sigma-Aldrich, Dorset, UK), were analysed for apoptosis and cell death. First, a 2D dot plot representing cell size and granularity was created for each sample **(Figure 2.6A)**. This is derived from the Forward (cell size) and Side scatter (granularity) values (FSC versus SSC) and is useful for cell population gating according to physical characteristics of cells (P1) and thus for the exclusion of cell debris which have lower forward scatter than living cells **(see Section 2.8.1.2)**. Next, the cell gate

(P1) population of cells, was displayed as a quadrant two-dimensional (2D) dot plot, representing the fluorescent Area (A) scale (Annexin V APC 660/20 nm-A(rea)) which is indicative of the number of apoptotic cells binding Annexin V (Annexin V positive cells) according to the red fluorescence emitted by Cy^{TM}5 dye conjugated to Annexin V antibody (BD Pharmingen^{TM}, BD Biosciences, San Jose, CA) and the fluorescent Area (A) scale (DAPI UV 440/40 nm-A(rea)) which is indicative of the number of dead cells (DAPI positive cells) according to the blue fluorescence emitted by DAPI dye (Sigma-Aldrich, Dorset, UK), with gates Q3, Q4, Q2 and Q1 gating on viable non-apoptotic cells (DAPI (-) Annexin V (-) cells), early apoptotic cells that bind Annexin V (DAPI (-) Annexin V (+) cells), late apoptotic/dead cells that are binding Annexin V and taking up DAPI (DAPI (+) Annexin V (+) cells) and dead cells that take up DAPI but do not bind Annexin V (DAPI (+) Annexin V (-) cells), with 0.3%, 5.5%, 82.4% and 11.8% respectively **(Figure 2.6F and Chapter 4, Section 4.2.5.2, Figure 4.15)**. The gating of cells was initially acquired using the reference wild-type cell line (N/TERT) and the five different controls **(Figure 2.6A, B, C, D, E, F)**.

Samples were analysed in duplicates and statistical analysis was performed using the Microsoft Excel's software for student's *t* test analysis **(see Section 2.16)**.

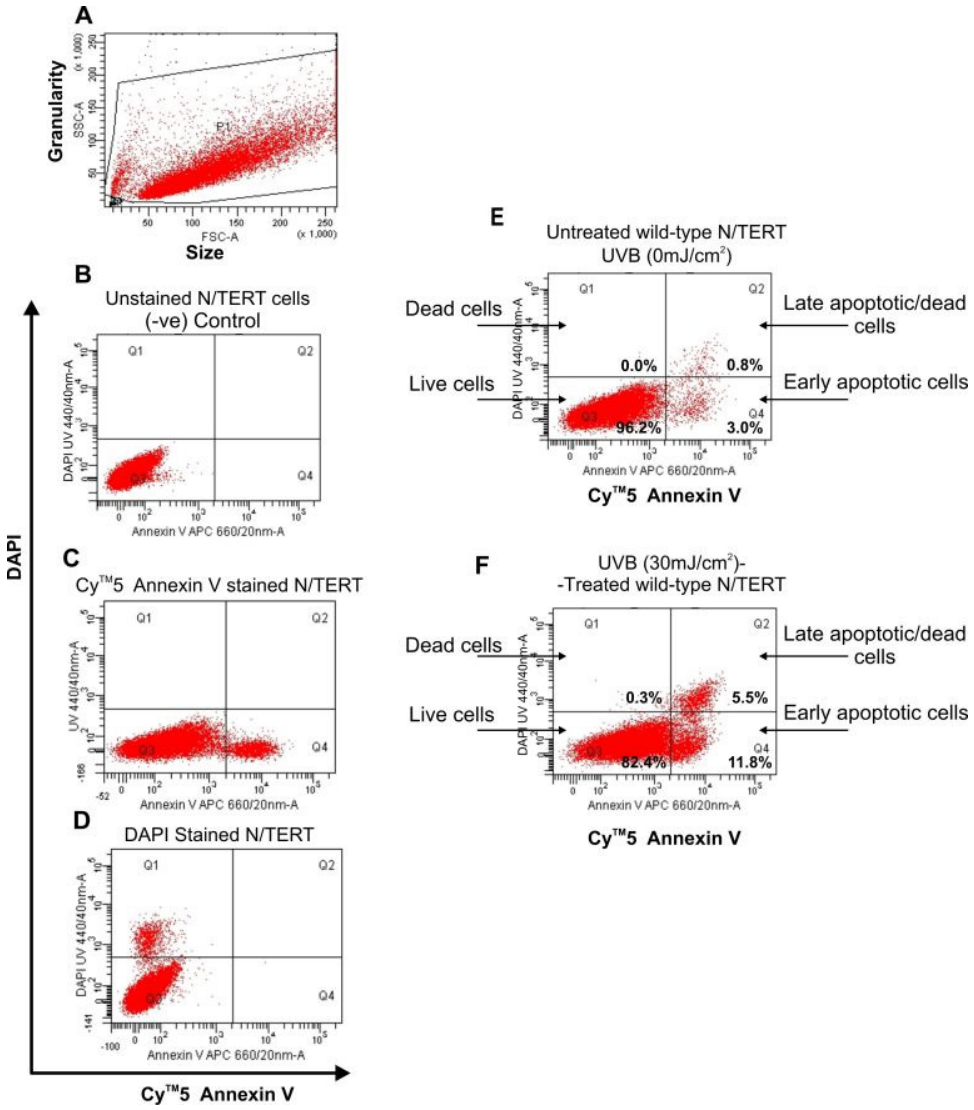

Figure 2.6: Cy™5 Annexin V staining and flow cytometry analysis.

(A) Initial cell population gating (P1) for each sample is placed on FSC versus SSC (cell size versus granularity) 2D dot plot. Debris appear to the left of cell analysis gate (P1). **(B, C, D, E, F)** This cell population gate (P1) is then displayed as quadrant two dimensional (2D) dot plots using the Annexin V APC 660/20 nm-A(rea) versus DAPI UV 440/40 nm-A(rea) (red fluorescence emitted by Cy™5 dye conjugated to Annexin V antibody which is indicative of the number of apoptotic cells binding Annexin V versus blue fluorescence emitted by DAPI which is indicative of the number of dead cells), with gates Q3, Q4, Q2 and Q1 gating on live non-apoptotic cells (DAPI (-) Annexin V (-) cells), early apoptotic cells that bind Annexin V (DAPI (-) Annexin V (+) cells), late apoptotic/dead cells that are binding Annexin V and taking up DAPI (DAPI (+) Annexin V (+) cells) and dead cells that take up DAPI but do not bind Annexin V (DAPI (+) Annexin V (-) cells), with 0.3%, 5.5%, 82.4% and 11.8% respectively **(F)**. **(B, C, D, E, F)** Controls used to set up compensation and quadrants for flow cytometry analysis: **(B)** unstained N/TERT cells, **(C)** N/TERT cells stained with Cy™5 Annexin V antibody alone, **(D)** N/TERT cells stained with DAPI alone, **(E)** untreated (wild-type N/TERT) populations stained with Cy™5 Annexin V antibody and DAPI, used to define the basal level of apoptotic and dead cells **(F)** positive control staining with Cy™5 Annexin V antibody and DAPI, on a cell line which is induced to undergo apoptosis, that is UVB-treated N/TERT cells.

2.8.2 FACS sorting

Fluorescence-activated cell sorting (FACS) **(Figure 2.7)** is a specialized type of flow cytometry **(Section 2.8.1)** which is used to separate cells according to subtype or epitope expression (cells labeled with fluorescently tagged antibodies, fluorescent dyes or fluorescent expressing proteins) for further biological studies. Thus, FACS provides a method for sorting a heterogeneous mixture of biological cells into two or more containers, one cell at a time, based upon the specific light scattering and fluorescent characteristics of each cell, typically through a process which is known as electrostatic droplet deflection (Willis, 2004).

After the sample is hydrodynamically focused **(see Section 2.8.1.2)**, into a thin stream so that cells pass singly through an exit nozzle (flow cell) the stream is in laminar flow in air. The further away from the flow cell, the more unstable the stream becomes, eventually breaking up into droplets. To sort accurately, the stream needs to be precisely and reproducibly forming droplets at the same point. This is done by acoustic waves applied to the nozzle; the waves travel down the stream allowing droplet formation and break-off point to be stabilised. Thus through hydrodynamic focusing and the stabilised break-off, a particle or cell of interest passing in the stream will be partitioned into individual droplets (http://flow.csc.mrc.ac.uk/).

Therefore, after hydrodynamic focusing each particle or cell is probed with a beam of light from the laser and a computer registers its physical and fluorescent properties **(see Section 2.8.1.2)** and the scatter and fluorescence signal is compared to the predetermined sort criteria set on the computer **(Figure 2.7A, B, C, D)**. If the cell matches the selection criteria, an electric charge is applied to the stream. Electrostatic charging actually occurs at a precise moment called the 'break-off point', which describes the instant the droplet containing the cell of interest separates from the stream. Thus, when the cell to be sorted reaches the break-off point, an electric charge is applied to the stream and as the drop leaves the stream and is no longer attached to the stream the charge on the stream is reset to zero and the droplet with the cell of interest retains the applied charge (http://flow.csc.mrc.ac.uk/), (www.abdserotec.com/uploads/Flow-Cytometry.pdf). The droplets eventually pass through a strong electrostatic field (a pair of charged metal plates), and are deflected left or right based on their charge (deflected

away from the plate of opposite charge) and collected to collection tubes or into a waste container.

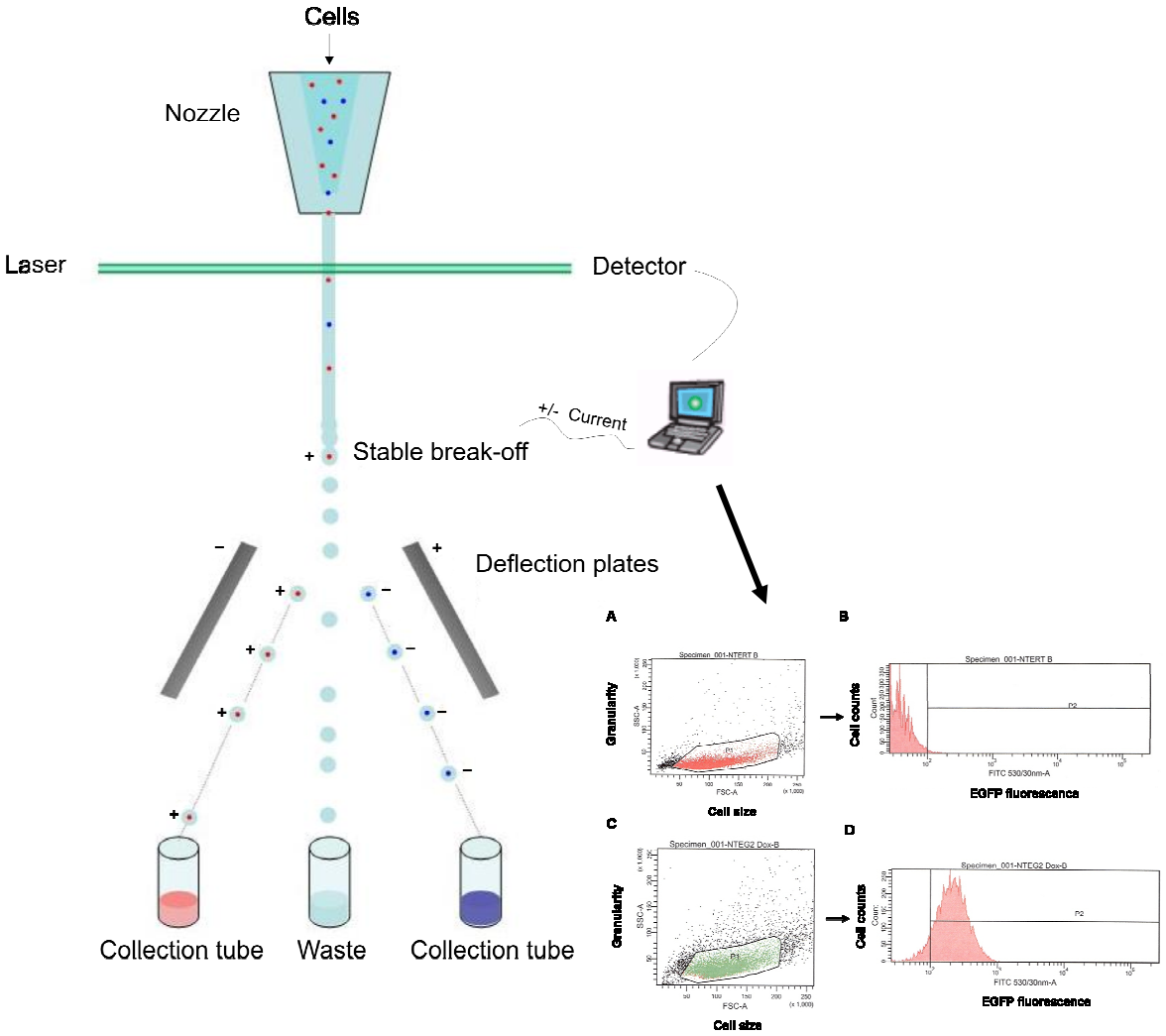

Figure 2.7: Fluorescent Activated Cell Sorting (FACS).

A schematic of fluorescence activated cell sorting (FACS). Sort criteria for EGFP-expressing cells are shown in panels **A-D**. **(A)** A normal non-EGFP expressing wild-type cell line (i.e. N/TERT) is used to select for cells (P1) according to size (FSC) and granularity (SSC) as shown in the 2D dot plot. **(B)** The same cells are used to detect levels of background auto-fluorescence as plotted in the histogram. The threshold for green fluorescence (GFP fluorescence) is set accordingly (set of the gates), for the discrimination of EGFP negative from positive (P2) cells. **(C)** An inducible EGFP expressing cell line (N/TERT-EGFP-GLI2ΔN, NTEG2 Dox-) is the cell line of interest used for sorting, and thus cells are firstly selected (P1) according to the FSC and SSC profiles as obtained previously. **(D)** The cells are then selected (gated) according to the levels of green fluorescence (EGFP fluorescence) (P2). All cells detected within the specified range of FSC and SSC (P1) **(C)**, and green fluorescence positivity (P2) **(D)**, will satisfy the sorting criteria and will thus be sorted in the collection tubes.
Modified from http://flow.csc.mrc.ac.uk/.

All fluorescent activated cell sorting (FACS) runs (sorting based on enhanced green fluorescence protein - EGFP levels), in my study, were performed in a BD FACSAria Cell Sorter fitted with a Blue Argon Laser 488 nm, violet diode 405 nm, and red diode 633 nm (BD Biosciences, San Jose, CA), by Gary Warnes at FACS Lab of Cell and Molecular Science, Barts and the London Queen Mary's School of Medicine and Dentistry, Whitechapel, London, UK.

N/TERT wild-type cells **(see Section 2.1.3)** and stable expressing-EGFP and EGFP-GLI2ΔN transduced (4 days after infection) N/TERT keratinocytes **(see Section 2.3.5.1)**, or selected **(see Section 2.4)** and inducible expressing EGFP-GLI2ΔN (NTEG2 Dox-, removal of Dox for 5 days) transduced N/TERT keratinocytes **(see Section 2.3.5.2)**, plated in either 6 or 10 cm dishes, were trypsinised **(see Section 2.1.8)** and centrifuged at 1,000 rpm for 5 minutes. After washing each pellet with 10 ml 1x sterile PBS (PAA, Somerset, UK) and centrifuging at 1,000 rpm for 5 minutes, cell pellets were resuspended in 2 ml of 1x sterile PBS (PAA, Somerset, UK) each, and were then passed through a 70 μm strainer (BD Falcon Cell strainers, BD Biosciences, San Jose, CA) (minimise doublets and clumps). Cells were transferred in sterile 5 ml polystyrene dual-position snap-cap round bottom FACS tubes (BD Falcon tubes, BD Biosciences, San Jose, CA), which were kept on ice and were given for FACS analysis. N/TERT wild-type cells were used for obtaining basal levels of green fluorescence (background auto-fluorescence), and all cells above this basal threshold were considered as being EGFP positive fluorescent cells and were thus collected in either sterile 5 ml polystyrene dual-position snap-cap round bottom FACS tubes (BD Falcon tubes, BD Biosciences, San Jose, CA) or in sterile 1.5 ml microcentrifuge tube (Eppendorf, Cambridge, UK, depending on the number of the collected cells, containing 1 ml and 500 μl respectively, of the appropriate normal culture medium for each cell line. Collected cell were either plated immediately after collection in 24, 12 or 6-well plates or in T25 flask, containing normal growth medium (growth medium depending on the cell line), or were centrifuged at 1,000 rpm for 5 minutes and then the pellet was resuspended in 2 ml of culture medium and plated in the appropriate normal culture medium for each cell line. FACS sorted and replated cells were either used in experiments or were cryopreserved **(Section 2.1.10)**.

2.9 Hoechst-33342 staining and replating

For Hoechst-33342 staining and replating cells were seeded at equal densities and as soon as they reached 50-60% confluence they were washed, trypsinised and stained with 10 μg/ml Hoechst-33342 (Sigma-Aldrich, Dorset, UK) (2 ml 1x sterile PBS + 2 μl 10 mg/ml Hoechst-33342; 1:1000 dilution) **(see Appendix I)** following the same procedure as described in **Section 2.8.1.3**. Cells were then counted using a haemocytometer **(Section 2.1.9.1)** and were reseeded in 10 cm dishes at a density of $3x10^5$ cells/dish. Digital bright-field and fluorescent images were captured 24, 48, 72 hr, (~ 30-60 % confluent throughout the experiment) after plating using a fluorescence microscope **(Section 2.2)**.

2.10 DAPI staining and Binucleate cells counting

For DAPI staining and binucleate cells counting, equal number $1.2x10^5$ N/TERT, SINCE, and SINEG2 cells were seeded per well in a 6 well plate. 72 hours after plating (~ 40-60 % confluent), cells were washed 1x in 1x sterile PBS (PAA, Somerset, UK) and were fixed in 4% (v/v) Formaldehyde/Formalin (Fisher, Leicestershire, UK) solution **(Appendix I)** for 20 minutes at room temperature and were either stored at 4^oC until required or were immediately stained with DAPI. Cells were washed 2x in 1 ml per well of 1x sterile PBS (PAA, Somerset, UK) and were incubated in 1 ml per well of 1x sterile PBS (PAA, Somerset, UK) containing 200 ng/ml DAPI (Sigma-Aldrich, Dorset, UK) **(Appendix I)** for 10 minutes at room temperature in the dark. Finally cells were washed 1x in 1 ml of 1x sterile PBS (PAA, Somerset, UK) per well and were then covered in 1-2 ml of 1x sterile PBS (PAA, Somerset, UK) per well.

Digital bright-field and fluorescent images (~ 15 images (fields) per cell line in two replicate wells) were captured using a fluorescence microscope **(see Section 2.2)**. The bi-nucleated (tetraploid) cells per field (image) were counted using Adobe Photoshop CS4 Extended. The percentage of bi-nucleated cells per field was derived by counting the number of cells with two nuclei over the total number of cells per field. Thus, the percentage of bi-nucleated cells per field (x) was calculated as follows: x = Number of Bi-nucleate Cells x 100 / Total Number of Cells. For example if a field of cells had a

total amount of 80 cells, of which, 9 were bi-nucleated, then x = 9 x 100 / 80, then x = 11.25 %. An average of approximately 300 - 350 cells were counted for each cell line in total. Only bi-nulceated cells were counted in this analysis, while all multi-nucleated cells were included in the total number of cells per field. Cells undergoing mitosis were also counted as two mononuclear cells.

2.11 Absolute Quantitative Real-time PCR (qRT-PCR) and Semi-Quantitative PCR

Polymerase chain reaction (PCR) is a commonly used method to amplify DNA sequences of interest and can be used to detect mRNA expression by amplification of a target region of a gene's cDNA, using oligonucleotide primers complementary to flanking cDNA sequences.

Absolute quantitative real-time PCR (qRT-PCR) is used for the accurate quantification of the copy number of a gene of interest in a given cell sample. The template of a qRT-PCR reaction can be cDNA, converted from isolated total RNA **(see Section 2.11.1)** by reverse transcription as described in **Section 2.11.2**. qRT-PCR is a kinetic PCR reaction which provides real time information about the amplification of cDNA template **(Figure 2.8A)**. The template cDNA is mixed with Syber (SYBR) Green I Master (Roche, Burgess Hill, UK), which is an asymmetrical fluorescent dye that stably binds to random sites of double stranded DNA. During cDNA amplification **(Figure 2.8A)** the qRT-PCR instrument records the level of green fluorescence emitted by double strand DNA-bound SYBR Green I Master (Roche, Burgess Hill, UK), and these readings are repeated for each PCR cycle. Therefore, a real-time cDNA amplification curve (fluorescence/time or cycle, y/x axis) is finally produced based on the levels of fluorescence present in each amplification cycle **(Figure 2.8A)**. By comparing these values to a standard curve produced by serial dilutions of a known amount of cDNA template **(see Section 2.11.6)**, it is possible to calculate the absolute template copy number in the unknown samples. This method differs qualitatively and quantitatively from conventional semi-quantitative PCR **(see Section 2.11.8)**, since only the former can accurately quantify the copy number of template cDNA present in the original

sample, while the latter indicates the final amplified PCR products. Although semi-quantitative PCR can offer information about the presence or absence of a specific product, the relative abundance of copy number is often subjective since it is based on visual confirmation and/or manual signal analysis. Furthermore, by using qRT-PCR the specificity of product amplification is also confirmed by melting analysis performed at the end of the qRT-PCR run **(Figure 2.8B)**. During melting analysis, the qPCR amplified products are initially melted at 95^{o}C followed by a cooling to 65^{o}C where all qPCR products become double stranded through annealing after 30 sec, emitting high fluorescence signal. Then qPCR products become gradually melted and single stranded, when subjected to increasing temperature incubations from 65^{o}C up to 99^{o}C and the green fluorescence signal is acquired continuously. The fluorescent signal will suddenly drop once the melting temperature (DNA product denaturation; dsDNA conversion to two single strands where SYBR Green I (Roche, Burgess Hill, UK) is not bound to) for a specific qPCR product is reached, thus producing a melting curve (fluorescence intensity/temperature, (y/x axis), which is also depicted as a single peak representing the product's melting temperature (fluorescence intensity/temperature, (y/x axis) **(Figure 2.8B)**. Therefore, a single peak indicates the presence of a single amplified product, whereas multiple peaks indicate the presence of multiple unspecific PCR products that melt at different temperatures.

Absolute quantitative Real Time-PCR (qRT-PCR) in this study was performed using Light Cycler® 480 SYBR green I Master (Roche, Burgess Hill, UK). Semi-quantitative PCR (PCR) in this study was performed using Verity 96-well Thermal Cycler (Applied Biosystems, Carlsbad, CA).

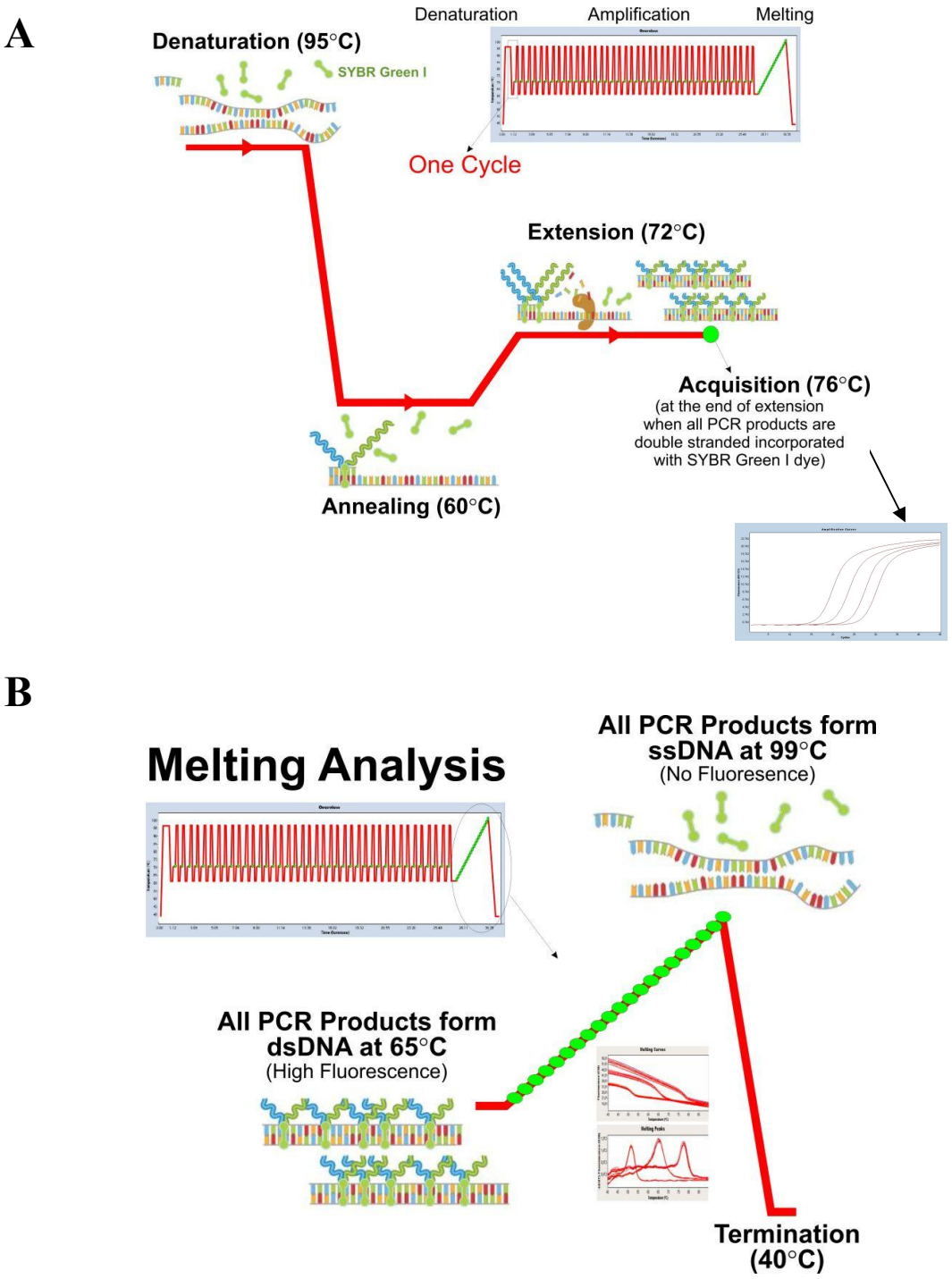

Figure 2.8: Amplification and melting analysis in qRT-PCR.

(A) Amplification cycle. Each amplification cycle consists of three cycling temperature steps including denaturation (95°C), primer annealing (60°C), and extension (72°C). Fluorescence is acquired at the end of extension step at 76°C when all products are double stranded and after a number of cycles the amplification curve for each sample is obtained. **(B)** Melting analysis. Modified from Dr Muy-Teck Teh, LightCycler LC480 Protocol for Absolute Gene Quantification, Clinical and Diagnostic Oral Sciences, Institute of Dentistry, Barts and the London School of Medicine and Dentistry, London, UK.

2.11.1 Total RNA Extraction from cultured cells

Cells were seeded in 6 cm dishes (~ $5x10^5$ cells/dish) and total RNA was extracted either 24 or 48 hours after plating. The work surface and pipettes were prepared with RNase Zap (Ambion, Cambridgeshire, UK) to remove enzymes that digest RNA and all steps were performed at room temperature. Total RNA was extracted from cells using RNeasy Mini Kit (Qiagen, West Sussex, UK). Semi-confluent cultures (50-65% confluent dishes) were harvested in 350 µl of RLT lysis buffer (Qiagen, West Sussex, UK) containing 10 µl/ml β-mercaptoethanol (β-ME) (Sigma-Aldrich, Dorset, UK). RLT buffer acts to lyse the cells (Qiagen, West Sussex UK) and contains guanidine isothiocyanate, which deactivates RNase enzymes that would otherwise degrade extracted RNA. Next, cell lysates were collected in eppendorf tubes (Eppendorf, Cambridge, UK) and were either snap frozen in dry ice and kept at -80^{o}C for long-term storage, or processed immediately to the next step. Cell lysates were homogenized by passing them through QIAshredder columns inside 2 ml collection tubes (Qiagen, West Sussex, UK) and centrifuged at 13,200 rpm for 2 minutes followed by column removal. Next, 350 µl of 70% (v/v) ethanol (Fisher, Leicestershire, UK) **(see Appendix I)** was added to each lysate and mixed by pipetting, to precipitate RNA. Then, the 350 µl of sample were loaded into an RNeasy Mini Spin column inside 2 ml collection tubes (Qiagen, West Sussex, UK) and centrifuged at 10,000 rpm for 15 seconds. Upon centrifugation RNA was adhered to the column and the flow-through was discarded.

Then the columns were rinsed by loading 700 µl RW1 buffer (Qiagen, West Sussex, UK) and centrifuging at 10,000 rpm for 15 seconds. Then, the columns were washed again by adding 500 µl RPE buffer (Qiagen, West Sussex, UK) and centrifuging at 10,000 rpm for 15 seconds. This was repeated with a further 500 µl RPE buffer, but centrifuged at 10,000 rpm for 1 minute to dry the column. Finally, the column was transferred to a fresh RNase-free microcentrifuge tube (Qiagen, West Sussex, UK) and the RNA was eluted by adding 20-30 µl RNase-free water (Qiagen, West Sussex, UK) to the column and centrifuging for 10,000 rpm for 1 min. The RNA concentration was measured with NanoDrop^{TM} ND-1000 (ThermoScientific, Cambridgeshire, UK) **(see Section 2.3.2)** and RNA was stored at -80°C until required.

2.11.2 Reverse Transcriptase cDNA Synthesis

Reverse transcriptase is an enzyme that transcribes single stranded RNA into double stranded DNA. Reverse transcriptases were first identified in tumour viruses (Baltimore, 1970; Temin & Mizutani, 1970). The reverse transcriptase used in this study in order to convert total RNA into complementary DNA (cDNA) (First-strand cDNA synthesis) is the AMV (Avian Myeloblastosis Virus - tumour virus) Reverse Transcriptase (Promega, Hampshire, UK) that synthesizes single-stranded cDNA from total isolated RNA (Dasgupta et al., 2006).

Purified RNA (1-3 μg of total isolated RNA, as described in **Section 2.11.1**) was reverse transcribed into cDNA with the Reverse Transcription Kit (Promega, Hampshire, UK) with very few modifications to manufacturer's protocol. Initially, isolated RNA and the components of the Reverse Transcription Kit (Promega, Hampshire, UK) were defrosted and a mastermix was prepared in an RNase-free eppendorf tube (Eppendorf, Cambridge, UK), as well as 1 μg/10 μl RNA from the RNA sample was prepared (i.e. Sample 1 RNA concentration ng/μl: 1 μg RNA = 3 μl from the RNA sample → 3 μl RNA + 7 μl RNase-free water = 10 μl thus final concentration 1 μg/10 μl = 0.1 μg/μl = 100 ng/μl) in an RNase-free eppendorf tube (Eppendorf, Cambridge, UK). A typical reverse transcription reaction to convert 1 μg of total RNA contained the following (all reagents were supplied with Reverse Transcription Kit from Promega, Hampshire, UK):

Component	Amount
$MgCl_2$, 25mM	4.0 µl
Reverse Transcription 10xBuffer	2.0 µl
dNTPs Mixture, 10mM	2.0 µl
Oligo$(dT)_{15}$ Primers (0.5 µg/µl)	0.5 µl
Random Primers (0.5 µg/µl)	0.5 µl
RNAsin®	0.5 µl
AMV Reverse Trascriptase (15 units/µl)	1.0 µl
Nuclease-free water	4.5 µl
Mastermix	**15 µl**
RNA*	10 µl (1 µg; 100 ng/µl RNA)
Total	**25 µl**

**** For more than 1µg of RNA, the reaction volume was increased accordingly***

Mastermix 15 µl was added in 10 µl RNA sample. Reaction (25 µl) was mixed by vortexing and then pulse centrifuged, before incubating at room temperature for 10 minutes. This allowed the hybridisation of Oligo$(dT)_{15}$ and random primers to the RNA. The transcripts were reverse transcribed to cDNA by incubating at 42^{o}C for 30 minutes. AMV reverse trascriptase was inactivated and prevented from binding to cDNA by incubating at 75^{o}C for 5 minutes. Then samples were centrifuged at 8,000 rpm for 5 sec. Finally, the Reverse Transciption mixture (25 µl) was diluted (1:3) with 50 µl of Nuclease-free molecular biology grade H_2O (Reverse Transcription Kit, Promega, Hampshire, UK or Sigma-Aldrich, Dorset, UK) (i.e. 25 µl + 50 µl → 75 µl final volume) and kept in ice if being used immediately in downstream PCR applications, or stored at -20^{o}C until required.

2.11.3 Primer design

The cDNA accession numbers of genes of interest were obtained using the online NCBI database, and were then used in Roche's Universal Probe Library tool for primer design (https://www.roche-applied-science.com/sis/rtpcr/upl/index.jsp?id=UP030000).

Primer sequences **(see Table 2.3)** were selected on the basis of size (70-120 bp) and were all verified on BLAST tool (http://blast.ncbi.nlm.nih.gov/Blast.cgi) to ensure high specificity to target product.

Primer sequences for BCL-2 (Regl et al., 2004b) and GLI2 a/β (Regl et al., 2002) were chosen from previously published papers, as well as POLR2A and YAP1 (Gemenetzidis et al., 2009). E-cadherin primers were kindly provided by Dr Adrian Biddle, Centre for Cutaneous Research, Institute of Cell and Molecular Science, Barts and the London School of Medicine and Dentistry, London, UK), and Involucrin (IVL), Integrin β1, POLR2A and YAP1 were kindly provided by Dr Muy-Teck Teh, Clinical and Diagnostic Oral Sciences, Institute of Dentistry, Barts and the London School of Medicine and Dentistry, London, UK).

2.11.4 Primer preparation and validation by qRT-PCR

The primers used in this study were either custom-designed, as described in **Section 2.11.3** and ordered from Sigma-Aldrich, Dorset, UK, or were purchased as pre-designed and validated primers from Qiagen, West Sussex, UK. The preparation of custom primers is described below.

The lyophilised forward and reverse primers were each diluted in the necessary volume of sterile 1x TE buffer (1x Tris-EDTA buffer; 10 mM Tris, 1 mM EDTA pH 8.0) as stated by Sigma-Aldrich (Dorset, UK) primer concentration datasheet, to obtain a final primer concentration of 100 μM per primer. This original solution was mixed thoroughly by vortexing and pulse spin at a table-top microcentrifuge and was stored at -20^{o}C until required. This original solution is referred to as the stock primer solution. The 500 μl working primer aliquots were prepared by 1:20 dilution of the forward and reverse primer in the same solution to obtain a final concentration of 5 μM for each

primer (25 µl of Forward primer + 25 µl of Reverse primer + 450 µl of nuclease-free water (Sigma-Aldrich, Dorset, UK) = 500 µl of F+R primers at 5 µM each). Working primer aliquots were mixed thoroughly by vortexing and pulse spin at a table-top microcentrifuge and were stored at -20^{o}C until required. For each 10 µl qRT-PCR reaction, only 1 µl of the working primer solution was used (1:10 dilution; 1 µl of F + R primers at 5 µM each + 9 µl of qRT-PCR reaction = 10 µl of qRT-PCR reaction, 0.5 µM final primer concentration for each primer). For the preparation of standard curves where 50 µl of qRT-PCR reaction is prepared for each given gene **(see Section 2.11.6)**, the concentration for each primer is increased up to 0.7 µM (1:7.14 dilution; 7 µl of F + R primers at 5 µM each + 43 µl of qRT-PCR reaction = 50 µl of qRT-PCR reaction, 0.7 µM final primer concentration for each primer).

For the preparation of commercially available Qiagen primers (10x QuantiTect Primer assay, Qiagen, West Sussex, UK), the vial with the lyophilised mix of forward and reverse primer pair was centrifuged at a table-top microcentrifuge and was reconstituted in 1.1 ml sterile 1x TE buffer (1x Tris-EDTA buffer; 10 mM Tris, 1 mM EDTA pH 8.0), mixed thoroughly by vortexing and aliquoted in 200 µl working aliquots and stored at -20^{o}C until required (working primer solution). Each 10x QuantiTect Primer assay is sufficient for 200 x 50 µl reactions as stated by Qiagen (West Sussex, UK), indicating that for each 50 µl reaction, 5 µl of the 10x QuantiTect Primer assay are used. Therefore, in this study for each 10 µl qRT-PCR reaction, only 1 µl of the working primer solution (1:10 dilution; 1 µl of F + R primers 10x QuantiTect Primer assay + 9 µl of qRT-PCR reaction = 10 µl of qRT-PCR reaction with 1x QuantiTect Primer assay) was used. The primer concentrations and sequences are proprietary and were not disclosed within the Qiagen (West Sussex, UK) product information.

To validate that the selected primers are specific for the gene of interest (amplify only one product), a qRT-PCR run was set up using cDNA from the target cell line (i.e. N/TERT) and/or a cocktail of oral human normal and neoplastic keratinocytes (provided by Dr Muy-Teck Teh, Clinical and Diagnostic Oral Sciences, Institute of Dentistry, Barts and the London School of Medicine and Dentistry, London, UK) as templates. Primer pair and cDNA, prepared as described in **Section 2.11.1** and **Section 2.11.2**, and Light Cycler® 480 SYBR Green I Master (Roche, Burgess Hill, UK) were defrosted and Syber (SYBR) Green I Master Mix reaction (qRT-PCR) was performed. Light Cycler®

480 SYBR Green I Master (2x concentrated) (Roche, Burgess Hill, UK) is a ready to use hot-start Taq DNA polymerase reaction buffer containing dNTP mix (dUTP instead of dTTP), SYBR Green I dye, and $MgCl_2$, containing also $6x10^{-6}$% Blue dye Bromophenol Blue (BPB) (Sigma-Aldrich, Dorset, UK) to visually assist sample loading in qPCR 96-well white opaque plates (Roche, Burgess Hill, UK). A 0.001% BPB solution was prepared (80 µl of 1.5% BPB in 1 ml dH_2O (nuclease-free water, Sigma-Aldrich, Dorset, UK)) and 30 µl from this solution were added in 5 ml bottle of 2x SYBR Green I Master (Roche, Burgess Hill, UK) ($6x10^{-6}$ % Blue dye Bromophenol Blue). Then 1 ml aliquots were prepared and kept at -20^{o}C until required and once defrosted were kept at 4^{o}C for 1 month. A qRT-PCR reaction for each pair of primers was therefore prepared as follows:

Component	Amount
2x SYBR Green I MASTER	4 µl
5 µM F/R Primer	1 µl
dH_2O (nuclease-free water)	4.5 µl (0.5 µl extra to correct for pipetting error)
Master Mix	**9.5 µl**

Only 9 µl were used from the master mix to correct for pipetting error, and were added on top of the template cDNA.

Master Mix	9 µl
Template cDNA	2 µl
Total volume/well	**10 + 1 µl** (1 µl extra to compensate for evaporation during preparation)

First, 2 µl of the template cDNA were loaded in each well of the 96-well plate (Roche, Burgess Hill, UK). An extra well with 2 µl of nuclease-free dH_2O (Sigma-Aldrich, Dorset, UK) instead of template cDNA was loaded as a negative control. After the master mix was prepared, it was thoroughly mixed by vortexing and then 9 µl were used for each sample and for negative control. Next, the plate was covered with a sealing foil provided by Roche, Burgess Hill, UK, and was centrifuged for 30 sec at 3,000 rpm

(centrifuge plate for 30 sec using a bench top centrifuge and hold down the quick spin button for 30 sec until reaches the 3,000 rpm), prior to starting the absolute quantitative Real Time-PCR (qRT-PCR) run on Light Cycler® 480 instrument (Roche, Burgess Hill, UK).

The samples were run on a typical qRT-PCR amplification protocol **(Table 2.2)** including an initial incubation at 95°C for 5 minutes, to allow for the activation of polymerase, linearization of cDNA, and the reduction of primer dimers in the PCR mixture. This is followed by 45 cycles of **(see Section 2.11, Figure 2.8A)**:

- 95°C for 10 sec to allow DNA denaturation so that the double stranded DNA is opened into two single strands (single-stranded DNA).
- 60°C for 6 sec for primer annealing to allow the forward and reverse primers to bind to the single stranded DNA.
- 72°C typically for 6 sec for product elongation (incubation time here dependent on the length of the product; 1 sec/25 base pairs). This will allow sufficient time for the elongation of the newly synthesised DNA strand.

Fluorescence readings were acquired at 76°C for 1 sec (at the end of the extension), once per cycle, when all PCR products are double stranded **(see Figure 2.8A)**. Samples were then subjected to a melting curve analysis **(Table 2.2)**, which begins after the final qPCR amplification cycling step, to confirm amplification specificity of the PCR products **(see Section 2.11, Figure 2.8B)**. Melting analysis is performed by 1 cycle of:

- 95°C for 30 sec in order to melt all qPCR products and to become single-stranded qPCR products (denaturation).
- 65°C for 30 sec in order to cool down and all qPCR products through annealing to become double stranded after 30 sec and thus the fluorescence signal is maximum.
- 65°C to 99°C gradual heating of qPCR products. During this gradual heating (0.11°C/1 sec), fluorescence is continuously acquired (65°C, dsDNA qPCR products, high fluorescence to 99°C, ssDNA qPCR products, no fluorescence) to generate a melting curve to determine the melting profiles (number of peaks and melting temperature for each peak) of qPCR products in each well. Therefore, a

single peak indicates the presence of a single amplified product, whereas multiple peaks indicate the presence of multiple unspecific PCR products that melt at different temperatures.

Melting analysis run, terminates at 40^{o}C. After confirmation of a single melting peak following melting curve analysis, amplified PCR products were further visualised by agarose gel electrophoresis as described below in **Section 2.11.5 (see Chapter 3, Section 3.2.1.3, Figure 3.2A i, ii and Figure 3.2B i, ii)**.

Table 2.2: Conditions for qRT-PCR amplification and melting analysis.

Stage	Function	Temperature (^{o}C)	Time	Number of cycles
1 Denaturation	Initial Denaturation	95	5 min	1
2 Amplification	Denaturation	95	10 sec	45
	Annealing	60	6 sec	
	Extension	72	6 sec	
	Fluorescence acquisition	76	1 sec	
3 Melting analysis	Melting	95	30 sec	1
	Cooling/Annealing	65	30 sec	
	Gradual heating (0.11 ^{o}C/sec) and Fluorescence acquisition	65-99	continuous	
4 Termination	Cooling/Termination	40	30 sec	1

2.11.5 Agarose gel electrophoresis

Agarose gel electrophoresis is a method used to separate DNA or RNA. Nucleic acid molecules are separated by size. This is achieved by moving negatively charged nucleic acid molecules through an agarose matrix with an electric field (electrophoresis) that forces the DNA to migrate toward the positive potential (anode). Thus, shorter molecules move faster and migrate further than longer ones because of the separating effect of the gel.

Amplified qPCR products were run on 2% Agarose gel for visualisation of product size and the validation of single-product amplification **(see Chapter 3, Section 3.2.1.3, Figure 3.2A ii and Figure 3.2B ii)**. Agarose gel was prepared by diluting 2 g of agarose (Sigma-Aldrich, Dorset, UK) in 100 ml of 1x TAE (Tris base/Acetic acid/EDTA) buffer (1x TAE; 50 ml 10x TAE buffer from Invitrogen (Paisley, UK) + 450 ml dH_2O = 500 ml). The 500 ml mixture was heated to boiling temperature and was then allowed to cool down to 60^oC prior to adding 1 µg/ml Ethidium Bromide (Sigma-Aldrich, Dorset, UK). Ethidium bromide intercalates with DNA and this causes the ethidium bromide molecule to strongly fluoresce when exposed to UV light. This allows for the location of DNA to be visualised on the gel under UV light.

Once the agarose gel was solidified, it was placed in a gel tank, which was pre-filled with 1x TAE running buffer (Invitrogen, Paisley, UK). The amplified qPCR products were loaded typically at 2 µl/well, while in the case that product amplification was less efficient, up to 5 µl/well of the qPCR product were used. For semi-quantitative PCR **(Section 2.11.8)**, the whole reaction volume of 10 µl was used for visualisation of the PCR amplified products. The qPCR amplified products were mixed in 1:1 ratio with 2x loading dye buffer (75% (v/v) Glycerol, 0.075% (v/v) Bromophenol Blue, 0.075% (v/v) Xylene Cyanol; all supplied by Sigma-Aldrich, Dorset, UK) **(see Appendix I)** (i.e. 5 µl PCR product + 5 µl 2x loading dye = 10 µl total volume) and were loaded in each well of the pre-prepared agarose gel. The samples were run against 1 Kb plus DNA ladder (1 µg/ml) (Invitrogen, Paisley, UK) to estimate the product size. The 1 Kb plus DNA ladder (1 µg/ml) (Invitrogen, Paisley, UK) was initially diluted 1:2.5 in 2x loading dye buffer (250 µl of DNA ladder + 375 µl of 2x loading dye buffer = 600 µl) to finally obtain a concentration of 0.4 µg/µl (working solution), and stored at -20^oC until

required. 5 µl of the 1 Kb plus ladder (Invitrogen, Paisley, UK) working solution were used per well. The samples were run at a constant voltage of 120 V for ~ 30 min until DNA migration was evident. qPCR products were visualised by UV light and a gel image was captured in the Autochemi imaging system (UVP, Upland, CA).

2.11.6 Generation of standard curves

Absolute quantification for a single gene is achieved by performing a standard curve using PCR product standard dilution series. The gene copy number of an unknown sample will be calculated based on the standard curve of that gene. The Light Cycler® 480 operating software (Roche, Burgess Hill, UK) will automatically calculate the gene copy numbers in unknown samples based on the standard curve fitting, using a novel non-linear algorithm.

To acquire a standard curve for each gene, the primer pair (5 µM) **(see Section 2.11.4)** was initially mixed with SYBR green I Master (2x concentrated) (Roche, Burgess Hill, UK) and a template cDNA (cocktail from a wide range of oral human normal and neoplastic derived keratinocytes, provided by Dr Muy-Teck Teh, Clinical and Diagnostic Oral Sciences, Institute of Dentistry, Barts and the London School of Medicine and Dentistry, London, UK and/or N/TERT target cell line) in the following reaction mixture followed by vortexing:

Component	Amount
2x SYBR Green I MASTER	20 µl
dH_2O (nuclease-free water)	20 µl
Template cDNA	5 µl
5 µM F/R Primer	7 µl
Total volume	**50 + 2 µl** (2 µl extra to compensate for evaporation during preparation)

Only 50 µl were used from the master mix/template cDNA mixture to correct for pipetting error, and were added in each well. The qPCR-96 well plate was centrifuged for 30 sec at 3,000 rpm as described in **Section 2.11.4**, prior to starting the absolute quantitative Real Time-PCR (qRT-PCR) run on Light Cycler® 480 instrument (Roche,

Burgess Hill, UK). The above qRT-PCR reactions were run on a typical amplification protocol as described in **Section 2.11.4** and **Table 2.2**.

2.11.6.1 Purification of qPCR product

Amplified qPCR product (double-stranded DNA) was then purified using QIAquick PCR Purification kit (Qiagen, West Sussex, UK) in order to obtain the amplified product for the specific gene of interest and to use it as template for the serial dilutions, which are necessary for the establishment of the standard curve.

The amplified qPCR product (1 volume) was mixed by pipetting up and down with 5x volume of PB buffer (Qiagen, West Sussex, UK) (i.e. 50 µl qPCR product + 250 µl PB buffer) in an 1.5 ml microcentrifuge tube (Eppendorf, Cambridge, UK) and the colour of the mixture was turned to yellow. The mixture was placed in a QIAquick spin column inside 2 ml collection tube (Qiagen, West Sussex, UK) and was spun at 13,200 rpm on a table top centrifuge for 1 minute. Upon centrifugation DNA was adhered to the column and the flow-through was discarded. QIAquick spin column inside 2 ml collection tube was then washed once in 750 µl PE buffer (Qiagen, West Sussex, UK), before centrifugation at 13,200 rpm for 1 minute. After centrifugation the flow-through was discarded and the QIAquick spin column inside 2 ml collection tube was further spun at 13,200 rpm for 1 minute to completely dry the filter. After centrifugation the 2 ml collection tube was discarded and the QIAquick spin column (Qiagen, West Sussex, UK) was placed in a clean 1.5 ml microcentrifuge tubes (Eppendorf, Cambridge, UK). To elute bound DNA, 20-30 µl of dH_2O (nuclease-free water, Sigma-Aldrich, Dorset, UK) were added to the centre of the QIAquick spin column (Qiagen, West Sussex, UK) and let to stand for 1 min, before centrifugation at 13,200 rpm for 1 minute. After centrifugation the QIAquick spin column (Qiagen, West Sussex, UK) was discarded and the eluted DNA (20-30 µl) was collected in the 1.5 ml microcentrifuge tube (Eppendorf, Cambridge, UK).

2.11.6.2 Calculation of the total number of copies in the purified qPCR product

Purified DNA concentration was measured using 2 µl from the eluted DNA (20-30 µl) and a NanoDrop™ ND-1000 Spectrophotometer (ThermoScientific, Cambridgeshire,

UK) as described in **Section 2.3.2**, of which ideally the concentration should be above 15 ng/µl.

Purified DNA concentration was used to calculate the absolute copy number of amplified qPCR products contained in the remaining eluted DNA sample (18-28 µl; 2 µl used for DNA concentration measurement) using the equation below (based on the Avogadro's constant where 1 mole 6.02 x 10^{23}):

$$\frac{\textbf{6.02 x } 10^{23} \textbf{ molecules/mole}}{\textbf{(base pair) (660 g/mole of base pair) (1x}10^{9}\textbf{ ng/g)}} \textbf{ x DNA conc. (ng/µl) x vol. (µl)} = \textbf{Number of molecules or number of copies of template in the sample.}$$

- **base pair**: qPCR product size, product length i.e. GLI2 a/β amplicon size 194 bp
- **660 g/mole**: average weight of one bp
- **1x10^9 ng/g**: in order to convert g/mole into ng/mole
- **DNA conc. (ng/µl)**: concentration of the eluted DNA
- **vol. (µl)**: qPCR template volume (eluted DNA volume)

2.11.6.3 Standard serial dilutions

To make standard dilution series of the of the purified qPCR product, a stock solution of a concentration of 10^{11} copies per 2 µl (because 2 µl will be used for qPCR reaction **(see Section 2.11.6.4)** by multiplying the number of copies of template in the sample **(see Section 2.11.6.2)** by 2, then dividing by 10^{11}copies minus the original volume (18-28 µl) in order to obtain the volume of nuclease-free dH_2O (Sigma-Aldrich, Dorset, UK) needed to be added to make 10^{11} copies/2 µl concentration stock. This was made by using the following equation:

$$\left[\frac{\left(\frac{\text{Number of copies of template in the sample}}{6.02 \times 10^{14}} \times \text{DNA conc.} \times \text{vol.} \right) \times 2}{10^{11}} \right] - \text{vol.} = \text{Volume required to dilute original stock DNA to give } 10^{11} \text{ per 2 µl concentration}$$

Then the 10^{11} copies/2 µl concentration stock was diluted using 25 µg/ml tRNA (Sigma-Aldrich, Dorset, UK; 25 µg/ml: 25 µl from stock 10 mg/ml tRNA into 10 ml dH_2O - nuclease-free (Sigma-Aldrich, Dorset, UK) to make 250 µg/10ml or 25 µg/ml solution (1:400 dilution) and kept it at -20°C until required). tRNA was used as a DNA carrier in order to prevent the qPCR products from sticking to the walls of the 1.5 ml microcentrifuge eppendorf tubes (Eppendorf, Cambridge, UK). The serial 100-fold and 10-fold dilutions (10^2 - 10^9 cDNA copies/ 2 µl) of the 10^{11} copies/2 µl amplified qPCR products were prepared in tRNA carrier as follows:

- 10^{11}/2 µl (DNA copies/2 µl) stock.
- To make 10^9/2 µl from 10^{11}, 2 µl of 10^{11} were added into 198 µl tRNA (25 µg/ml); 1:100 dilution.
- To make 10^7/2 µl from 10^9, 2 µl of 10^9 were added into 198 µl tRNA (25 µg/ml); 1:100 dilution.
- To make 10^6/2 µl from 10^7, 20 µl of 10^7 were added into 180 µl tRNA (25 µg/ml); 1:10 dilution.
- To make 10^5/2 µl from 10^6, 20 µl of 10^6 were added into 180 µl tRNA (25 µg/ml); 1:10 dilution.
- To make 10^4/2 µl from 10^5, 20 µl of 10^5 were added into 180 µl tRNA (25 µg/ml); 1:10 dilution.
- To make 10^3/2 µl from 10^4, 20 µl of 10^4 were added into 180 µl tRNA (25 µg/ml); 1:10 dilution.
- To make 10^2/2 µl from 10^3, 20 µl of 10^3 were added into 180 µl tRNA (25 µg/ml); 1:10 dilution.

Standard dilution series were thoroughly mixed by vortexing stored at -20°C until required.

2.11.6.4 Standard curve qRT-PCR reaction

A qRT-PCR run was prepared, using the standard dilution series range of 10^2-10^6 for each gene. A single qRT-PCR reaction was prepared as follows:

Component	Amount
2x SYBR Green I MASTER	4 µl
5 µM F/R Primer	1 µl
dH_2O (nuclease-free water)	4.5 µl (0.5 µl extra to correct for pipetting error)
Master Mix	**9.5 µl**

Only 9 µl were used from the master mix to correct for pipetting error, and were added on top of the template cDNA.

Master Mix	9 µl
Template cDNA	2 µl
Total volume/well	**10 + 1 µl** (1 µl extra to compensate for evaporation during preparation)

First, standards were defrosted and mixed thoroughly by vortexing, before loading 2 µl of the template cDNA in each well of the 96-well plate (Roche, Burgess Hill, UK). An extra well with 2 µl of nuclease-free dH_2O (Sigma-Aldrich, Dorset, UK) instead of template cDNA was loaded as a negative control. After the master mix was prepared, it was thoroughly mixed by vortexing and then 9 µl were used for each sample and for negative control. Next, the plate was covered with a sealing foil provided by Roche, Burgess Hill, UK, and was centrifuged for 30 sec at 3,000 rpm (centrifuge plate for 30 sec using a bench top centrifuge and hold down the quick spin button for 30 sec until reaches the 3,000 rpm), prior to starting the absolute quantitative Real Time-PCR (qRT-PCR) run on Light Cycler® 480 instrument (Roche, Burgess Hill, UK). The samples

were run on a typical qRT-PCR amplification protocol as described in **Section 2.11.4 and Table 2.2**.

Amplification curves for each dilution series were obtained **(see Chapter 3, Section 3.2.1.3, Figure 3.2B iii)** and standard curves for each given gene were thus calculated by the LightCycler® 480 qPCR software program (Roche, Burgess Hill, UK) **(see Chapter 3, Section 3.2.1.3, Figure 3.2B iv)**, and were thereafter used for absolute copy number quantitative PCR **(see Section 2.11.7)**.

2.11.7 Gene Amplification by qRT-PCR

All qRT-PCR experiments for the expression analysis of genes (gene amplification) used in this study were performed according to the protocols described in **Section 2.11.4** and **Section 2.11.6.4**. In addition all primers and primer sequences are listed in primer table **(Table 2.3)**.

Using the GeNorm algorithm analysis method (Vandesompele et al., 2002), and the LightCycler® 480 Relative Quantification Software program (Roche, Burgess Hill, UK) (with built-in multiple reference genes normalisation algorithm, Roche, Burgess Hill, UK), of the 8 reference genes (GAPDH, RPLPO, YAP1, UBC, HPRT1, POLR2A, ESD, 18S), two were identified as being most reliable and stable reference genes: polymerase (RNA) II (DNA directed) polypeptide A (POLR2A) and Yes-associated protein 1 (YAP1) across a large panel of normal and cancer human cells and tissues (the analysis of housekeeping genes was performed by Dr Muy-Teck Teh, Clinical and Diagnostic Oral Sciences, Institute of Dentistry, Barts and the London School of Medicine and Dentistry, London, UK (Gemenetzidis et al., 2009)). POLR2A and YAP1 were used as reference genes for all subsequent qRT-PCR experiments to calculate target gene expression levels. Given that the LightCycler® 480 Relative Quantification Software program (Roche, Burgess Hill, UK) was fast, convenient and produces highly similar results to the GeNorm analysis method, all subsequent data analysis was performed using the LightCycler® 480 qPCR software program (Roche, Burgess Hill, UK) to expedite work flow. Samples were analysed in triplicates and values of

statistical significance were calculated using GraphPad's InStat Software (V2-04a; Graph-Pad Software, San Diego, CA) for student's *t* test analysis **(see Section 2.16)**.

Table 2.3: Primer table. *** N/A: Non/Applicable**

Genes	Forward (F) and Reversed (R) Primer Nucleotide Sequence (5'-3')	Product (bp)
BCL2-F **BCL2-R**	TGGACAACCATGACCTTGGACAATCA TCCATCCTCCACCAGTGTTCCCATC	198
CDKN1A-F **CDKN1A-R**	*N/A. Commercially available by Qiagen, West Sussex, UK Cat. No: QT00062090	79
c-MYC-F **c-MYC-R**	TTTTTCGGGTAGTGGAAAACC GAGGTCATAGTTCCTGTTGGTG	80
E-Cadherin-F **E-Cadherin-R**	GAACGCATTGCCACATACAC AGCACCTTCCATGACAGACC	160
GLI2 α/β-F **GLI2 α/β-R**	GGGTCAACCAGGTGTCCAGCACTGT GATGGAGGGCAGGGTCAAGGAGTTT	194
GLI2-F **GLI2-R**	*N/A. Commercially available by Qiagen, West Sussex, UK Cat. No: QT00018648	116
Integrin β1-F **Integrin β1-R**	CGATGCCATCATGCAAGT AGTGAAACCCGGCATCTG	95
IVL-F **IVL-R**	TGCCTGAGCAAGAATGTGAG TTCCTCATGCTGTTCCCAGT	83
POLR2A-F **POLR2A-R**	GCAAATTCACCAAGAGAGACG CACGTCGACAGGAACATCAG	72
SNAIL1-F **SNAIL1-R**	GCTGCAGGACTCTAATCCAGA ATCTCCGGAGGTGGGATG	84
SNAIL2-F **SNAIL2-R**	ACAGCGAACTGGACACACAT GATGGGGCTGTATGCTCCT	113
SOX2-F **SOX2-R**	GGGGGAATGGACCTTGTATAG GCAAAGCTCCTACCGTACCA	85
WNT11-F **WNT11-R**	TGTGCTATGGCATCAAGTGG GCACCTGTGCAGACACCA	108
WNT5A-F **WNT5A-R**	*N/A. Commercially available by Qiagen, West Sussex, UK Cat. No: QT00025109	105
WNT7A-F **WNT7A-R**	GGGACTATGAACCGGAAAGC CCAGAGCTACCACTGAGGAGA	103
YAP1-F **YAP1-R**	CCCAGATGAACGTCACAGC GATTCTCTGGTTCATGGCTGA	82

2.11.8 Gene Amplification by semi-quantitative PCR

Semi-quantitative PCR analysis was performed in Verity 96-well Thermal Cycler (Applied Biosystems, Carlsbad, CA) for the visualisation of GLI2 (whole gene amplification or α/β isoform specific amplification) gene mRNA expression. The cDNA template samples were prepared in 0.2 ml PCR tubes (Eppendorf, Cambridge UK) for ease of use. The PCR reaction for each gene was prepared as previously described in **Section 2.11.4** and **Section 2.11.6.4**. Each PCR reaction therefore contained the following:

Component	Amount
2x SYBR Green I MASTER	4 µl
5 µM F/R Primer	1 µl
dH_2O (nuclease-free water)	4.5 µl (0.5 µl extra to correct for pipetting error)
Master Mix	**9.5 µl**

Only 9 µl were used from the master mix to correct for pipetting error, and were added on top of the template cDNA.

Master Mix	9 µl
Template cDNA	2 µl
Total volume/PCR tube	**10 + 1 µl** (1 µl extra to compensate for evaporation during preparation)

First, 2 µl of the template cDNA were loaded in each 0.2 ml PCR tubes (Eppendorf, Cambridge UK). An extra 0.2 ml PCR tube (Eppendorf, Cambridge UK) with 2 µl of nuclease-free dH_2O (Sigma-Aldrich, Dorset, UK) instead of template cDNA was also prepared as a negative control. After the master mix was prepared, it was thoroughly mixed by vortexing and then 9 µl were used for each sample and for negative control. Next, samples were run on the same PCR amplification protocol as previously described in **Section 2.11.4**, **Table 2.2** with the only difference that the thermal cycles were reduced to 36 for GLI2 full-length and POLR2A, and to 27 and 30 for GLI2 a/β and

POLR2A respectively, to avoid saturation of PCR product amplification. Once the PCR thermal cycles were finished, the samples were maintained at a constant temperature of 4^{o}C until they were used for agarose gel electrophoresis in order to visualise the expression levels of each gene as described in **Section 2.11.5**. The whole volume of the PCR reaction (10 µl) was loaded on 2% agarose gel following 1:1 ratio with 2x loading dye buffer **(see Appendix I)** (10 µl of PCR product + 10 µl of 2x loading dye buffer). All samples were run against 1 Kb plus DNA ladder (Invitrogen, Paisley, UK) at a constant voltage of 120 V for ~ 30 min, until DNA separation was evident. PCR products were visualised by UV light and a gel image was captured in the Autochemi imaging system (UVP, Upland, CA).

2.12 Protein extraction and Western Blotting analysis

Different methods of protein isolation were utilised, depending on the distribution of the protein in the cell. Two different buffers where used for total protein isolation, including mainly 1x RIPA buffer (which is a very strong lysis buffer) and 1x Reporter Lysis Buffer (Promega, Southampton, UK) (a weaker reporter lysis buffer) in some cases. For nuclear and cytosolic protein isolation, the Nuclear Extraction Kit (Imgenex, San Diego, CA) was chosen for β-catenin protein analysis, since β-catenin is located in the membrane and the cytoplasm (where it is degraded) and upon activation of WNT signalling pathway it accumulates in the cytoplasm and translocates to the nucleus and forms a complex with TCF/LEF transcription factor and thus activates transcription of target genes.

2.12.1 Total Protein Extraction from cultured cells

For total protein extraction, equal number $3x10^5$ - $1x10^6$ of N/TERT, SINCE, and SINEG2 cells were seeded in 10 cm dishes, and harvested either 24, 48 or 72 hr after plating (semi-confluent). Similarly, equal number $3x10^5$ or $1x10^5$ of N/TERT and NTEG2 cells were seeded in 10 cm dishes, and harvested either 72 hr or 6 days after plating, respectively (semi-confluent) (48 hr or 5 days after doxycycline removal respectively). Doxycycline was removed in all NTEG2 cells 24 hr after plating (NTEG2 Dox-).

Total cell proteins were extracted from cultured cells in 1x RIPA buffer. Culture media was aspirated from cells in 10 cm petri dishes, and cells were washed twice in ice-cold 10 ml PBS **(Appendix I)**, and then incubated in ice-cold 100-500 µl 1x RIPA buffer (50 mM Tris base, pH 7.3, 150 mM NaCl, 0.1% (v/v) SDS, 1% (v/v) Nonidet P-40, 10 mM sodium orthovanadate (Na_3VO_4 - phosphatase inhibitor); all from Sigma-Aldrich, Dorset, UK) **(see Appendix I)** (lysis buffer volume was depending on the confluence of the cells). Lysis buffer also contained freshly added protease inhibitor cocktail 1x CM EDTA-free (complete mini EDTA-free protease inhibitor cocktail tablets, Roche Diagnostics, Burgess Hill UK) **(see Appendix I)**, to prevent degradation of proteins of interest by proteases after cell lysis. Cells were kept on ice for 20 minutes prior to collecting the cell lysates. The protein was harvested, by scraping, in 1.5 ml

microcentrifuge tubes (Eppendorf, Cambridge, UK), and cell lysates were then centrifuged at 14,000 rpm at 4°C for 20 min in a microcentrifuge, to remove cell debris. Supernatants were then collected as whole protein lysates and transferred to clean in 1.5 ml microcentrifuge tubes (Eppendorf, Cambridge, UK). The supernatants were snap frozen in dry ice before being stored at -80°C until required. The protein concentration of the supernatant was determined by using Dc Protein Assay Kit (BioRad, Hertfordshire, UK) **(Section 2.12.4.2)**.

Alternatively, total cell proteins were extracted from cultured cells in 1x Reporter Lysis Buffer (Promega, Southampton, UK). Culture media was aspirated from cells in 10 cm petri dishes, and cells were washed twice in ice-cold 10 ml PBS **(Appendix I)**, and then incubated in 100-300 µl 1x Reporter Lysis Buffer (Promega, Southampton, UK) (for 1 ml 1x Reporter Lysis Buffer; 200 µl 5x Reporter Lysis Buffer (Promega, Southampton, UK) diluted in 800 µl sterile distilled water (PAA, Somerset, UK) - 1:5 dilution) (lysis buffer volume was depending on the confluence of the cells). Lysis buffer also contained freshly added protease inhibitor cocktail 1x CM EDTA-free (complete mini EDTA-free protease inhibitor cocktail tablets, Roche Diagnostics, Burgess Hill UK) **(see Appendix I)**. Cells were kept on ice for 20 minutes prior to collecting the cell lysates. The protein was harvested, by scraping, in 1.5 ml microcentrifuge tubes (Eppendorf, Cambridge, UK), and cell lysates were then centrifuged at 14,000 rpm at 4°C for 20 min in a microcentrifuge, to remove cell debris. Supernatants were then collected as whole protein lysates and transferred to clean in 1.5 ml microcentrifuge tubes (Eppendorf, Cambridge, UK). The supernatants were snap frozen in dry ice before being stored at -80°C until required. The protein concentration of the supernatant was determined by using the Bio-Rad Protein Assay System (BioRad, Hertfordshire, UK) **(Section 2.12.4.2)**.

2.12.2 Total Protein Extraction from UV and non-UV treated cells

For total protein extraction, equal number $3x10^5$ of N/TERT, SINCE, and SINEG2 cells were seeded in 6 cm dishes, and were either mock treated or UVB treated 24 or 48 hr after plating (semi-confluent) **(see Section 2.13)**. 24 hr after UVB treatment, mock and UVB treated cells were harvested.

Total cell proteins were extracted from UV and non-UV treated cultured cells in 1x RIPA buffer. For the extraction of total protein from UV irradiated cells **(see Section 2.13)**, culture media from each of the 6 cm petri dishes were collected to include any dead or apoptotic cells that may be floating in the medium following irradiation. Control non-UV treated cells were processed similarly. Therefore, supernatants (culture media) were collected in 15 ml falcon tubes and cells were centrifuged at 1,100 rpm for 5 minutes. At the same time, the culture dishes were placed on ice and the cells attached in the 6 cm petri dishes were washed with 5 ml of ice-cold PBS **(Appendix I)** and were lysed in 50-100 µl of ice-cold 1x RIPA buffer **(see Appendix I)**, (lysis buffer volume was depending on the confluence of the cells). Lysis buffer also contained freshly added protease inhibitor cocktail 1x CM EDTA-free (complete mini EDTA-free protease inhibitor cocktail tablets, Roche Diagnostics, Burgess Hill UK) **(see Appendix I)**. Once the centrifugation of floating dead cells was finished, the supernatant was discarded and cells were washed with 5 ml of ice-cold PBS and cells were spun again at 1,100 rpm for 5 minutes. The supernatant was discarded and the cell pellet was directly lysed by the addition of 50-100 µl ice-cold 1x RIPA buffer **(see Appendix I)**, containing also a freshly added protease inhibitor cocktail 1x CM EDTA-free (complete mini EDTA-free protease inhibitor cocktail tablets, Roche Diagnostics, Burgess Hill UK) **(see Appendix I)**. The solution was mixed thoroughly by repeated pipetting. The lysed pellets were now added to the 6 cm culture dishes, which contain the previously lysed attached cells (total 100-200 µl ice-cold 1x RIPA buffer, depending on confluence). The culture dishes were incubated on top of ice for an additional 20 minutes for complete lysis. The protein was harvested, by scraping, in 1.5 ml microcentrifuge tubes (Eppendorf, Cambridge, UK), and cell lysates were then centrifuged at 14,000 rpm at 4°C for 20 min in a microcentrifuge, to remove cell debris. Supernatants were then collected as whole protein lysates and transferred to clean in 1.5 ml microcentrifuge tubes (Eppendorf, Cambridge, UK). The supernatants were snap frozen in dry ice before being stored at -80°C until required. The protein concentration of the supernatant was determined by using Dc Protein Assay Kit (BioRad, Hertfordshire, UK) **(Section 2.12.4.2)**.

2.12.3 Subcellular Protein Extraction from cultured cells

Cells for whole protein extraction and cells for subcellular fractionation were cultured at the same time in separate 10 cm dishes, for each experiment. When cells reached 50-70% confluence they were harvested for whole protein (half of the 10 cm dishes) using 1x RIPA buffer, containing also a freshly added protease inhibitor cocktail 1x CM EDTA-free (complete mini EDTA-free protease inhibitor cocktail tablets, Roche Diagnostics, Burgess Hill UK) **(Appendix I)** as described in **Section 2.12.1**, while fractionation was performed in the cells in the remaining 10 cm dishes, by sequential extraction of cytosolic and nuclear proteins using the Nuclear Extraction Kit (Imgenex, San Diego, CA).

Culture media was aspirated from cells in each 10 cm petri dish, and cells were washed twice with 5 ml of ice-cold 1x PBS/PMSF (Imgenex, San Diego, CA) **(see Appendix I)**. Cells were harvested by scraping from the 10 cm petri dishes and were transferred in 15 ml falcon tubes, followed by centrifugation at 1,000 rpm for 5 minutes in a cold centrifuge. After centrifugation, the supernatant was discarded and the pellet from each 10 cm dish was kept in ice.

In order to obtain the cytoplasmic fraction, the pellet was resuspended in 1 ml of ice-cold 1x Hypotonic Buffer (Imgenex, San Diego, CA) **(see Appendix I)** by pipetting up and down several times and was transferred to a pre-chilled 1.5 ml microcentrifuge tube (Eppendorf, Cambridge, UK). The resuspended cells were kept on ice for 15 min. Then 50 μl of detergent solution (Imgenex, San Diego, CA) was added to the resuspended cells and cells were vortexed vigorously for 10 sec. The cells were centrifuged for 30 sec at 14,000 rpm at 4°C in a microcentrifuge. The supernatant, which is the cytoplasmic fraction, was carefully removed into a pre-chilled 1.5 ml microcentrifuge tube (Eppendorf, Cambridge, UK) and stored at -80°C until required. The remaining pellet is the nuclear fraction.

In order to collect the nuclear fraction, the nuclear pellet was resuspended in 100 μl Nuclear Lysis Buffer (Imgenex, San Diego, CA) **(see Appendix I)** by pipetting up and down. The suspension was vortexed vigorously and was incubated at 4°C for 30 minutes on a rocking platform. After incubation, the suspension was vortexed again for

30 sec and was centrifuged at 14,000 rpm for 10 min at 4°C in a microcentrifuge. Then the supernatant, which is the nuclear fraction, was transferred into a pre-chilled 1.5 ml microcentrifuge tube (Eppendorf, Cambridge, UK) and stored at -80°C until required.

2.12.4 Protein measurement using colorimetric assays and spectrometry

2.12.4.1 Spectrometry

Spectrometry is widely used for the accurate determination of the concentration of a given chemical. The instrument that is commonly used to measure the amount of protein in a given solution is the spectrophotometer, or a microplate reader. The measurement of concentration of a given substance relies on the property of chemical structures to absorb light (absorption). Absorption refers to the physical process of absorbing light (electromagnetic energy) and is the way by which the energy of a photon is taken up by matter, typically the negatively charged electrons of an atom (basic unit of matter). Absorption is mathematically quantified as absorbance (or optical density) and is calculated by the detection instrument. A light source illuminates the sample of interest with a specified wavelength (maximum absorbance wavelength) (i.e. specified by a monochromator) and a light detector which is placed on the other side of the beam and measures how much of the initial light is transmitted through the actual sample and therefore, how much of the initial light is absorbed by the sample. The amount of light absorbed is therefore proportional to the amount of the chemical compound present in the sample. This method has many applications including the detection of protein and nucleic acid concentrations.

2.12.4.2 Colorimetric assays and protein measurement

Assays for the detection of protein are also known as colorimetric assays and their detection requires the presence of light in the visible spectrum 380-700 nm. For example, Bio-Rad Protein Assay System (Bradford assay) (BioRad, Hertfordshire, UK) can be used for the determination of protein concentration by using a standard spectrophotometer or microplate reader **(see Section 2.12.4.1)** which illuminates the samples with a light at 595 nm wavelength. The determination of protein concentration is based on the absorbance of Coomassie® Brilliant Blue G-250 dye - green colour -

(Bio-Rad Protein Assay Reagent, BioRad, Hertfordshire, UK) which changes to blue by binding to protein in the sample. The bound, and therefore blue, form of the dye has a maximal absorption rate at 595 nm. Therefore the increase of absorbance is proportional to the amount of bound dye (blue) and therefore to the amount of protein present in the original sample. Similar to this principle, the Dc Protein Assay Kit (BioRad, Hertfordshire, UK) is based on the reaction of protein with an alkaline copper tartrate solution and Folin reagent which leads to the development of blue colour with maximum absorbance at 750 nm (also measured at 650 nm).

Protein concentrations were measured either using the Bio-Rad Protein Assay System (Bradford Assay) (BioRad, Hertfordshire, UK) or the Dc (Detergent compatible) protein Assay Kit (BioRad, Hertfordshire, UK), depending on which extraction buffer was used.

Protein concentrations of cell lysates harvested in 1x Reporter Lysis Buffer (Promega, Southampton, UK) were measured using the Bio-Rad Protein Assay System (BioRad, Hertfordshire, UK). First, a protein standard curve **(Figure 2.9A)** was generated by using bovine serum albumin (BSA) protein samples (New England Biolabs (NEB), Manchester, UK) of known concentrations, which had been diluted in the same lysis buffer (1x Reporter Lysis Buffer, Promega, Southampton, UK) as the samples to be analysed. Stock BSA concentration 10 mg/ml (NEB, Manchester, UK) was diluted 1:10 (1 mg/ml) in 1x Reporter Lysis Buffer (Promega, Southampton, UK); 100 µl BSA stock + 900 µl 1x Reporter Lysis Buffer = 1 ml total volume, and was aliquoted in 100 µl per 1.5 ml microcentrifuge tubes (Eppendorf, Cambridge, UK) which were either kept in ice or being stored at -80^{o}C until required. Next, the 5x Bio-Rad Protein Assay Reagent (Bio-Rad Protein Assay System, Hertfordshire, UK) was diluted in dH_2O (6 ml of 5x Bio-Rad Protein Assay Reagent in 24 ml dH_2O). A series of different protein dilutions in a final volume of 2 ml was made to contain the following concentrations: 0, 1, 2, 4, 8, 12, 16, 20, 30, and 40 µg/2 ml. A sample protein dilution, prepared in a 15 ml falcon tube, contained the following: 2 µl BSA (1 µg/µl) + 2 µl 1x Reporter Lysis Buffer + 2 ml of 1x Bio-Rad Protein Assay Reagent, to give for example a concentration of 2 µg/2 ml (1 µg/ml). All samples were thoroughly mixed by vortexing and were incubated for 10 minutes at room temperature. The intensity of the solution colour in each 15 ml falcon tube was proportional to the amount of protein. Next, samples were transferred

from the 15 ml falcon tubes to 1.5-3.0 ml cuvettes (Plastibrand, Sigma-Aldrich, Dorset, UK) and the absorbance (optical density) of each sample was measured at 595 nm at a Beckman Coulter DU800 spectrophotometer (Beckman Coulter, High Wycombe, UK). After obtaining absorbance values, a standard curve was plotted (where x = BSA protein concentration (μg/2 ml) and y = absorbance (optical density) at 595 nm), and the equation of the line of the best fit was acquired from Microsoft Excel, as well as the R^2 value which is a quantitative value known as goodness of fit. R^2 values close to 1 indicate a good fit **(Figure 2.9A)**.

To measure the protein concentration in unknown samples, 2 μl of protein lysates were mixed with 2 μl of 1x Reporter Lysis buffer (Promega, Southampton, UK) and 2 ml of 1x Bio-Rad Protein Assay Reagent (BioRad, Hertfordshire, UK). Next, the same procedure as the one mentioned above was followed. After obtaining absorbance values for all unknown samples, the standard curve equation (i.e. y = 0.031x; where y is the optical density and x is the quantity of protein) **(Figure 2.9A)** was used to calculate the amount of protein that was initially present in 2 ml of solution. Since 2 μl of the protein lysate were initially added, the protein concentration of unknown samples (mg/ml or μg/μl) was deduced. For example, if absorbance = 0.465, then the protein contained in 2 ml of solution is 15 μg (according to equation x = 0.465/0.031). If 2 μl of lysate were initially added, then protein concentration of unknown sample is 15 μg / 2 μl = 7.5 μg/μl.

Protein concentrations of cell lysates harvested in 1x RIPA buffer, Hypotonic and Nuclear Buffers (Imgenex, San Diego, CA) were measured using the Dc Protein Assay Kit (BioRad, Hertfordshire, UK). First, a protein standard curve **(Figure 2.9B)** for each buffer was generated by using bovine serum albumin (BSA) protein samples (NEB, Manchester, UK) of known concentrations which had been diluted in the same lysis buffer as the samples to be analysed. First, BSA protein samples of different concentrations (final volume of 10 μl in lysis buffer) were added in each of 10 wells of a clear, flat bottomed 96-well plate (Nunc, Roskilde, Denmark). The BSA protein amounts (1 mg/ml; prepared from a 10 mg/ml stock solution as I described above using the appropriate lysis buffer) that were used in each well were as follows: 0, 0.5, 1, 1.5, 2, 3, 4, 5, 6, 7, 8 and 9 μg. A sample protein dilution, prepared in a 1.5 ml microcentrifuge eppendorf tube (Eppendorf, Cambridge, UK), contained the following:

2 µl BSA (1 µg/µl) + 8 µl lysis buffer, to give for example a concentration of 2 µg/10 µl or 0.2 µg/µl. Next, 25 µl of Reagent A (Reagent A; 20 µl Reagent S for each ml of Reagent A, i.e. Reagent S 20 µl + Reagent A 980 µl = 1 ml Reagent A, Dc Protein Assay Kit, BioRad, Hertfordshire, UK) was added in each well. Following gentle rocking, 200 µl of Reagent B (Dc Protein Assay Kit, BioRad, Hertfordshire, UK) were added on top and mixed well. Plates were then incubated at room temperature for 15 minutes, prior to measuring the absorbance (optical density) of each sample. The intensity of the solution colour in each well was proportional to the amount of protein. Thus, absorbances were measured at 650 nm in VICTOR^2 Multilabel Counter; Wallac Oy, Turku, Finland. After obtaining absorbance values, a standard curve was plotted (where x = BSA protein concentration (µg/10 µl) and y = absorbance (optical density) at 650 nm), and the equation of the line of the best fit was acquired from Microsoft Excel, as well as the R^2 value **(Figure 2.9B)**.

To measure the protein concentration in unknown samples, 1 or 2 µl of protein lysates were mixed with 9 or 8 µl of lysis buffer respectively (total volume 10 µl). Next, the same procedure as the one mentioned above was followed. After obtaining absorbance values for all unknown samples, the standard curve equation (i.e. $y = 0.0205x + 0.0385$; where y is the optical density and x is the quantity of protein) **(Figure 2.9B)** was used to calculate the amount of protein that was initially present in 10 µl of lysis buffer. According to whether 1 or 2 µl of the protein lysate was added, the protein concentration of unknown samples (mg/ml or µg/µl) can be deduced. For example, if absorbance = 0.125, then the protein contained in 10 µl of solution is 4.2 µg (according to equation x = (0.125-0.0385) / 0.0205). If 2 µl of lysate were initially added, then protein concentration of unknown sample is 4.2 µg / 2 µl = 2.1 µg/µl.

A

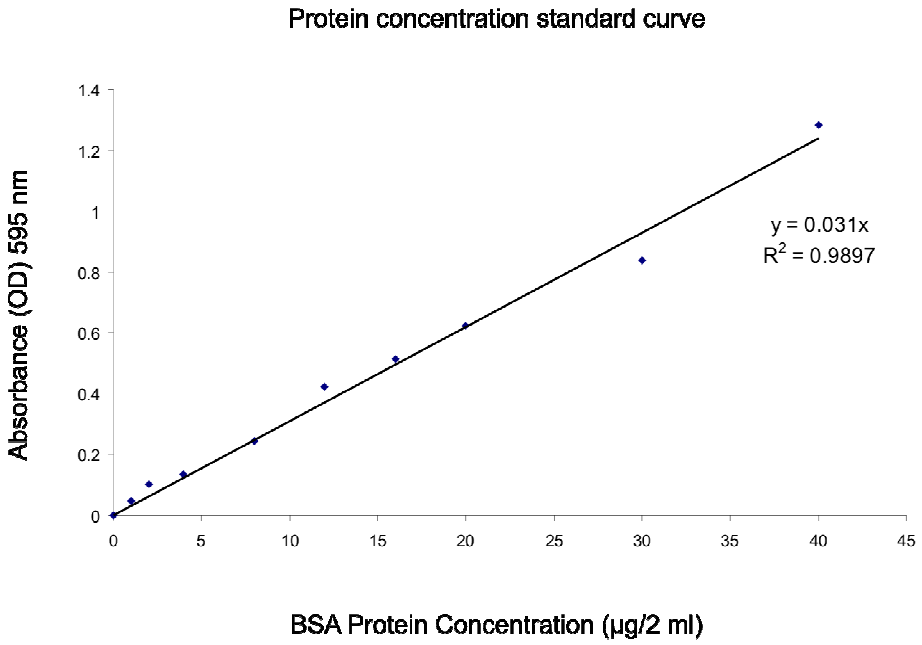

B

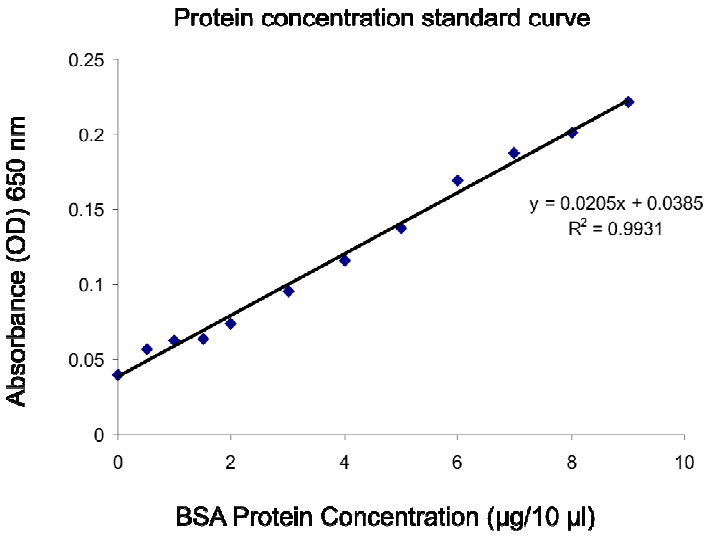

Figure 2.9: Protein concentration standard curves.

(A) Example of a Bio-Rad Protein Assay standard curve. **(B)** Example of a Dc Protein Assay standard curve.

2.12.5 Western Blotting analysis

Western blotting can be used to estimate the abundance of a specific protein in a cellular sample. Following extraction, proteins are firstly denatured to break any protein-protein interactions. Then, denatured proteins are run in a sodium dodecyl sulphate (SDS) gel which allows their efficient separation according to their molecular size. SDS applies a negative charge to denatured proteins on the gel, thus allowing the protein to be separated in the polyacrylamide gel by means of electrophoresis. When proteins are sufficiently separated on the SDS-polyacrylamide gel, they are then transferred to nitrocellulose membranes which are specialised membranes, with a high affinity for protein binding. Since SDS applies a negative charge to separated proteins on the gel, it allows the protein to be transferred from the SDS-polyacrylamide gel to the membrane by means of electrophoresis. Following transfer, the protein of interest can be accurately detected by incubating the membrane with a highly specific antibody (primary antibody) raised against the protein of interest. Next, a secondary antibody raised in the same species as the primary one, is used in order to detect the primary antibody, which is now bound on the protein of interest. Secondary antibodies are typically coupled to horseradish peroxidase (HRP) for their easy detection. Bound secondary antibodies can therefore be detected by chemi-luminescence due to a chemical reaction with the addition of ECL plus (GE Healthcare, Buckinghamshire, UK). Chemiluminescence is the emission of light as a result of a chemical reaction and it differs from fluorescence **(see Section 2.8.1.1)** in that the electronic excited state is derived from the product of a chemical reaction, rather than the more typical way of creating electronic excited states namely absorption **(see Section 2.12.4.1)**. HRP reacts with a lumigen PS-3 acridan substrate in the ECL plus solution and converts it to an acridinium ester intermediate. The ester intermediate reacts with peroxide in alkaline conditions to emit a light signal that is detected using an autoradiography film (Veitch, 2004).

2.12.5.1 SDS-Polyacrylamide Gel Electrophoresis (PAGE)

Extracted proteins were diluted in 5x SDS sample buffer (0.31 M Tris-HCl, pH 6.8, 0.25 M DTT (dithiothreitol), 0.1% (v/v) Bromophenol Blue, 50% (v/v) Glycerol, 10% (w/v) SDS; all supplied by Sigma-Aldrich, Dorset, UK) **(see Appendix I)** and briefly denatured for 5 min at 100°C, before loading on either standard freshly made 8% or

10% SDS-polyacrylamide mini gels (with a 5% stacking gel) **(see Appendix I)** or pre-cast 4-12% NuPAGE® (Invitrogen, Paisley, UK) mini gels. In most experiments the standard freshly made 8% or 10% SDS-polyacrylamide mini gels (with a 5% stacking gel) were used instead of the pre-cast 4-12% NuPAGE® (Invitrogen, Paisley, UK) mini gels. First, according to the protein concentration (μg/μl) obtained from protein measurement **(Section 2.12.4)** the amount of protein and of sample buffer was calculated as follows: to load 5 μg per lane from a protein sample with 0.5 μg/μl protein concentration, 10 μl from the protein sample will be taken and will be mixed with 2.5 μl 5x sample buffer (1:4 ratio; 10 μl lysate / 4 = 2.5 μl sample buffer) and were kept on ice until denaturation and loading step. Then, either a freshly made 8% or 10% SDS-polyacrylamide mini gel (with a 5% stacking gel) **(see Appendix I)** that was prepared in a Mighty Small dual gel Caster (Hoefer, Holliston, MA) or a pre-cast 4-12% NuPAGE® (Invitrogen, Paisley, UK) mini gel, were assembled into a Mighty Small II complete gel elecrophoresis tank (Hoefer, Holliston, MA) or into a Novex Mini-cell gel electrophoresis tank (Invitrogen, Paisley, UK), respectively, according to manufacturer's instructions. The Mighty Small II complete gel elecrophoresis tank (Hoefer, Holliston, MA) was filled with standard 1x SDS based running buffer (25 mM Tris base, 192 mM Glycine, 0.1% SDS; all from Sigma-Aldrich, Dorset, UK) (1x SDS running buffer; 100 ml 10x SDS running buffer + 900 ml dH_2O = 1 L) **(see Appendix I)** and the Novex Mini-cell gel electrophoresis tank (Invitrogen, Paisley, UK) with NuPAGE® MES-SDS running buffer (Invitrogen, Paisley, UK). Equal protein amount (μg) (briefly denatured) for each sample, was loaded into the lanes of the gel, ranging from 2 μg up to 30 μg and in one case 60 μg. In addition, 10 μl of Precision Plus Protein (All Blue Standards) standard molecular weight marker (Bio-Rad Laboratories, Hertfordshire, UK) was loaded into one lane of the gel, in order to determine protein size.

Gels were typically run (proteins were separated) at a constant rate of 90 V, until molecular weight marker (Precision Plus Protein All Blue Standards; Bio-Rad Laboratories, Hertfordshire, UK) separation was evident, after which point voltage was increased to 120 V until the dye front reached the base of the gel or even for longer if the protein of interest was of a high molecular weight.

2.12.5.2 Immunoblot analysis

Proteins were then transferred from the either the SDS-polyacrylamide gel or from the pre-cast 4-12% NuPAGE® (Invitrogen, Paisley, UK) gel to a Hybond-C extra nitrocellulose membrane (Amersham, GE Healthcare, Buckinghamshire, UK) in a Bio-Rad transfer tank (Bio-Rad Laboratories, Hertfordshire, UK) containing 1x Transfer Buffer (25 mM Tris base, 192 mM Glycine, 20% (v/v) methanol; all supplied by Sigma-Aldrich, Dorset, UK, whereas methanol was obtained by Fisher, Leicestershire, UK) (1x Transfer buffer; 100 ml 10x Transfer buffer + 200 ml methanol + 700 ml dH_2O = 1 L) **(see Appendix I)** at a constant current of 400 mA for 90 minutes or at constant 20 V for overnight transfer at 4^oC.

After transfer, the membrane was removed and immediately immersed in 1x TBS (1x TBS; 100 ml 10x TBS + 900 ml dH_2O = 1 L) or 1x TBS containing 0.1% Tween-20 (Sigma-Aldrich, Dorset UK) (TBS/T; 1x TBS/T; 100 ml 10x TBS + 899 ml dH_2O + 1 ml Tween-20 = 1 L) **(see Appendix I)** or 1x PBS containing 0.1% Tween-20 (Sigma-Aldrich, Dorset UK) (PBS/T; 1x PBS/T; 100 ml 10x PBS + 899 ml dH_2O + 1 ml Tween-20 = 1 L) **(see Appendix I)** and kept in the fridge if not immediately used.

The success of the transfer was estimated by checking that the protein marker was present on the membrane, as well as by performing Ponceau staining. Ponceau S (Sigma-Aldrich, Dorset UK) is a sodium salt routinely used for the rapid, but reversible, detection of protein bands on nitrocellulose membranes. To visualise protein, the nitrocellulose membrane was rinsed 2x with dH_2O and was then immersed in Ponceau S (diluted 1:10 in dH_2O) (Sigma-Aldrich, Dorset UK) for a few seconds until protein bands were visible. Next, the membrane was rinsed 2x in dH_2O and then was thoroughly washed with TBS/T or PBS/T until no protein bands were anymore visible. Membrane was then stored for short time at 4^oC in TBS, TBS/T or PBS/T for future use, or was immediately used for immunoblotting.

The membrane was then blocked in 5% (w/v) non-fat dry milk in TBS, TBS/T or PBS/T **(see Appendix I)**, according to **Table 2.4,** for 30 min at room temperature under continuous agitation on a rocking platform. The membrane has a high affinity for protein binding and therefore during membrane blocking, the milk proteins will cover all the sites of the membrane, which are not occupied by cellular proteins. This way, the

primary antibodies will not bind at non-specific sites of the membrane, and will thus only recognise the proteins of interest.

Next, the membrane was probed with 6-10 ml of primary antibody diluted in either 3% milk TBS/T or PBS/T or 5% milk TBS, TBS/T or PBS/T, for 2 hours at room temperature or was incubated overnight at 4^{o}C according to **Table 2.4,** under continuous agitation on a rocking platform. Primary antibodies used are listed in antibody table **(Table 2.4)**.

The membrane was washed 3x in 3% milk TBS/T or PBS/T or 5% milk TBS, TBS/T or PBS/T (same buffer as the primary antibody) for 5 minutes each wash, under continuous agitation on a rocking platform at room temperature, prior to incubation with secondary antibody. Secondary antibody was diluted in 12-15 ml of 3% milk TBS/T or PBS/T or 5% milk TBS, TBS/T or PBS/T (same buffer as the primary antibody) and membranes were incubated under continuous agitation on a rocking platform for 1.5 hours at room temperature, according to **Table 2.4**. Secondary antibodies used were polyclonal rabbit anti-mouse immunoglobulin/HRP (DakoCytomation, Cambridgeshire, UK), polyclonal goat anti-rabbit immunoglobulin/HRP (DakoCytomation, Cambridgeshire, UK) and polyclonal rabbit anti-goat immunoglobulin/HRP (DakoCytomation, Cambridgeshire, UK).

The membrane was washed again 3x for 5 minutes in 3% milk TBS/T or PBS/T or 5% milk TBS/T or PBS/T (same buffer as the primary antibody), under continuous agitation on a rocking platform at room temperature, except for the membrane probed for anti-active-β-catenin antibody which was washed in TBS containing 0.05% Tween-20. The membranes were then rinsed 2 x with 1x TBS (1x TBS; 100 ml 10x TBS + 900 ml dH_2O = 1 L) or 1x PBS (1x PBS; 100 ml 10x PBS + 900 ml dH_2O = 1 L) **(see Appendix I)** prior to immunodetection.

Immunodetection (visualisation of protein bands) was performed with enhanced chemi-luminescence detection reagent ECL plus (Amersham, GE Healthcare, Buckinghamshire, UK) according to manufacturer's instructions, using 1 ml of reagent per membrane. The membrane was wrapped in plastic bag (Medium Duty 250 Gauge Polythene, Layflat Tubing, Davpak, Derby, UK) and the resulting chemi-luminescence was visualised by exposing the membrane to light-sensitive Hyperfilm (Amersham, GE

Healthcare, Buckinghamshire, UK) for 1 sec to 30 min, depending on band intensity, in a dark room (illuminated by a safety light). The film was developed using a Hyperprocessor automatic autoradiography film processor (Amersham, GE Healthcare, Buckinghamshire, UK) or manually by immersing the film briefly in developer (Kodak, New York, USA), rinsing briefly in tap water and then immersing in fixer (Kodak, New York, USA), rinsing briefly in tap water and leaving it to dry. Following autoradiography the membrane was briefly washed 2 x in 1x TBS or 1x PBS **(see Appendix I)**, before being stored in either 1x TBS or 1x PBS at 4^{o}C.

Table 2.4: Antibodies and conditions for Western Blotting.

Antigen	Supplier and Antibody (Cat. No)	Blocking conditions	Primary antibody dilution, dilution buffer and incubation	Secondary antibody dilution, dilution buffer and incubation
14-3-3σ	14-3-3σ (N-14) sc-7681, goat polyclonal, Santa Cruz, Heidelberg, Germany	5% milk PBS/T, 30 min, *RT	1:500 in 5% milk PBS/T, overnight at 4°C	1:2000 in 5% milk PBS/T, $1^{1/2}$ hr at RT
Active-β-catenin	Anti-Active-β-catenin (anti-ABC), clone 8E7, 05-665, mouse monoclonal, Upstate, Lake Placid, NY, USA	5% milk TBS, 30 min, RT	1:400 in 5% milk TBS, overnight at 4°C	1:1000 in 5% milk TBS, $1^{1/2}$ hr at RT
BCL-2	Bcl-2 (100) sc-509, mouse monoclonal, Santa Cruz, Heidelberg, Germany	5% milk TBS/T, 30 min, RT	1:1000 in 3% milk TBS/T, overnight at 4°C	1:1000 in 3% milk TBS/T, $1^{1/2}$ hr at RT
Caspase-3	Caspase-3 9662, rabbit polyclonal, Cell Signalling, Danvers, MA, USA	5% milk TBS/T, 30 min, RT	1:1000 in 5% milk TBS/T, overnight at 4°C	1:5000 in 5% milk TBS/T, $1^{1/2}$ hr at RT
c-MYC	c-Myc (9E10) sc-40, mouse monoclonal, Santa Cruz, Heidelberg, Germany	5% milk TBS/T, 30 min, RT	1:1000 in 5% milk TBS/T, overnight at 4°C	1:1000 in 5% milk TBS/T, $1^{1/2}$ hr at RT
EGFP	GFP ab-290, rabbit polyclonal, Abcam , Cambridge, UK	5% milk PBS/T, 30 min, RT	1:1000 in 5% milk PBS/T, 2 hr at RT or overnight at 4°C	1:1000 in 5% milk PBS/T, $1^{1/2}$ hr at RT
GAPDH	GAPDH ab9485, rabbit polyclonal, Abcam , Cambridge, UK	5% milk TBS/T, 30 min, RT	1:1000 in 5% milk TBS/T, 2 hr at RT	1:1000 in 5% milk TBS/T, $1^{1/2}$ hr at RT

GLI2	GLI2 (H300) sc-28674, rabbit polyclonal, Santa Cruz, Heidelberg, Germany	5% milk TBS/T, 30 min, RT	1:5000 or 1:500 in 3% milk TBS/T, overnight at 4°C	1:2000 in 3% milk TBS/T, $1^{1/2}$ hr at RT
Lamin-β1	Lamin-β1 sc-28674, rabbit polyclonal, Imgenex, San Diego, CA, USA	5% milk TBS/T, 30 min, RT	1:500 in 5% milk TBS/T, overnight at 4°C	1:1000 in 5% milk TBS/T, $1^{1/2}$ hr at RT
$p21^{WAF1/CIP1}$	p21 (187) sc-817, mouse monoclonal, Santa Cruz, Heidelberg, Germany	5% milk TBS/T, 30 min, RT	1:500 in 3% milk TBS/T, overnight at 4°C	1:1000 in 3% milk TBS/T, $1^{1/2}$ hr at RT
p53	p53 (DO1), mouse monoclonal, CRUK	5% milk TBS/T, 30 min, RT	1:10000 in 5% milk TBS/T, 2 hr at RT	1:1000 in 5% milk TBS/T, $1^{1/2}$ hr at RT
β-actin	Anti-β-actin (AC-15) A 1978, mouse monoclonal, Sigma-Aldrich, Dorset, UK	5% milk TBS/T, 30 min, RT	1:100000 or 1:1000000 in 5% milk TBS/T, 2 hr at RT	1:1000 or 1:2000 in 5% milk TBS/T, $1^{1/2}$ hr at RT
β-catenin	beta-catenin (CAT-5H10) 13-8400, mouse monoclonal, Zymed, San Fransisco, CA, USA	5% milk TBS/T, 30 min, RT	1:5000 in 5% milk TBS/T, 2 hr at RT	1:1000 in 5% milk TBS/T, $1^{1/2}$ hr at RT

***RT: Room Temperature**

2.12.5.3 Western Blot Membrane Stripping for Reprobing

Hybond-C extra nitrocellulose membrane (Amersham, GE Healthcare, Buckinghamshire, UK) can be re-used to probe with other antibodies, for detection of another protein of interest, by stripping the membrane. Thus, an additional protein of a similar molecular size can be detected following the removal of the primary antibody

binding (membrane stripping). In addition, in case where a primary polyclonal antibody (less specific then monoclonal ones with multiple unspecific bands) is used, stripping is necessary to avoid background signal in subsequent blots, even if the molecular sizes of proteins of interest are completely different. This method is also used in the case where the second ('new') antibody to be used is raised in the same species as the 'older' one. Membrane stripping will thus clear the membrane of any primary antibody bound to its target proteins from the first immunoblotting, and will therefore prevent its repeated detection by the subsequent incubation with secondary antibody. This is particularly useful in cases of detection of housekeeping gene products, such as β-actin protein, which is used to confirm equal protein loading between samples.

Previously probed membranes were stripped, by incubating the membrane with 15-20 ml (sufficient volume to ensure that membrane is completely covered) Restore Plus Western Blot Stripping Buffer (Pierce, Thermo Fisher Scientific, Nortumberland, UK). Membranes were incubated in Restore Plus for 15-30 minutes at room temperature, followed by thorough washing 3x for 5 minutes in TBS/T or PBS/T at room temperature to completely remove the stripping buffer, under continuous agitation on a rocking platform. Membranes were then blocked and re-probed with primary and secondary antibody according to **Section 2.12.5.2** and **Table 2.4**.

2.13 UVB-irradiation

Initially, the growth medium of semi-confluent (50-65%) cells grown in 6 cm or 10 cm dishes was aspirated. The culture dishes were then inserted in the ultraviolet cross-linker (UVP, Cambridge, UK) and the lids were removed. Cells were irradiated with UVB at different doses (10-30 mJ/cm^2), and fresh growth medium was replaced immediately after UVB exposure. Routine calibration was performed to ensure UVB emission peak at 312 nm which is physiologically relevant to skin photobiology. Similar procedure was followed for the control cells except the UVB-exposure step (non-UVB treated control cells).

UVB and non UVB-treated cells, 24 hours after UVB exposure, were either used for whole protein extraction **(Section 2.12.2)** followed by western blot analysis **(Section**

2.12.5) in order to check the levels of several cell cycle or apoptotic proteins such as p53, $p21^{WAF1/CIP1}$, Bcl-2 and Caspase-3 **(Section 2.12.5.2, Table 2.4)**, or were used for PI (Propidium Iodide) **(Section 2.8.1.4)** or $Cy^{TM}5$ Annexin V antibody staining **(Section 2.8.1.5)**, both followed by flow cytometry analysis, in order to check apoptosis and cell death.

2.14 M-FISH

M-FISH (multiplex-fluorescent in situ hybridization) **(Figure 2.10)** is a molecular cytogenetic method that allows colour karyotyping of human chromosomes by painting each chromosome with a unique colour and thus allows the examination of the 24 human chromosomes in metaphase cells (spectral karyotyping). The simultaneous and unequivocal discrimination of all human chromosomes in different colours is of great clinical importance and allows the cytogenetic analysis of numerical (i.e. aneuploidy) and structural (i.e. translocations, terminal and interstitial deletions, insertions, amplifications) chromosomal aberration in pre- and postnatal diagnostics and cancer cytogenetics (Schrock et al., 1996; Speicher et al., 1996; Speicher & Ward, 1996; McNeil & Ried, 2000; Strefford et al., 2001; Trask, 2002; Strachan & Read, 2004b).

The M-FISH technique requires the preparation of metaphase chromosome spreads and the usage of a 24-colour chromosome painting probe. Thus, cells of interest need to be treated with colcemid in order to obtain metaphase cells. Colcemid, a closely related to, but less-toxic compound than colchicine, is a mitotic inhibitor, which inactivates spindle fiber formation (depolymerises microtubules and thus limits microtubule formation), and thus arresting cells in metaphase (chromosomes do not align in the spindle fiber and there is no chromosome segregation) **(see Chapter 4, Section 4.2.6, Figure 4.19)**, allowing cell harvest and metaphase spread preparation and karyotyping to be performed (Taylor, 1965; Sluder, 1991; Rieder & Palazzo, 1992).

Next, already prepared metaphase spreads are hybridised with the labelled DNA probe, the WCP® (Whole Chromosome Paint) DNA probe (24-colour chromosome painting probe, combination of fluorophore-labelled painting probe), which involves the precise

annealing of denatured (single stranded) DNA probe to target chromosomal DNA in specimens that are fixed and mounted to slides (in situ hybridisation). The WCP® DNA probes (Vysis, Abbott Molecular, Maidenhead Berkshire, UK) are directly labelled with five different fluorophores in a combinatorial labelling format to provide 24 distinct colours (one colour for each human chromosome) when analysed with SpectraVysion Imaging System (Vysis, Abbott Molecular, Maidenhead Berkshire, UK). Thus, once pure DNA (human chromosomes) has been isolated (i.e. through FACS), a fluorochrome must be incorporated into the DNA probe in a reaction known as labelling (i.e. probes can be labelled by using PCR) **(Figure 2.10a)** (McNeil & Ried, 2000; Trask, 2002). The fluorophores that are directly attached to the WCP® DNA probes (Vysis, Abbott Molecular, Maidenhead Berkshire, UK) include: SpectrumAqua™, SpectrumGreen™, SpectrumGold™, SpectrumRed™ and SpectrumFRed™. Cot-1® DNA is also included in the probe mixture (24-colour chromosome painting probe, combination of fluorophore-labelled painting probe) to suppress the hybridisation of sequences that are common to various chromosomes (repetitive sequences of the genome) and thus to avoid non-specific hybridisation of the WCP® DNA probe (Vysis, Abbott Molecular, Maidenhead Berkshire, UK) **(Figure 2.10a)**. Cot-1® DNA is enriched in repetitive sequences and by binding to repetitive sequences in the fluorescently tagged probes, it suppress their hybridisation to target chromosomes.

Visualisation of the M-FISH hybridisation requires a fluorescence microscope with a set of optical filters spaced across the spectral interval 350-770 nm that give a high degree of discrimination between all possible fluorochrome pairs and a highly sensitive area imager, a camera. Thus, in order to evaluate a metaphase spread, six images are captured in six different filters (the five fluorochromes used for probe labelling and DAPI used to counterstain all chromosomes), and are analysed by a specific software, which generates a composite image in which each chromosome is given a different pseudocolour depending on the fluorophore composition **(Figure 2.10b)** and allows karyotyping (Schrock et al., 1996; Speicher et al., 1996; Trask, 2002; Strachan & Read, 2004b).

The M-FISH hybridisation and analysis for this study were performed in Dr Yong-Jie Lu's laboratory at Centre for Molecular Oncology and Imaging, Institute of Cancer, Barts and the London School of Medicine and Dentistry, Charterhouse square, London.

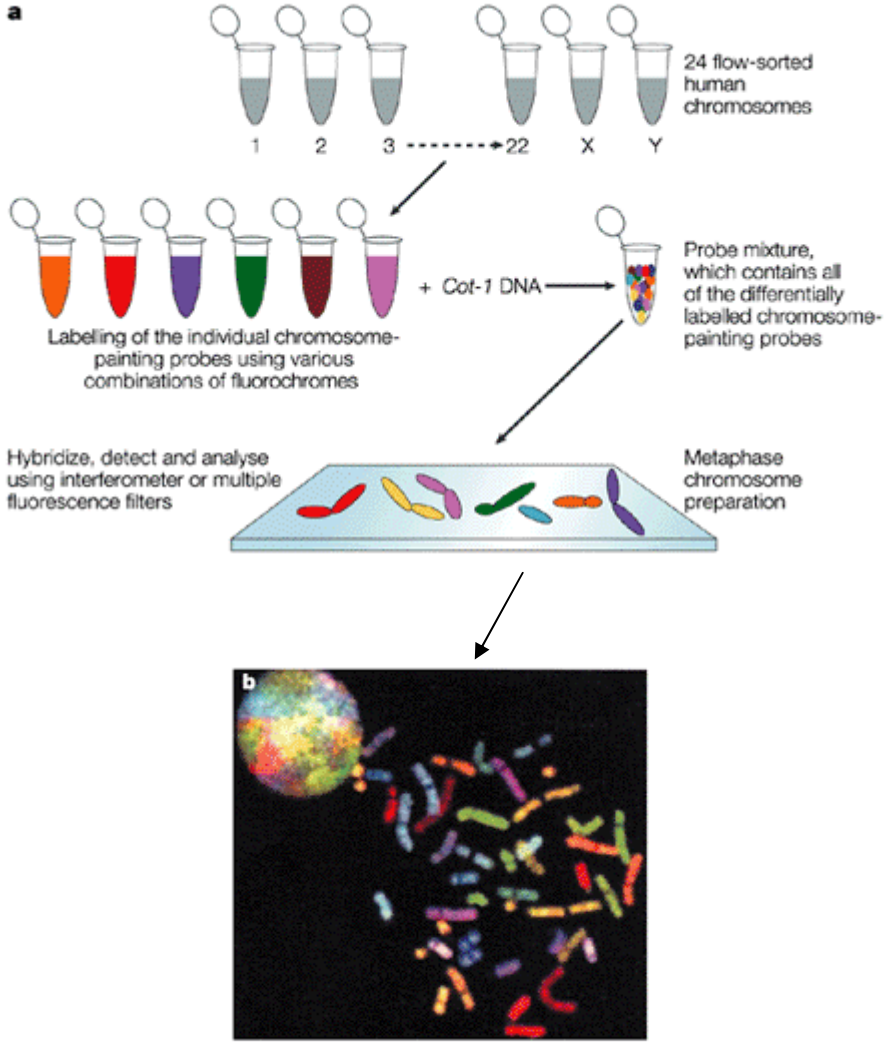

Figure 2.10: Principle of M-FISH.

(a) First, 24 flow-sorted human chromosomes (chromosomes 1-22, X and Y) are combinatorially labelled with at least one, and as many as five, fluorochrome combinations to create a unique spectral colour for each chromosome pair. Aliquotes of the 'painted' chromosomes are pooled together with an excess of Cot-1 DNA which is used to suppress repetitive sequences in the genome. The M-FISH probe mixture is then hybridised to a metaphase chromosome preparation at 37°C for 24-72 hours. Next, detection of the hybridised sample takes place by washing slides to remove unbound nucleotides and also by using DAPI counterstaining of chromosomes. Visualisation of the M-FISH hybridisation requires the use of a fluorescence microscope with a series of excitation and emission filters corresponding to different fluorochromes and a camera. Images for each metaphase spread are captured in five different filters and are analysed by a specific computer software, which generates a composite image, in which each chromosome is given a different pseudocolour depending on the fluorophore composition **(b)**, as well as in DAPI filter. Modified from (McNeil & Ried, 2000; Trask, 2002).

2.14.1 Colcemid treatment of cells

2.14.1.1 Colcemid treatment and cell cycle analysis

N/TERT, SINCE and SINEG2 cells were plated at $7.8x10^5$ cells per 10 cm dish, in four replicates (a total of twelve 10 cm dishes containing 10 ml RM+ growth medium per dish) and incubated at 37°C in a humidified atmosphere of 10% (v/v) CO_2/90% (v/v) air. Medium was replaced every two days and 72 hours after plating (~ 60-75% confluent) N/TERT, SINCE and SINEG2 cells were either treated in duplicates for each cell line with 0.04 μg/ml colcemid **(+)** (Invitrogen, Paisley, UK) (4 μl from 10 μg/ml stock colcemid solution in HBSS-Hank's Buffered Salt Solution (Invitrogen, Paisley, UK) in 1 ml RM+ growth medium; 1:250 dilution) for 2 hours and 15 minutes (six 10 cm dishes) or mock treated **(-)** in duplicates for each cell line (six 10 cm dishes), and were all incubated at 37°C in a humidified atmosphere of 10% (v/v) CO_2/90% (v/v) air. After the 2 hours and 15 minutes incubation, cells treated with colcemid **(+)** along with the mock treated **(-)** cells, were either harvested and Hoechst-33342 (Sigma-Aldrich, Dorset, UK) stained followed by flow cytometry analysis both for DNA content and green fluorescence (EGFP) according to **Section 2.8.1.3**, or were fixed and PI stained followed by flow cytometry analysis for DNA content according to **Section 2.8.1.4**, in order to check the cell cycle prior to metaphase spreads preparation.

2.14.1.2 Colcemid treatment and preparation of metaphase slides

N/TERT, SINCE and SINEG2 cells were plated at $1x10^6$ cells per T75 flask in 20 ml RM+ growth medium per flask and incubated at 37°C in a humidified atmosphere of 10% (v/v) CO_2/90% (v/v) air. Medium was replaced every two days and 72 hours after plating (~ 60-75% confluent) N/TERT, SINCE and SINEG2 cells were treated with 0.04 μg/ml colcemid **(+)** (Invitrogen, Paisley, UK) (4 μl from 10 μg/ml stock colcemid solution in HBSS-Hank's Buffered Salt Solution (Invitrogen, Paisley, UK) in 1 ml RM+ growth medium; 1:250 dilution) for 2 hours and 15 minutes, and were incubated at 37°C in a humidified atmosphere of 10% (v/v) CO_2/90% (v/v) air. After the 2 hours and 15 minutes incubation, all cells treated with colcemid **(+)** were collected and used for the preparation of metaphase slides **(see Section 2.14.2)**.

2.14.2 Metaphase slide preparation

N/TERT, SINCE and SINEG2 cells, treated with colcemid **(+) (Section 2.12.4.1)**, were washed once with 1x sterile PBS (PAA, Somerset, UK) and then trypsinised until all the cells had detached **(see Section 2.1.8)**. The trypsin reaction was inhibited by transferring the trypsinised cells to 50 ml falcon tubes containing complete RM+ growth medium at a ratio of 1:1 (v/v) trypsinised cells to RM+ culture medium. Cells were then centrifuged at 1,000 rpm for 6 minutes. The supernatant was aspirated very carefully so as to avoid discarding cells and each pellet was resuspended in 8-10 ml (depending on cell number) pre-warmed (incubated at 37^{o}C) 0.075 M KCl (Sigma-Aldrich, Dorset, UK) **(Appendix I)**, mixed completely and incubated at 37^{o}C in a humidified atmosphere of 10% (v/v) CO_2/90% (v/v) air, for 20 minutes. KCl is a hypotonic solution, which has lesser osmotic pressure than the solution on the other side of the cell's membrane. Osmotic pressure is the pressure applied by a solution to prevent the inward flow of water across a semi-permeable membrane. Therefore, KCl hypotonic solution flows into the cell and thus disrupts the cell's membrane and increases cell volume. Then, 1 ml of fix solution (100% methanol (Fisher, Leicestershire, UK) : 100% acetic acid (Fisher, Leicestershire, UK) = 3 : 1 ratio) **(Appendix I)** was added in each resuspended pellet and it was completely mixed by using a plastic Pasteur pipette. Next, cells were centrifuged at 1,100 rpm for 6 minutes, the supernatant was gently discarded by using a plastic Pasteur pipette, and 10 ml of fix solution **(Appendix I)** was added in each pellet, mixed completely using a plastic Pasteur pipette, followed by incubation at room temperature for 15 minutes. Resuspended cell pellets were then centrifuged at 1,100 rpm for 6 minutes and the supernatant was gently discarded by using a plastic Pasteur pipette. Again 10 ml of fix solution **(Appendix I)** was added in each pellet, mixed completely using a plastic Pasteur pipette, and incubated at room temperature for 15 minutes. Resuspended cell pellets were either stored at 4^{o}C or were immediately used for the preparation of metaphase slides. Resuspended cells were centrifuged at 1,100 rpm for 6 minutes and the supernatant was gently discarded by using a plastic Pasteur pipette. 10-20 drops of fix solution **(Appendix I)** were added in each pellet (depending on cell number), using a plastic Pasteur pipette and mixed completely. Then, two drops of fix solution with cells were dropped on each slide (new, cleaned and pre-treated microscope glass slides), using a plastic Pasteur pipette. The new microscope glass slides (Berliner Glas KG Herbert Kubatz, Berlin, Germany) that were used for the

metaphase cells were cleaned by 100% ethanol (Fisher, Leicestershire, UK) and then treated in 100% acetic acid (Fisher, Leicestershire, UK) overnight at room temperature in a fume hood. Then, slides were washed using distilled water and were kept in the distilled water at 4^{o}C until used for dropping the cell suspension. The water was allowed to drain from the slide so that a thin film of water remains and then 2-3 drops of the cell suspension were dropped down the length of the slide, starting at the frosted end. The slide was held at a 45º angle while dropping the cell suspension and then slides were placed at a 45º angle and were left to air dry (metaphase slides). Slides (metaphase slides) were then stored at -20^{o}C. Metaphase cells on the slides were evaluated under a light microscope **(Section 2.2)** for cell density and metaphase spreading. Metaphase slides should have optimum cell density so that the density is neither too sparse or too high, and also optimum spreading (not inadequate or over-spreading) so that the cell boundaries and the majority of chromosomes are distinguishable. The resulting metaphase cells should have minimal overlaps and no visible cytoplasm surrounding the chromosomes, with chromosomes appearing flat and gray **(see Chapter 4, Section 4.2.6, Figure 4.21)**.

2.14.3 Hybridisation

The metaphase slides were taken from -20^{o}C and according to the characteristics mentioned above **(Section 2.14.2)**, a target area (approximately 22 mm x 22 mm) with good quality metaphase cells in each metaphase slide was selected and marked with a pencil on the side of the slide. Slides were then heated on a hot plate at 65^{o}C for 30 minutes, followed by enzymatic treatment (protease treatment). Enzymatic treatment changes the accessibility of the chromosomal DNA, by removing the cytoplasmic proteins of the cell membrane, since for optimum hybridisation to occur the chromosomal DNA must be readily accessible to the DNA M-FISH probes. Therefore, 40 µl of the RNase A (Sigma-Aldrich, Dorset, UK) working solution **(Appendix I)** was applied to the target region of each slide and a 22 x 50 mm glass coverslip (VWR, Leicestershire, UK) was applied. Next, the slides were placed in a pre-warmed (to 37^{o}C) humidified box (Vysis, Abbott Molecular, Maidenhead Berkshire, UK) and incubated at 37^{o}C for 30 minutes. The humidified box (pre-hybridisation sealed box) (Vysis, Abbott Molecular, Maidenhead Berkshire, UK) was containing 3-4 filter papers soaked in 2x

Saline Sodium Citrate (SSC) (Vysis, Abbott Molecular, Maidenhead Berkshire, UK) solution **(Appendix I)** so as to be humid, and it was warmed in a 37^{o}C incubator. After incubation, the glass coverslip was removed and the slides were washed 2x for 5 minutes each in 2x SSC (Vysis, Abbott Molecular, Maidenhead Berkshire, UK) solution **(Appendix I)** inside a glass Coplin jar. Then, the slides were placed in another pre-warmed (in 37^{o}C water bath) glass Coplin jar containing the pepsin (Vysis, Abbott Molecular, Maidenhead Berkshire, UK) working solution **(Appendix I)** at 37^{o}C (in 37^{o}C water bath) for 5 minutes. Next, the slides were washed 2x for 5 minutes each in 1x PBS **(Appendix I)** inside a glass Coplin jar and were then placed in another glass Coplin jar containing the formaldehyde (Fisher, Leicestershire, UK) fixation solution **(Appendix I)** at room temperature for 2 minutes. Slides were then washed 2x for 5 minutes each in 1x PBS **(Appendix I)** inside a glass Coplin jar and were dehydrated by being placed sequentially in glass Copling jars containing 70% (v/v) **(Appendix I)**, 85% (v/v) **(Appendix I)** and 100% (v/v) ethanol (Fisher, Leicestershire, UK) **(Appendix I)** for 2 minutes in each one, and were left to air dry.

The next step was the denaturation of the slides in order for the double stranded DNA to become single stranded due to high temperatures, which occurs when the hydrogen bonds between the strands are broken at high temperatures. The slides were immersed in a pre-warmed to 72±1^{o}C glass Coplin jar containing the denaturation solution **(Appendix I)** for 2 minutes at 72±1^{o}C (in 72±1^{o}C water bath) in a fume hood. The glass Coplin jar containing the denaturation solution **(Appendix I)** was placed in a 72±1^{o}C water bath in a fume hood approximately 30 minutes prior to use to bring the denaturation solution to 72±1^{o}C. Slides were then dehydrated by being placed sequentially in glass Copling jars containing 70% (v/v) **(Appendix I)**, 85% (v/v) **(Appendix I)** and 100% (v/v) ethanol (Fisher, Leicestershire, UK) **(Appendix I)** for 1 minute in each one, and were placed on a 46^{o}C heat plate to evaporate remaining ethanol and warm the slide.

Next, SpectraVysion^{TM} DNA probe (Vysis, Abbott Molecular, Maidenhead Berkshire, UK) was hybridised to the chromosomes in the target area of the slides and was allowed to anneal. Thus, 10 μl of the denatured SpectraVysion^{TM} DNA probe (Vysis, Abbott Molecular, Maidenhead Berkshire, UK) were applied in the dark to the target area in each slide (slides have already being placed on a 46^{o}C heat plate) and a 22 x 22 mm

glass coverslip (VWR, Leicestershire, UK) was applied. Then, the glass coverslip was sealed with rubber cement to prevent evaporation during hybridisation and the slides were placed in the pre-warmed (to 37^{o}C) humidified box (hybridisation box) (Vysis, Abbott Molecular, Maidenhead Berkshire, UK), containing 3-4 filter papers soaked in 2x Saline Sodium Citrate (SSC) (Vysis, Abbott Molecular, Maidenhead Berkshire, UK) solution **(Appendix I)** so as to be humid, and incubated at 37^{o}C for either 48 or 72 hours. Prior to use, the SpectraVysion^{TM} DNA probe (Vysis, Abbott Molecular, Maidenhead Berkshire, UK) was taken from -20^{o}C, was defrosted at room temperature and then was centrifuged 2-3 seconds using a microcentrifuge. The probe (Vysis, Abbott Molecular, Maidenhead Berkshire, UK) was then warmed at 37^{o}C for 5 minutes using a water bath in order for the probe to become resolubilised. Then, the probe (Vysis, Abbott Molecular, Maidenhead Berkshire, UK) was vortexed and centrifuged 2-3 seconds to bring all the contents to the bottom of the tubes and 35 μl were transferred in a 0.5 ml microcentrifuge tubes (Eppendorf, Cambridge, UK) in darkness. At the same time that the slides were placed to denaturation solution **(Appendix I)**, the DNA probe (Vysis, Abbott Molecular, Maidenhead Berkshire, UK) was also placed in 80±1^{o}C water bath for 5 minutes in the dark so as to become denatured. The denaturation of the probe (Vysis, Abbott Molecular, Maidenhead Berkshire, UK) was timed so that it is approximately the same time as the specimen slide denaturation.

After 48 or 72 hours of hybridisation the slides were washed to remove any excess probe that is non-specifically bound, and were prepared for capturing images. The glass coverslips were removed from the slides and the slides were immediately immersed in a pre-warmed to 72±1^{o}C glass Coplin jar containing 0.4x SSC/0.3% NP-40 (NP-40 was supplied by Vysis, Abbott Molecular, Maidenhead Berkshire, UK) wash solution **(Appendix I)** for 2 minutes at 72±1^{o}C (in 72±1^{o}C water bath) in the dark. The slides were initially agitated for 1-3 seconds and were then left for 2 minutes in 0.4x SSC/0.3% NP-40 wash solution **(Appendix I)**. The glass Coplin jar containing the 0.4x SSC/0.3% NP-40 wash solution **(Appendix I)** was placed in a 72±1^{o}C water bath approximately 30 minutes prior to use to bring the wash solution to 72±1^{o}C. Next, the slides were immersed in a glass Coplin jar containing 2x SSC/0.1% NP-40 wash solution **(Appendix I)** for 5 sec - 1 min at room temperature in the dark. The slides were initially agitated for 1-3 seconds and were then left for 5 sec - 1 min in 2x SSC/0.1% NP-40 wash solution **(Appendix I)**. Slides were then drained by tiling in darkness and

20 µl DAPI III counterstain (Vysis, Abbott Molecular, Maidenhead Berkshire, UK) were applied to the target area of each slide in darkness and a 22 x 22 mm glass coverslip (VWR, Leicestershire, UK) was applied. The slides were left at 4^{o}C for 30 minutes and then images were captured. Slides were stored for short term at 4^{o}C.

M-FISH was visualised by fluorescence microscopy (Strefford et al., 2001; Mao et al., 2008). The whole hybridisation target area of the slide was scanned in order to locate high quality metaphase spreads by using the yellow or red filter set, using an Olympus Provis AX70 (Olympus, London, UK) fluorescent microscope with an M-FISH filter configuration (Vysis, Abbott Molecular, Maidenhead Berkshire, UK) (a series of excitation and emission filters corresponding to different fluorochromes **(Section 2.8.1.1)**). Next, M-FISH images of metaphase spreads were auto-captured in six different filters, by acquiring the images in the following fluorophore **(see Section 2.8.1.1)** sequences: 1st Spectrum Gold (excitation 530 nm and emission 555 nm), 2nd Spectrum Far Red (excitation 655 nm and emission 675 nm), 3rd Spectrum Aqua (excitation 433 nm and em 480 nm), 4th Spectrum Red (excitation 592 nm and emission 612 nm), 5th Spectrum Green (excitation 497 nm and emission 524 nm) and 6th DAPI (excitation 367 nm and emission 452 nm), using a Photometric Sensys Camera (Perceptive Scientific Inc., Chester, UK) and a composite image representing each of the six fluorophore image captures was presented in the monitor. This sequence of image capture is important in order to minimise photodegradation effects on the five probe fluorophores, thereby providing higher quality images. M-FISH images of metaphase spreads were analysed using the computer software SpectroVision (Vysis, Abbott Molecular, Maidenhead Berkshire, UK) which generates a pseudocolored image for each metaphase spread, where each chromosome has a different pseudocolour depending on its fluorophore composition **(Figure 2.10b)** and thus allows the karyotypic analysis. More than ten M-FISH karyotypes were analysed for each cell line.

2.15 Luciferase reporter assays on stable and inducible cell lines

Genetic reporter systems have contributed greatly to the study of eukaryotic gene expression and regulation. Reporter genes, such as firefly luciferase, are frequently used

as indicators of transcriptional activity in cells. Typically, a reporter gene is joined to a promoter sequence in an expression vector that is transferred into cells. Following transfer, the cells are assayed for the presence of the reporter by directly measuring the reporter protein itself or the enzymatic activity of the reporter protein.

In this study, luciferase reporter assay (Bright-Glo^{TM} Luciferase Assay System, Promega, Southampton, UK) was used to detect and measure the activity of the OT promoter, and indirectly the transcriptional activity of β-catenin. The OT-β-catenin-responsive promoter (OT) is an improved version of TOPFLASH, which contains the TCF-4 binding sites **(CCTTTGATC)** (Korinek et al., 1997; He et al., 1998; Shih et al., 2000). The OT promoter drives the expression of a luciferase gene to facilitate the detection of promoter activity, and indirectly β-catenin protein transcriptional activity. Thus, luciferase is used as a reporter gene to provide information about the activity of the promoter that drives its expression.

Therefore, pSIN-OT-Luciferase (pSIN-OT-Luc) retroviral vector contains a luciferase gene downstream of the OT promoter, which is comprised of three repeats of the wild-type Tcf-4 binding site **(CCTTTGATC) (Figure 2.11 i and Section 2.1.1, Section 2.3.1)**. Tcf-4 binds in a sequence-specific fashion to the regulatory sequences (Tcf-4 binding sites of the OT promoter) of specific target genes (in this case luciferase gene), while β-catenin supplies a transactivation domain and thus transcriptional activation of target genes occurs only when Tcf-4 is associated with β-catenin. Therefore, β-catenin through binding to Tcf-4 (protein-protein interaction) activates the OT promoter which then drives the expression of luciferase (Luc) gene **(Figure 2.11 ii)**. The latter is an enzyme that catalyses the mono-oxygenation of the beetle luciferin protein (lyophilised Bright-Glo^{TM} Luciferase Assay Substrate provided by (Promega, Southampton, UK)) in the presence of ATP (Adenosine Triphosphate), Mg^{2+} (Magnesium), and O_2 (Molecular Oxygen) **(Figure 2.11 ii)**. This leads to the production of luciferin protein with luminescent properties **(Figure 2.11 ii)**. The levels of luciferase enzyme are thus measured by detection of luminescence by standard microplate readers **(Figure 2.11 ii)**. Luminescence or otherwise bioluminescence is the emission of light as a result of a chemical reaction and it differs from fluorescence **(see Section 2.8.1.1)** in that the electronic excited state is derived from the product of a chemical reaction, rather than the more typical way of creating electronic excited states namely absorption **(see**

Section 2.12.4.1). Bioluminescence is a subset of chemiluminescence **(see Section 2.12.5)**, where the light producing reaction occurs inside a cell. In the context used herein, luminescence indirectly reports the activity levels of the OT promoter, and therefore the relative abundance of transcriptionally active β-catenin.

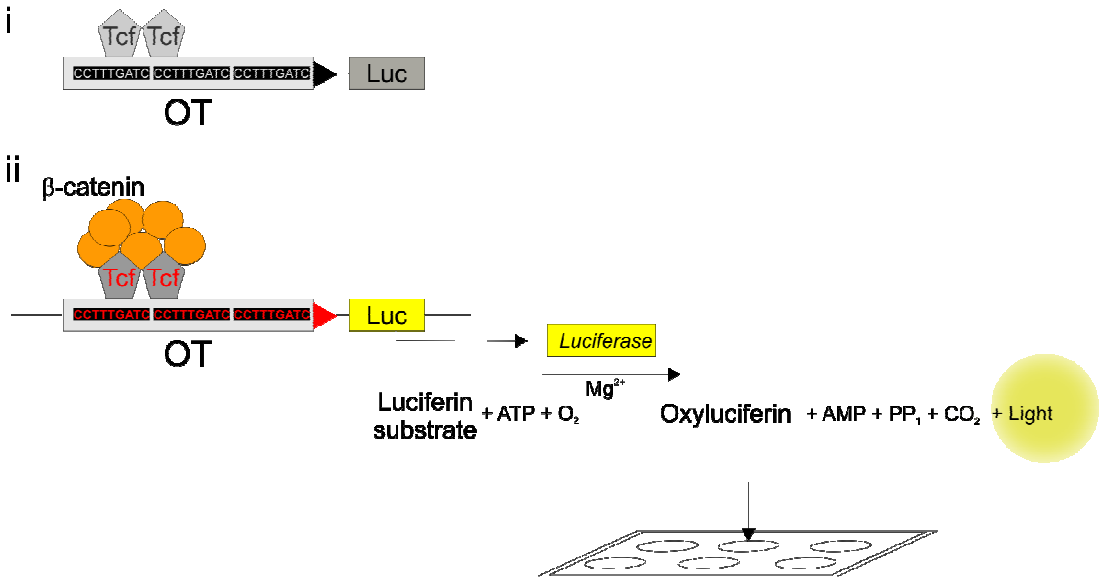

Figure 2.11: Principle of luciferase reporter assay.

(i) pSIN-OT-Luciferase (pSIN-OT-Luc) retroviral vector contains a luciferase gene downstream of the OT promoter, which is comprised of three repeats of the wild-type Tcf-4 binding site **(CCTTTGATC) (Section 2.1.1 and Section 2.3.1)** (Shih et al., 2000). **(ii)** Tcf-4 binds to the Tcf-4 binding sites of the OT promoter and β-catenin through binding to Tcf-4 (protein - protein interaction) activates the OT promoter which then drives the expression of luciferase (Luc) gene. Firefly luciferase is an enzyme that catalyzes an oxidation reaction (Luciferin substrate + ATP + O_2 → Oxyluciferin + AMP + PP_1 + CO_2 + Light) to yield light, usually in the green to yellow region, typically 550-570 nm. Mono-oxygenation of the beetle luciferin protein is catalyzed by luciferase in the presence of ATP (Adenosine Triphosphate), Mg^{2+} (Magnesium), and O_2 (Molecular Oxygen) and this leads to the production of oxyluciferin protein with luminescent properties. The levels of luciferase enzyme measured by luminometer. **PP_1**, pyrophosphate; **AMP**, adenosine monophosphate; **CO_2**, carbon dioxide.

For the luciferase reporter assay, NTERT, SINEG2, SINCE cells, were transduced, as previously described **(see Section 2.3, Section 2.3.5.1 and Section 2.3.5.3)** with pSIN-

OT-Luciferase (pSIN-OT-Luc) retroviral plasmid, and were left to express the transgene for 72 hr prior to harvesting for luciferase activity and protein content measurement **(Section 2.12.4)**. Transduced cells were split according to **Section 2.1.8** and seeded in 6-well plates ($16.8x10^4$ cells/well), in triplicates (n=3 for each cell type), 48 hr after viral infection. The next day (72 hr post-infection) cells were lysed and examined for luciferase activity and protein content **(Section 2.12.4)**.

N/TERT and NTEG2 cells were transduced, as previously described **(see Section 2.3, Section 2.3.5.1 and Section 2.3.5.3)** with pSIN-OT-Luciferase (pSIN-OT-Luc) retroviral vector and were left to express the transgene for 5 days prior to harvesting for luciferase activity and protein content measurement **(Section 2.12.4)**. Transduced cells were splitted according to **Section 2.1.8** and seeded in 6-well plates ($4.2x10^4$ cells/well), in triplicates (n=3 for each cell type), 48 hr after viral infection. The next day (72 hr post-infection) doxycycline was removed from transduced cells for another 48 hr (NTEG2 Dox-). Day 5 post-transduction, cells were lysed and examined for luciferase activity and protein content **(Section 2.12.4)**.

The seeded NTERT, SINCE, SINEG2 and N/TERT, NTEG2 cells in 6-well plates, after 3 and 5 days post-infection respectively, had reached ~ 40-50% confluence and were washed once with 2 ml sterile PBS (PAA, Somerset, UK). Cells in each well were then incubated in 55 µl of 1x Reporter Lysis Buffer (Promega, Southampton, UK) (5x Reporter Lysis Buffer (Promega, Southampton, UK) diluted in sterile distilled water (PAA, Somerset, UK) - 1:5 dilution) for 10 min at room temperature to allow cell lysis. The protein was harvested in 1.5 ml microcentrifuge tubes (Eppendorf, Cambridge, UK).

All cell lysates were assayed for luciferase activity using the Bright-Glo™ Luciferase Assay System (Promega, Southampton, UK). Cell lysates were vortexed for 5 sec and from each 55 µl cell lysate, 50 µl were transferred to the luminometer plate well (opaque, flat bottomed white 96-well plate, Nunc, Roskilde, Denmark), while the rest 5 µl were kept in ice and used for protein concentration measurement using the Bio-Rad Protein Assay System (BioRad, Hertfordshire, UK) **(Section 2.12.4)**, or were stored at -80°C if were not immediately measured. Bright-Glo™ Assay reagent (LAR) (Promega, Southampton, UK) (the lyophilised Bright-Glo™ Luciferase Assay Substrate (Promega,

Southampton, UK) was reconstituted with 10 ml of Bright-Glo™ Luciferase Assay Buffer (Promega, Southampton, UK) until completely dissolved and it was aliquoted and stored at -80°C) was thawed, kept in dark, equilibriated to room temperature since luciferase activity is temperature dependent, and vortexed. LAR (Promega, Southampton, UK) was added in each well of the luminometer plate at equal volume (50 µl) to the cell lysate and samples were mixed by quick pipetting. Luminencence was measured immediately (to avoid loss of luminescence signal) after exposure for 20 sec for each well, using a FLUOSTAR OPTIMA microplate reader (BMG LABTECH, Aylesbury, UK). Prior to luminescence measurement the plate was briefly shaken for 7 sec by the FLUOSTAR OPTIMA microplate reader (BMG LABTECH, Aylesbury, UK) to ensure complete sample mixing with the LAR (Promega, Southampton, UK) reagent.

Luminescence data of each sample were normalized to protein content (luciferase/µg) (i.e. protein concentration µg/µl of cell lysate x 50 µl of volume of cell lysate = protein µg in 50 µl cell lysate → luminescence/protein µg in 50 µl cell lysate = luciferase/µg).

Samples were analysed in duplicates or triplicates and statistical analysis was performed using the Microsoft Excel's software for student's *t* test analysis **(see Section 2.16)**.

2.16 Statistical analysis

Almost all experiments have been repeated at least three times and statistical analysis was performed using either the Microsoft Excel's software for student's *t* test analysis or the GraphPad's InStat Software (V2-04a; Graph-Pad Software, San Diego, CA) for student's *t* test analysis. Statistical significance was expressed as a probability value (P) which represents the probability of two comparing groups being the same. The smaller the P value the more significant the differences between two comparing groups (* $P \leq 0.05$ - significant, ** $P \leq 0.01$ - very significant, *** $P \leq 0.001$ - extremely significant).

2.17 Organotypic cultures and Immunohistochemistry

In order to mimic physiological skin conditions *in vitro*, NTEG2 induced and uninduced keratinocytes were grown in organotypic three-dimensional cultures, by Nafeesa Ali at Centre for Cutaneous Research, Institute of Cell and Molecular Science, Barts and the London School of Medicine and Dentistry, London, UK, under conditions that can support the proliferation and differentiation of epidermal keratinocytes and mimic their *in vivo* pattern of growth and differentiation (Contard et al., 1993; Ojeh et al., 2001). Therefore, a three-dimension *in vitro* functional reconstruction of skin epithelium can be achieved by the culture of keratinocytes on the papillary surface of the de-epidermalised dermis (DED) either in the presence or absence of extra fibroblasts, which allows a better representation of the *in vivo* situation, compared to monolayer culture models. The procedure entails the culture of primary fibroblasts, preferentially derived from the tissue of interest (i.e. skin fibroblasts), within the reticular side of the DED. After fibroblasts are established and have migrated within the DED (usually within 24 hours), skin keratinocytes are placed on the papillary surface of the DED, and are then allowed to grow for an initial period of 24 - 48 hours. After this stage, the organotypic rafts are raised to the air-liquid interface to allow keratinocyte differentiation and the induction of tissue keratinisation.

The organotypic keratinocyte cultures were performed as previously described (Ojeh et al., 2001) by Nafeesa Ali at Centre for Cutaneous Research, Institute of Cell and Molecular Science, Barts and the London School of Medicine and Dentistry, London, UK. Briefly, glycerol-preserved skin (Euro Skin Bank, Beverwijk, Holland) was washed three to five times in 1x PBS and incubated in 1x PBS containing 1% antibiotic-antimycotic solution (PAA, Somerset, UK) at 37^{o}C in a humidified atmosphere of 10% (v/v) CO_2/90% (v/v) air for up to 10 days. Epidermis was then mechanically removed using forceps, and de-epidermalised dermis (DED) was cut into 6 sections (I, II, III, IV, V, and VI) of 1.5 x 1.5 cm squares each one and placed in a 6-well culture plate. The DED was placed in three of the six wells (I, II, III) with the papillary dermal surface on the underside and in the other three (IV, V, VI) on topside. Stainless steel rings were placed on top of the dermis of the I, II, III wells, and normal human dermal fibroblasts ($5x10^5$ cells) were seeded into the rings on the reticular dermal surface. On IV, V, VI wells some culture medium was added, to prevent the DED from drying. After a 24 h-

incubation, the DED was inverted on I, II, III wells, to orient the papillary dermal surface on top before the rings were replaced and keratinocytes ($3x10^5$cells) were seeded inside the rings (N/TERT cells seeded on I and IV wells and NTEG2 (induced and uninduced) cells seeded on II, III, V, VI wells). After 2 days, the DED composite was raised to the air-liquid interface in the same orientation, by placing on stainless steel grids for 14 days. The medium was refreshed every 2-3 days. After 14 days, the composites were removed from the grids, fixed in 4% (v/v) formaldehyde and embedded in paraffin wax. Paraffin processed tissue sections were cut at 4 μm thickness and transferred on to microscope slides.

Immunohistochemistry is a method to detect the abundance and the localisation of a protein of interest, within a tissue. This is achieved by the use of highly specific antibodies that have been raised against a protein/antigen of interest. The first step of immunohistochemistry includes the successful blocking of antigen sites on the tissue, which serves to increase the specificity of the subsequent antibody binding by using serum (i.e. goat serum). Next, the primary antibody is used to detect the protein of interest within the tissue (skin section). After washing off unbound primary antibody with buffer, the secondary antibody which detects the primary antibody is applied to skin section. Secondary antibody is raised in the same species as the primary one and is typically conjugated to enzyme or a fluorochrome for the easy detection. In this study, enzyme conjugated secondary antibodies were used for the detection of antigen abundance in normal and BCC **(Section 2.18)** human biopsies. Such secondary antibodies are directly conjugated to an enzyme, usually horseradish peroxidase or alklaline phosphatase. For enzyme-linked secondary antibody, a substrate (i.e. DAB; 3,3'- diaminobenzidine) is applied, which is converted into an insoluble coloured product by the respective enzyme. This reaction leads to the production of brown stain wherever the secondary, and hence the primary, antibodies are bound and indirectly indicate the levels of a target protein present in the tissue sample.

Thus, β-catenin was immunostained with a mouse monoclonal antibody (Zymed, San Fransisco, CA) on tissue sections as described (Ghali et al., 1999) and the reaction product was visualised using diaminobenzidine (DAB) as a chromogenic substrate. In addition, deparaffinised sections were counterstained with haematoxylin (blue dye that

stains cell nucleus) and eosin (red dye that stains cytoplasm, collagen) for histological examination.

2.18 BCC tissues and Immunohistochemistry

A cohort of 16 patients' tissue samples (BCC paraffin blocks) comprising normal skin epithelium, and tissues derived from diverse human BCC subtypes, including nodular, superficial, infiltrative and morpheaform along with a $p21^{WAF1/CIP1}$ primary antibody ($p21^{WAF1/CIP1}$ (DCS60), 2946, mouse monoclonal antibody; Cell Signaling, Danvers, MA; 1:125 dilution) were supplied to the pathology lab at the Pathology Department of the Institute of Cancer, Barts and the London School of Medicine and Dentistry, Charterhouse square, London, UK. Tissue processing and immunohistochemistry **(see Section 2.17)** were performed by Dr Mohammed Ikram at the Pathology Department of the Institute of Cancer, Barts and the London School of Medicine and Dentistry, Charterhouse square, London, UK.

Briefly, 4 μm tissue sections were cut from the BCC blocks and transferred on to charged microscope slides. The slides were dried in a 37^{o}C oven over night and then run on Ventana discovery platform (Ventana Molecular Discovery Systems S.A., France) with an automated protocol including deparaffinisation, primary antibody incubation, secondary antibody incubation, DAB application, Haematoxylin and Bluing Reagent counterstaining and finally slides cleaning.

After the run was completed the slides were placed in soapy tap water and rinsed under the tap for 1 min and then placed in dH_2O. Next, the slides were immersed in a series of solvents (3 min to each one) such as ethanol and xylene, to ensure that samples were completely dehydrated prior to examination. Finally, slides were mounted and cover slipped and stored at room temperature.

CHAPTER THREE

3 RESULTS

Generation and characterisation of stable and inducible GLI2ΔN-expressing human N/TERT keratinocyte cell lines

3.1 Introduction

The importance of the Sonic Hedgehog (SHH) pathway as a causative agent in Basal Cell Carcinomas (BCC) is well known in the literature. Taking into account the difficulty of culturing basal cell carcinomas *in vitro*, the molecular mechanisms involved in human BCC formation are poorly understood.

In the present study, a constitutively active form of human GLI2-β isoform (GLI2 - a SHH mediator gene) that lacks the N-terminal repressor domain (Tanimura et al., 1998), GLI2ΔN-β (GLI2ΔN), and h/TERT (human telomerase reverse transcriptase) immortalised human skin keratinocytes (N/TERT-1) (Dickson et al., 2000) were used in order to generate and characterise N/TERT cell lines, either stably or conditionally expressing an EGFP-GLI2ΔN fusion protein, and to investigate the effects of GLI2ΔN overexpression in human keratinocytes.

The telomerase immortalised cell line, N/TERT-1 (N/TERT) (Dickson et al., 2000) was chosen to examine GLI2ΔN effects, because of its genotype, which is comparable to primary human keratinocytes. This line retains a functional p53/p21$^{WAF1/CIP1}$ pathway, contrarily to other keratinocyte cell lines such as HaCaT (Boukamp et al., 1988; Lehman et al., 1993), and while it has a potentially unlimited lifespan because of abrogated senescence, it is neither tumour derived nor malignant. There are only two genetic hits involved in its creation, that is ectopic telomerase expression and spontaneous downregulation/loss of p16^{INK4a} (Dickson et al., 2000; Rheinwald et al., 2002). In addition, N/TERT keratinocytes retain normal differentiation characteristics and are able to give rise to stratified epithelium in organotypic cultures (Dickson et al., 2000).

The reason for choosing isoform β out of the four GLI2 isoforms, is because GLI2-β mRNA expression is the predominant isoform in human BCCs (Tojo et al., 2003). Moreover, the truncated human GLI2-β/N-terminal deleted (GLI2ΔN), chosen for this study, is a valuable tool to mimic the activated form of GLI2 (Eichberger et al., 2006). The human full length GLI2 shows relatively weaker transactivation *in vitro*, compared to GLI2*, and unlike full length GLI2, GLI2* is able to produce basal cell carcinoma-

like downgrowths originating directly from the epidermis of transgenic mice (Roessler et al., 2005).

In addition, the use of the active form of GLI2, is a way of partly mimicking SHH signalling. Expression of the constitutively active form of Gli2 (ΔNG2) *in vitro* shows increased transcriptional activity and has the ability to induce transcriptional activation of all the Shh target genes, in isolated presomitic mesoderms, compared to the full-length Gli2 (Sasaki et al., 1999; Buttitta et al., 2003). *In vivo*, in transgenic mice, ΔNG2, unlike full-length Gli2, is also able to mimic Shh-induced gene expression in dorsal neural tube (Sasaki et al., 1999). Interestingly, transgenic mice with overexpression of the N-terminal deletion of Gli2 in the epidermis under the control of K5 promoter, not only develop BCCs but also a variety of other skin tumours resembling human trichoblastomas, cylindromas, basaloid follicular hamartomas, in contrast to mice with epidermal overexpression of the full-length Gli2 that develop only BCCs (Sheng et al., 2002). The difference between the transgenic mice overexpressing full length Gli2 (K5-Gli2) and those overexpressing the N-terminal deleted Gli2 (K5-Gli2ΔN2), is not only restricted to the occurrence of multiple skin tumour types in K5-Gli2ΔN2 mice compared to the single tumour type in K5-Gli2 mice, but is also reflected on their phenotype which is characterised by (a) earlier development of visible skin abnormalities, (b) highly variable tumour growth rates, and (c) preference for different body sites (Sheng et al., 2002). Furthermore, in mice, hair follicle development requires Shh-dependent Gli2 activator function in the epidermis (Mill et al., 2003). In the absence of Shh, only the constitutively active form of Gli2 (ΔNGli2) (under the control of K5 promoter), that closely resembles the human GLI2ΔN, can rescue the follicular development, activate Shh-responsive gene expression, and promote cell proliferation by inducing cyclin-D1 and cyclin-D2 expression in $Shh^{-/-}$ transgenic mice (Mill et al., 2003).

Therefore, since continued HH signalling, is required for BCC-like growth, proliferation and survival in transgenic mice (Hutchin et al., 2005), and is also implicated in human BCC development and in many other cancers (Ruiz i Altaba et al., 2002b; Pasca di Magliano & Hebrok, 2003; Beachy et al., 2004; Daya-Grosjean & Couve-Privat, 2005; Rubin & de Sauvage, 2006), GLI2ΔN could be a useful tool to partly mimic the

constitutive activation of HH signalling and to study the molecular mechanism of human BCC carcinogenesis *in vitro*.

3.2 Results

3.2.1 Generation and characterisation of EGFP-GLI2ΔN stable cell line

3.2.1.1 Generation of EGFP-GLI2ΔN stable cell line

The stable N/TERT cell lines expressing the EGFP-GLI2ΔN (EGFP-GLI2ΔN fusion protein) and the EGFP (Enhanced Green Fluorescent Protein) protein were generated according to the procedures described in Materials and Methods **(Chapter 2, Section 2.1.5 and Section 2.3.5.1)**. Due to lack of selectable markers, transduced cells were sorted by FACS for green fluorescence (EGFP fluorescence) and collected **(Chapter 2, Section 2.8.2)**, in order to enhance the percentage of cells that have been efficiently transduced.

3.2.1.2 Expression levels of the SINCE and SINEG2 constructs

The SINEG2 cell line was characterised for the expression of EGFP-GLI2ΔN fusion protein, by fluorescence microscopy **(Chapter 2, Section 2.2)**, flow cytometry **(Chapter 2, Section 2.8)**, and western blot analysis **(Chapter 2, Section 2.12)**. Representative pictures of EGFP (SINCE) and EGFP-GLI2ΔN (SINEG2) expressing cell lines are shown in **Figure 3.1A**.

Both cell lines were initially sorted for green fluorescence emission using FACS **(Chapter 2, Section 2.8.2)**, after transduction with EGFP and EGFP-GLI2ΔN retroviral vectors. N/TERT wild-type cells were used for obtaining basal levels of green fluorescence intensity **(Figure 3.1B i)**, and all cells above this basal threshold were considered as being positive and were thus collected and replated in normal growth medium. Flow cytometry of sorted cells confirmed the existence of a high fluorescence subpopulation (86.2% EGFP+) of SINCE cells **(Figure 3.1B ii)**, and the existence of a high fluorescence subpopulation (95.2% EGFP+) of SINEG2 cells **(Figure 3.1B iii)**, but of lower green fluorescence intensity compared to SINCE cells.

Further immunoblotting against EGFP **(Figure 3.1C)**, revealed a band at the predicted size for the EGFP-GLI2ΔN fusion protein (~ 180 kDa). β-actin was used as loading control.

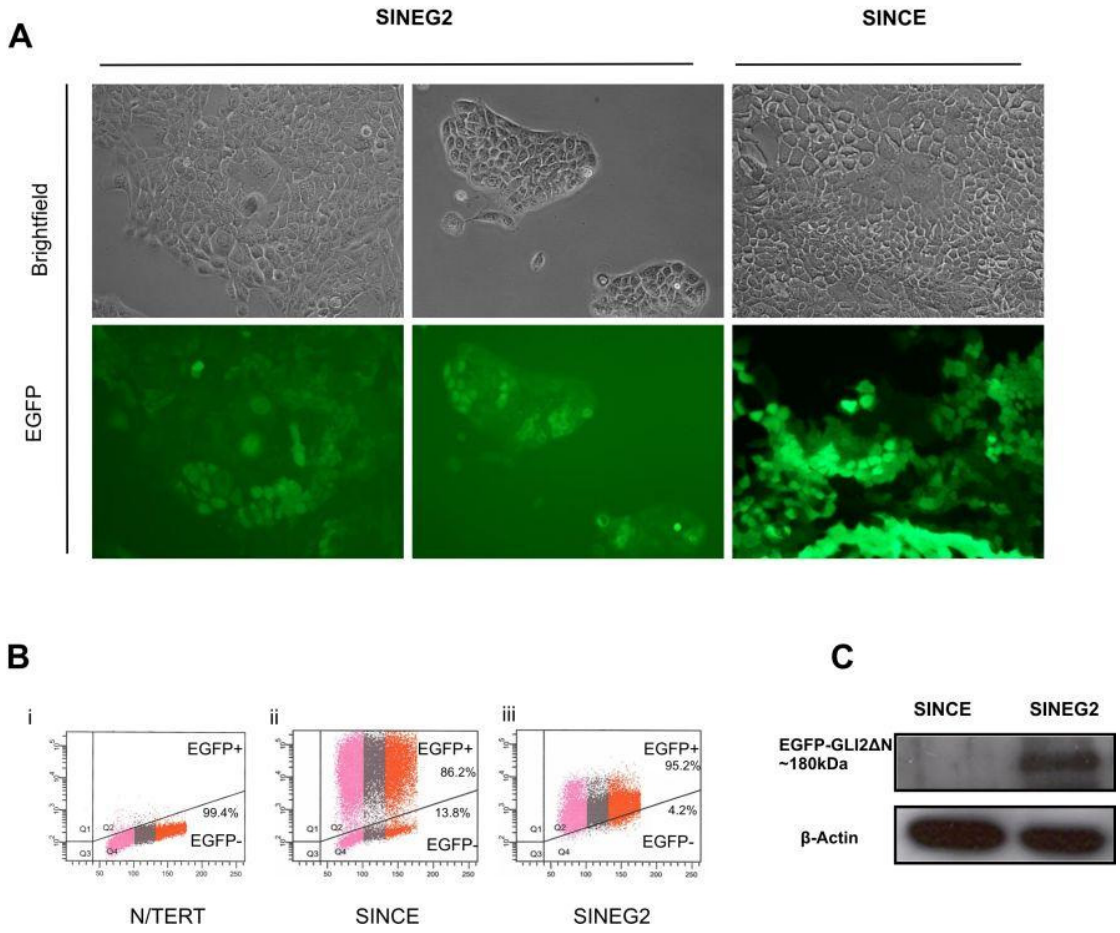

Figure 3.1: EGFP-GLI2ΔN stable expression in N/TERT human keratinocytes.

(A) Representative pictures of EGFP-GLI2ΔN fusion protein and EGFP stably expressing N/TERT cells were taken at x20 magnification, under brightfield and UV excitation for EGFP fluorescence, showing clear expression of EGFP-GLI2ΔN (SINEG2) and EGFP (SINCE) proteins. The EGFP-GLI2ΔN fusion protein localisation is mainly nuclear and partly cytoplasmic. **(B)** Flow cytometry analysis of wild-type N/TERT cells **(i)**, used as reference cell line, against both SINCE **(ii)** and SINEG2 **(iii)** cell line, showing the presence of distinct populations of EGFP expressing cells. **(C)** Immunoblotting of SINCE and SINEG2 cell protein extracts against anti-EGFP antibody revealed the presence of a band at the predicted size of EGFP-GLI2ΔN fusion protein at ~ 180 kDa. β-actin (~ 42 kDa) confirmed equal protein loading for both samples.

3.2.1.3 Transcription and endogenous protein levels of GLI2 in N/TERT human keratinocytes

To obtain information on the transcription levels of GLI2 in N/TERT keratinocytes, the mRNA expression levels of GLI2 were examined by quantitative real-time PCR (qRT-PCR) **(Chapter 2, Section 2.11)**. Specific intron spanning primers were used, to detect full length GLI2 (GLI2) mRNA as well as mRNA templates that correspond only to α and β isoforms of GLI2 (GLI2 α/β) **(Chapter 2, Section 2.11.3 and Section 2.11.7, Table 2.3)**. GLI2 full length and GLI2 α/β primers specificity and efficient amplification was confirmed by melting peak analysis **(Chapter 2, Section 2.11.4) (Figure 3.2A i and Figure 3.2B i)** and further visualized on a 2% DNA agarose gel, showing amplification of a single product of the corresponding size **(Chapter 2, Section 2.11.5) (Figure 3.2A ii and Figure 3.2B ii)**.

The qRT-PCR amplification products were purified and 10-fold serial dilutions were made in order to generate a standard curve **(Chapter 2, Section 2.11.6)**. This allowed accurate quantification of the absolute mRNA copy number of each target gene in qRT-PCR analytical runs using LightCycler 480 software **(Chapter 2, Section 2.11.7)**. Representative amplification curves of serially diluted GLI2 full length **(Figure 3.2A iii)** and GLI2 α/β **(Figure 3.2B iii)** products, and the resulting standard curves are shown **(Figure 3.2A iv and Figure 3.2B iv)**.

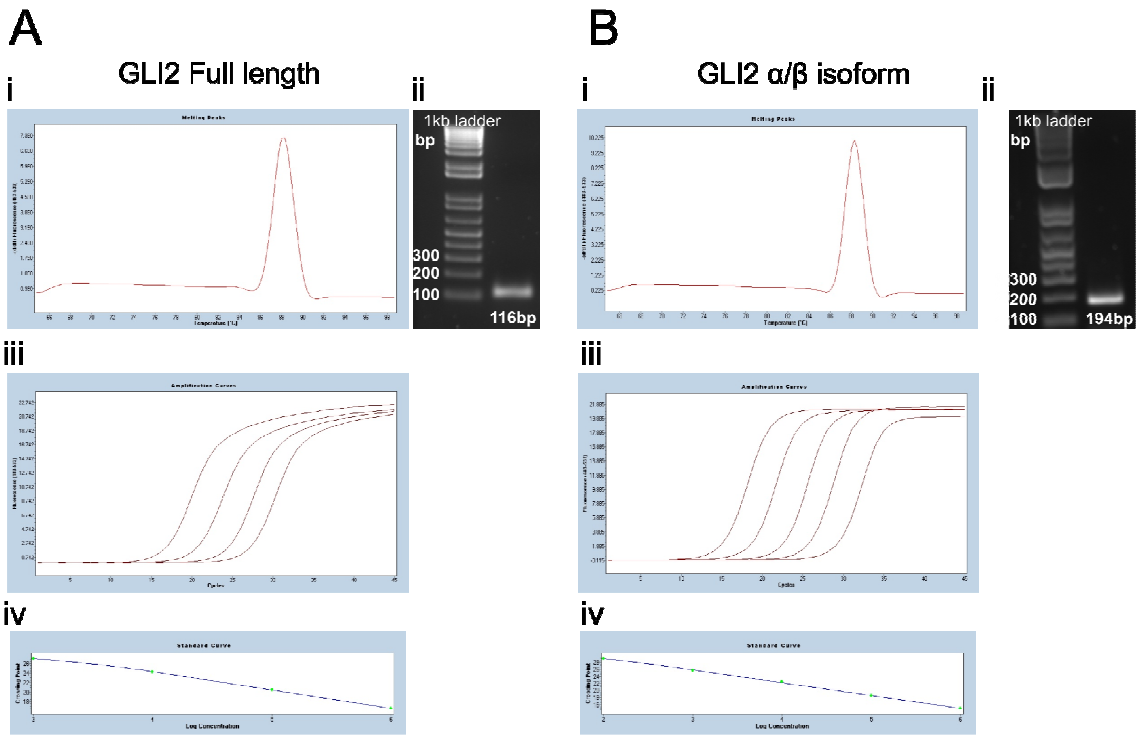

Figure 3.2: Validation of GLI2 specific primers and standard curves creation.

(A) Melting curve analysis **(i)** showed the presence of a single peak which signifies the presence of a single product, produced by qRT-PCR. qRT-PCR products were run on 2% agarose gel **(ii)** to confirm the presence of a single product of 116 bp. Ten fold serial dilutions of GLI2 full length template was used to generate a standard curve comprising 1000-100,000 copies. qRT-PCR amplification curves **(iii)** and the resulting standard curve **(iv)** are shown. **(B)** Melting curve analysis **(i)** showed the presence of a single peak which signifies the presence of a single product produced by qRT-PCR. qRT-PCR products were run on a 2% agarose gel **(ii)** to confirm the presence of a single product of 194 bp. Ten fold serial dilutions of GLI2 α/β isoforms template was used to generate a standard curve comprising 100-100,000 copies. qRT-PCR amplification curves **(iii)** and the resulting standard curve **(iv)** are shown.

To examine GLI2 transcription levels, RNA was harvested from N/TERT, SINCE, and SINEG2 keratinocytes **(Chapter 2, Section 2.11.1)**. cDNA from these samples was subjected to qRT-PCR using GLI2 full length and α/β isoform specific primers **(Chapter 2, Section 2.11.7)**. Relative mRNA copy numbers were obtained after normalization with two housekeeping genes, POLR2A (polymerase (RNA) II (DNA directed) polypeptide A) and YAP1 (Yes-associated protein 1). Results show the clear mRNA expression of both full length GLI2 (*** *P≤0.001*) **(Figure 3.3A i)** and GLI2 α/β (*** *P≤0.001*) **(Figure 3.3B i)** genes in SINEG2 cells, while endogenous transcription levels in N/TERT and SINCE control cells were low but detectable **(Figure 3.3A i and Figure 3.3B i)**. The higher abundance of GLI2 α/β over GLI2 full length in SINEG2 cells probably reflects the fact that SINEG2 cell line is transduced with retroviral construct bearing only the β isoform of GLI2ΔN. The fold difference of GLI2 mRNA induction between SINEG2 and control N/TERT and SINCE cells, is likely to be an overestimation of the actual differences in mRNA copy numbers, since GLI2 endogenous levels of both N/TERT and SINCE cells were very low, consistent with the very low expression of GLI2 in normal human skin (O'Driscoll et al., 2006). A semi-quantitative approach **(Chapter 2, Section 2.11.8)** was also used to display the clear induction of GLI2 and GLI2 α/β transcription in SINEG2 keratinocytes **(Figure 3.3A ii and Figure 3.3B ii)**.

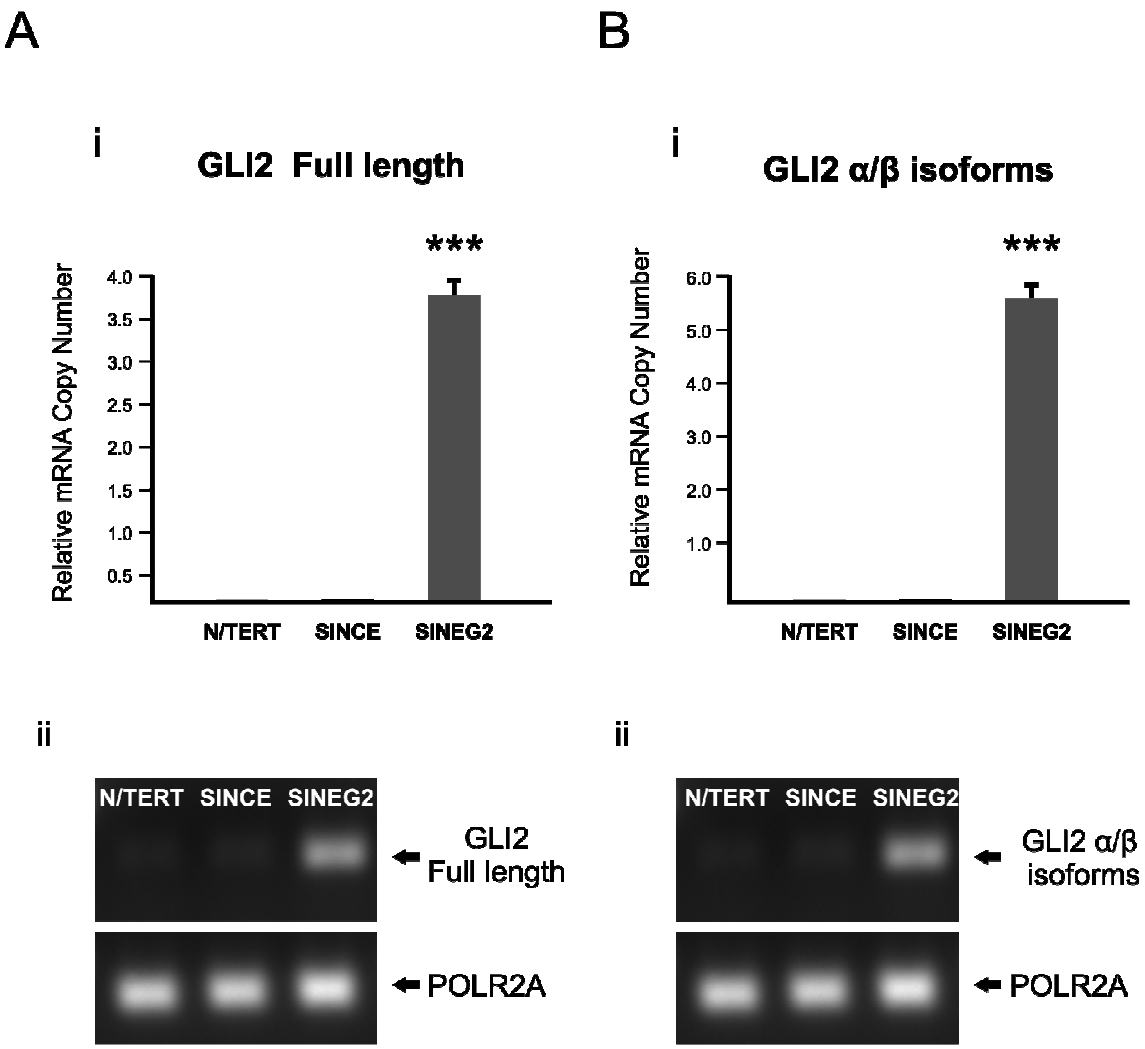

Figure 3.3: Quantification of GLI2 mRNA expression in N/TERT keratinocytes.

(A) RNA was harvested from N/TERT, SINCE, and SINEG2 cells to examine the levels of GLI2 expression using primers specific for full length GLI2. Quantitative RT-PCR analysis of GLI2 full length expression **(i)** and semi-quantitative PCR **(ii)** analysis, show the presence of high levels of GLI2 mRNA expression in SINEG2 cells compared to N/TERT and SINCE, cells where GLI2 mRNA expression is low but detectable. Each bar represents a mean ± s.e.m of triplicate samples. *** *P≤0.001*. **(B)** RNA was harvested from N/TERT, SINCE, and SINEG2 cells to examine the levels of GLI2 expression using primers to amplify α/β isoforms of GLI2. Quantitative RT-PCR analysis of GLI2 α/β isoforms expression **(i)** and semi-quantitative PCR **(ii)** analysis show the presence of high GLI2 α/β expression in SINEG2 cells compared to N/TERT and SINCE cells where GLI2 α/β mRNA expression is low but detectable. Each bar represents a mean ± s.e.m of triplicate samples. *** *P≤0.001*. POLR2A (polymerase (RNA) II (DNA directed) polypeptide A) was used as a housekeeping gene control for all samples in semi-quantitative PCR.

Since the transcriptional activity of GLI2 was low in N/TERT as well as in SINCE control keratinocytes, the endogenous protein levels were examined. Total protein extracts from N/TERT, SINCE and SINEG2 keratinocytes were immunoblotted against anti-GLI2 antibody **(Chapter 2, Section 2.12.1 and Section 2.12.5)**. Expectedly, GLI2 protein levels were only detectable in SINEG2 keratinocytes **(Figure 3.4A)**. Immunoblotting revealed the presence of exogenous EGFP-GLI2ΔN protein at the predicted size of ~ 180 kDa, but also showed the presence of endogenous GLI2 protein at around ~ 150 kDa **(Figure 3.4A)**. In order to confirm the presence of endogenous GLI2 protein at the predicted molecular size (~ 150 kDa) as previously shown for SINEG2 cells **(Figure 3.4A)**, high concentrations of N/TERT and SINCE protein extracts (30 μg of protein lysates) were separately immunoblotted against anti-GLI2 antibody **(Figure 3.4B)**. Low but detectable levels of GLI2 protein were found **(Figure 3.4B)** at the same molecular size (~ 150 kDa) as in SINEG2 cells. This is in line with the very low transcription levels detected in both N/TERT and SINCE cells, as well as with the high rate of GLI2 protein turnover (Bhatia et al., 2006; Huntzicker et al., 2006; Pan et al., 2006).

The above data suggested that exogenous GLI2ΔN protein had an effect on the regulation of endogenous protein in SINEG2 cells. At this point, it is difficult to delineate the reason for endogenous GLI2 upregulation, but this data may suggest the presence of a positive feedback loop whereby exogenous GLI2ΔN stimulates the expression of endogenous GLI2. Alternatively, the presence of excessive EGFP-GLI2ΔN protein in SINEG2 cells may cause a significant delay to the rapid proteasome mediated degradation of the endogenous GLI2 protein levels.

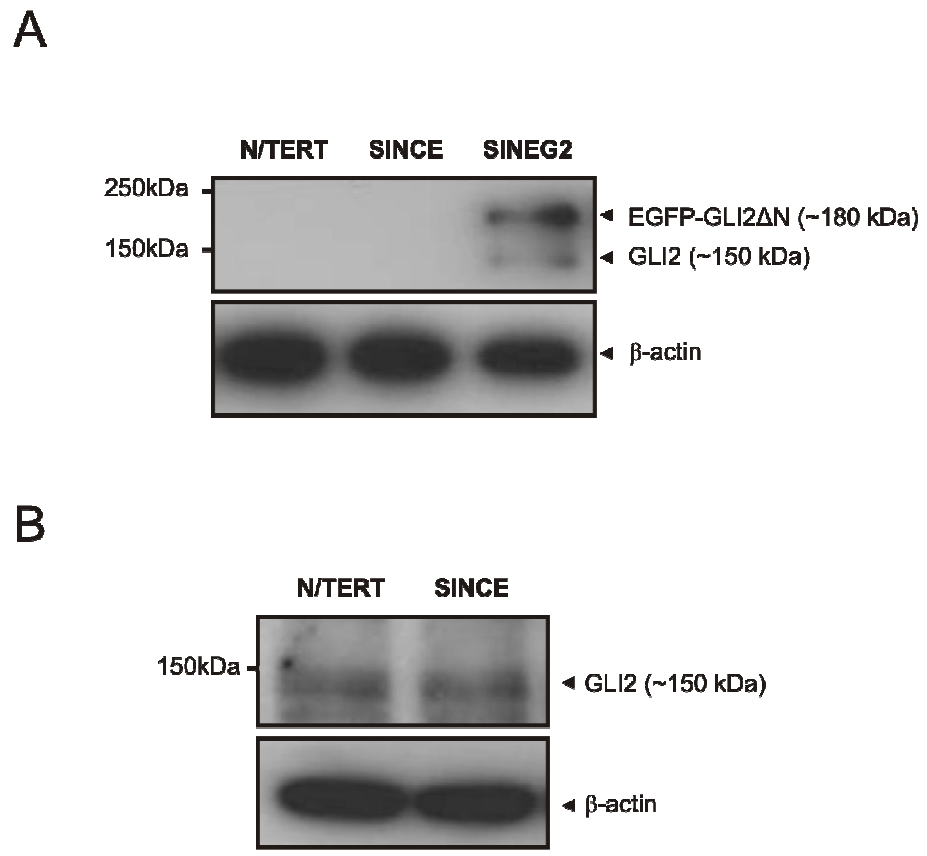

Figure 3.4: Detection of GLI2 endogenous and EGFP-GLI2ΔN exogenous protein levels.

(A) N/TERT, SINCE, and SINEG2 cells were harvested and total protein was immunoblotted against anti-GLI2 antibody and anti-β-actin as a protein loading control. Endogenous GLI2 (~ 150 kDa) and exogenous EGFP-GLI2ΔN (~ 180 kDa) proteins were detected in SINEG2 cells while GLI2 endogenous levels were almost absent from N/TERT and SINCE control cells. **(B)** N/TERT and SINCE protein lysates of higher protein concentration (30 μg protein lysates), were separately immunoblotted against anti-GLI2 antibody to confirm the presence of endogenous GLI2 protein at the predicted molecular size of approximately ~ 150 kDa. Again, β-actin was used as protein loading control.

3.2.1.4 Gene targets of GLI2ΔN in N/TERT human keratinocytes

The expression profile of SINEG2 keratinocytes was further examined by investigating the expression (either mRNA or protein levels) status **(Chapter 2, Section 2.11 and Section 2.12)** of two genes that have been shown to be either positively or negatively regulated both in response to GLI2ΔN and in human BCCs. The anti-apoptotic gene, BCL-2 (B-cell lymphoma 2), was previously identified as direct transcriptional target of GLI2 transcription factor (Regl et al., 2004b). In addition, GLI2 and BCL-2 are often co-expressed in human basal cell carcinomas (Regl et al., 2004b). Consistently the mRNA expression levels of BCL-2 were significantly elevated by 11-fold in SINEG2 keratinocytes, compared to N/TERT and SINCE controls (** $P \leq 0.01$) **(Figure 3.5A)**.

Inducible expression of GLI2ΔN in HaCaT keratinocytes results in downregulation of c-MYC (Regl et al., 2004a; Eichberger et al., 2006), and more importantly, c-MYC mRNA and protein levels are significantly suppressed in human BCCs (Bonifas et al., 2001; Regl et al., 2002; O'Driscoll et al., 2006; Asplund et al., 2008). SINEG2 keratinocytes displayed a similar expression pattern, whereby c-MYC mRNA expression **(Figure 3.5B)**, as well as protein levels **(Figure 3.5C)**, were reduced when compared to N/TERT and SINCE keratinocytes (* $P \leq 0.05$).

Therefore, SINEG2 keratinocytes display an expression pattern for BCL-2 and c-MYC that is similar to what is previously reported in other systems, as well as to the molecular signature of human basal cell carcinomas.

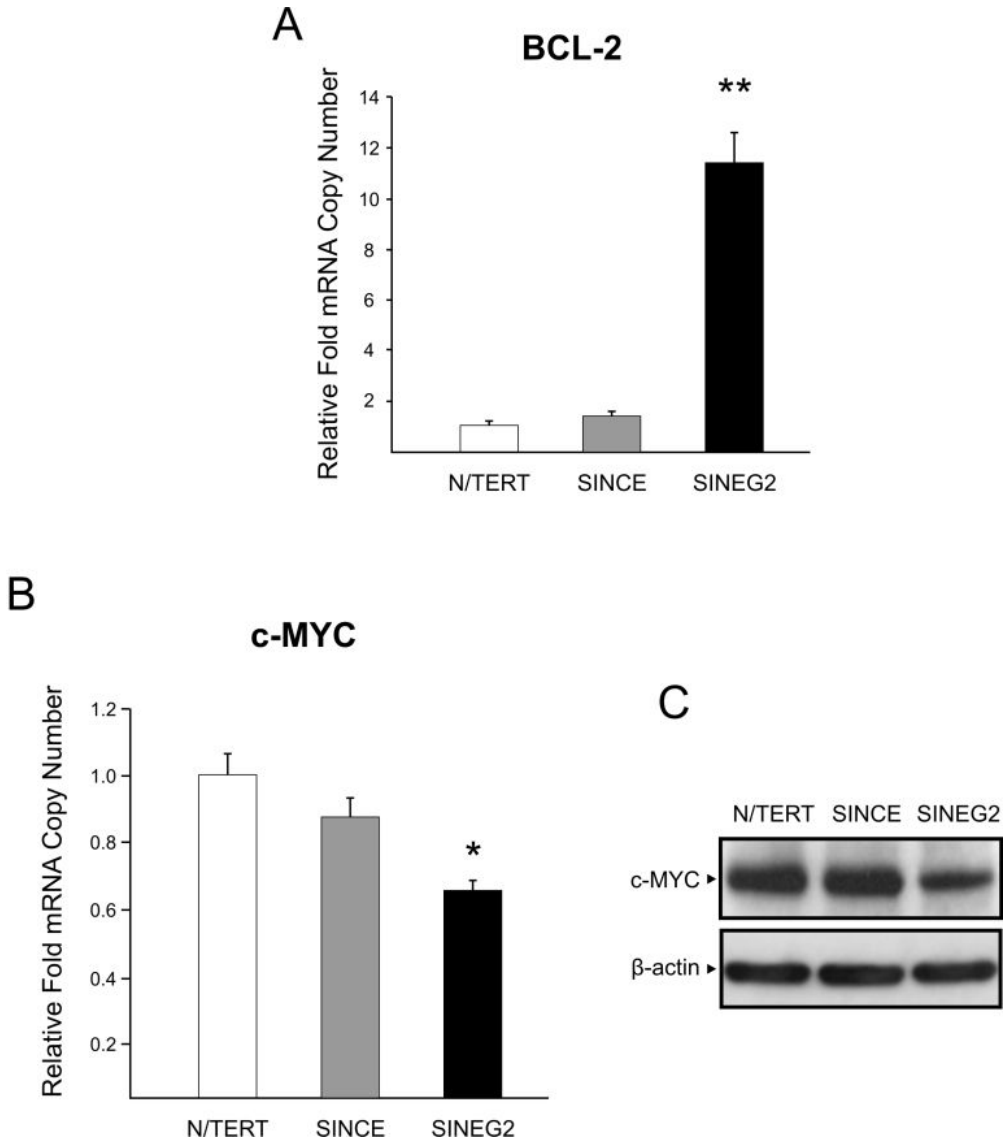

Figure 3.5: BCC associated markers expression in SINEG2 keratinocytes.

RNA was harvested from N/TERT, SINCE, and SINEG2 cells to examine the levels of BCL-2 **(A)** and c-MYC **(B)** expression by qRT-PCR, using primers specific for each gene. Quantitative RT-PCR analysis of BCL-2 and c-MYC show an increase and a decrease respectively in SINEG2 cells, compared to N/TERT and SINCE control cells. Each bar represents mean fold induction/or suppression relative to N/TERT (arbitrary value of 1) ± s.e.m of triplicate samples. ** $P \leq 0.05$*, *** $P \leq 0.01$*. **(C)** N/TERT, SINCE, and SINEG2 cells were harvested and total protein was immunoblotted against anti-c-MYC antibody (~ 60 kDa) and anti-β-actin (~ 42 kDa) as a protein loading control. SINEG2 cells show a significant decrease of the c-MYC protein levels compared to N/TERT and SINCE cells.

3.2.2 Generation and characterisation of EGFP-GLI2ΔN inducible cell line

3.2.2.1 Generation

The preparation of the inducible cell line, NTEG2, provided by Dr Giuseppe Trigiante (Centre for Cutaneous Research, Institute of Cell and Molecular Science, Barts and the London School of Medicine and Dentistry, London, UK), was based on the RevTet-OFF regulatory system (Clontech Laboratories, Palo Alto, CA), as previously described in Materials and Methods **(Chapter 2, Section 2.1.6 and Section 2.3.5.2)**. In the retrovirus-mediated tet-regulated gene expression system (RevTet-Off system), transcription of the gene of interest (in this study EGFP-GLI2ΔN fusion gene) is turned off in the presence of Doxycycline (a derivative of tetracycline) (Dox+), while transcription of this gene (EGFP-GLI2ΔN fusion gene) is turned on in the absence of Doxycycline (Dox-) **(Figure 3.6)**. For the generation of the NTEG2 cell line, heterogeneous cell populations were used in order to avoid any clone specific effects.

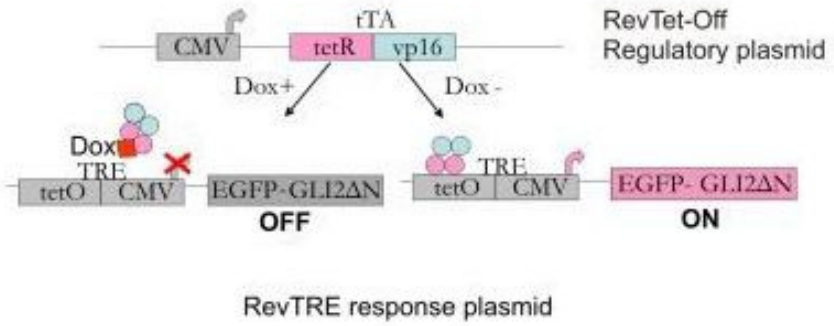

Figure 3.6: Generation of NTEG2 inducible cell line (RevTet-Off system).

Diagram illustrating the principle of induction and/or repression of EGFP-GLI2ΔN fusion protein under the control of Doxycycline (Dox). Tetracycline controlled transactivator (tTA) (RevTet-Off Regulatory plasmid) binds to tetracycline response element (TRE) (RevTRE Response plasmid) to activate transgene transcription mediated by the CMV promoter in the absence of doxycycline. tTA binding is repressed in the presence of doxycycline. The tTA regulatory element is a fusion tetracycline-dependent protein which consists of the tetR and the vp16. tetR is a tetracycline repressor found in *E.Coli*, while vp16 is a transcriptional activator protein isolated from Herpes Simplex Virus. In the absence of Doxycycline (Dox-), the tTA binds to the TRE which consists of the tetO and a CMV promoter. The tetO operator consists of an array of direct repeats which are recognized by the tetR protein. Binding of the tTA (tetR + vp16) to the tetO sequence leads to the activation of the CMV promoter, which then drives the expression of the transgene (EGFP-GLI2ΔN fusion protein). In the presence of Doxycycline (Dox+), the tetracycline repressor (tetR) is inactivated, tetO becomes inactive, and therefore the CMV promoter is silenced.

3.2.2.2 Selection of NTEG2 cells

Different concentrations of G418 and Hygromycin B selection were used, in order to identify the optimal concentration for selection **(Chapter 2, Section 2.4) (Figure 3.7)**. The minimum antibiotic concentration that induced massive cell death after 3 days and total cell death after 8 days was chosen for each antibiotic. The final concentrations used for selection of the NTEG2 cell line, were 500 μg/ml for G418 and 100 μg/ml for Hygromycin B, and for maintenance 250 μg/ml and 50 μg/ml respectively.

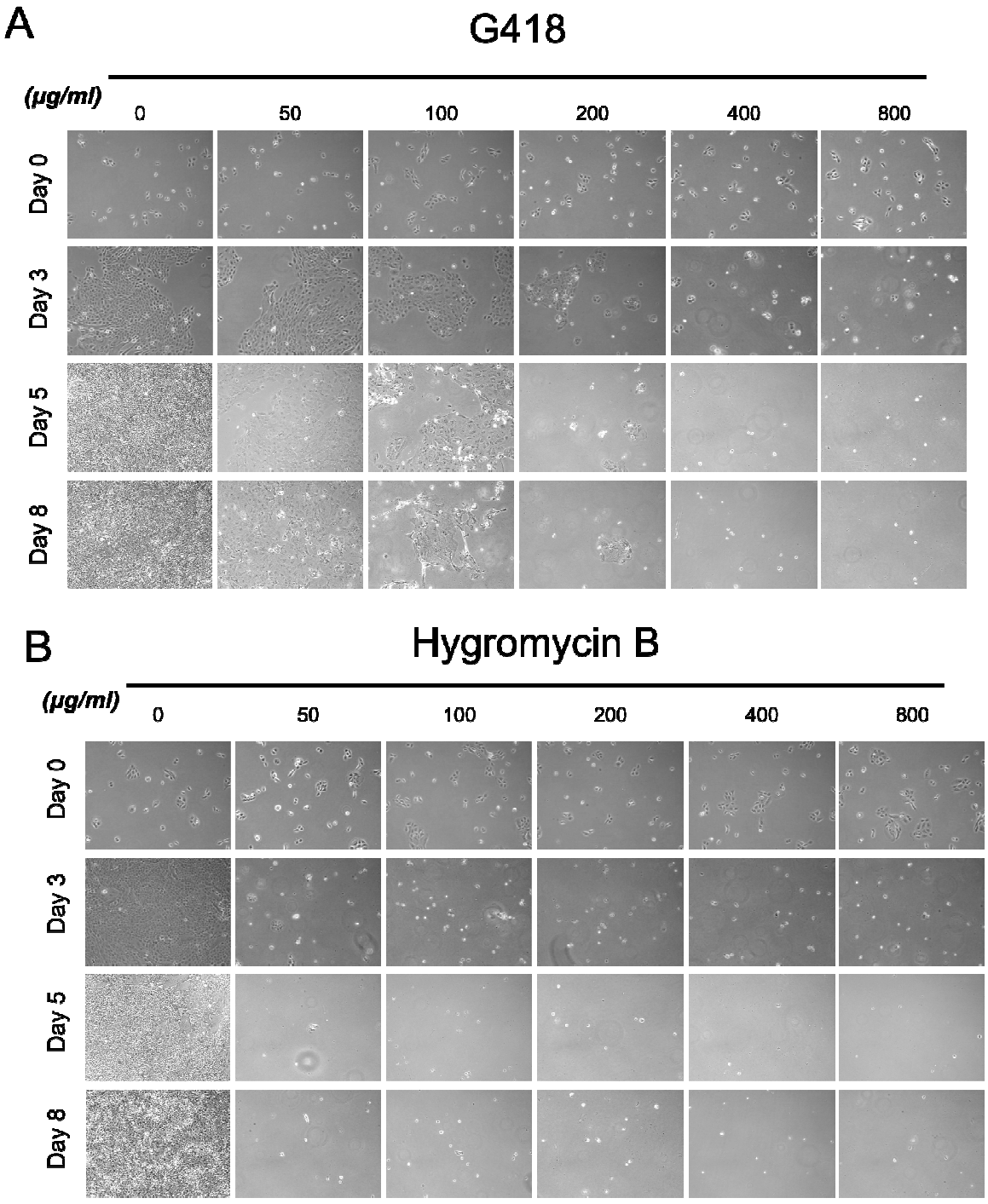

Figure 3.7: Antibiotic selection of N/TERT cell line.

N/TERT cells were seeded in equal densities and cultured in normal growth medium with 0, 50, 100, 200, 400, 800 µg/ml of either G418 **(A)** or Hygro B **(B)** for the total period of 8 days. The minimum antibiotic concentration that induced massive cell death after 3 days and total cell death after 8 days was chosen for antibiotic selection of NTEG2 inducible cell line.

3.2.2.3 FACS Sorting

Following 8-11 days of drug selection, and induction for 5 days, NTEG2 (NTEG2 Dox-) cells were sorted by FACS **(Chapter 2, Section 2.8.2)**, and all EGFP positive and negative cells were gated as shown previously **(Figure 3.1B i)** using N/TERT as a reference cell line to obtain baseline values of green fluorescence. All EGFP+ cells were collected, replated and cultured under the presence of doxycycline.

3.2.2.4 Doxycycline optimisation

Pilot experiments were carried out, in order to optimise the concentration of doxycycline which provides the best ratio of induction/suppression of EGFP-GLI2ΔN expression, without inducing any cytotoxic effects on the NTEG2 cell line **(Chapter 2, Section 2.5)**. Initially, NTEG2 cells were grown in the absence of doxycycline (Dox) for 48 or 72 hours, for transgene induction.

Next, cells were grown in the presence of different Dox concentrations (1, 100, 1000, 10000 ng/ml) and EGFP-GLI2ΔN suppression was investigated by flow cytometry analysis after 48 hours **(Figure 3.8A)** and 5 days **(Figure 3.8B)**. The presence of Dox suppressed transgene expression in a dose-dependent manner. Fluorescence levels were reduced by 2 fold after 48 hours incubation in the presence of maximum Dox concentration (10000 ng/ml) **(Figure 3.8A)**. After 5 days of doxycycline treatment, an even stronger suppression was observed, where EGFP-GLI2ΔN fluorescence levels reached ~ 8% (4 fold suppression) **(Figure 3.8B)**. Data are representative of two independent experiments.

To further confirm that Dox efficiently suppressed EGFP-GLI2ΔN protein levels, NTEG2 cells were incubated in 40 ng/ml, 1 μg/ml, and 10 μg/ml of Dox for 6 days (Dox (+) cells), and protein extracts were prepared and immunoblotted against anti-EGFP antibody **(Figure 3.8C)**. At the same time another set of NTEG2 cells was initially treated with 40 ng/ml, 1 μg/ml, and 10 μg/ml of Dox for 24 hr and was thereafter cultured in the absence of Dox for 5 days (Dox (-) cells) and protein extracts were prepared and immunoblotted against anti-EGFP antibody **(Figure 3.8C)**. Consistent with flow cytometry analysis, EGFP-GLI2ΔN protein suppression showed a dose-dependent effect. The concentration range between 40 ng/ml and 10 μg/ml of Dox,

is sufficient to suppress EGFP-GLI2ΔN. However, total suppression was not observed indicating the presence of background levels of EGFP-GLI2ΔN protein in control NTEG2 Dox (+) cells.

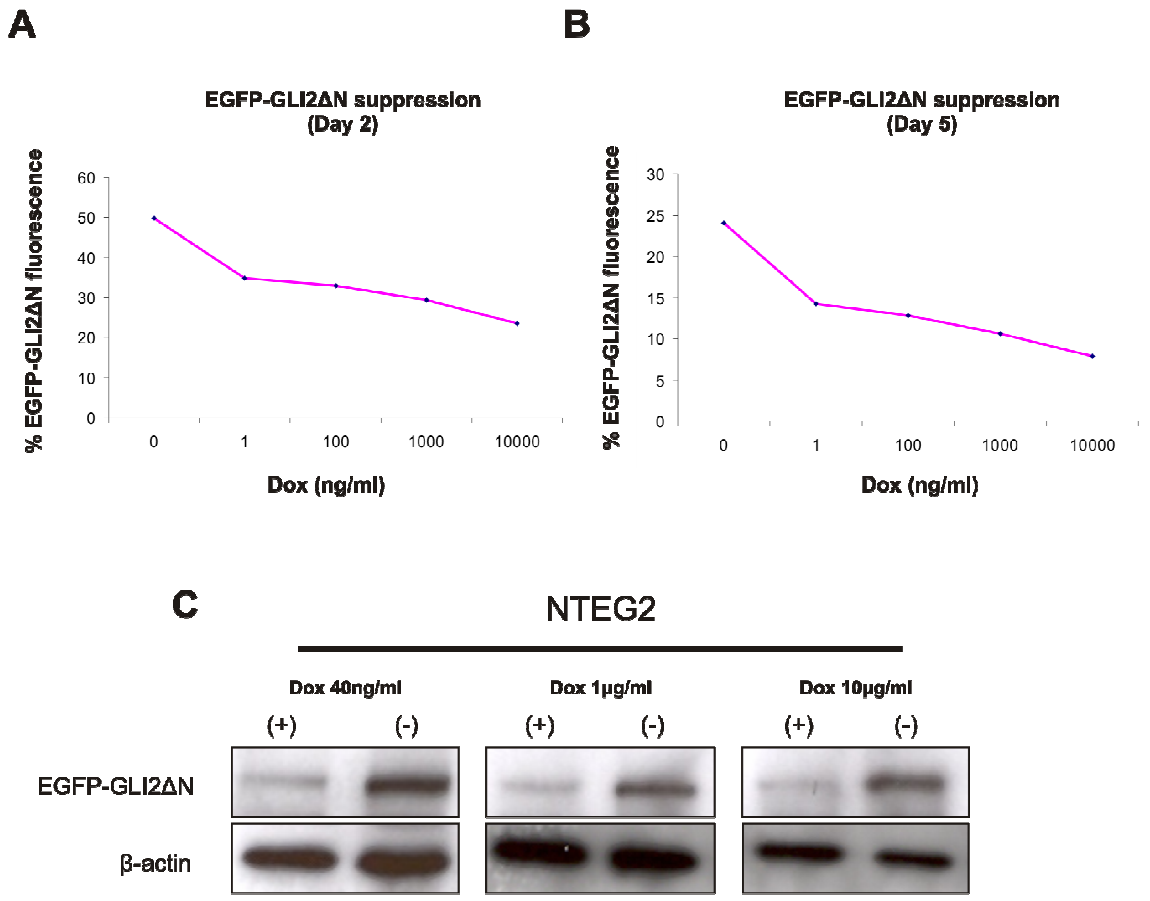

Figure 3.8: Doxycycline optimisation.

NTEG2 cells were grown for 48 or 72 hours in the absence of Dox. Next, cells were treated with different concentrations of Dox (1, 100, 1000, 10000 ng/ml) and EGFP-GLI2ΔN expression was analysed by flow cytometry analysis after 48 hours **(A)** and 5 days **(B)**. A dose-dependent suppression of EGFP-GLI2ΔN fluorescence is observed in response to Dox treatment. Data are representative of two independent experiments. **(C)** NTEG2 cells were treated with 40 ng/ml, 1 µg/ml, and 10 µg/ml of Dox for 6 days (Dox (+) cells and at the same time another set of NTEG2 cells was were treated with 40 ng/ml, 1 µg/ml, and 10 µg/ml of Dox for 24 h which was thereafter cultured in the absence of Dox for 5 days (Dox (-) cells). Protein extracts were prepared prior to immunoblotting analysis against anti-EGFP antibody. β-actin was used as protein loading control. Clear EGFP-GLI2ΔN protein suppression is observed in this range of Dox concentration (40 ng/ml - 10 µg/ml). Strongest transgene suppression was observed with 10 µg/ml of Dox.

In order to rule out the possibility that Dox is inducing any cytotoxic effects on NTEG2 cell line, a cytotoxicity assay was performed **(Chapter 2, Section 2.7.1.1)**. N/TERT cells were grown in the absence or presence of Dox (1, 10, 100, 1000, 10000 ng/ml) for 48 hours and 5 days, and cell cytotoxicity was measured by Alamar Blue™ reduction **(Chapter 2, Section 2.7.1 and Section 2.7.1.1) (Figure 3.9)**. Results showed that this range of Dox concentration did not significantly affect the growth rate of N/TERT cells **(Figure 3.9)**. Data are representative of two independent experiments each of them consisting of duplicate samples.

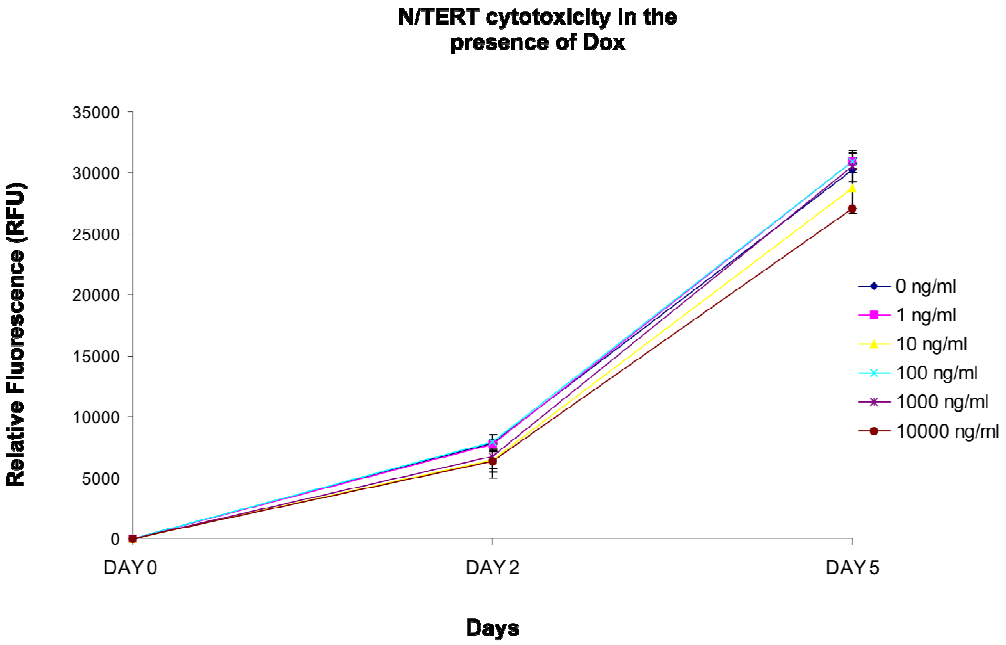

Figure 3.9: N/TERT cytotoxicity in the presence of Dox.

N/TERT cells were grown in the absence or presence of Dox (1, 10, 100, 1000, 10000 ng/ml) for 48 hours and 5 days, and fluorescence intensity produced by Alamar Blue™ reduction was measured in order to assess Dox mediated cytotoxicity. The increasing concentrations of Dox did not induce significant effects in the growth rate of N/TERT cells. Each data point in the graphs represents a mean ± s.e.m of duplicate samples, relative to the baseline values obtained at Day 0. All the values for all the different time points were subtracted from the mean value of Day 0.

3.2.2.5 Expression levels of NTEG2

Significant induction of protein levels was evidenced under fluorescent microscopy **(Chapter 2, Section 2.2)**, 5 days after removal of Dox, as shown in **Figure 3.10A ii, iii**, while no induction of EGFP-GLI2ΔN fusion protein was observed in NTEG2 cells under the presence of doxycycline (**Figure 3.10A i)**.

Subsequent flow cytometry analysis **(Chapter 2, Section 2.8)** of NTEG2 cells showed an increased percentage of EGFP+ cells when Dox was removed (**Figure 3.10B ii)**, but also a small baseline induction of fluorescence even in Dox treated cells (**Figure 3.10B i)**.

Immunoblotting **(Chapter 2, Section 2.12)** for EGFP-GLI2ΔN fusion protein confirmed GLI2ΔN induction in NTEG2 cells upon removal of Dox in comparison with baseline leak **(Figure 3.10C)**. β-actin was used as loading control.

Because pooled (FACS sorted EGFP+) NTEG2 cells were used, variation was observed in the levels of GLI2ΔN expression (EGFP intensity), between different clones in NTEG2 culture (compare **Figure 3.10A ii** and **Figure 3.10A iii**). To control for this variation, the levels of EGFP-GLI2ΔN induction/suppression were always measured by flow cytometry and immunoblotting prior to carrying out experiments, to ensure similar levels of GLI2ΔN expression between experiments.

The GLI2 transcription factor is normally present in both the cytoplasm and the nucleus, and its subcellular localisation and stability is dependent upon Hedgehog (HH) signalling and stimulation (Murone et al., 2000; Roessler et al., 2003; Barnfield et al., 2005; Pan et al., 2006; Varjosalo et al., 2006). Accordingly, I found that EGFP-GLI2ΔN was detected in both the cytoplasm and the nucleus of both SINEG2 **(Figure 3.1A)** and NTEG2 cells **(Figure 3.10A ii, iii)**.

GLI2 transcription factor undergoes rapid proteasome mediated degradation, as a barrier to human tumourigenesis (Bhatia et al., 2006; Huntzicker et al., 2006; Pan et al., 2006). This suggests that constitutive activation of the transgene may be necessary to achieve maximum levels of EGFP-GLI2ΔN accumulation. In line with this, in this study it is

observed that while EGFP intensity is similar in both the stable and inducible cell lines (by flow cytometry analysis), the proportion of EGFP positive cells in SINEG2 stable cell line, is significantly higher than that observed in the induced NTEG2 cells (compare **Figure 3.1B iii** with **Figure 3.10B ii**).

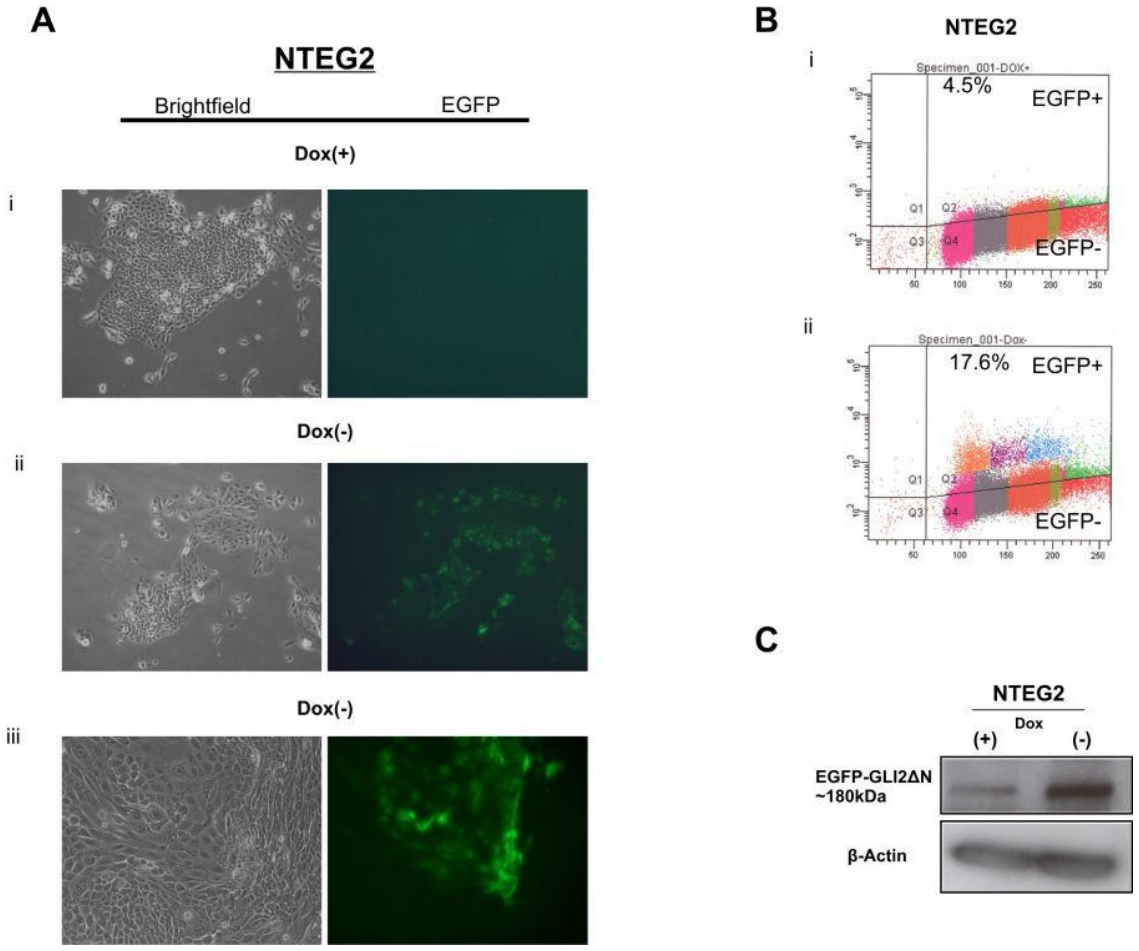

Figure 3.10: Characterisation of NTEG2 inducible cell line.

(A) Representative pictures of NTEG2 cells in the presence **(i)** or absence **(ii, iii)** of doxycycline. Varying levels of EGFP-GLI2ΔN expression were observed possibly due to the heterogeneity of NTEG2 cell population. **(B)** Flow cytometry analysis of NTEG2 cell line in the presence or absence of doxycycline. Clear induction of EGFP-GLI2ΔN is shown in Dox (-) cells **(ii)** while background activity of EGFP-GLI2ΔN is also evidenced in the presence of doxycycline **(i)** represented by the small population detected above threshold levels of fluorescence obtained from wild-type N/TERT cells. **(C)** Immunoblotting analysis of NTEG2 cells in the presence or absence (5 days) of doxycycline against anti-EGFP antibody. Significant induction of the transgene is observed in Dox (-) cells, while background levels of induction are also present, as evidenced by previous flow cytometry analysis. β-actin confirms equal protein loading for both samples.

3.2.3 The effect of GLI2ΔN on cell morphology and growth

3.2.3.1 Cell morphology

Stable expression of GLI2ΔN in N/TERT keratinocytes resulted in the manifestation of a phenotype that contains a morphologically heterogeneous cell population that was different from wild-type N/TERT and SINCE control keratinocytes. These phenotypic differences became more obvious at approximately ten days after infection (eight days after FACS sorting). No differences between the morphologies of N/TERT and SINCE cells were detected before and after FACS sorting, indicating that the phenotypic differences in SINEG2 cells were GLI2ΔN specific. SINEG2 cells display a compact morphology and tend to give rise to tight colonies **(Figure 3.11C-H)** compared to N/TERT and SINCE cells that tend to form more loosely associated colonies which are well spread in culture **(Figure 3.11A, B)**. Although the majority of SINEG2 keratinocytes comprising such colonies, appear to be very cohesive, it can be noted that few cells mainly located at the periphery of such colonies, are more loosely attached **(Figure 3.11D, E)**. These loosely attached cells are not always associated with tight colonies and can also be found scattered throughout the culture **(Figure 3.11H)** or forming loose colonies **(Figure 3.11I)**. A high proportion of SINEG2 keratinocytes, forms islands of compact colonies that do not appear to merge, even in confluent cultures. However, a smaller number of colonies appear to be joined **(Figure 3.11D, E, H)** by groups of keratinocytes that have characteristics resembling the peripheral cells of tight colonies. This may suggest a more migratory behaviour for peripheral keratinocytes, which are able to detach from the bulk of tight colonies and mediate or initiate the apparent colony merging. However, all these morphological differences were less pronounced when the cells were seeded at higher densities.

Importantly, these phenotypic characteristics (tight, round, smooth colonies consisting of small with high nuclear to cytoplasmic ratio cells) are also observed in a proportion of human epidermal keratinocyte clones, that appear to be relatively undifferentiated and posses a capacity of self-renewal. Such clones of keratinocytes (holoclones) are considered to be the *in vitro* analogue of keratinocyte stem cells (Barrandon & Green, 1987).

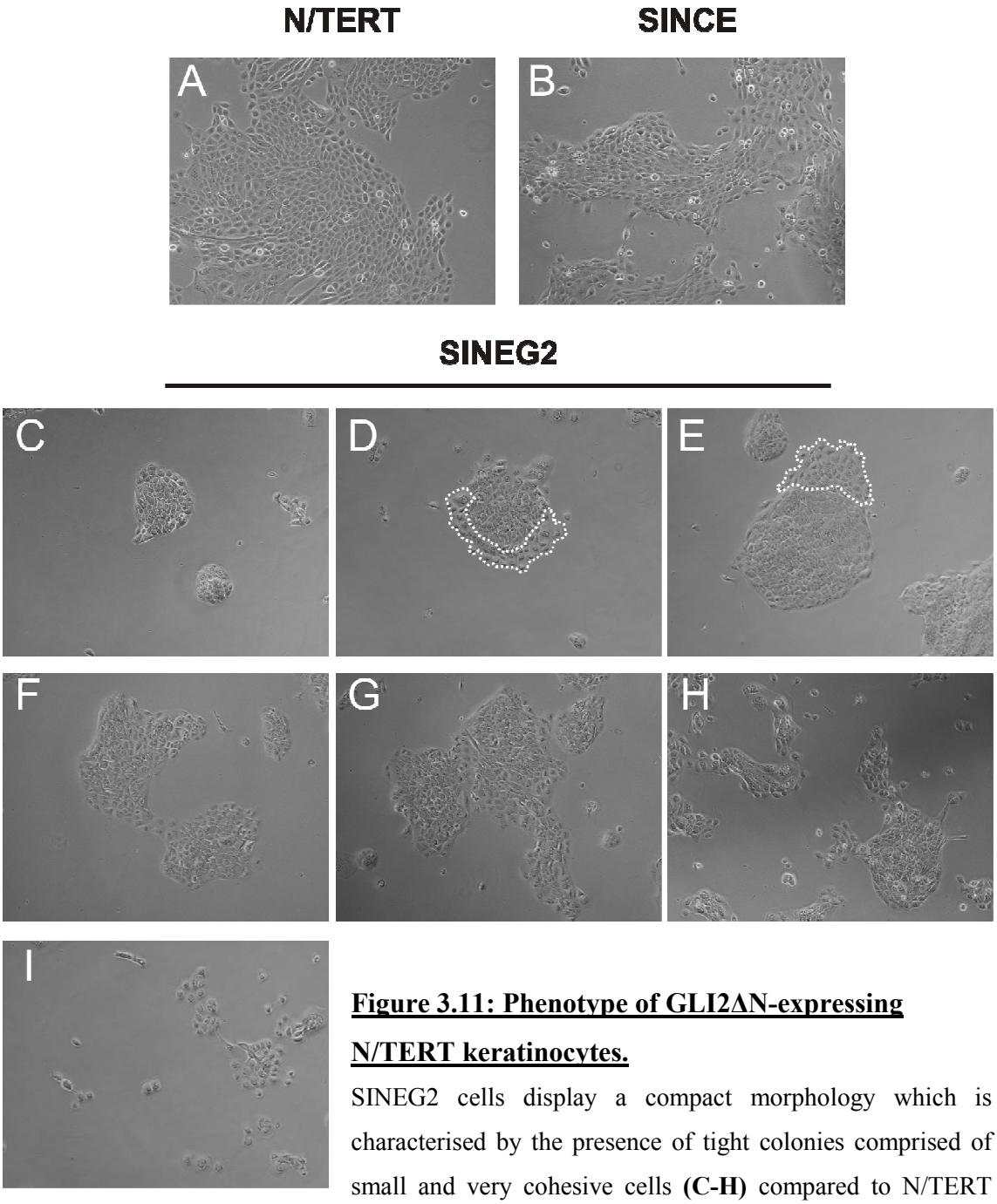

Figure 3.11: Phenotype of GLI2ΔN-expressing N/TERT keratinocytes.

SINEG2 cells display a compact morphology which is characterised by the presence of tight colonies comprised of small and very cohesive cells **(C-H)** compared to N/TERT and SINCE cells **(A, B)**. The presence of more loose keratinocytes can be noted in the periphery of some colonies **(D, E)**, scattered throughout the culture **(H)**, and in more loose colonies **(I)**. Although SINEG2 cells form compact islands of keratinocytes, in the same culture other colonies can be found joined together **(F, G)**. Peripheral cells which appear to be more detached from the main colony might have a more migratory phenotype which might be responsible for the colony joining **(F, G)**.

Confluent N/TERT and SINCE cultures (initially seeded at low density) show a uniform growth pattern, and contain cells with high nuclear/cytoplasmic ratio as well as large and more flattened cells indicating the presence of proliferative and differentiating keratinocytes respectively **(Figure 3.12 i A, B)**. In contrast, cultures of SINEG2 keratinocytes grown for the same period of time retain the compact morphology and are characterised by round colonies with smooth perimeters **(Figure 3.12 i C, D)**. Again, a smaller proportion of SINEG2 derived keratinocyte colonies, are found joined together, while retaining a tight morphology and the presence of peripheral loosely attached keratinocytes **(Figure 3.12 i E)**.

To obtain a clearer picture depicting the growth patterns of the whole culture, N/TERT, SINCE and SINEG2 keratinocytes were seeded at low densities (clonal growth) and were allowed to grow until N/TERT and SINCE control cells reached confluence. By staining keratinocytes with Rhodamine B **(Chapter 2, Section 2.6)**, it is clear that while N/TERT and SINCE keratinocytes can form a uniform monolayer culture, the vast majority of GLI2ΔN expressing keratinocytes form tightly packed colonies **(Figure 3.12 ii)**. This again shows that this is not a localised effect in small proportion of the culture, but a rather strong phenotypic outcome of GLI2ΔN overexpression.

A similar effect was observed with inducible expression of GLI2ΔN in distinct colonies, but the overall effect was considerably weaker **(Figure 3.10A ii)**. This apparent discrepancy could be attributed to several factors. The inducible system used to overexpress GLI2ΔN resulted in weaker expression of the transgene when compared to stable transduction of N/TERT keratinocytes. Furthermore, the background activation of the uninduced control N/TERT cells may have led to an underestimation of the effect produced by GLI2ΔN. Last, the transient short-term (maximum of five days) induction of GLI2ΔN using the inducible system, combined with the low levels of transgene expression may not be sufficient to elicit the strong phenotype observed in stably transduced keratinocytes.

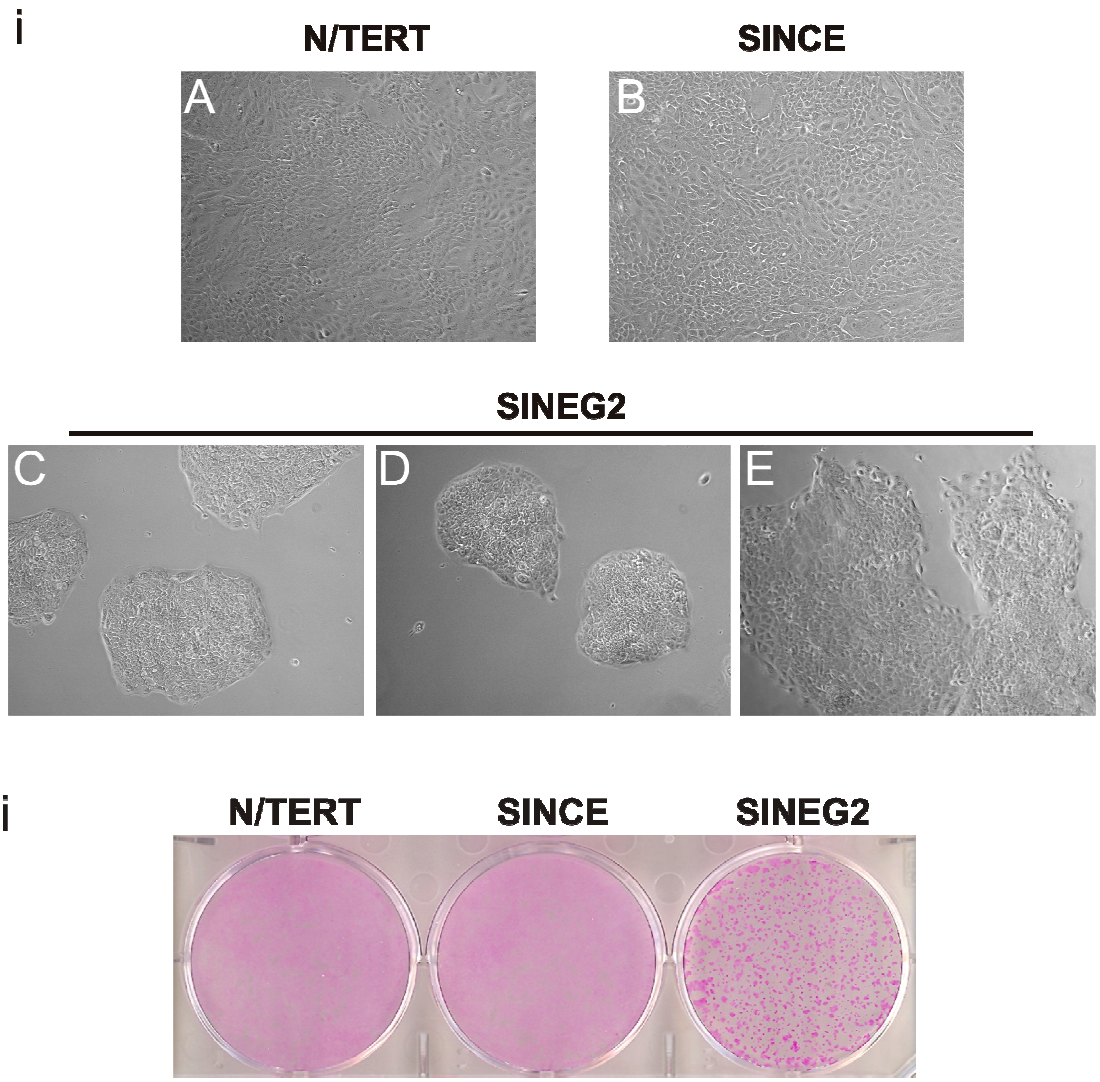

Figure 3.12: GLI2ΔN induces changes in cell morphology of N/TERT keratinocytes.

(i) Confluent cultures of N/TERT, SINCE, and SINEG2 keratinocytes are shown **(A-E)**. SINEG2 keratinocytes tend to have a compact morphology and form tightly packed colonies with smooth perimeters **(C, D)** compared to N/TERT and SINCE cells that display a well spread monolayer culture **(A, B)**. Although very few large joined colonies are found together in SINEG2 monolayer culture, they still retain a tight and highly compact phenotype **(E)**. **(ii)** NTERT, SINCE, and SINEG2 keratinocytes were seeded at low density and were allowed to grow until control NTERT and SINCE keratinocytes became confluent. Next, cells were stained with Rhodamine B to macroscopically examine the colony forming efficiency and colony morphology of cells. In contrast to control NTERT and SINCE cells which formed a spread and confluent monolayer culture, SINEG2 keratinocytes grew into small, tightly packed, round colonies which are easily discernable with Rhodamine B staining.

3.2.3.1.1 Integrin β1, involucrin and SOX2 expression in GLI2ΔN-expressing N/TERT cells

This basal-like phenotype of SINEG2 keratinocytes in culture could be attributed to a disruption of the differentiation process probably, due to downregulation and/or upregulation of differentiation and stem cell genes respectively. Consistently with the resistance to differentiation of BCC cells (Murphy et al., 1984; Said et al., 1984; Sumitomo et al., 1986; Miller, 1991a), it has been previously shown in confluent GLI2 expressing HaCaT keratinocytes, that GLI2 represses genes that are involved in differentiation (Regl et al., 2004a), as well as opposing differentiation in organotypic cultures (Snijders et al., 2008). However, integrin beta 1 (ITGB1) gene, which is a marker of undifferentiated keratinocytes in the basal layer of the epidermis (Adams & Watt, 1991; Jones et al., 1995) and of which both *in vitro* and *in vivo* loss is associated with the onset of keratinocyte terminal differentiation (De Strooper et al., 1989; Peltonen et al., 1989; Adams & Watt, 1990; Nicholson & Watt, 1991; Hotchin et al., 1995), was found to be upregulated both in confluent and high-calcium confluent contact inhibited GLI2 HaCaT keratinocytes (Regl et al., 2004a). This suggests that while control cells arrest and downregulate β1 integrin levels upon confluence or high-calcium confluent induced differentiation, GLI2 HaCaT cells oppose this effect (no cell cycle arrest and suppression of differentiation markers) and maintain an immature population of keratinocytes with high β1 integrin levels (result of disrupted differentiation). Alternatively, the upregulation of β1 integrin levels can be a result of GLI2 induced expression independently of any differentiation stimulus (high-calcium confluence) in which case, it can contribute to the suppression of keratinocyte differentiation (one of the causes of disrupted differentiation).

In order to confirm which of these two possibilities occurs, GLI2ΔN along with control cells were grown in normal culture conditions (sub-confluent) without any extra stimulus for differentiation and RNA was harvested **(Chapter 2, Section 2.11.1)**. Expression analysis **(Chapter 2, Section 2.11)** showed that SINEG2 keratinocytes exhibit increased mRNA levels of β1 integrin gene (~ 2-fold) compared to N/TERT and SINCE cells (*** $P \leq 0.001$) **(Figure 3.13A)**, in line with the results of a previous large-scale microarray analysis in GLI2 HaCaT cells (Eichberger et al., 2006). This suggests that integrin β1 induction is likely to be a result of GLI2ΔN overexpression, rather than

an outcome of suppressed differentiation observed in confluent or high-calcium confluent cultures.

Involucrin (IVL gene) is the major soluble cytoplasmic protein precursor of the cornified envelope (stratum corneum) in human stratified squamous epithelia and is expressed in the mature cells of the upper stratum spinosum and stratum granulosum layers of human epidermis **(see Chapter 1, Section 1.1.1)** (Rice & Green, 1977; Murphy et al., 1984; Candi et al., 2005). Therefore, since involucrin is a well established marker for keratinocyte terminal differentiation *in vivo* and *in vitro* (Rice & Green, 1979; Watt, 1983), its mRNA levels were checked both in control and SINEG2 keratinocytes. Expression analysis **(Chapter 2, Section 2.11)** showed that SINEG2 keratinocytes exhibit decreased mRNA levels of involucrin (~ 5-fold), compared both to N/TERT and SINCE control cells (*** $P \leq 0.001$) **(Appendix II)**, further confirming the undifferentiated phenotype of SINEG2 keratinocytes.

The undifferentiated phenotype of SINEG2 keratinocytes could also be accompanied by an expression profile that is reminiscent of that observed in the more immature populations of keratinocyte stem cells. This will not be a surprise knowing that in skin SHH/GLI pathway is implicated in the maintenance and regulation of the epidermal stem cell population residing in the epidermal basal layer (interfollicular epidermis) and the hair follicle bulge (Callahan & Oro, 2001; Adolphe et al., 2004; Blanpain & Fuchs, 2006; Zhou et al., 2006), while *in vitro* it is also suggested that SHH/GLI signalling has a potential role in the maintenance and proliferation of human putative epidermal stem cells (Fan & Khavari, 1999; Kameda et al., 2001; Zhang & Kalderon, 2001; Zhou et al., 2006). In addition, GLI1 overexpression in N/TERT keratinocytes induces and suppresses a number of stem and non stem cell associated genes respectively (Kasper et al., 2006b; Neill et al., 2008). At the same time, BCCs which are characterised as undifferentiated tumours (expression of keratins 5 and 14 which are mainly expressed by basal cells (Stoler et al., 1988; Coulombe et al., 1989; Fuchs, 2008)) (Miller, 1991a; Crowson, 2006), manifest a stem cell gene profile similar to that expressed by the cells of the interfollicular epidermis and hair follicle bulge region, such as keratins 15 and 19, and α2 and β1 integrins (Lane et al., 1991; Miller, 1991a; Jones & Watt, 1993; Jones et al., 1995; Pentel et al., 1995; Kruger et al., 1999; Lyle et al., 1999; Morris et al., 2004; Tumbar et al., 2004; Crowson, 2006).

Additionally, integrin β1 which was found to be overexpressed upon GLI2ΔN induction **(Figure 3.13A)**, is not only a marker for undifferentiated cells, but it is also a valuable marker to enrich for epidermal keratinocyte stem cells *in vitro*, by selecting the cells with the highest levels of β1 integrins (Jones & Watt, 1993; Jones et al., 1995). In addition, its high levels are required for the maintenance of human epidermal stem cell compartment *in vitro* (Zhu et al., 1999), suggesting either a possible role of GLI2ΔN in this process or an ability of GLI2ΔN to induce a stem cell associated phenotype and gene expression in N/TERT keratinocytes.

Consistent with this notion, another well characterised stem cell associated gene, SOX2 (SRY (sex determining region Y)-box 2), was found to be dramatically upregulated in SINEG2 keratinocytes (~ $3x10^3$-fold), compared to both N/TERT and SINCE controls (**** $P \leq 0.001$*) **(Figure 3.13B)**, similarly to what was found by Snijders et al. (Snijders et al., 2008) in GLI2ΔN HaCaT keratinocytes. The relative fold mRNA induction could be an overestimate due to the very low background levels of SOX2 mRNA observed in control N/TERT and SINCE keratinocytes (Ct value > 31). Nevertheless, this remarkable induction in GLI2ΔN expressing N/TERT keratinocytes, suggests that SOX2 may be a direct downstream target of GLI2ΔN in human keratinocytes. This is also strengthened by the fact that a number of potential GLI2 consensus-binding sites are present in SOX2-promoter (Snijders et al., 2008). However, this remains to be elucidated by more specifically designed assays to prove protein (GLI2) - chromatin (SOX2 promoter) interaction. Importantly, in mice, it was very recently found that Gli2 can regulate the expression of SOX2 in developing neuroepithelial cells via direct binding to the SOX2 enhancer region (Takanaga et al., 2009). Loss of Gli2 (Gli2ΔC or Gli2 shRNA) suppresses the expression of SOX2, and induces premature neuronal differentiation of developing neuroepithelial cells (Takanaga et al., 2009), further supporting the role of GLI2 in opposing differentiation and possibly in the maintenance of stem cells.

SOX2 is a transcription factor which is involved in organ development and in determining stem cell fate and properties. SOX2 plays a key role in maintaining embryonic stem cell pluripontency both in mice (Masui et al., 2007; Niwa, 2007) and human (Fong et al., 2008), in regulating neural and retinal cell progenitors (Graham et al., 2003; Taranova et al., 2006) and in development of the sensory organs of the inner

ear (Kiernan et al., 2005). In addition, SOX2 in the epithelial context, is required for the differentiation of endodermal progenitor cells of the mouse tongue into taste bud cells (highly expressed) versus keratinocytes, while it is also expressed in the basal epithelial cells of the tongue (Okubo et al., 2006). Its overexpression in basal epithelial cells of the tongue in transgenic mice, causes complete suppression of the differentiation of the filiform keratinocytes (Okubo et al., 2006). Consistently, expression of SOX2 gene, has also been reported in poorly differentiated tumours such as breast, as well as in gliomas which are also associated with activated hedgehog signalling and GLI1/2 overexpression (Kinzler et al., 1987; Dahmane et al., 2001; Kubo et al., 2004; Sterling et al., 2006; Clement et al., 2007; Ben-Porath et al., 2008; Chen et al., 2008; Kameda et al., 2009).

These results point to the fact that the expression profile of SINEG2 keratinocytes may be directly linked to the phenotypic characteristics observed in culture. Excepting that the expression patterns of SINEG2 cell line come in agreement with previous observations in other cell lines, these results show a novel phenotypic outcome induced by GLI2ΔN, which could be, at least partly, attributed to the basal stem-cell like expression signature displayed in SINEG2 keratinocytes and can suggest that GLI2 might block keratinocyte differentiation by upregulating stem cell genes.

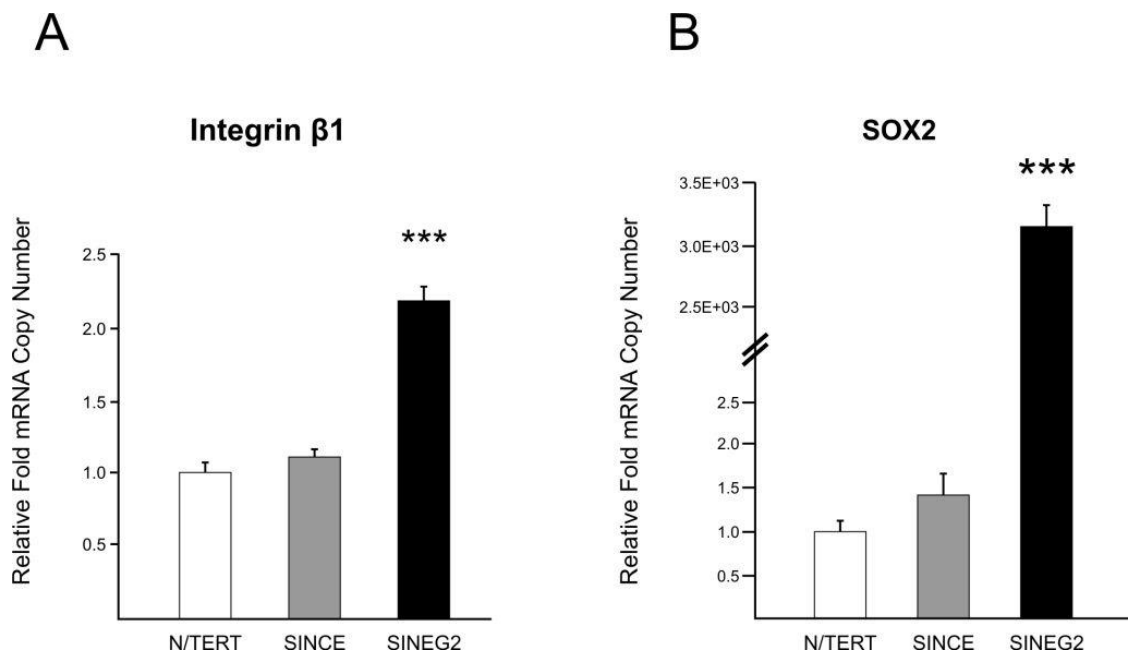

Figure 3.13: GLI2ΔN induces the expression of basal undifferentiated keratinocyte and stem cell associated genes.

RNA was harvested from N/TERT, SINCE, and SINEG2 cells to examine the levels of Integrin β1 **(A)** and SOX2 **(B)** mRNA expression using primers specific for each gene. Quantitative RT-PCR analysis of Integrin β1 and SOX2 showed an increase in expression of both genes in SINEG2 cells compared to N/TERT and SINCE control cells. Each bar represents mean fold induction relative to N/TERT (arbitrary value of 1) ± s.e.m of triplicate samples. *** *P≤0.001*.

3.2.3.2 Cell growth

Normally, cells in culture undergo three phases that describe their rate of cell growth. Cells, when first introduced into culture, do not begin to divide immediately but there is a delay in time that is called the lag and is referred to as the 'lag phase' growth (sparse cells). During this time, there is very little change in the number of cells, but a lot of synthetic activity occurs that both supports the cells and prepares them for future cell division (Martin, 1994).

Following the lag phase, most of the cell population divides continuously for a limited period of time and two new cells are created every time a cell divides. The increase in cell number during this phase is logarithmic and so called 'log phase' growth (subconfluent cells) (Martin, 1994).

This does not continue indefinitely and the rate of growth of the population slows down. This final phase of growth is known as the 'plateau' or 'stationary phase' (confluent cells), in which only some cells in culture are proceeding through the cell cycle and dividing. When the cells are contact inhibited, the growth in the plateau phase is zero and the graph will appear flat for this phase (Martin, 1994). Therefore, normal cells grown *in vitro* undergo cell cycle arrest as soon as they reach confluence, a process frequently suppressed in tumourigenic cells.

Due to the diverse morphological characteristics of SINEG2 keratinocytes, the effect of GLI2ΔN expression in the growth rate of N/TERT keratinocytes was examined.

First, the proliferation rates of N/TERT, SINCE, and SINEG2 keratinocytes were assessed during the period of 7 days by the use of Alamar Blue™ proliferation assay **(Chapter 2, Section 2.7.1 and Section 2.7.1.2) (Figure 3.14A)**. The rate of Alamar Blue™ reduction is quantified by fluorescence emission, and directly reflects the amount of viable cells in culture. The results indicated a clear reduction in the proliferation rate of SINEG2 keratinocytes compared to both N/TERT and SINCE controls. N/TERT and SINCE control cells have reached confluence by day 4, and hence the growth curve representing their growth rate has thereafter reached a plateau. On the other hand, SINEG2 cells were still at the log phase of cell growth, suggesting a significant reduction in cell numbers.

At the same time, the proliferation rates of all three cell lines were also assessed by the rate of MTT reduction **(Chapter 2, Section 2.7.2)** that reflects a measure of viable cells **(Figure 3.14B)**, to further validate the above findings. Again, GLI2ΔN expressing keratinocytes showed a pronounced delay in cell growth and could not reach the proliferation rate of neither N/TERT nor SINCE keratinocytes by the end of the time-course. By day 7, N/TERT and SINCE cells start reaching the resting phase, while SINEG2 cells are still in the log phase.

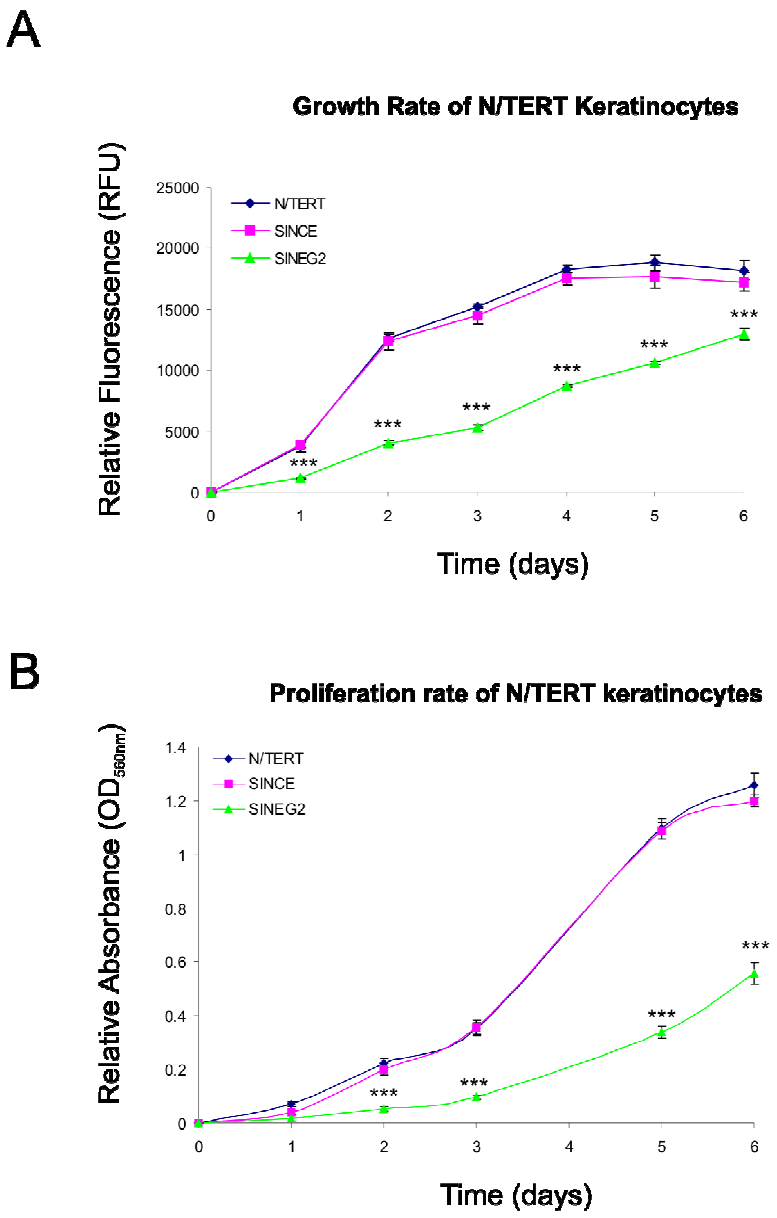

Figure 3.14: Growth characteristics of GLI2ΔN expressing N/TERT keratinocytes.

(A) N/TERT, SINCE, and SINEG2 keratinocytes were grown for a period of seven days and their growth rates were measured by the fluorescence intensity produced by Alamar Blue™ reduction. SINEG2 display a significantly reduced growth rate compared to both N/TERT and SINCE control keratinocytes. **(B)** The proliferation rate of keratinocytes was also assayed by the rate of MTT reduction during the period of seven days in culture. Again, GLI2ΔN expressing N/TERT keratinocytes display a significantly slower growth rate compared to both N/TERT and SINCE control keratinocytes. Each data point in the graphs represents a mean ± s.e.m of six replicate samples, relative to the baseline values obtained at Day 0. All the values for all the different time points were subtracted from the mean value of Day 0. *** *P≤0.001*.

However, it is important to note that both these assays give an indication of the amount of viable cells, solely depending upon of a cell's intrinsic metabolic activity and therefore, its ability to reduce chemical reagents. Consequently, if the metabolic activity of a given population is altered, the calculation of cell growth could potentially be inaccurately measured.

Therefore, the growth potential of N/TERT, SINCE, and SINEG2 keratinocytes was also investigated during long term culture by assessing the number of population doublings for each given cell line **(Chapter 2, Section 2.7.3) (Figure 3.15)**. Population Doublings (PD) represent the number of times the cell population doubles in number, during the course of culture. Cells were passaged every four days for the total period of 16 days and the number of cumulative population doublings for each cell line was calculated as described in Materials and Methods **(Chapter 2, Section 2.7.3 and Section 2.1.9.2)**.

It was observed that GLI2ΔN expressing keratinocytes had undergone significantly less population doublings (10 PD), compared to N/TERT and SINCE (14 PD both), further confirming their reduced proliferation rate. The marked reduction in population doublings shown here, suggests fewer mitotic divisions for GLI2ΔN expressing keratinocytes, possibly as a result of either a slow cell cycle, or inappropriate execution of mitosis.

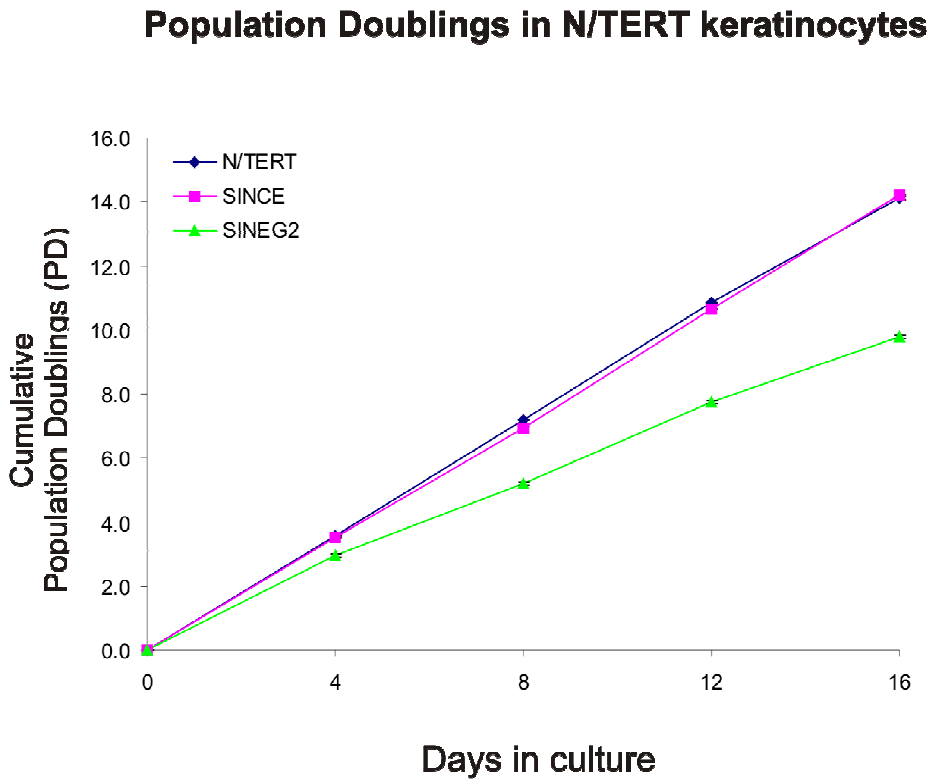

Figure 3.15: The effect of GLI2ΔN in long term culture.

N/TERT, SINCE, and SINEG2 cells were serially passaged every 4 days for a total of 16 consecutive days. Equal numbers of keratinocytes were seeded and the total output of cells was measured at the end of each time point to obtain population doublings values. GLI2ΔN expressing N/TERT keratinocytes have undergone significantly less population doublings after 16 days in culture compared to the N/TERT and SINCE cells, reflecting their reduced growth rate. Each data point in the graph represents the PD which was calculated by using the mean ± s.e.m of three replicate measurements, as described in Materials and Methods **(Chapter 2, Section 2.7.3 and Section 2.1.9.2)**.

3.3 Discussion

3.3.1 Generation, expression and characterisation of GLI2ΔN in N/TERT human keratinocytes

Differential expression of the SHH effector, GLI2, is an important step in the formation of human Basal Cell Carcinoma, since upregulation of GLI2 is frequently observed in human BCCs (Mullor et al., 2001; Regl et al., 2002; Tojo et al., 2003; Ikram et al., 2004; Regl et al., 2004b; O'Driscoll et al., 2006; Asplund et al., 2008; Yu et al., 2008). In addition, targeted overexpression of Gli2 in epidermal cells of transgenic mice can induce the formation of BCC or BCC-like tumours (Grachtchouk et al., 2000; Sheng et al., 2002; Hutchin et al., 2005; Huntzicker et al., 2006). The *in vitro* equivalent of such a model would require the forced induction of an active form of GLI2 oncogene in the context of epidermal keratinocytes. Herein, overexpression of the constitutively active form of human GLI2-β isoform (GLI2ΔN) (most prevalent isoform in human BCCs) (Tanimura et al., 1998; Tojo et al., 2003) was achieved in immortalised human epidermal keratinocytes N/TERT-1 (N/TERT) (Dickson et al., 2000), using both a stable and an inducible system. N/TERT keratinocytes are derived from normal human foreskin keratinocytes, and were subsequently immortalised by ectopic expression of h/TERT and have spontaneous downregulation/loss of $p16^{INK4a}$ (Dickson et al., 2000; Rheinwald et al., 2002). The employment of this cell line is advantageous in the aspect that it has a functional $p53/p21^{WAF1/CIP1}$ pathway contrarily to the highly aneuploid HaCaT keratinocytes (Boukamp et al., 1988; Lehman et al., 1993), and retains normal differentiation mechanisms (Dickson et al., 2000).

Stable transduction of N/TERT keratinocytes with pSINEGFP-GLI2ΔN resulted in the generation of a cell line that showed strong transgene mRNA expression and production of high protein levels of EGFP-GLI2ΔN **(Figure 3.1)**. The use of high efficiency mediated gene transfer method described here, allows strong and long term induction of transgene expression without the undesirable effects of antibiotic selection (Deng et al., 1997). However, maximum purity of EGFP-GLI2ΔN transduced keratinocytes was achieved by FACS.

It has been previously shown by in situ-hybridization, that GLI2 mRNA is mainly expressed in the interfollicular epidermis and the outer root sheath of hair follicles in normal skin, and in BCC tumour islands (Ikram et al., 2004). During the characterisation of stably transduced keratinocytes, it was observed that N/TERT and SINCE (EGFP alone transduced) keratinocytes showed low but detectable mRNA levels of endogenous GLI2 (Ct value GLI2 > 31, Ct value GLI2 a/β > 25), as well as very low endogenous GLI2 protein levels **(Figure 3.3)**. This is in line with endogenous mRNA copy number of GLI2 that also detected in trace amounts (Ct value > 32) in human primary skin keratinocytes (Regl et al., 2002), as well as in normal human skin (O'Driscoll et al., 2006). The detection of low endogenous GLI2 protein levels is consistent with the fact that in normal cells, GLI2 protein undergoes rapid proteasome mediated degradation as a barrier to tumourigenesis (Bhatia et al., 2006; Huntzicker et al., 2006; Pan et al., 2006).

In addition to the high levels of ectopic GLI2ΔN protein, SINEG2 keratinocytes also displayed elevated levels of endogenous GLI2 protein **(Figure 3.4)**. This may suggest the presence of a positive feedback loop whereby exogenous GLI2ΔN stimulates the expression of endogenous GLI2. In support of this, the induction of GLI2ΔN in HaCaT keratinocytes, results in a rapid elevation of GLI1 mRNA, followed by stimulation of endogenous GLI2 mRNA expression (Regl et al., 2002). This suggests that GLI2ΔN may be indirectly involved in an autoregulatory mechanism, possibly through its direct downstream target GLI1 (Ikram et al., 2004). At the same time, it is possible that the presence of excessive EGFP-GLI2ΔN protein in SINEG2 cells may cause a significant delay to the rapid proteasome mediated degradation of the endogenous GLI2 protein levels.

Induction of GLI2ΔN can result in the activation and/or suppression of a plethora of genes in HaCaT keratinocytes, as previously reported (Regl et al., 2004a; Eichberger et al., 2006). In accordance with previous observations, SINEG2 keratinocytes displayed a dramatic upregulation in the transcription levels of anti-apoptotic factor BCL-2 **(Figure 3.5A)**, a direct downstream target of GLI2 both in human primary and HaCaT keratinocytes (Regl et al., 2004b). Consistently, BCL-2 and GLI2 are often co-expressed in BCC tumours (Regl et al., 2004b). Furthermore, both the mRNA and protein levels of c-MYC **(Figure 3.5B, C)** have been reported to be suppressed in

human BCCs (Bonifas et al., 2001; Regl et al., 2002; Asplund et al., 2008; Kriegl et al., 2009), as well as in response to transient induction of GLI2ΔN in HaCaT keratinocytes (Regl et al., 2004a; Eichberger et al., 2006). SINEG2 keratinocytes also displayed a significant reduction in c-MYC protein and mRNA levels compared to wild-type and EGFP transduced N/TERT keratinocytes. Thus, both BCL-2 and c-MYC, BCC molecular markers, that have been previously shown to be activated and suppressed respectively, upon GLI2ΔN activation in other *in vitro* systems, were appropriately regulated in my system. These results indicate the relevance of this *in vitro* model system to HH/GLI induced gene expression patterns in BCC.

The development of an inducible RevTet-OFF system provides significant benefit to the investigation of GLI2ΔN mediated effects, by allowing the induction of the transgene only at desired time points, upon removal of doxycycline **(Figure 3.6)**. This is especially useful since the induction and subsequent repression of transgene expression can significantly increase the specificity of any downstream observations. However, there are several disadvantages associated with the generation of the N/TERT inducible system (NTEG2) described here.

First, it is worth mentioning that the presence of high, but non-toxic **(Figure 3.9)**, levels of doxycycline did not result in complete suppression of the transgene **(Figure 3.8)**. This led to the undesirable effect of background GLI2ΔN activation in uninduced control cells **(Figure 3.8 and Figure 3.10)**. Given the very low endogenous levels of GLI2 present in normal N/TERT keratinocytes, as mentioned above, even a small background activation of the transgene may lead to the underestimation of any downstream effects produced in induced GLI2ΔN NTEG2 keratinocytes. Furthermore, the protein levels of GLI2ΔN after removal of doxycycline were considerably lower compared to SINEG2 stably transduced keratinocytes. This could be attributed to the fact that the CMV promoter driving the expression of GLI2ΔN in NTEG2 cells, is under the control of a tetracycline response element, as opposed to the constitutively active CMV promoter present in the pSINEGFP-GLI2ΔN construct, that was used to generate the SINEG2 cell line. Last, in an effort to avoid any clone specific effects, the NTEG2 cells were generated as a polyclonal population of transduced keratinocytes. This could have led to the apparent heterogeneity in terms of EGFP-GLI2ΔN expression. Despite the drawbacks associated with the generation of this cell line, the data obtained by the

use of either the inducible or the stably transduced N/TERT cell lines, were comparable and highly reproducible.

3.3.2 Localisation of GLI2ΔN in N/TERT keratinocytes

The intracellular localisation of GLI2ΔN in N/TERT keratinocytes was primarily nuclear both in stable and inducible cell line **(Figure 3.1 and Figure 3.10)**. However, a smaller proportion of cells displayed cytoplasmic localisation of the protein. These observations are consistent with previous reports showing that there is nuclear/cytoplasmic shuttling of GLI2 depending on hFu and hSuFu proteins respectively, which is required for protein degradation (Murone et al., 2000; Barnfield et al., 2005; Varjosalo et al., 2006). This also provides evidence that exogenous GLI2ΔN protein is regulated in a similar fashion to the endogenous wild-type GLI2 protein. This is in line with the fact that the active form of GLI2 (GLI2ΔN) can only partly mimic the activated SHH/GLI pathway, since GLI2 subcellular localisation and stability is dependent upon SHH signalling stimulation (Pan et al., 2006).

3.3.3 GLI2ΔN opposes contact inhibition

Sustained induction of GLI2ΔN in stably transduced N/TERT keratinocytes (SINEG2) produced a strong phenotype that was mainly related to the colony formation of keratinocytes **(Figure 3.11 and Figure 3.12)**. SINEG2 cells tend to grow by forming tight colonies of cohesive keratinocytes, as opposed to the more spread monolayer cultures observed in normal N/TERT and SINCE controls. Interestingly, basal cell carcinomas are characterised by their tight and compact morphology. Recently, it was also shown that forced expression of GLI1, a downstream target of GLI2, can also induce tight colony formation in N/TERT keratinocytes (Neill et al., 2008). Normal cells grown *in vitro* undergo cell cycle arrest as soon as they reach confluence, a process frequently suppressed in tumourigenic cells. Therefore, despite their highly compact appearance, SINEG2 colonies tend to grow to a considerable size, possibly indicating that these cells are irresponsive to contact inhibition mechanisms. In support of that, inducible expression of GLI2ΔN in contact inhibited (confluent) cultures of HaCaT keratinocytes is sufficient to stimulate DNA synthesis (G1-S progression), re-entry to

the cell cycle and to regulate the mRNA levels of specific cell cycle genes (Regl et al., 2004a). In addition, the expression of G1-S and G2-M phase progression genes was examined in contact-inhibited primary human keratinocytes showing similar results as in HaCaT cells (Regl et al., 2004a).

Further evidence comes from the fact that SHH stimulation can oppose growth arrest of primary epidermal keratinocytes in response to extracellular calcium as well as to ectopic expression of CDKI $p21^{WAF1/CIP1}$ (Fan & Khavari, 1999). Keratinocytes undergo terminal differentiation during epithelial cell renewal **(see Chapter 1, Section 1.1.1)**, which is preceded by cell growth arrest (Potten & Morris, 1988; Fuchs, 1990; Fuchs, 1993; Steven & Steinert, 1994; Fuchs, 2008). This process can be efficiently reproduced *in vitro,* in response to elevated concentrations of extracellular calcium (Hawley-Nelson et al., 1980; Hennings et al., 1980; Boyce & Ham, 1983; Pillai et al., 1990; Li et al., 1995; Bikle et al., 2004; Xie et al., 2005). The relevance of calcium-induced differentiation *in vitro* to the *in vivo* situation is evidenced by the steep gradient of calcium within the epidermis, with the highest levels in the uppermost suprabasal (most differentiated-nucleated) layers (Menon et al., 1985; Bikle et al., 2004). Application of high extracellular calcium concentration both in mice and human primary epidermal keratinocytes in culture, inhibits the rate of DNA synthesis and induces the production of differentiation markers, such as K1, K10, involucrin and loricrin (Fuchs, 1990; Fuchs, 1993; Steven & Steinert, 1994; Candi et al., 2005; Fuchs, 2008). Thus, Fan and Khavari (Fan & Khavari, 1999) showed that the presence of activated SHH signalling in confluent primary human epidermal keratinocytes opposes the cell cycle inhibitory effects (G0/G1 arrest) of this *in vitro* stimulus of epithelial differentiation. Another important cell cycle regulator, which is known to be responsible for mediating cell growth arrest prior to terminal keratinocyte differentiation and of other cell types, and thus irreversible commitment to differentiation, is CDKI $p21^{WAF1/CIP1}$ (Jiang et al., 1994; Steinman et al., 1994; Missero et al., 1995; Missero et al., 1996; Tron et al., 1996; Di Cunto et al., 1998; Todd & Reynolds, 1998; Topley et al., 1999; Dotto, 2000). The same study showed that SHH overexpressing primary human keratinocytes can also antagonize the growth inhibitory effects (G1 arrest) induced by ectopic expression of $p21^{WAF1/CIP1}$ (Fan & Khavari, 1999).

3.3.4 Morphological heterogeneity in N/TERT GLI2ΔN-expressing colonies

The strong phenotype induced by GLI2ΔN in N/TERT keratinocytes, is mainly characterised by the presence of large compact, cohesive colony islands, comprised of small dense cells with a high ratio of nuclear to cytoplasmic volume **(Figure 3.11 and Figure 3.12)**. However, there is a considerable degree of heterogeneity in SINEG2 cultures. In addition to tightly packed keratinocyte colonies, SINEG2 cultures also contain more loosely attached cells that can be either found scattered throughout the culture, arranged in small loose colonies, or at the peripheries of bigger compact colonies. Although normal N/TERT and SINCE keratinocyte cultures may contain such keratinocyte populations, their presence becomes more pronounced in a background of tightly packed colonies, observed in SINEG2 culture.

Primary human epidermal keratinocytes also display significant heterogeneity in culture, and their morphology is closely linked to their proliferative and self-renewal capacity (Barrandon & Green, 1987). Specifically, epidermal keratinocytes can form regular, round, large, compact colonies with smooth perimeters consisting of small, tightly-packed cells (holoclones), smaller highly irregular colonies with loosely packed large-flattened cells (paraclones), as well as colonies with intermediated features of both holoclones and paraclones, with smaller size than holoclones and irregular perimeter (meroclones). Each has different capacities for multiplication, and they can be distinguished by the marked difference in the frequency with which they give rise to terminal progeny. Holoclones have the ability of self-renewing and the greatest growth potential since under standard conditions fewer than 5% of the colonies formed by the cells of a holoclone abort and terminally differentiate. In contrast, paraclones may grow rapidly at first but they have a short replicative lifespan in total, since after 15 cell generations cells uniformly become growth arrested and terminally differentiated. The meroclone contains a mixture of cells of different proliferative potential, dividing only for limited generations and is considered as a transitional stage between the holoclones and the paraclones, as it gives rise to paraclones with appreciable frequency and are consumed by this conversion. The transitions from holoclone to meroclone to paraclone are unidirectional, and the result is progressively restricted growth potential (Barrandon & Green, 1987).

It is therefore thought that the cells of a holoclone are the *in vitro* analogue of keratinocyte stem cells (Barrandon & Green, 1987), according to the definition of Lajtha (Lajtha, 1979) that stem cells are cell types capable of extensive self renewal throughout adult life and also have the ability to produce daughters that undergo terminal differentiation, while the cells of the meroclone and paraclone are early and late transit-amplifying cells (differentiated) respectively. It has also been shown that keratinocyte cultures containing holoclones, when they are grafted to humans they can regenerate epidermis that persists for years (Gallico et al., 1984) indicating the self renewing capacity of holoclones, as well as that stem cells are not lost in culture.

Thus, it is apparent that at least some of the morphological characteristics of holoclones (regular, large compact with smooth perimeter colonies consisting of small dense cells), described in normal epidermal keratinocytes, can be observed in a large proportion of SINEG2 keratinocyte colonies and thus SINEG2 cells resemble in some aspects the phenotypical stem cell characteristics.

A similar hierarchy has been suggested for cells derived from a number of different epithelial tumours. It has been reported that cell lines derived from head and neck squamous cell carcinoma epithelial tumours show patterns resembling those of primary normal keratinocytes, in that they can form heterogeneous colonies *in vitro* (holoclone/ meroclone/paraclone series of colony morphologies), with malignant holoclones being round colonies consisting of tightly packed cells, smaller than the cells of malignant meroclones or paraclones, highly proliferative and solely responsible for regenerating each cell line (Locke et al., 2005; Harper et al., 2007). Similar phenomenon was observed in a breast and prostate carcinoma cell lines (Locke et al., 2005; Li et al., 2008). Moreover, in prostate carcinoma cell lines, holoclones can not only regenerate all distinguishable colony types, but can also initiate serially transplantable tumours in nude mice (Li et al., 2008).

Importantly, malignant holoclone derived cells, retain the expression of normal keratinocyte associated stem cell genes, including β1 integrin, E-cadherin and β-catenin compared to malignant meroclone and paraclone derived cells (Locke et al., 2005; Harper et al., 2007; Li et al., 2008).

In addition to epithelial tumours, another example of tumour heterogeneity *in vitro* is that of a non epithelial tumour such as glioma, the generation of which, is closely linked to GLI gene amplification (Kinzler et al., 1987). Human glioma derived cells can give rise (a) to tight round-shaped colonies with small and compact cells, (b) to intermediate colony less smooth than the tight colony, composed of inner cells closely packed, and of peripheral cells with flat plasma migrated out and finally (c) to the loose colony, which is the most irregular one and is composed of scattered flat plasma cells (Zhou et al., 2009). Each of them resembles holoclones, meroclones and paraclones of primary epidermal keratinocytes respectively, while similar morphological heterogeneity is also observed in SINEG2 keratinocytes *in vitro*.

In addition to their self renewal capacity and regeneration of all different colony types, glioma derived holoclones are poorly differentiated and display an expression profile reminiscent of that observed in neural stem cells, in contrast to paraclones and meroclones. In particular, they show elevated levels of neural stem cell associated genes including NESTIN and SOX2, which have also been shown to be expressed in response to GLI1 and GLI2ΔN respectively (Kasper et al., 2006b; Snijders et al., 2008; Zhou et al., 2009). Thus, Zhou et al. (Zhou et al., 2009) indicates that colony morphology is reliable in distinguishing colonies enriched for stem cells ('cancer stem cells') from glioma cell lines, as it has been previously stated for other epithelial tumour cell lines (Locke et al., 2005; Harper et al., 2007; Li et al., 2008; Zhou et al., 2009).

Morphological heterogeneity is typical of malignant cell lines and tumours and has usually been attributed to genetic instability and the selection for cells that can adapt to the tumour microenvironment (clonal evolution) (Weiss, 2000). However, studies since 1977, due to the similarity of normal stem cells and a subpopulation of tumourigenic cells within the tumour in terms of self renewal capacity, extensive proliferative potential and the ability to give rise to phenotypically heterogeneous cells that exhibit various degrees of differentiation, suggest an underlying stem cell related pattern (Hamburger & Salmon, 1977). Recent evidence, including the studies mentioned above, strongly support the notion that the cancer stem cell model plays a major role in tumour heterogeneity (Hamburger & Salmon, 1977; Reya et al., 2001) and that tumourigenic cells can be thought of as cancer stem cells that undergo an aberrant and poorly

regulated process of organogenesis analogous to what normal stem cells do (Reya et al., 2001).

The cancer stem cell theory initially predicted that cancer arises from a normal stem cell that has acquired an ability for uncontrolled proliferation and therefore capable of initiating a tumour. The resultant cancer stem cell will continuously replenish the tumour population with more committed progenitors that are responsible for tumour expansion but not tumour maintenance, as well as with more differentiated cells of little growth potential (Lobo et al., 2007). This hypothesis can be supported by a study of Holland et al. (Holland et al., 2000), which demonstrated that glioma tumour development in mice, a brain tumour which is linked to GLI gene overexpression (Kinzler et al., 1987), arises from a nestin-positive progenitor population rather than from differentiated astrocytes, upon activation of Ras and Akt in both subpopulations.

Initial studies by Bonnet and Dick (Bonnet & Dick, 1997), showed that a small proportion of acute myeloid leukaemia (AML) cells that are characterised by a $CD34^+$ $CD38^-$ expression profile similar to normal haematopoietic stem cells, are highly clonogenic *in vitro* and are the only cells capable of transferring the disease from human patients to sublethally irradiated non-obese diabetic (NOD) severe combined immunodeficient (SCID) mice. Thus, the fact that only a minute proportion of tumour cells were able to initiate cancer formation, when transplanted into nude mice, further supported the idea that the disease is initiated and maintained by a small subset of tumour cells, namely cancer stem cells (Bonnet & Dick, 1997; Reya et al., 2001). Moreover, the common expression signature between normal and cancer haematopoietic stem cells (Bonnet & Dick, 1997), has fuelled attempts to provide a functional link between a stem cell expression profile and the tumour initiation potential of putative cancer stem cells. Others studies, have focused on the phenotypic similarities between normal and cancer stem cells, showing that only holoclone derived prostate tumour cells are capable of initiating tumours, when transplanted into NOD/SCID mice (Li et al., 2008).

However, the recent demonstration that adult fibroblasts can be reprogrammed into pluripotent embryonic stem cell-like cells, raises the possibility that combined expression of stem cell associated factors and specific oncogenes could also induce a

non differentiated state in cancer cells (Takahashi et al., 2007; Yu et al., 2007). Therefore, it cannot be definitively determined whether the stem cell signature in several tumours is inherited from stem cell-of-origin, or is reactivated during the course of tumour progression (Ben-Porath et al., 2008). In addition, despite the suggested stem cell origin of tumours, the ability of more committed progenitor cells to initiate tumour formation after genetic manipulation, indicating that cancer cells can undergo progressive de-differentiation during their development, has led further studies to refer to cancer stem cells as being any cell within a tumour that possesses the capacity to self-renew and to give rise to heterogeneous lineages of cancer cells that comprise the tumour (Clarke et al., 2006).

Nevertheless, the mutagenic background already present in malignant cells makes it very difficult to draw any parallels between stem cells in normal tissues and those of malignant tumours. Given that genomic instability, that generates the genetic and epigenetic changes, is a widespread feature in many malignancies, and that homeostatic control mechanisms are frequently perturbed, it is difficult to attribute tumour heterogeneity to a stem cell pattern similar to that observed in normal healthy tissues.

In addition, despite the demonstration that cancer arises from a very small number of tumour cells (~ $1/10^6$), recent studies have thrown a lot of doubt on that model, by making assay modifications regarding the immune systems of recipient mice, in an effort to create an environment similar to what normal human tumour cells would be expected to encounter in an immunocompatible background (Clarke et al., 2006). Notably, as little as 10 pre-B/B lymphoma cells were sufficient to initiate lymphomas when transplanted back to syngenic animals, while enrichment for cells expressing stem cell associated markers did not preferentially increase tumour incidence (Kelly et al., 2007). More recently, by using NOD/SCID *Il2rg*$^{-/-}$ mice that lack natural-killer cell activity, a study demonstrated that 1 in 9 cells could induce the formation of melanomas in mice, contradicting the previously reported estimate of 1 in 46,700 cells (Quintana et al., 2008). More importantly, the same study concluded that melanoma tumours could arise from all cell subtypes irrespectively of stem cell gene expression status (Quintana et al., 2008). Therefore, it is obvious from these studies that modifications in xenotransplantation assays can dramatically increase the detectable frequency of cells with tumourigenic potential.

Although the abundance of tumour initiating cells may be higher that previously thought, in some types of cancer, still the possibility that some human cancers follow a cancer-stem cell model cannot be ruled out, and their tumourigenic properties need to be further investigated, since their characterisation will provide additional insight into the molecular mechanisms of cancer initiation and maintenance. However, cells should be interrogated by optimised and multiple methods, and given that even normal adult stem cells are still poorly characterised due to the lack of specific stem cell markers, expression of potential stem cell or cancer stem cell markers should always be linked to functional assays, such as *in vivo* regeneration of the tissue of origin (Clarke et al., 2006).

3.3.5 GLI2ΔN opposes epithelial differentiation

Differentiation of human epidermis is associated with a series of morphological and biochemical changes as cells (transit-amplifying cells) migrate from the proliferative and mitotic basal cell layer through the non proliferative, post-mitotic but metabolically active spinous, granular and corneum layers where the terminal phase of maturation is completed (Fuchs, 1990). Keratinocytes in each of these layers are expressing different molecular markers such as keratins, involucrin, filaggrin, and loricrin **(see Chapter 1, Section 1.1.1)** (Fuchs, 1990; Fuchs, 1993; Candi et al., 2005; Fuchs, 2008).

Defective terminal differentiation in culture is a consistent characteristic of malignantly transformed keratinocytes (Rheinwald & Beckett, 1980). Human BCCs are thought to be derived from keratinocytes of the basal stem cell layer of the epidermis (interfollicular epidermis) which are negative for markers of differentiation **(see Chapter 1, Section 1.3.6)** (Miller, 1991a; Owens & Watt, 2003; Daya-Grosjean & Couve-Privat, 2005; Crowson, 2006; Fuchs, 2008). Also due to the activation role of SHH in hair follicle morphogenesis and the striking relation between BCCs and deregulation of the SHH pathway in BCC tumourigenesis (Dahmane et al., 1997; Oro et al., 1997; Grachtchouk et al., 2000; Nilsson et al., 2000; Sheng et al., 2002; Daya-Grosjean & Couve-Privat, 2005; Hutchin et al., 2005; Huntzicker et al., 2006), BCCs are also thought to be derived from undifferentiated cells of hair follicles (Kruger et al., 1999; Owens & Watt, 2003; Hutchin et al., 2005; Blanpain & Fuchs, 2006; Crowson,

2006; Huntzicker et al., 2006; Mancuso et al., 2006). However, a very recent study by Youssef et al. (Youssef et al., 2010), using conditional overexpression of a constitutive active form of mouse smoothened gene in transgenic mice under the control of specific promoters, favours the notion that BCCs arise from the undifferentiated cells of the basal layer of the epidermis (interfollicular epidermis).

Consistently with the resistance to differentiation of BCC cells (Murphy et al., 1984; Said et al., 1984; Sumitomo et al., 1986; Miller, 1991a), it has been previously shown in confluent GLI2 expressing HaCaT keratinocytes, using cDNA-array technology, that GLI2 represses genes that are expressed in differentiating or terminally differentiated keratinocytes or are involved in promoting keratinocyte differentiation (Regl et al., 2004a). GLI2 expressing keratinocytes are also shown to maintain basal expression patterns in response to high-calcium induced differentiation, and to repress the expression of epidermal differentiation genes (cytokeratin 1, cytokeratin 10, involucrin, SPRR2A, loricrin) in primary human epidermal and in confluent HaCaT keratinocytes (Regl et al., 2004a). Snijders et al. (Snijders et al., 2008) also showed that GLI2 expressing HaCaT keratinocytes oppose differentiation in organotypic cultures, due to the fact that very few and sparse individual cells in the GLI2-expressing reconstructs stained positively for cytokeratin 10/13 and involucrin but not at all for loricrin (differentiation markers), compared to the uniform staining observed in the upper, more differentiated layers of the epidermis formed by control cells.

By contrast, GLI2 expression both in confluent and high-calcium confluent contact inhibited HaCaT keratinocytes led to increased mRNA levels of integrin beta1 (ITGB1) gene (Regl et al., 2004a), which is a marker of undifferentiated keratinocytes in the basal layer of the epidermis (Adams & Watt, 1991; Jones et al., 1995).

In line with these previous studies, SINEG2 cells maintained basal-like phenotype in culture **(Figure 3.11 and Figure 3.12)**, and the mRNA levels of involucrin were downregulated **(Appendix II)**, whereas the mRNA levels of integrin β1 were upregulated, compared to the control cells **(Figure 3.13A)**, suggesting that induction of β1 integrin by GLI2ΔN in normal culture conditions (sub-confluent) contributes to the suppression of keratinocyte differentiation.

Integrins primarily serve as link between the extracellular matrix and the cytoskeleton, by mediating the attachment of cells to the extracellular matrix (Hynes, 1992), but are also believed to play a role in cell-cell adhesion, migration, programmed cell death, tissue organization and differentiation (Adams & Watt, 1989; Adams & Watt, 1990; Carter et al., 1990; Larjava et al., 1990; Tenchini et al., 1993; Brakebusch et al., 1997). Integrins are heterodimeric transmembrane receptors consisting of one **α** and a **β** subunit and the combination of the **α** and **β** subunit determines the ligand specificity of the integrin receptor (van der Flier & Sonnenberg, 2001).

In skin, several integrin receptors are expressed by the epidermal keratinocytes including $\alpha_2\beta_1$ (collagen receptor), $\alpha_3\beta_1$ (laminin 5 receptor), $\alpha_6\beta_4$ (laminin receptor), $\alpha_5\beta_1$ (fibronectin receptor) (Watt, 2002). Basal keratinocytes attach to the underlying basement membrane that contains a range of extracellular matrix proteins including laminin, fibronectin and type IV collagen, via integrins and in normal undamaged epidermis integrin expression is confined mainly to the basal layer of proliferating keratinocytes and outer root sheath of hair follicles including the bulge, but are largely absent from the suprabasal layers of terminally differentiating cells (Adams & Watt, 1991; Jones et al., 1995; Lyle et al., 1998; Huelsken et al., 2001; Watt, 2002). However, during wound healing or in certain pathological conditions such as psoriasis, there is expression of integrins in the suprabasal, differentiating cell layers and is generally associated with hyperproliferation and/or abnormal terminal differentiation (Hertle et al., 1992; Watt & Hertle, 1994). Immunofluorescence studies have shown that β1 integrins are not only found as clusters interspersed with hemidesmosomes on the basal surface of the basal cells (focal adhesions) in the epidermis, but also around the entire periphery of these cells (De Strooper et al., 1989; Peltonen et al., 1989; Jensen et al., 1999; van der Flier & Sonnenberg, 2001).

Studies in human BCCs have shown that there is selective expression of β1 integrins in a manner resembling that of human epidermis (Peltonen et al., 1989; Miller, 1991a; Pentel et al., 1995). Localisation of β1 integrins was demonstrated to the peripheral layer containing the basal cells with the most intense staining on the surface of the cells that interfaced with the basement membrane (Peltonen et al., 1989). However, in areas of fragmentation and discontinuity, a suprabasal intercellular staining pattern of integrin receptors was observed instead of an epithelial-mesenchymal interface expression

pattern, suggesting that these areas may represent sites of invasion of this locally destructive tumour (Peltonen et al., 1989).

In culture, keratinocytes synthesize and deposit the major basement membrane components (i.e. fibronectin, laminin, collagen IV), even though the proteins are not organized into a recognizable basement membrane (Alitalo et al., 1982; Brown & Parkinson, 1983; Kubo et al., 1984; O'Keefe et al., 1984; Oguchi et al., 1985; Bohnert et al., 1986), supporting the idea that epidermal keratinocytes are responsible for the synthesis of at least some of the components of the basement membrane in human skin (Brown & Parkinson, 1983).

In human epidermis, irreversible withdrawal from the cell cycle in the basal layer (Potten & Morris, 1988), along with loss of integrins expression from the cell surface (De Strooper et al., 1989; Peltonen et al., 1989) and loss of adhesiveness to a range of extracellular matrix proteins, initiate terminal differentiation (Adams & Watt, 1990).

In addition, when normal human keratinocytes are placed in suspension as single cells they withdraw from the cell cycle, and undergo terminal differentiation (Green, 1977) in a two stage process. In the first stage, there is loss of integrin-ligand binding ability that occurs on commitment to terminal differentiation (Adams & Watt, 1990; Hotchin & Watt, 1992; Hotchin et al., 1993). This ensures that early terminal differentiation is linked to detachment of keratinocytes from the underlying basement membrane and migration to the suprabasal layers (Adams & Watt, 1990). In the second stage, on overt terminal differentiation, integrins are lost from the cell surface (Adams & Watt, 1990; Hotchin et al., 1995) and there is a decrease in the transcription levels of the integrin genes (Nicholson & Watt, 1991; Hotchin & Watt, 1992). This can be partially inhibited by extracellular matrix proteins such as fibronectin (Adams & Watt, 1989) or by adhesion-blocking antibodies to β1 integrins (Adams & Watt, 1990; Watt et al., 1993). It thus appears that ligation of β1 integrins is a negative regulator of terminal differentiation. However, it seems that the inhibition of terminal differentiation by β1 integrins is not simply a consequence of β1 mediated adhesion, but it appears that the mechanism by which β1 integrins regulate the onset of terminal differentiation is distinct from the mechanism by which they mediate keratinocyte adhesion. Integrin-mediated keratinocyte adhesion and spreading to the extracellular matrix involves

clustering of integrins in focal contacts and polymerization of the actin cytoskeleton (Hynes, 1992). In contrast, the inhibition of suspension-induced terminal differentiation does not involve or require neither receptor clustering nor polymerization of the actin cytoskeleton (Watt et al., 1993; Levy et al., 2000). Even though there are potential limitations of suspension induced terminal differentiation, the loss of the cell surface integrins and the decrease in β1 integrins mRNA levels that occur in suspension do parallel the *in vivo* situation (De Strooper et al., 1989; Peltonen et al., 1989; Adams & Watt, 1990; Adams & Watt, 1991; Nicholson & Watt, 1991; Hotchin & Watt, 1992).

The implication of β1 integrins in the regulation of differentiation and proliferation of keratinocytes, is shown also by studies in mice in which ectopic expression of α2, α5 and β1 integrin in the suprabasal layers of transgenic mice resulted in hyperproliferation, perturbed keratinocyte differentiation and a psoriasis-like phenotype (Carroll et al., 1995). In addition, conditional ablation of β1 integrin gene in mouse epidermis caused severe hair loss due to reduced proliferation of hair matrix keratinocytes, lack of hair follicles and sebaceous glands decreased proliferation of the interfollicular epidermis and blistering (Brakebusch et al., 2000; Raghavan et al., 2000). However, mice lacking the $\alpha_3\beta_1$ integrin show no evidence of reduced epidermal proliferation or abnormal differentiation suggesting that removal of all β1 integrins is required for a decrease in proliferation and an increase in the proportion of differentiating cells (DiPersio et al., 2000). *In vitro*, β1-null keratinocytes were characterised by poor adhesion to extracellular matrix proteins and a 5-fold increase in the proportion of terminally differentiated cells compared to β1-positive keratinocytes (Grose et al., 2002). On the other hand, *in vivo* β1-null keratinocytes do not all undergo spontaneous terminal differentiation like cultured keratinocytes that are held in suspension, probably due to the maintenance of the intercellular contacts, and to the presence of an abnormal, but existing basement membrane (Grose et al., 2002).

Therefore, the basal-like phenotype of GLI2-expressing cells *in vitro* and in organotypic cultures, along with the increase and decrease of the transcription levels of the integrin β1 and involucrin genes respectively, and the GLI2 predominant expression in region of normal skin and BCC where undifferentiated and proliferating cells are located (Ikram et al., 2004), suggests that GLI2 opposes differentiation.

3.3.6 GLI2ΔN induces stem cell expression pattern in N/TERT keratinocytes

Stem cells (SC) are the subpopulation of keratinocytes that are responsible for renewing the epidermis throughout adult life giving rise to the differentiating cells of the interfollicular epidermis (IFE), hair follicles (HF) and sebaceous glands (SG) (Watt, 2001; Watt, 2002; Blanpain et al., 2007). Thus, it appears to be at least three distinct niches of skin epidermal stem cells, the follicle bulge, the base of the sebaceous glands and the basal layer of the epidermis and it also seems that these three progenitor populations share a few common expression markers such as K5, K14, p63, E-cadherin, $\alpha_3\beta_1$ and $\alpha_6\beta_4$ integrins as well as reduced levels of desmosomes and increased levels of adherens junctions **(see Chapter 1, Section 1.1.5)** (Fuchs, 2008).

In skin, SHH/GLI pathway is implicated in the maintenance and regulation of the epidermal stem cell population residing in the epidermal basal layer (interfollicular epidermis) and the hair follicle bulge (Callahan & Oro, 2001; Adolphe et al., 2004; Blanpain & Fuchs, 2006; Zhou et al., 2006), whereas continuous activation of this pathway is associated with the initiation and growth of many types of human cancer (Beachy et al., 2004). Thus, constitutive activation of the SHH/GLI pathway in skin, could disrupt the epidermal homeostasis and lead to tumourigenesis with a phenotype that resembles stem cell characteristics (stem-like tumour phenotype), such as BCCs, which have been suggested to arise from epidermal basal layer or hair follicle stem cells (Miller, 1991a; Kruger et al., 1999; Owens & Watt, 2003; Daya-Grosjean & Couve-Privat, 2005; Hutchin et al., 2005; Blanpain & Fuchs, 2006; Crowson, 2006; Huntzicker et al., 2006; Mancuso et al., 2006), with a very recent study in transgenic mice favouring more the stem cells of the basal layer as the cell of origin of BCCs **(see Chapter 1, Section 1.3.6)** (Youssef et al., 2010).

This notion is further supported not only by the continuous proliferation, slow growth and resistance to differentiation of human BCC cells (expression of keratins 5 and 14 which are mainly expressed by basal cells (Stoler et al., 1988; Coulombe et al., 1989; Fuchs, 2008)) (Miller, 1991a; Crowson, 2006), but also by the fact that human BCCs manifest a stem cell gene profile similar to that expressed by the cells of the interfollicular epidermis and hair follicle bulge region, such as keratins 15 and 19, and

α2 and β1 integrins (Lane et al., 1991; Miller, 1991a; Jones & Watt, 1993; Jones et al., 1995; Pentel et al., 1995; Kruger et al., 1999; Lyle et al., 1999; Morris et al., 2004; Tumbar et al., 2004; Crowson, 2006). In addition, BCCs display a reduced or even absent EGFR1 (epidermal growth factor receptor 1) expression compared with normal epidermis (Nazmi et al., 1990; Krahn et al., 2001; O'Driscoll et al., 2006; Rittie et al., 2007), of which low expression is another characteristic of epidermal stem cells (Fortunel et al., 2003; Jensen & Watt, 2006). Similarly, human BCCs also exhibit reduced expression of c-MYC proto-oncogene (Bonifas et al., 2001; Regl et al., 2002; O'Driscoll et al., 2006; Asplund et al., 2008), of which low expression is thought to be necessary for epidermal stem cell maintenance (Gandarillas & Watt, 1997; Arnold & Watt, 2001; Watt et al., 2008).

Stem cell gene expression patterns have also been reported in other poorly differentiated tumours such as breast, as well as in gliomas which are also associated with activated hedgehog signalling and GLI1/2 overexpression (Kinzler et al., 1987; Dahmane et al., 2001; Kubo et al., 2004; Sterling et al., 2006; Clement et al., 2007; Ben-Porath et al., 2008; Chen et al., 2008; Kameda et al., 2009).

In vitro studies also suggest that SHH/GLI signalling has a potential role in the maintenance and proliferation of human putative epidermal stem cells of the skin (Fan & Khavari, 1999; Kameda et al., 2001; Zhang & Kalderon, 2001; Zhou et al., 2006). In addition, Shh is also involved in the proliferation and cell-fate specification of several stem cells such as neural and mesenchymal stem cells (Palma & Ruiz i Altaba, 2004; Kondo et al., 2005).

Therefore, both these *in vitro* and *in vivo* studies, suggest that despite the reported effects of GLI2 in suppressing genes associated with differentiation, the more basal phenotype observed in SINEG2 keratinocytes could also be partly explained by an induction of stem cell genes by GLI2 and thus block of differentiation. Interestingly, GLI1 overexpression in N/TERT keratinocytes can induce the expression of a network of stem cell associated genes, including K19, K15, TNC and NESTIN (Kasper et al., 2006b), as well as it reduces the levels of the negative stem cell marker CD71 gene, which encodes the transferrin receptor (Tani et al., 2000; Kasper et al., 2006b) and the levels of the epidermal growth factor receptor (EGFR), consistent with the acquisition

of a stem cell gene expression profile (Fortunel et al., 2003; Jensen & Watt, 2006; Neill et al., 2008). In addition, inducible expression of GLI2 in HaCaT keratinocyte also resulted in the upregulation SOX2 neural stem cell marker (Snijders et al., 2008), and induction of epidermal stem cell marker integrin β1 in HaCaT keratinocytes (Regl et al., 2004a; Eichberger et al., 2006).

In agreement with these studies, SINEG2 keratinocytes displayed a dramatic upregulation in the transcription levels of SOX2 **(Figure 3.13B)**, as well as an increase in the mRNA levels of β1 integrin gene **(Figure 3.13A)**.

3.3.6.1 Integrin β1 stem cell marker

Due to the major role of integrins in regulating differentiation and also due to their increased levels of expression in regions where stem cells are suggested to be located (Jones & Watt, 1993; Jones et al., 1995; Lyle et al., 1998; Jensen et al., 1999), it is plausible to suggest that integrins could provide a valuable marker for epidermal keratinocyte stem cells. Indeed, both in cultures of primary human keratinocytes (Jones & Watt, 1993) and in keratinocytes isolated directly from neonatal foreskin epidermis (Jones et al., 1995), it is possible to enrich for stem cells by selecting the cells that have the highest levels of β1 integrins (Watt, 1998; Watt, 2002). Stem cells (20%) express 2-fold higher levels of β1 integrins than do transit-amplifying cells (20%), which is also accompanied by a 4-fold higher colony forming efficiency of the high β1 integrin cells compared to the low β1 integrin expressing cells (Jones & Watt, 1993; Jones et al., 1995). In addition, cells with characteristics of stem and transit-amplifying cells can be identified and isolated on the basis of their adhesive properties both in human (Jones & Watt, 1993; Jones et al., 1995) and mice (Bickenbach & Chism, 1998). Human basal cells, that express high levels of β1 integrins and adhere rapidly to fibronectin, type IV collagen and the extracellular matrix deposited by cultured keratinocytes (KECM), were enriched for cells capable of forming large, actively growing colonies, a typical characteristic of stem cells *in vitro* (Jones & Watt, 1993; Jones et al., 1995). Human basal cells that express lower levels of β1 integrins and adhere more slowly to the extracellular matrix proteins, tend to form small (fewer than 32 cells), abortive colonies in which the cells underwent terminal differentiation after 1 to 5 rounds of division

within 14 days, as indicated by expression of involucrin protein, and thus displaying characteristics of transit-amplifying cells (Jones & Watt, 1993; Jones et al., 1995). Therefore, both cultured human keratinocytes and keratinocytes isolated directly from skin hold the same relationship between increased β1 integrin expression, enhanced adhesiveness and high proliferative potential *in vitro* (Jones & Watt, 1993; Jones et al., 1995), while keratinocytes directly prepared from skin, selecting for high β1 integrin expression and rapid adhesion to type IV collagen were also able to reconstitute an epidermis when grafted onto nude mice (Jones et al., 1995). Moreover, high levels of β1 integrins are required for the maintenance of human epidermal stem cell compartment *in vitro*. Zhu et al. (Zhu et al., 1999), by retrovirally introducing a dominant negative integrin mutation into human epidermal keratinocytes (downregulation of β1 protein expression and β1-mediated adhesion function), and carrying out clonogenic assays, showed that reduction of β1 integrin levels stimulate keratinocytes to exit from the stem cell compartment, and behave like transit-amplifying cells forming small, abortive colonies and differentiating within a few rounds of division, accompanied by reduced activation of mitogen-activated protein kinase (MAPK) (Zhu et al., 1999).

3.3.6.2 SOX2 stem cell marker

SOX genes are transcription factors, that belong to a superfamily of genes, characterised by a homologous sequence known as the high-mobility-group (HMG) box, and they are conserved throughout the animal kingdom, while playing key roles in a number of developmental processes (Pevny & Lovell-Badge, 1997; Wegner, 1999). SOX genes have been identified on the basis of their homology to the HMG box of the testis-determining gene Sry, also referred to as the Sry box (Sox stands for Sry-related HMG box), which gene resides on the Y chromosome of the mouse and human (Gubbay et al., 1990; Sinclair et al., 1990; Pevny & Lovell-Badge, 1997; Kamachi et al., 2000). The mammalian SOX family comprises 20 genes, almost all of which show at least 50% amino acid similarity with the HMG box in Sry and can be divided into 10 subgroups on the basis of sequence similarity and genomic organization (Bowles et al., 2000; Kamachi et al., 2000).

This HMG box is a DNA binding domain, which mediates DNA-binding of Sox proteins to specific DNA sequences in the promoter or the enhancer of other genes and thus renders them transcription factors which either activate or repress target genes (Wegner, 1999; Kamachi et al., 2000). All SOX factors appear to recognize only a similar and specific DNA binding motif, while the L-shaped HMG domain binds to DNA in the minor groove and the DNA strand exhibits a bend, a widened in the minor groove and is helically unwound (Werner et al., 1995; Werner & Burley, 1997; Wegner, 1999; Wilson & Koopman, 2002). Thus, SOX proteins may have an extra role apart from functioning as classical transcription factors, since they also seem to function as architectural components of chromatin by organizing local chromatin structure and allowing other transcription factors to bind the major groove and/or facilitating the formation of protein complexes (Pevny & Lovell-Badge, 1997; Wegner, 1999; Wilson & Koopman, 2002; Dong et al., 2004).

It is currently accepted that the binding of SOX proteins to DNA is weaker than for most of the classical transcription factors. Thus, the transcription activity of SOX proteins requires recruitment of other protein partners, which stabilise the binding of the transcription factor complex to DNA (Kamachi et al., 2000; Wilson & Koopman, 2002). Thus, this combination of SOX factors with different protein partners (cell-type- or tissue-specific partner proteins) in order to direct gene expression, required for a specific cell type (cell specificity of SOX proteins), is the way by which each SOX factor recognizes each appropriate target gene or set of target genes, given that all SOX factors recognize the same core binding motif (Pevny & Lovell-Badge, 1997; Kamachi et al., 1999; Kamachi et al., 2000; Wilson & Koopman, 2002). This notion is also strengthened by the fact that each given cell type can co-express a number of SOX factors, while a single SOX factor is expressed in a variety of cellular contexts, is able to regulate different set of target genes in different tissues, and is able to participate in the differentiation of a wide variety of cells in embryonic development (Pevny & Lovell-Badge, 1997; Kamachi et al., 2000; Wilson & Koopman, 2002). Moreover sequences outside the HMG box may facilitate protein-protein interaction between the SOX and partner factors and also influence partner selection and thus the specificity of SOX proteins (Kamachi et al., 1999; Wilson & Koopman, 2002).

SOX2 (SRY (sex determining region Y)-box 2), is a transcription factor which is involved in organ development and in determining stem cell fate and properties by being paired off with cell-type- or tissue-specific partner factors (Kamachi et al., 1999; Kamachi et al., 2000; Boyer et al., 2005). SOX2 plays a key role in maintaining embryonic stem cell pluripontency, both in mice (Avilion et al., 2003; Masui et al., 2007; Niwa, 2007) and human (Boyer et al., 2005; Fong et al., 2008), in regulating neural and retinal cell progenitors (Zappone et al., 2000; Graham et al., 2003; Kondo & Raff, 2004; Taranova et al., 2006), and in development of the sensory organs of the inner ear (Kiernan et al., 2005). SOX2 is also expressed in the endoderm of foregut-derived organs, including tongue, oesophagus, trachea and proximal lung and stomach (Que et al., 2007).

In addition, SOX2 in the epithelial context, is required for the differentiation of endodermal progenitor cells of the mouse tongue into taste bud cells (highly expressed) versus keratinocytes, while it is also expressed in the basal epithelial cells of the tongue (Okubo et al., 2006). Its overexpression in basal epithelial cells of the tongue in transgenic mice, causes complete suppression of the differentiation of the filiform keratinocytes (Okubo et al., 2006). Similarly, constitutive overexpression of SOX2 in mouse neural stem cells inhibits their differentiation and results in the maintenance of progenitor characteristics (Graham et al., 2003), while its inhibition or its complete depletion by RNA interference results in their premature exit from the cell cycle and differentiation into neurons (Graham et al., 2003; Kondo & Raff, 2004), indicating the essential role of SOX2 in maintaining stem cells in different tissues.

Like other developmental regulatory factors, the improper functioning of SOX genes has been linked to a number of severe clinical disorders, indicating that the expression of SOX factors in different tissues is functionally significant. SOX2 mutations have been shown to cause anopthalmia (Fantes et al., 2003), a severe structural malformation of the eye, while heterozygous loss of function of SOX2 is associated with anopthalmia-oesophageal-genital (AEG) syndrome (Williamson et al., 2006).

It has also been shown that there is a link between SOX factors and cancer (Xia et al., 2000; Dong et al., 2004). Although SOX genes such as SOX1, SOX2, SOX3 etc. are expressed during early development, they are almost absent, or expressed at low levels

in adult tissues, while they are found highly overexpressed in different types of cancer supporting the hypothesis that cancer progression often reflects a reversal of normal development (Gure et al., 2000; Dong et al., 2004). SOX2 has been found amplified in many different types of cancer, including small cell lung and prostate cancer (Gure et al., 2000; Sattler et al., 2000) which are also associated with activated hedgehog signalling and GLI1/2 overexpression (Watkins et al., 2003; Karhadkar et al., 2004; Sanchez et al., 2004; Sheng et al., 2004; Bhatia et al., 2006; Thiyagarajan et al., 2007). Interestingly, SOX9, a master regulator gene for cartilage differentiation was found to have an unexpected but essential role in the development and maintenance of the mice hair in skin (Vidal et al., 2005). Sox9 was found to be expressed in the outer root sheath, as well as in the bulge of the hair follicle (hair stem cell compartment) during hair development, indicating a role of it in the maintenance of hair bulge stem cells (Vidal et al., 2005). Its crucial role in hair differentiation was also demonstrated by the fact that skin deleted for Sox9 (Sox9 knockout mice), developed initially abnormal hair and followed by complete loss of external hair (alopecia) (Vidal et al., 2005). Most importantly, Sox9 showed a dramatic protein reduction both in mice $Shh^{-/-}$ and in $Gli2^{-/-}$ sections, while basal cell carcinoma samples from K5:ΔNGli2 mice were expressing high levels of Sox9, suggesting an activation of Sox9 by Gli2 (Vidal et al., 2005). Consistently SOX9 was found upregulated in four out of four human BCC tumours (Vidal et al., 2005), as well as in all subtypes of human BCC tested in another study (Vidal et al., 2008). In addition, expression of SOX2 gene, has also been reported in poorly differentiated tumours such as breast, as well as in gliomas which are also associated with activated hedgehog signalling and GLI1/2 overexpression (Kinzler et al., 1987; Dahmane et al., 2001; Kubo et al., 2004; Sterling et al., 2006; Clement et al., 2007; Ben-Porath et al., 2008; Chen et al., 2008; Kameda et al., 2009).

Therefore, the remarkable induction of SOX2 in GLI2ΔN expressing N/TERT keratinocytes **(Figure 3.13B)**, suggests that SOX2 may be a direct downstream target of GLI2ΔN in human keratinocytes. This is also strengthened by the fact that a number of potential GLI2 consensus-binding sites are present in SOX2-promoter (Snijders et al., 2008). Importantly in mice, it was very recently found that Gli2 can regulate the expression of SOX2 in developing neuroepithelial cells via direct binding to the SOX2 enhancer region (Takanaga et al., 2009). Loss of Gli2 (Gli2ΔC or Gli2 shRNA) suppresses the expression of SOX2, and induces premature neuronal differentiation of

developing neuroepithelial cells (Takanaga et al., 2009), further supporting the role of GLI2 in opposing differentiation and possibly in the maintenance of stem cells.

3.3.7 GLI2ΔN downregulates c-MYC

Another important trait of SINEG2 keratinocytes is that of reduced c-MYC proto-oncogene mRNA and protein levels **(Figure 3.5B, C)**. Although significant, this finding was not unprecedented since c-MYC transcription is repressed in response to inducible expression of GLI2ΔN in HaCaT keratinocytes (Regl et al., 2004a; Eichberger et al., 2006) and it nicely correlates with the expression pattern of human BCCs, which show significant c-MYC reduction in both mRNA (Bonifas et al., 2001; Regl et al., 2002; O'Driscoll et al., 2006) and protein levels (Asplund et al., 2008).

c-MYC is an oncoprotein known to induce proliferation (G1 to S phase transition), transformation and apoptosis in mammalian cells (DePinho et al., 1991; Amati & Land, 1994). Overexpression of c-MYC induces proliferation and neoplastic transformation in many cell types, while downregulation of c-MYC accompanies differentiation of a range of cell types (DePinho et al., 1991). In addition, the level of c-MYC mRNA decreases when human keratinocytes undergo suspension or TPA induced terminal differentiation *in vitro* (Gandarillas & Watt, 1995; Hurlin et al., 1995). Consistently, in human interfollicular epidermis c-MYC protein is predominantly detected in the basal cell layers (proliferative cells), while it is almost undetectable in the terminally differentiating suprabasal layers (Bull et al., 2001). In human hair follicles, c-MYC protein was detected both in the bulb (base of the follicle) which contains a highly proliferative population of hair follicle epithelial cells and in the bulge, a region which is believed to contain stem cells, consistent with the proposed role of c-MYC as a key regulator of keratinocyte cell proliferation (Bull et al., 2001). Surprisingly, c-MYC protein was also detected in the terminally differentiating matrix cells that lie above the bulb and give rise to the hair fiber, suggesting, according to the authors, that c-MYC downregulation may not be essential for hair matrix cells to terminally differentiate (Bull et al., 2001).

Unexpectedly, a novel biological role of c-MYC in promoting differentiation of human keratinocytes *in vitro*, was revealed by Gandarillas and Watt (Gandarillas & Watt, 1997). When c-MYC (MycER - C-terminus of Myc is fused to the ligand binding domain of a mutant oestrogen receptor and thus c-MYC is only active when cells are exposed to 4-hydroxy-Tamoxifen (4OHT)) was overexpressed in primary human keratinocytes, keratinocyte proliferation was decreased and accompanied by induction of terminal differentiation, increased percentage of abortive colonies, and a decrease in the levels of β1 integrin, contradicting the expected hyperproliferative or apoptotic response observed in other cell types (Gandarillas & Watt, 1997). In the same study, when keratinocyte stem cells were distinguished from transit-amplifying cells through FACS, according to their β1 integrin expression levels (high and low respectively), it was clear that c-MYC over-expressing cells contained significantly less stem cells compared to the controls, as evidenced by the reduced clonogenic capacity of both $\beta1^{high}$ and $\beta1^{low}$ c-MYC over-expressing cells *in vitro*; indicating that overexpression of c-MYC has led to the depletion of epidermal stem cells from keratinocyte culture (Gandarillas & Watt, 1997). Moreover, when keratinocytes overexpressing c-MycER were seeded on dead, de-epidermalized dermis, they formed an abnormal epidermis. The reconstructed epidermis of c-MycER keratinocytes was mainly characterised by premature differentiation, as evidenced by decreased and increased number of proliferating cells and cells initiating terminal differentiation in the basal layer respectively, and abnormal accumulation of cells in the final stages of terminal differentiation (Gandarillas & Watt, 1997; Watt et al., 2008). This suggests that low levels of c-MYC are required for stem cells to proliferate, while sustained or high levels of c-MYC drive keratinocytes from the stem to the transit amplifying compartment, and thus stimulate terminal differentiation, rendering c-MYC a strong regulator of stem cell maintenance (Gandarillas & Watt, 1997).

Thus, in an attempt to combine the findings that c-MYC can stimulate both proliferation and terminal differentiation in human keratinocytes, it has been proposed by Gandarillas and Watt (Gandarillas & Watt, 1997) that since stem cells are often quiescent *in vivo*, activation of c-MYC leads to stem cell proliferation; sustained or high level c-MYC activation stimulates proliferating stem cells to enter the transit amplifying proliferating compartment and initiate terminal differentiation as a fail-safe mechanism to prevent uncontrolled proliferation of epidermal stem cells, and thereby to

protect the epidermis from the potentially oncogenic effects of sustained c-MYC activation (Watt et al., 2008).

This model was supported by further studies both *in vitro* and *in vivo* (Watt et al., 2008). *In vitro* it was shown that leucine-rich repeats and immunoglobulin-like domains 1 (Lrig1), which is an EGF receptor antagonist and a putative stem cell marker, maintains epidermal stem cells in a quiescent non-dividing state, partly by negatively regulating c-MYC transcription (reduced activation of c-MYC in response to EGF) (Jensen & Watt, 2006). Downregulation of Lrig1 triggers stem cell proliferation as a result of EGF stimulation and of c-MYC expression - moderate increase in c-MYC which is not sufficient to stimulate terminal differentiation, consistent with the notion that low levels of c-MYC are required for keratinocyte stem cell maintenance and proliferation (Jensen & Watt, 2006).

In vivo, constitutive over-expression of wild-type c-Myc (Waikel et al., 2001) or inducible c-MycER (Arnold & Watt, 2001), targeted via keratin 14 promoter to the basal layer of the epidermis and the hair follicles of transgenic mice skin, causes progressive and irreversible changes of the epidermis (Watt et al., 2008). Sustained overexpression of c-Myc for 5 months resulted in (i) gradual loss of the hair in adult mice, (ii) epidermal hyperplasia and in some areas complete epidermal loss, (iii) development of spontaneous ulcerated lesions in areas of chronic mechanical stress such as behind the ears, due to severe impairment in wound healing probably as a result of impaired migration of keratinocytes in response to wounding, and finally in (iv) reduction of the number of stem cells in the 3 month old c-Myc mice compared to the control, as judged by the 75% reduction of the label retaining cells (LRCs) (Waikel et al., 2001). In addition, β1 integrin which is essential for the stem cell maintenance was found unusually reduced in the epidermis of the c-Myc overexpressing mice, which in combination with the other phenotypic differences, suggests a depletion of epidermal stem cells by high levels of c-Myc (Waikel et al., 2001).

Continuous activation of c-Myc by the application of 4OHT (c-MycER) for 1 month in the basal layer of the transgenic mice epidermis and hair follicles via the keratin 14 promoter, caused stimulation of proliferation, as judged by the increase in the number of Ki67 positive cells, predominantly in the basal layer of the interfollicular epidermis, but

also in the outer root sheath of the hair follicles, thickening and hyperproliferation of the epidermis, and increased numbers of sebocytes along with development of abnormal hair follicles with often missing hair fibers (Arnold & Watt, 2001). However, it did not cause impaired terminal differentiation of the interfollicular epidermis which would reflect a possible neoplastic conversion of basal cells (Arnold & Watt, 2001). Instead, keratinocytes were terminally differentiated into interfollicular epidermis with increased number of suprabasal layers - reflecting that the thickening is due to increased number of differentiating layers rather than basal layers, and into sebaceous glands at the expense of the hair lineage differentiation (Arnold & Watt, 2001). Most importantly, activation of c-Myc even by a single application of 4OHT was as efficient as repeated doses in inducing the phenotype, while this c-Myc-induced phenotype continued to develop even after grafting of treated skin to untreated immunocompromised recipient mice (Arnold & Watt, 2001). Therefore, both these *in vivo* studies suggest that elevated expression of c-Myc depletes the epidermal stem cells by recruitment of stem cells into the cell cycle, irreversible exit from the stem cell compartment and stimulation of terminal differentiation.

Alternatively, epidermal deletion of c-Myc via the K5 promoter resulted in impaired wound healing, thinning of the interfollicular epidermis and premature differentiation possibly due to a proliferation defect (Zanet et al., 2005). Furthermore, there was insufficient expansion of the stem cell compartment (impaired stem cell self-renewal) as measured by a reduction in the number of BrdU label retaining cells, further suggesting that low levels of c-Myc are required for stem cell maintenance (Zanet et al., 2005). Therefore, in the absence of c-Myc, stem cells might be able to divide but their daughters cannot amplify and thus undergo premature differentiation. Thus stem cells would be triggered to divide and differentiate more frequently to replenish the epidermis and their compartment might be depleted over time (Zanet et al., 2005). However, in another study where c-Myc was selectively deleted in adult epidermis via 4OHT activation of K5 promoter, there were no abnormalities in the overall epidermal morphology, the thickness and the hair follicles and sebaceous glands appeared normal (Oskarsson et al., 2006). There were also no changes in proliferation or expression of differentiation markers suggesting that loss of c-Myc in some extent might be compensated by expression of other Myc genes such as N-Myc (Oskarsson et al., 2006). The discrepancy between those two studies might be due to the use of a non-inducible

transgene that already eliminates c-Myc during embryogenesis (Zanet et al., 2005), rather than in the adult epidermis (Oskarsson et al., 2006).

Finally, c-MycER over-expression in the suprabasal, post-mitotic cell layers of the mice epidermis via the involucrin promoter, disrupts the differentiation programme and triggers proliferation of the differentiated post-mitotic keratinocytes (Pelengaris et al., 1999). This leads to induction of papillomatosis together with angiogenesis, changes that both resemble hyperplastic actinic keratosis, a commonly observed human precancerous epithelial lesion, revealing the oncogenic potential of c-Myc (Pelengaris et al., 1999). However, the phenotype is entirely reversible on withdrawal of 4OHT, suggesting that cells with activated c-MycER upon withdrawal of 4OHT are being lost from the tissue through terminal differentiation and thus the differentiation compartment will be replenished by a pool of stem cells that are not expressing c-MycER (Arnold & Watt, 2001). Moreover, c-MycER induced lesions did not convert into malignant tumours indicating that further mutations might need to be acquired, for complete transformation and tumourigenesis (Pelengaris et al., 1999).

Overall, both from studies in human keratinocytes in culture and in various mice models it can be concluded that within the epidermis, c-MYC can act both as an agent that promotes differentiation of stem cells as well as an oncogene, depending on where in the epidermis it is expressed, the levels and the duration of its expression as well as the time of the observation (Watt et al., 2008).

Therefore, low levels of c-MYC might also contribute to the undifferentiated stem cell like phenotype of GLI2ΔN expressing cells and possibly to the role of GLI2ΔN in opposing differentiation and in the induction or maintainance of stem cell characteristics in cells, resembling in some aspects the gene expression of basal cell carcinomas.

3.3.8 Poor adhesion of GLI2ΔN-expressing cells to the extracellular surface in culture

Another property of keratinocyte stem cells is that of strong adhesion to the extracellular matrix. Immature populations of basal epidermal keratinocytes have been

identified by differential expression of β1 integrins (Jones & Watt, 1993; Jones et al., 1995). Positive fractions of integrin β1 human epidermal keratinocytes have shown a superior capacity for rapid adhesion to extracellular matrices (Collagen IV, Fibronectin and extracellular matrix deposited by cultured keratinocytes) (Jones & Watt, 1993; Jones et al., 1995). It will be therefore expected that SINEG2 cells, that exhibit high levels of integrin β1 compared to the controls, will adhere more efficiently to the extracellular surface during culture conditions. However, it was observed that even though SINEG2 cells displayed a very cohesive phenotype (cell-cell interaction), at the same time they displayed a significant delay in terms of adhesion to substrate (culture vessel) (cell-substrate interaction) and were also very easily detached by trypsinisation, compared to control N/TERT and SINCE cells. Often, GLI2ΔN keratinocytes needed more than 18 hours to completely attach to the substrate, with a few cells permanently remaining in suspension. This difference between the SINEG2 cell-cell and cell-substrate interactions is probably due to the different set of proteins, such as cadherins (adherens-junctions and desmosomes) and integrins (focal adhesions and hemidesmosomes) respectively, which are responsible for the implementation of those two processes (Garrod, 1993; Nievers et al., 1999; van der Flier & Sonnenberg, 2001). Given that the mechanism by which β1 integrins regulate the onset of terminal differentiation is distinct from the mechanism by which they mediate keratinocyte adhesion (Watt et al., 1993; Levy et al., 2000), and since the attachment efficiency of SINEG2 in culture vessels coated with any of the integrin β1 ligands such as collagen, laminin or fibronectin was not examined in my study, a possible explanation for this deficiency could be the improper production of basement membrane proteins by SINEG2 cells, as well as the possible absence of other integrins necessary for anchorage to the basement membrane from SINEG2 cells.

Consistent with these notions, and with the decreased ability of SINEG2 keratinocytes for attachment to culture substrate, is also the poor adhesion to collagen/fibroblast layers, that was recently observed in GLI2ΔN-expressing HaCaT GLI2 keratinocyte tissue reconstructs (Snijders et al., 2008), suggesting a defect in the structural link between the GLI2-expressing keratinocytes and the extracellular matrix. Indeed, the expression of components of the basement membrane zone in GLI2-expressing HaCaT GLI2 cells was abnormal. There was complete loss of integrin β4 (ITGB4), compared to the linear pattern in the basal keratinocyte layer of the controls, and only a few, and not

limited to the basal layer HaCaT GLI2 cells, were expressing laminin 5γ-2 (LAMC2 - a major constituent of the basement membrane zone), while in controls the staining was intense in the cytoplasm of keratinocytes in the basal layer and at the dermal-epidermal junctions (Snijders et al., 2008).

Malignant transformation is characterised by disruption of cytoskeletal organization, decreased adhesion, and altered adhesion dependent responses (Mizejewski, 1999). Thus altered epidermal integrin expression (downregulation, upregulation and/or altered distribution in the epidermis) may contribute to a transformed cell phenotype (Mizejewski, 1999; Watt, 2002). Focal or generalized loss of integrins is a feature of oral squamous cell carcinoma (Bagutti et al., 1998), while focal $\alpha_6\beta_4$ integrin loss in tumours such as oral squamous cell carcinoma tend to correlate with loss of basement membrane proteins and has been proposed to participate in invasion (Downer et al., 1993).

Integrin β4 participates in the formation of hemidesmosomes (Dowling et al., 1996), which are protein complexes in the inner basal surface of keratinocytes in the epidermis, and are anchoring the cell to the underlying basement membrane, by connecting the intermediate keratin filaments with the extracellular matrix (Borradori & Sonnenberg, 1999; Nievers et al., 1999; van der Flier & Sonnenberg, 2001). Thus $\alpha_6\beta_4$ integrin, as a component of hemidesmosomes, is primarily concentrated in the basement membrane zone and genetic ablation of the α6 or β4 integrin gene in mice resulted in a complete absence of hemidesmosomes, creating large blisters between the dermis and the epidermis, displaying only a very fragile attachment to the basal lamina and exhibiting signs of degeneration and tissue disorganization (Dowling et al., 1996; Georges-Labouesse et al., 1996; van der Neut et al., 1996). In addition, the existence of clusters of basal keratinocytes found in the suprabasal layers of the β4-null mouse epidermis, suggests that either there is clonal expansion of keratinocytes that have escaped detachment-induced cell death, or that basal cells became catapulted into the suprabasal layers, due to disrupted basement membrane adhesion (Dowling et al., 1996; Watt, 2002).

Interestingly, the observations that GLI2 overexpression disrupts both the normal adhesion capacity of cells to attach to the extracellular surface and the normal

expression pattern of keratinocyte-derived proteins linking the epithelium to the stroma, made from GLI2ΔN overexpressing N/TERT (SINEG2) keratinocytes *in vitro*, and from reconstructs of HaCaT GLI2ΔN-overexpressing keratinocytes respectively, correlate with the findings in human BCCs. Although histochemical studies in human BCCs have shown a continuous band of collagen and laminin around nodular islands of BCC, indicating an intact basement membrane in micronodular or more aggressive BCC subtypes such as infiltrative, morpheaform and basosquamous, there are broad regions of discontinuity or absence of this basement membrane (Miller, 1991a; Crowson, 2006). In addition, occasional discontinuities have been observed with fingerlike cytoplasmic projections extended into the stroma of these regions (Miller, 1991a). These observations suggested that in nodular BCC subtype, epidermal tumour cells following local invasion, may cease migration and produce distinct continuous basal lamina, similar to that of the normal dermal-epidermal junction (a barrier for further invasion), while in more aggressive BCC subtypes there is loss of the basal lamina in foci of ongoing tumour invasion (McArdle et al., 1984; Miller, 1991a). Thus, factors that might contribute to this initial local invasion of all BCC subtypes including nodular BCCs, as well as in the ongoing invasion of the more aggressive BCCs, are the (i) discontinuity of the basement membrane zone due to its impaired formation from the epidermal tumour cells, (ii) the induction of factors from the epidermal tumour cells which stimulate fibroblasts from the stroma to proliferate and release of collagenase, an enzyme which is required for the initiation of collagen breakdown and is thus important in the pathogenesis of soft tissue destruction *in vivo* (Bauer et al., 1977; Hernandez et al., 1985), along with (iii) the upregulation of transmembrane matrix metalloproteinases (MMPs) in epidermal tumour cells, which are able to degrade all kinds of proteins of the extracellular matrix (Miller, 1991a; Nagase & Woessner, 1999; Westermarck & Kahari, 1999; Crowson, 2006; Page-McCaw et al., 2007).

Comparable to the *in vitro* studies, the existence of retraction spaces observed around the human nodular and superficial BCC tumour islands with mucin deposition (slit-like retractions of the palisaded basal cells from the subjacent stroma), indicates reduced adhesion between keratinocytes of the basement membrane and the stroma (BCC loosely adhere to the collagen), probably due to collagenase upregulation by adjacent fibroblasts and thus reduction of collagen, as well as to mucin production from the epidermal tumour cells and to the absence of type VII collagen anchoring fibrils

(another component of the basement membrane secreted by fibroblasts, which connects the basement membrane to the stromal collagen) (Miller, 1991a; Hollingsworth & Swanson, 2004; Crowson, 2006).

The existence of these retraction spaces also within the basement membrane in all types of human BCCs, is suggestive of a decrease in numbers of hemidesmosomes (Miller, 1991a), the formation of which requires the presence of integrin β4 (Dowling et al., 1996), which in turn is markedly suppressed in GLI2ΔN expressing keratinocytes (Snijders et al., 2008). Indeed, hemidesmosomes cover the 45% of the basal area in normal basal cells, while in BCCs including nodular ones, they occupy only 7% (Miller, 1991a), further suggesting an impaired tumour cell-basement membrane and basement membrane-stroma attachment.

3.3.9 GLI2ΔN overexpression does not accelerate proliferation in culture

Contradictory to the oncogenic properties of GLI2ΔN transcription factor, its overexpression resulted in significant reduction of N/TERT keratinocyte proliferation **(Figure 3.14 and Figure 3.15)**. The marked reduction in cell proliferation could be attributed to a variety of factors including cell cycle arrest, impaired or delayed mitosis, apoptosis and/or cell death, or poor adhesion to the substrate.

Notably, this ability of SINEG2 cells resembles the slow growing nature of human basal cell carcinomas as well as the slow cycling status of keratinocytes stem cells (Miller, 1991a; Potten & Booth, 2002; Crowson, 2006). The ability to grow at slow rates, but for longer period of time is an attribute characterising stem cells *in vitro* (Potten & Booth, 2002). However, much like any immortalised cell line, the nature of N/TERT keratinocytes, does not allow the identification of a distinct population of cells with ability for prolonged growth *in vitro*. Therefore, the effect of GLI2ΔN overexpression, in the cell cycle dynamics and the long term proliferative potential, of finitely replicating primary human epidermal keratinocytes, could be of great interest.

A reduced growth rate in response to GLI2ΔN overexpression was also previously reported in HaCaT keratinocytes (Snijders et al., 2008). However, large scale expression

microarray analysis in the same cell line, carried out from another group, has revealed that several proliferation associated genes (i.e. CCND1, E2F1, CCNB1, PCNA), are upregulated in transcript levels in response to transient induction of GLI2ΔN (Regl et al., 2004a). This study was conducted in confluent, contact inhibited keratinocytes strongly suggesting that GLI2ΔN is stimulating cell cycle re-entry, opposing contact inhibition (Regl et al., 2004a). In addition, qRT-PCR analysis of the levels of expression of some of these associated genes (i.e. CCND1, CCNB1) in contact-inhibited human primary keratinocytes confirmed the proliferative expression profile of the contact-inhibited GLI2-expressing cells (Regl et al., 2004a). Thus, the differences in proliferation associated gene expression are likely to be reflecting the inability of normal control keratinocytes to proliferate under confluent conditions, compared to GLI2ΔN expressing cells, and do not predict that GLI2ΔN overexpression can confer any proliferative advantage (more rapid cell cycle) under normal steady state culture conditions, compared to the controls. In support, while at post confluent HaCaT keratinocytes expression of GLI2ΔN induces a two-fold increase in BrdU-incorporation (DNA synthesis) compared to control cells, at sub-confluence there is no difference in BrdU-incorporation between GLI2ΔN-expressing HaCaT cells and controls (Regl et al., 2002). In addition, induction of GLI2ΔN in tissue reconstructs, increases the proportion of Ki-67 (proliferation marker) positive keratinocytes compared to the controls, but does not induce an increase in the mitotic index of HaCaT keratinocytes, as judged by phosphohistone H3-PHH3 staining (Hendzel et al., 1997; Snijders et al., 2008).

However, the same group (Regl et al., 2004a) using the same cell line (GLI2ΔN HaCaT) performed another, larger scale expression microarray analysis in non-confluent HaCaT cells and showed that some proliferation associated genes are upregulated in response to inducible expression of GLI2ΔN (Eichberger et al., 2006). Strikingly though, the same GLI2ΔN HaCaT cell line that was used by Eichberger et al. (Eichberger et al., 2006) for microarray analysis, not only had no proliferative advantage (more rapid cell cycle) compared to the control, but instead it showed a reduced growth rate in culture, as reported by Snijders et al. (Snijders et al., 2008).

The proliferative activity in normal epidermis is restricted to the basal layer, since only the innermost basal layer of the epidermal cells has the capacity for DNA synthesis and mitosis (Fuchs, 1990). All keratinocytes leaving the basal membrane shift to program of

gene expression leading to terminal differentiation (Fuchs, 1990). Thus, keratinocytes in the suprabasal layers of the epidermis are postmitotic and any proliferative activity in the suprabasal layers could indicate an impaired differentiation program. Accordingly, Snijders et al. (Snijders et al., 2008) showed that induction of GLI2ΔN results in inappropriate keratinocyte proliferation across all epithelial layers, as opposed to control HaCaT keratinocytes where proliferation (only a few cells) is strictly confined to the basal layers of reconstructed epithelium. Therefore, although keratinocytes are inappropriately in cycle in all layers of the epithelium, GLI2ΔN expression did not result in accelerated cell division (Snijders et al., 2008).

The reasons behind the observed delay in the growth of SINEG2 keratinocytes will be discussed more extensively in the next chapter **(Chapter 4, Section 4.3.1.1)**. Although it is possible that poorly adhering SINEG2 keratinocytes resume normal cell cycle later than N/TERT and SINCE keratinocytes, loss of cells either through apoptosis or cell death is not likely to be responsible for this effect as none of the associated features (i.e. membrane blebbing, floating or necrotic cells, increase in trypan blue positive cells) were observed during routine keratinocyte culture.

3.4 Summary

In this chapter, evidence is provided for the efficient stable transduction of N/TERT keratinocytes with pSINEGFP-GLI2ΔN which results in the generation of a cell line that showed strong transgene mRNA expression and production of high protein levels. Similarly, in the inducible system significant induction of GLI2ΔN protein levels were observed, but without avoiding a background GLI2ΔN activation in uninduced control cells. In addition, previously established gene targets of GLI2ΔN and BCC molecular markers, such as BCL-2 and c-MYC, were appropriately regulated in my system, indicating the relevance of my *in vitro* model system to HH/GLI induced gene expression patterns in human BCC. Importantly, GLI2ΔN-expressing keratinocytes manifest a phenotype with a considerable degree of heterogeneity, which is mainly characterised by compact, undifferentiated, basal-like keratinocyte colonies, similar to the undifferentiated phenotype of human BCCs. This basal-like phenotype of SINEG2 keratinocytes is in accordance with, and can be attributed to, the ability of GLI2ΔN to suppress differentiation, through the downregulation of genes responsible for the onset of differentiation such as c-MYC, of differentiation markers such as involucrin and of stem cell markers such as integrin β1 and SOX2, as observed in my study and which is in line with previous studies. Moreover, in this chapter it was observed that GLI2ΔN overexpression disrupts the normal adhesive capacity of cells to attach to the extracellular surface, as judged by the delay that cells display in terms of adhesion to the substrate and their easy detachment upon trypsinisation, compared to the control cells. Finally, overexpression of GLI2ΔN in human N/TERT keratinocytes does not seem to accelerate proliferation in culture, as revealed by the reduced growth rate of SINEG2 keratinocytes compared to control cells.

CHAPTER FOUR

4 RESULTS

GLI2ΔN overexpression induces numerical and structural chromosomal instability in N/TERT human keratinocytes

4.1 Introduction

Although little is known about the role of the SHH/GLI2 on the cell cycle, several mechanisms have been proposed for the interactions of SHH/GLI signalling with important cell cycle mediators that promote cell proliferation, including cyclin D1, cyclin B1 and CDC25B (M-phase inducer phosphatase 2), which have been described more extensively in **Chapter 1, Section 1.3.7** (Barnes et al., 2001; Ruiz i Altaba et al., 2002a; Pasca di Magliano & Hebrok, 2003; Wetmore, 2003; Daya-Grosjean & Couve-Privat, 2005; Aberger & Frischauf, 2006; Athar et al., 2006; Benazeraf et al., 2006; Kasper et al., 2006a).

In support of that, loss of Shh or Gli2 function in mice leads to a significant decrease in the rate of cell proliferation in the developing hair follicle (Mill et al., 2003). In addition, SHH expression can oppose growth arrest (G1 arrest) of primary human epidermal keratinocytes in response to extracellular calcium as well as to ectopic expression of CDKI $p21^{WAF1/CIP1}$ (Fan & Khavari, 1999). Accordingly, inducible expression of GLI2ΔN in contact inhibited (confluent) cultures of HaCaT and primary human keratinocytes is sufficient to stimulate DNA synthesis (G1-S progression), re-entry to the cell cycle and to regulate the mRNA levels of specific cell cycle genes involved in G1-S and G2-M phase progression, such as cyclin D1 (CCND1), E2F transcription factor 1 (E2F1) and cyclin B1 (CCNB1) respectively **(see Chapter 3, Section 3.3.3)** (Regl et al., 2002; Regl et al., 2004a). Moreover, a larger scale expression microarray analysis, that was performed using the same cell line (GLI2ΔN HaCaT), further showed that some proliferation associated genes, including E2F1 and cyclin B1, are upregulated in response to inducible expression of GLI2ΔN **(see Chapter 3, Section 3.3.9)** (Eichberger et al., 2006).

However, it has not yet been reported that keratinocytes expressing GLI2 have an accelerated proliferation rate in normal culture conditions. Instead, the same inducible GLI2ΔN HaCaT cell line that was used by Eichberger et al. (Eichberger et al., 2006) for microarray analysis, showed no proliferative advantage (more rapid cell cycle) compared to the control, whereas it showed a reduced growth rate in culture, as reported by Snijders et al. (Snijders et al., 2008). Similarly, a reduced growth rate in response to

GLI2ΔN overexpression was observed in my system **(see Chapter 3, Section 3.2.3.2, Figure 3.14 and Figure 3.15) (see Chapter 3, Section 3.3.9)**.

Therefore, in this chapter, I have investigated the effect of GLI2ΔN, on the cell cycle of N/TERT keratinocytes, and on checkpoints genes that control the cell cycle, the regulation of which is important for the maintenance of genomic integrity and necessary to impose the appropriate limitations to uncontrolled proliferation (Sherr, 1996). In addition, factors such as cell cycle arrest, impaired or delayed mitosis, apoptosis and/or cell death, which might have contributed in the reduced rate of N/TERT keratinocytes proliferation upon GLI2ΔN induction, are also examined in this chapter.

4.2 Results

4.2.1 GLI2ΔN induces G2/M increase, tetraploidy and polyploidy in Human Keratinocytes

4.2.1.1 GLI2ΔN induces G2/M increase

Several oncogenes have been implicated in the regulation of cell cycle specific genes, promoting cell survival and increased proliferation rate. However, the oncogenic stress response can vary depending upon the different cell context. It has been shown that oncogenic Ras activation can increase the proliferation of aberrant cells, but can also lead to growth arrest and/or senescence when induced in primary cells with intact tumour suppressor responses (Di Micco et al., 2006; Sarkisian et al., 2007).

Therefore, I sought to investigate the effects of GLI2ΔN oncoprotein expression in N/TERT cells which have a functional p53/p21$^{WAF1/CIP1}$, diploid genome and retain normal epidermal keratinocyte differentiation in organotypical cultures (Dickson et al., 2000).

Flow cytometry analysis was used, after Hoechst-33342 staining **(see Chapter 2, Section 2.8.1 and Section 2.8.1.3)** (Shapiro, 1981a; Shapiro, 1981b), to investigate the effect of stable EGFP-GLI2ΔN expression on the cell cycle of N/TERT keratinocytes. Equal number of N/TERT, SINCE, and SINEG2 cells were seeded and harvested after 48 hrs (~ 60% confluent) for flow cytometry analysis both for DNA content and green fluorescence (EGFP) which corresponds to exogenous EGFP protein and EGFP-GLI2ΔN fusion protein. GLI2ΔN-expressing keratinocytes, showed a significant increase in the G2/M population, when compared to both EGFP control and wild-type N/TERT cells **(Figure 4.1A i)**.

Then, the same approach was used to investigate the cell cycle of NTEG2 cells, after the induction of EGFP-GLI2ΔN, by removal of dox for 5 days **(Figure 4.2A i)**. Cells were stained with Hoechst-33342 and analysed both for DNA content and green fluorescence (EGFP) which corresponds to exogenous EGFP-GLI2ΔN fusion protein **(see Chapter 2, Section 2.8.1 and Section 2.8.1.3)**. After gating on EGFP+/- cells and doublet discrimination with width and area parameters, using N/TERT as a reference cell line,

the cell cycle of EGFP+/- cells was determined. The EGFP negative (Dox+) and positive (Dox-) populations were discriminated and their cell cycle profiles were obtained. EGFP positive (Dox-) cells, show a marked increase in G2/M phase, compared to EGFP negative (Dox+) cells, which comes in total agreement with the results obtained from stable expression of GLI2ΔN in N/TERT keratinocytes, suggesting a strong correlation between EGFP-GLI2ΔN fusion protein expression and an increase in G2/M phase.

Experiments for both cell lines were repeated three separate times, and average values are presented in the tables shown in **Figure 4.1A ii** and **Figure 4.2A ii**, and in graphs plotted **Figure 4.1B** and **Figure 4.2B**, to indicate the statistically significant (** *P≤0.01)* differences in the percentages of G2/M populations in both cell lines examined.

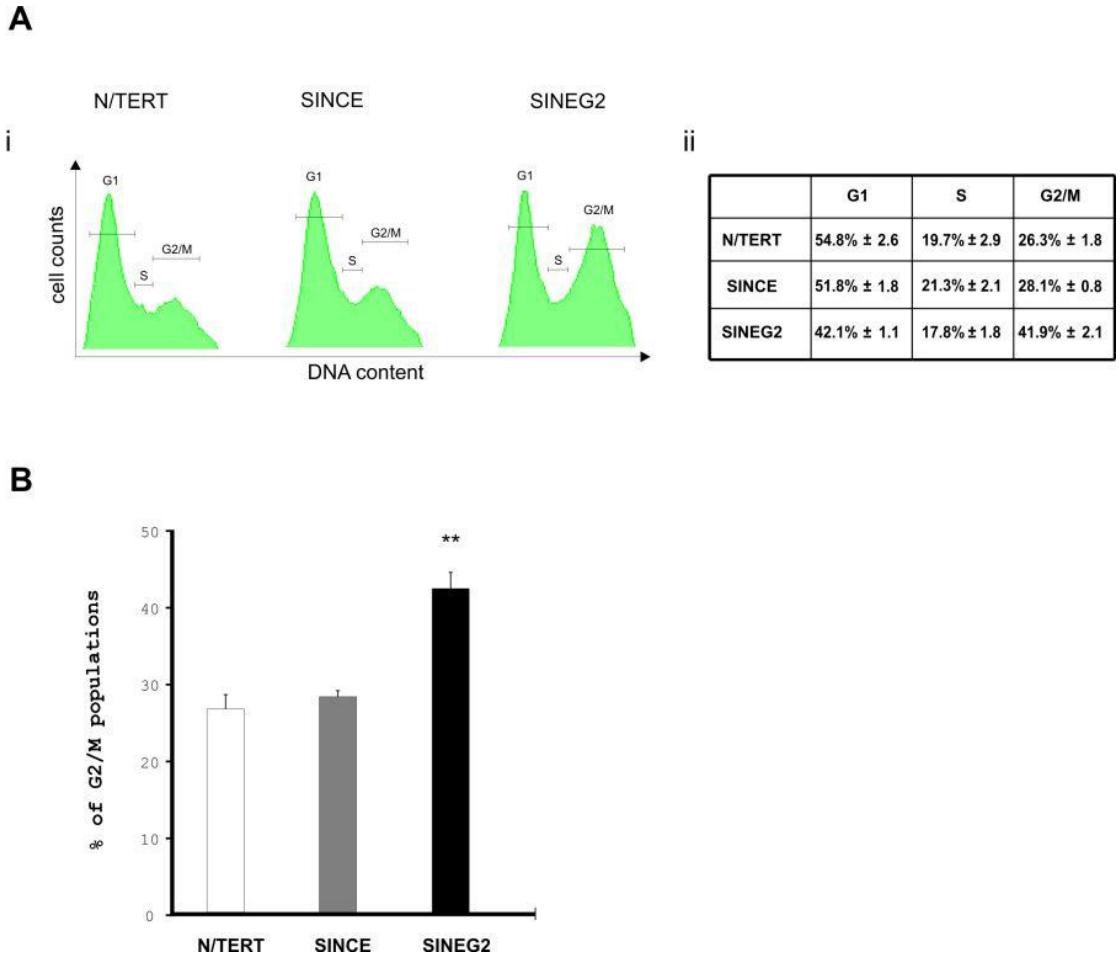

	G1	S	G2/M
N/TERT	54.8% ± 2.6	19.7% ± 2.9	26.3% ± 1.8
SINCE	51.8% ± 1.8	21.3% ± 2.1	28.1% ± 0.8
SINEG2	42.1% ± 1.1	17.8% ± 1.8	41.9% ± 2.1

Figure 4.1: Stable expression of GLI2ΔN induces G2/M arrest in N/TERT cells.

(A) Flow cytometry analysis of stable EGFP-GLI2ΔN cell line (SINEG2) against both N/TERT and SINCE control cells after Hoechst-33342 staining **(i)**. After doublet discrimination with width and area parameters, cells were discriminated according to DNA content and the cell cycle profile was obtained. A significant increase in the cell population at the G2/M boundary is evidenced in the SINEG2 cell line, compared to both N/TERT and SINCE cells. Average values of three independent experiments are presented **(ii)**. **(B)** Graphical presentation of the percentage of G2/M populations, to indicate the significant differences in the presence or absence of EGFP-GLI2ΔN expression. Each bar represents the mean values ± s.e.m of three independent experiments. ** *P≤0.01*.

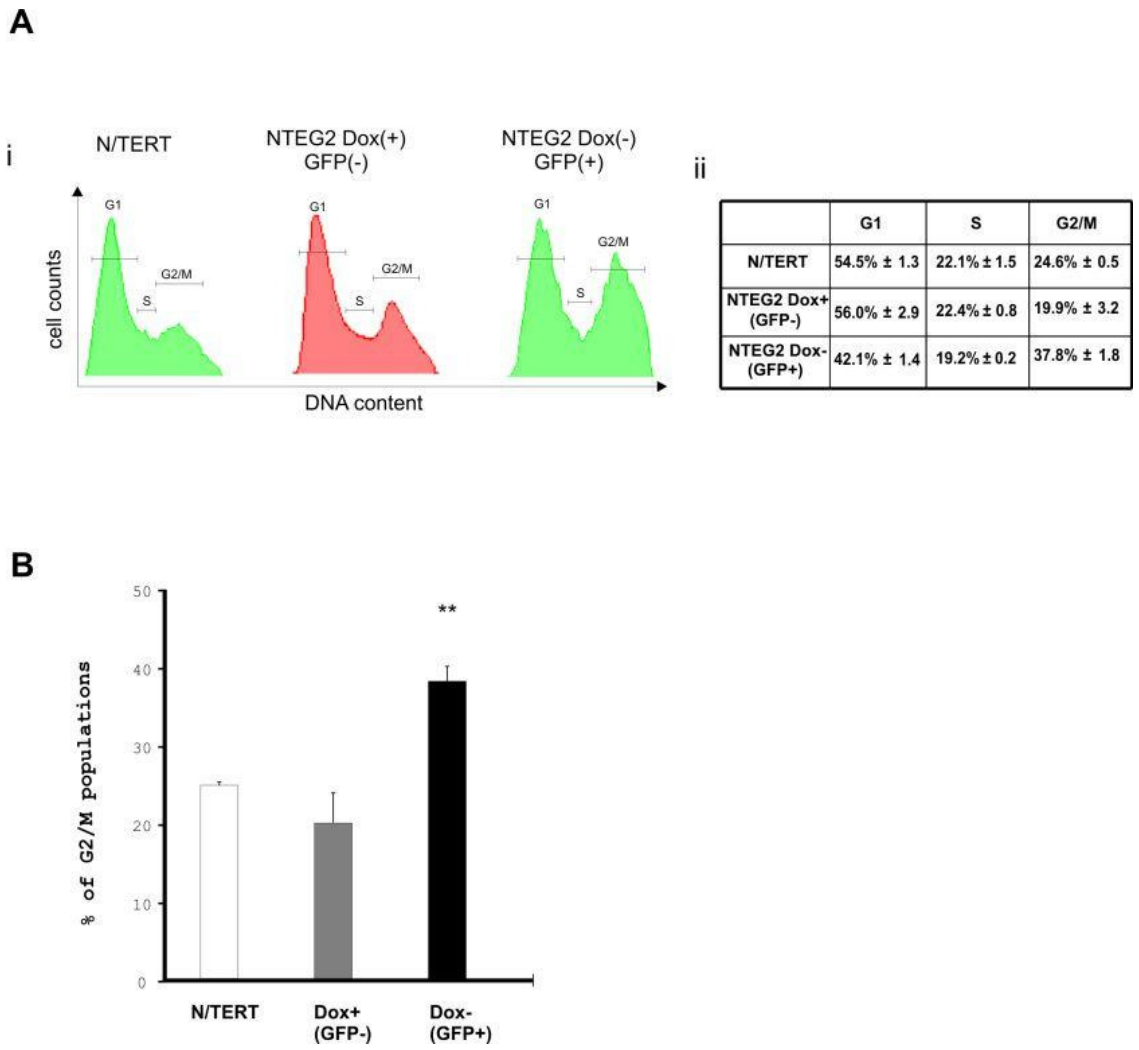

	G1	S	G2/M
N/TERT	54.5% ± 1.3	22.1% ± 1.5	24.6% ± 0.5
NTEG2 Dox+ (GFP-)	56.0% ± 2.9	22.4% ± 0.8	19.9% ± 3.2
NTEG2 Dox- (GFP+)	42.1% ± 1.4	19.2% ± 0.2	37.8% ± 1.8

Figure 4.2: Inducible expression of GLI2ΔN induces G2/M arrest in N/TERT cells.

(A) Flow cytometry analysis of NTEG2 cell line **(i)**. After gating on EGFP+/- cells and doublet discrimination with width and area parameters, using N/TERT as a reference cell line, the cell cycle of EGFP+/- cells was determined. EGFP negative cells were obtained from Dox+ samples and were compared to EGFP positive cells obtained from NTEG2 cells, in the absence of doxycycline for 5 days (Dox- samples). A G2/M phase increase is evidenced in EGFP positive (Dox-) populations, compared to the EGFP negative (Dox+) populations. Average values of three independent experiments are presented **(ii)**. **(B)** Graphical presentation of the percentage of G2/M populations, to indicate the significant differences in the presence or absence of EGFP-GLI2ΔN expression. Each bar represents the mean values ± s.e.m of three independent experiments. ** *P≤0.01*.

4.2.1.2 GLI2ΔN does not cause increased cell death or apoptosis

Given the slow growth profile of stable GLI2ΔN-expressing cells (SINEG2), observed in **Chapter 3, Section 3.2.3.2 (Figure 3.14 and Figure 3.15)**, and the increase in their G2/M phase **(Figure 4.1)**, compared both to N/TERT and SINCE control cells, it was investigated whether there is any evidence of increased apoptosis or cell death, by using Annexin V staining and flow cytometry analysis **(see Chapter 2, Section 2.8.1 and Section 2.8.1.5)**.

Apoptosis, or programmed cell death, is a normal physiologic process, which occurs during embryonic development as well as in the maintenance of tissue homeostasis (Taylor et al., 2008). Apoptosis can be detected by different methods including, Annexin V staining (early stage of apoptosis) (Vermes et al., 1995), PI-staining and flow cytometry analysis to detect cells with sub-G1 content (late stage of apoptosis) (Riccardi & Nicoletti, 2006), and caspase activation (late stage of apoptosis) (Riedl & Shi, 2004). During apoptosis, cells acquire certain morphological features, including shrinkage, loss of plasma membrane (membrane blebbing), condensation of the cytoplasm and the nucleus (pyknosis), followed by DNA fragmentation (Taylor et al., 2008). Annexin V, is a Ca^{2+} dependent phospholipid-binding protein that has a high affinity for membrane phosholipid phosphatidylserine (PS), and binds to cells with exposed PS (Raynal & Pollard, 1994). In apoptotic cells, the membrane phosholipid phosphatidylserine (PS) is translocated from the inner to the outer leaflet of the plasma membrane, thereby exposing PS to the external cellular environment and thus enabling the binding of Annexin V to it (Koopman et al., 1994; Martin et al., 1995). Due to the fact that externalisation of PS occurs in the earlier stages of apoptosis (Martin et al., 1995), Annexin V staining is used to identify apoptosis at an earlier stage, compared to assays based on nuclear changes (DNA fragmentation), such as propidium iodide staining. DAPI (Kubista et al., 1987; Barcellona et al., 1990) was also used for staining along with Annexin V in order to discriminate late apoptotic or dead cells which have lost membrane integrity from early apoptotic cells which still have intact membranes, by dye exclusion **(see Chapter 2, Section 2.8.1.5)**.

Equal number of N/TERT, SINCE, and SINEG2 cells were seeded and harvested after 48 hrs for Annexin V ($Cy^{TM}5$ Annexin V) and DAPI staining, followed by flow

cytometry analysis. Results clearly show that upon induction of GLI2ΔN oncogene, there is no difference in any of the three different subpopulations of cells (live, early apoptotic, late apoptotic/dead cells), between control and GLI2ΔN-expressing cells **(Figure 4.3)**. Therefore, activation of GLI2ΔN in N/TERT cells does not cause any increased apoptosis or cell death.

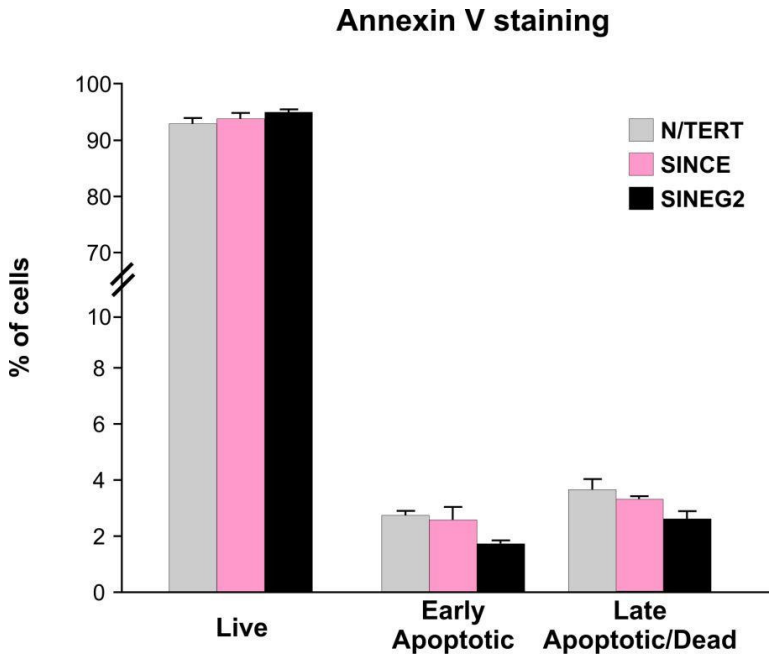

Figure 4.3: Annexin V staining in N/TERT, SINCE and SINEG2 cells.

N/TERT, SINCE and SINEG2 cells were stained with Cy™5 Annexin V and DAPI for the detection of apoptotic and dead cells respectively. The percentage of cells representing the early (Annexin V (+) DAPI (-)) and late (Annexin V (+) DAPI (+)) apoptotic or dead populations, do not show significant differences between all three different cell lines. Expectedly, the percentage of cells in the remaining live (Annexin V (-) DAPI (-)) populations are similar in both control and GLI2ΔN-expressing cells, suggesting that GLI2ΔN upregulation does not cause cell death or apoptosis in N/TERT keratinocytes. Each bar represents the mean values ± s.e.m of three independent experiments each of which consisted of duplicate samples.

4.2.1.3 GLI2ΔN induces numerical chromosomal instability in human N/TERT keratinocytes

The marked increase of cells in G2/M phase could indicate a G2/M block, and thus a G2/M checkpoint activation, and/or an increase of cells with DNA content of 4N (G2/M phase), indicating abnormal accumulation of tetraploid/bi-nucleated cells in response to GLI2ΔN induction.

Thus, in order to investigate the cell cycle profile of stable GLI2ΔN over-expressing N/TERT cells more extensively, propidium iodide staining (Krishan, 1990) was used for flow cytometry analysis **(see Chapter 2, Section 2.8.1 and Section 2.8.1.4)**. Equal number of N/TERT, SINCE, and SINEG2 cells were seeded and stained for propidium iodide, followed by flow cytometry analysis for DNA content. The cell area parameters were increased in order to check for the existence of cells with DNA content more than 4N, where N is the haploid number, which represents one complete set of chromosomes (23 chromosomes). Doublets were excluded by adjustment of the width and area parameters.

In addition, propidium iodide staining in permeabilised cells facilitates the discrimination of cells with reduced DNA content, due to DNA fragmentation (sub-G1 populations). When cells are permeabilised, the apoptosis-mediated fragmented DNA multimers leak out of the cell, and therefore the resulting stained by propidium iodide sub-G1 populations, represent late apoptotic/dead cells (cells with fragmented DNA), and thus used for detection of later stages of apoptosis **(see Chapter 2, Section 2.8.1.4)** (Riccardi & Nicoletti, 2006).

The sub-G1 population for all three cell lines was at basal levels, with no significant differences **(Figure 4.4 i, ii, iii)**, indicating that overexpression of GLI2ΔN does not seem to cause any cell death or apoptosis, reconfirming the data from **Section 4.2.1.2**. However, GLI2ΔN expressing N/TERT cells again showed an increase in G2/M phase and a 3 fold increase in the cell population containing DNA 8N **(Figure 4.4 iii)** compared both to N/TERT and SINCE control cells **(Figure 4.4 i, ii)**. This 8N population represents cells, which are known as polyploid cells, cells that have acquired more than two homologous sets of chromosomes. Polyploid populations (8N) are

represented by a clear peak appearing at the far right of the flow cytometry trace **(see inset Figure 4.4 iii)**. Data are representative of three independent experiments.

Further flow cytometry analysis in Hoechst-33342 stained cells, showed that SINEG2 cells have a significant increase in the percentage of polyploid cells (>4N and 8N), compared to N/TERT and SINCE cells **(Figure 4.5 i, ii)**. Four independent experiments, each of them consisting of duplicate or triplicate samples, were carried out with both Hoechst-33342 and Propidium Iodide staining, and similar results were obtained.

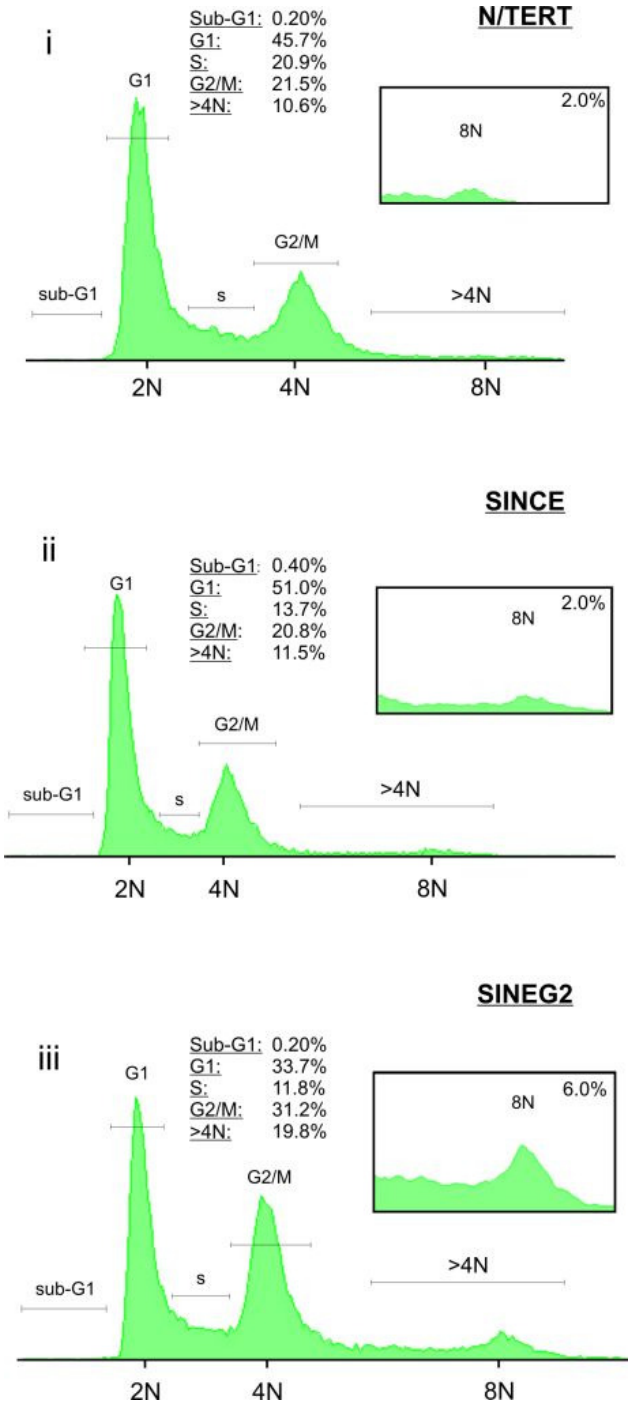

Figure 4.4: GLI2ΔN induces polyploidy in N/TERT keratinocytes.

Propidium iodide staining, followed by flow cytometry analysis to obtain cell cycle distribution of N/TERT **(i)**, SINCE **(ii)**, and SINEG2 **(iii)** cells. Sub-G1 trace was negligible for all cell lines examined. Flow cytometry analysis revealed a G2/M phase increase in SINEG2 cells **(iii)** and a 3 fold increase in the percentage of cells with DNA content 8N, represented by a clear peak appearing at the far right of the flow cytometry trace **(see inset, iii)**. **N**: haploid number. Data are representative of three independent experiments.

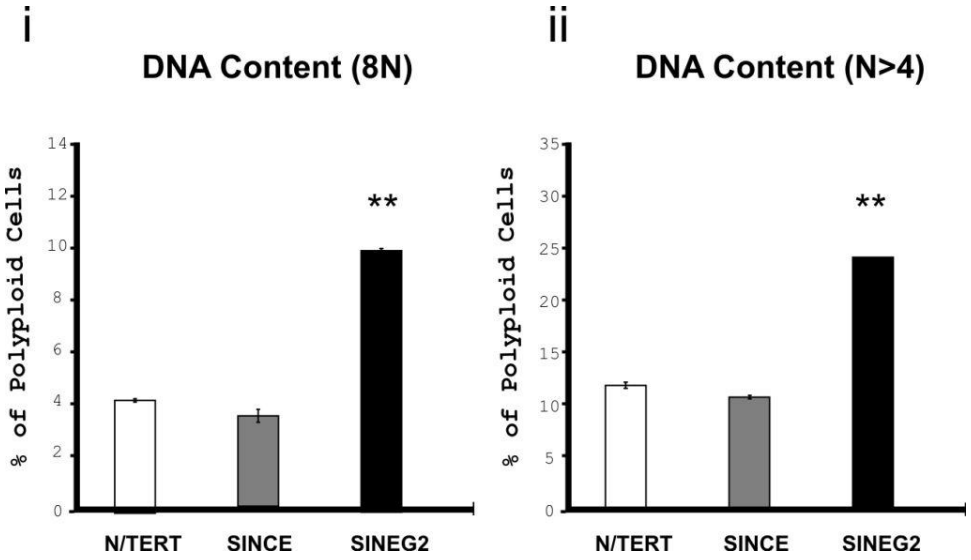

Figure 4.5: GLI2ΔN induces polyploidy in N/TERT keratinocytes.

Graphical representation of the percentage of polyploid **(i)** 8N and **(ii)** >4N cells, for each cell line after Hoechst-33342 staining and flow cytometry analysis. SINEG2 cells have significantly higher *(** P≤0.01)* percentage of polyploid cells in culture. Each bar represents the mean values ± s.e.m of duplicate samples. ** *P≤0.01*. **N**: haploid number.

These results suggest that the increase in G2/M population, observed both by Hoechst-33342 staining **(Figure 4.1 and Figure 4.2)**, and by propidium iodide staining **(Figure 4.4),** might be due to the increase of bi-nucleated/tetraploid cells (DNA content 4N) upon GLI2ΔN induction, which precede the formation of polyploid and aneuploid cells and can lead to genomic/chromosomal instability (Storchova & Pellman, 2004; Ganem et al., 2007). Tetraploidy, is a feature that is commonly seen in human cancer, including human BCCs (Miller, 1991a; Rajagopalan & Lengauer, 2004; Shi & King, 2005; Olaharski et al., 2006; Weaver & Cleveland, 2006; Ganem et al., 2007; Storchova & Kuffer, 2008), and has been reported as an early step in human tumourigenesis and as a contributing factor in the generation of aneuploid tumours (Shackney et al., 1989; Galipeau et al., 1996; Storchova & Pellman, 2004; Zhivotovsky & Kroemer, 2004; Fujiwara et al., 2005; Ganem et al., 2007; Storchova & Kuffer, 2008; Holland & Cleveland, 2009).

Tetraploidy and polyploidy can result from a variety of alterations **(Figure 4.6)** (Storchova & Pellman, 2004); either as a result of (a) endoreplication - DNA replication in the absence of complete mitosis, a normal developmental program, observed in the megakaryocyte (Ravid et al., 2002), yielding mononucleated tetraploid cells, which lead to the formation of terminally differentiated non-dividing polyploid cells, (b) cell fusion due to viruses (Vignery, 2000; Taylor, 2002; Duelli & Lazebnik, 2007), yielding binucleated tetraploid cells, (c) centrosome overduplication (centrosome amplification), yielding either mononucleated or binucleated tetraploid cells (Nigg, 2002; Fukasawa, 2007), (d) failure in centrosome duplication, yielding mononucleated tetraploid cells (Nigg, 2002; Fukasawa, 2007), (e) DNA damage (Olive et al., 1996; Waldman et al., 1996; Bunz et al., 1998), or as a result of (f) abortive cell cycle - a failure in executing a crucial step in the cell division process, yielding either mononucleated tetraploid cells due to karyokinesis failure, or bi-nucleated tetraploid cells due to cytokinesis failure. Abortive cell cycle may arise from a wide variety of defects in different aspects of cell division, such as failure of spindle assembly and chromosome segregation, cytokinesis failure, and microtubule stabilisation or destabilisation by agents such as taxol or nocodazole respectively (Andreassen et al., 1996; Minn et al., 1996; Lanni & Jacks, 1998; Andreassen et al., 2001b; Storchova & Pellman, 2004; Zhivotovsky & Kroemer, 2004). In all the aforementioned situations, apart from the developmental process of megakaryocytes, tetraploid cells can either undergo bipolar and symmetric divisions, leading to the formation of polyploid cells, or multipolar and asymmetric divisions, yielding aneuploid progenies with chromosome complements that are not a simple multiple of the haploid set (gain and loss of chromosomes), depending on the centrosome clustering **(Figure 4.6)** (Storchova & Pellman, 2004; Quintyne et al., 2005; Basto et al., 2008; Kwon et al., 2008). Aneuploidy is consistently observed in virtually all cancers, including human BCCs (Buchner et al., 1985; Miller, 1991a; Herzberg et al., 1993; Fortier-Beaulieu et al., 1994; Lengauer et al., 1997; Lengauer et al., 1998; Staibano et al., 2001; Ashton et al., 2005; Weaver & Cleveland, 2006; Storchova & Kuffer, 2008).

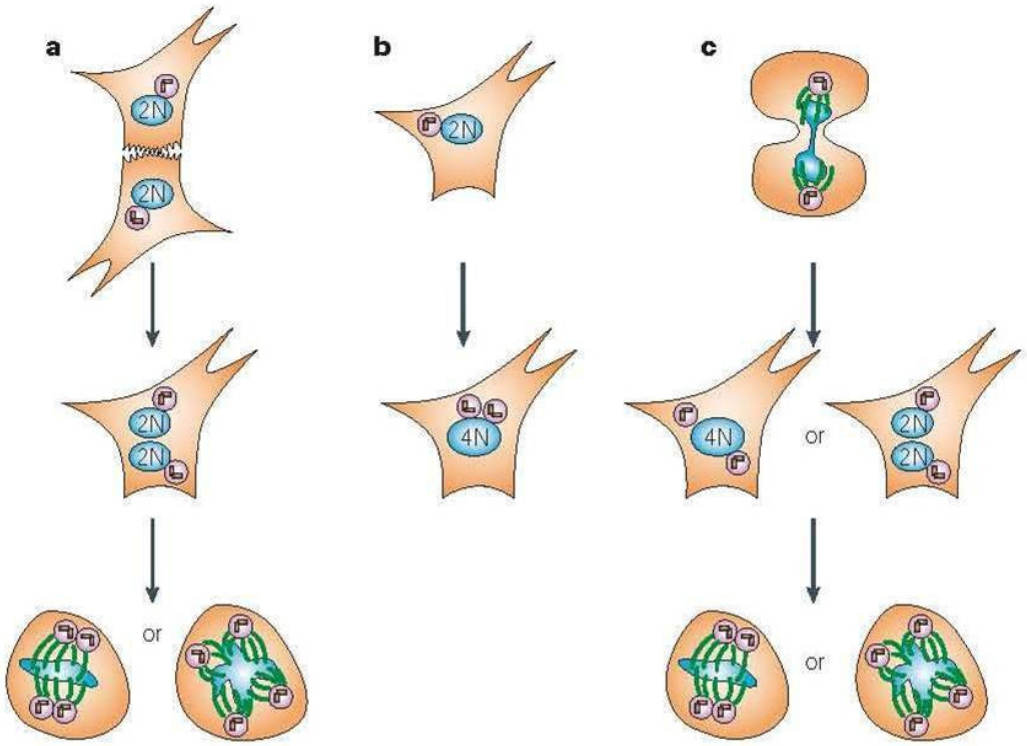

Figure 4.6: Several routes to tetraploidy, polyploidy and aneuploidy.

Tetraploidy and polyploidy can result from a variety of alterations; **(a)** Cell fusion, **(b)** Endoreplication, **(c)** Abortive cell cycle. Tetraploid cells can either undergo bipolar and symmetric divisions **(a)**, **(c)**, leading to the formation of polyploid cells, or multipolar and asymmetric divisions **(a)**, **(c)**, yielding aneuploid progenies with chromosome complements that are not a simple multiple of the haploid set (gain and loss of chromosomes), depending on the centrosome clustering (Storchova & Pellman, 2004).

In order to examine if there are any tetraploid, polyploid or aneuploid phenotypic characteristics in my cell culture, and in order to verify (quantify) that there is an increase in tetraploid cells in SINEG2 cultures, two different experiments were carried out.

First, SINEG2 cells were stained with Hoechst-33342 in suspension for 1 hour, were replated in culture for 24, 48 and 72 hours **(see Chapter 2, Section 2.9)**, and representative pictures were taken **(Figure 4.7)**. The presence of enlarged, bi-nucleated and multi-nucleated cells in SINEG2 culture **(Figure 4.7 a, b, c, d)**, provided further support for the existence of tetraploid and polyploid / aneuploid cells respectively, indicating a failure in the cytokinesis process. An example of a tetraploid cell (4N) is shown in **Figure 4.7 c**, pointed out by a black arrow, a polyploid cell (8N) is shown in **Figure 4.7 d (ii)** pointed out by a red arrow, an aneuploid cell (3N) is shown in **Figure 4.7 c,** pointed out by a red arrow, and an example of a cell undergoing karyokinesis with no cytokinesis is shown in **Figure 4.7 a, i (see inset)**, pointed out by a red arrow.

Second, N/TERT, SINCE and SINEG2 cells were plated, fixed, stained with DAPI, and bi-nucleated cells (tetraploids) in all three cell lines were counted under the fluorescent microscope **(see Chapter 2, Section 2.10)**. More than 300 cells were counted for each different cell line. The percentage of bi-nucleated cells per field was derived by counting the number of cells with two nuclei over the total number of cells per field **(see Chapter 2, Section 2.10)**. Cells undergoing mitosis were counted as two mononuclear cells. SINEG2 cultures showed a significantly elevated percentage (~ 3.5 fold increase) of bi-nucleated cells (~ 19%), compared to both control cell lines (~ 5%) **(Figure 4.8)**. This difference in bi-nucleated cells (~ 14%), is consistent with the differences in G2/M populations between control (N/TERT, SINCE) and SINEG2 keratinocytes (~ 11-15%), as evidenced from flow cytometry analysis **(Figure 4.1 and Figure 4.4)**. This suggests that the accumulation of SINEG2 cells at G2/M (DNA content, 4N), observed by flow cytometry, is mostly due to the presence of bi-nucleated tetraploid cells as a result of a cytokinesis defect, rather than due to the activation of G2/M checkpoint of diploid cells. This is further supported by the fact that, when at least some of these cells eventually divide, they give rise to cells with DNA content N>4, and 8N, rather than to normal diploid keratinocytes **(Figure 4.4 and Figure 4.7)**. However, it cannot be excluded completely that there might be a transient arrest of diploid cells due to the activation of

the mitotic spindle checkpoint. Therefore, the G2/M peak in the cell cycle profile of the SINEG2 cells **(Figure 4.4 iii)** consists of **(a)** G2/M diploids (diploid cells in G2/M phase undergoing division), **(b)** bi-nucleated/tetraploid cells **(Figure 4.8)**, cells that have acquired more than two homologous sets of chromosomes (4N) after an abortive cell cycle (i.e. cytokinesis failure of a G2/M diploid cell) which are now in a G1 biochemical state, **(c)** bi-nucleated/tetraploid cells (4N) in a G1 biochemical state **(Figure 4.8)**, that arise from the bipolar and symmetric divisions of the octoploid/polyploid (8N) cells, and possibly to a lesser extent of **(d)** diploid cells undergoing a transient mitotic arrest. Accordingly, the 8N peak in the cell cycle profile of the SINEG2 cells **(Figure 4.4 iii)** consists of G2/M tetraploids (tetraploid cells in G2/M phase undergoing division) and polyploid cells, cells that have acquired more than two homologous sets of chromosomes (8N) after an abortive cell cycle (i.e. cytokinesis failure of a G2/M tetraploid cell) and are now in a G1 biochemical state.

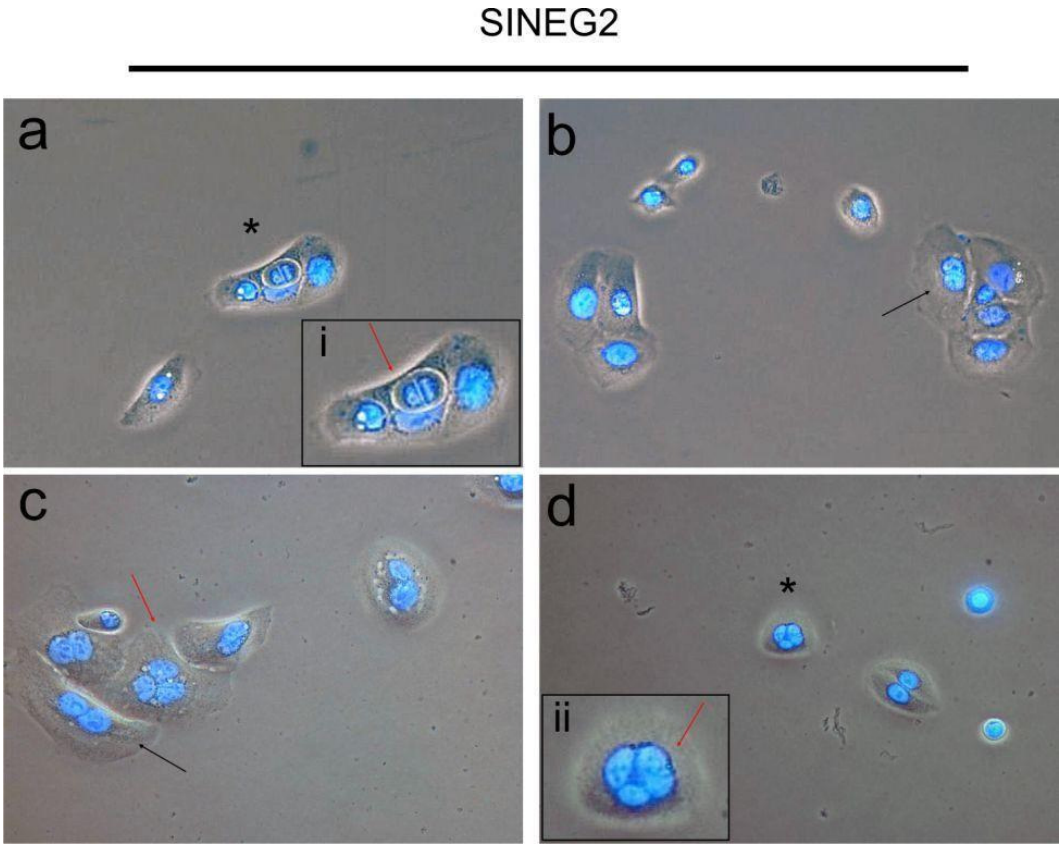

Figure 4.7: Phenotypic characteristics of tetraploid, polyploid and aneuploid cells in GLI2ΔN-expressing keratinocytes.

Representative pictures taken from Hoechst-33342 stained SINEG2 cell line at x20 magnification, showing the presence of bi- and multi-nucleated cells. Black arrows indicate bi-nucleated cells (4N) and red arrows indicate multi-nucleated (>4N) cells. DNA was detected by Hoechst-33342 staining (blue). Insets **a (i)** and **d (ii),** show magnified images indicated by asterisk, of the nuclear region of the corresponding photos. Black arrow in picture **c** points out a tetraploid cell (4N); Red arrow in picture **c** points out an aneuploid cell (3N); Black arrow in picture **d (ii)** points out a polyploid cell (8N); Inset **a (i)** is an example of a cell undergoing karyokinesis with no cytokinesis.

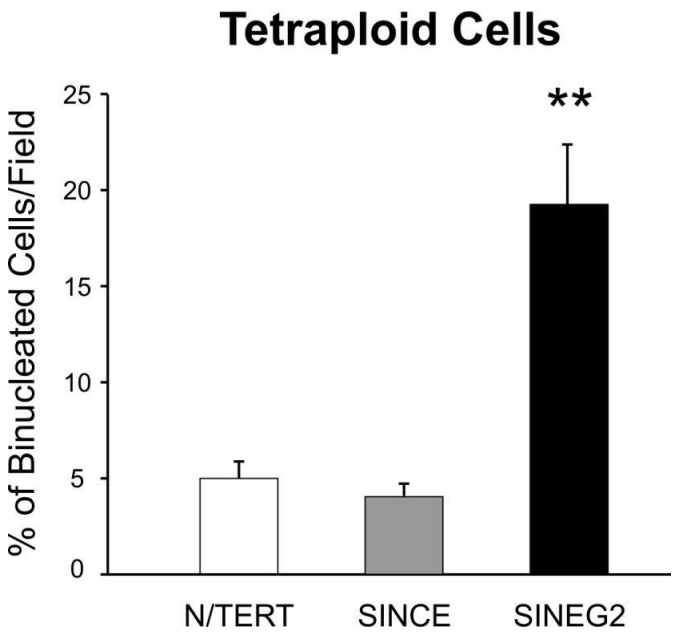

Figure 4.8: GLI2ΔN increases bi-nucleated cells in culture.

N/TERT, SINCE and SINEG2 cells were stained with DAPI to visualize nuclear DNA. By calculating the average percentage of bi-nucleated cells per field, it was evidenced that SINEG2 cells display a significant increase (~ 3.5 fold) in the population of bi-nucleated (tetraploid) cells. Each bar represents the mean values of bi-nucleated cells per field ± s.e.m of 7 fields for N/TERT and SINCE, and 13 fields for SINEG2. Total count ~ 300 cells per cell line. ** *P≤0.01*.

4.2.1.4 14-3-3σ (14-3-3 sigma) is downregulated in GLI2ΔN-expressing keratinocytes

The scope of my study was not to find out how the tetraploids arise, but how they survive and are maintained in culture, and whether these populations could give rise to cells with structural chromosomal instability. However, recently a study from Wilker et al. (Wilker et al., 2007) demonstrated that 14-3-3σ (stratifin) is an important regulator of the mitotic cap-independent translation (Pyronnet et al., 2001; Cormier et al., 2003; Holcik & Sonenberg, 2005; Wynshaw-Boris, 2007), and its loss leads to the improper mitotic cap-independent translation of PITSLRE/CDK11^{p58} (endogenous internal ribosomal entry site (IRES)-dependent form of the cyclin-dependent kinase Cdk11) protein and improper localisation of Polo-like kinase-1 (Plk1) (loss of Polo-like kinase-1 protein in the midbody during mitosis, a protein which is required for cytokinesis). Both these proteins are important executioners of mitosis (Neef et al., 2003; Liu et al., 2004b; Petretti et al., 2006; Hu et al., 2007), and the deregulation of PITSLRE/CDK11^{p58} mitotic cap-independent translation by 14-3-3σ knockdown, leads to cytokinesis failure and accumulation of binucleate cells (Wilker et al., 2007).

In addition, the ability of 14-3-3 proteins to bind to a variety of functionally diverse signalling proteins including kinases and phosphatases, allows them to play important roles in a wide range of regulatory processes, including cell-cycle regulation (Yaffe, 2002; Hermeking, 2003). 14-3-3σ is a direct transcriptional target of p53 after DNA damage (Hermeking et al., 1997), of which elevated levels enforce a G2/M cell cycle arrest by binding and sequestering Cdc2/cyclin B1 complexes in the cytoplasm (Hermeking et al., 1997; Chan et al., 1999b), and are required for the maintenance of a stable G2/M cell cycle arrest after DNA damage (Chan et al., 1999b). Moreover, 14-3-3σ is also thought to be a negative regulator of G1/S progression by binding to, and inhibiting the activities of both CDK2 and CDK4 (Laronga et al., 2000). Importantly, 14-3-3σ is abundantly expressed in the differentiated suprabasal layers of human epidermis, and its downregulation results in immortalization of primary human keratinocytes, suggesting a role of 14-3-3σ downregulation in maintaining epidermal stem cells and promoting cell transformation (Dellambra et al., 2000). Consistent with the latter, 14-3-3σ is frequently lost in many cancers including breast and prostate, either due to hypermethylation of its promoter (transcriptional silencing), or induction

of its proteasomal degradation (Ferguson et al., 2000; Umbricht et al., 2001; Hermeking, 2003; Lodygin et al., 2004; Lodygin & Hermeking, 2005; Mhawech et al., 2005; Lodygin & Hermeking, 2006). Similarly, human BCCs, exhibit partial or complete loss of 14-3-3σ protein expression, due to CpG-hypermethylation of the 14-3-3σ promoter (Lodygin et al., 2003).

Therefore, due to the accumulation of binucleated/tetraploid cells, probably due to cytokinesis failure, in SINEG2 cultures **(Figure 4.8)**, and taking into account that human BCCs exhibit low or event absent protein levels of 14-3-3σ, as well as the role of 14-3-3σ in facilitating cytokinesis, I checked the protein levels of 14-3-3σ. 14-3-3 sigma was found to be downregulated in GLI2ΔN-expressing keratinocytes compared to both N/TERT and SINCE controls **(Figure 4.9)**, suggesting a possible contribution of the low levels of 14-3-3σ in the production and accumulation of tetraploid cells in SINEG2 keratinocytes, as well as in the progression of these cells through G1/S and G2/M phases of the cell cycle, yielding polyploid and aneuploid cells.

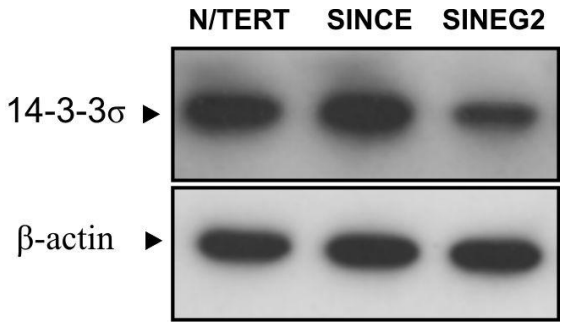

Figure 4.9: GLI2ΔN downregulates 14-3-3 sigma.

Immunoblotting analysis for 14-3-3σ (~ 30 kDa) protein, on N/TERT, SINCE, SINEG2 whole cell lysates. β-actin (~ 42 kDa), was used as loading control. SINEG2 cells show a remarkable decrease in the 14-3-3σ protein levels, compared both to N/TERT and SINCE control cells.

4.2.2 GLI2ΔN enhances the survival of tetraploid/polyploid human keratinocytes

The mechanism that has been suggested to be responsible for the restricted growth potential and the elimination of the tetraploid/polyploid cells, is the so-called "tetraploidy checkpoint" (Zhivotovsky & Kroemer, 2004). Tetraploid/polyploid cells resulting either from karyokinesis or cytokinesis failure, show limited growth potential in the absence of anti-apoptotic activation. Tetraploids that result from karyokinesis failure normally undergo a transient G2/M cell cycle arrest, and through a process which is known as 'mitotic slippage', they escape this G2/M arrest and permanently arrest in G1 phase, following activation of a p53/p21$^{WAF1/CIP1}$-dependent checkpoint, known as the "tetraploidy checkpoint", which finally triggers apoptosis. Similarly, tetraploids arising from cytokinesis failure permanently arrest in G1 phase, following activation of the p53/p21$^{WAF1/CIP1}$-dependent checkpoint and subsequent activation of apoptosis (Lane, 1992; Lanni & Jacks, 1998; Andreassen et al., 2001a; Andreassen et al., 2001b; Borel et al., 2002; Margolis et al., 2003; Storchova & Pellman, 2004; Zhivotovsky & Kroemer, 2004; Castedo et al., 2006) **(Figure 4.10)**. It has been previously suggested that overexpressed BCL-2 inhibits apoptosis after a failed cell division, resulting in the generation of tetraploid/polyploid cells with enhanced survival, while it can also favour multipolar and asymmetric divisions of tetraploid cells, which leads to aneuploidy and numerical chromosomal instability **(Figure 4.10)** (Minn et al., 1996; Nelson et al., 2004; Zhivotovsky & Kroemer, 2004; Castedo et al., 2006).

Thus, in order to check if this 'tetraploidy checkpoint' is functional in the p53 wild-type-GLI2ΔN expressing N/TERT keratinocytes, and to further investigate the cause of the cell cycle effects presented, the protein levels of the anti-apoptotic protein BCL-2 (Bcl-2), which has been shown to be direct target of GLI2ΔN in HaCaT keratinocytes (Regl et al., 2004b), were examined. In addition, the levels of p53 which has been observed to be partially responsible for the limited life-span of polyploid cells, were examined. Next, the protein levels of p21$^{WAF1/CIP1}$ (p21) cyclin dependent kinase (CDK) inhibitor – a direct transcriptional target of p53 (el-Deiry et al., 1994) – were investigated in order to look further into the control of G1 phase of these cells. N/TERT, SINCE and SINEG2 whole protein lysates **(Chapter 2, Section 2.12.1)** were

immunoblotted **(Chapter 2, Section 2.12.5)** against anti-p53, anti-Bcl-2 and anti-$p21^{WAF1/CIP1}$ antibodies, while β-actin was used as a loading control **(Figure 4.11)**.

Bcl-2 protein was massively up-regulated in SINEG2 cell line, which could explain the apoptotic resistance/survival of tetraploid/polyploid populations, especially in the absence of p53 checkpoint activation. Indeed, there was no detection of p53 protein stabilisation in SINEG2 cells compared to SINCE and wild-type N/TERT cells. However, $p21^{WAF1/CIP1}$ protein was almost absent from GLI2ΔN expressing cells, indicating abnormal G1 checkpoint control, and the ability of GLI2ΔN to downregulate indirectly $p21^{WAF1/CIP1}$ in a p53-independent manner. In addition, $p21^{WAF1/CIP1}$ protein plays a pivotal role in centrosome overduplication (Duensing et al., 2006) and in preventing endoreduplication and tetraploidisation (Stewart et al., 1999), and thus its downregulation could explain the occurrence and maintenance of a high percentage of tetraploid/polyploid cells in SINEG2 culture. The experiment was repeated three separate times giving identical results, clearly suggesting that the 'teraploidy checkpoint' is not functional in GLI2ΔN-expressing cells.

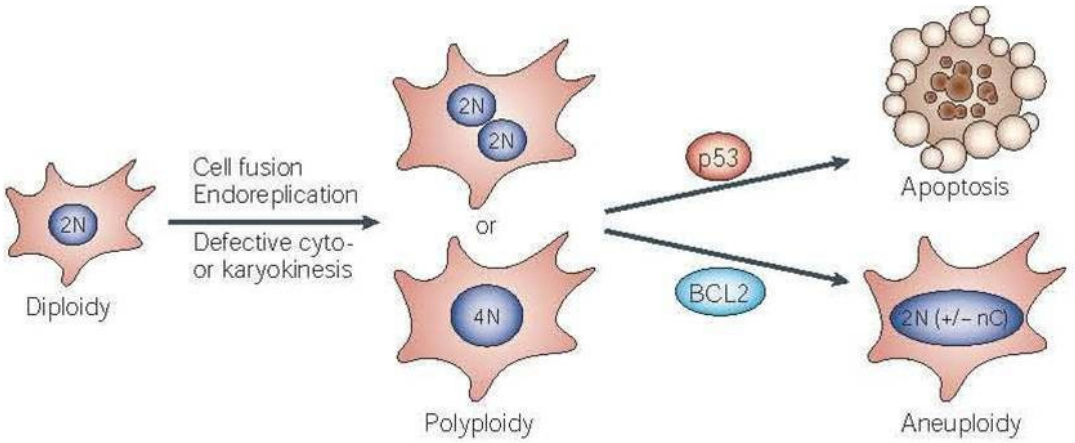

Figure 4.10: The fate of tetraploid/polyploid cells.

Tetraploid/polyploid cells normally undergo apoptosis, following the activation of a p53/p21$^{WAF1/CIP1}$-dependent checkpoint. In the presence of an anti-apoptotic factor, such as BCL-2 and due to its overexpression, there is inhibition of apoptosis, which favours multipolar and asymmetric divisions and therefore results in aneuploidy and numerical chromosomal instability. nC is the number of chromosomes (Zhivotovsky & Kroemer, 2004).

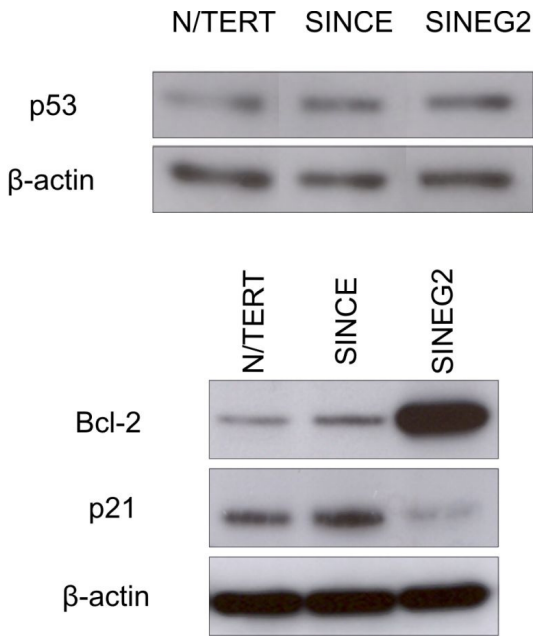

Figure 4.11: Dysfunctional 'tetraploidy checkpoint' in GLI2ΔN-expressing human keratinocytes.

Immunoblotting analysis for p53 (~ 53 kDa), Bcl-2 (~ 26 kDa), and $p21^{WAF1/CIP1}$ (~ 21 kDa) proteins, on N/TERT, SINCE, SINEG2 whole cell lysates. β-actin (~ 42 kDa), was used as loading control. SINEG2 cells show similar levels of p53 protein compared to N/TERT and SINCE, a remarkable increase of the anti-apoptotic Bcl-2 protein, and a significant decrease of the CDK inhibitor $p21^{WAF1/CIP1}$ protein levels.

4.2.3 GLI2ΔN downregulates $p21^{WAF1/CIP1}$ in a p53-independent manner

In response to a range of stresses, including oncogene overexpression and DNA damage, p53 becomes stabilised and activated, followed by activation of its targets and causing cells to undergo either cell cycle arrest and/or apoptosis (Vousden & Lu, 2002; Brown & Attardi, 2005).

Thus, the tumour suppressor p53 and its direct transcriptional target, $p21^{WAF1/CIP1}$, have been found to be primarily associated with both DNA damage checkpoints (G1/S and G2/M checkpoints), and to act as a backup mechanism in the mitotic checkpoint control, by inducing cell cycle arrest and/or apoptosis, preventing the survival of tetraploid cells yielded from defects during mitosis **(see Chapter 1, Section 1.3.7.1 and Chapter 4, Section 4.2.2)** (Kuerbitz et al., 1992; el-Deiry et al., 1994; Brugarolas et al., 1995; Cross et al., 1995; Minn et al., 1996; Bunz et al., 1998; Khan & Wahl, 1998; Lanni & Jacks, 1998; Wang et al., 1998; Chehab et al., 1999; Andreassen et al., 2001a; Andreassen et al., 2001b; Taylor & Stark, 2001; Borel et al., 2002; Margolis et al., 2003; Sherr, 2004; Castedo et al., 2006). Inactivation of checkpoint genes can result in gene mutations, chromosome damage, ploidy abnormalities, defective apoptosis, all of which can contribute to genomic instability and carcinogenesis (Paulovich et al., 1997; Lengauer et al., 1998; Stewart et al., 1999; Nowak et al., 2002; Zhivotovsky & Kroemer, 2004; Jefford & Irminger-Finger, 2006; Lobrich & Jeggo, 2007).

Since p53 protein levels were unchanged in the presence of tetraploid populations in GLI2ΔN-expressing keratinocytes **(Figure 4.11)**, it was investigated whether non-mutated p53 could still be normally activated by other stimuli, such as UVB (solar ultraviolet B radiation)-induced DNA damage (Maltzman & Czyzyk, 1984; Cox & Lane, 1995; Maccubbin et al., 1995). UV (ultraviolet) light (UVB irradiation, 280-320 nm) is known to induce immunosuppression and DNA breaks and local DNA damages in exposed cells (skin keratinocytes) (Brash & Haseltine, 1982; Grossman & Leffell, 1997; Soehnge et al., 1997; Lodish et al., 1999a; Erb et al., 2005; Erb et al., 2008). However, the cells including skin cells have important mechanisms to protect them against genomic instability and subsequent tumour formation due to persistent DNA damage, in which p53 tumour suppressor and its targets play a critical role (anti-cancer activity) (Soehnge et al., 1997). p53 nuclear phosphoprotein, known as the 'guardian of

the genome' is stabilised and activated after DNA damage, and induces arrest in cell proliferation at the G1/S and G2/M phases, through the activation of cyclin-dependent kinase inhibitors, such as p21 $^{WAF1/CIP1}$ and 14-3-3σ, in order to provide sufficient time for DNA damage repair (Levine et al., 1991a; Lane, 1992; Levine, 1997; Vousden & Lu, 2002; Lobrich & Jeggo, 2007). Cyclin-dependent kinases (CDKs), along with their cyclin partners, are responsible for the transitions of the eukaryotic cell cycle and are positive regulators that facilitate cell cycle progression (Cox & Lane, 1995; Sherr & Roberts, 1995; Taylor & Stark, 2001; Lobrich & Jeggo, 2007). Both p21 $^{WAF1/CIP1}$ and 14-3-3σ, direct transcriptional targets of p53, are cyclin-dependent kinase inhibitors (CKIs) (negative regulators of cell cycle), which bind and inhibit kinase activity of various cyclin/cyclin-dependent kinase complexes and thus stop either G1/S or G2/M cell cycle progression after DNA damage (Gu et al., 1993; Harper et al., 1993; Xiong et al., 1993; el-Deiry et al., 1994; Cox & Lane, 1995; Hermeking et al., 1997; Chan et al., 1999b; Laronga et al., 2000; Taylor & Stark, 2001; Lobrich & Jeggo, 2007). If DNA repair is not possible, then the DNA damaged cells are eliminated through apoptosis under the control of p53 gene (Levine et al., 1991a; Levine, 1997; Ashkenazi, 2002; Vousden & Lu, 2002; Zhivotovsky & Kroemer, 2004; Brown & Attardi, 2005; Erb et al., 2008; Taylor et al., 2008).

Therefore the protein levels of p53 and the levels of its downstream direct target, p21$^{WAF1/CIP1}$, were also examined after UVB treatment, in order to further investigate if the downregulation of p21$^{WAF1/CIP1}$ upon GLI2ΔN induction, is p53-independent, as observed in **Section 4.2.2**.

SINCE and SINEG2 cells were either mock treated **(-)** or exposed to UVB irradiation (10 mJ/cm^2) **(+) (Chapter 2, Section 2.13)**, 48 hours (~ 65% confluent) after plating. Cells were harvested 24 hours after UVB irradiation, and whole protein lysates **(Chapter 2, Section 2.12.2)** were immunoblotted **(Chapter 2, Section 2.12.5)** against anti-p53 and anti-p21 antibodies, while β-actin was used as a loading control **(Figure 4.12)**. Although p53 was upregulated upon UVB treatment both in SINEG2 and SINCE control cells, p21$^{WAF1/CIP1}$ was only upregulated in control cells, but not in GLI2ΔN expressing keratinocytes. This observation clearly suggests that (a) p53 is functional and is induced by UVB-mediated DNA damage in both SINCE and SINEG2 cells, but not in the presence of tetraploid cells, and that (b) p53-mediated induction of p21$^{WAF1/CIP1}$

after UVB irradiation is only functional in SINCE control cells and not in GLI2ΔN-expressing cells. This further confirms that the downregulation of $p21^{WAF1/CIP1}$ by GLI2ΔN induction, occurs in a p53-independent manner, not only in the presence of tetraploid cells, but also in response to UVB-induced DNA damage.

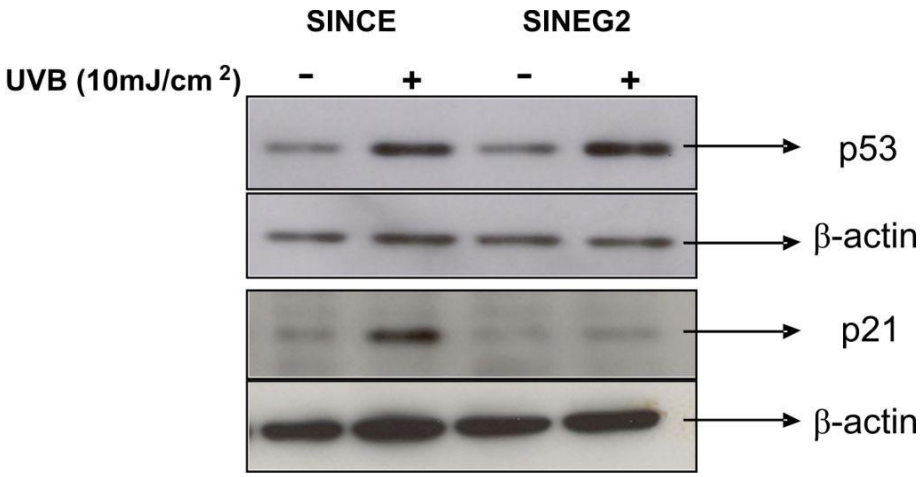

Figure 4.12: GLI2ΔN-mediated p21 downregulation is p53 independent in UVB treated cells.

Immunoblotting analysis for p53 and p21 proteins on UV (+) and non-UV (-) SINCE and SINEG2 whole cell lysates. β-actin was used as loading control. p53 protein is upregulated both in SINCE control and in SINEG2 cells upon UVB exposure, while p21 is only increased in control cells and not in GLI2ΔN-expressing cells after UVB-induced DNA damage.

4.2.4 $p21^{WAF1/CIP1}$ expression in human BCCs

The data presented here **(see Chapter 3, Section 3.2.1.4)**, as well as in previous studies, suggest that the overexpression of GLI2ΔN in cultured human epidermal keratinocytes can induce expression patterns that are very similar to those observed in human BCC tumours *in vivo*. In addition to showing increased and suppressed BCL-2 and c-MYC expressions respectively **(Chapter 3, Section 3.2.1.4, Figure 3.5)**, SINEG2 keratinocytes showed a remarkable suppression in $p21^{WAF1/CIP1}$ protein levels **(Figure 4.11 and Figure 4.12)**. Therefore, it was investigated whether this *in vitro* finding was physiologically relevant to the *in vivo* situation in human BCC tumours, since GLI2 and BCL-2 have already been shown to be co-expressed in human BCCs (Regl et al., 2004b), and c-MYC to be largely downregulated (Bonifas et al., 2001; Regl et al., 2002; O'Driscoll et al., 2006; Asplund et al., 2008).

Thus, the protein expression levels of $p21^{WAF1/CIP1}$ (p21) were examined in a cohort of 16 patients' tissue samples comprising normal skin epithelium, and tissues derived from diverse human BCC subtypes, including nodular, superficial, infiltrative and morpheaform. Tissue processing and immunohistochemistry were performed by Dr Mohammed Ikram at the Pathology Department of the Institute of Cancer, Barts and the London School of Medicine and Dentistry, Charterhouse square, London, UK **(see Chapter 2, Section 2.18)**.

The expression of $p21^{WAF1/CIP1}$ (p21) in normal epidermis showed a diffuse pattern with p21 protein being mainly detected in the non-proliferating suprabasal layers of the epithelium with very few positive stained cells in the basal layer **(Figure 4.13A)**. In contrast, $p21^{WAF1/CIP1}$ (p21) was largely absent from human BCC tumour islands in all the three different subtypes, with the exception of individual positively stained cells **(Figure 4.13B, C, D)**. The clear downregulation of p21 was even more evident in superficial BCCs, where p21 expression is suddenly lost in the developing tumour, when compared to the immediately adjacent normal epithelium **(Figure 4.13C)**, suggesting that p21 is massively downregulated in tumour cells. Overall, these data show that GLI2ΔN-mediated p21 downregulation *in vitro*, absolutely correlates with the p21 expression pattern in human BCCs *in vivo*.

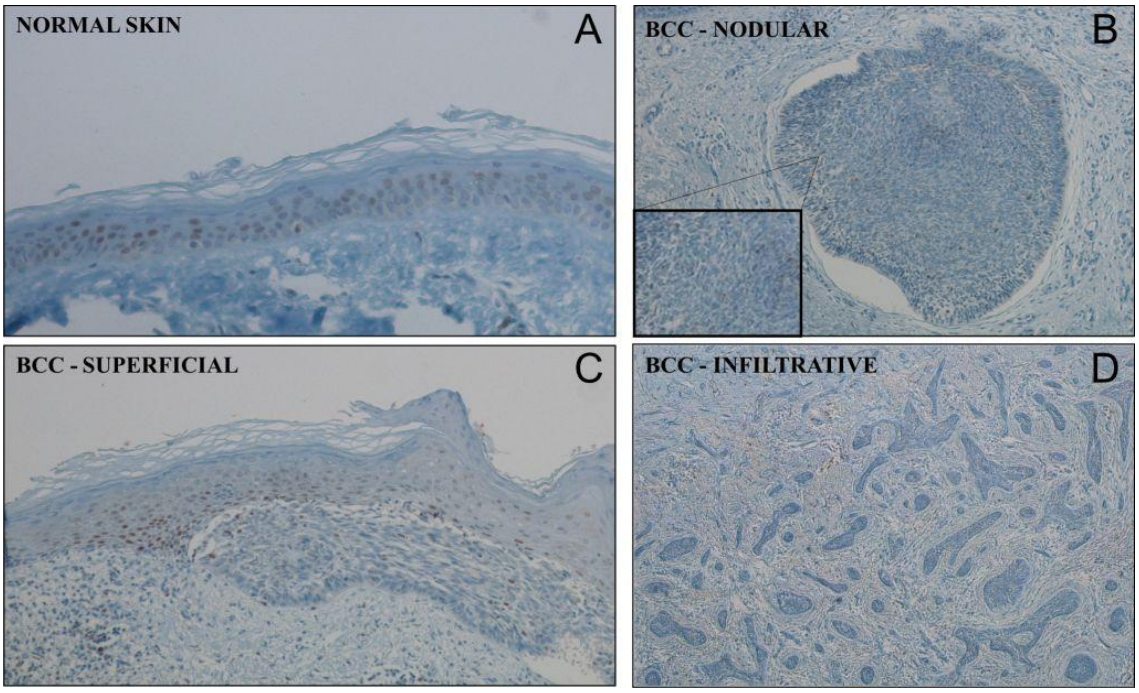

Figure 4.13: $p21^{WAF1/CIP1}$ is almost absent in human BCCs.

Representative pictures from the immunohistochemistry for $p21^{WAF1/CIP1}$ protein on a panel of formalin fixed, paraffin embedded **(A)** normal human skin, **(B)** nodular human BCC, **(B inset)** magnified region of nodular BCC, **(C)** superficial human BCC and **(D)** infiltrative human BCC, showing the clear downregulation of $p21^{WAF1/CIP1}$ in human BCC tumours, compared both to normal control skin **(A)** and to normal epidermis adjacent to the BCC tumour **(C)**.

4.2.5 GLI2ΔN expressing cells are resistant to UVB-induced apoptosis

Apoptosis, as I mentioned in **Section 4.2.1.2**, is a normal physiologic process, which occurs during embryonic development, as well as in maintenance of tissue homeostasis (Taylor et al., 2008), while its deregulation (inactivation) leads to a variety of human pathologies, including cancer (Hanahan & Weinberg, 2000; Igney & Krammer, 2002; Brown & Attardi, 2005). Apoptosis can be mediated either by intrinsic or extrinsic pathways, depending on the origin of death stimuli, while cross-talk between them is possible. The intrinsic pathway is mediated by mitochondria, and is triggered in response to an oncogene, defective cell cycle, and/or DNA damage (death stimuli that are generated from within the cell), whereby the extrinsic pathway is mediated by the binding of an extracellular death ligand (i.e. FASL) to its cell-surface death receptor (i.e. FAS) **(Figure 4.17)** (Ashkenazi, 2002; Green & Kroemer, 2004; Riedl & Shi, 2004; Green, 2005; Taylor et al., 2008).

Since there was no activation of apoptosis upon GLI2ΔN oncogene induction (oncogenic stress), which was followed by subsequent tetraploidy and polyploidy formation (abortive cell cycle) **(Figure 4.3 and Figure 4.11)**, I checked if GLI2ΔN-expressing keratinocytes are also resistant in another stimulus, which also causes p53-mediated apoptosis, such as UV light (UVB treatment) (Levine, 1997). Ultraviolet (UV) radiation is the carcinogenic factor in sunlight (Soehnge et al., 1997). Although, together solar ultraviolet B (UVB, 280-320nm) irradiation with solar ultraviolet A (UVA, 320-400nm) irradiation can initiate transformation of skin epidermal cells and accelerate carcinogenesis, UVA has been shown to be less effective than UVB, concerning the transforming potential (less carcinogenic) (Grossman & Leffell, 1997; Soehnge et al., 1997; Erb et al., 2008). Thus, UVB irradiation is known to be one of the main risk and etiological factors in human skin BCC formation, since the most frequent mutations found in particular genes in human BCCs, have the 'UV signature' of UV-light mediated mutations (Grossman & Leffell, 1997; Soehnge et al., 1997; Brash & Ponten, 1998; Armstrong & Kricker, 2001; de Gruijl et al., 2001; Ehrhart et al., 2003). These specific mutations in DNA, are consistently associated with UV radiation, and are characterised by C (cytosine) to T (thymine) or CC to TT transitions at dipyrimidine sites, induced by UVB-radiation (Brash & Haseltine, 1982; Grossman & Leffell, 1997). Therefore, these C to T transition mutations serve as molecular fingerprints for DNA

damaged by UVB, and are found in the two genes that are most correlated with human BCC development, the p53 and PTCH genes (Grossman & Leffell, 1997; Soehnge et al., 1997; Brash & Ponten, 1998; de Gruijl et al., 2001; Ling et al., 2001; Dicker et al., 2002; Lacour, 2002; Daya-Grosjean & Couve-Privat, 2005; Reifenberger et al., 2005; Epstein, 2008). UVB irradiation is known to be responsible for a 65-75% of p53 mutations and a 40-50% of PTCH mutations in human sporadic BCCs (Demirkan et al., 2000; Lacour, 2002; Bolshakov et al., 2003; Daya-Grosjean & Couve-Privat, 2005; Reifenberger et al., 2005). The importance of p53 inactivation in skin carcinogenesis is highlighted by the fact that homozygous or heterozygous p53 knockout mice develop skin tumours much earlier than wild-type mice upon UV radiation (Jiang et al., 1999; Erb et al., 2005).

In my system (N/TERT keratinocytes), the p53/p21$^{WAF1/CIP1}$ pathway is functional and not mutated contrarily to other keratinocyte cell lines such as HaCaT (Boukamp et al., 1988; Lehman et al., 1993; Dickson et al., 2000; Rheinwald et al., 2002). Thus, p53 was shown to be upregulated upon UVB-induction both in GLI2ΔN-expressing and control keratinocytes **(Figure 4.12)**. On the other hand, p21$^{WAF1/CIP1}$ was only upregulated in the control cells after UVB-induction **(Figure 4.12)**, while it was downregulated before **(Figure 4.11)** and after **(Figure 4.12)** UVB treatment in SINEG2 cells, compared to the control cells, indicating a defective cell cycle/growth arrest that prevents the UVB-DNA damaged SINEG2 cells to be repaired (uncontrolled cell proliferation). At the same time, BCL-2 (anti-apoptotic factor, antagonist of p53-mediated apoptosis) was found to be highly upregulated before **(Figure 4.11)** and after **(Figure 4.18)** UVB treatment in GLI2ΔN-expressing keratinocytes compared to the controls, suggesting also a defective apoptosis procedure in the non-repaired UVB-DNA damaged SINEG2 keratinocytes (loss of apoptosis). Thus, I checked if GLI2ΔN-expressing cells are resistant not only in cell cycle failure-mediated apoptosis as observed in **Figure 4.3**, but also in UVB-mediated apoptosis, which would be consistent with the resistance in apoptosis, mediated by intrinsic or extrinsic pathways, of human BCCs (Regl et al., 2004b; Erb et al., 2005; Erb et al., 2008; Kump et al., 2008). Three different apoptotic assays were carried out for this purpose including (i) PI staining, (ii) Annexin V staining, both of which were followed by flow cytometry analysis, and (iii) detection of caspase-3 activation.

4.2.5.1 PI staining in UV and non-UV SINEG2 keratinocytes

Propidium iodide (PI) staining in permeabilised cells facilitates the discrimination of cells with reduced DNA content, due to DNA fragmentation (sub-G1 populations). When cells are permeabilised, the apoptosis-mediated fragmented DNA multimers leak out of the cell, and therefore the resulting stained by propidium iodide sub-G1 populations, represent late apoptotic/dead cells (cells with fragmented DNA), and thus used for detection of later stages of apoptosis (Riccardi & Nicoletti, 2006).

Equal number of SINCE and SINEG2 cells were seeded and were either mock treated **(-)** or exposed to UVB irradiation (10 mJ/cm^2) **(+) (see Chapter 2, Section 2.13)**, 72 hours (~ 65% confluent) after plating. Cells were harvested 24 hours after UVB irradiation, and stained with propidium iodide, followed by flow cytometry analysis in order to detect cells with sub-G1 content **(see Chapter 2, Section 2.8.1.4) (Figure 4.14)**. Results clearly show that SINCE control keratinocytes showed increased apoptosis/death in response to UVB (10 mJ/cm^2) **(+)** (7.1%) **(Figure 4.14 ii)**, compared to mock treated SINCE cells (0.40%) **(Figure 4.14 i)**, as evidenced by the marked increase in the percentage of sub-G1 populations (P3). Contrarily, in response to the same dose of UVB irradiation (10 mJ/cm^2), SINEG2 keratinocytes displayed only a marginal increase in the percentage of sub-G1 (P3) keratinocytes **(+)** (2.7%) **(Figure 4.14 iv)**, compared to the mock treated SINEG2 cells **(-)** (0.2%) **(Figure 4.14 iii)**, suggesting a resistance of GLI2ΔN-expressing keratinocytes in late UVB-mediated apoptosis and cell death.

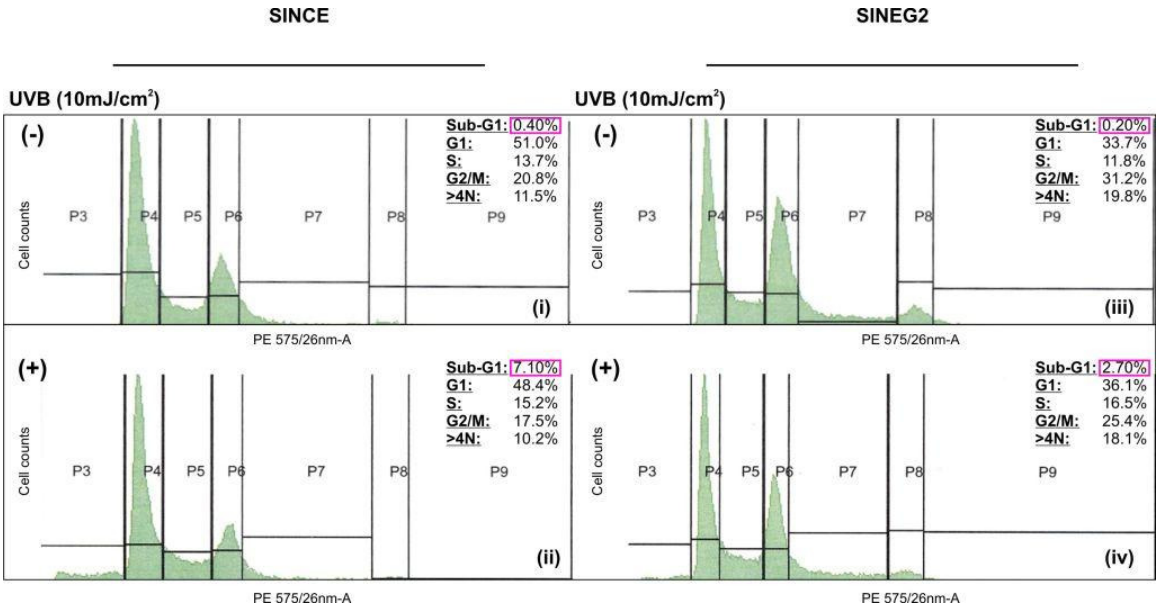

Figure 4.14: Induction of GLI2ΔN protects against UVB-induced apoptosis and cell death.

SINCE **(i, ii)** and SINEG2 **(iii, iv)** keratinocytes were either mock treated (-), or UVB irradiated (10 mJ/cm^2) (+), and were allowed to grow for 24 hours prior to staining with propidium iodide and flow cytometry analysis. SINCE keratinocytes **(ii)** showed increased apoptosis/death in response to UVB (10 mJ/cm^2) (+), as evidenced by the marked increase in the percentage of sub-G1 populations (P3). In contrast, SINEG2 keratinocytes **(iv)** displayed a marginal increase in the percentage of sub-G1 (P3) keratinocytes in response to the same dose of UVB irradiation, suggesting a resistance of GLI2ΔN-expressing cells to apoptosis and cell death.

4.2.5.2 Annexin V staining in UV and non-UV SINEG2 keratinocytes

Annexin V staining is used to identify apoptosis at an earlier stage (early apoptotic marker) (Vermes et al., 1995), compared to assays based on nuclear changes (DNA fragmentation) such as propidium iodide staining **(see Chapter 2, Section 2.8.1.5 and Chapter 4, Section 4.2.1.2)**. DAPI (Kubista et al., 1987; Barcellona et al., 1990) is also used for staining along with Annexin V in order to discriminate late apoptotic or dead cells which have lost membrane integrity, from early apoptotic cells which still have intact membranes, by dye exclusion. Two different doses of UVB radiation were used (10 mJ/cm^2 and 30 mJ/cm^2) **(see Chapter 2, Section 2.13)**, in order to check if the resistance observed in SINEG2 cells in UVB 10 mJ/cm^2-mediated apoptosis **(Figure 4.14)** is also retained in higher doses of UVB irradiation (30 mJ/cm^2).

Firstly, in order to check if the assay is functional in wild-type N/TERT keratinocytes, N/TERT keratinocytes were seeded, were mock treated (no UVB) 24 hr after plating and were allowed to grow for another 24 hours. Cells were analysed by flow cytometry (non-stained) in order to obtain values of background fluorescence **(Figure 4.15 i)**. Then, mock, no UVB-treated (0 mJ/cm^2) N/TERT cells were stained with DAPI and Cy^{TM}5 Annexin V antibody prior to flow cytometry analysis and based on background fluorescence values, keratinocyte populations were further distributed into live (Q3) DAPI (-) Annexin V (-), early apoptotic (Q4) DAPI (-) Annexin V (+), late apoptotic/dead (Q2) DAPI (+) Annexin V (+), and dead (Q1) DAPI (+) Annexin V (-) cells **(Figure 4.15 ii)**. Next, two different UVB doses were used in order to verify that the percentage of early apoptotic cells is proportionally increased along with the UVB dose **(Figure 4.15 iii, iv)**. N/TERT keratinocytes were irradiated with UVB (10 mJ/cm^2) 24 hr after plating and were allowed to grow for 24 hours prior to staining with DAPI and Cy^{TM}5 Annexin V for flow cytometry analysis. A clear apoptotic response can be seen in UVB irradiated keratinocytes as evidenced by the increase of early apoptotic (6.0%) populations **(Figure 4.15 iii)**. N/TERT keratinocytes were also irradiated with UVB (30 mJ/cm^2) 24 hr after plating and were allowed to grow for 24 hours prior to staining with DAPI and Cy^{TM}5 Annexin V for flow cytometry analysis. The apoptotic response of N/TERT keratinocytes is further enhanced, as evidenced by significant increases in early apoptotic (11.8%), as well as in late apoptotic/dead (5.5%) keratinocyte populations **(Figure 4.15 iv)**.

Secondly, equal number of N/TERT, SINCE and SINEG2 cells were seeded and were either mock treated (0 mJ/cm^2) or exposed to UVB irradiation (10 mJ/cm^2 and 30 mJ/cm^2), 24 hours (~ 65% confluent) after plating. Cells were harvested 24 hours after UVB irradiation, and stained with both DAPI and Cy^{TM}5 Annexin V antibody, followed by flow cytometry analysis resulting in the discrimination of early apoptotic DAPI (-) Annexin (+) and late apoptotic/dead DAPI (+) Annexin (+) populations **(Figure 4.16)**. Results show that SINEG2 keratinocytes display a reduction in the percentage of early apoptotic and late apoptotic/dead cells not only in response to low (10 mJ/cm^2), but also to high (30 mJ/cm^2) doses of UVB irradiation (~ 9% early apoptotic cells), compared to both N/TERT (~ 24% early apoptotic cells) and SINCE (~ 24% early apoptotic cells) control keratinocytes **(Figure 4.16)**.

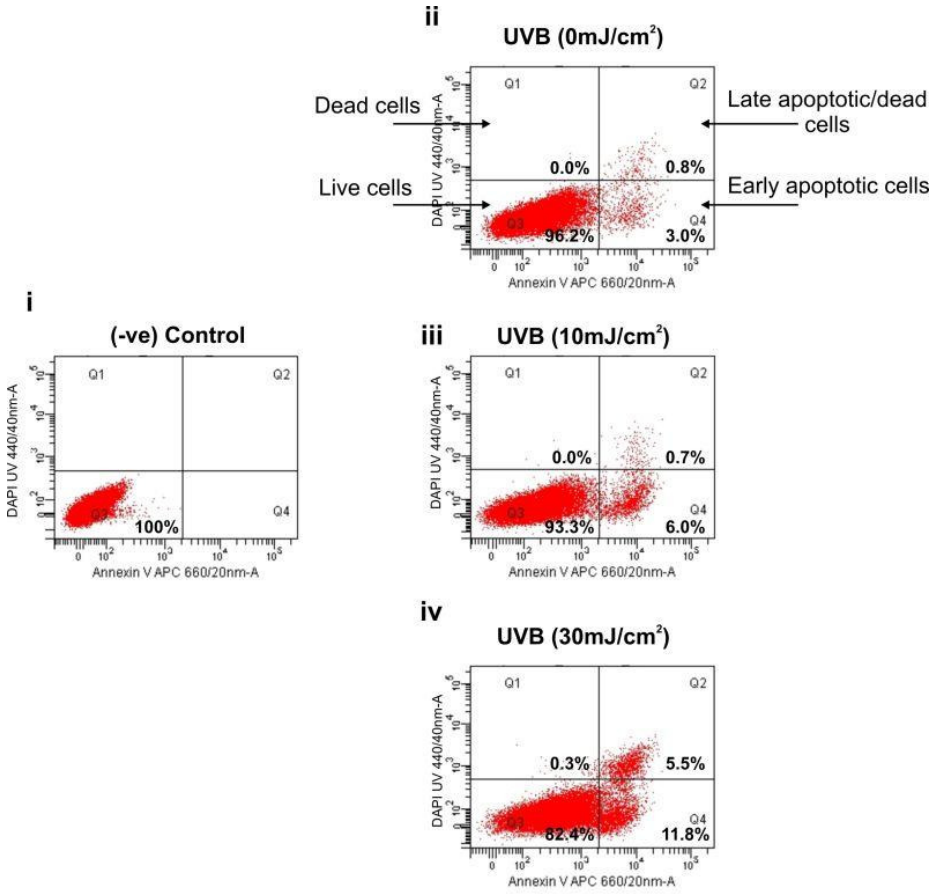

Figure 4.15: Cy™5 Annexin V staining in control and UVB-treated N/TERT keratinocytes.

(i) N/TERT keratinocytes were mock treated (no UVB) and were allowed to grow for 48 hours after plating. Cells were analysed by flow cytometry (non-stained) in order to obtain values of background fluorescence (x axis; APC/Annexin V, y axis; DAPI). **(ii)** Next, mock, no UVB-treated (0 mJ/cm^2) N/TERT cells were stained with DAPI and Cy™5 Annexin V antibody prior to flow cytometry analysis and based on background fluorescence values, keratinocyte populations were further distributed into live (Q3) DAPI (-) Annexin V (-), early apoptotic (Q4) DAPI (-) Annexin V (+), late apoptotic/dead (Q2) DAPI (+) Annexin V (+), and dead (Q1) DAPI (+) Annexin V (-) cells. **(iii)** N/TERT keratinocytes were irradiated with UVB (10 mJ/cm^2) 24 hr after plating and were allowed to grow for 24 hours prior to staining with DAPI and Cy™5 Annexin V antibody for flow cytometry analysis. A clear apoptotic response can be seen in UVB irradiated keratinocytes as evidenced by the increase of early apoptotic populations. **(iv)** N/TERT keratinocytes were irradiated with UVB (30 mJ/cm^2) 24 hr after plating and were allowed to grow for 24 hours prior to staining with DAPI and Cy™5 Annexin V for flow cytometry analysis. The apoptotic response of N/TERT keratinocytes is further enhanced, as evidenced by significant increases in early apoptotic, as well as in and late apoptotic/dead keratinocyte populations.

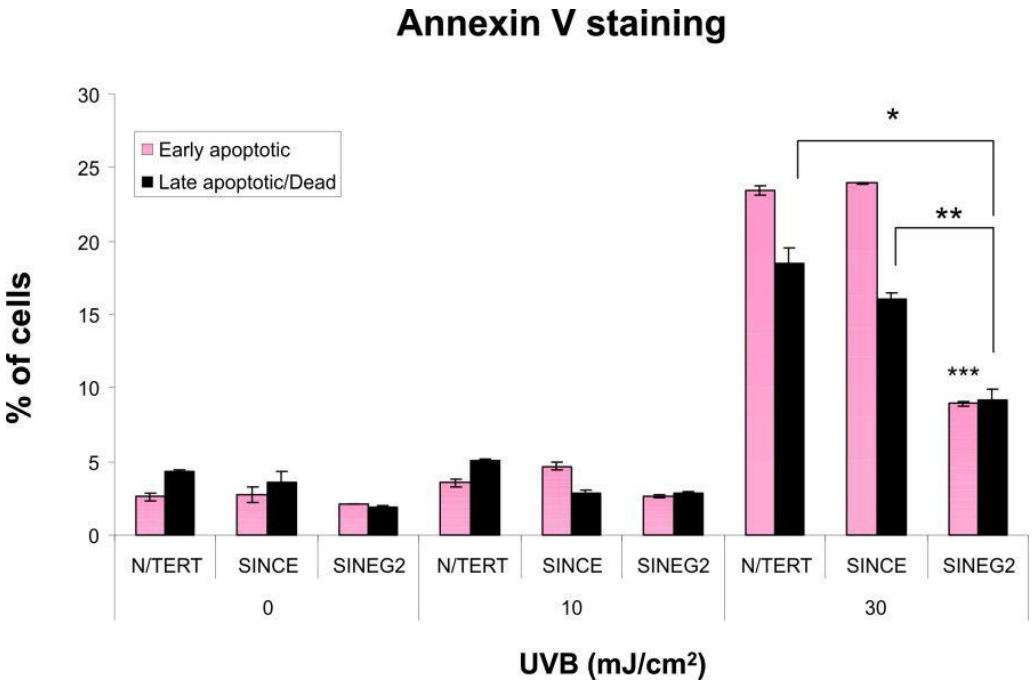

Figure 4.16: GLI2ΔN-expressing cells are resistant in apoptosis mediated by high doses of UVB.

N/TERT, SINCE, and SINEG2 keratinocytes were either mock treated (0 mJ/cm^2), or UVB irradiated with 10 or 30 mJ/cm^2. Cells were allowed to grow for 24 hours prior to harvesting and staining with both DAPI and Cy^{TM}5 Annexin V antibody for the discrimination of early apoptotic (DAPI (-) Annexin V (+)) and late apoptotic/dead (DAPI (+) Annexin V (+) and DAPI (+) Annexin V (-)) populations. SINEG2 keratinocytes display a reduction in the percentage of early and late apoptotic/dead populations in response to low and high dose of UVB irradiation (10 and 30 mJ/cm^2) compared to both N/TERT and SINCE control keratinocytes. Each bar represents the mean values ± s.e.m of duplicate samples. * *P≤0.05*, ** *P≤0.01*, *** *P≤0.001*.

4.2.5.3 Reduced Caspase-3 activation in SINEG2 keratinocytes

Caspases (Cysteine aspartic acid proteases) are a conserved family of enzymes that control all steps of apoptosis either mediated by the intrinsic or the extrinsic pathway **(Figure 4.17)**, by initiating and executing the intracellular cascade of events that result in protein and nucleic acid cleavage and ultimately, in the irreversible commitment of a cell to die (Riedl & Shi, 2004; Taylor et al., 2008). Caspases are produced in every cell as inactive precursors called procaspases, and must undergo proteolytic activation during apoptosis by specific initiation mechanisms including (i) exposure to another activated caspase, (ii) autocatalysis, or (iii) association with an activator protein such as Apaf-1 (apoptotic-protease-activating factor-1) and cytochrome c (Hengartner, 2000; Riedl & Shi, 2004). The apoptotic caspases can be divided into two types: the 'initiator' caspases (i.e. caspase-2, -8, -9 and -10) and the 'effector' or 'executioner' caspases (i.e. caspase-3, -6 and -7). The initiator caspases are auto-activated (self-cleavage) and their activation is facilitated by specific activator proteins. Then, initiator caspases act by activating effector caspases through cleavage at specific internal Asp residues (Riedl & Shi, 2004). Once activated, the effector caspases, proteolytically cleave a broad set of target proteins, that are major components of the cytoskeleton and the nuclear envelope, play central role in the breakdown of nuclear DNA, and are involved in essential functions within the cell, all of which lead to cell death (Riedl & Shi, 2004; Taylor et al., 2008).

In order to further confirm the resistance of GLI2ΔN-expressing cells in UVB-induced apoptosis, the protein levels of Caspase-3, which is a critical executioner of apoptosis, were examined in SINEG2 and SINCE control cells. The reason for choosing caspase-3 instead of any other caspases is because the activation of the effector caspase-3 during apoptosis can be mediated both by the cell intrinsic pathway, of which BCL-2 is an antagonist and by the cell extrinsic pathway of which c-FLIP is an antagonist (**Figure 4.17)**.

The anti-apoptotic gene, BCL-2 (B-cell lymphoma 2) and its protein product, belongs to the BCL-2 superfamily consisting of proteins with pro-apoptotic (BAX, BAK, BID, NOXA, PUMA) and anti-apoptotic (BCL-2, BCL-X_L) activities, of which a dynamic equilibrium is necessary for the proper execution of apoptosis (Cory & Adams, 2002;

Youle & Strasser, 2008). BCL-2 membrane protein, is residing at the mitochondrial, nuclear and endoplasmic reticulum membranes, and is one of the major anti-apoptotic factor of the intrinsic pathway of apoptosis (p53-dependent apoptosis), while its overexpression inhibits cell death and contributes to tumour formation, including skin carcinogenesis (Vaux et al., 1988; Hockenbery et al., 1990; Hockenbery, 1995; Rodriguez-Villanueva et al., 1998; Jiang & Milner, 2003; Lessene et al., 2008; Youle & Strasser, 2008). In normal human epidermis, BCL-2 is exclusively expressed in the basal layer of the epidermis (Rodriguez-Villanueva et al., 1995; Delehedde et al., 1999), and is directly controlled by GLI1 in primary human keratinocytes (Bigelow et al., 2004). It has also been identified as a direct transcriptional target of GLI2 transcription factor (Regl et al., 2004b) and thus, consistent with this finding, BCL-2 was found to be upregulated in GLI2ΔN-expressing keratinocytes **(Chapter 3, Section 3.2.1.4, Figure 3.5A and Chapter 4, Section 4.2.2, Figure 4.11)**. In addition, BCL-2 undergoes an increase in expression in many cancers (Igney & Krammer, 2002; Lessene et al., 2008), including human BCCs (Rodriguez-Villanueva et al., 1995; Delehedde et al., 1999; Regl et al., 2004b).

c-FLIP (c (cellular)-FAS-associated death domain-like IL (interleukin)-1-converting enzyme-like inhibitory protein) is a protein-deficient caspase homolog, which in contrast to caspases lacks the key features that are required for the proteolytic activity of caspases and the subsequent substrate catalysis (Tschopp et al., 1998). c-FLIP is a cytoplasmic inhibitor of the extrinsic apoptotic pathway at the level of caspase-8, since it binds to FADD (FAS-associated death domain) and caspase-8, and thus prevents both the binding of caspase-8 to various death receptors and its activation (Irmler et al., 1997; Tschopp et al., 1998; Ashkenazi, 2002; Opferman, 2008). The ratio of c-FLIP to caspase-8 is critical for the assembly of the DISC (death-inducing signalling complex), and therefore for the balance between proliferation and apoptosis which is required for tissue homeostasis (Tschopp et al., 1998). Upregulation of c-FLIP has been associated with diverse hematologic cancer cell lines (Shain et al., 2002; Thomas et al., 2002), while high c-FLIP levels have been detected in certain tumour cell lines that are resistant to apoptosis mediated by death receptors (Hahne et al., 1996; Irmler et al., 1997), suggesting that abnormal regulation of c-FLIP expression may contribute to tumourigenesis (Tschopp et al., 1998). According to the latter, c-FLIP was found to be a direct target of GLI2, and to be highly expressed in human BCCs (Kump et al., 2008),

suggesting that c-FLIP induced by GLI2 is responsible for the resistance of BCCs to apoptosis mediated by the extrinsic pathway.

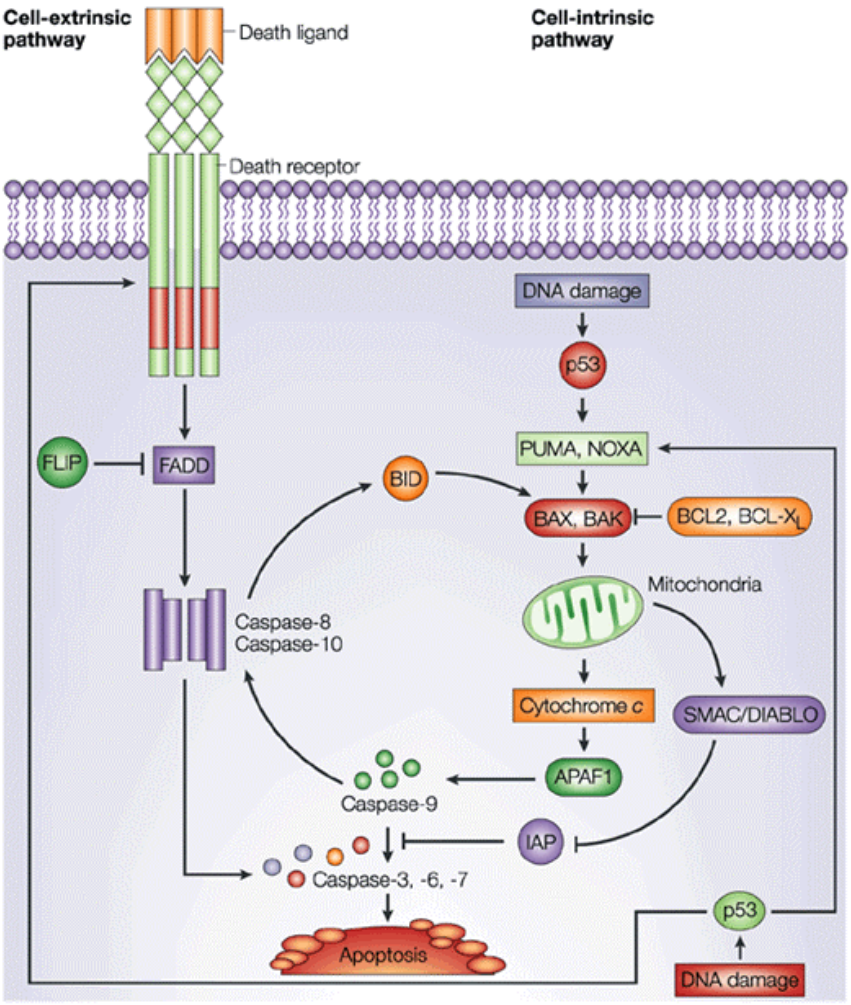

Figure 4.17: Apoptosis signalling pathways.

Apoptosis can be mediated either by the intrinsic or the extrinsic pathway, depending on the origin of the death stimulus. The intrinsic pathway, is p53-dependent, mediated by mitochondria, and is triggered in response to an oncogenic stress and/or DNA damage. In response to apoptotic stimuli, there is activation of pro-apoptotic proteins of the BCL-2 superfamily (PUMA, NOXA, BAX and BAK), which in turn cause the release of several proteins such as cytochrome c, SMAC (second mitochondria-derived activator of caspases) / DIABLO (direct inhibitor of apoptosis (IAP)-binding protein with low pI) from the intermembrane space of mitochondria, into the cytoplasm. Cytochrome c binds to and activates the APAF1 (apoptotic-protease-activating factor-1) protein in the cytoplasm that mediates the activation of the apoptosis-initiating protease caspase-9, which in turns cleaves and activates the executioner proteases caspase-3, -6, and 7. The extrinsic pathway is mediated by the binding of an extracellular death ligand to its cell-surface death receptor, which leads to the formation of a death-inducing signalling complex (DISC), that involves FADD (FAS-associated death domain) and caspase 8, -10, which then cleaves and activates the effector caspase-3, -6, -7. The extrinsic pathway can crosstalk to the intrinsic pathway through the caspase 8-mediated cleavage of BID (BCL-2 superfamily member), which then triggers the release of mitochondrial proteins. BCL-2 and its relative BCL-X_L are prosurvival proteins (anti-apoptotic) that antagonize intrinsic-pathway mediated apoptosis, and c-FLIP antagonizes death ligand/receptor-mediated apoptosis (Ashkenazi, 2002).

Therefore, in order to confirm the involvement of BCL-2 in the resistance of SINEG2 cells in UVB-mediated apoptosis and to check the levels of cleaved active caspase-3, equal number of SINCE and SINEG2 cells were seeded and were either mock **(-)** treated (0 mJ/cm^2) or exposed to UVB irradiation **(+)** (10 mJ/cm^2) **(see Chapter 2, Section 2.13)**, 24 hours (~ 65% confluent) after plating **(Figure 4.18B)**. SINCE and SINEG2 keratinocytes were harvested for total protein **(see Chapter 2, Section 2.12.2)**, 24 hr after UVB 10 mJ/cm^2 **(+)**, or mock **(-)** 0 mJ/cm^2 treatment. Total protein extracts were immunoblotted **(see Chapter 2, Section 2.12.5)** against anti-Bcl-2 (top panel) and anti-full length and cleaved Caspase-3 (middle panel) antibodies, while β-actin (bottom panel) was used as protein loading control **(Figure 4.18B)**. Normally, upon UVB treatment full length caspase-3 (~ 35 kDa) is proteolytically processed into a large fragment (~ 19 kDa) and a smaller one (~ 17 kDa) and then induces apoptosis. The absence of activated (cleaved) Caspase-3 and the high levels of Bcl-2 expression in SINEG2 cells following UVB-irradiation, compared to SINCE control cells, further confirm the resistance of SINEG2 keratinocytes to p53-mediated apoptosis, probably as a consequence of high BCL-2 expression directly induced by GLI2ΔN.

Due to the fact that caspase-3 protein is a late apoptotic marker compared to Annexin V protein, the same batch of cells was also checked for Annexin V protein levels **(Figure 4.18A)**. Equal number of SINCE and SINEG2 cells were seeded and were either mock treated (0 mJ/cm^2) or exposed to UVB irradiation (10 mJ/cm^2) **(see Chapter 2, Section 2.13)**, 24 hours (~ 65% confluent) after plating. Cells were harvested 24 hours after UVB irradiation, and stained with both DAPI and Annexin V antibody, followed by flow cytometry analysis **(see Chapter 2, Section 2.8.1.5)**, resulting in the discrimination of early apoptotic DAPI (-) Annexin (+) and late apoptotic/dead DAPI (+) Annexin (+) populations. Results show that SINEG2 keratinocytes display a reduction in the percentage of early apoptotic cells in response to UVB irradiation (~ 1.0% early apoptotic cells), compared to SINCE (~ 4.0% early apoptotic cells) control keratinocytes **(Figure 4.18A)**.

Overall, the results indicate that GLI2ΔN-expressing keratinocytes are resistant both in early **(Figure 4.18A)** and late **(Figure 4.18B)** UVB mediated apoptosis, and suggest that BCL-2 is central in apoptosis prevention by GLI2ΔN overexpression.

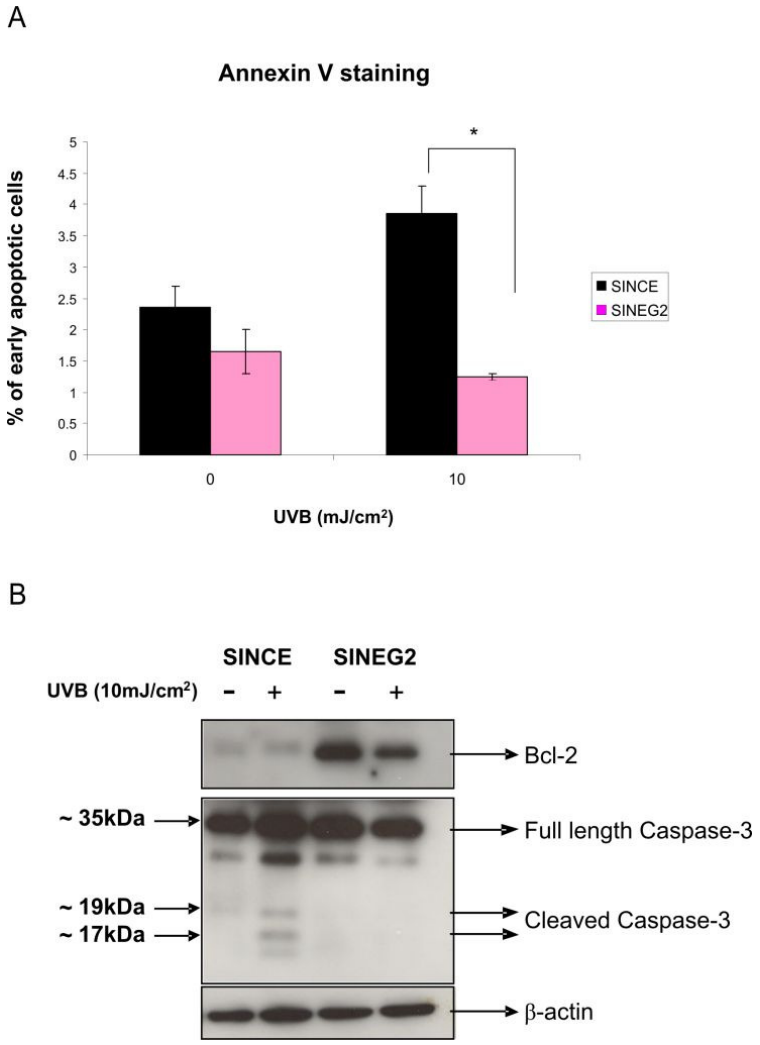

Figure 4.18: GLI2ΔN-expressing cells are resistant both in UVB-mediated early and late apoptosis.

(A) SINCE and SINEG2 keratinocytes were either mock (0 mJ/cm^2) or UVB (10 mJ/cm^2) treated. Cells were allowed to grow for 24 hr prior to staining with Annexin V and DAPI staining, for the discrimination of early apoptotic and late apoptotic/dead cells respectively. The results clearly indicate that SINEG2 cells are less susceptible to UVB-induced early apoptosis compared to SINCE control cells. Each bar represents mean values ± s.e.m of duplicate samples. * *P≤0.05*. **(B)** SINCE and SINEG2 keratinocytes were harvested for total protein, 24 hr after UVB 10 mJ/cm^2 (+), or mock (-) 0 mJ/cm^2 treatment. Total protein extracts were immunoblotted against anti-Bcl-2 (~ 26 kDa) (top panel) and anti-full length (~ 35 kDa) and cleaved Caspase-3 (~ 19, 17 kDa) (middle panel) antibodies. β-actin (bottom panel) was used as protein loading control. The absence of activated (cleaved) Caspase-3 in SINEG2 cells, a late apoptotic marker, following UVB-irradiation, further confirms the apoptotic resistance of SINEG2 keratinocytes compared to SINCE cells.

4.2.6 GLI2ΔN induces numerical and structural chromosomal instability as revealed by 24 colour FISH karyotyping analysis

Cancer is a complex disease, with multiple genes in diverse pathways involved in its initiation, progression, invasion and metastasis (Jefford & Irminger-Finger, 2006). In fact, it is widely accepted that the sequential accumulation of mutations that activate oncogenes and disrupt tumour suppressor genes, combined with multiple cycles of clonal selection and evolution facilitate the process of carcinogenesis (Nowell, 1976; Cahill et al., 1999; Hanahan & Weinberg, 2000; Jefford & Irminger-Finger, 2006). One of the hallmarks of cancer is genetic/genomic instability and is reflected in the heterogeneity seen within individual tumours and among tumours of the same type (Cahill et al., 1999; Hanahan & Weinberg, 2000; Mitelman et al., 2003). Genomic instability refers to a set of events capable of causing unscheduled alterations either of a temporary or permanent nature within the genome (Jefford & Irminger-Finger, 2006). Thus, genomic instability is the failure to transmit an accurate copy of the entire genome from one cell to its two daughter cells (Zhivotovsky & Kroemer, 2004). Although it has been debated for years if genomic instability is a cause or a consequence of tumourigenesis, it now appears that genomic instability not only possibly drives tumourigenesis, but is at least a factor in tumour progression by generating mutations in oncogenes and tumour suppressor genes (Cahill et al., 1999; Nowak et al., 2002; Jefford & Irminger-Finger, 2006; Halazonetis et al., 2008; Negrini et al., 2010). Spontaneous mutations happen once every hundred thousand cell divisions and cancers initially were thought to develop, because cells acquire a discrete small number of key mutations. However, recent findings by large scale sequencing projects in many different types of human cancers and cancer cell lines, show that most tumours harbour much more mutations responsible for tumourigenesis, than initially thought, further supporting the existence of genomic instability, which might facilitate and drive tumour development by increasing the spontaneous mutation rate (Sjoblom et al., 2006; Storchova & Kuffer, 2008; Negrini et al., 2010).

Genomic instability can be divided into two major groups; instability occurring at the chromosomal level (CIN-chromosomal instability), and at the nucleotide level (MSI-microsatellite instability) (Zhivotovsky & Kroemer, 2004; Jefford & Irminger-Finger, 2006). Instability at the nucleotide level occurs due to faulty DNA repair pathways such

as base excision repair and nucleotide excision repair, and includes instability of microsatellite repeat sequences (MSI) caused by defects in the mismatch repair pathway due to mutations in, or silencing of, DNA-mismatch-repair genes (Lengauer et al., 1998; Zhivotovsky & Kroemer, 2004; Jefford & Irminger-Finger, 2006). Chromosomal instability (CIN), defines the existence of accelerated rate of chromosomal alterations, and it can be classified into (i) structural chromosomal instability - inversions, deletions, amplifications, duplications, and translocations of chromosomal segments that arise from breaks in DNA and defects in the repair mechanisms including homologous and non-homologous end joining, and (ii) numerical chromosomal instability - gains or losses of whole chromosomes, including monoploidy, polyploidy, aneuploidy that originate from errors in chromosome separation during cell division (mitosis) **(see Chapter 1, Section 1.3.7.1, Figure 1.19)** (Richardson & Jasin, 2000; Khanna & Jackson, 2001; Zhivotovsky & Kroemer, 2004; Jefford & Irminger-Finger, 2006; Lobrich & Jeggo, 2007; Pellman, 2007; Aguilera & Gomez-Gonzalez, 2008). Cancer cells, often display numerical changes in the whole chromosomes, coupled with structural chromosomal alterations which are an established cause of cancer, and of which the most frequent in cancer genotypes are the translocations (Solomon et al., 1991; Lengauer et al., 1998; Saunders et al., 2000; Nowak et al., 2002; Albertson et al., 2003; Futreal et al., 2004; Jefford & Irminger-Finger, 2006; Pellman, 2007).

Inactivation of checkpoint genes (i.e. due to an oncogene overexpression) can result in gene mutations, chromosome damage, ploidy abnormalities, all of which can contribute to genomic instability and carcinogenesis **(see Chapter 1, Section 1.3.7.1, Figure 1.19)** (Paulovich et al., 1997; Lengauer et al., 1998; Stewart et al., 1999; Nowak et al., 2002; Liu et al., 2004a; Jefford & Irminger-Finger, 2006; Lobrich & Jeggo, 2007). Moreover, another important factor that can favour genomic instability is disabled apoptosis. The processes that lead either to structural or to numeric chromosomal instability tend to induce apoptosis as a default pathway that aborts damaged cells after DNA damage, polyploidisation, or asymmetric cell division (Ashkenazi, 2002; Nelson et al., 2004; Zhivotovsky & Kroemer, 2004; Castedo et al., 2006; Ganem et al., 2007; Taylor et al., 2008). Defective apoptosis increases the probability for these cells to survive, further accumulate genomic changes and become selected and generate cancers (Zhivotovsky & Kroemer, 2004).

In addition, ploidy abnormalities (monoploidy, polyploidy, aneuploidy) are widespread features of human cancer. Tetraploidy, is a feature that is commonly seen in human cancer, including human BCCs (Miller, 1991a; Rajagopalan & Lengauer, 2004; Shi & King, 2005; Olaharski et al., 2006; Weaver & Cleveland, 2006; Ganem et al., 2007; Storchova & Kuffer, 2008), and has been reported as an early step in human tumourigenesis and as a contributing factor in the generation of aneuploid tumours (transient intermediates on the road to aneuploidy and tumourigenesis) (Shackney et al., 1989; Galipeau et al., 1996; Barrett et al., 2003; Storchova & Pellman, 2004; Zhivotovsky & Kroemer, 2004; Fujiwara et al., 2005; Olaharski et al., 2006; Ganem et al., 2007; Storchova & Kuffer, 2008; Holland & Cleveland, 2009). Aneuploidy, is consistently observed in virtually all cancers, including human BCCs (Buchner et al., 1985; Miller, 1991a; Herzberg et al., 1993; Fortier-Beaulieu et al., 1994; Lengauer et al., 1997; Lengauer et al., 1998; Staibano et al., 2001; Ashton et al., 2005; Carless et al., 2006; Weaver & Cleveland, 2006; Storchova & Kuffer, 2008), and it can be either a result of a transient chromosome missegregation event at some point in the development of the tumour that leads to a stably propagated and inherited abnormal karyotype (stably aneuploid tumour cells), or a result of an underlying chromosomal instability that leads to an increased rate of gain or loss of whole chromosomes during cell division (unstable aneuploid tumour cells) (Lengauer et al., 1997; Lengauer et al., 1998; Saunders et al., 2000; Lingle et al., 2002; Holland & Cleveland, 2009). In proof of the latter, not only many cancers are aneuploid, but individual cells within the same tumour manifest karyotypic (numerical and structural variations) and phenotypic (metastatic capacity, drug sensitivity, growth rates, morphology) heterogeneity, reflecting the persistent generation of new chromosomal variations, an inevitable consequence of chromosomal instability (Nowell, 1976; Shapiro et al., 1981; Frentz & Moller, 1983; Frentz et al., 1985; Cowan, 1992; Duesberg et al., 1998; Cahill et al., 1999; Jin et al., 2001; Mitelman et al., 2003; Saunders, 2005; Negrini et al., 2010). Thus, this heterogeneity, might suggest that tumour cells are the progeny of a genetically unstable single cell (due to a 'mutator' that generate genomic instability), which continues to acquire chromosomal abnormalities over time, including those (i.e. gene mutations) that cause cancer (Nowell, 1976; Duesberg et al., 1998; Cahill et al., 1999).

Tetraploid cells (DNA content 4N) caused by replication of genomic DNA but without proper cell division, precede the formation of polyploid and aneuploid cells. In addition,

the uncontrolled proliferation of chromosomally unstable tetraploid cells, triggers numerical chromosomal instability (rate of change in chromosome number due to increased rate of chromosome missegregation), aneuploidy (state of an altered chromosome number), and cell transformation and tumourigenesis (Storchova & Pellman, 2004; Fujiwara et al., 2005; Duelli et al., 2007; Ganem et al., 2007; Holland & Cleveland, 2009). Most importantly, tetraploid cells apart from being more susceptible to chemically induced, as well as spontaneous transformation, than diploid cells, are also more prone to acquire structural genomic instability both *in vitro* (tetraploid-derived cells exhibit structural chromosomal rearrangements) and *in vivo* (Fujiwara et al., 2005; Duelli et al., 2007). According to the latter, mice tetraploid-derived tumours display large-scale numerical and structural (non-reciprocal translocations, double minute chromosomes) chromosomal aberrations, indicating that tetraploidy and uncontrolled proliferation promotes further aneuploidy and chromosomal instability (Fujiwara et al., 2005; Holland & Cleveland, 2009).

Since upon GLI2ΔN induction in human keratinocytes there is increased tetraploidisation, along with ploidy abnormalities (polyploidy, aneuploidy), inactivation of cell cycle genes that control the proliferation of tetraploid cells and defective apoptosis, I investigated whether GLI2ΔN overexpression can also induce structural genomic instability in human keratinocytes, to promote malignant transformation, and if tetraploid populations which are more susceptible to acquire structural genomic alterations, could give rise to tetraploid and/or aneuploid progenies with structural chromosomal rearrangements.

Therefore, in order to detect any structural chromosomal abnormalities and to further confirm the numerical chromosomal abnormalities in GLI2ΔN-expressing keratinocytes, a technique known as M-FISH (multiplex-fluorescent in situ hybridization) was used. M-FISH is a molecular cytogenetic method that allows colour karyotyping of human chromosomes by painting each chromosome with a unique colour **(Chapter 2, Section 2.14)** (Schrock et al., 1996; Speicher et al., 1996; Speicher & Ward, 1996; McNeil & Ried, 2000; Strefford et al., 2001; Trask, 2002; Strachan & Read, 2004b).

As described in Materials and Methods **(Chapter 2, Section 2.14)**, M-FISH technique requires the preparation of metaphase chromosome spreads and the usage of a 24-colour chromosome painting probe. Thus, equal number of N/TERT, SINCE, and SINEG2 keratinocytes were seeded and were either mock treated **(-)** or treated with colcemid **(+)** for 2 hours and 15 minutes **(Chapter 2, Section 2.14.1 and Section 2.14.2)**, 72 hrs (~ 60-75% confluent) after plating. Colcemid, a closely related to, but less-toxic compound than colchicine, is a mitotic inhibitor, which inactivates spindle fiber formation (depolymerises microtubules and thus limits microtubule formation), and thus arresting cells in metaphase **(Figure 4.19)**, allowing cell harvest and karyotyping to be performed (Taylor, 1965; Sluder, 1991; Rieder & Palazzo, 1992).

Then, some of the N/TERT, SINCE and SINEG2 cells treated with colcemid **(+)** along with the mock treated **(-)** cells, were harvested and Hoechst-33342 stained followed by flow cytometry analysis both for DNA content and green fluorescence (EGFP) **(Chapter 2, Section 2.14.1.1) (Figure 4.20)**, in order to check the cell cycle prior to metaphase spreads preparation. Consistent with previous observations **(Section 4.2.1.1 and Section 4.2.1.3, Figure 4.1, Figure 4.2 and Figure 4.4, Figure 4.8)**, SINEG2 keratinocytes showed a significant increase in G2/M populations (P5) **(Figure 4.20 v, vi)**, when compared to either SINCE **(Figure 4.20 iii, iv)** or N/TERT control keratinocytes **(Figure 4.20 i, ii)**. In addition to the increased percentage of G2/M (tetraploid cells), SINEG2 keratinocytes display a nearly 3-fold increase in >4N and 8N (P15) polyploid populations **(Figure 4.20 v, vi)**, compared to both N/TERT **(Figure 4.20 i, ii)** and SINCE **(Figure 4.20 iii, iv)** control cells, which is in agreement with previous experiments **(Section 4.2.1.3, Figure 4.4, Figure 4.5 and Figure 4.8)**. This effect is evident either with **(+)** 2 hours and 15 minutes or without **(-)** treatment of keratinocytes with colcemid.

As a result of its inhibitory activity, colcemid induced a partial arrest of control keratinocytes in G2/M phase (P5) **(Figure 4.20 ii, iii)**. In addition, the dividing populations with DNA content 8N (P15) were also arrested after treatment with colcemid in control keratinocytes **(Figure 4.20 ii, iii)**. It is noteworthy that the effect of colcemid on SINEG2 keratinocytes produced slightly different results. The G2/M population (P5) of SINEG2 cells showed no increase after colcemid treatment **(Figure 4.20 v, vi)**. However, there was significant arrest in cells with DNA content 8N (P15)

(Figure 4.20 v, vi). As previously mentioned **(Section 4.2.1.3)**, the cell populations with DNA content 4N (P5) of SINEG2 keratinocytes (depicted in flow cytometry as a G2/M peak), is largely composed of bi-nucleated/tetraploid keratinocytes (~ 19%) **(Figure 4.8)**, while the 8N (P15) population partially represents the mitotic tetraploid population (G2/M tetraploids undergoing division). Since colcemid acts to inhibit the mitotic process, it seems that SINEG2 keratinocytes with DNA content 4N (P5) (G2/M peak; bi-nucleated/tetraploid cells) were not affected by the treatment, as opposed to the dividing tetraploid keratinocytes (8N) (P15), which showed a significant arrest as a result of the mitotic block induced by colcemid treatment. Data are representative of two independent experiments either using Hoechst-33342 **(Chapter 2, Section 2.14.1.1)** or PI staining **(see Chapter 2, Section 2.14.1.1)**, each of them consisting of duplicate samples.

The rest of the N/TERT, SINCE and SINEG2 cells treated with colcemid **(+)** for 2 hours and 15 minutes, were harvested, fixed and used in order to prepare metaphase spreads on slides **(Figure 4.21)**, according to the protocols described in Materials and Methods **(Chapter 2, Section 2.14.1.2 and Section 2.14.2)**. Already prepared metaphase spreads were hybridised with the labelled DNA probe **(see Chapter 2, Section 2.14.3)**. Pictures were taken for each hybridised metaphase spread in five different filters, and were analysed by a specific software, which generates a composite image in which each chromosome is given a different pseudocolour depending on the fluorophore composition, as well as in DAPI filter **(see Chapter 2, Section 2.14.3)** (Schrock et al., 1996; Speicher et al., 1996; Trask, 2002; Strachan & Read, 2004b). M-FISH analysis revealed a stable near-diploid male karyotype with the presence of an extra chromosome 20 (trisomy 20) in all three keratinocyte cell lines N/TERT, SINCE and SINEG2 and in all metaphases analysed. Therefore, each of these three cell lines has a karyotype of (47,XY,+20) (two sets of chromosomes per cell, with an additional copy of chromosome 20) **(Figure 4.22, Figure 4.23 and Figure 4.24)**. Trisomy 20 was a widespread feature, which was further confirmed by 10K SNP (Single Nucleotide Polymorphisms) array analysis, performed by Dr Muy-Teck Teh, Clinical and Diagnostic Oral Sciences, Institute of Dentistry, Barts and the London School of Medicine and Dentistry, London, UK **(see Appendix III)**. No structural chromosome aberrations clonal or non-clonal were detected in the control N/TERT and SINCE keratinocyte cell lines **(Figure 4.22 and Figure 4.23)**.

However SINEG2 keratinocytes manifested both numerical and structural chromosome aberrations **(Figure 4.25, Figure 4.26, Figure 4.27, Figure 4.28, Figure 4.29 and Figure 4.30)**. Based on metaphase chromosome counting, approximately 7% of SINEG2 cells had DNA content 8N (94 chromosomes, (94, XXYY, +20, +20)) **(Figure 4.25)**, representing (G2/M tetraploids) tetraploids in metaphase (G2/M tetraploids), and ~ 60% were near-tetraploid aneuploid cells with random gains and losses of chromosomes (i.e. 73 chromosomes) **(Figure 4.26)**, in contrast to control cells of which only ~ 10% had DNA content 8N (tetraploids in metaphase). The structural chromosomal rearrangements were found in ~ 36% (5/14 metaphases) of SINEG2 keratinocytes **(Figure 4.27, Figure 4.28, Figure 4.29 and Figure 4.30)**, including non-reciprocal unbalanced translocations and double minute chromosomes. Chromosomal translocation is a chromosome abnormality, caused by rearrangement of segments between non-homologous chromosomes, due to chromosome breakage. Non-reciprocal translocations, are one-way translocations in which two chromosomes break and only one segment from each chromosome joins together with another non-homologous chromosome, while the other segment from each chromosome is lost or joins with additional chromosomes (Lengauer et al., 1998; Albertson et al., 2003). Reciprocal translocations involve the breakage of two non-homologous chromosomes, and the exchange of segments between those two non-homologous chromosomes. Translocations can also be either balanced – no portions of the genome are lost or gained during exchange of chromosome material, or unbalanced – unequal exchange of chromosome material resulting in extra or missing portions of the genome (Lengauer et al., 1998; Albertson et al., 2003). Double minute chromosomes, are restricted regions of the genome which have been separated from the main chromosome body and amplified, and the amplified sequences present in small acentric fragments (double minutes) interspersed in the genome (Lengauer et al., 1998; Albertson et al., 2003; Gebhart, 2005). A clonal (detected in two or more metaphases) chromosome rearrangement, t(7;14), was found in three SINEG2 metaphases (~ 21%) **(Figure 4.27, Figure 4.28 and Figure 4.29)**. Interestingly, this specific translocation was detected both in a diploid cell (portion of the genome (7p) is gained - partial trisomy of chromosome 7p) **(Figure 4.27)**, and in two near-tetraploid aneuploid cells **(Figure 4.28 and Figure 4.29)**. A non clonal unbalanced translocation t(9;14) was also detected in a near-tetraploid aneuploid SINEG2 keratinocyte. In addition, double minutes originating from chromosome 8 were observed in one cell **(Figure 4.30)**.

Overall, these results suggest that GLI2ΔN induces a level of genomic instability in N/TERT human keratinocytes, and strikingly the presence of the clonal translocation t(7;14) in a diploid cell and the presence of a pair of t(7;14) in near-tetraploid aneuploid cells, suggest that the ability of GLI2ΔN to induce structural chromosomal aberrations is independent of its ability to induce tetraploidisation which however definitely seems to contribute to the overall chromosomal instability that GLI2ΔN-expressing cells exhibit.

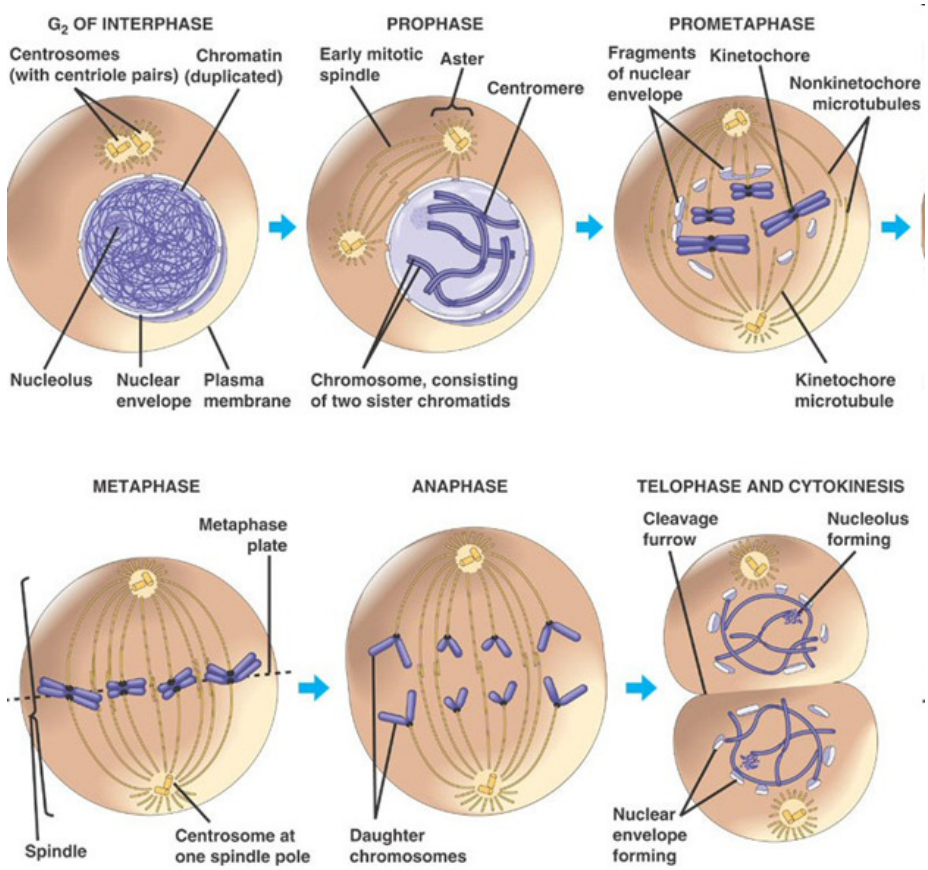

Figure 4.19: Stages of Mitosis.

Mitosis (M phase) is the process of nuclear division plus cytokinesis, which results in the production of two identical daughter cells from a single parent cell. M phase starts at the end of G2 phase and ends at the start of the next G1 phase. It includes the five stages of nuclear division (mitosis), as well as cytoplasmic division (cytokinesis). The five stages of nuclear division are the prophase, prometaphase, metaphase, anaphase and telophase. **Interphase**, where the cell prepares itself for cell division, is preceeding of all the stages of mitosis, and is not part of mitosis. Interphase is divided into three phases, G1 (first gap), S (synthesis), and G2 (second gap). A cell grows during G1 phase, continues to grow as it duplicates its chromosomes during S phase and grows more and prepares for mitosis during G2 phase. In **prophase**, the chromatin, which is diffuse in interphase, condenses into chromosomes. Each chromosome has duplicated in S phase and now consists of two sister chromatids bound together at the centromere. The mitotic spindle begins to form in the cytoplasm. In **prometaphase**, the nuclear envelope disassembles and microtubules invade the nuclear space. During metaphase the chromosomes align at the equatorial plate (metaphase plate) and are held in place by microtubules (kinetochore microtubules) attached to the mitotic spindle and to part of the centromere. In **anaphase**, chromosomes have separated into their two sister chromatids which are moving to opposite poles (each chromatid now called a chromosome). In **telophase**, daughter chromosomes arrive at the poles and the kinetochore microtubules disappear. The condensed chromatin expands and the nuclear envelope reappears. During **cytokinesis**, the cytoplasm divides by a process known as cleavage, where the cell membrane pinches inward to form a cleavage furrow, where the metaphase plate used to be, which gradually narrows and finally breaks leaving two separate daughter cells (Alberts et al., 1994; Lodish et al., 1999b; Strachan & Read, 2004a). royaleb.wordpress.com/2009/04/27/mitosis/.

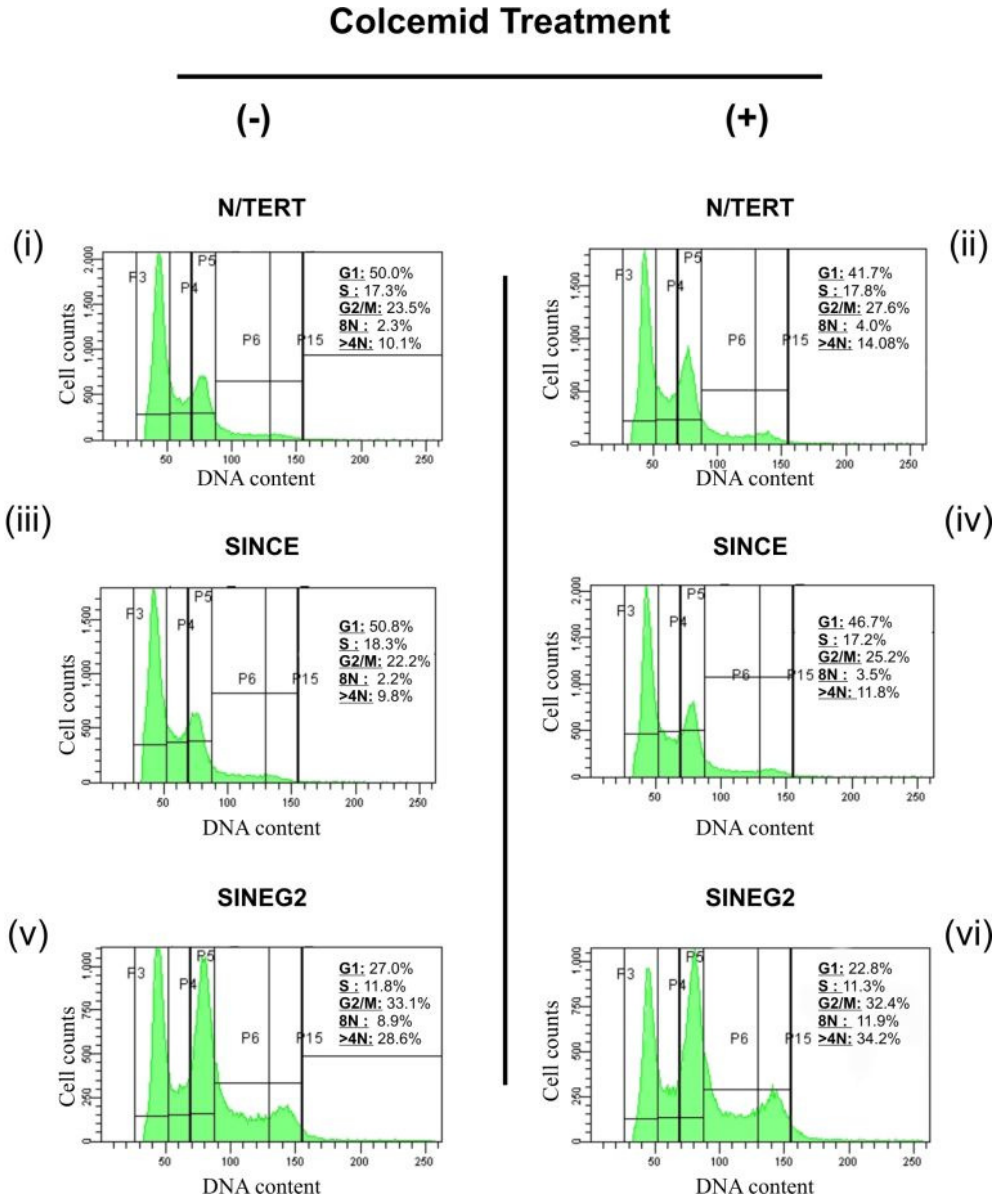

Figure 4.20: Colcemid treatment and cell cycle analysis in N/TERT, SINCE and SINEG2 cells.

Flow cytometry analysis of SINEG2 **(v, vi)** keratinocytes with (+) or without (-) colcemid treatment for 2 hours and 15 minutes, against both N/TERT **(i, ii)** and SINCE **(iii, iv)** control cells, after Hoechst-33342 staining. After doublet discrimination with width and area parameters, cells were discriminated according to DNA content and cell cycle profile was obtained. A significant increase in the cell population at the G2/M-4N (P5) and G2/M-8N (P15) boundaries, is evidenced in the SINEG2 **(v, vi)** cell line, with (+) or without (-) colcemid treatment, compared to both N/TERT **(i, ii)** and SINCE **(iii, iv)** cells. Colcemid treatment induces mitotic arrest both in G2/M populations (P5) and in cell populations with DNA content 8N (P15) in control N/TERT **(i, ii)** and SINCE **(iii, iv)** cells. In contrast, colcemid treatment induces mitotic arrest only in SINEG2 **(v, vi)** populations with DNA content 8N (P15), and not in G2/Mphase (P5) of SINEG2 **(v, vi)** keratinocytes. **N**: haploid number. Data are representative of two independent experiments.

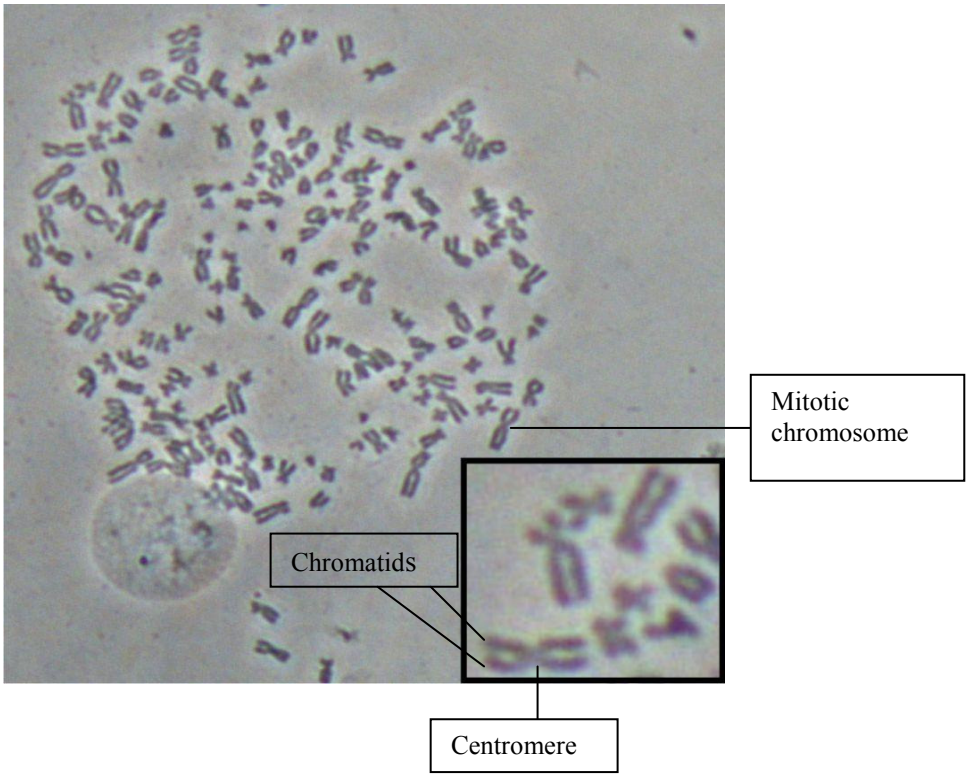

Figure 4.21: Metaphase spread.

Representative picture of a metaphase spread taken from SINEG2 cell line at x20 magnification, showing individual replicated and condensed mitotic chromosomes. The two sister chromatids of the mitotic chromosomes are joined at the centromere and are distinct. **Inset** shows magnified chromosomes from this particular metaphase spread.

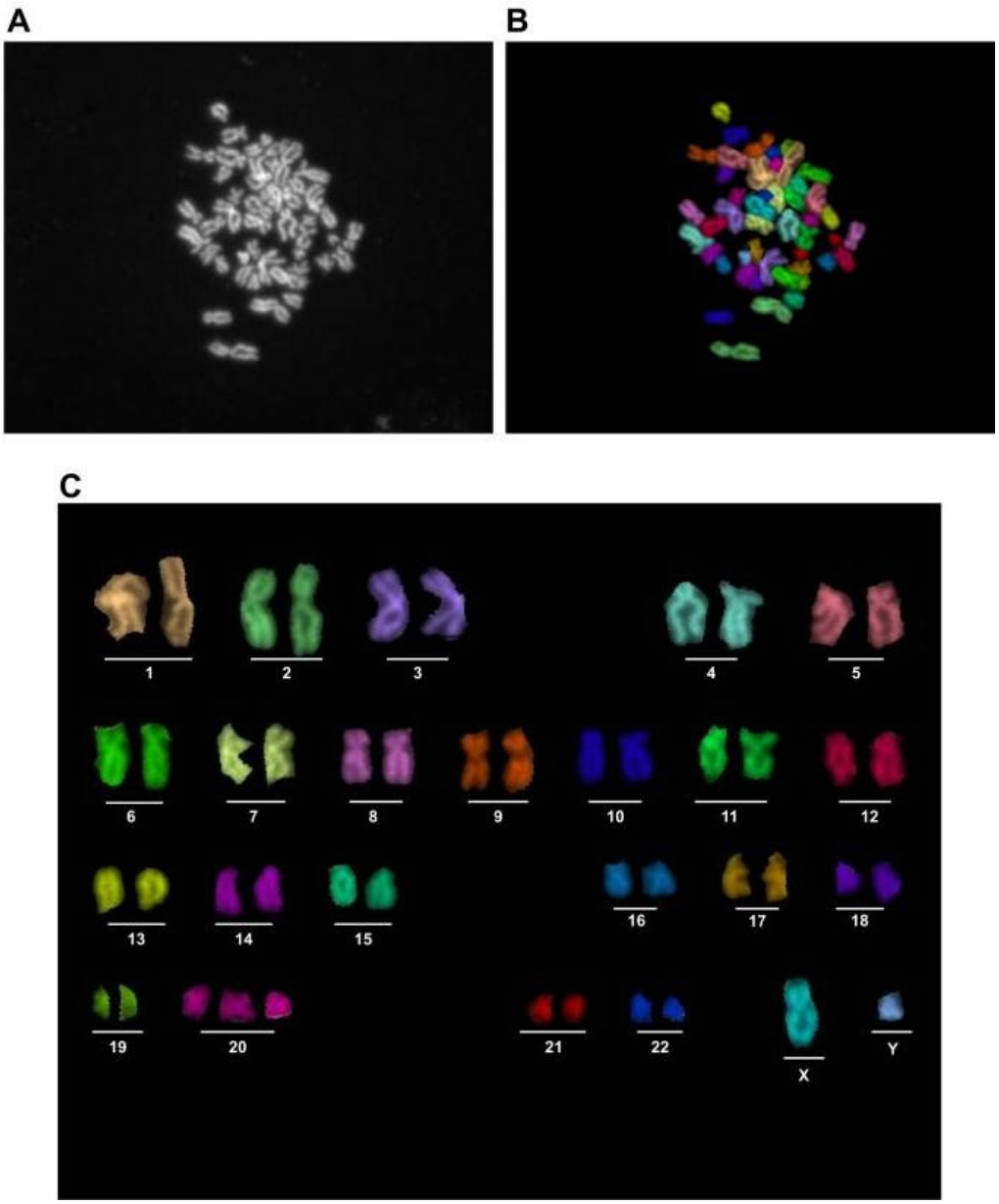

Figure 4.22: A representative karyotype of an N/TERT keratinocyte after DNA hybridised of the metaphase spread using M-FISH.

(A) N/TERT male metaphase spread as a DAPI image. **(B)** The same metaphase spread hybridised with colour-coded chromosome probes and captured as a pseudocoloured image. **(C)** Final M-FISH karyotype for the N/TERT cell (47, XY, +20).

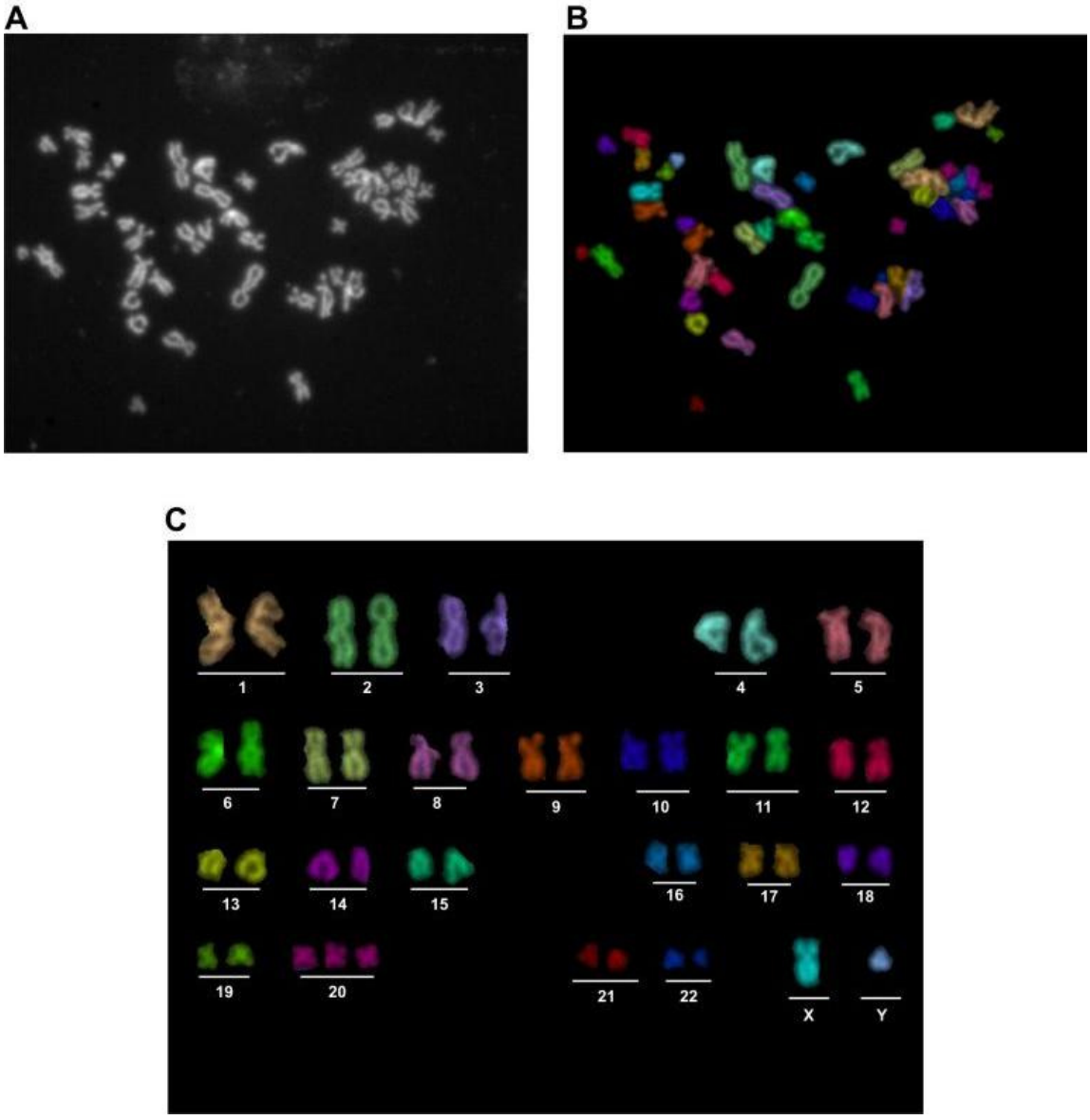

Figure 4.23: A representative karyotype of a SINCE keratinocyte after DNA hybridised of the metaphase spread using M-FISH.

(A) SINCE male metaphase spread as a DAPI image. **(B)** The same metaphase spread hybridised with colour-coded chromosome probes and captured as a pseudocoloured image. **(C)** Final M-FISH karyotype for the SINCE cell (47, XY, +20).

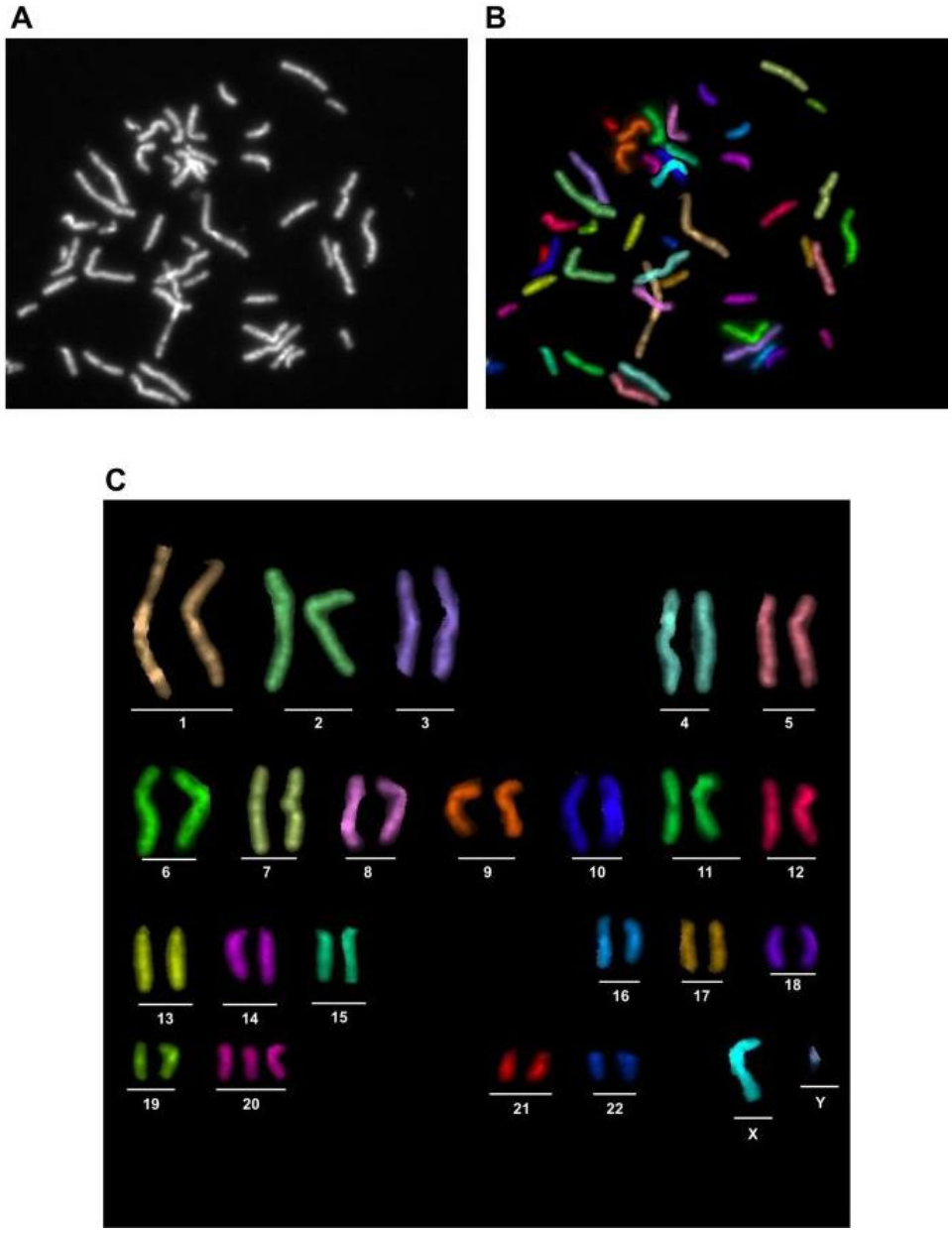

Figure 4.24: A representative karyotype of a SINEG2 keratinocyte after DNA hybridised of the metaphase spread using M-FISH.

(A) SINEG2 male metaphase spread as a DAPI image. **(B)** The same metaphase spread hybridised with colour-coded chromosome probes and captured as a pseudocoloured image. **(C)** Final M-FISH karyotype for the SINEG2 cell (47, XY, +20).

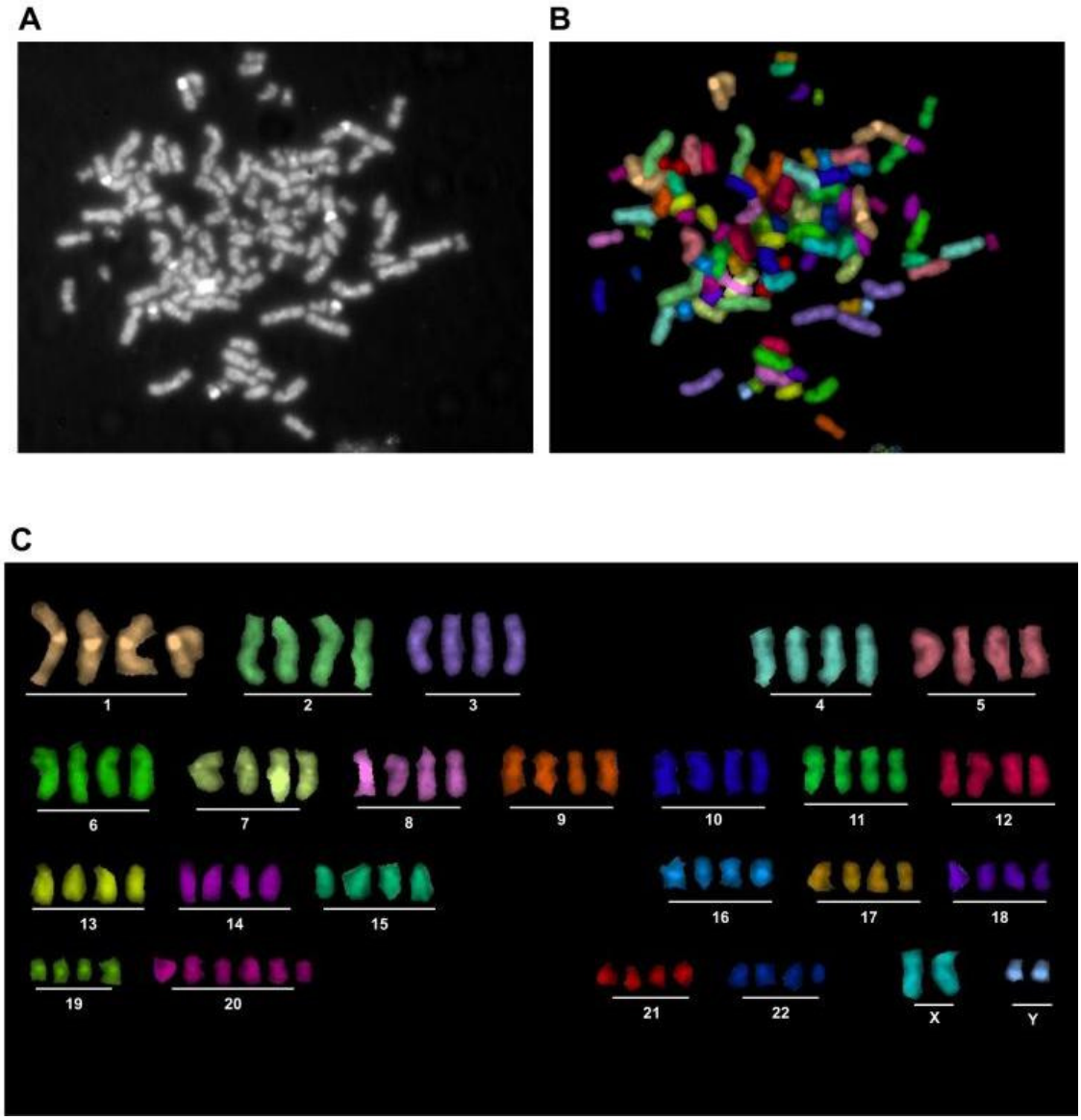

Figure 4.25: A representative karyotype of a SINEG2 keratinocyte after DNA hybridised of the metaphase spread using M-FISH.

(A) SINEG2 male metaphase spread as a DAPI image. **(B)** The same metaphase spread hybridised with colour-coded chromosome probes and captured as a pseudocoloured image. **(C)** Final M-FISH karyotype for the SINEG2 cell (94, XXYY, +20, +20). A representative metaphase spread and karyotype of a tetraploid SINEG2 cell with DNA content 8N (4 sets of chromosomes) in metaphase (G2/M tetraploid).

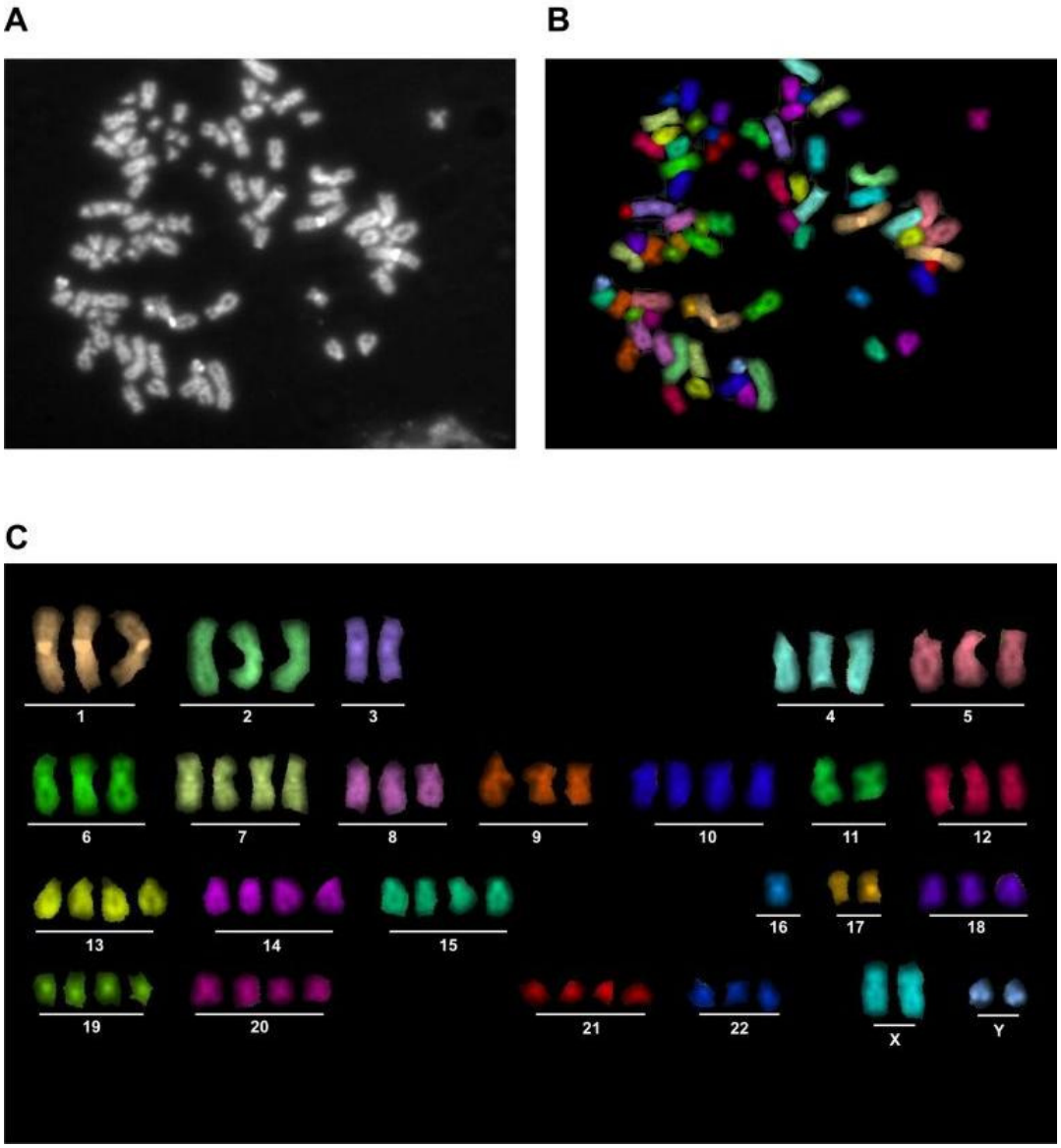

Figure 4.26: A representative karyotype of a SINEG2 keratinocyte after DNA hybridised of the metaphase spread using M-FISH.

(A) SINEG2 male metaphase spread as a DAPI image. **(B)** The same metaphase spread hybridised with colour-coded chromosome probes and captured as a pseudocoloured image. **(C)** Final M-FISH karyotype for the SINEG2 cell. A representative metaphase spread and karyotype of an aneuploid (near-tetraploid aneuploid) SINEG2 cell displaying 73 chromosomes with losses and gains of many chromosomes. This is an example of a tetraploid cell that might have undergone multipolar and asymmetric divisions, yielding aneuploid progenies.

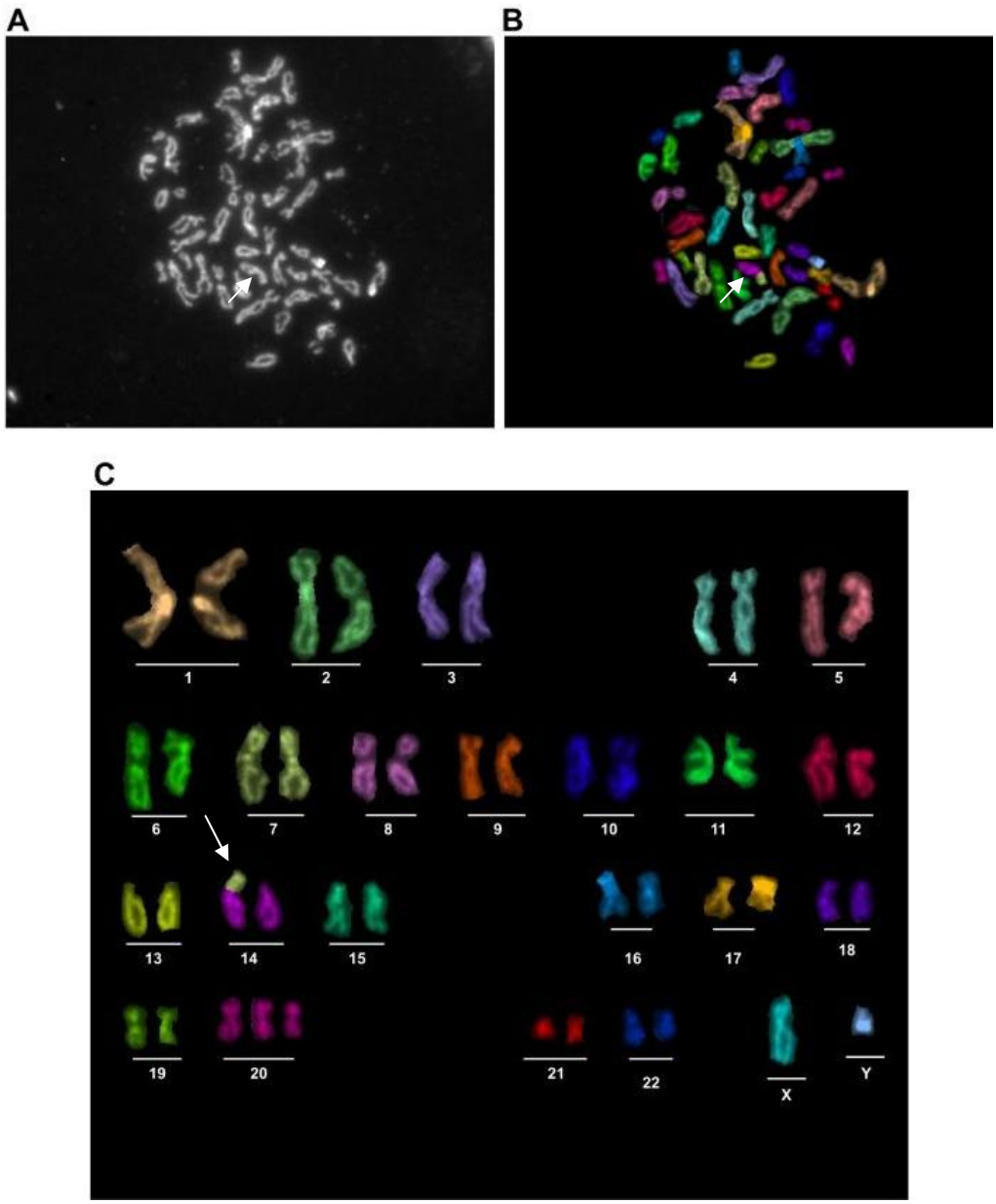

Figure 4.27: A representative karyotype of a SINEG2 keratinocyte after DNA hybridised of the metaphase spread using M-FISH.

(A) SINEG2 male metaphase spread as a DAPI image. **(B)** The same metaphase spread hybridised with colour-coded chromosome probes and captured as a pseudocoloured image. **(C)** Final M-FISH karyotype for the SINEG2 cell (47, XY, -7, +del7q, -14, +der(14)t(7;14) +20). A representative metaphase spread and karyotype of a diploid SINEG2 cell show the clonal non-reciprocal unbalanced translocation t(7;14) (white arrows).

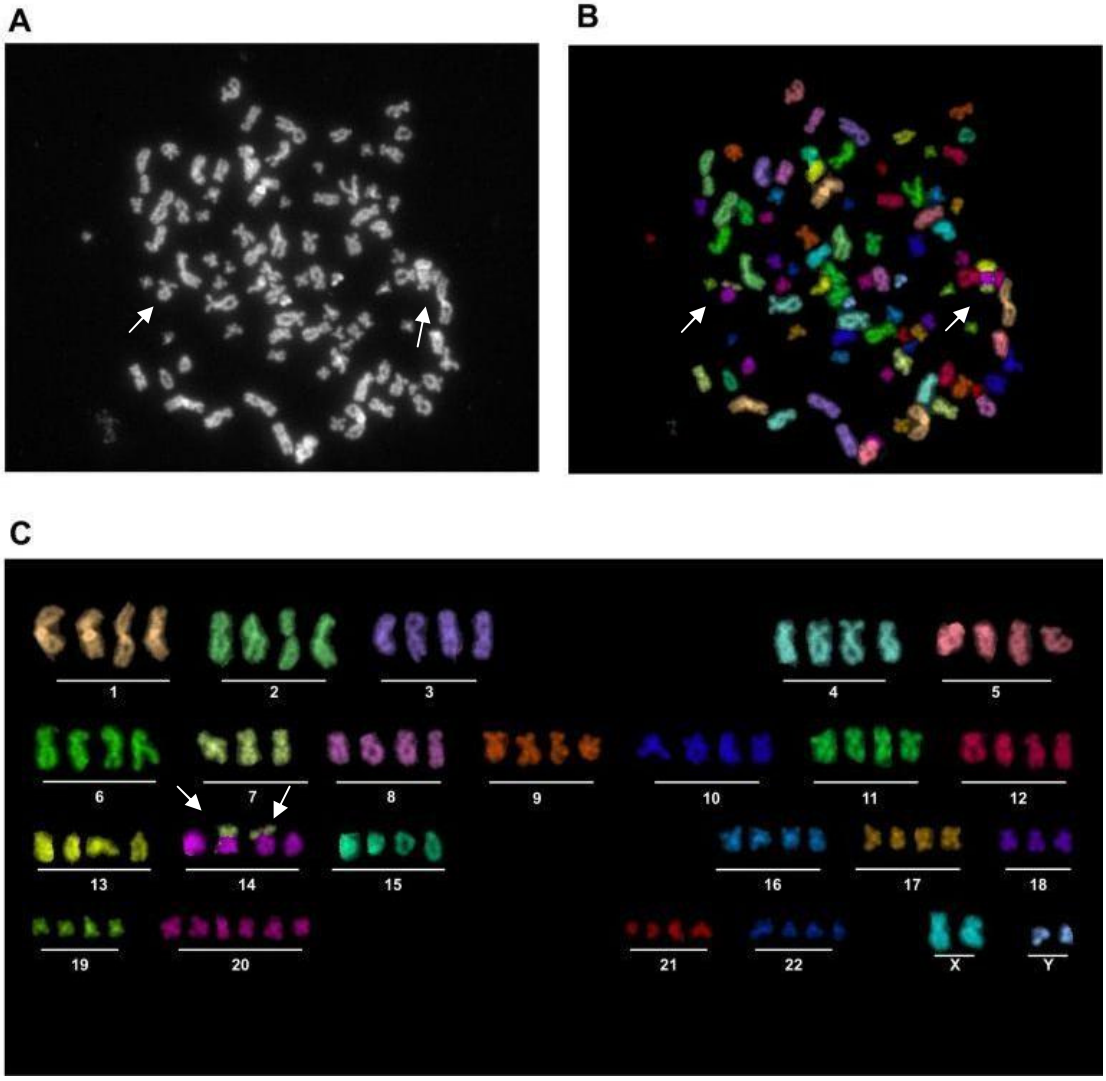

Figure 4.28: A representative karyotype of a SINEG2 keratinocyte after DNA hybridised of the metaphase spread using M-FISH.

(A) SINEG2 male metaphase spread as a DAPI image. **(B)** The same metaphase spread hybridised with colour-coded chromosome probes and captured as a pseudocoloured image. **(C)** Final M-FISH karyotype for the SINEG2 cell. A representative metaphase spread and karyotype of an aneuploid (near-tetraploid aneuploid) SINEG2 cell show the clonal translocation t(7;14) (white arrows).

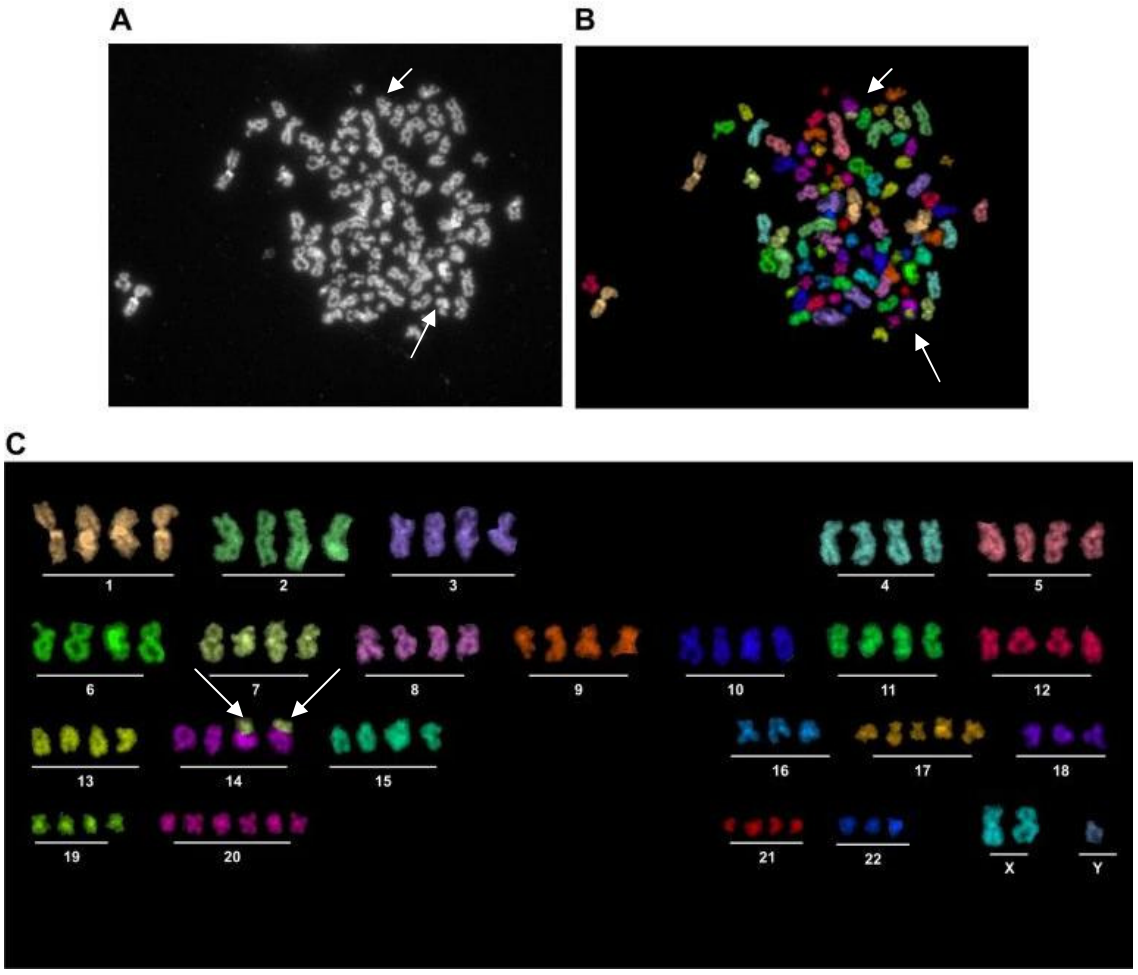

Figure 4.29: A representative karyotype of a SINEG2 keratinocyte after DNA hybridised of the metaphase spread using M-FISH.

(A) SINEG2 male metaphase spread as a DAPI image. **(B)** The same metaphase spread hybridised with colour-coded chromosome probes and captured as a pseudocoloured image. **(C)** Final M-FISH karyotype for the SINEG2 cell. A representative metaphase spread and karyotype of an aneuploid (near-tetraploid aneuploid) SINEG2 cell show the clonal translocation t(7;14) (white arrows).

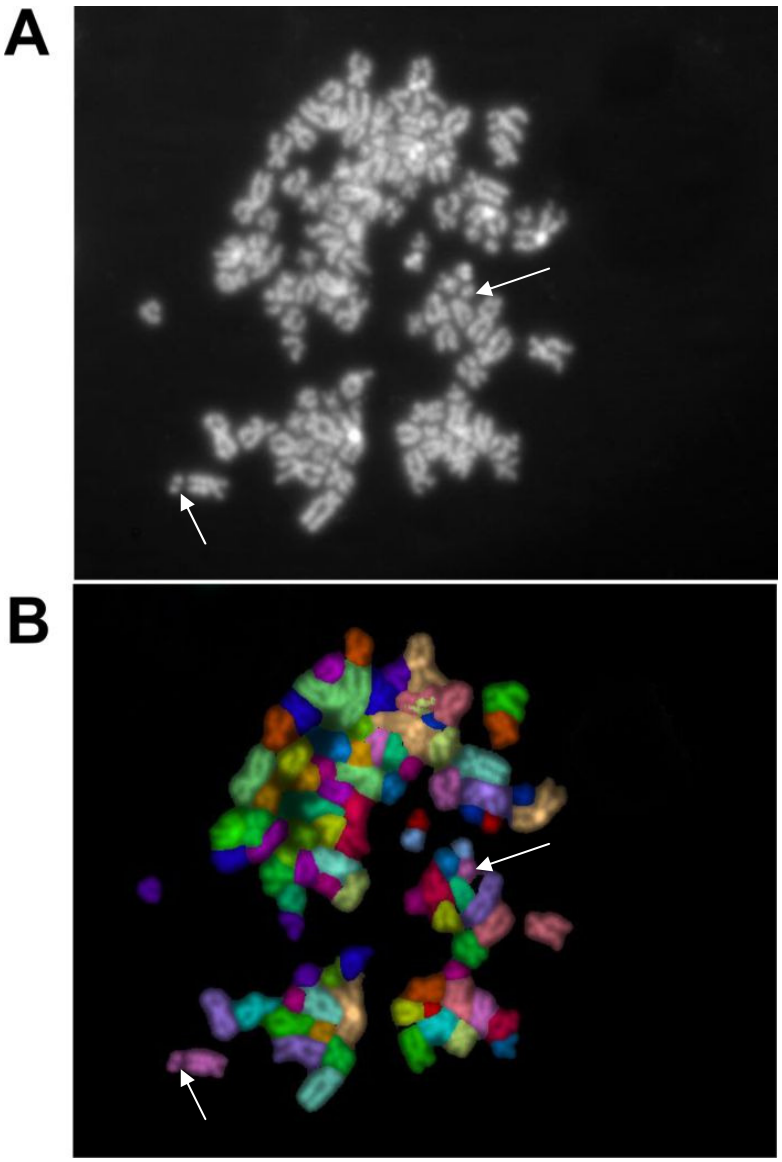

Figure 4.30: A representative picture of a SINEG2 keratinocyte after DNA hybridised of the metaphase spread using M-FISH.

(A) SINEG2 male metaphase spread as a DAPI image. **(B)** The same metaphase spread hybridised with colour-coded chromosome probes and captured as a pseudocoloured image. A representative metaphase spread of an aneuploid (near-tetraploid aneuploid) SINEG2 cell shows the presence of double minute chromosomes (white arrows). M-FISH analysis reveals that the origin of the double minute chromosomes is chromosome 8.

4.3 Discussion

4.3.1 GLI2ΔN induces numerical chromosomal instability in human N/TERT keratinocytes

4.3.1.1 GLI2ΔN-induced tetraploidy is responsible for the observed delay in the growth of SINEG2 keratinocytes

The general consensus regarding the SHH/GLI signalling pathway in skin is that it drives cell proliferation and hence its members are proto-oncogenes. The genetic analysis of Gorlin or nevoid basal cell carcinoma (NBCC) syndrome, an autosomal dominant hereditary disease which predisposes patients to the early development of multiple BCCs (Gorlin, 1987; Gorlin, 1995), has been shown that is linked to deregulation of the PTCH/SMO interaction due to inactivating PTCH (Patched) mutations, and thus leading to constitutive activation of the SHH/GLI pathway promoting proliferation in the absence of the ligand (Hahn et al., 1996b; Johnson et al., 1996; Unden et al., 1996; Gailani & Bale, 1997; Unden et al., 1997; Booth, 1999; Happle, 1999; Ling et al., 2001; Daya-Grosjean & Couve-Privat, 2005). In addition, inactivation of PTCH and activation of SMO (Smoothened) mutations occur frequently in sporadic BCCs and in BCCs associated with xeroderma pigmentosum, whereas both sporadic and hereditary human BCCs contain p53 mutations (Barbareschi et al., 1992; Shea et al., 1992; Gailani et al., 1996; Unden et al., 1996; Gailani & Bale, 1997; Grossman & Leffell, 1997; Ponten et al., 1997; Unden et al., 1997; Xie et al., 1998; Bodak et al., 1999; Ling et al., 2001; Dicker et al., 2002; Lacour, 2002; Daya-Grosjean & Couve-Privat, 2005; Reifenberger et al., 2005; Teh et al., 2005). Furthermore, direct overexpression of Gli2, as well as of other members of the SHH/GLI signalling pathway, in mice, directly leads to BCC or BCC-like tumour susceptibility (Fan et al., 1997; Oro et al., 1997; Xie et al., 1998; Grachtchouk et al., 2000; Nilsson et al., 2000; Sheng et al., 2002; Hutchin et al., 2005; Huntzicker et al., 2006; Youssef et al., 2010).

However, despite the identification of the genetic hits involved in BCC development, little is known about the molecular mechanisms involved in the transformation of epidermal keratinocytes in response to HH/GLI signalling. In this respect, several mechanisms have been proposed in different organisms, including interactions of

SHH/GLI signalling with important cell cycle mediators that promote cell proliferation, such as cyclin D1, cyclin B1 and CDC25B (M-phase inducer phosphatase 2) **(see Chapter 1, Section 1.3.7)** (Barnes et al., 2001; Ruiz i Altaba et al., 2002a; Pasca di Magliano & Hebrok, 2003; Wetmore, 2003; Daya-Grosjean & Couve-Privat, 2005; Aberger & Frischauf, 2006; Athar et al., 2006; Benazeraf et al., 2006; Kasper et al., 2006a). In mouse skin, loss of Shh or Gli2 function, leads to a significant decrease in the rate of cell proliferation in the developing hair follicle (Mill et al., 2003), while recent works by Regl et al. (Regl et al., 2004a) and Eichberger et al. (Eichberger et al., 2006), using cDNA-array based gene expression techniques, have shown that inducible overexpression of GLI2ΔN in either confluent or sub-confluent human skin epidermal HaCaT keratinocytes, induces a number of genes involved in G1-S phase and G2-M phase progression of the cell cycle **(see Chapter 1, Section 1.3.7 and Chapter 4, Section 4.1)**. On the other hand, it has not been reported that keratinocytes expressing GLI2 have an accelerated proliferation rate in normal culture conditions, and no one has shown the cell cycle profile of keratinocytes expressing GLI2. Instead, a reduced growth rate in response to GLI2ΔN overexpression was observed in N/TERT keratinocytes in my system **(see Chapter 3, Section 3.2.3.2, Figure 3.14 and Figure 3.15) (see Chapter 3, Section 3.3.9)**, while the same inducible GLI2ΔN HaCaT cell line that was used by Eichberger et al. (Eichberger et al., 2006) for microarray analysis, had no proliferative advantage (no faster cell cycle) compared to the control, it showed a reduced growth rate in culture, as reported by Snijders et al. (Snijders et al., 2008).

Several reasons might have contributed to the observed delay in the growth of SINEG2 keratinocytes in my study, including cell cycle arrest, impaired or delayed mitosis and apoptosis and/or cell death. However, the GLI2ΔN induction in N/TERT keratinocytes, did not result in increased apoptosis or cell death, as judged by the Annexin V and Annexin V / DAPI positive cells **(Figure 4.3)**, and by the propidium iodide stained cells with sub-G1 content **(Figure 4.4)**. In addition, cell cycle analysis of N/TERT keratinocytes expressing GLI2ΔN, showed that SINEG2 keratinocytes displayed an increase in the G2/M phase, representing bi-nucleated/tetraploid cells **(Figure 4.1, Figure 4.2 and Figure 4.8)**, as well as an increase in the cells with DNA content >4N and 8N, representing G2/M-tetraploid (tetraploids undergoing division), polyploid and aneuploid cells **(Figure 4.4, Figure 4.5 and Figure 4.7)**. Taken together these findings, indicate that overexpression of GLI2ΔN interferes with normal cell cycle completion

through the G2/M phase and mitotic division, possibly due to cytokinesis failure and therefore increasing the chromosomal complement of the cells. Hence, a proportion of GLI2ΔN cells fail to divide upon completion of mitosis (cytokinesis failure) yielding bi-nucleated tetraploid cells (a dividing cell giving rise to one G1 bi-nucleated daughter cell instead of two G1 daughter cells), a fact that might contribute to the low cell counts obtained from long term culture, and explain the significant reduction of cumulative population doublings in GLI2ΔN overexpressing keratinocytes.

It has been previously shown that either bi-nucleated or mono-nucleated tetraploid, polyploid and aneuploid cells exhibit a prolonged mitosis compared to diploid cells (Gisselsson et al., 2008; Storchova & Kuffer, 2008; Yang et al., 2008b). Therefore, overexpression of GLI2ΔN leads to delayed exit form mitosis of tetraploid cell, and allows the generation of polyploid and aneuploid progenies with enhanced viability. This observation is highly consistent with Sotillo et al. (Sotillo et al., 2007), which showed that inducible overexpression of Mad2 oncogene in MEF cells from transgenic mice, leads to the accumulation of bi-nucleated tetraploid and mono-nucleated aneuploid MEFs, with a much slower growth rate than their normal counterparts (Sotillo et al., 2007).

Recently, it has also been demonstrated that the chromosome complement and the amount of centrosomes present during division, are both very important determinants of the duration of mitosis in human normal and cancer cells (Yang et al., 2008b). In the same study, it was shown that the duration of the mitotic process was proportional to the modal chromosome number of each cell (i.e. 4N bi-nucleated cells, originated from cytokinesis failure due to cytochalasin treatment, took longer (>2x) than 2N diploid cells to enter anaphase) (Yang et al., 2008b). While the slower rate of mitotic progression was attributed both to the increased chromosome and centrosome numbers, the latter showed to have a much stronger influence since diploid cells with artificially introduced additional centrosomes were 3x slower than tetraploid cells with artificially normalised centrosome numbers, compared to normal diploid cells (Yang et al., 2008b).

Abnormally increased centrosome numbers can lead to the formation of multipolar spindles (defect in chromosome segregation), which have been shown to display significant mitotic delay and to be responsible for the longer duration of mitosis in

tetraploid, polyploid and aneuploid cells, due to the delay in satisfaction of the spindle assembly checkpoint (SAC) (SAC prolongs mitosis until all kinetochores are stably attached to spindle microtubules) (Rieder et al., 1994; Gisselsson et al., 2008; Storchova & Kuffer, 2008; Yang et al., 2008b). The prolongation in the division of bi-nucleated tetraploid cells can be alleviated when the spindle assembly checkpoint is abrogated through the introduction of a dominant-negative form of Mad2 (Mad2-ΔC), further supporting the role of SAC in impairing the mitotic process (Yang et al., 2008b). Although cells with multipolar spindles are stalled in mitosis, this transient block imposed by the SAC is eventually bypassed, and cells are allowed to complete either multipolar (mainly transformed cells) or bipolar divisions and exit mitosis (mitotic slippage) (Gisselsson et al., 2008; Yang et al., 2008b).

Therefore, the existence of tetraploid, polyploid and aneuploid cells in GLI2ΔN-expressing keratinocyte cultures, followed by prolonged mitosis, could explain why overall SINEG2 keratinocytes exhibit a reduced growth rate in culture.

4.3.1.2 Ploidy abnormalities (tetraploidy, aneuploidy) induced by GLI2ΔN in N/TERT keratinocytes are hallmarks of cancer

The increase of bi-nucleated/tetraploid cells (DNA content 4N), observed upon GLI2ΔN induction in N/TERT keratinocytes **(Figure 4.1, Figure 4.2, Figure 4.4 and Figure 4.8)**, apart from being a possible explanation for the slow growth rate of keratinocytes, it may also contribute to cell transformation and carcinogenesis by preceding the formation of polyploid and aneuploid cells and leading to genomic/chromosomal instability (Storchova & Pellman, 2004; Ganem et al., 2007). Tetraploidy is a feature that is commonly seen in human cancer, including human BCCs (Miller, 1991a; Rajagopalan & Lengauer, 2004; Shi & King, 2005; Olaharski et al., 2006; Weaver & Cleveland, 2006; Ganem et al., 2007; Storchova & Kuffer, 2008), and has been reported as an early step in human tumourigenesis and as a contributing factor in the generation of aneuploid tumours (Shackney et al., 1989; Galipeau et al., 1996; Storchova & Pellman, 2004; Zhivotovsky & Kroemer, 2004; Fujiwara et al., 2005; Ganem et al., 2007; Storchova & Kuffer, 2008; Holland & Cleveland, 2009).

4.3.1.2.1 Aneuploidy and cancer

Aneuploidy is often caused by errors in chromosome partitioning during mitosis, due to defects in mitotic checkpoint signalling, sister chromatid cohesion defects, merotelic attachment, and due to acquisition of extra centrosomes leading either to multipolar mitotic divisions and thus whole chromosome missegregation, and unequal distribution of chromosomes in daughter cells, or to centrosome clustering into two groups that will allow cells to divide in a bipolar fashion but with increased risk of incorrect kinetochore microtubule attachments and thus leading to aneuploidy **(Figure 4.31)** (Fukasawa, 2007; Holland & Cleveland, 2009). Each centrosome consists of two centrioles and in order to ensure bipolar mitotic spindle formation, the single centrosome of a cell duplicates precisely once prior to mitosis (Hinchcliffe & Sluder, 2001). Thus, during centrosome duplication the two centrioles separate, followed by *de novo* synthesis of a single daughter centriole adjacent to each of the older centrioles during S phase (Hinchcliffe & Sluder, 2001). Extra centrosome acquisition, can be due to centrosome malfunctions, such as centrosome overduplication, centrosome fragmentation and loss of centriole cohesion in a diploid cell, or generation of tetraploidy (Nigg, 2002; Fukasawa, 2007; Holland & Cleveland, 2009).

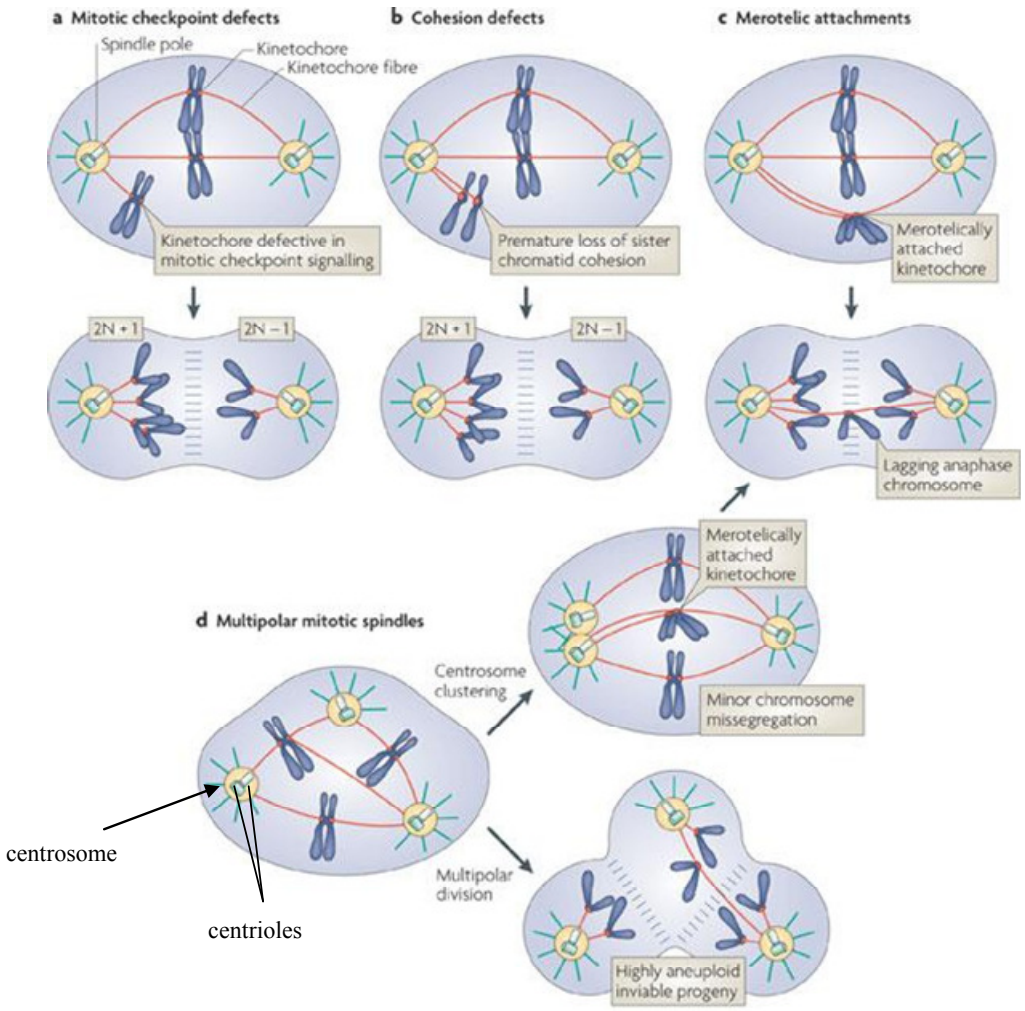

Figure 4.31: Roads to aneuploidy.

There are several pathways by which cells might gain or loose chromosomes, and thus generate aneuploidy; **(a) Defects in mitotic checkpoints**, which allow cells to enter anaphase in the presence of unattached or misaligned chromosomes, **(b) Cohesion defects**, leading to premature loss of sister chromatid cohesion and chromosome missegregation, **(c) Merotelic attachments**, occur when one kinetochore is attached to microtubules from both poles of the spindle, leading to chromosome missegregation and to exclusion of the lagging chromatid from both daughter cells during cytokinesis, **(d) Acquisition of extra centrosomes**, leading to multipolar mitotic spindle formation, followed either by centrosome clustering where cells are allowed to divide in a bipolar fashion but with an increased risk of merotelic attachments, or by multipolar mitotic divisions producing three or more highly aneuploid daughter cells (Holland & Cleveland, 2009). Centrosomes **(black arrow)** are small cytoplasmic organelles that are the microtubule (cytoskeletal protein)-organizing centre of animal cells (nucleation and organization of microtubules) and are also crucial in the organization of spindle poles and the completion of cytokinesis. Each centrosome consists of a pair of centrioles **(black lines)** which are open-ended cylinders comprised of nine sets of triplet microtubules linked together and embedded in a matrix of pericentriolar material (Doxsey, 2001; Duensing & Munger, 2001; Hinchcliffe & Sluder, 2001; Nigg, 2002).

Aneuploidy is consistently observed in virtually all cancers, including human BCCs, both in early stages of many tumour types (probably a result of mutations, in a set of genes that are specifically involved in maintaining chromosome stability, or in other genes and through other mechanisms i.e. radiation which damages the spindle apparatus and causes aneuploidy (Duesberg & Rasnick, 2000; Li et al., 2000)) and in mature tumours, and this is why it has been proposed to play a role both in tumourigenesis and in tumour progression (Buchner et al., 1985; Miller, 1991a; Herzberg et al., 1993; Fortier-Beaulieu et al., 1994; Lengauer et al., 1997; Lengauer et al., 1998; Staibano et al., 2001; D'Assoro et al., 2002; Nowak et al., 2002; Ashton et al., 2005; Carless et al., 2006; Weaver & Cleveland, 2006; Storchova & Kuffer, 2008). Thus, apart from the fact that aneuploidy precedes transformation as it is found in pre-cancerous lesions of the cervix (Ried et al., 1999; Duensing & Munger, 2004), head and neck (Ai et al., 2001), colon (Ried et al., 1999; Cardoso et al., 2006), oesophagus (Doak et al., 2004), bone marrow (Amiel et al., 2005), breast (Medina, 2002) and skin (Dooley et al., 1993), it also disrupts global transcription by causing misregulation of growth-promoting and growth-restricting genes (Upender et al., 2004), further supporting the notion that it might have a role in tumourigenesis (Weaver & Cleveland, 2006).

In addition, aneuploidy can be either a result of a transient chromosome missegregation event at some point in the development of the tumour that leads to a stably propagated and inherited abnormal karyotype (stably aneuploid tumour cells), or a result of an underlying chromosomal instability that leads to an increased rate of gain or loss of whole chromosomes during cell division (unstable aneuploid tumour cells) (Lengauer et al., 1997; Lengauer et al., 1998; Saunders et al., 2000; Lingle et al., 2002; Holland & Cleveland, 2009). Hence, the karyotypic/chromosomal instability of a cancer cell, is proportional to its degree of aneuploidy (ratio of the ploidy of a given cell versus the ploidy of a normal cell of the same species), suggesting that the more aneuploid the cell (abnormal number of chromosomes), the more unstable is the karyotype (Lengauer et al., 1997; Duesberg et al., 1998; Duesberg & Rasnick, 2000). Although it is not yet clear how aneuploidy can trigger tumourigenesis, the most likely scenario is that aneuploidy, due to changes in chromosome copy number, allows oncogene amplification or loss of tumour-suppressor genes (Torres et al., 2008; Holland & Cleveland, 2009). There are also non-neoplastic aneuploidies, which typically involve the loss or the gain of only

one or very few chromosomes (Harnden et al., 1976; Galloway & Buckton, 1978; Duesberg & Rasnick, 2000).

The notion that aneuploidy might have a causative role in cancer lies back in 1914, when Theodor Boveri (Boveri, 2008) first suggested that malignancy is due to a disorder in the chromosome constitution of the cell (abnormal chromosome constitution / aneuploidy), that this karyological disorder is initiated most commonly by abnormalities of mitosis (multipolar mitosis) and that centrosomes malfunction might be involved and be the major source of instability (Balmain, 2001; Hardy & Zacharias, 2005; Bignold et al., 2006; Boveri, 2008; Harris, 2008a; Harris, 2008b; Holland & Cleveland, 2009). However, even if for more than 100 years aneuploidy has been proposed to drive / promote tumour formation (Boveri, 2008), it is still hotly debated whether aneuploidy is a cause or a consequence of malignant transformation, mainly due to the genetic complexity of aneuploid cells (Storchova & Pellman, 2004; Weaver & Cleveland, 2006; Holland & Cleveland, 2009). Each aneuploid tumour, is aneuploid on its own way and has its own particular abnormal chromosome content, and thus its own abnormal characteristics, a fact that complicates the identification of mutations that result in aneuploidy, or the identification of general features common to aneuploid tumour cells (Storchova & Pellman, 2004; Pellman, 2007). In addition, although aneuploidy correlates with transformation, the difficulty of generating experimentally aneuploidy, without causing other cellular defects such as DNA damage (i.e. suppressing genes that they do not participate in cellular functions other than chromosome segregation, or using drugs that are not mutagenic), partly restricts the testing and the confirmation of the hypothesis that aneuploidy drives/causes tumourigenesis (Weaver & Cleveland, 2006).

However, a recent study made by Weaver et al., (Weaver et al., 2007), using mouse cells and mice with reduced levels of the mitosis-specific, centromere-linked motor protein CENP-E (involved in aligning chromosomes normally on the mitotic spindle and in modulating the spindle checkpoint), is in favour of the idea that chromosome missegregation and its associated aneuploidy drives malignant transformation as Boveri had initially proposed (Pellman, 2007). Cells and mice with reduced levels of the CENP-E were shown to develop aneuploidy (single-chromosomal aneuploidy, near-diploid aneuploidy) and chromosomal instability *in vitro* and *in vivo*, as well as to

develop spontaneous tumourigenesis *in vivo* in aged mice, but only at a modest frequency (Weaver et al., 2007). Most strikingly though, aneuploidy from whole single-chromosome loss (or gain) in heterozygous CENP-E knockout mice, was reported to strongly delay *in vivo* tumourigenesis after loss of the p19/ARF tumour-suppressor gene (Weaver et al., 2007). This observation suggests that low levels of aneuploidy and chromosomal instability, due to reduction of CENP-E, promote tumour initiation and progression, whereas high levels, due to an additional genetic damage (loss of the p19/ARF), are protective (Weaver et al., 2007).

Therefore, although it is clear from this and from other studies that aneuploidy is able to trigger tumourigenesis, as well as to increase the risk of neoplastic transformation and to facilitate tumour progression (Weaver & Cleveland, 2006; Holland & Cleveland, 2009), many factors might affect the overall outcome of aneuploidy. The balance between aneuploid cells to become tumourigenic or growth-arrested following cell death, may be controlled by the different paths to aneuploidy (i.e. through single-chromosomal missegregation or tetraploidy intermediate), the different cell types, the different genetic contexts and the levels of genomic instability (Pellman, 2007). High levels of genomic instability in a near-diploid aneuploid cell would be fatal to the cell, and would decrease the fitness of this cell, compared to a diploid cell with intact genome (Cahill et al., 1999). Thus, the 'just right' levels of genomic instability that will still be compatible with survival and sufficient enough to generate new genomic variants are required in a cell, in order for the cell to become transformed (Cahill et al., 1999; Storchova & Kuffer, 2008).

4.3.1.2.2 Tetraploidy and cancer

Separately from chromosome missegregation, or abnormal centrosome numbers during mitosis that can result in aneuploidy, tetraploidy (genome doubling) is an alternative mechanism through which diploid cells can evolve into highly aneuploid cells, by chromosomal loss from a tetraploid intermediate (Shackney et al., 1989; Ganem et al., 2007; Storchova & Kuffer, 2008; Torres et al., 2008; Holland & Cleveland, 2009).

Most importantly, tetraploidy is not just a harmless side effect of cancer-promoting chromosome instability, but it has its own tumourigenic potential, since only tetraploid

(generated by transient exposure to an actin inhibitor, dihydrocytochalasin B (DCB), that prevents remodelling of the cytoskeleton and thus causes failure of cytokinesis), and not diploid, p53 null mouse mammary epithelial cells promote tumourigenesis after subcutaneous injection into nude mice (Fujiwara et al., 2005). Also, tetraploid p53 null cells and not diploid p53 null cells promoted chemically-induced *in vitro* transformation (Fujiwara et al., 2005). In addition, Duelli et al. (Duelli et al., 2007) recently showed that only tetraploid, generated by MPMVE viral-induced cell-cell fusion, and not diploid human fibroblasts co-expressing E1A and HRAS1 oncogenes, are able to promote tumourigenesis when transplanted into nude mice (Ganem et al., 2007; Holland & Cleveland, 2009). In both these studies, tetraploidy in culture increased the proportion of highly aneuploid cells (whole-chromosome aneuploidy), and of cells with structural chromosomal rearrangements (Fujiwara et al., 2005; Duelli et al., 2007), whereas mice tetraploid-derived tumours also displayed large-scale structural chromosomal aberrations (Fujiwara et al., 2005).

Further evidence, supporting the notion that tetraploids are transient intermediates on the road to aneuploidy, and of which uncontrolled proliferation might promote cellular transformation and tumourigenesis (at least in some tumour types), is multifold and comes from studies of tissue cultured cells, animal models, and from human patients (Shackney et al., 1989; Storchova & Pellman, 2004; Ganem et al., 2007; Storchova & Kuffer, 2008; Holland & Cleveland, 2009). First, some tumours have a tetraploid or near-tetraploid DNA content (tetraploid, near-tetraploid, polyploid karyotypes) (Kaneko & Knudson, 2000; Mitelman et al., 2003; Rajagopalan & Lengauer, 2004; Storchova & Pellman, 2004; Weaver & Cleveland, 2006; Storchova & Kuffer, 2008), while the number of chromosomes in some tumour cells is often very high, which is difficult to explain by a repeated accumulation of chromosomes at each division (Storchova & Kuffer, 2008). Second, the majority of tumours contain aneuploid cells that possess multiple centrosomes, which might reflect a previous history of cell division failures and tetraploidy (i.e. cytokinesis failure), without of course excluding the possibility of centrosome overduplication (Lingle et al., 1998; Pihan et al., 1998; Brinkley, 2001; Doxsey, 2001; D'Assoro et al., 2002; Nigg, 2002; Fukasawa, 2005; Saunders, 2005; Fukasawa, 2007). Centrosome abnormalities have been reported to arise at early stages of tumour formation and to expand parallel to tumour progression (Pihan et al., 2001; Shono et al., 2001; Pihan et al., 2003). Third, multipolar mitosis of tetraploid cells, that

have acquired extra centrosomes, leads to aneuploidy (Andreassen et al., 1996; Andreassen et al., 2001b; Borel et al., 2002; Margolis et al., 2003; Storchova & Pellman, 2004).

Fourth, tumour suppressor proteins, such as breast cancer type 2 susceptibility protein (BRCA2), large tumour suppressor homologue 1 (LATS1) and adenomatous polyposis coli (APC), that have been found to be inactivated in human cancers (aneuploid tumours), have been shown to be implicated in cytokinesis (BRCA2 and LATS1), whereas their inactivation leads to cytokinesis failure and increases the percentage of tetraploid/polyploid cells (BRCA2, LATS1 and APC) (Daniels et al., 2004; Yang et al., 2004; Caldwell et al., 2007; Ganem et al., 2007; Storchova & Kuffer, 2008; Holland & Cleveland, 2009). In addition, lack of the kinesin motor protein KIF4, which has been reported to be necessary for cytokinesis (Zhu & Jiang, 2005), from mouse embryonic stem cells, results in increased tetraploidy/polyploidy, subsequent aneuploidy, and enhanced tumourigenesis *in vivo* when cells lacking KIF4 were injected subcutaneously into nude mice (Mazumdar et al., 2006). Importantly KIF4 was found to be absent, or expressed at low levels in 35% of tested human tumour samples (Mazumdar et al., 2006). Fifth, the two proteins p53 and Rb, (along with p21 and p16) that have been implicated in the prevention of further proliferation of tetraploid and aneuploid cells (Minn et al., 1996; Lanni & Jacks, 1998; Andreassen et al., 2001a; Andreassen et al., 2001b; Borel et al., 2002; Meraldi et al., 2002; Margolis et al., 2003), are commonly absent or non-functional in human cancers (Weinberg, 1995; Sherr, 1996; Sherr & McCormick, 2002; Storchova & Pellman, 2004; Ganem et al., 2007; Storchova & Kuffer, 2008).

Finally but most importantly, consistent with the causative role of tetraploidy at least in some types of cancer, and with the long-standing hypothesis that a tetraploid intermediate has a crucial role in the development of aneuploidy and chromosomal instability (aneuploidy develops through chromosomal loss from a tetraploid intermediate) in some solid tumours (Shackney et al., 1989), an increase in tetraploid population of cells have been detected in early-stage cancers either in mice or human model systems (Cowell & Wigley, 1980; Ornitz et al., 1987; Levine et al., 1991b; Galipeau et al., 1996; Southern et al., 1997; Barrett et al., 2003; Olaharski et al., 2006; Storchova & Kuffer, 2008; Holland & Cleveland, 2009). Studies from human patients

with a premalignant condition known as Barrett's oesophagous that leads to the development of esophageal adenocarcinoma (early dysplasia to malignancy), have revealed inactivation/loss of p16 gene, followed by loss of p53 gene and a significant increase of tetraploid cells (increase of 4N populations in diploid cells), before gross aneuploidy occurs (Galipeau et al., 1996; Barrett et al., 1999). This suggests that tetraploid populations in premalignant cells are predisposed to further genomic/chromosomal instability during neoplastic progression, leading to the evolution of aneuploid cells, and through clonal expansion to progression to cancer (Galipeau et al., 1996; Reid et al., 1996; Barrett et al., 1999; Barrett et al., 2003; Maley et al., 2004; Maley, 2007). Similarly, studies from human patients with either normal, low or high-grade squamous intraepithelial lesions, showed that tetraploidy and chromosomal instability occur during the early stages of cervical carcinogenesis, predisposing cervical cells to the formation of aneuploidy (Olaharski et al., 2006). Further evidence, to the notion that polyploid/aneuploid cells are commonly found in tumours of all stages, and that tetraploid cells occur as an early step in tumourigenesis preceding aneuploidy, comes also from studies using mice models of pancreatic cancer (Ornitz et al., 1987; Levine et al., 1991b). Expression of SV40 (simian virus 40) in mouse pancreatic cells leads to a multistep pathway of neoplastic progression, characterised by a progression from normal pancreas to hyperplasia, to dysplasia, and ultimately to carcinoma, accompanied by accumulation of tetraploid cells in the early stages of tumour formation, and the subsequent appearance of aneuploid cells (diploid (normal, hyperplasia) to tetraploid (dysplasia) to aneuploid (neoplastic tissues) (Ornitz et al., 1987).

Therefore, according to all these studies described above, there is compelling evidence to suggest that the uncontrolled proliferation of tetraploid cells is able to promote / enhance cellular transformation and tumour formation, probably due to the increased chromosomal instability that tetraploid cells provoke, both in mammalian and in yeast cells (i.e. tetraploidy in mammalian cells → acquisition of extra centrosomes → errors in the division of tetraploid cells and/or multipolar divisions (defect in chromosome segregation, whole chromosome mis-segregation i.e. multipolar mitosis leads to chromosomal instability due to unsynchronized sister-chromatid separation, high frequency of non-disjunction, and subsequent occurrence of diplochromosomes - sister chromatids remain attached in their centromeres (Gisselsson et al., 2008)) → gain/loss

of chromosomes (oncogene amplification and/or reduction of tumour suppressor genes due to changes in copy number) → aneuploidy → further chromosomal instability due to the unbalanced gene expression of the aneuploid cells (gene expression imbalances might lead to an increase in the rate of spontaneous DNA damage, by altering cellular processes that produce or repair the normally low level of spontaneous DNA damage) → acquisition of transforming mutations that promote cancer) → selection → cancer (Nowell, 1976; Cowell & Wigley, 1980; Shackney et al., 1989; Mayer & Aguilera, 1990; Cahill et al., 1999; Fujiwara et al., 2005; Storchova et al., 2006; Ganem et al., 2007; Storchova & Kuffer, 2008). Although multiple centrosomes, which lead to the formation of multipolar spindles and consequently to aneuploidy and chromosomal instability, can arise either in a diploid cell (centrosome overduplication / amplification) or through the formation of a tetraploid cell (cell fusion and/or failure in cytokinesis) (Nigg, 2002; Fukasawa, 2007), there is probably a striking difference in the fate of those two cells. A diploid cell with increased chromosomal instability (acquisition of extra centrosomes) would probably die after losing multiple chromosomes in a multipolar division (aberrant mitosis) (producing highly unstable aneuploid progeny but not viable), while a tetraploid/polyploid cell by doubling the genome, might have a higher chance of survival after multipolar divisions, because of a higher redundancy in chromosomal content (producing unstable aneuploid progeny but still viable and able to generate new genomic variants) (Shackney et al., 1989; Storchova & Kuffer, 2008).

The extra sets of chromosomes in tetraploid cells and/or near-tetraploid aneuploid cells, might mask (protect against) the effects of deleterious mutations, by the buffering effects of the extra normal chromosomes (Ganem et al., 2007; Storchova & Kuffer, 2008; Holland & Cleveland, 2009). This possibly allows cells to survive for longer in the presence of ongoing DNA damage and allow more time for cells to acquire and accumulate growth-promoting and transforming mutations, providing another explanation for the tumour-promoting activity of tetraploidy and subsequent aneuploidy (Shackney et al., 1989; Ganem et al., 2007; Storchova & Kuffer, 2008; Holland & Cleveland, 2009). Consistently, two studies based on budding yeast evolution experiments, have clearly shown the positive effects that ploidy seems to exhibit on fitness of the cells (Paquin & Adams, 1983; Thompson et al., 2006). Haploid mutator budding yeast (mismatch repair defective) had no growth advantage versus haploid non-mutators. In contrast, diploid mutator had a growth advantage not only over diploid

non-mutators, but also over haploid mutators in long-term evolution experiments, suggesting that in the presence of increased mutations, increased ploidy can offer an overall growth advantage (Thompson et al., 2006; Ganem et al., 2007).

4.3.1.2.3 Possible mechanisms through which GLI2ΔN induces tetraploidy in human N/TERT keratinocytes

As mentioned in **Section 4.2.1.3**, tetraploidy can result from a variety of alterations **(Figure 4.6)** (Storchova & Pellman, 2004) including (a) endoreplication (Ravid et al., 2002), (b) cell fusion due to viruses (Vignery, 2000; Taylor, 2002; Duelli & Lazebnik, 2007), (c) centrosome overduplication (centrosome amplification) (Nigg, 2002; Fukasawa, 2007), (d) failure in centrosome duplication (Nigg, 2002; Fukasawa, 2007), (e) DNA damage (Olive et al., 1996; Waldman et al., 1996; Bunz et al., 1998), or as a result of (f) abortive cell cycle due to defects in different aspects of cell division, such as failure of spindle assembly and chromosome segregation (failure in karyokinesis), microtubule stabilisation or destabilisation by agents such as taxol or nocodazole, respectively (failure in karyokinesis), and cytokinesis failure (Andreassen et al., 1996; Minn et al., 1996; Lanni & Jacks, 1998; Andreassen et al., 2001b; Storchova & Pellman, 2004; Zhivotovsky & Kroemer, 2004).

In addition, defects in some genes can lead to tetraploidisation, which subsequently leads to aneuploidy, chromosomal instability and tumourigenesis (Storchova & Kuffer, 2008; Holland & Cleveland, 2009). Thus, apart from some tumour suppressor genes which have been linked to tetraploidisation and its tumourigenic potential **(see Section 4.3.1.2.2)** (inactivation of tumour suppressor proteins, such as BRCA2, LATS1, and APC) (Daniels et al., 2004; Yang et al., 2004; Caldwell et al., 2007; Ganem et al., 2007; Storchova & Kuffer, 2008; Holland & Cleveland, 2009), there are also several established oncogenes that have been reported to induce tetraploidisation (Storchova & Kuffer, 2008; Holland & Cleveland, 2009). For instance, overexpression of Aurora A kinase in human and mouse cell lines, which has a role in bipolar spindle formation and is frequently overexpressed in human cancers (breast, colon, ovarian, pancreatic) (Meraldi et al., 2004), results in cytokinesis failure and accumulation of bi-nucleated/tetraploid cells and subsequent centrosome amplification (Meraldi et al., 2002). In addition, overexpression of Aurora A in the mammary gland of mice leads to

an increase in the generation of tetraploidy, chromosomal instability and subsequent formation of mammary tumours (Zhang et al., 2004; Wang et al., 2006). This specific phenotype induced by overexpression of Aurora A in cell lines as well as in the mammary gland of mice models was significantly exacerbate, and the tumour incidence in these mice models was significantly increased, in a p53 mutation background (absence of the tumour suppressor p53 protein) (Meraldi et al., 2002; Wang et al., 2006).

Similarly, overexpression of Eg5 (Kif11) in mice, a motor protein that belongs to the BimC family of kinesin-related proteins and has a role in bipolar spindle formation and is often overexpressed in tumours (Carter et al., 2006; Saijo et al., 2006), resulted both in accumulation of mono-nucleated tetraploid and polyploid cell in mouse embryonic fibroblasts from the transgenics, and in the formation of tumours in mice models with widespread aneuploidy and chromosomal instability (Castillo et al., 2007). Accordingly, Mad2, a central component of the spindle assembly checkpoint that blocks separation of sister chromatids until microtubule attachment to kinetochore is complete, and which is inhibited by the retinoblastoma tumour suppressor (Rb) pathway, has also been reported to be expressed at high levels in a number of human cancers (retinoblastoma, B-cell lymphoma, neuroblastoma, liver and lung cancer) (Hernando et al., 2004). Conditional overexpression of Mad2 in mice, resulted in the accumulation of bi-nucleated tetraploid and aneuploid cells (numerical chromosomal instability), and to a significant increase in the number of chromosomal breaks, end-to-end fusions (dicentric chromosomes) and other structural chromosomal aberrations (structural chromosomal instability) (Sotillo et al., 2007). Importantly, transgenic mice overexpressing Mad2, developed a wide range of tumours with extensive chromosomal rearrangements (Sotillo et al., 2007). Finally, high-risk HPV type 16 E6 and E7 oncoproteins can induce abnormal centrosome numbers followed by nuclear atypias (multi-nucleation) (Duensing et al., 2000; Duensing et al., 2001; Duensing & Munger, 2003), as well as both structural and numerical chromosomal instability (Duensing & Munger, 2002; Patel et al., 2004), in primary human keratinocytes. E6 oncoprotein induces the degradation of p53 protein, while E7 can abrogate the suppressive function of Rb tumour suppressor, and also limit the function of $p21^{WAF1/CIP1}$ (Vousden, 1994; Jones et al., 1997; Duensing & Munger, 2003). Overexpression of both E6 and E7 oncogenes in primary human epidermal keratinocytes induces tetraploidy, possibly as a result of the transcriptional deregulation

of many mitosis regulatory genes (Patel et al., 2004). In addition, primary human keratinocytes overexpressing either E6 or E7 or both, resulted in increased tetraploidy, and subsequent polyploidy, after nocodazole treatment, possibly due to the downregulation of p53/p21$^{WAF1/CIP1}$ and Rb proteins (Thomas & Laimins, 1998; Patel et al., 2004). An important observation is that primary human keratinocytes overexpressing HPV type oncoproteins are allowed to enter anaphase despite the formation of multipolar spindles, and they can further display structural chromosomal aberrations, as evidenced by the presence of DNA breaks and anaphase bridges (Duensing & Munger, 2002).

Similar to all these reports, in my study, overexpression of GLI2ΔN in human N/TERT keratinocytes, an oncogene which is frequently overexpressed in human cancers related with aneuploidy and chromosomal instability **(see Section 4.3.1.2.1)**, including human BCCs, prostate and breast cancers, osteosarcomas and oral squamous cell carcinomas (Mullor et al., 2001; Regl et al., 2002; Ruiz i Altaba et al., 2002b; Tojo et al., 2003; Beachy et al., 2004; Ikram et al., 2004; Rajagopalan & Lengauer, 2004; Regl et al., 2004b; Sanchez et al., 2004; Bhatia et al., 2006; O'Driscoll et al., 2006; Perez-Ordonez et al., 2006; Sterling et al., 2006; Weaver & Cleveland, 2006; Thiyagarajan et al., 2007; Asplund et al., 2008; Snijders et al., 2008; Storchova & Kuffer, 2008; Yu et al., 2008; Hirotsu et al., 2010), resulted in accumulation of bi-nucleated/tetraploid cells due to cytokinesis failure **(Figure 4.1, Figure 4.2, Figure 4.4 and Figure 4.8)**, presence of polyploid and aneuploid cells **(Figure 4.4, Figure 4.5 and Figure 4.7)**, and both numerical and structural chromosomal instability **(Figure 4.25, Figure 4.26, Figure 4.27, Figure 4.28, Figure 4.29 and Figure 4.30),** revealing new mechanisms by which GLI2 might exert its tumourigenic effect. Two possible mechanisms could be responsible for the GLI2ΔN-induced tetraploidisation. First, GLI2ΔN might trigger tetraploidisation, by indirectly downregulating 14-3-3σ (stratifin) **(Figure 4.9)**. 14-3-3 sigma (14-3-3σ) is an important regulator of the mitotic cap-independent translation (Pyronnet et al., 2001; Cormier et al., 2003; Holcik & Sonenberg, 2005; Wynshaw-Boris, 2007), and its loss leads to the improper mitotic cap-independent translation of PITSLRE/CDK11^{p58} (endogenous internal ribosomal entry site (IRES)-dependent form of the cyclin-dependent kinase Cdk11) protein and improper localisation of Polo-like kinase-1 (Plk1) (loss of Polo-like kinase-1 protein in the midbody during mitosis, a protein which is required for cytokinesis). Both these proteins are important

executioners of mitosis (Neef et al., 2003; Liu et al., 2004b; Petretti et al., 2006; Hu et al., 2007), and the deregulation of PITSLRE/CDK11^{p58} mitotic cap-independent translation by 14-3-3σ knockdown, leads to cytokinesis failure and accumulation of binucleate/tetraploid cells as reported by Wilker et al. (Wilker et al., 2007). Second, GLI2ΔN might trigger tetraploidisation, by indirectly downregulating p21$^{WAF1/CIP1}$ (p21) cyclin dependent kinase (CDK) inhibitor **(Figure 4.11)**. p21$^{WAF1/CIP1}$ protein plays a pivotal role in centrosome homeostasis, as well as in the prevention of polyploidisation (Stewart et al., 1999; Duensing et al., 2006). Although many studies have shown that p21 deficiency causes the development of abnormal centrosome numbers (Fukasawa et al., 1996; Bunz et al., 1998; Mantel et al., 1999; Matsumoto et al., 1999; Tarapore et al., 2001), it is not clear whether the accumulation of extra centrosomes in the absence of p21 is a solely secondary phenomenon of cell division failure and polyploidisation, or if it can also be a genuine phenomenon. However, a recent study by Duensing et al. (Duensing et al., 2006) using a novel marker for maternal centrioles, Cep170, showed that knock-down of p21 protein expression in murine myeloblasts, triggers the development of excessive centriole numbers in the presence of only one or two maternal centrioles (overduplication of centrioles), and to a much lesser extent, the accumulation of centrioles in p21-deficient cells due to cytokinesis failure and polyploidisation. Therefore, the downregulation of p21$^{WAF1/CIP1}$ by GLI2ΔN in human N/TERT keratinocytes, might induce centrosome overduplication followed by cytokinesis failure, and resulting in genome doubling and increased bi-nucleated tetraploidy (Fukasawa, 2007).

A low, but detectable proportion of wild-type N/TERT and SINCE control populations was presented with DNA content N>4 and 8N **(Figure 4.4, Figure 4.5 and Figure 4.8)**. This suggests the presence of spontaneously arising tetraploid and polyploid cells within the normal population. This is in agreement with a recent report by Shi and King (Shi & King, 2005), showing that human N/TERT keratinocytes have low rates of chromosomal non-disjunction during normal bipolar mitoses (both copies of a chromosome segregate to the same daughter cell), which leads to the generation of bi-nucleated tetraploid progenies (~ 2%) due to cytokinesis failure (cleavage furrow regression), instead of aneuploid progenies (Shi & King, 2005; Ganem et al., 2007). The majority of these wild-type p53 N/TERT tetraploid cells (60%) do not proceed to the next division, and from the rest 40% that proceeds to the next cell division only 35%

form multipolar spindle (Shi & King, 2005). In contrast, in the p53-suppresed HeLa (human cervical cancer) cells (~ 8% bi-nucleated tetraploid cells due to chromosome non-disjunction and cytokinesis failure), bi-nucleated/tetraploid cells almost universally divide, and from these, 94% form multipolar spindle (Shi & King, 2005). The fact that the majority of N/TERT bi-nucleated tetraploids did not proceed to the next division, suggests the existence of a checkpoint (though a leaky checkpoint in N/TERT cells, since a minority of tetraploid cells proceed to the next division, probably due to p16 downregulation that N/TERT immortalised cells exhibit (Dickson et al., 2000)) and thus, activation of oncogenes and/or loss of tumour suppressor genes might be necessary at a subsequent step, enabling bi-nucleated/tetraploid cells to proliferate inappropriately and/or to promote multipolar division, which can give rise to highly aneuploid progenies (Margolis, 2005; Shi & King, 2005). Consistently, a recent study by Thompson and Compton (Thompson & Compton, 2008) showed that elevating chromosome missegregation rates alone in human cultured cells is not sufficient to convert stable, near-diploid cells into highly aneuploid cells with karyotypes that resemble those of tumour cells. Therefore, the overexpression of GLI2ΔN oncogene not only can trigger tetraploidisation, but also may allow the propagation of arising tetraploids and of the resulting aneuploids.

4.3.1.3 Uncontrolled proliferation of tetraploid and aneuploid cells through impaired cell cycle arrest and apoptosis

In the absence of anti-apoptotic activation, tetraploid and aneuploid cells, in a variety of cell types, show limited growth potential as they normally undergo cell cycle arrest and/or apoptosis following activation of p53 and several p53-targeted genes (i.e. p21) **(see Section 4.2.2)** (Lane, 1992; Lanni & Jacks, 1998; Andreassen et al., 2001a; Andreassen et al., 2001b; Borel et al., 2002; Chen et al., 2003; Margolis et al., 2003; Storchova & Pellman, 2004; Zhivotovsky & Kroemer, 2004; Castedo et al., 2006). Tetraploidy activates cell death pathways and most of the resulting tetraploid cells undergo apoptosis, which seems to be mainly p53-dependent and mitochondrial-mediated (Chen et al., 2003; Castedo et al., 2006; Ganem et al., 2007; Storchova & Kuffer, 2008).

4.3.1.3.1 GLI2ΔN upregulates BCL-2 in N/TERT keratinocytes

It has been previously suggested that overexpressed BCL-2 inhibits apoptosis after a failed cell division (human and mouse cells treated either with nocodazole-mitotic inhibitor or cytochalasin-cytokinesis inhibitor), resulting in the generation of tetraploid cells with enhanced survival, while defective apoptosis due to BCL-2 overexpression can also favour multipolar and asymmetric divisions of tetraploid cells, which leads to aneuploidy and numerical chromosomal instability (Minn et al., 1996; Nelson et al., 2004; Zhivotovsky & Kroemer, 2004; Castedo et al., 2006). BCL-2 is one of the major anti-apoptotic factors of the intrinsic pathway of apoptosis (p53-dependent apoptosis) **(see Section 4.2.5.3)** (Hockenbery et al., 1990; Hockenbery, 1995; Youle & Strasser, 2008), and it has also been identified as a direct transcriptional target of GLI2 transcription factor (Regl et al., 2004b). Consistently, BCL-2 was found to be upregulated in GLI2ΔN-expressing keratinocytes **(Chapter 3, Section 3.2.1.4, Figure 3.5A and Chapter 4, Figure 4.11)**, while SINEG2 cells did not exhibit any increased apoptotic activity (oncogenic stress and/or cell cycle failure-mediated apoptosis) compared to the N/TERT and SINCE control cells **(Figure 4.3 and Figure 4.4)**. This suggests that the enhanced survival of tetraploid GLI2ΔN-expressing cells and the subsequent formation of GLI2ΔN aneuploid progenies may be attributed to the increased levels of BCL-2.

In addition, overexpression of BCL-2 in human N/TERT keratinocytes upon GLI2ΔN induction, may not only be contributing to the enhanced survival of tetraploid and aneuploid cells, but also to the resistance of GLI2ΔN-keratinocytes to UVB-mediated apoptosis (p53-dependent apoptosis) observed in my study **(see Section 4.2.5 and Figure 4.14, Figure 4.16, Figure 4.18)** and consistent with the resistance to apoptosis, mediated by intrinsic or extrinsic pathways, of human BCCs (Regl et al., 2004b; Erb et al., 2005; Erb et al., 2008; Kump et al., 2008). Accordingly, Rodriguez-Villanueva et al. (Rodriguez-Villanueva et al., 1998) using a transgenic mouse model with human BCL-2 overexpressed in the epidermis under the control of human keratin 1 promoter, showed both *in vivo* and *in vitro* that keratinocytes with increased levels of BCL-2 had a reduced rate of apoptosis upon UVB treatment, and were more susceptible to skin tumour formation in response to chemical carcinogens compared to control keratinocytes, suggesting that impaired apoptosis is a critical step in tumour

development. Similarly, in human BCCs, which are resistant in apoptosis (Regl et al., 2004b; Erb et al., 2005; Erb et al., 2008; Kump et al., 2008) and UVB is known to be one of the main risk and etiological factor (Grossman & Leffell, 1997; Soehnge et al., 1997; Armstrong & Kricker, 2001; de Gruijl et al., 2001; Ehrhart et al., 2003; Erb et al., 2008), both GLI2 and BCL-2 are co-expressed (Regl et al., 2004b), while increased levels of BCL-2 have also been reported (Rodriguez-Villanueva et al., 1995; Delehedde et al., 1999; Regl et al., 2004b). In support of the role of GLI2ΔN in apoptotic resistance of human BCCs through the upregulation of BCL-2, and c-FLIP **(see Section 4.2.5.3)** (Kump et al., 2008), Ji et al. (Ji et al., 2008) showed that Gli2 gene silencing *in vivo* renders cells susceptible to apoptosis (increases cell death). In this study, mouse Gli2 gene was silenced in a mouse BCC-like tumour cell line (K5-Gli2ΔN2) that constitutively express high levels Gli2ΔN2, and is originated from a K5-Gli2ΔN2-induced trichoblastoma (Ji et al., 2008). When the Gli2 knock down cells were injected subcutaneously into nude mice, they gave rise to tumours of a much slower growth rate, partly due to the increased susceptibility to apoptosis of tumour cells, compared to the tumours arising from control cells (Ji et al., 2008). Finally, BCL-2 undergoes an increase in expression in many other cancers (Igney & Krammer, 2002; Lessene et al., 2008), further supporting the notion that its overexpression inhibits cell death and contributes to tumour formation, including skin carcinogenesis (Vaux et al., 1988; Hockenbery et al., 1990; Hockenbery, 1995; Rodriguez-Villanueva et al., 1998; Jiang & Milner, 2003; Lessene et al., 2008; Youle & Strasser, 2008).

4.3.1.3.2 GLI2ΔN downregulates $p21^{WAF1/CIP1}$ and 14-3-3σ in a p53-independent manner in human N/TERT keratinocytes

The tumour suppressor p53 and its direct transcriptional target $p21^{WAF1/CIP1}$ (el-Deiry et al., 1994), have been found to be primarily associated with both DNA damage checkpoints (G1/S and G2/M checkpoints), and to act as a backup mechanism in the mitotic checkpoint control, either by inducing cell cycle arrest and/or apoptosis, preventing the survival of tetraploid cells yielded from defects during mitosis **(see Chapter 1, Section 1.3.7.1 and Chapter 4, Section 4.2.2, Section 4.2.3)** (Kuerbitz et al., 1992; el-Deiry et al., 1994; Brugarolas et al., 1995; Cross et al., 1995; Minn et al., 1996; Bunz et al., 1998; Khan & Wahl, 1998; Lanni & Jacks, 1998; Wang et al., 1998;

Chehab et al., 1999; Andreassen et al., 2001a; Andreassen et al., 2001b; Taylor & Stark, 2001; Borel et al., 2002; Margolis et al., 2003; Sherr, 2004; Castedo et al., 2006).

Therefore, p53 tumour suppressor and its targets play a critical role (anti-cancer activity) in the mechanisms that protect cells, including skin cells, against genomic instability which can be caused due to DNA damage (i.e. DNA breaks either due to replication errors, UVB radiation or oncogene amplification), and subsequent tumour formation due to persistent DNA damage (Soehnge et al., 1997). Stabilisation and activation of p53 after DNA damage, induces arrest in cell proliferation at the G1/S and G2/M phases, through the activation of its direct transcriptional targets such as $p21^{WAF1/CIP1}$ and 14-3-3σ cyclin-dependent kinase inhibitors (negative regulators of cell cycle), in order to provide sufficient time for DNA damage repair (Levine et al., 1991a; Lane, 1992; el-Deiry et al., 1994; Hermeking et al., 1997; Levine, 1997; Dhar et al., 2000; Khanna & Jackson, 2001; Vousden & Lu, 2002; Lobrich & Jeggo, 2007). If DNA repair is not possible, then the DNA damaged cells are eliminated through apoptosis under the control of p53 gene (Levine et al., 1991a; Levine, 1997; Ashkenazi, 2002; Vousden & Lu, 2002; Zhivotovsky & Kroemer, 2004; Brown & Attardi, 2005; Erb et al., 2008; Taylor et al., 2008). Therefore, the downregulation of p21 before **(Figure 4.11),** and after UVB treatment **(Figure 4.12)**, and the downregulation of 14-3-3 sigma **(Figure 4.9)**, indirectly by GLI2ΔN, may relax the DNA damage checkpoints, possibly allowing cells with DNA breaks to propagate unrepaired to the next cell cycles, yielding cells with structural chromosomal abnormalities, enhancing their survival, and thus triggering genomic instability and tumour formation.

Similarly, in response to ploidy abnormalities, even if p53 and $p21^{WAF1/CIP1}$do not primarily participate in checkpoint function in mitosis, they both play a role as a backup mechanism, so-called "tetraploidy checkpoint", in cells that have evaded transient mitotic arrest, imposed by an abortive cell cycle **(see Section 4.2.2)** (Minn et al., 1996; Lanni & Jacks, 1998; Andreassen et al., 2001a; Andreassen et al., 2001b; Borel et al., 2002; Margolis et al., 2003; Storchova & Pellman, 2004; Zhivotovsky & Kroemer, 2004). Although the universality and the existence of a so called "tetraploidy checkpoint" has been debated (Uetake & Sluder, 2004; Wong & Stearns, 2005) and suggested that the fate of tetraploid cells depends on the cell type and genetic context, it is widely acknowledged that tetraploid cells at least in some cell types, resulting either

from karyokinesis or cytokinesis failure or both, permanently arrest in G1 phase, an arrest which mainly depends on p53 and $p21^{WAF1/CIP1}$, as well as on Rb function (Andreassen et al., 2001b; Borel et al., 2002; Margolis et al., 2003; Ganem et al., 2007; Storchova & Kuffer, 2008). Activation of p53 and $p21^{WAF1/CIP1}$ upon tetraploidisation, finally triggers apoptosis as I mentioned earlier, and thereby prevents the propagation of errors of defective mitosis and the generation of polyploid cells, possible precursors of aneuploid cells and chromosomal instability (Lane, 1992; Minn et al., 1996; Lanni & Jacks, 1998; Andreassen et al., 2001a; Andreassen et al., 2001b; Borel et al., 2002; Chen et al., 2003; Margolis et al., 2003; Storchova & Pellman, 2004; Zhivotovsky & Kroemer, 2004; Fujiwara et al., 2005; Castedo et al., 2006). Therefore, even if a 'tetraploidy checkpoint' that senses the ploidy abnormality exists and triggers permanent arrest in tetraploid cells, or tetraploidy due to aberrant mitosis causes damages in the mitotic apparatus and/or cytoskeleton, DNA damages, or centrosome abnormalities (centrosome damage / centrosomal stress) which in turn activates G1 arrest and cell death, the resulted G1 arrest will be in both cases p53 and $p21^{WAF1/CIP1}$ dependent (Aylon et al., 2006; Srsen et al., 2006; Ganem et al., 2007; Storchova & Kuffer, 2008). However, neither loss of p53 nor Rb suppression leads to gross aneuploidy that often accompanies tumourigenesis in the absence of other metabolic defects, further suggesting that p53 and Rb are not responsible for the formation of tetraploid and aneuploid cells, but are members of G1 surveillance mechanisms that normally would prevent the cell cycle progression of the arising tetraploid and aneuploid cells (Borel et al., 2002; Bunz et al., 2002; Margolis et al., 2003).

The reduction of $p21^{WAF1/CIP1}$ protein levels in combination with the lack of p53 stabilisation, observed in my stable GLI2ΔN expressing cell line **(Figure 4.11)**, first indicates an abnormal G1 checkpoint control, whereby cells are allowed to progress through S phase after aberrant mitotic exit. This implies that a proportion of arising tetraploid cells in this culture evade to a G1-like biochemical state and were allowed to reinitiate DNA replication, as indicated by the presence of cells with DNA content 8N (polyploid cells and tetraploid mitotic cells) and DNA content >4N (aneuploid cells), leading to numerical chromosomal instability **(Figure 4.4, Figure 4.5 and Figure 4.7)**. In addition, $p21^{WAF1/CIP1}$ protein plays a pivotal role in centrosome overduplication **(see Section 4.3.1.2.3)** (Duensing et al., 2006), and in preventing endoreduplication and tetraploidisation (Stewart et al., 1999), and thus its downregulation could explain the

occurrence and maintenance of a high percentage of tetraploid and polyploid cells in SINEG2 culture **(Figure 4.4, Figure 4.5 and Figure 4.8)**. The absence of $p21^{WAF1/CIP1}$ in DNA damaged (γ irradiation) human colorectal cancer cells leads to the escape of cells from the growth inhibition normally conferred by p53/p21, followed by DNA synthesis (endoreduplication) and giving rise to polyploid cells, while its absence in human haematopoietic cells causes re-replication, centrosome overduplication and polyploidy in response to nocodazole treatment (Mantel et al., 1999; Zhivotovsky & Kroemer, 2004). However, the activation of $p21^{WAF1/CIP1}$ and inhibition of cyclin E/cdk2 activity prevents endoreduplication and polyploidy in human colon cancer cells in response to nocodazole (Stewart et al., 1999). In addition, Shen et al. (Shen et al., 2005) showed, using a mouse model and a mouse cell line, that ATM (DNA damage checkpoint protein kinase mutated in ataxia telangiectasia) and p21 cooperate to impede tumourigenesis by suppressing aneuploidy development, while p21 acts as a tumour suppressor specifically in a genetically unstable background ($ATM^{-/-}$), by suppressing further numerical chromosomal instability. $ATM^{-/-}p21^{-/-}$ mice had an increased frequency of tumour development (carcinomas and sarcomas) with aneuploidy and intratumoural heterogeneity (chromosomal instability), as judged by cytogenetic analysis (Shen et al., 2005). Loss of p21 in $ATM^{-/-}$ mouse embryonic fibroblasts exacerbated the percentage of tetraploid, polyploid and aneuploid metaphases and thus the development of further numerical chromosomal instability (Shen et al., 2005).

Furthermore, ectopic overexpression of $p21^{WAF1/CIP1}$ in p53-defective human brain tumour cells, inhibits proliferation, aneuploidy and tumourigenicity of the cells (Chen et al., 1996). Overexpression of $p21^{WAF1/CIP1}$ *in vitro* resulted in reduced cell proliferation as demonstrated by increased cell doubling time and G1-arrested cell cycle, in inhibition of the accumulation of aneuploid cells upon nocodazole treatment, and in reduced tumourigenic potential as indicated by the loss of anchorage-independent growth in soft agar (Chen et al., 1996). Subcutaneous injection of control cells and cells overexpressing $p21^{WAF1/CIP1}$ in nude mice, further supported the alteration of the malignant phenotype of $p21^{WAF1/CIP1}$-expressing cells, and the prevention of tumour formation *in vivo*, since no tumour was observed post cell implantation in mice, compared to the control cells that formed large tumours (Chen et al., 1996). In addition, although there are conflicting data in the role of $p21^{WAF1/CIP1}$ as a tumour suppressor in skin carcinogenesis, several studies have shown that loss of $p21^{WAF1/CIP1}$ in

keratinocytes with chemical-induced carcinogenesis, or in keratinocytes overexpressing oncogenes such as ras, or in keratinocytes missing genes such as c-myc and Notch1 while overexpressing ras, is able to enhance neoplasia (Missero et al., 1996; Philipp et al., 1999; Topley et al., 1999; Weinberg et al., 1999; Dotto, 2000; Weinberg & Denning, 2002; Nicolas et al., 2003; Oskarsson et al., 2006).

Therefore, the role p53 and $p21^{WAF1/CIP1}$ to protect cells from genomic instability, either caused by UVB-induced DNA damage or ploidy abnormalities, and subsequent tumourigenesis, is further supported by the fact that many human cancers associated with tetraploidy and aneuploidy have commonly the p53, $p21^{WAF1/CIP1}$ and Rb proteins absent or non-functional (Weinberg, 1995; Sherr, 1996; Sherr & McCormick, 2002; Storchova & Pellman, 2004; Bott et al., 2005; Ganem et al., 2007; Storchova & Kuffer, 2008), including human BCCs which have very frequently inactivated p53 mutations mainly caused by UVB radiation (Demirkan et al., 2000; Lacour, 2002; Bolshakov et al., 2003), and almost absence of $p21^{WAF1/CIP1}$ protein as observed in my study **(Figure 4.13)**. Similarly, 14-3-3σ is frequently lost in many cancers including breast and prostate (Ferguson et al., 2000; Umbricht et al., 2001; Hermeking, 2003; Lodygin et al., 2004; Lodygin & Hermeking, 2005; Mhawech et al., 2005; Lodygin & Hermeking, 2006), including human BCCs which exhibit partial or complete loss of 14-3-3σ protein expression (Lodygin et al., 2003).

Second, the reduced levels of $p21^{WAF1/CIP1}$ protein, along with the unchanged levels of p53 protein, underscore the fact that GLI2ΔN negatively regulates $p21^{WAF1/CIP1}$ independently of p53 **(Figure 4.11)**. In accordance, when keratinocytes were exposed to UVB irradiation, which is known to stimulate p53-mediated induction of $p21^{WAF1/CIP1}$ (Levine et al., 1991a; Lane, 1992; Levine, 1997; Vousden & Lu, 2002; Lobrich & Jeggo, 2007), p53 was upregulated both in SINEG2 and SINCE control cells, whereas $p21^{WAF1/CIP1}$ was only upregulated in control cells, but not in GLI2ΔN expressing keratinocytes **(Figure 4.12)**. This observation further confirms that the downregulation of $p21^{WAF1/CIP1}$ by GLI2ΔN induction occurs in a p53-independent manner, not only in the presence of tetraploid cells, but also in response to UVB-induced DNA damage. Consistently, transcription of $p21^{WAF1/CIP1}$ has been reported to be downregulated upon inducible GLI2ΔN induction in confluent contact-inhibited and sub-confluent HaCaT keratinocytes (Regl et al., 2004a; Eichberger et al., 2006), which are known to harbour

inactivated p53 mutations (both alleles of the HaCaT cell line are mutated in the p53 gene) (Boukamp et al., 1988; Lehman et al., 1993), and thus further confirm the ability of GLI2ΔN to downregulate $p21^{WAF1/CIP1}$ in a p53-independent manner. In support of the latter, GLI1 a downstream target of GLI2 in human keratinocytes (Regl et al., 2002; Ikram et al., 2004), has also been reported to negatively regulate $p21^{WAF1/CIP1}$ independent of p53 in human gastric carcinoma cells (Ohta et al., 2005). SHH and GLI1 have been found to be highly expressed in human gastric carcinoma cells and tissues (Ohta et al., 2005). Knock-down of GLI1 in human gastric carcinoma cells resulted in a significant increase in the proportion of cells in G1 phase and in the upregulation of transcription and protein levels of $p21^{WAF1/CIP1}$ but not of p53 (Ohta et al., 2005). Similar results were obtained by treatment of human gastric cells with cyclopamine in order to inhibit SHH/GLI signalling, whereas Gli1 expression suppressed the cyclopamine-induced increase in $p21^{WAF1/CIP1}$ (Ohta et al., 2005). The authors suggested the possibility of SHH/GLI pathway to cross talk with other signalling pathways including PI(3)K (phosphatidylinositol-3-OH kinase), which have been shown to repress the expression of $p21^{WAF1/CIP1}$ in a p53-independent manner in tumour cells (Massague, 2004; Seoane et al., 2004; Ohta et al., 2005).

In view of the strongly activating properties of the GLI2ΔN transcription factor (constitutively active form of GLI2 lacking the N-terminal repressor domain), repression of $p21^{WAF1/CIP1}$ and of 14-3-3σ in my system is likely to be indirect, possibly by GLI2ΔN specific and direct activation of a transcriptional repressor, such as FOXE1 (forkhead transcription factor) (Eichberger et al., 2004; Eichberger et al., 2006), which has been shown to have a repressor function (Zannini et al., 1997; Perrone et al., 2000) and to be specifically expressed in basal undifferentiated keratinocytes of the epidermis and highly expressed in human BCCs (Eichberger et al., 2004). In addition, GLI2ΔN could regulate p21 and 14-3-3σ in post-translational level by activating proteins necessary for their protein degradation. Finally, another possible explanation for the downregulation of p21 and 14-3-3σ upon GLI2ΔN induction, could be the CpG hypermethylation of their promoter (epigenetic mechanism). Many gene promoters have CpG islands, which are regions of DNA with higher concentration of CpG sites (Cytosine-phosphate-Guanine sites - regions of DNA where a cytosine nucleotide occurs next to a guanine nucleotide in the linear sequence of bases) (Jaenisch & Bird, 2003; Lodygin & Hermeking, 2005; Lodygin & Hermeking, 2006). Cytosines in CpG

islands are methylated (addition of a methyl group) by methyltransferases (DNMTs) to form a 5-methylcytosine, allowing the recognition by specific proteins that recruit chromatin remodelling factors and histone deacetylases resulting in decreased transcriptional activity of the chromatin (Jaenisch & Bird, 2003; Lodygin & Hermeking, 2005; Lodygin & Hermeking, 2006). CpG islands, often in cancer cells acquire abnormal hypermethylation, which results in transcriptional silencing and leads to the loss of gene function (i.e. loss of a tumour suppressor gene function through an epigenetic mechanism) (Jaenisch & Bird, 2003; Lodygin & Hermeking, 2005; Lodygin & Hermeking, 2006).

Strikingly, methyltransferases which are over-expressed in many types of human tumour cells (Robertson et al., 1999), have been reported to cooperate with oncogenes including c-fos in the transformation of primary mouse fibroblasts cells, suggesting that oncogenes transform cells through alterations in DNA methylation by overexpressing DNMTs (Bakin & Curran, 1999). Accordingly, loss of Rb (retinoblastoma tumour suppressor protein), following activation of E2F1 transcription factor has been shown to promote aberrant expression of DNMT in human and murine prostate epithelial cells (McCabe et al., 2005). Most importantly, 14-3-3 sigma which is downregulated in GLI2ΔN-expressing keratinocytes, has been reported to be frequently lost in many cancers such as breast and prostate due to hypermethylation of its promoter (Ferguson et al., 2000; Umbricht et al., 2001; Hermeking, 2003; Lodygin et al., 2004; Lodygin & Hermeking, 2005; Mhawech et al., 2005; Lodygin & Hermeking, 2006), while human BCCs exhibit partial or complete loss of 14-3-3σ protein expression, due to CpG-hypermethylation of the 14-3-3σ promoter (Lodygin et al., 2003). Similarly, p21, which is suppressed upon GLI2ΔN induction in human keratinocytes and is lost in many cancers including prostate cancer, was also found to be inactivated in metastatic prostatic cancer human cell lines (where HH/GLI activation has been previously shown to be implicated **(see Chapter 1, Section 1.3.5)** (Karhadkar et al., 2004; Sheng et al., 2004; Bhatia et al., 2006; Thiyagarajan et al., 2007)), by promoter hypermethylation (Bott et al., 2005).

Therefore, it is plausible to imagine that GLI2ΔN downregulates p21 or 14-3-3σ or both, by inducing the overexpression of DNMTs, followed by gene promoter hypermethylation and thus gene silencing. It would be interesting to treat SINEG2 and

control cells with either 5-azacytidine (azacytidine) or 5-aza-2'deoxycytidine (decitabine), which are demethylating agents (Issa & Kantarjian, 2005; Gore et al., 2006), and check if expression of p21 and/or 14-3-3σ is reactivated in SINEG2 cells.

4.3.2 Downregulation of $p21^{WAF1/CIP1}$ and 14-3-3σ might contribute to the GLI2ΔN-mediated resistance to differentiation *in vitro* and *in vivo*

In normal human epidermis, BCL-2 is exclusively expressed in the basal layer of the epidermis (Rodriguez-Villanueva et al., 1995; Delehedde et al., 1999), while 14-3-3σ is abundantly expressed in the differentiated suprabasal layers of human epidermis (Dellambra et al., 2000). The distribution of both BCL-2 and 14-3-3σ protein in normal human skin indicates that the overexpression of BCL-2 and the downregulation of 14-3-3σ upon GLI2ΔN induction, might contribute to the undifferentiated phenotype observed in SINEG2 keratinocytes **(see Chapter 3, Section 3.2.3.1 and Section 3.2.3.1.1, Figure 3.13)**.

Similarly, the expression of $p21^{WAF1/CIP1}$ in normal human epidermis showed a diffuse pattern, with $p21^{WAF1/CIP1}$ protein being mainly detected in the non-proliferating suprabasal layers of the epithelium with very few positive stained cells in the basal layer **(Figure 4.13A),** consistent with the role of $p21^{WAF1/CIP1}$ in promoting G1 arrest (cell growth arrest) of keratinocytes prior to terminal keratinocyte differentiation and thus irreversible commitment to differentiation **(see Chapter 3, Section 3.3.3)** (Potten & Morris, 1988; Steinman et al., 1994; Missero et al., 1995; Missero et al., 1996; Tron et al., 1996; Di Cunto et al., 1998; Todd & Reynolds, 1998; Topley et al., 1999; Dotto, 2000). Therefore, the downregulation of $p21^{WAF1/CIP1}$ observed upon GLI2ΔN induction *in vitro* **(Figure 4.11)**, further confirms the undifferentiated phenotype of SINEG2 cells, and it also supports the notion that GLI2ΔN suppresses keratinocyte differentiation through the downregulation of genes responsible for the onset of differentiation, including $p21^{WAF1/CIP1}$, c-MYC **(see Chapter 3, Section 3.2.1.4, Figure 3.5B and Section 3.3.7)** and of differentiation markers such as involucrin **(see Chapter 3, Section 3.2.3.1.1, Appendix II and Section 3.3.5)** and 14-3-3σ (stratifin), as well as through the upregulation of stem cell markers such as integrin β1 and SOX2 **(see**

Chapter 3, Section 3.2.3.1.1, Figure 3.13, Section 3.3.6, Section 3.3.6.1 and Section 3.3.6.2). Importantly, it has been suggested that similar to c-MYC, suppression of $p21^{WAF1/CIP1}$ and 14-3-3 sigma, are implicated in the maintenance of epidermal stem cells (Topley et al., 1999; Dellambra et al., 2000; Dotto, 2000). Downregulation of 14-3-3σ results in immortalization of primary human keratinocytes (escape senescence by maintenance of telomerase activity and by downregulating p16), indicating a role in maintaining epidermal stem cells and promoting cell transformation (Dellambra et al., 2000). Mouse keratinocytes derived from $p21^{-/-}$ mice have been reported to contain a significantly increased number of cells with clonogenic potential and high rates of adherence, lesser commitment to differentiation, and the ability to generate all types of terminally differentiated keratinocytes that are present *in vivo* (interfollicular epidermis and hair follicles) (Topley et al., 1999).

Consistent with the undifferentiated phenotype of human BCCs (Miller, 1991a; Crowson, 2006), different subtypes of human BCCs showed almost absence of $p21^{WAF1/CIP1}$ protein, with the exception of individual positively stained cells **(Figure 4.13B, C, D)**, indicating that GLI2ΔN-mediated $p21^{WAF1/CIP1}$ downregulation *in vitro* **(Figure 4.11 and Figure 4.12)**, absolutely correlates with the $p21^{WAF1/CIP1}$ expression pattern in human BCCs *in vivo*. Similarly, 14-3-3σ protein which was found to be downregulated in GLI2ΔN-expressing keratinocytes **(Figure 4.9)**, is partially or completely lost in human BCCs due to CpG-hypermethylation of the 14-3-3σ promoter (Lodygin et al., 2003). These observations further strengthen the notion that overexpression of GLI2ΔN in cultured human keratinocytes can elicit gene expression patterns, similar to those observed in human BCCs *in vivo*. However, it is possible that the downregulation of $p21^{WAF1/CIP1}$ and 14-3-3σ protein in human BCCs reflect the expression pattern of the suggested cell of origin for these tumours, which is the undifferentiated basal epidermal stem cell **(see Chapter 1, Section 1.3.6)**. Even if that is the case, the expression of GLI2ΔN may contribute to the maintenance of this gene expression signature. Finally, the possibility that the suppression of p21 protein in human BCCs is due to the frequently observed p53 inactivation mutations (Barbareschi et al., 1992; Shea et al., 1992; Grossman & Leffell, 1997; Ponten et al., 1997; Soehnge et al., 1997; de Gruijl et al., 2001; Ling et al., 2001; Dicker et al., 2002; Lacour, 2002; Daya-Grosjean & Couve-Privat, 2005; Reifenberger et al., 2005; Epstein, 2008), cannot be ruled out.

4.3.3 GLI2ΔN induces structural chromosomal instability in human N/TERT keratinocytes

Stable overexpression of GLI2ΔN in human N/TERT keratinocytes causes chromosomal instability, which is one of the major hallmarks of cancer **(see Section 4.2.6)** (Hanahan & Weinberg, 2000), including both numerical (tetraploidy, polyploidy, aneuploidy) **(Figure 4.25 and Figure 4.26)**, and structural chromosome aberrations, such as chromosomal translocations and double minute chromosome, as observed using M-FISH and karyotype analysis **(Figure 4.27, Figure 4.28 Figure 4.29 and Figure 4.30)**.

Consistent with my data, overexpression of other oncogenes, such as Mad2 in mice **(see Section 4.3.1.2.3)**, apart from resulting in the accumulation of tetraploid and aneuploid cells (numerical chromosomal instability), also showed also a significant increase in the number of DNA breaks and structural chromosomal aberrations (structural chromosomal instability) (Sotillo et al., 2007). Importantly, transgenic mice overexpressing Mad2, developed a wide range of tumours with extensive chromosomal rearrangements (Sotillo et al., 2007). My results are also in agreement with previous studies **(see Section 4.3.1.2.2)**, which have shown that the proliferation of tetraploid, compared to diploid cells in culture, in the presence of an oncogene or in the absence of tumour suppressor gene, give rise to the accumulation of both numerical (aneuploidy) and structural chromosomal abnormalities (i.e. non-reciprocal translocations, double minute chromosomes) (Fujiwara et al., 2005; Duelli et al., 2007; Holland & Cleveland, 2009). Similarly, mice tetraploid-derived tumours display large-scale numerical and structural chromosomal aberrations (Fujiwara et al., 2005). Therefore, since uncontrolled tetraploidy in these studies, is coupled with massive chromosomal instability (numerical and structural) (Fujiwara et al., 2005; Duelli et al., 2007) and *in vitro* chemically induced transformation (Fujiwara et al., 2005), as well as with spontaneous *in vivo* transformation (Fujiwara et al., 2005; Duelli et al., 2007), it would be interesting to check if GLI2ΔN-expressing keratinocytes that exhibit both uncontrolled tetraploidy and numerical and structural chromosomal instability, have also a potential to *in vitro* transformation, by assaying the growth of the cells in soft agar, which is a known attribute of many transformed cells (Traul et al., 1979; Traul et al., 1981).

However, it remains yet unclear how increased ploidy (tetraploidy) promotes structural chromosomal abnormalities. Taking into account that structural chromosome abnormalities (i.e. translocations) have been suggested to arise from breaks in DNA (DNA double strand breaks) during DNA replication or mitosis and improper DNA repair (Paulovich et al., 1997; Lengauer et al., 1998; Richardson & Jasin, 2000; Khanna & Jackson, 2001; Zhivotovsky & Kroemer, 2004; Jefford & Irminger-Finger, 2006; Lobrich & Jeggo, 2007; Pellman, 2007; Aguilera & Gomez-Gonzalez, 2008; Nambiar et al., 2008), two major sources of chromosomal rearrangements have been recommended (Ganem et al., 2007; Storchova & Kuffer, 2008; Holland & Cleveland, 2009).

First, tetraploidy might increase the rate of spontaneous DNA damage and breakage (Ganem et al., 2007; Storchova & Kuffer, 2008). The acquisition of double the amount of DNA content of a tetraploid cell, might result in twice the amount of spontaneous DNA damage during S phase, which leads to increased requirement for, or even saturation, of DNA repair processes, as observed in budding-yeast tetraploids (increased requirement of tetraploid cells for homologous recombination genes compared to diploid cells, given that the length of the cell cycle, and specifically S phase is not increased with higher ploidy) and possibly inefficient repair (Storchova et al., 2006; Ganem et al., 2007; Storchova & Kuffer, 2008). Indeed, wild-type yeast tetraploid cells have been reported to accumulate DNA damage and to be more sensitive to agents that damage DNA by inducing double-strand-breaks (not sensitive to UV light), compared to their diploid counterparts (Storchova et al., 2006). Similarly, human tetraploid fibroblasts appear to be more sensitive to DNA damaging agents (ionizing radiation) relative to normal diploid fibroblasts (Hau et al., 2006). Moreover, whole chromosome missegregation in tetraploid cells and subsequent near-tetraploid aneuploidy, which may lead to unbalanced gene expression, might also cause an increase in the rate of spontaneous DNA damage, by altering the expression of genes which are involved in cellular processes that produce or repair the normally low level of spontaneous DNA damage (Ganem et al., 2007). Furthermore, abnormal mitosis and mitotic arrest induced in human cells by transient nocodazole (or colcemid) treatment leads to the accumulation of DNA breaks in both diploid and tetraploid cells (Quignon et al., 2007). Prolonged nocodazole treatment in human cells, results in the accumulation of DNA breaks in the arising tetraploid cells originated through mitotic slippage, and in the absence of DNA damage checkpoint activation and apoptosis, leads to the formation of

mitotic tetraploid cells with structural chromosomal rearrangements (Quignon et al., 2007). Finally, the possibility that chaotic multipolar mitosis may directly break chromosomes (Jannink et al., 1996; Storchova & Kuffer, 2008), as well as the likelihood that aberrant cytokinesis (i.e. premature cytokinesis) can lead to the trap, damage and break of chromosomes through the cleavage furrow machinery (Jannink et al., 1996; Mendoza & Barral, 2008; Storchova & Kuffer, 2008), cannot be excluded.

Second, tetraploidy as I mentioned in **Section 4.3.1.2.2** may enhance the fitness of cells containing broken or rearranged chromosomes, through the buffering effect of extra normal chromosomes, and thus give to these cells a proliferative advantage (Ganem et al., 2007; Storchova & Kuffer, 2008).

Strikingly though, even if structural chromosomal abnormalities such as double minute chromosomes **(Figure 4.30)** and translocations **(Figure 4.28 and Figure 4.29)** were found in near-tetraploid aneuploid cells upon GLI2ΔN induction, the clonal translocation t(7;14) was not only present in near-tetraploid aneuploid cells, but also in a diploid SINEG2 keratinocyte **(Figure 4.27)**. This observation suggests that the ability of GLI2ΔN to induce structural chromosomal aberrations is independent of its ability to induce tetraploidisation which however definitely seems to contribute to the overall chromosomal instability that GLI2ΔN-expressing cells exhibit.

The existence of this clonal translocation in a diploid SINEG2 cell can be explained by the fact that GLI2ΔN in human N/TERT keratinocytes, downregulates and upregulates crucial components of the DNA damage checkpoints and apoptosis, respectively, such as p21 and 14-3-3 sigma and BCL-2 **(Figure 4.9 and Figure 4.11)**, which are responsible for the detection of cells with DNA breaks, and the activation of repair mechanisms, or if repair is not possible, their elimination through apoptosis **(see Section 4.2.6 and Section 4.3.1.3.2)** (Dhar et al., 2000; Richardson & Jasin, 2000; Khanna & Jackson, 2001; Zhivotovsky & Kroemer, 2004; Lobrich & Jeggo, 2007; Aguilera & Gomez-Gonzalez, 2008; Taylor et al., 2008). Therefore, GLI2ΔN, by relaxing the DNA damage checkpoints and inhibiting the apoptotic machinery, possibly allows diploid cells (as well as tetraploid and aneuploid cells) with DNA breaks, originated by spontaneous replication errors or by other causes, to propagate unrepaired to the next cell cycles, yielding cells with structural chromosomal abnormalities

(dicentric chromosomes, translocations, double minute chromosomes), with enhanced survival and with the potential of clonal selection and transformation. Furthermore, GLI2ΔN might downregulate proteins that are involved in DNA repair mechanisms and thus further increasing subsequent genomic instability (Lobrich & Jeggo, 2007; Aguilera & Gomez-Gonzalez, 2008; Negrini et al., 2010). Another possible alternative, responsible for the presence of chromosomal rearrangements could be telomere dysfunction (telomere attrition) (Artandi et al., 2000; Zhivotovsky & Kroemer, 2004; Jefford & Irminger-Finger, 2006). Telomere (cap the ends of chromosomes, thereby preventing them from being recognized as double strand breaks) shortening or mutation of telomere binding proteins cause telomere uncapping, that can lead to end-to-end fusions and to the formation of dicentric chromosomes (chromosomes that carry two centromeres, which can also been formed by unrepaired DNA breaks), leading to breakage-fusion-bridge (BFB) cycles and subsequent generation of cells with structural chromosomal abnormalities (i.e. translocations) (Artandi et al., 2000; Zhivotovsky & Kroemer, 2004). However, telomere shortening is unlikely to occur in my system since N/TERT keratinocytes are stably expressing telomerase (h/TERT), which is responsible for telomere elongation (Dickson et al., 2000; Rheinwald et al., 2002).

Finally, GLI2ΔN oncogene might induce structural chromosomal rearrangements and thus structural chromosomal instability, through a mechanism that causes DNA breaks and involves DNA replication stress (Aguilera & Gomez-Gonzalez, 2008; Halazonetis et al., 2008; Negrini et al., 2010). DNA replication stress is defined as inefficient DNA replication that causes DNA replication forks to progress slowly or stall. In the absence of the S-phase checkpoint activation replication forks can collapse, the replisome disassembles (dissociation of the replication proteins from the DNA), which in turn leads to formation of DNA breaks (Lobrich & Jeggo, 2007; Aguilera & Gomez-Gonzalez, 2008). Therefore, GLI2ΔN oncogene might induce stalling and collapse of DNA replication forks, leading to the formation of DNA breaks and to subsequent formation of chromosomal rearrangements and genomic instability, by impairing the DNA damage response (G1/S and G2/M checkpoints) and apoptotic pathways (Halazonetis et al., 2008; Negrini et al., 2010). In support of the latter, several studies have reported the presence of DNA breaks induced by replication stress (as judged by the allelic imbalances (loss of heterozygosity) in common fragile sites - specific genomic sites which are prone to DNA breaks, when DNA replication is compromised

and are also associated with hotspots for translocations, gene amplifications and other chromosomal alterations (Aguilera & Gomez-Gonzalez, 2008)) in both human precancerous lesions and human cancers, in the absence of telomere attrition or mutations in genes responsible for genome integrity in precancerous lesions, but in the presence of activated oncogenes (Bartkova et al., 2005; Gorgoulis et al., 2005; Halazonetis et al., 2008; Negrini et al., 2010). The formation of DNA breaks in precancerous lesions is followed by activation of DNA damage response mechanisms and apoptosis, whereas loss of p53 function is accompanied by the ability of cells to escape apoptosis and/or senescence effects and subsequent conversion of precancerous lesions to cancerous (Bartkova et al., 2005; Gorgoulis et al., 2005; Halazonetis et al., 2008; Negrini et al., 2010). In addition, overexpression of several oncogenes such as RAS, cyclin E and E2F1 in various cell types and model systems resulted in the presence of DNA replication stress (prematurely terminated replicated forks) and the induction of DNA breaks (Gorgoulis et al., 2005; Bartkova et al., 2006; Di Micco et al., 2006; Halazonetis et al., 2008; Negrini et al., 2010).

Overall, regardless of the mechanism by which chromosomal rearrangements do occur in SINEG2 cultures, their presence is reflective of genomic instability, and their importance is underscored by the fact that structural chromosomal abnormalities are an established cause of cancer and are often found in many cancer cells (Solomon et al., 1991; Lengauer et al., 1998; Saunders et al., 2000; Nowak et al., 2002; Albertson et al., 2003; Mitelman et al., 2003; Futreal et al., 2004; Jefford & Irminger-Finger, 2006; Mitelman et al., 2007; Pellman, 2007). Both chromosomal translocations and double minute chromosomes, observed in GLI2ΔN-expressing keratinocytes, are frequently observed in many cancers (Barker, 1982; Solomon et al., 1991; Cowan, 1992; Lengauer et al., 1998; Albertson et al., 2003; Mitelman et al., 2003; Gebhart, 2005; Jefford & Irminger-Finger, 2006; Mitelman et al., 2007; Nambiar et al., 2008). Unbalanced translocations lead to breakpoint gene alterations, as well as to chromosome arm copy-number changes. Thus, unbalanced chromosomal rearrangements may result in the gain of genetic material - i.e. partial trisomy of 7p **(Figure 4.27)**, containing tumour-growth promoting genes, or loss of genetic material encoding tumour suppressor genes. Balanced translocations lead to either deregulation of genes in one of the breakpoints or to the formation of a hybrid chimeric gene which occurs through the fusion of two genes, generating a hybrid protein with altered properties (Rowley, 2001; Greaves &

Wiemels, 2003; Mitelman et al., 2007). Two of the most well-characterised examples of balanced translocations, have been reported in hematologic malignancies and are the t(9;22)(q34;q11) (CML-chronic myelogenous leukaemia) and t(8;14)(q24;q32) (Burkitt's lymphoma) **(Figure 4.32A, B)** (Rowley, 2001; Greaves & Wiemels, 2003; Mitelman et al., 2007; Nambiar et al., 2008). The t(9;22)(q34;q11) results in the Philadelphia chromosome, which originates by the fusion of the BCR (gene A) and ABL (gene B) genes, resulting to a hybrid BCR-ABL fusion protein, with increased tyrosine kinase activity (encodes an unregulated, cytoplasm targeted tyrosine kinase that allows the cells to proliferate without being regulated by cytokines and thus allows the cells to become cancerous) **(Figure 4.32b)** (Rowley, 2001; Mitelman et al., 2007; Nambiar et al., 2008). The t(8;14)(q24;q32) results in the abnormal timing and levels of MYC gene expression, due to the juxtaposition of the IGH (immunoglobulin heavy chain gene) promoter region (gene A promoter) next to the coding region of MYC oncogene (gene B coding region) **(Figure 4.32a)**. Thus, MYC gene is constitutively activated, because its expression is driven by immunoglobulin promoter/enhancer elements (Rowley, 2001; Mitelman et al., 2007; Nambiar et al., 2008).

Double minute chromosomes **(Figure 4.30)** along with the homogeneously staining regions (HSR-amplified sequences incorporated into chromosomes as tandem arrays or inverted repeats), are defined as the cytogenetic equivalents of amplified DNA sequences, extrachromosomally amplified copies and intrachromosomally amplified copies respectively, possibly containing a gene or genes that give selective advantage to the progression of the cancer (Barker, 1982; Cowell, 1982; Solomon et al., 1991; Lengauer et al., 1998; Albertson et al., 2003; Gebhart, 2005). Although the mechanisms that generate double minute chromosomes are not fully understood, similarly to translocations, it has been suggested that replication errors and DNA double strand breaks near the amplified segment in cells lacking robust checkpoints, followed by incorrect or/no repair of DNA breaks and in some cases by breakage-fusion-bridge cycles, may be involved (Solomon et al., 1991; Lengauer et al., 1998; Singer et al., 2000; Savelyeva & Schwab, 2001; Gebhart, 2005; Albertson, 2006). A classic example of gene amplification in tumour cells is the amplification of N-myc oncogene that occurs in ~ 30% of advanced neuroblastomas. In normal cells N-myc is localised as a single copy on chromosome 2, whereas tumour cells with amplification have up to several hundred copies generally located in an HSR (direct tandem repeats) on another

chromosome (chromosome 11) (Seeger et al., 1985; Solomon et al., 1991; Lengauer et al., 1998; Savelyeva & Schwab, 2001; Albertson et al., 2003; Gebhart, 2005; Albertson, 2006). Another example is the amplification of EGFR oncogene that occurs in 40% of gliomas, and is present in double minute chromosomes (Vogt et al., 2004; Albertson, 2006) .

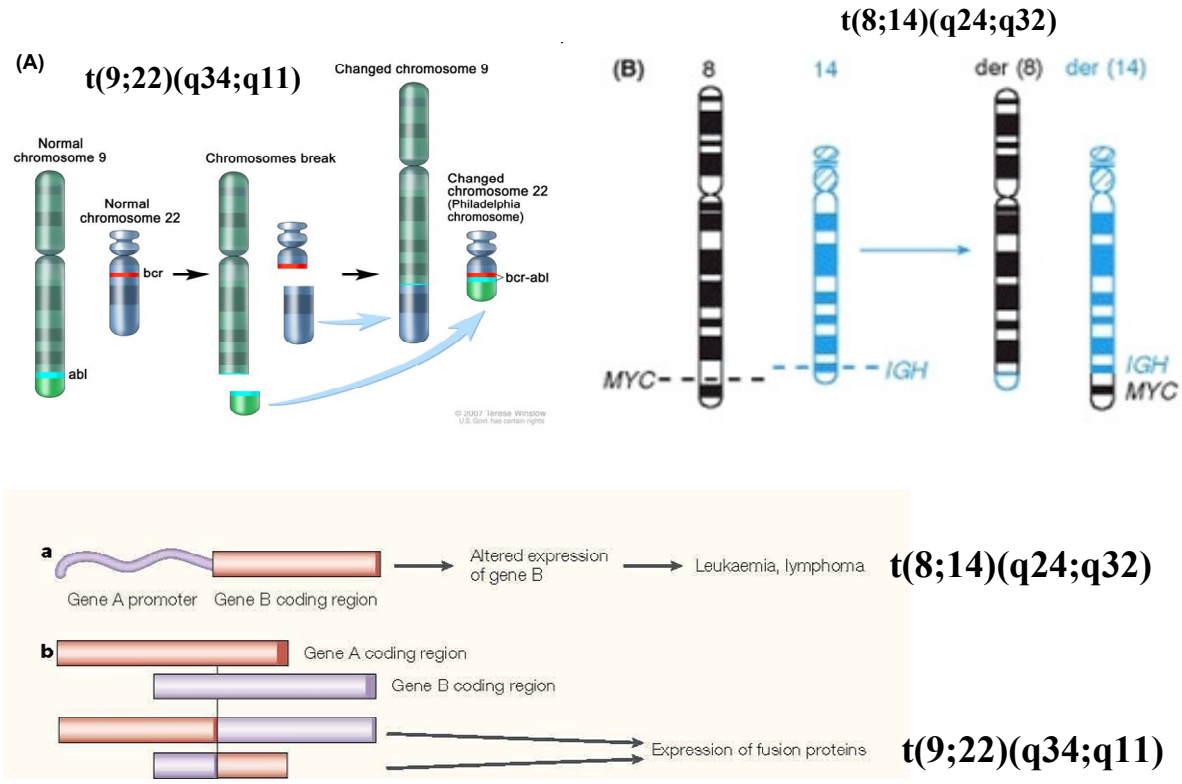

Figure 4.32: Chromosomal translocations and their consequences.

(A) The Philadelphia chromosome in chronic myelogenous leukaemia, which originates through the translocation t(9;22)(q34;q11), **(b)** results in the formation of a fusion/chimeric protein BCR-ABL with an enhanced function (enhanced tyrosine kinase activity) (Rowley, 2001). **(B)** The translocation t(8;14)(q24;q32), the most common translocation in Burkitt's lymphoma **(a)** results in the deregulation of MYC gene through its juxtaposition next to the promoter of the immunoglobulin heavy chain (IGH) gene (Rowley, 2001). Modified from
www.meb.uni-bonn.de/cancer.gov/CDR0000257989.html
http://www.ncbi.nlm.nih.gov/bookshelf/br.fcgi?book=hmg&part=A2342

In contrast to the stepwise model of carcinogenesis requiring multiple genetic alterations, human BCCs have been shown experimentally (*in vivo* human-tissue cancer models) to be able to originate by only one hit (overexpression of SHH and thus deregulation of SHH/GLI pathway) (Fan et al., 1997; Khavari, 2006). This observation may account for the fact that BCC is the most common malignancy, as well as for the absence of precursor lesions in arising BCCs and their failure to metastasize, compared to other cancers with more aggressive behaviour (Miller, 1991a; Wong et al., 2003; Daya-Grosjean & Couve-Privat, 2005; Crowson, 2006). However, genetically engineered human tissue cancer models have their limitations and restrictions, and thus the possibility that cytogenetic disruptions might facilitate the more rapid emergence of these cancers by altering core oncogenic networks cannot be excluded. According to the latter, while human cells initially had been reported to become transformed after a long latent period without widespread genetic changes, due to coexpression of the SV40 large T antigen (oncogene), the telomerase catalytic subunit hTERT and oncogenic ras, later examination showed that a majority of these cells had increased tetraploidy, non-diploid aneuploid karyotype and structural chromosomal translocations (Hahn et al., 1999; Li et al., 2000; Zimonjic et al., 2001).

The techniques that are used for the detection of genomic instability *in vitro* and *in vivo* are of great importance. Recently, it was shown by Mao et al. (Mao et al., 2008) that diploid cancer cell lines that have previously been described with cytogenetically normal diploid karyotypes, had all subtle genomic copy number changes as revealed by high resolution 500K SNP (single-nucleotide polymorphism) array analysis. This observation indicates that also other tumours previously reported with normal karyotypes might have subtle genetic alterations.

Therefore, although human BCCs, and especially nodular ones, are considered quite stable as observed by 10K SNP microarray (loss of heterozygosity study) (Teh et al., 2005), other cytogenetic studies have shown that there is a reasonable degree of genomic instability, still smaller compared to other cancers, which increases in the more aggressive forms of BCCs (Ashton et al., 2005; Carless et al., 2006). Overall, the incidence of tetraploidy and subsequent aneuploidy in human BCCs is 9-40%, whereas different subgroups of BCC, mainly the more aggressive ones (i.e. superficial, infiltrative) have been shown to have much higher aneuploidy rates such as 50-80%

(Frentz & Moller, 1983; Buchner et al., 1985; Miller, 1991a; Herzberg et al., 1993; Fortier-Beaulieu et al., 1994; Staibano et al., 2001; Ashton et al., 2005; Carless et al., 2006; Weaver & Cleveland, 2006). More recently, it was shown that aneuploidy may be a risk factor for the frequent local recurrence of human BCC tumours (development of secondary BCCs) (Janisson-Dargaud et al., 2008). In this case study, comparing patients with recurrent (group 1) and non-recurrent BCC (group 2) with a follow-up time ≥ 5 years, a significant association between recurrences and an abnormal DNA content (aneuploidy) was observed (Janisson-Dargaud et al., 2008). The majority (78%) of patients who experienced local recurrences had aneuploid primary tumours (nodular and superficial BCCs) (group 1), while aneuploidy was observed only in 32% of patients with tumours without recurrence (group 2) (Janisson-Dargaud et al., 2008). These observations along with my data, suggest that activation of GLI2ΔN is able to induce a degree of genomic instability and according to the extent to which the SHH/GLI pathway is deregulated and the genetic background in which this disruption occurs, may influence subsequent genetic events that lead to tumour progression (Hoban et al., 2006). This is consistent with the study of Grachtchouk et al. (Grachtchouk et al., 2003), which showed that different levels of SHH/GLI signalling activity can result in distinct tumour types in skin, and it also provides an explanation for the wide phenotypic diversity of human BCCs (several histological subtypes associated with more or less aggressive phenotypes) (Hoban et al., 2006).

The oncogenic activity of GLI2 interferes with a multitude of biological processes, leading to the inhibition of apoptosis, resistance to growth arrest, and suppression of epithelial differentiation, as observed by me and others (Aberger & Frischauf, 2006; Snijders et al., 2008). Therefore, at least in the case of GLI2, three of the most important obstacles that potential tumour cells need to evade, are overcome by the activation of a single oncogene. It therefore follows that simple activation of GLI2 alone might suffice for the generation of a more indolent type of tumours, such as nodular BCCs, without the presence of widespread genomic instability (no need for persistent generation of new chromosomal variations), while the progression to more aggressive BCC variants may have a stronger requirement for additional genetic changes, as previously suggested.

However, it is nearly impossible to exclude the occurrence of a transient state of instability during an undefined period of tumour's history (i.e. human BCC), since every investigation is a snap-shot that captures only an instantaneous picture of the life of the tumour (Heim et al., 1988; Lengauer et al., 1998). Thus, a diploid or near-diploid homogeneous tumour that is observed at the time of analysis, might have been preceded by a population of uncontrolled tetraploid cells that become aneuploid with increased numerical and structural chromosomal instability (acquisition of genetic alterations necessary for cell transformation-activation of growth promoting genes) and increased chromosome loss, forming heterogeneous populations, which through a process known as genomic convergence (clonal adaptation) are eliminated all apart from one or a few clones that have been selected and form the pseudo monoclonal near-diploid homogeneous tumour (Nowell, 1976; Heim et al., 1988; Shackney et al., 1989; Cahill et al., 1999; Fukasawa, 2005).

Overall, it is important to note that the effects of GLI2ΔN observed in a human keratinocyte cell line *in vitro* cannot be readily assimilated to the genotype of BCC tumours *in vivo*. The former demonstrates the ability of GLI2ΔN oncogene to disturb the mitotic process and therefore lead to genomic instability regardless of the influences of the surrounding environment, while the latter is the outcome of sequential intrinsic and extrinsic events that collectively may lead to the generation of a tumour that is genetically more stable compared to other malignant neoplasms. This is an important observation as it highlights the potential importance of GLI2 oncogene activation in the initiation and/or promotion of genomic instability in other biological settings. The upregulation of GLI2 in tumour cells with a more permissive or molecularly aberrant background, compared to those of BCC, could further promote genomic instability. This view is supported by the fact that GLI2 oncogene is significantly upregulated in numerous human tumours that, contrarily to BCC, are known to display a high degree of genomic instability (Ruiz i Altaba et al., 2002b; Beachy et al., 2004; Sanchez et al., 2004; Bhatia et al., 2006; Perez-Ordonez et al., 2006; Sterling et al., 2006; Weaver & Cleveland, 2006; Thiyagarajan et al., 2007; Snijders et al., 2008; Storchova & Kuffer, 2008; Hirotsu et al., 2010).

4.4 Summary

In this chapter it is shown that over-expression of GLI2ΔN can interfere with normal cell cycle control of human N/TERT keratinocytes, and induces significant ploidy abnormalities, which could be partly responsible for their reduced growth rate, without causing any cell death or increased apoptosis. Upon GLI2ΔN induction in human N/TERT keratinocytes, there is (i) increased tetraploidisation, followed by subsequent polyploidy and aneuploidy, (ii) inactivation of cell cycle genes such as $p21^{WAF1/CIP1}$ and 14-3-3σ that control the generation of tetraploid cells, as well as the proliferation of tetraploid and DNA damaged cells, with no change in p53 protein levels and (iii) defective apoptosis, possibly through the upregulation of the anti-apoptotic protein BCL-2, which is responsible for the elimination of tetraploid / polyploid / aneuploid cells **(Figure 4.33)**. Consistently with the downregulation of $p21^{WAF1/CIP1}$ *in vitro*, $p21^{WAF1/CIP1}$ protein in this study was also found to be almost absent in human BCC tumours. In addition, in this chapter, evidence was provided for the ability of GLI2ΔN to induce not only numerical chromosomal instability in human keratinocytes, but also structural genomic instability, as judged by the structural chromosomal aberrations observed in GLI2ΔN-expressing keratinocytes, using M-FISH karyotype analysis **(Figure 4.33)**. Furthermore, ultraviolet B (UVB, 290-320 nm) is known to be one of the most important etiological factors in BCC formation. In this study, it is shown that GLI2ΔN induction in human N/TERT keratinocytes, renders cells resistant, not only to tetraploidy-mediated apoptosis, but also to UVB-mediated apoptosis possibly through the activation of BCL-2 gene and protein upregulation, whereas the upregulation of p53 and the concomitant downregulation of $p21^{WAF1/CIP1}$ protein after UVB treatment in GLI2ΔN-expressing keratinocytes further confirms that GLI2ΔN downregulates $p21^{WAF1/CIP1}$ in a p53-independent manner. Collectively, these observations give new insights into the possible mechanisms through which GLI2ΔN might exert its tumourigenic potential.

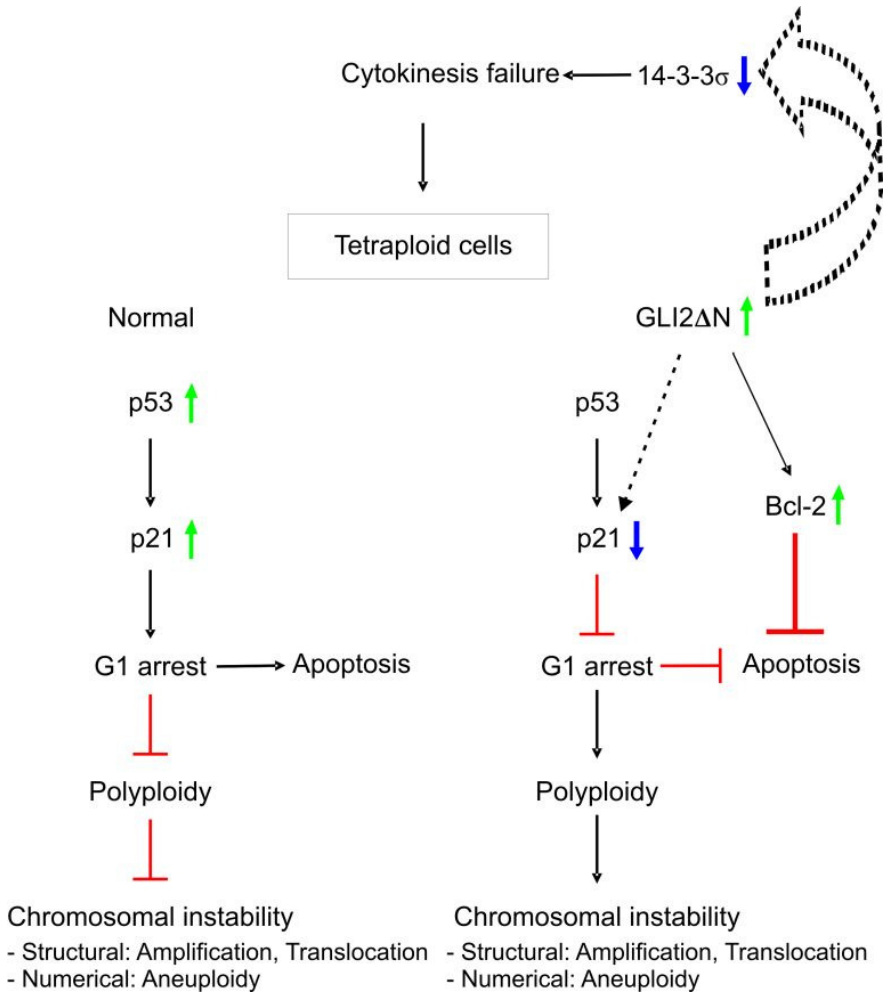

Figure 4.33: GLI2ΔN induces numerical and structural chromosomal instability.

Diagram illustrating a potential mechanism for the effects of GLI2ΔN in genomic integrity. Under normal conditions (left-hand panel), spontaneously arising tetraploid cells are blocked by the stabilisation of p53 followed by activation of p21, resulting in G1/S arrest and apoptosis. Upon GLI2ΔN induction (left-hand panel), there is accumulation of bi-nucleated tetraploid cells (increased tetraploidisation), possibly due to cytokinesis failure through the downregulation of 14-3-3σ. Tetraploid cells, in the presence of GLI2ΔN, proliferate to the next cell cycles and have enhanced survival, due to the absence of p53 stabilisation, the downregulation of p21 and the upregulation of Bcl-2, which overall inhibit G1/S arrest and apoptosis, resulting in the presence of polyploid and aneuploid cells and of near-tetraploid aneuploid cells with structural chromosomal aberrations (translocations and double minute chromosomes). The ability of GLI2ΔN to cause structural chromosomal instability in human N/TERT keratinocytes is independent from its ability to induce tetraploidisation, as judged by the clonal translocation observed in a diploid cell.

CHAPTER FIVE

5 RESULTS

HH/GLI2ΔN and WNT/β-catenin interactions in N/TERT human keratinocytes

5.1 Introduction

In skin, the Shh pathway plays a pivotal role in maintaining the stem cell population, and in regulating the development of hair follicles, adult hair cycle, and sebaceous glands (Parisi & Lin, 1998; St-Jacques et al., 1998; Chiang et al., 1999; Wang et al., 2000b; Callahan & Oro, 2001; Allen et al., 2003; Ellis et al., 2003; Oro & Higgins, 2003; Schmidt-Ullrich & Paus, 2005; Athar et al., 2006; Blanpain & Fuchs, 2006; Zhou et al., 2006), while Wnt/β-catenin signalling pathway also plays an important role in hair follicle morphogenesis, hair follicle stem cell maintenance and/or activation, and hair shaft differentiation (Gat et al., 1998; DasGupta & Fuchs, 1999; Huelsken et al., 2001; Alonso & Fuchs, 2003a; Lowry et al., 2005; Schmidt-Ullrich & Paus, 2005; Blanpain & Fuchs, 2006; Blanpain et al., 2007; Watt & Collins, 2008). Previous studies in normal skin of transgenic mice, have shown that Wnt/β-catenin is required upstream of the Bmp and Shh in placode formation during hair follicle morphogenesis, and thus specifying the hair follicle fate in the undifferentiated basal epidermis and initiate hair bud formation (Gat et al., 1998; Huelsken et al., 2001; Andl et al., 2002; Lo Celso et al., 2004; Silva-Vargas et al., 2005; Blanpain & Fuchs, 2006). Then, it subsequently activates Shh signalling, which is required for the proliferation and expansion of follicle epithelium in order to assemble a mature follicle (St-Jacques et al., 1998; Chiang et al., 1999; Mill et al., 2003; Lo Celso et al., 2004; Silva-Vargas et al., 2005; Blanpain & Fuchs, 2006).

However in different contexts, such as in *Xenopus*, Wnt signalling can also be a downstream effector of Shh/Gli signalling pathway (Mullor et al., 2001). Gli2, the key transcriptional regulator of Hh signalling, affects ventro-posterior mesodermal development by regulating *Wnt* genes, such as Wnt8 and Wnt11 (Mullor et al., 2001).

In mice, constitutive activation of β-catenin promotes hair follicle-like tumours such as pilomatricomas and trichofolliculomas, or BCC-like tumours (Gat et al., 1998; Nicolas et al., 2003; Lo Celso et al., 2004), similar to those induced by Gli1 and Gli2 - Shh pathway genes (Grachtchouk et al., 2000; Nilsson et al., 2000; Sheng et al., 2002; Hutchin et al., 2005; Huntzicker et al., 2006). In human pilomatricomas (hair matrix cell tumourigenesis), stabilising mutations of β-catenin have also been identified (Chan et

al., 1999a; Kajino et al., 2001; Moreno-Bueno et al., 2001; Xia et al., 2006), while human BCCs show increased levels of GLI2 and GLI1 - SHH genes (Dahmane et al., 1997; Ghali et al., 1999; Mullor et al., 2001; Regl et al., 2002; Tojo et al., 2003; Ikram et al., 2004; Regl et al., 2004b; O'Driscoll et al., 2006; Asplund et al., 2008; Yu et al., 2008), as well as increased activation of WNT genes such as WNT2, WNT5A (Bonifas et al., 2001; Mullor et al., 2001; Saldanha et al., 2004; O'Driscoll et al., 2006; Yu et al., 2008), and accumulation of nuclear β-catenin (Yamazaki et al., 2001; El-Bahrawy et al., 2003; Saldanha et al., 2004; Yang et al., 2008a).

In addition, compared to normal skin, human BCCs exhibit increased protein and mRNA levels of LEF-1, which belongs to the family of TCF/LEF transcription factors, and is an important nuclear binding partner for β-catenin in skin (O'Driscoll et al., 2006; Asplund et al., 2008; Kriegl et al., 2009). In line with this, human BCCs also exhibit increased mRNA levels of matrix metalloproteinases (MMP), which are known targets of β-catenin-TCF/LEF signalling and are involved in cell invasion (O'Driscoll et al., 2006; Yu et al., 2008).

Therefore, even though little is known about SHH/GLI and WNT/β-catenin interactions in human tumourigenesis, studies in different organisms have shown that parallels and crosstalk between HH and WNT signalling, occur both during development and tumourigenesis, as described more extensively in the main introduction **(Chapter 1, Section 1.5.3)**.

In the absence of WNT signal, cytoplasmic β-catenin (non-E-cadherin bound) (CTNNB1) is phosphorylated and targeted for degradation by a complex of proteins including axin, adenomatous polyposis coli (APC) protein, glycogen synthase kinase (GSK)-3β and β-TrCP. In the presence of WNT signal, the degradation machinery is inhibited, β-catenin accumulates in the cytoplasm and translocates to the nucleus, where it interacts with the TCF/LEF transcription factor and activates gene expression (Polakis, 2000; Huelsken & Behrens, 2002; Nelson & Nusse, 2004; Klaus & Birchmeier, 2008; MacDonald et al., 2009). Aberrant WNT/β-catenin signalling, due to mutations of the pathway components, that lead to cytoplasmic β-catenin stabilisation and its subsequent nuclear translocation, has been found to be implicated not only in human skin cancer (pilomatricoma), but also in many other human cancers, as described

in the main introduction **(Chapter 1, Section 1.5.2)** (Polakis, 2000; Giles et al., 2003; Polakis, 2007; Fuerer et al., 2008; Klaus & Birchmeier, 2008).

Therefore, in this chapter, I have investigated whether GLI2ΔN is able to activate mediators of the Wnt/β-catenin pathway in human N/TERT keratinocytes, and to regulate β-catenin localisation and transcriptional activation.

5.2 Results

5.2.1 HH/GLI2ΔN and WNT/β-catenin interactions

5.2.1.1 GLI2ΔN induces nuclear re-localisation of β-catenin in N/TERT cells

In the present study, I investigated whether GLL2ΔN expression can alter the sub-cellular distribution of β-catenin by means of its re-localisation to the nucleus, which is an important step required for the transcriptional activation of downstream genes, since β-catenin is very tightly controlled and undergoes rapid degradation in the cytoplasm.

SINCE and SINEG2 cells were seeded at equal densities and harvested for whole, cytoplasmic and nuclear protein fractions **(see Chapter 2, Section 2.12.1 and Section 2.12.3)**. Cell lysates were then subjected to immunoblotting for β-catenin **(see Chapter 2, Section 2.12.5) (Figure 5.1)**. GAPDH and Lamin B1 were used as cytoplasmic and nuclear markers respectively, to confirm successful fractionation. β-actin was used as loading control. The distribution of β-catenin was altered in SINEG2 cells **(Figure 5.1 ii)**. Increased nuclear, and decreased cytoplasmic β-catenin, was observed in SINEG2 cells, compared to SINCE cells **(Figure 5.1 i)**, indicating protein re-localisation from the cytoplasm to the nucleus. Overall levels of β-catenin were similar in both SINCE and SINEG2 cell lines **(Figure 5.1 iii)**.

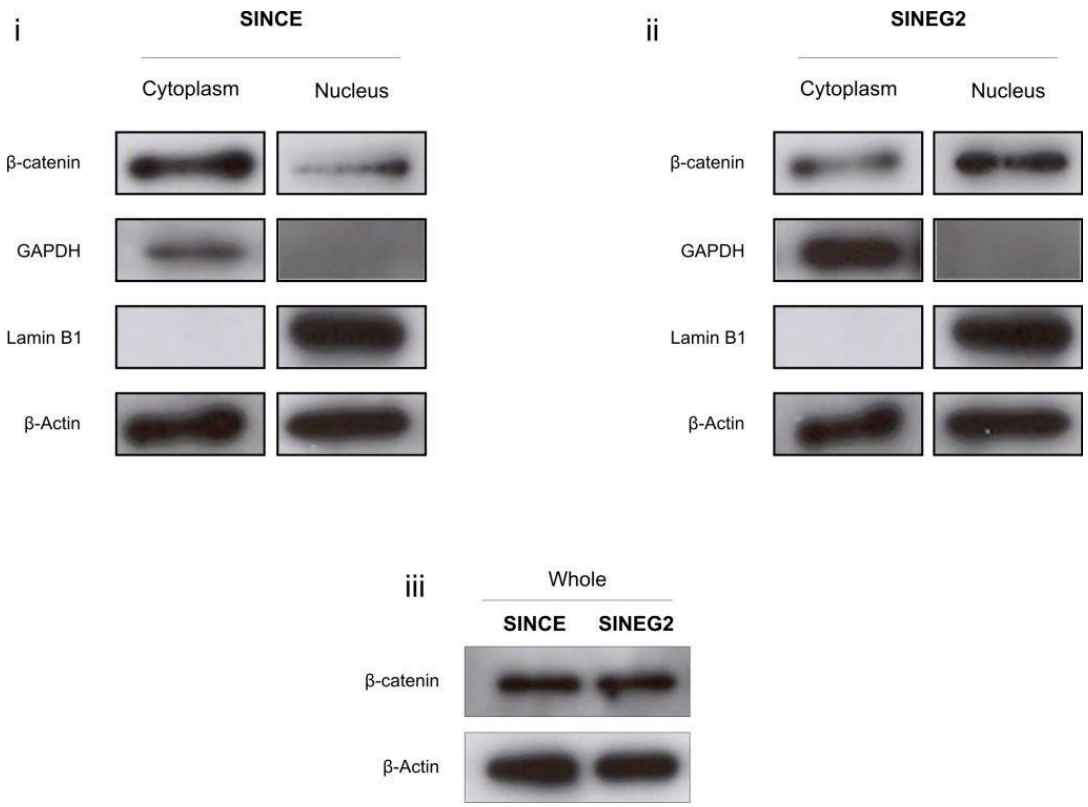

Figure 5.1: GLI2ΔN induces nuclear translocation of β-catenin.

Immunoblotting analysis after whole, cytoplasmic and nuclear protein fractionation on SINCE **(i)** and SINEG2 **(ii)** cell lines. Whole, cytoplasmic and nuclear protein fractions were prepared and samples were run on SDS PAGE gel. Membrane was probed against β-catenin antibody (~ 92 kDa), to examine its subcellular distribution. Lamin-B1 (~ 66 kDa) and GAPDH (~ 35 kDa) antibodies were used as nuclear and cytoplasmic markers respectively, to confirm successful fractionation. β-actin (~ 42 kDa) was used as loading control. β-catenin was found to be mainly localised in the cytoplasm of SINCE control cells with little protein being present in the nucleus **(i)**. In contrast, β-catenin distribution was altered in EGFP-GLI2ΔN expressing SINEG2 cells, indicating β-catenin translocation from the cytoplasm to the nucleus **(ii)**. Overall levels of β-catenin were similar in both SINEG2 and SINCE control cells **(iii)**.

5.2.1.2 GLI2ΔN expression causes β-catenin nuclear relocalisation in organotypic cultures.

In order to mimic physiological skin conditions *in vitro*, NTEG2 induced and uninduced cells were grown in organotypic three-dimensional cultures, by Nafeesa Ali at Centre for Cutaneous Research, Institute of Cell and Molecular Science, Barts and the London School of Medicine and Dentistry, London, UK, under conditions that can support the proliferation and differentiation of epidermal keratinocytes and mimic their *in vivo* pattern of growth and differentiation **(see Chapter 2, Section 2.17)** (Contard et al., 1993; Ojeh et al., 2001). The localisation of β-catenin following conditional expression of GLI2ΔN in N/TERT keratinocytes (NTEG2 induced), was investigated by immunohistochemistry on organotypic sections **(Figure 5.2 i)**, using an anti-β-catenin antibody. In experiments carried out by Nafeesa Ali at Centre for Cutaneous Research, Institute of Cell and Molecular Science, Barts and the London School of Medicine and Dentistry, London, UK, strong membranous, with limited nuclear, staining of β-catenin was detected in uninduced NTEG2 control cells **(Figure 5.2 i)**. Conversely, in the NTEG2, GLI2ΔN induced cells **(Figure 5.2 ii)**, β-catenin was no longer predominantly membranous, but instead mainly nuclear in a subset of cells, and prevalently so in the basal layer of the organotypic cultures. The data generated using this *in vitro* skin model support the results obtained using stable EGFP-GLI2ΔN expressing cells, further suggesting an active role for GLI2ΔN in the nuclear relocalisation of β-catenin in human keratinocytes.

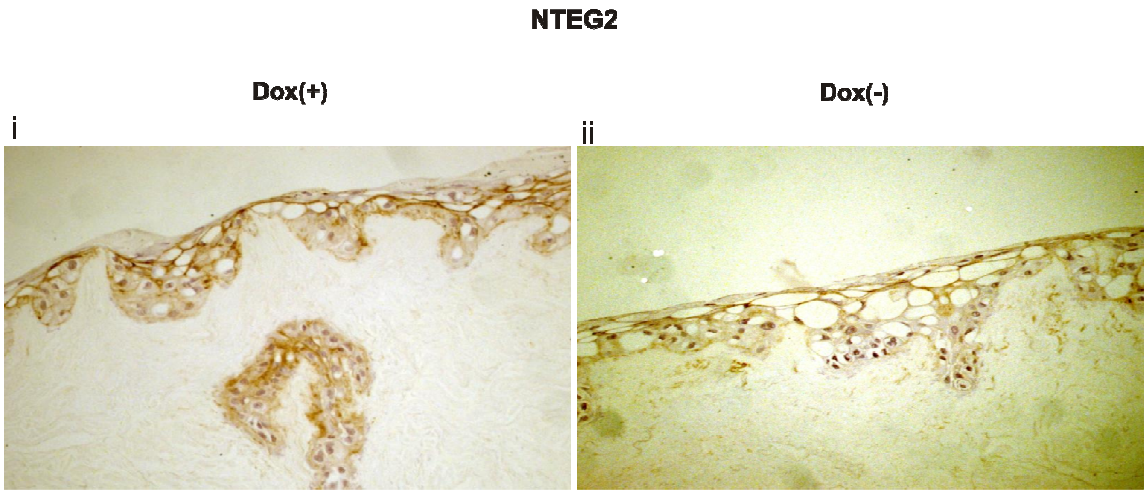

Figure 5.2: GLI2ΔN expression causes β-catenin nuclear relocalisation in organotypic cultures.

NTEG2 cells (Dox+ / Dox-) were grown on organotypic three dimensional cultures by Nafeesa Ali at Centre for Cutaneous Research, Institute of Cell and Molecular Science, Barts and the London School of Medicine and Dentistry, London, UK). Paraffin-embedded sections from organotypic cultures of NTEG2 (Dox+) and NTEG2 (Dox-) were stained using anti-β-catenin antibody. Increased nuclear staining of β-catenin was observed in induced NTEG2 organotypic culture **(ii)**. Strong staining of nuclear β-catenin was present mainly in the basal layer of NTEG2 (Dox-) **(ii)**, compared to membranous localisation of β-catenin in NTEG2 (Dox+) **(i)** organotypic cultures.

5.2.1.3 GLI2ΔN induces β-catenin dependent transactivation

WNT pathway activation leads to the inhibition of β-catenin degradation, followed by its stabilisation to the cytoplasm, and its subsequent translocation to the nucleus, where it associates with the T-cell factor/lymphoid enhancer (TCF/LEF) family of transcription factors (McArdle et al., 1984; Behrens et al., 1996; Molenaar et al., 1996; Polakis, 2000; Huelsken & Behrens, 2002; Arce et al., 2006). This results in the transactivation of WNT target genes, including cyclin D1, c-Myc, MMP26, MMP7, PPAP-δ and AF17, which have been linked to increased cell proliferation, invasion and tumour metastasis (He et al., 1998; Brabletz et al., 1999; He et al., 1999; Shtutman et al., 1999; Lin et al., 2001; Marchenko et al., 2002). To test whether the increased nuclear β-catenin, due to the GLI2ΔN activation, is also transcriptionally active, the well characterised OT-β-catenin responsive promoter (improved version of TOPFLASH) containing the TCF-4 binding sites **(CCTTTGATC)**, was used (Korinek et al., 1997; He et al., 1998; Shih et al., 2000).

Initially, the levels of EGFP-GLI2ΔN induction in NTEG2 cell line, 48 hr and 5 days after removal of Dox were investigated, by immunoblotting against anti-EGFP antibody **(Figure 5.3A)**. β-actin was used as protein loading control. N/TERT cells were also used as internal controls, due to background activation levels of GLI2ΔN in Dox+ NTEG2 cells, as evidenced on **Figure 5.3A**.

Both N/TERT and NTEG2 cells were transduced with SIN-OT-Luc retrovirus containing the OT-β-catenin responsive promoter, in order to assess the transcriptional activity of β-catenin **(see Chapter 2, Section 2.1.7 and Section 2.3.5.3)**. Cells were left to express the transgene for 72 hr, and harvested 48 hr after removal of Dox. This time point was selected instead of 5 days, in order to achieve maximum expression of the transgene (OT promoter) with insignificant difference in the induction of EGFP-GLI2ΔN fusion protein **(Figure 5.3A)**. Next, cells were lysed and luciferase activity and total protein content were measured **(see Chapter 2, Section 2.15 and Section 2.12.4)**. NTEG2 (Dox-) cells showed a significant increase (~ 2.4 fold) in β-catenin transcriptional activation when compared to NTEG2 (Dox+) (** $P \leq 0.01$) and N/TERT cells (*** $P \leq 0.001$) **(Figure 5.3B)**. The increase in activity observed in uninduced NTEG2 cells (NTEG2 Dox+), compared to N/TERT cells can possibly be attributed to

incomplete repression of GLI2ΔN in the presence of Dox. Three independent experiments, each of them consisting either of duplicate or triplicate samples, were carried out and similar results were obtained.

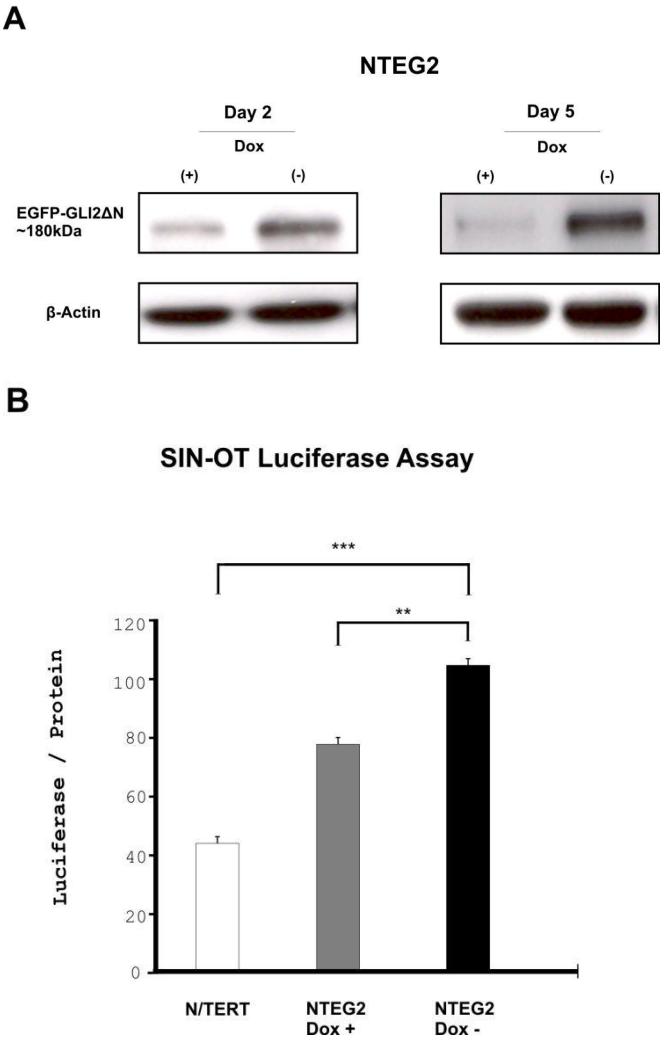

Figure 5.3: Inducible GLI2ΔN expression causes β-catenin transcriptional activation.

(A) Immunoblotting of NTEG2 inducible cell line lysates against anti-EGFP antibody, in the presence or absence of doxycycline, for 48 hr and 5 days. Results indicated high levels of EGFP-GLI2ΔN fusion protein induction before the experiment. Also, immunoblotting analysis revealed a small difference in protein induction/repression levels between the two time points. β-actin was used as protein loading control. 48 hr of doxycycline withdrawal was the time-point of choice in order to achieve significant induction of EGFP-GLI2ΔN and maximum expression of SIN-OT-Luc reporter vector. **(B)** N/TERT and NTEG2 cells were transduced with SIN-OT-Luciferase vector and expressed the transgene for 72 hr, followed by doxycycline removal for another 48 hr. Day 5 post-transduction, lysates were prepared and examined for luciferase activity and protein content. OT-β-catenin responsive promoter was significantly induced in NTEG2 Dox- cells (~ 2.4 fold) compared to both N/TERT (*** *P≤0.001*) and NTEG2 Dox+ (** *P≤0.01*) cells. The increase in luciferase activity observed in uninduced NTEG2 cells (NTEG2 Dox+), compared to N/TERT cells can possibly be attributed to incomplete repression of GLI2ΔN in the presence of Dox. Each bar represents a mean ± s.e.m of normalised to protein content triplicate samples.

Due to the continuous phosphorylation of β-catenin in the cytoplasm, followed by subsequent proteasome-mediated degradation, the levels of active, dephosphorylated β-catenin protein are kept at very low levels (Aberle et al., 1997; Behrens et al., 1998; Jiang & Struhl, 1998; Latres et al., 1999; Amit et al., 2002; Liu et al., 2002; van Es et al., 2003; Nusse, 2005; Klaus & Birchmeier, 2008; MacDonald et al., 2009). Therefore, the levels of active-β-catenin in the NTEG2 induced cells were examined. NTEG2 induced cells were lysed 48 hr after Dox removal **(see Chapter 2, Section 2.12.1)** and subjected to immunoblotting for EGFP and active-β-catenin **(see Chapter 2, Section 2.12.5) (Figure 5.4)**, with β-actin as loading control. The levels of active free β-catenin protein were significantly higher in the induced NTEG2 cells (NTEG2 Dox-), compared to uninduced control cells (NTEG2 Dox+), further indicating the activation of β-catenin.

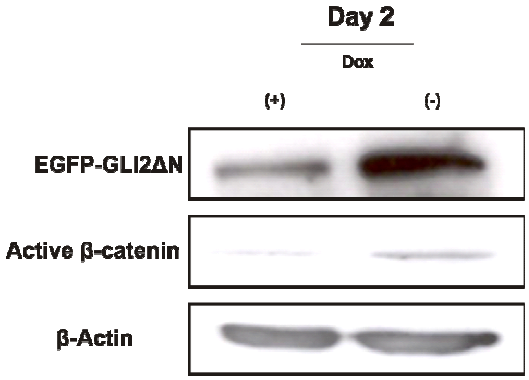

Figure 5.4: GLI2ΔN expression causes an increase in active β-catenin levels.

Active (dephosphorylated) β-catenin levels (~ 92 kDa) are increased in induced NTEG2 cells compared to the uninduced control cells. Active β-catenin levels in cell lysates from induced and uninduced NTEG2 cells were analysed by immunoblotting with anti-active-β-catenin antibody. The EGFP-GLI2ΔN protein levels after 48 hr removal of doxycycline are also shown for reference and β-actin was used as loading control.

Then, β-catenin transactivation assay was repeated in the stably expressing cell line SINEG2, for further confirmation. N/TERT, SINCE, and SINEG2 cells were transduced with the SIN-OT-Luc retrovirus **(see Chapter 2, Section 2.1.7 and Section 2.3.5.3)** and were left to express the transgene for 72 hr prior to harvesting for luciferase activity and protein content measurement **(see Chapter 2, Section 2.15 and Section 2.12.4)**. Again, GLI2ΔN expressing keratinocytes showed a significant increase in the transactivation of β-catenin (~ 2.4 fold), when compared to both N/TERT (** *P≤0.01*) and SINCE cells (** *P≤0.01*) **(Figure 5.5B)**. The levels of GLI2ΔN expression in the cells are reported for reference **(Figure 5.5A)**. Three independent experiments, each of them consisting either of duplicate or triplicate samples, were carried out and similar results were obtained.

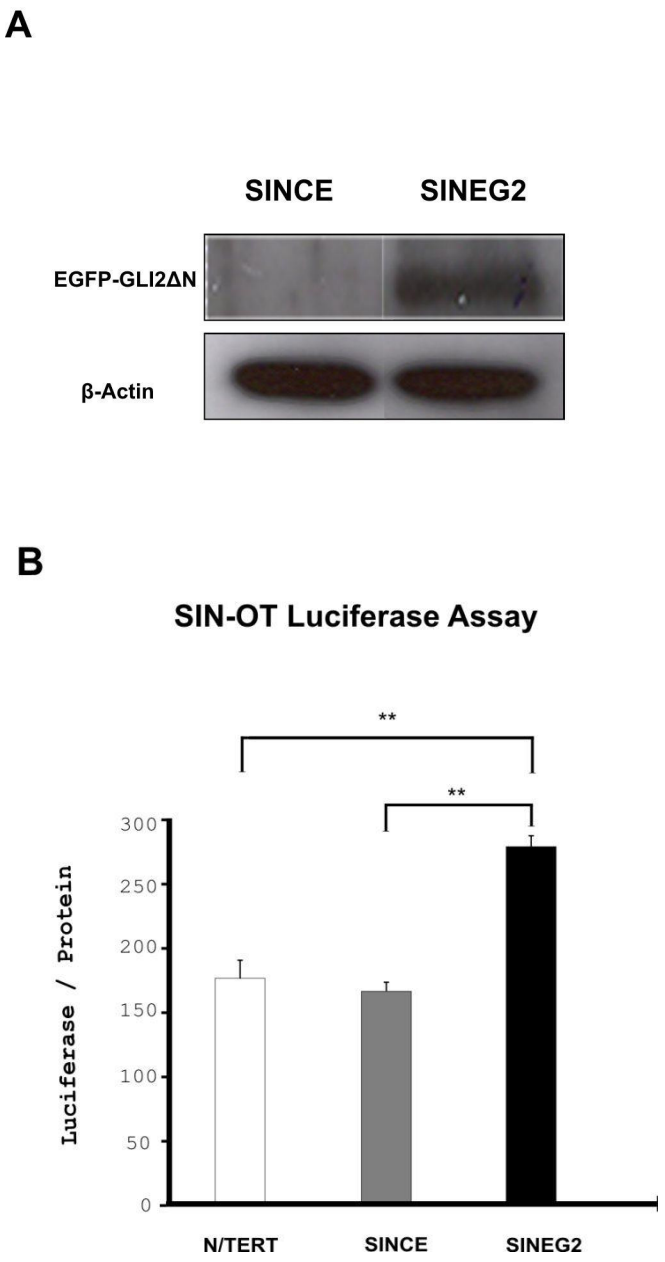

Figure 5.5: Stable GLI2ΔN expression in N/TERT keratinocytes causes β-catenin transcriptional activation.

(A) Immunoblotting of SINEG2 and SINCE protein lysates against anti-EGFP antibody, indicating high levels of EGFP-GLI2ΔN expression. β-actin was used as loading control. **(B)** N/TERT, SINCE, and SINEG2 cells were transduced with SIN-OT-Luc retrovirus and expressed the transgene for 72 hr. Lysates were prepared and examined for luciferase activity and protein content. OT-β-catenin responsive promoter was significantly induced in EGFP-GLI2ΔN stably expressing cells (~ 2.4 fold), when compared to both SINCE and N/TERT controls (** *P≤0.01*). Each bar represents a mean ± s.e.m of normalised to protein content triplicate samples.

5.2.1.4 GLI2ΔN induces the expression of WNT genes in human N/TERT keratinocytes

It has been previously reported that WNT genes are activated in human BCCs (*in vivo* tumourigenesis) (Bonifas et al., 2001; Mullor et al., 2001; Saldanha et al., 2004; O'Driscoll et al., 2006; Yu et al., 2008), where GLI2 is highly expressed (Mullor et al., 2001; Regl et al., 2002; Tojo et al., 2003; Ikram et al., 2004; Regl et al., 2004b; O'Driscoll et al., 2006; Asplund et al., 2008; Yu et al., 2008), as well as in frog embryo animal cap explants injected with Gli2 and Gli3 mRNA (embryonic development) (Mullor et al., 2001), and in rat kidney epithelial cells upon Gli1 induction (*in vitro* transformation) (Li et al., 2007).

Thus, in order to determine whether aberrant GLI2ΔN expression may be influencing the canonical Wnt/β-catenin pathway through alterations in WNT ligand expression in human N/TERT keratinocytes, quantitative RT-PCR analysis of different WNT ligands was performed **(see Chapter 2, Section 2.11 and Section 2.11.7)**. Stable expression of GLI2ΔN in human N/TERT keratinocytes, results in the upregulation of WNT5A (~ 5 fold) **(Figure 5.6A)**, WNT7A (~ 3 fold) **(Figure 5.6B)** and WNT11 (~ 400 fold) **(Figure 5.6C)** genes, compared to wild-type and EGFP-expressing N/TERT keratinocytes (*** $P \leq 0.001$), suggesting a possible implication of these WNT genes in the nuclear translocation of β-catenin, and its subsequent transcriptional activation upon GLI2ΔN induction. The relative fold mRNA induction of WNT11 could be an overestimation, due to the very low background levels of WNT11 mRNA observed in control N/TERT and SINCE keratinocytes (Ct >31).

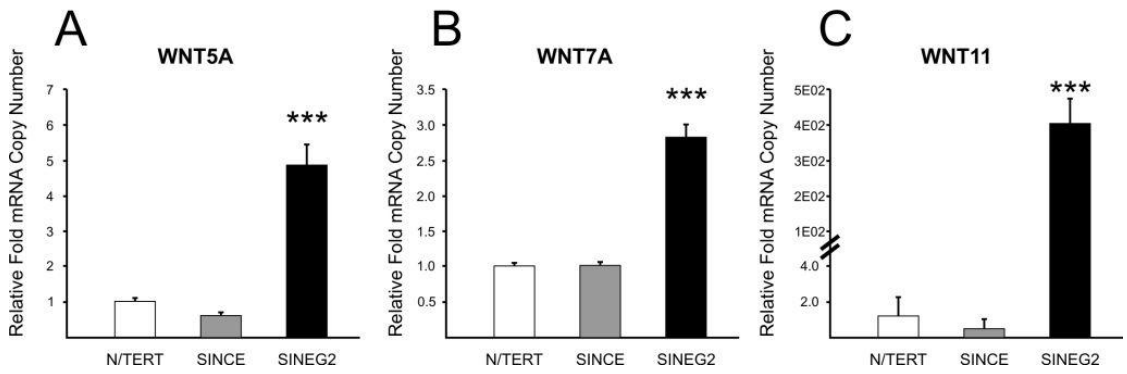

Figure 5.6: Stable GLI2ΔN expression in N/TERT keratinocytes induces WNT genes expression.

RNA was harvested from N/TERT, SINCE, and SINEG2 cells to examine the levels of WNT5A **(A)**, WNT7A **(B)**, and WNT11 **(C)** mRNA expression using primers specific for each gene. Quantitative RT-PCR analysis of WNT5A, WNT7A and WNT11 showed an increase in expression of all the three genes in SINEG2 cells compared to N/TERT and SINCE control cells. Each bar represents mean fold induction relative to N/TERT (arbitrary value of 1) ± s.e.m of triplicate samples. *** *P≤0.001*.

5.2.1.5 GLI2ΔN induces the expression of SNAIL1, SNAIL2 but not of E-CADHERIN genes

In addition to its function in Wnt signalling pathway and to its presence in the cytoplasm, β-catenin also exists in a different functional pool in the epithelial cell membrane, where it tightly binds to the intracellular cytoplasmic domain of the transmembrane protein E-cadherin (epithelial cadherin), and to the actin binding protein α-catenin and forms the cadherin-catenin complex (E-cadherin/β-α-catenin complex), necessary for calcium-dependent cell-cell adhesion interactions **(see Chapter 1, Section 1.4.1)** (McCrea & Gumbiner, 1991; Gumbiner, 2000; Jamora & Fuchs, 2002; Cavallaro & Christofori, 2004; Nelson & Nusse, 2004; Gumbiner, 2005; Brembeck et al., 2006). Serine/threonine phosphorylation of β-catenin (CTNNB1) or E-cadherin (CDH1), results in increased stabilisation of the cadherin-catenin complex (Lickert et al., 2000; Bek & Kemler, 2002), while tyrosine phosphorylation of E-cadherin or β-catenin is correlated with loss of cadherin mediated cell-cell adhesion, and an increase in the level of cytoplasmic β-catenin for the latter (Roura et al., 1999; Fujita et al., 2002; Lilien et al., 2002; Cavallaro & Christofori, 2004; Nelson & Nusse, 2004).

Still it is not clear if the roles of β-catenin in cell-cell adhesion and Wnt signalling, both in development and tumourigenesis, are either largely independent from each other, or interrelated, since evidence occurs for both possibilities in different cell contexts (Cavallaro & Christofori, 2004; Gottardi & Gumbiner, 2004; Nelson & Nusse, 2004; Bienz, 2005; Brembeck et al., 2006). According to the latter, loss of E-cadherin during developmental epithelial-mesenchymal transitions or during tumour progression (Birchmeier & Behrens, 1994; Gumbiner, 1996; Thiery, 2002; Pecina-Slaus, 2003; Cavallaro & Christofori, 2004; Nelson & Nusse, 2004; Gumbiner, 2005; Hugo et al., 2007), could promote loss of cell-cell adhesion, release of the membranous β-catenin to the cytoplasm, accumulation of β-catenin in the cytoplasm and subsequent translocation to the nucleus (increased Wnt/β-catenin signalling).

Recently, Li et al. (Li et al., 2007) showed that Gli1 acts both through Wnts and Snail (Snail homologue 1 of *Drosophila*) to switch β-catenin during rat kidney epithelial transformation. Snail belongs to a family of zinc-finger transcription factors and it was originally identified in *Drosophila* as a factor in the control of gastrulation and essential

for mesoderm formation (Nieto, 2002). Snail1 or Snail (Snail homologue 1 of *Drosophila*), and its close family member Snail2 or Slug (Snail homologue 2 of *Drosophila*) are both expressed in fibroblasts and have a major role not only to the mesoderm formation, but also in the formation of neural crest, both of which processes require large-scale cell movements, and delamination from the tissue of origin triggered by epithelial-mesenchymal transitions (EMT), followed by migration (Nieto, 2002). In addition, Snail and Slug not only trigger EMT during development, but also during tumourigenesis and progression of epithelial malignant tumours, while at the same time there is evidence for their implication in regulating cell death or survival (Batlle et al., 2000; Hajra et al., 2002; Nieto, 2002; Thiery, 2002; Nelson & Nusse, 2004; Hugo et al., 2007). Moreover, Snail1 has been found to be a direct target of Gli1 in rat kidney epithelial cells (Louro et al., 2002; Li et al., 2006), and to act as transcriptional suppressor of E-cadherin gene, by direct binding to the E-boxes of E-cadherin promoter, resulting in EMT activation and converting epithelial cells to mesenchymal during development and tumour progression (Batlle et al., 2000; Cano et al., 2000).

Thus, according to Li et al. (Li et al., 2007), Snail is a downstream target of Gli1, which downregulates E-cadherin, and synergistically with Wnt activation, promotes β-catenin cytoplasmic and nuclear relocalisation, in rat kidney epithelial cells. Since GLI2 is an upstream regulator of GLI1 (Ding et al., 1998; Bai et al., 2002; Regl et al., 2002; Mill et al., 2003; Ikram et al., 2004), it is plausible to imagine that this may have a positive contribution to the β-catenin accumulation in the cytoplasm and its subsequent translocation to the nucleus.

Therefore, in order to test if the nuclear translocation of β-catenin in the N/TERT keratinocytes upon GLI2ΔN induction, observed in our study, is not only due to the WNT genes activation, but also due to the induction of SNAIL1 (human SNAIL homologue 1 of *Drosophila*) directly by GLI2ΔN or mediated through GLI1 activation, following subsequent suppression of E-cadherin, quantitative RT-PCR analysis of SNAIL1, SNAIL2 (human SNAIL homologue 2 of *Drosophila*) and E-cadherin genes was performed **(Chapter 2, Section 2.11 and Section 2.11.7)**. Stable expression of GLI2ΔN in human N/TERT keratinocytes, results in upregulation of SNAIL1 (~ 2.8 fold) **(Figure 5.7A)**, and to a lesser extent, of SNAIL2 (~ 1.7 fold) **(Figure 5.7B),** while the transcription levels of E-cadherin were unchanged **(Figure 5.7C)**, compared to wild-

type and EGFP-expressing N/TERT keratinocytes (** *P≤0.01*). This suggests that even though both SNAIL1 and SNAIL2 are upregulated in GLI2ΔN expressing cells, there is no downregulation of E-cadherin and thus membranous-β-catenin bound to E-catherin is not contributing to the β-catenin cytoplasmic stabilisation, accumulation, and subsequent translocation to the nucleus upon GLI2ΔN induction.

Figure 5.7: Stable GLI2ΔN expression in N/TERT keratinocytes induces SNAIL1 and SNAIL2 genes expression with no effect in the expression of E-cadherin gene.

RNA was harvested from N/TERT, SINCE, and SINEG2 cells to examine the levels of SNAIL1 **(A)**, SNAIL2 **(B)**, and E-cadherin **(C)** mRNA expression using primers specific for each gene. Quantitative RT-PCR analysis of SNAIL1, SNAIL2 and E-cadherin showed an increase in expression of both SNAIL genes in SINEG2 cells compared to N/TERT and SINCE control cells, but no difference in expression of E-cadherin gene. Each bar represents mean fold induction relative to N/TERT (arbitrary value of 1) ± s.e.m of triplicate samples. ** *P≤0.01*.

5.3 Discussion

5.3.1 GLI2ΔN mediates β-catenin nuclear translocation and transcriptional activation in human N/TERT keratinocytes

WNT/β-catenin signalling pathway plays crucial role in a wide range of developmental processes during embryogenesis and during adult tissue homeostasis, while uncontrolled WNT/β-catenin signalling, due to mutations of the pathway components, or due to interactions with other inappropriately activated signalling cascades, which might cause constitutive activation of β-catenin (cytoplasmic accumulation / nuclear relocalisation), is an important event in the genesis of many cancers (Clevers, 2006; Klaus & Birchmeier, 2008; MacDonald et al., 2009).

Studies in different organisms, have shown that parallels and crosstalk between HH and WNT signalling occur both during development and tumourigenesis (Taipale & Beachy, 2001; Alonso & Fuchs, 2003a; Beachy et al., 2004; Hooper & Scott, 2005; Blanpain & Fuchs, 2006; Watt & Collins, 2008). However, due to the complexity and context-dependency of both HH and WNT pathways during development and tumourigenesis in different organisms, still little is known about SHH and WNT interactions in human carcinogenesis.

In normal skin, both Hh and Wnt pathways are implicated in hair follicle morphogenesis and adult hair cell cycle (Millar, 2002; Schmidt-Ullrich & Paus, 2005; Blanpain & Fuchs, 2006). Wnt/β-catenin is required upstream of Shh in placode formation, during hair follicle morphogenesis (Gat et al., 1998; Huelsken et al., 2001; Andl et al., 2002; Lo Celso et al., 2004; Silva-Vargas et al., 2005; Blanpain & Fuchs, 2006), while Shh signalling is required for the proliferation and expansion of follicle epithelium in order to assemble a mature follicle (St-Jacques et al., 1998; Chiang et al., 1999; Mill et al., 2003; Silva-Vargas et al., 2005; Blanpain & Fuchs, 2006).

Active Wnt/β-catenin signalling in adult transgenic mice was found to activate Shh/Gli signalling, and to promote *de novo* hair follicle morphogenesis (Gat et al., 1998; Lo Celso et al., 2004; Silva-Vargas et al., 2005; Ito et al., 2007), while constitutive

activation of β-catenin results in the development of hair follicle tumours such as pilomatricomas and trichofolliculomas (Gat et al., 1998; Lo Celso et al., 2004).

Human BCCs show, (a) increased levels of SHH effector genes such as GLI1 and GLI2 (Dahmane et al., 1997; Ghali et al., 1999; Mullor et al., 2001; Regl et al., 2002; Tojo et al., 2003; Ikram et al., 2004; Regl et al., 2004b; O'Driscoll et al., 2006; Asplund et al., 2008; Yu et al., 2008), (b) increased levels of WNT genes such as WNT2β, WNT5a and WNT7β (Bonifas et al., 2001; Mullor et al., 2001; Saldanha et al., 2004; O'Driscoll et al., 2006; Yu et al., 2008), as well as (c) accumulation of nuclear β-catenin (Yamazaki et al., 2001; El-Bahrawy et al., 2003; Saldanha et al., 2004; Yang et al., 2008a), (d) increased protein and mRNA levels of the β-catenin nuclear binding partner, LEF-1 (O'Driscoll et al., 2006; Asplund et al., 2008; Kriegl et al., 2009), and (e) increased mRNA levels of several matrix metalloproteinases (MMPs), which are known targets of β-catenin-TCF/LEF-1 signalling and are involved in cell invasion (O'Driscoll et al., 2006; Yu et al., 2008).

In my study, a new connection between Hh and Wnt pathways in human epidermal cells was found for the first time, demonstrating that β-catenin is a downstream effector of SHH/GLI pathway and that GLI2ΔN is a novel regulator of β-catenin, as judged by the fact that, upon constitutive activation of SHH/GLI2 signalling, by overexpressing GLI2ΔN oncogene in cultured human keratinocytes, there is subsequent activation of Wnt/β-catenin pathway.

β-catenin, the downstream mediator of the canonical WNT pathway, is usually confined to the cell membrane in an adhesion complex including E-cadherin (McCrea et al., 1991; Peifer et al., 1992; Kemler, 1993; Nelson & Nusse, 2004; Bienz, 2005) and in the cytoplasm. The cytoplasmic concentration of non-E-cadherin bound β-catenin, in the absence of Wnt ligand, is tightly controlled by cellular phosphorylation and proteasomal-mediated degradation mechanisms, which modulate its nuclear re-localisation and hence its transcriptional activity (Aberle et al., 1997; Behrens et al., 1998; Jiang & Struhl, 1998; Latres et al., 1999; Amit et al., 2002; Liu et al., 2002; van Es et al., 2003; Nusse, 2005; Klaus & Birchmeier, 2008; MacDonald et al., 2009).

The overexpression of GLI2ΔN has a marked effect on β-catenin localisation. This study provides evidence of nuclear accumulation of β-catenin induced by stable expression of GLI2ΔN in N/TERT human keratinocytes **(Figure 5.1)**. This nuclear re-localisation of β-catenin was also observed after inducible GLI2ΔN induction in three dimensional organotypic cultures **(Figure 5.2)**, a model that mimics patterns of proliferation and differentiation of normal human skin *in vivo* (Contard et al., 1993; Ojeh et al., 2001). Strong nuclear localisation of β-catenin was observed in a subset of the GLI2ΔN-induced cells in the basal layer of the organotypic skin cultures, compared to the membranous staining of the uninduced control cells. In line with the nuclear translocation of β-catenin in GLI2ΔN expressing cells, elevated levels of active-β-catenin (non-phosphorylated) were also observed in GLI2ΔN induced human N/TERT keratinocytes **(Figure 5.4)**. Furthermore, it is shown that β-catenin re-localisation to the nucleus, results in its transcriptional activation, both in stable and inducible GLI2ΔN expressing cells, as determined by the transactivation of the OT-β-catenin responsive promoter **(Figure 5.3 and Figure 5.5)**. It is worth mentioning here that recently Park et al. (Park et al., 2009) showed that telomerase can interact with BRG1 (protein-protein interaction) which in turn binds to β-catenin (protein-protein interaction) and enhances its transcriptional activity as judged by the activation of TOPFLASH and several WNT-dependent genes such as cyclin-D1, c-myc and Axin 2. Knowing that N/TERT keratinocytes, used in my study, have been immortalised with human telomerase reverse transcriptase (h/TERT) (Dickson et al., 2000) it is possible that these cells have intrinsically enhanced activity of the OT-β-catenin responsive promoter. However, even if this is the case it would not have an impact on the overall result **(Figure 5.3 and Figure 5.5)** since all three cell lines (controls and GLI2ΔN-expressing cells) used in my experiments contain the same genetic background and therefore expressing similar levels of h/TERT.

These observations suggest a direct link between the SHH/GLI2 and the WNT/β-catenin signalling pathway, and are in keeping with previous reports describing Hh/Gli-Wnt/β-catenin crosstalk, both during embryonic processes in the frog embryo (Mullor et al., 2001), and *in vitro* transformation of rat kidney epithelial cells (Li et al., 2007). Mullor et al. (Mullor et al., 2001) has reported that expression of different Wnts, including Wnt5A, 7B, 8 and 11 are induced in *Xenopus* animal cap explants injected with Gli2 and Gli3 mRNA, while Wnt 8 and Wnt 11 are required for Gli2/3-induced ventro-

posterior mesodermal development, as judged by the blockade of this morphogenetic response to Gli2, upon inhibition of Wnt signalling. Furthermore, Li et al. (Li et al., 2007) demonstrates that Gli1 induces Wnts (Wnt2b, 4, 7) and promotes β-catenin cytoplasmic and nuclear relocalisation in rat kidney epithelial cells, during epithelial transformation. Inhibition of Wnt/β-catenin signalling, by using a dominant negative form of Tcf4, represses the Gli1-mediated transformation of rat kidney epithelial cells *in vitro*, as indicated by the reduced foci formation in soft agar (Li et al., 2007). In addition, Alvarez-Medina et al. (Alvarez-Medina et al., 2009) showed that Shh pathway is required upstream of the canonical Wnt/β-catenin signalling, to control neural progenitor proliferation in chick embryos. Therefore, in developing vertebrate nervous system, the cell cycle progression of the neural progenitors is co-ordinately regulated, by activated Shh signalling which subsequently activates Wnt/β-catenin pathway, followed by activation of cyclin-D1 (Wnt/β-catenin target gene) and thus progression through the G1 phase of the cell cycle (Alvarez-Medina et al., 2009).

Most recently, in line with my data, it was demonstrated that canonical WNT/β-catenin signalling is essential for the tumourigenic response to deregulated HH signalling (BCC carcinogenesis, basaloid follicular hamartomas), both in mice and humans, and it is downstream of HH signalling in basaloid follicular hamartomas in transgenic mice (Roop & Toftgard, 2008; Yang et al., 2008a). Yang et al. (Yang et al., 2008a), first established that there is significant molecular resemblance between human superficial basal cell carcinoma and the human embryonic hair bud, by using early-stage follicle lineage markers, including K17, Sox9 and CDP. Then, by using a mouse model with conditional activation of Hh signalling in skin, achieved by using the human M2SMO oncogene (activated smoothened mutant) (Xie et al., 1998; Grachtchouk et al., 2003) under the K5 promoter regulation, further molecular similarity was confirmed between the embryonic mouse hair buds and the *de novo* epithelial hair buds formed in the M2SMO mice skin, in a normally hairless region (Yang et al., 2008a). Conditional expression of M2SMO in the skin of transgenic mice for longer, resulted in the progression of the *de novo* epithelial hair buds to form basaloid follicular hamartomas, a benign hair follicle tumour associated with deregulated Hh signalling both in mice and humans (Grachtchouk et al., 2003; Jih et al., 2003). The presence of active Wnt/β-catenin signalling induction upon deregulated Hh signalling in M2SMO-expressing mice, was first established by the increased levels of nuclear β-catenin both in the

M2SMO-induced mouse epithelial buds, and in the peripheral cells of the M2SMO-induced mouse follicular hamartomas (Yang et al., 2008a). Similarly, nuclear β-catenin was also detected in the normal mouse and human embryonic epithelial hair buds, consistent with the notion that Wnt/β-catenin pathway is activated during early stages of hair follicle morphogenesis, as well as in the neoplastic cells of the human superficial BCCs (Yang et al., 2008a). Secondly, non-phosphorylated (active) β-catenin was detected in protein lysates from M2SMO-transgenic mouse skin, while little or no expression was detected in the protein lysates from the control non-transgenic hairless mouse skin (Yang et al., 2008a). Finally, increased expression of Wnt ligands, including Wnt 4, 5a, and 11, and Wnt/β-catenin signalling target genes, including Axin2 and cyclin-D1, were observed in M2SMO-expressing mice, while inhibition of the canonical Wnt/β-catenin pathway in M2SMO-expressing mice by using the DKK inhibitor, resulted in suppression of both epithelial hair bud formation and basaloid follicular hamartoma, as well as in expression of β-catenin only in the cytoplasm (Yang et al., 2008a).

Thus, both the data from my study in GLI2ΔN-expressing human N/TERT keratinocytes, which are consistent with gene and protein expression profiling data of human BCCs (Yamazaki et al., 2001; El-Bahrawy et al., 2003; O'Driscoll et al., 2006; Asplund et al., 2008; Yu et al., 2008; Kriegl et al., 2009), and the analysis reported by Yang et al. (Yang et al., 2008a) in M2SMO-expressing mice, which is also consistent with the presence of nuclear β-catenin in a subset of BCC-like tumours in conditional Ptch1-inactivated mice (Adolphe et al., 2006), suggest that activated canonical Wnt/β-catenin signalling is required downstream of HH/GLI pathway during skin tumourigenesis both *in vitro* and *in vivo*, whereas this relationship between the two signalling pathways is reversed during hair follicle development (epithelial hair bud formation) **(Figure 5.8)** (Roop & Toftgard, 2008).

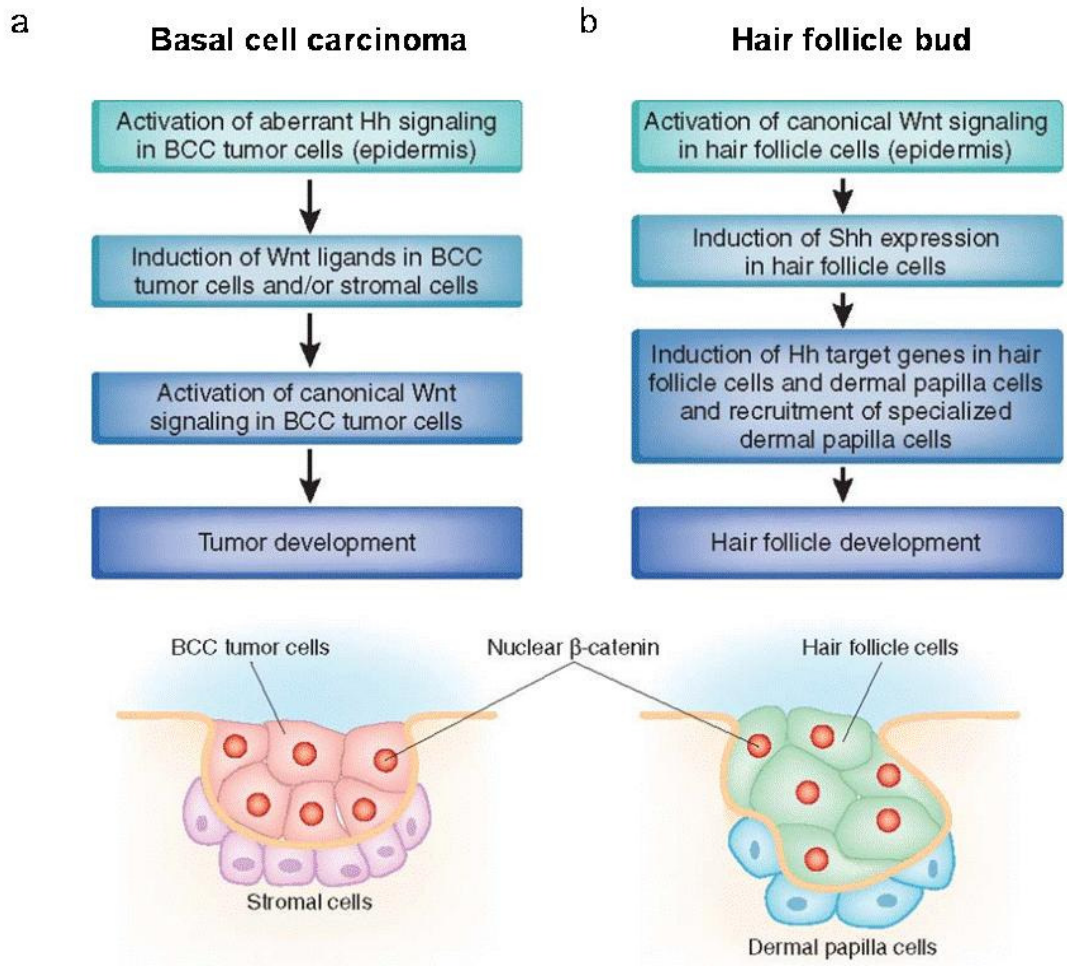

Figure 5.8: Signalling events in basal cell carcinoma and hair follicle buds.

(a) In basal cell carcinoma uncontrolled Hh signalling leads to the induction of the canonical Wnt/β-catenin signalling, which is essential for subsequent tumour development. **(b)** In hair follicle buds activation of Wnt/β-catenin signalling precedes, and leads to, the induction of Hh/Gli signalling, which is required for the proliferation and expansion of follicle epithelium in order to assemble a mature hair follicle (Roop & Toftgard, 2008).

Furthermore, the strong nuclear localisation of β-catenin, that was observed in the basal layer of the organotypic skin cultures **(Figure 5.2)**, the most proliferative layer of the epidermis (Fuchs, 1990), is consistent with the known WNT/β-catenin signalling role in cell proliferation, since nuclear β-catenin localisation has been found to peak in the G2/M cell cycle phase (Olmeda et al., 2003). In line with this, increased ectopic epidermal expression of β-catenin in basal keratinocytes results in *de novo* hair follicle morphogenesis and tumour formation in transgenic mice models (Gat et al., 1998; Xia et al., 2001; Nicolas et al., 2003; Lo Celso et al., 2004; Hardman et al., 2005; Silva-Vargas et al., 2005; Ito et al., 2007). Furthermore, the nuclear localisation of β-catenin, observed in a proportion of cells in the basal layer of the organotypic skin cultures is consistent with the invasive pattern of both β-catenin and its nuclear binding partner LEF-1 in human BCCs. This pattern displayed an intense nuclear expression at the invasive margins (basaloid cells), whereas cells in the tumour centre lack nuclear expression of both β-catenin and LEF-1 (Kriegl et al., 2009), suggesting a possible contribution to the ability of human BCCs to invade locally **(see Chapter 3, Section 3.3.8)**, possibly through the activation of matrix metalloproteinases (MMPs) by β-catenin/LEF-1. MMPs (matrixins) are enzymes, which are able to degrade all kinds of the extracellular matrix proteins and are essential during development and tissue remodelling, whereas their upregulation is often found in human diseases and cancer (Nagase & Woessner, 1999; Westermarck & Kahari, 1999; Curran & Murray, 2000; Stamenkovic, 2000; Page-McCaw et al., 2007). Similarly, accumulation of nuclear β-catenin was preferentially observed in the outer-most cells of the undifferentiated basaloid follicular hamartomas, which were formed in response to ectopic Hh signalling in the epidermis of transgenic mice (mice expressing M2SMO oncogene-activated smoothened mutant), followed by subsequent Wnt/β-catenin signalling activation (Yang et al., 2008a).

In addition, it is also believed that in the most proliferative layer of the epidermis, the basal layer, a subpopulation of keratinocytes, known as epidermal stem cells, reside **(Chapter 1, Section 1.1.5 and Section 1.1.5.1)** (Potten, 1974; Fuchs, 2008). Thus, the fact that only a small proportion of epidermal keratinocytes with activated Hh signalling, exhibit active Wnt/β-catenin signalling in my study, as well as in the analysis reported by Yang et al. (Yang et al., 2008a), suggests that the ability to respond to Hh signalling with increased Wnt/β-catenin expression and subsequent BCC formation, is

restricted to a small subset of epidermal cells (Roop & Toftgard, 2008). This small population of cells is thought to correspond to the stem cell compartment, where activation of Wnt/β-catenin and Shh signalling is found during normal skin development, and is required for their maintenance **(Chapter 1, Section 1.5.1 and Chapter 3, Section 3.3.6)** (Callahan & Oro, 2001; Adolphe et al., 2004; Beachy et al., 2004; Blanpain & Fuchs, 2006; Zhou et al., 2006; Roop & Toftgard, 2008). This is consistent with the notion that constitutive activation of the SHH/GLI pathway in skin and subsequent activation of Wnt/β-catenin pathway (signalling pathways with major developmental functions), could disrupt epidermal homeostasis and lead to tumourigenesis, with a phenotype that resembles stem cell characteristics (stem-like tumour phenotype), such as BCCs, which have been suggested to arise from epidermal basal layer or hair follicle stem cells **(see Chapter 1, Section 1.3.6 and Chapter 3, Section 3.3.6)**, and have been considered as an one-hit tumour, due to the lack of multiple genetic alterations, and their biologically mild behavioural characteristics (slow growing, locally invade, rarely metastasize) **(Chapter 1, see Section 1.2.1)** (Miller, 1991a; Fan et al., 1997; Oro et al., 1997; Kruger et al., 1999; Grachtchouk et al., 2000; Nilsson et al., 2000; Sheng et al., 2002; Owens & Watt, 2003; Hutchin et al., 2005; Blanpain & Fuchs, 2006; Crowson, 2006; Huntzicker et al., 2006; Mancuso et al., 2006; Youssef et al., 2010). Thus, in line with this, arguments are in favour of stem cells being the appealing candidates as the 'cell of origin' of BCC, because of their pre-existing capacity of self-renewal and unlimited proliferative capacity, which are prerequisites for the extra genetic hit (one-hit) that will transform the normal cell into a cancer cell (Beachy et al., 2004; Khavari, 2006; Youssef et al., 2010).

In support of these arguments, and of previous studies showing that stabilised Wnt/β-catenin signalling is required for hair follicle SC maintenance and activation **(Chapter 1, Section 1.5.1)** (DasGupta & Fuchs, 1999; Van Mater et al., 2003; Lo Celso et al., 2004; Lowry et al., 2005; Blanpain & Fuchs, 2006), a recent report by Malanchi et al. (Malanchi et al., 2008) demonstrated that in murine skin β-catenin signalling is essential for maintaining a population of cells in early epidermal tumours, characterised by phenotypic and functional similarities to normal bulge skin stem cells (including expression of CD34 and SOX9). This population contains cells referred to as cancer stem cells **(see Chapter 3, Section 3.3.4** (Beachy et al., 2004)**)**, with high tumourigenic capacity, indicated by the initiation of secondary tumours, which resembled the

architecture of the parental tumours, while ablation of β-catenin gene in the already established parental early epidermal tumours, results in the loss of this subpopulation of cells and complete tumour regression characterised by extensive terminal differentiation (Malanchi et al., 2008).

Finally, the nuclear translocation of β-catenin and its subsequent transcriptional activation might not only be mediated by the TCF/LEF-1 transcription factors, as it is observed by the increased activity of the OT-β-catenin responsive promoter, which contains the binding sites of the TCF-4, in GLI2ΔN-expressing keratinocytes **(Figure 5.3)**, but also by the SOX transcription factors. SOX factors belong to the superfamily of the high mobility group DNA binding factors, same as the TCF/LEF-1 transcription factors **(see Chapter 3, Section 3.3.6.2 and Chapter 1, Section 1.4.2)**. The binding of both SOX and TCF/LEF-1 factors to DNA is weaker than for most transcription factors, and thus recruitment of other protein partners (cell-type or tissue specific) is required for their transcriptional activity (Pevny & Lovell-Badge, 1997; Kamachi et al., 1999; Kamachi et al., 2000; Wilson & Koopman, 2002). SOX2, is a transcription factor, which is involved in organ development and in determining stem cell fate and properties, while it has been consistently reported to be upregulated in poorly differentiated tumours such as breast, as well as in gliomas which are also associated with activated hedgehog signalling and GLI1/2 overexpression **(see Chapter 3, Section 3.2.3.1.1 and Section 3.3.6.2)** (Kinzler et al., 1987; Dahmane et al., 2001; Kubo et al., 2004; Sterling et al., 2006; Clement et al., 2007; Ben-Porath et al., 2008; Chen et al., 2008; Kameda et al., 2009). Interestingly, a recent study demonstrated that β-catenin is a transcription partner for SOX2, and that SOX2 and β-catenin act in synergy in the transcription regulation of cyclin-D1, and therefore facilitating the G1/S transition and increasing the proliferation of breast cancer cells (Chen et al., 2008). Thus, due to the massive upregulation and high availability of SOX2 **(Chapter 3, Section 3.2.3.1.1, Figure 3.13)**, along with the nuclear accumulation of β-catenin in GLI2ΔN-expressing keratinocytes **(Figure 5.1)**, it is plausible to imagine that this might be another mechanism of β-catenin-mediated transcriptional activation, giving more insights to the tumourigenic role of GLI2.

5.3.2 β-catenin is not a transcriptional activator of c-MYC in N/TERT human keratinocytes

As I mentioned in the main introduction **(Chapter 1, Section 1.4.2)**, the transcriptional targets of TCF/LEF-1- β-catenin complex are diverse, and cell-type and context specific (Logan & Nusse, 2004; Vlad et al., 2008; MacDonald et al., 2009). Therefore, while different MMPs (matrixins), are known targets of β-catenin in colon and other epithelial cancers (Brabletz et al., 1999; Marchenko et al., 2002), and they have been found to be upregulated in human BCCs (Miller, 1991a; O'Driscoll et al., 2006; Yu et al., 2008) and GLI2-expressing HaCaT keratinocytes (Regl et al., 2004a; Eichberger et al., 2006), c-MYC which is a well established target of β-catenin in colon cancer cells (He et al., 1998; Klaus & Birchmeier, 2008), is downregulated both in human BCCs (Bonifas et al., 2001; Regl et al., 2002; O'Driscoll et al., 2006; Asplund et al., 2008) and in GLI2ΔN-expressing N/TERT keratinocytes **(Chapter 3, Section 3.2.1.4, Figure 3.5B, C),** whereas nuclear β-catenin is expressed in both. Similarly, c-myc was not found upregulated by stabilised β-catenin or Gli1-induced β-catenin in rat kidney epithelial cells (Kolligs et al., 1999; Li et al., 2007), and is repressed in response to inducible expression of GLI2ΔN in HaCaT keratinocytes (Regl et al., 2004a; Eichberger et al., 2006).

Collectively these findings along with my data, suggest that c-MYC is not a transcriptional target of β-catenin or β-catenin is not a transcriptional activator of c-MYC in human keratinocytes *in vitro*, consistent with their diverse roles observed in skin, both *in vitro* and *in vivo* **(see Chapter 3, Section 3.3.7 and Chapter 1, Section 1.5.1)** (Watt & Collins, 2008), and with the undifferentiated basal-like phenotype and stem-cell gene expression pattern, observed in GL2ΔN-expressing N/TERT keratinocytes **(Chapter 3, Section 3.2.3.1, Figure 3.11, Figure 3.12, Appendix II and Section 3.2.3.1.1, Figure 3.13)**. *In vitro*, putative epidermal stem cells express lower levels of c-MYC (Gandarillas & Watt, 1997; Jensen & Watt, 2006) and higher levels of β-catenin (Zhu & Watt, 1999), compared to the transit-amplifying cells, while for the expansion of the epidermal stem cell compartment, stabilised β-catenin expression and low levels of c-MYC are required (Gandarillas & Watt, 1997; Zhu & Watt, 1999), since ectopic overexpression of c-MYC in primary human keratinocytes *in vitro* promotes their terminal differentiation (Gandarillas & Watt, 1997). *In vivo*, in the presence of

stabilised β-catenin, there is expansion of the epidermal stem cell compartment and induction of *de novo* hair follicle formation (Gat et al., 1998; Lo Celso et al., 2004; Silva-Vargas et al., 2005; Ito et al., 2007), while overexpression of c-myc, depletes the epidermal stem cell compartment and induces differentiation of keratinocytes into interfollicular epidermis and sebaceous glands (Arnold & Watt, 2001; Waikel et al., 2001).

The different effects that c-MYC and β-catenin exert in the lineage selection of epidermal stem cells, was further confirmed in an immortalised human sebocyte cell line, which can be induced to differentiate into mature sebocytes by growing the cells to high density (Lo Celso et al., 2008). Stabilised β-catenin stimulates interfollicular epidermis differentiation, as indicated by the increased number of positive stained cells for involucrin and cornifin, while c-MYC stimulates sebaceous gland differentiation, as indicated by the increase in the number and size of cytoplasmic lipid droplets, present in the c-MycER transduced sebocyte cells following two days tamoxifen treatment to activate c-MYC (Lo Celso et al., 2008). Interestingly, Indian Hedgehog (Ihh) which is usually upregulated in mice and human sebaceous glands, human differentiated immortalised sebocyte cells and in human and mouse sebaceous tumours (Niemann et al., 2003; Takeda et al., 2006), was found to be a direct target gene of c-MYC (c-MYC binds to the promoter of Ihh in primary human keratinocytes) (Lo Celso et al., 2008), while it is known that β-catenin increases Shh expression during ectopic hair follicle formation in transgenic mice (Gat et al., 1998; Lo Celso et al., 2004; Silva-Vargas et al., 2005). Additional data on the mutual antagonism between c-Myc and β-catenin in the lineage specification in the epidermis, came from bitransgenic mice that co-expressed both stabilised β-cateninER and activated c-MycER under the control of K14 promoter (Lo Celso et al., 2008). In these bitransgenic mice, there was inhibition of β-catenin-mediated formation of ectopic hair follicles in the interfollicular epidermis by c-Myc, whereas β-catenin blocked c-Myc-induced sebocyte terminal differentiation (Lo Celso et al., 2008).

Therefore, future studies with the GLI2ΔN-expressing keratinocytes are required, in order to evaluate already existing, and to identify new, candidate target genes of β-catenin, which are probably implicated in the tumourigenic role of GLI2ΔN both *in vitro* and *in vivo*.

5.3.3 GLI2ΔN may mediate β-catenin activation through WNT genes upregulation

WNTs, which are secreted lipid-modified glycoproteins, activate both canonical and non-canonical Wnt pathways, and are involved in multiple developmental events during embryogenesis and adult tissue homeostasis, whereas their upregulation has been associated with cancer **(see Chapter 1, Section 1.4)** (Wodarz & Nusse, 1998; Huelsken & Behrens, 2002; Logan & Nusse, 2004; Hausmann et al., 2007). However, prior to the discovery of the Frizzled and LRP co-receptor, and due to the fact that Wnt proteins are hydrophobic/insoluble proteins, Wnt proteins were difficult to manipulate. Therefore, all the initial studies on the effects of Wnt proteins, were solely based on gene transfer experiments in different animal models or cell culture systems, without regard to the cellular context in which they were overexpressed (van Amerongen et al., 2008). Thus, based on these early studies, Wnts were classified into two functional categories, the 'canonical' Wnts (including Wnt1, and Wnt8) and the 'non-canonical' Wnts (including Wnt5A and Wnt11) (van Amerongen et al., 2008). However, further studies using purified active Wnt proteins and identifying Wnt ligand receptors, suggested that Wnt themselves are not intrinsically canonical or non-canonical, but that their signalling output (activation of canonical or non-canonical pathways) is determined by distinct sets of receptors (Frizzleds and LRPs) (Umbhauer et al., 2000; Holmen et al., 2002; Liu et al., 2003; Tamai et al., 2004; Liu et al., 2005; van Amerongen et al., 2008).

Wnt5A, is one of the Wnts with dual signalling capabilities, since prior to the existence of soluble active Wnt proteins, it was found to be associated with non-canonical Wnt signalling (Wnt/Ca^{2+} pathway) and to inhibit Wnt/β-catenin pathway either by promoting the degradation of β-catenin protein (Topol et al., 2003), or by inhibiting β-catenin-TCF-mediated transcription (Ishitani et al., 1999; Ishitani et al., 2003). Recently, Mikels and Nusse (Mikels & Nusse, 2006a) showed, by using purified active soluble Wnt5a protein, that Wnt5a functions according to receptor availability. When Wnt5a binds to Frizzled 4 and LRP5, it activates canonical Wnt/β-catenin pathway, as judged by co-expression of Frizzled 4 and LRP5 in Wnt5a-treated human embryonic kidney cells and subsequent activation of a β-catenin responsive luciferase reporter construct (Mikels & Nusse, 2006a). In contrast, when Wnt5a binds to the single-pass transmembrane receptor Ror2 (orphan tyrosine kinase 2), it inhibits canonical Wnt/β-

catenin signalling without affecting β-catenin protein levels, but rather affecting the β-catenin-TCF-mediated transcription and also without inducing increased cellular calcium levels (Mikels & Nusse, 2006a). Consistently, co-injection of Wnt5a RNA with Frizzled 4 RNA, and co-injection of Wnt5a RNA with Frizzled 5 RNA, leads to the activation of Wnt/β-catenin target genes in *Xenopus* animal caps, and in the activation of Wnt/β-catenin signalling in *Xenopus* embryos inducing axis duplication respectively (He et al., 1997; Umbhauer et al., 2000).

Similarly to Wnt5A, Wnt7A is also a dual signalling Wnt, depending on receptor availability. When, Frizzled 5 is expressed in human endometrial cells, treated with purified active soluble Wnt7a protein, there is activation of the canonical Wnt/β-catenin pathway, whereas when Frizzled 10 is expressed in Wnt7a-treated human endometrial cells, there is activation of the non-canonical Wnt pathway, the planar cell polarity pathway (Carmon & Loose, 2008). Wnt11 has also been found to be implicated in the non-canonical planar cell polarity pathway in *zebrafish* (Marlow et al., 2002), while it was recently found that Wnt11 is a direct target of the canonical Wnt/β-catenin pathway in mouse myoblast cell lines and in mouse developing heart, which in turn activates the non-canonical planar cell polarity pathway, essential for the cell movements required for morphogenesis of the cardiac outflow tract (Zhou et al., 2007). At the same time, Wnt11 activates the canonical Wnt/β-catenin signalling cascade in the early *Xenopus* embryo, required for axis formation (Tao et al., 2005), further suggesting a possible activation of different receptors in each of these organisms. Interestingly, both Wnt11-Frizzled 5 and Wnt5A-Frizzled 5 fusion proteins, caused axis duplication, when separately injected as mRNA in *Xenopus* embryos, indicating an activated canonical Wnt pathway, while both Wnt11-Frizzled 5 and Wnt5A-Frizzled 5 fusion proteins synergised with LRP6 to activate Wnt/β-catenin pathway, indicated by increased transcriptional activity of the TOPFlash reporter promoter in human embryonic kidney cells (Holmen et al., 2002).

Gene expression studies, both in embryonic mouse skin and in normal human keratinocytes, have shown that all the three Wnt5a, Wnt7a and Wnt11 genes are expressed in embryonic mouse skin (Reddy et al., 2001), while in normal human keratinocytes only Wnt5a and Wnt7a are expressed, along with several Frizzled receptors including Frizzled 4 and Frizzled 5 (Yang et al., 2006). Importantly, Wnt5a

was found upregulated in mouse hair follicles at early morphogenetic stages (dermal condensation), but not at the earliest (promotion of placode), as confirmed by in situ hybridization, while both Wnt5a and Wnt11 are expressed in specific subsets of cells in mature anagen hair follicle (outer root sheath and outer layers of the inner root sheath), in mouse skin (Reddy et al., 2001). Therefore, these observations suggest that Wnt5a has a crucial role in hair follicle morphogenesis. Strikingly,the same study showed that Wnt5a is not expressed in early hair follicle morphogenesis in the absence of Shh (Shh -/- mouse embryos), strongly suggesting that Wnt5a is a target of Shh in hair follicle morphogenesis, and although in the earliest stages of hair follicle development (placode promotion) the Wnt genes (Wnt10a and Wnt 10b) are upstream of the Shh, in later stages (dermal condensation) Wnt genes (Wnt5a) lie downstream of the Shh (Reddy et al., 2001).

Analysis of gene expression in human BCCs by using both PCR and cDNA microarrays, revealed that several WNT and Frizzled genes are upregulated including, WNT5A, WNT7A, WNT11 and Frizzled 5 (Bonifas et al., 2001; Mullor et al., 2001; Saldanha et al., 2004; O'Driscoll et al., 2006; Yu et al., 2008). Therefore, since these WNT genes are known to be implicated in the activation of the canonical Wnt/β-catenin pathway, I checked whether these WNTs were increased in GLI2ΔN-epressing cells and found upregulation of WNT5A, 7A and 11 **(Figure 5.6)**; consistent with the results obtained from gene analysis in human BCCs and in M2SMO-induced basaloid follicular hamartoma in mice (Yang et al., 2008a). In addition, my results are in line with previous studies in different organisms, which have reported that Wnt genes are activated, in frog embryo animal cap explants injected with Gli2 and Gli3 mRNA (embryonic development) (Mullor et al., 2001), and in rat kidney epithelial cells upon Gli1 induction (*in vitro* transformation) (Li et al., 2007).

Therefore, given that the availability of different Frizzled receptors to the WNT ligand binding can influence the output of the WNT signal, it would be interesting to examine whether, and which, FZD receptors are overexpressed in response to GLI2ΔN induction in human N/TERT keratinocytes. In addition, the fact that the expression of several WNT ligands is induced in response to GLI2ΔN overexpression raises the possibility that at least some of these WNT genes are direct downstream targets of GLI2 transcription factor. By using chromatin immunoprecipitation experiments, it can be

examined whether there is any direct protein (GLI2) : DNA (WNT genes promoters) interactions, thus offering a possible explanation for the activation of WNT genes, and especially that of WNT11, which showed remarkable induction in response to GLI2ΔN upregulation. It is also important to understand, whether overexpression of WNT genes is solely responsible for β-catenin activation. A direct approach would be to block WNT ligand binding to FZD and LRP5/LRP6 receptors, by using DKK1 inhibitor, and then assess the levels of β-catenin transcriptional activity. Finally, it will be interesting to investigate whether any of the dual signalling Wnts that were found upregulated in mine, and previous studies, upon activation of the HH/GLI2 signalling, activate the non-canonical Wnt pathways, which might be important and have a role in HH/GLI2-mediated BCC tumourigenesis.

5.3.4 GLI2ΔN induces expression of molecular markers of EMT, without mediating suppression of E-cadherin or any morphological changes *in vitro*

The fact that Gli1 was found to be an upstream regulator of Snail (Snail homologue 1 of *Drosophila*) (Louro et al., 2002; Li et al., 2006), which is a transcriptional repressor of E-cadherin, and to act both through Wnts and Snail to promote nuclear signalling of β-catenin during epithelial transformation (Li et al., 2007), and also knowing that GLI2 is an upstream regulator of GLI1 (Ding et al., 1998; Bai et al., 2002; Regl et al., 2002; Mill et al., 2003; Ikram et al., 2004), suggest that these interactions may have a positive effect on β-catenin translocation to the nucleus of GLI2ΔN-expressing human N/TERT keratinocytes, thereby providing a further mechanism for the SHH/GLI-WNT/β-catenin crosstalk. The roles of β-catenin in cell-cell adhesion and Wnt signalling **(see Chapter 1, Section 1.4 and Chapter 5, Section 5.2.1.5)**, both in development and tumourigenesis, can be both independent from each other, or interrelated, since evidence occurs for both possibilities in different cell contexts (Cavallaro & Christofori, 2004; Gottardi & Gumbiner, 2004; Nelson & Nusse, 2004; Bienz, 2005; Brembeck et al., 2006), Thus, according to the latter, the nuclear relocalisation and transcriptional activation of β-catenin in the nucleus of GLI2ΔN-expressing keratinocytes, might not only be due to the WNT genes activation, but also due to the direct (GLI2ΔN→ SNAIL1), or indirect (GLI2ΔN→ GLI1→ SNAIL1) induction of SNAIL1, resulting in

subsequent suppression of E-cadherin, which might lead in the release of membranous β-catenin in the cytoplasm.

However, my results suggested that there is no contribution of the membranous E-cadherin bound β-catenin to the accumulation of the cytoplasmic β-catenin and its subsequent translocation to the nucleus since the upregulation of both SNAIL1 and its close family member SNAIL2 genes upon GLI2ΔN induction in N/TERT keratinocytes, was not accompanied by suppression of E-cadherin gene **(Figure 5.7)**.

The unchanged transcription levels of E-cadherin **(Figure 5.7)** are consistent with the phenotypic characteristics of GLI2ΔN-expressing cells. E-cadherin is required to hold epithelial cells together, while downregulation of E-cadherin expression leads to loss of cell-cell adhesion **(see Chapter 1, Section 1.4.1)** (Gumbiner, 1996; Gumbiner, 2005). Downregulation of E-cadherin expression often occurs both during normal developmental epithelial-mesenchymal transitions (EMT) and during tumour progression, when cells change their epithelial morphology to a motile mesenchymal one (i.e. spindle like morphology with abundant membrane extensions and long filaments resembling filopodia, fibroblast-like phenotype (Lee et al., 2006)) (Birchmeier & Behrens, 1994; Gumbiner, 1996; Thiery, 2002; Pecina-Slaus, 2003; Cavallaro & Christofori, 2004; Nelson & Nusse, 2004; Gumbiner, 2005; Hugo et al., 2007). Most of the GLI2ΔN-expressing cells do not exhibit any of these mesenchymal characteristics as described in **Chapter 3, Section 3.3.4**, and are mainly characterised by the presence of large compact, cohesive colony islands, comprised of small dense cells with a high ratio of nuclear to cytoplasmic volume **(Chapter 3, Section 3.2.3.1, Figure 3.11 and Figure 3.12)**. Similarly, Yang et al. (Yang et al., 2008a) reported no downregulation of E-cadherin in the M2SMO-induced buds, compared to the normal embryonic hair buds where suppression of E-cadherin was detected. These observations are also in keeping with the expression pattern of E-cadherin in human BCCs. While nodular and superficial BCCs express nuclear β-catenin (Yamazaki et al., 2001; El-Bahrawy et al., 2003; Saldanha et al., 2004; Yang et al., 2008a), they exhibit an epithelial cell phenotype with a palisading of columnar cells at the periphery of tumour nodules, and the expression of E-cadherin is preserved in most of these tumours (Kriegl et al., 2009). On the other hand, infiltrative BCCs, which are more locally invasive and aggressive, but not metastatic, represent morphologically EMT-like changes, including reduction of

cell-cell interactions and single cell dissociation, accompanied by reduced expression of E-cadherin (Pizarro et al., 1994; Pizarro et al., 1995; Fuller et al., 1996; Shirahama et al., 1996; Tada et al., 1996; Kooy et al., 1999; Pizarro, 2000; Tada et al., 2000; Saldanha et al., 2004), consistent with the role of E-cadherin in tumour cell invasion, but not with its role in metastasis **(see Chapter 1, Section 1.4.1)** (Birchmeier & Behrens, 1994; Hirohashi, 1998; Hirohashi & Kanai, 2003; Cavallaro & Christofori, 2004). However, there are a few cases in which E-cadherin is preserved even in infiltrative human BCCs, suggesting that other mechanisms in cancer cells can overcome the invasive-suppressor function of E-cadherin (Pizarro et al., 1994).

SNAIL1 and SNAIL2 are molecular markers for epithelial-mesenchymal transitions, which occur both during development, and during tumourigenesis and progression of epithelial malignant tumours, and act as transcriptional repressors of the E-cadherin gene **(see Section 5.2.1.5)** (Batlle et al., 2000; Cano et al., 2000; Hajra et al., 2002; Nieto, 2002; Thiery, 2002; Hugo et al., 2007). The fact that GLI2ΔN activates SNAIL1 and SNAIL2 *in vitro* **(Figure 5.7)**, suggests that although HH/GLI prepares cells for EMT, is not sufficient to complete the process in N/TERT human keratinocytes, since there is no downregulation of E-cadherin or any morphological signs of EMT-process. This does not necessary mean that activated HH/GLI pathway is incompatible with EMT and metastasis, but that the effect might be context dependent (Karhadkar et al., 2004; Sheng et al., 2004; Bhatia et al., 2006; Sterling et al., 2006; Thiyagarajan et al., 2007). Accordingly, human prostate cancer metastases have higher HH/GLI signalling activity than do the primary tumours from which they arose, while augmented Hh pathway activity (GLI1 overexpression) in mice prostate cancer cell lines resulted in increased levels of Snail, reduced levels of E-cadherin, and to a metastatic phenotype in mice inoculated subcutaneously with these cells **(see Chapter 1, Section 1.3.5)** (Karhadkar et al., 2004).

Another possibility would be, that since EMT largely depends on the interactions between the epithelial keratinocytes and the underlying mesenchyme (Radisky, 2005), the absence of this interaction *in vitro*, could abolish the effects of EMT related gene expression. Furthermore, it would be important to examine the protein levels of SNAIL in GLI2ΔN overexpressing keratinocytes and whether these are sufficient to suppress gene expression, since only stabilised forms of SNAIL can act as transcriptional

repressors of target genes. Even in the case of adequate protein stabilisation, it could be possible that the expression of E-cadherin is also regulated by other genes, thereby opposing SNAIL mediated suppression.

Alternatively, E-cadherin suppression could be a feature of isolated keratinocytes within the population, with an increased capacity to invade. In that case, suppression of E-cadherin would be undetectable in a monolayer *in vitro* system such as the one used here. It would be therefore interesting to investigate the expression pattern of E-cadherin in an organotypic model of epidermis, and observe whether its expression is altered in a specific subset of GLI2ΔN keratinocytes, and how this correlates with their ability to invade the tissue. In a recent study from Snijders et al. (Snijders et al., 2008), where GLI2-HaCaT-expressing keratinocytes were used, it was shown that inducible expression of GLI2 resulted in the invasion of GLI2-HaCaT keratinocytes into the collagen/fibroblast layers, as individual cells or small groups of cells. Surprisingly, the GLI2-HaCaT invading cells apart from having downregulated E-cadherin, which is associated with increased cell invasion, they also had downregulated the expression of GLI2 responsive genes, including BCL-2 and SOX2 (Snijders et al., 2008). However, the observations that the HH/GLI2 responsive genes are downregulated in the invading GLI2-HaCaT cells, and the suggestion from the authors that GLI2 activation needs to be downregulated/suppressed in order for the cells to invade, is contradictory to studies (in situ hybridisation and cDNA microarrays) in different subtypes of human BCCs, that have clearly shown that GLI2 is significantly upregulated in all the different BCC subtypes, including the aggressive ones consisting of the infiltrative and morpheaform/sclerosing (similar to infiltrative ones) human BCCs (Ikram et al., 2004; Crowson, 2006; O'Driscoll et al., 2006; Yu et al., 2008). In addition, SOX9, which is a downstream target of GLI2 **(see Chapter 3, Section 3.3.6.2)** (Vidal et al., 2005), was found to be upregulated in all subtypes of human BCC tested, including the infiltrative ones (Vidal et al., 2008). Therefore, at this stage, all these alternatives are equally likely to be the explanation of the non suppression of E-cadherin by SNAIL in my system, and further studies are required to discriminate between them.

Most importantly, the fact that in GLI2ΔN-expressing cells there is upregulation of SNAIL1, but not suppression of E-cadherin **(Figure 5.7)**, and thus no release of the membranous β-catenin, which could possibly contribute to the increased β-catenin

transcriptional activation, is in line with a recent study of Stemmer at al. (Stemmer et al., 2008). Stemmer at al. (Stemmer et al., 2008) demonstrated that SNAIL1 binds to β-catenin (protein-protein interactions), and promotes its transcriptional activity, through its carboxy-terminal zinc-finger domain, and not through its amino-terminal domain, which represses transcription of target genes, including E-cadherin, by recruiting histone deacetylases (Nieto, 2002). Therefore, SNAIL is a dual-function transcription factor, and suppression of E-cadherin by SNAIL is not required for the stimulation of β-catenin dependent transactivation in human embryonic kidney cells (Stemmer et al., 2008). In support of this, overexpression of SNAIL in human colorectal cancer cell lines leads to increased expression of Wnt target genes, including Axin2 and survivin, while knockdown (siRNA) of SNAIL in these cell lines resulted to reduced expression of WNT target genes, whereas no change in E-cadherin mRNA and protein levels was observed (Stemmer et al., 2008). This further suggests that endogenous SNAIL co-activates WNT target gene expression, without requiring suppression of E-cadherin by SNAIL (Stemmer et al., 2008). Interestingly, another study showed that upregulation of Axin2 by canonical Wnt/β-catenin signalling activation, increases/stabilises Snail1 protein levels (Axin2 sequesters GSK3β from the nucleus leaving Snail1 in its non-phosphorylated transcriptionally active form) leading to EMT in breast cancer cells (Yook et al., 2006).

Therefore, taking into account that the mechanisms by which SNAIL exerts its role as a co-activator of β-catenin and/or as a repressor of E-cadherin, are largely independent from each other and context specific, I suggest that GLI2ΔN-induced SNAIL1, may act as a co-activator of nuclear β-catenin rather than as a repressor of E-cadherin. Consistently, Gli1-induced mouse skin lesions, resembling infiltrating human BCCs, were found to have both increased expression of Snail and downregulation of E-cadherin (Li et al., 2006), while nodular human BCCs, which in most cases preserve E-cadherin, were also found to have increased expression of SNAIL (Louro et al., 2002).

Finally, with respect to Wnt signalling, the upregulation of SNAIL2 upon GLI2ΔN induction in human N/TERT keratinocytes **(Figure 5.7)**, is consistent with the study of Vallin et al. (Vallin et al., 2001), which suggested that Slug (SNAIL2) in *Xenopus* is a direct target of LEF-1/β-catenin complex, as judged by the presence of a functional binding site for LEF-1 in the promoter of Slug gene.

5.4 Summary

The SHH and WNT pathways play pivotal roles in development and stem cell maintenance in adult tissues. They are also implicated in the aetiology of various cancers such as colorectal and hepatoblastoma (WNT), medulloblastoma and BCC (SHH). The crosstalk between these pathways has not been fully investigated in human cells, although the potential benefits which would result from the targeted inhibition of either pathway, or both pathways, in the treatment of their associated cancers, makes them attractive targets. Most importantly, it is essential to be able to target tumour associated aberrant pathways without interfering significantly with the physiological relevant ones (Taipale & Beachy, 2001) and moreover, without stimulating undesirable cross-talk between pathways. Knowledge of the relationship between WNT and SHH would provide just this kind of information.

Thus, in this chapter, evidence is provided of SHH/GLI2 - WNT/β-catenin signalling interactions in human keratinocytes for the first time. Induction of GLI2ΔN in N/TERT keratinocytes promotes nuclear relocalisation of β-catenin and enhances its transcriptional activation, possibly through WNT genes upregulation and SNAIL1 induction, a co-activator of β-catenin. These results suggest, that WNT/β-catenin signalling is required downstream of SHH/GLI2 signalling, and that GLI2ΔN is a novel regulator of β-catenin, and may play an important role in its activation in human basal cell carcinoma.

CHAPTER SIX

6 CONCLUSIONS

Sonic Hedgehog signalling (SHH) activation plays an important role in the direction of embryonic development and it has been involved in the development of human malignancies. Abnormal SHH stimulation leads to increased transcriptional activation of its downstream effector, GLI2, which is implicated in the pathogenesis of a variety of human tumours, including human basal cell carcinoma (BCC). Nevertheless, little is still known about the molecular mechanisms underlying the tumourigenic role of GLI2 in human epidermal keratinocytes.

This study examined the effects of inducible and stable overexpression of GLI2ΔN (constitutively active form of GLI2 isoform β, lacking the N-terminal repressor domain) oncogenic transcription factor, on telomerase immortalised human epidermal keratinocytes (N/TERT). The findings showed that overexpression of GLI2ΔN in human N/TERT keratinocytes can produce gene expression patterns and phenotypic characteristics reminiscent of those observed in human BCC *in vivo* and of other systems reported *in vitro*. More specifically, overexpression of GLI2ΔN induced the expression of its downstream target BCL-2, while it also led to a reduction in the expression levels of c-MYC, which is an expression pattern previously reported in human BCCs. GLI2ΔN overexpression also produced a strong phenotype in human keratinocytes, which displayed significant heterogeneity in culture with the majority of cells being organised in small compact, undifferentiated, basal-like (stem cell-like) keratinocyte colonies resembling the undifferentiated phenotype of human BCCs. The macroscopic appearance of these cells (basal-like phenotype) was matched with a basal gene expression profile induced by GLI2ΔN, as was judged by the suppression of differentiation specific markers (an important hallmark of cancer), such as involucrin, of genes responsible for the onset of keratinocyte differentiation including $p21^{WAF1/CIP1}$, 14-3-3σ, and c-MYC, and of stem cell related genes such as integrin β1 and SOX2, which is keeping with previous reports on the effects of GLI2ΔN in other keratinocyte cell lines. Importantly, this expression pattern of GLI2ΔN-expressing keratinocytes is in line with the molecular signature of human BCCs. In addition, the overexpression of GLI2ΔN not only did not accelerate the proliferation rates of N/TERT keratinocytes, but instead led to a significant reduction in the growth rate of keratinocytes in culture, without causing any cell death or increased apoptosis.

Despite the similarities between GLI2ΔN overexpressing human keratinocytes *in vitro*, and human BCCs *in vivo*, this study unveiled a novel role for GLI2ΔN in cell cycle control and the maintenance of genomic integrity of human cells. It was found that expression of GLI2ΔN in N/TERT keratinocytes was alone sufficient to induce significant ploidy abnormalities, which is a hallmark of many cancers. These ploidy abnormalities could also be partly responsible for the reduced growth rate of GLI2ΔN-expressing keratinocytes, which however did not show any evidence of increased cell death or apoptosis in response to GLI2ΔN overexpression. Upon GLI2ΔN induction, N/TERT human keratinocytes displayed (i) increased tetraploidisation as evidenced by an increase in G2/M phase of the cell cycle and binucleate cell counting, followed by subsequent polyploidy and aneuploidy as evidenced by cell cycle analysis, (ii) inactivation of cell cycle regulator genes such as $p21^{WAF1/CIP1}$ and 14-3-3σ that control the generation of tetraploid cells, as well as the proliferation of tetraploid and DNA damaged cells, with no change in p53 protein levels and (iii) defective apoptosis, possibly through the upregulation of the anti-apoptotic protein BCL-2, which is responsible for the elimination of tetraploid / polyploid / aneuploid cells and is otherwise activated in response to tetraploidisation. This provided the first evidence that GLI2ΔN promotes the generation of tetraploid progenies in human keratinocytes propably via cytokinesis failure (binucleate tetraploids), while inactivating the growth inhibitory mechanisms that normally limit their survival and expansion, leading to aneuploidy and genomic instability. Consistently, GLI2ΔN overexpressing N/TERT keratinocytes showed evidence not only of numerical chromosomal instability, but also of structural genomic instability, another hallmark of many cancers, as was judged by structural chromosomal aberrations, such as translocations and double minute chromosomes, which were evident following M-FISH karyotype analysis.

Furthermore, consistent with the downregulation of $p21^{WAF1/CIP1}$ *in vitro*, $p21^{WAF1/CIP1}$ protein in this study was also found to be almost absent in human BCC tumours, while forced expression of GLI2ΔN in human N/TERT keratinocytes rendered cells resistant not only to tetraploidy-mediated apoptosis (cell cycle failure-mediated apoptosis), but also to UVB-mediated apoptosis (DNA damage-mediated apoptosis), consistent with the resistance of human BCCs in apoptosis mediated either by intrinsic or extrinsic pathways. The apoptotic resistance of GLI2ΔN overexpressing N/TERT keratinocytes to the strong apoptotic stimuli, UVB (UVB, 290-320 nm) irradiation, which is known to

be one of the most important etiological factors in BCC formation, is possibly achieved through the activation of BCL-2 gene and protein upregulation, whereas the upregulation of p53 and the concomitant suppression of $p21^{WAF1/CIP1}$ proteins after UVB treatment in GLI2ΔN-expressing keratinocytes, further confirms that downregulation of $p21^{WAF1/CIP1}$ upon GLI2ΔN induction occurs in a p53-independent manner. Tetraploidy, which has its own tumourigenic potential, along with aneuploidy, genomic instability and defective apoptosis, are all features of many human cancers in which GLI2 has been shown to be involved, including human BCCs. Therefore, collectively these observations provide new insights into how GLI2ΔN might exert its tumourigenic potential, and may explain why its upregulation is also implicated in a variety of human malignancies besides human BCCs.

The SHH and WNT pathways play pivotal roles in development and stem cell maintenance in adult tissues and their deregulation is often implicated in various cancers including colorectal cancer and hepatoblastoma (WNT), medulloblastoma and BCC (SHH). The activation of β-catenin is the most common alteration observed during aberrant WNT signalling and is often implicated in human carcinogenesis and metastasis. Athough little is known about SHH/GLI and WNT/β-catenin interactions in human tumourigenesis, several studies in different organisms have shown that parallels and crosstalk between HH and WNT signalling, occur both during development and tumourigenesis. This study provided evidence for the first time of a new connection between SHH/GLI2 and WNT/β-catenin pathways in human epidermal keratinocytes. GLI2ΔN induction in human N/TERT keratinocytes promoted the nuclear accumulation of β-catenin in keratinocyte cell culture and in the basal layer of organotypic skin rafts, similar to human BCCs where accumulation of nuclear β-catenin has been previously reported. In addition, several WNT and SNAIL genes were found to be upregulated upon GLI2ΔN induction, while β-catenin transcriptional activity was increased upon stable and conditional expression of GLI2ΔN, suggesting the activation of β-catenin-dependent transcription of WNT target genes. These observations also suggested that GLI2ΔN enhances the nuclear relocalisation and the transcriptional activation of β-catenin, possibly through WNT genes upregulation and SNAIL1 induction, a co-activator of β-catenin. Collectively, these data indicated that WNT/β-catenin signalling is required downstream of SHH/GLI2 signalling, and that GLI2ΔN is a novel regulator of β-catenin, and may play an important role in its activation in human basal cell

carcinoma and possibly in other cancers with aberrant activation of WNT/β-catenin pathway.

Overall, this study has provided multiple lines of evidence to support that GLI2 might exert its tumourigenic effect on human cells by affecting multiple processes such as epithelial differentiation, cell cycle control and the maintenance of genomic integrity, as well as the regulation of WNT/β-catenin pathway gene expression. More importantly, the effects of GLI2ΔN in human N/TERT keratinocytes are highly relevant to the biology of human BCCs, rendering this system a useful model for studying BCC biogenesis and survival *in vitro*.

References

Aberger F and Frischauf AM. (2006). *GLI Genes and Their Targets in Epidermal Development and Disease. In: Ariel Ruiz i Altaba (ed.). Hedgehog-Gli Signaling in Human Disease, pp 74-85.* Kluwer academic/plenum publishers.

Aberle H, Bauer A, Stappert J, Kispert A and Kemler R. (1997). beta-catenin is a target for the ubiquitin-proteasome pathway, *Embo J*, **16,** 3797-804.

Adams JC and Watt FM. (1989). Fibronectin inhibits the terminal differentiation of human keratinocytes, *Nature*, **340,** 307-9.

Adams JC and Watt FM. (1990). Changes in keratinocyte adhesion during terminal differentiation: reduction in fibronectin binding precedes alpha 5 beta 1 integrin loss from the cell surface, *Cell*, **63,** 425-35.

Adams JC and Watt FM. (1991). Expression of beta 1, beta 3, beta 4, and beta 5 integrins by human epidermal keratinocytes and non-differentiating keratinocytes, *J Cell Biol*, **115,** 829-41.

Adolphe C, Hetherington R, Ellis T and Wainwright B. (2006). Patched1 functions as a gatekeeper by promoting cell cycle progression, *Cancer Res*, **66,** 2081-8.

Adolphe C, Narang M, Ellis T, Wicking C, Kaur P and Wainwright B. (2004). An in vivo comparative study of sonic, desert and Indian hedgehog reveals that hedgehog pathway activity regulates epidermal stem cell homeostasis, *Development*, **131,** 5009-19.

Aguilera A and Gomez-Gonzalez B. (2008). Genome instability: a mechanistic view of its causes and consequences, *Nat Rev Genet*, **9,** 204-17.

Ahmed SA, Gogal RM, Jr. and Walsh JE. (1994). A new rapid and simple non-radioactive assay to monitor and determine the proliferation of lymphocytes: an alternative to [3H]thymidine incorporation assay, *J Immunol Methods*, **170,** 211-24.

Ai H, Barrera JE, Meyers AD, Shroyer KR and Varella-Garcia M. (2001). Chromosomal aneuploidy precedes morphological changes and supports multifocality in head and neck lesions, *Laryngoscope*, **111,** 1853-8.

Akiyoshi T, Nakamura M, Koga K, Nakashima H, Yao T, Tsuneyoshi M, Tanaka M and Katano M. (2006). Gli1, downregulated in colorectal cancers, inhibits proliferation of colon cancer cells involving Wnt signalling activation, *Gut*, **55,** 991-9.

Al-Daraji WI, Grant KR, Ryan K, Saxton A and Reynolds NJ. (2002). Localization of calcineurin/NFAT in human skin and psoriasis and inhibition of calcineurin/NFAT activation in human keratinocytes by cyclosporin A, *J Invest Dermatol*, **118,** 779-88.

Alberts B, Bray D, Lewis J, Raff M, Roberts K and Watson D. (1994). *The Mechanisms of Cell Division. Molecular Biology OF THE CELL, pp 911-946. 3rd ed.* Garland Publishing: New York, NY.

Albertson DG. (2006). Gene amplification in cancer, *Trends Genet*, **22,** 447-55.

Albertson DG, Collins C, McCormick F and Gray JW. (2003). Chromosome aberrations in solid tumors, *Nat Genet*, **34,** 369-76.

Alcedo J, Ayzenzon M, Von Ohlen T, Noll M and Hooper JE. (1996). The Drosophila smoothened gene encodes a seven-pass membrane protein, a putative receptor for the hedgehog signal, *Cell*, **86,** 221-32.

Alitalo K, Kuismanen E, Myllyla R, Kiistala U, Asko-Seljavaara S and Vaheri A. (1982). Extracellular matrix proteins of human epidermal keratinocytes and feeder 3T3 cells, *J Cell Biol*, **94,** 497-505.

Allen M, Grachtchouk M, Sheng H, Grachtchouk V, Wang A, Wei L, Liu J, Ramirez A, Metzger D, Chambon P, Jorcano J and Dlugosz AA. (2003). Hedgehog signaling regulates sebaceous gland development, *Am J Pathol*, **163,** 2173-8.

Alonso L and Fuchs E. (2003a). Stem cells in the skin: waste not, Wnt not, *Genes Dev*, **17,** 1189-200.

Alonso L and Fuchs E. (2003b). Stem cells of the skin epithelium, *Proc Natl Acad Sci U S A*, **100 Suppl 1,** 11830-5.

Alonso L and Fuchs E. (2006). The hair cycle, *J Cell Sci*, **119,** 391-3.

Alvarez-Medina R, Le Dreau G, Ros M and Marti E. (2009). Hedgehog activation is required upstream of Wnt signalling to control neural progenitor proliferation, *Development*, **136,** 3301-9.

Amati B and Land H. (1994). Myc-Max-Mad: a transcription factor network controlling cell cycle progression, differentiation and death, *Curr Opin Genet Dev*, **4,** 102-8.

Amiel A, Gronich N, Yukla M, Suliman S, Josef G, Gaber E, Drori G, Fejgin MD and Lishner M. (2005). Random aneuploidy in neoplastic and pre-neoplastic diseases, multiple myeloma, and monoclonal gammopathy, *Cancer Genet Cytogenet*, **162,** 78-81.

Amit S, Hatzubai A, Birman Y, Andersen JS, Ben-Shushan E, Mann M, Ben-Neriah Y and Alkalay I. (2002). Axin-mediated CKI phosphorylation of beta-catenin at Ser 45: a molecular switch for the Wnt pathway, *Genes Dev*, **16,** 1066-76.

Andl T, Reddy ST, Gaddapara T and Millar SE. (2002). WNT signals are required for the initiation of hair follicle development, *Dev Cell*, **2,** 643-53.

Andreassen PR, Lacroix FB, Lohez OD and Margolis RL. (2001a). Neither p21WAF1 nor 14-3-3sigma prevents G2 progression to mitotic catastrophe in human colon carcinoma cells after DNA damage, but p21WAF1 induces stable G1 arrest in resulting tetraploid cells, *Cancer Res*, **61,** 7660-8.

Andreassen PR, Lohez OD, Lacroix FB and Margolis RL. (2001b). Tetraploid state induces p53-dependent arrest of nontransformed mammalian cells in G1, *Mol Biol Cell*, **12,** 1315-28.

Andreassen PR, Martineau SN and Margolis RL. (1996). Chemical induction of mitotic checkpoint override in mammalian cells results in aneuploidy following a transient tetraploid state, *Mutat Res*, **372,** 181-94.

Arce L, Yokoyama NN and Waterman ML. (2006). Diversity of LEF/TCF action in development and disease, *Oncogene*, **25,** 7492-504.

Argyris TS. (1980a). Epidermal growth following a single application of 12-O-tetradecanoyl-phorbol-13-acetate in mice, *Am J Pathol*, **98,** 639-48.

Argyris TS. (1980b). Tumor promotion by abrasion induced epidermal hyperplasia in the skin of mice, *J Invest Dermatol*, **75,** 360-2.

Armstrong BK and Kricker A. (2001). The epidemiology of UV induced skin cancer, *J Photochem Photobiol B*, **63,** 8-18.

Arnold I and Watt FM. (2001). c-Myc activation in transgenic mouse epidermis results in mobilization of stem cells and differentiation of their progeny, *Curr Biol*, **11,** 558-68.

Artandi SE, Chang S, Lee SL, Alson S, Gottlieb GJ, Chin L and DePinho RA. (2000). Telomere dysfunction promotes non-reciprocal translocations and epithelial cancers in mice, *Nature*, **406,** 641-5.

Ashkenazi A. (2002). Targeting death and decoy receptors of the tumour-necrosis factor superfamily, *Nat Rev Cancer*, **2,** 420-30.

Ashton-Rickardt PG, Dunlop MG, Nakamura Y, Morris RG, Purdie CA, Steel CM, Evans HJ, Bird CC and Wyllie AH. (1989). High frequency of APC loss in

sporadic colorectal carcinoma due to breaks clustered in 5q21-22, *Oncogene*, **4,** 1169-74.

Ashton KJ, Carless MA and Griffiths LR. (2005). Cytogenetic alterations in nonmelanoma skin cancer: a review, *Genes Chromosomes Cancer*, **43,** 239-48.

Asplund A, Gry Bjorklund M, Sundquist C, Stromberg S, Edlund K, Ostman A, Nilsson P, Ponten F and Lundeberg J. (2008). Expression profiling of microdissected cell populations selected from basal cells in normal epidermis and basal cell carcinoma, *Br J Dermatol*, **158,** 527-38.

Aszterbaum M, Epstein J, Oro A, Douglas V, LeBoit PE, Scott MP and Epstein EH, Jr. (1999). Ultraviolet and ionizing radiation enhance the growth of BCCs and trichoblastomas in patched heterozygous knockout mice, *Nat Med*, **5,** 1285-91.

Athar M, Tang X, Lee JL, Kopelovich L and Kim AL. (2006). Hedgehog signalling in skin development and cancer, *Exp Dermatol*, **15,** 667-77.

Avilion AA, Nicolis SK, Pevny LH, Perez L, Vivian N and Lovell-Badge R. (2003). Multipotent cell lineages in early mouse development depend on SOX2 function, *Genes Dev*, **17,** 126-40.

Aylon Y, Michael D, Shmueli A, Yabuta N, Nojima H and Oren M. (2006). A positive feedback loop between the p53 and Lats2 tumor suppressors prevents tetraploidization, *Genes Dev*, **20,** 2687-700.

Aza-Blanc P and Kornberg TB. (1999). Ci: a complex transducer of the hedgehog signal, *Trends Genet*, **15,** 458-62.

Aza-Blanc P, Lin HY, Ruiz i Altaba A and Kornberg TB. (2000). Expression of the vertebrate Gli proteins in Drosophila reveals a distribution of activator and repressor activities, *Development*, **127,** 4293-301.

Aza-Blanc P, Ramirez-Weber FA, Laget MP, Schwartz C and Kornberg TB. (1997). Proteolysis that is inhibited by hedgehog targets Cubitus interruptus protein to the nucleus and converts it to a repressor, *Cell*, **89,** 1043-53.

Bagutti C, Speight PM and Watt FM. (1998). Comparison of integrin, cadherin, and catenin expression in squamous cell carcinomas of the oral cavity, *J Pathol*, **186,** 8-16.

Bai CB, Auerbach W, Lee JS, Stephen D and Joyner AL. (2002). Gli2, but not Gli1, is required for initial Shh signaling and ectopic activation of the Shh pathway, *Development*, **129,** 4753-61.

Bailleul B, Surani MA, White S, Barton SC, Brown K, Blessing M, Jorcano J and Balmain A. (1990). Skin hyperkeratosis and papilloma formation in transgenic mice expressing a ras oncogene from a suprabasal keratin promoter, *Cell*, **62,** 697-708.

Bakin AV and Curran T. (1999). Role of DNA 5-methylcytosine transferase in cell transformation by fos, *Science*, **283,** 387-90.

Bale AE and Yu KP. (2001). The hedgehog pathway and basal cell carcinomas, *Hum Mol Genet*, **10,** 757-62.

Balmain A. (2001). Cancer genetics: from Boveri and Mendel to microarrays, *Nat Rev Cancer*, **1,** 77-82.

Baltimore D. (1970). RNA-dependent DNA polymerase in virions of RNA tumour viruses, *Nature*, **226,** 1209-11.

Barbareschi M, Girlando S, Cristofolini P, Cristofolini M, Togni R and Boi S. (1992). p53 protein expression in basal cell carcinomas, *Histopathology*, **21,** 579-81.

Barcellona ML, Cardiel G and Gratton E. (1990). Time-resolved fluorescence of DAPI in solution and bound to polydeoxynucleotides, *Biochem Biophys Res Commun*, **170,** 270-80.

Barker N, Hurlstone A, Musisi H, Miles A, Bienz M and Clevers H. (2001). The chromatin remodelling factor Brg-1 interacts with beta-catenin to promote target gene activation, *Embo J*, **20,** 4935-43.

Barker PE. (1982). Double minutes in human tumor cells, *Cancer Genet Cytogenet*, **5,** 81-94.

Barnes EA, Kong M, Ollendorff V and Donoghue DJ. (2001). Patched1 interacts with cyclin B1 to regulate cell cycle progression, *Embo J*, **20,** 2214-23.

Barnfield PC, Zhang X, Thanabalasingham V, Yoshida M and Hui CC. (2005). Negative regulation of Gli1 and Gli2 activator function by Suppressor of fused through multiple mechanisms, *Differentiation*, **73,** 397-405.

Barrandon Y and Green H. (1985). Cell size as a determinant of the clone-forming ability of human keratinocytes, *Proc Natl Acad Sci U S A*, **82,** 5390-4.

Barrandon Y and Green H. (1987). Three clonal types of keratinocyte with different capacities for multiplication, *Proc Natl Acad Sci U S A*, **84,** 2302-6.

Barrandon Y, Morgan JR, Mulligan RC and Green H. (1989). Restoration of growth potential in paraclones of human keratinocytes by a viral oncogene, *Proc Natl Acad Sci U S A*, **86,** 4102-6.

Barrett MT, Pritchard D, Palanca-Wessels C, Anderson J, Reid BJ and Rabinovitch PS. (2003). Molecular phenotype of spontaneously arising 4N (G2-tetraploid) intermediates of neoplastic progression in Barrett's esophagus, *Cancer Res*, **63,** 4211-7.

Barrett MT, Sanchez CA, Prevo LJ, Wong DJ, Galipeau PC, Paulson TG, Rabinovitch PS and Reid BJ. (1999). Evolution of neoplastic cell lineages in Barrett oesophagus, *Nat Genet*, **22,** 106-9.

Bartek J and Lukas J. (2001). Mammalian G1- and S-phase checkpoints in response to DNA damage, *Curr Opin Cell Biol*, **13,** 738-47.

Bartkova J, Horejsi Z, Koed K, Kramer A, Tort F, Zieger K, Guldberg P, Sehested M, Nesland JM, Lukas C, Orntoft T, Lukas J and Bartek J. (2005). DNA damage response as a candidate anti-cancer barrier in early human tumorigenesis, *Nature*, **434,** 864-70.

Bartkova J, Rezaei N, Liontos M, Karakaidos P, Kletsas D, Issaeva N, Vassiliou LV, Kolettas E, Niforou K, Zoumpourlis VC, Takaoka M, Nakagawa H, Tort F, Fugger K, Johansson F, Sehested M, Andersen CL, Dyrskjot L, Orntoft T, Lukas J, Kittas C, Helleday T, Halazonetis TD, Bartek J and Gorgoulis VG. (2006). Oncogene-induced senescence is part of the tumorigenesis barrier imposed by DNA damage checkpoints, *Nature*, **444,** 633-7.

Basto R, Brunk K, Vinadogrova T, Peel N, Franz A, Khodjakov A and Raff JW. (2008). Centrosome amplification can initiate tumorigenesis in flies, *Cell*, **133,** 1032-42.

Bath-Hextall FJ, Perkins W, Bong J and Williams HC. (2007). Interventions for basal cell carcinoma of the skin, *Cochrane Database Syst Rev***,** CD003412.

Batlle E, Sancho E, Franci C, Dominguez D, Monfar M, Baulida J and Garcia De Herreros A. (2000). The transcription factor snail is a repressor of E-cadherin gene expression in epithelial tumour cells, *Nat Cell Biol*, **2,** 84-9.

Bauer EA, Gordon JM, Reddick ME and Eisen AZ. (1977). Quantitation and immunocytochemical localization of human skin collagenase in basal cell carcinoma, *J Invest Dermatol*, **69,** 363-7.

Beachy PA, Karhadkar SS and Berman DM. (2004). Tissue repair and stem cell renewal in carcinogenesis, *Nature*, **432,** 324-31.

Behrens J, Jerchow BA, Wurtele M, Grimm J, Asbrand C, Wirtz R, Kuhl M, Wedlich D and Birchmeier W. (1998). Functional interaction of an axin homolog, conductin, with beta-catenin, APC, and GSK3beta, *Science*, **280,** 596-9.

Behrens J, von Kries JP, Kuhl M, Bruhn L, Wedlich D, Grosschedl R and Birchmeier W. (1996). Functional interaction of beta-catenin with the transcription factor LEF-1, *Nature*, **382,** 638-42.

Bek S and Kemler R. (2002). Protein kinase CKII regulates the interaction of beta-catenin with alpha-catenin and its protein stability, *J Cell Sci*, **115,** 4743-53.

Belloni E, Muenke M, Roessler E, Traverso G, Siegel-Bartelt J, Frumkin A, Mitchell HF, Donis-Keller H, Helms C, Hing AV, Heng HH, Koop B, Martindale D, Rommens JM, Tsui LC and Scherer SW. (1996). Identification of Sonic hedgehog as a candidate gene responsible for holoprosencephaly, *Nat Genet*, **14,** 353-6.

Bellusci S, Furuta Y, Rush MG, Henderson R, Winnier G and Hogan BL. (1997). Involvement of Sonic hedgehog (Shh) in mouse embryonic lung growth and morphogenesis, *Development*, **124,** 53-63.

Ben-Porath I, Thomson MW, Carey VJ, Ge R, Bell GW, Regev A and Weinberg RA. (2008). An embryonic stem cell-like gene expression signature in poorly differentiated aggressive human tumors, *Nat Genet*, **40,** 499-507.

Benazeraf B, Chen Q, Peco E, Lobjois V, Medevielle F, Ducommun B and Pituello F. (2006). Identification of an unexpected link between the Shh pathway and a G2/M regulator, the phosphatase CDC25B, *Dev Biol*, **294,** 133-47.

Berman DM, Karhadkar SS, Hallahan AR, Pritchard JI, Eberhart CG, Watkins DN, Chen JK, Cooper MK, Taipale J, Olson JM and Beachy PA. (2002). Medulloblastoma growth inhibition by hedgehog pathway blockade, *Science*, **297,** 1559-61.

Berman DM, Karhadkar SS, Maitra A, Montes De Oca R, Gerstenblith MR, Briggs K, Parker AR, Shimada Y, Eshleman JR, Watkins DN and Beachy PA. (2003). Widespread requirement for Hedgehog ligand stimulation in growth of digestive tract tumours, *Nature*, **425,** 846-51.

Berx G, Cleton-Jansen AM, Nollet F, de Leeuw WJ, van de Vijver M, Cornelisse C and van Roy F. (1995). E-cadherin is a tumour/invasion suppressor gene mutated in human lobular breast cancers, *Embo J*, **14,** 6107-15.

Bhanot P, Brink M, Samos CH, Hsieh JC, Wang Y, Macke JP, Andrew D, Nathans J and Nusse R. (1996). A new member of the frizzled family from Drosophila functions as a Wingless receptor, *Nature*, **382,** 225-30.

Bhatia N, Thiyagarajan S, Elcheva I, Saleem M, Dlugosz A, Mukhtar H and Spiegelman VS. (2006). Gli2 is targeted for ubiquitination and degradation by beta-TrCP ubiquitin ligase, *J Biol Chem*, **281,** 19320-6.

Bhattacharya R, Kwon J, Ali B, Wang E, Patra S, Shridhar V and Mukherjee P. (2008). Role of hedgehog signaling in ovarian cancer, *Clin Cancer Res*, **14,** 7659-66.

Bickenbach JR. (1981). Identification and behavior of label-retaining cells in oral mucosa and skin, *J Dent Res*, **60 Spec No C,** 1611-20.

Bickenbach JR and Chism E. (1998). Selection and extended growth of murine epidermal stem cells in culture, *Exp Cell Res*, **244,** 184-95.

Bickenbach JR and Holbrook KA. (1987). Label-retaining cells in human embryonic and fetal epidermis, *J Invest Dermatol*, **88,** 42-6.

Bienz M. (2005). beta-Catenin: a pivot between cell adhesion and Wnt signalling, *Curr Biol*, **15,** R64-7.

Bigelow RL, Chari NS, Unden AB, Spurgers KB, Lee S, Roop DR, Toftgard R and McDonnell TJ. (2004). Transcriptional regulation of bcl-2 mediated by the sonic hedgehog signaling pathway through gli-1, *J Biol Chem*, **279,** 1197-205.

Bignold LP, Coghlan BL and Jersmann HP. (2006). Hansemann, Boveri, chromosomes and the gametogenesis-related theories of tumours, *Cell Biol Int*, **30,** 640-4.

Bikle DD, Oda Y and Xie Z. (2004). Calcium and 1,25(OH)2D: interacting drivers of epidermal differentiation, *J Steroid Biochem Mol Biol*, **89-90,** 355-60.

Birchmeier W and Behrens J. (1994). Cadherin expression in carcinomas: role in the formation of cell junctions and the prevention of invasiveness, *Biochim Biophys Acta*, **1198,** 11-26.

Blanpain C and Fuchs E. (2006). Epidermal stem cells of the skin, *Annu Rev Cell Dev Biol*, **22,** 339-73.

Blanpain C, Horsley V and Fuchs E. (2007). Epithelial stem cells: turning over new leaves, *Cell*, **128,** 445-58.

Blauwkamp TA, Chang MV and Cadigan KM. (2008). Novel TCF-binding sites specify transcriptional repression by Wnt signalling, *Embo J*, **27,** 1436-46.

Blewitt RW. (1980). Why does basal cell carcinoma metastasize so rarely?, *Int J Dermatol*, **19,** 144-6.

Bodak N, Queille S, Avril MF, Bouadjar B, Drougard C, Sarasin A and Daya-Grosjean L. (1999). High levels of patched gene mutations in basal-cell carcinomas from patients with xeroderma pigmentosum, *Proc Natl Acad Sci U S A*, **96,** 5117-22.

Bodmer WF, Bailey CJ, Bodmer J, Bussey HJ, Ellis A, Gorman P, Lucibello FC, Murday VA, Rider SH, Scambler P and et al. (1987). Localization of the gene for familial adenomatous polyposis on chromosome 5, *Nature*, **328,** 614-6.

Bohnert A, Hornung J, Mackenzie IC and Fusenig NE. (1986). Epithelial-mesenchymal interactions control basement membrane production and differentiation in cultured and transplanted mouse keratinocytes, *Cell Tissue Res*, **244,** 413-29.

Bolshakov S, Walker CM, Strom SS, Selvan MS, Clayman GL, El-Naggar A, Lippman SM, Kripke ML and Ananthaswamy HN. (2003). p53 mutations in human aggressive and nonaggressive basal and squamous cell carcinomas, *Clin Cancer Res*, **9,** 228-34.

Bonifas JM, Pennypacker S, Chuang PT, McMahon AP, Williams M, Rosenthal A, De Sauvage FJ and Epstein EH, Jr. (2001). Activation of expression of hedgehog target genes in basal cell carcinomas, *J Invest Dermatol*, **116,** 739-42.

Bonnet D and Dick JE. (1997). Human acute myeloid leukemia is organized as a hierarchy that originates from a primitive hematopoietic cell, *Nat Med*, **3,** 730-7.

Booth DR. (1999). The hedgehog signalling pathway and its role in basal cell carcinoma, *Cancer Metastasis Rev*, **18,** 261-84.

Borel F, Lohez OD, Lacroix FB and Margolis RL. (2002). Multiple centrosomes arise from tetraploidy checkpoint failure and mitotic centrosome clusters in p53 and RB pocket protein-compromised cells, *Proc Natl Acad Sci U S A*, **99,** 9819-24.

Borradori L and Sonnenberg A. (1999). Structure and function of hemidesmosomes: more than simple adhesion complexes, *J Invest Dermatol*, **112,** 411-8.

Botchkarev VA, Botchkareva NV, Nakamura M, Huber O, Funa K, Lauster R, Paus R and Gilchrest BA. (2001). Noggin is required for induction of the hair follicle growth phase in postnatal skin, *Faseb J*, **15,** 2205-14.

Botchkarev VA, Botchkareva NV, Roth W, Nakamura M, Chen LH, Herzog W, Lindner G, McMahon JA, Peters C, Lauster R, McMahon AP and Paus R. (1999). Noggin is a mesenchymally derived stimulator of hair-follicle induction, *Nat Cell Biol*, **1,** 158-64.

Bott SR, Arya M, Kirby RS and Williamson M. (2005). p21WAF1/CIP1 gene is inactivated in metastatic prostatic cancer cell lines by promoter methylation, *Prostate Cancer Prostatic Dis*, **8,** 321-6.

Boukamp P, Petrussevska RT, Breitkreutz D, Hornung J, Markham A and Fusenig NE. (1988). Normal keratinization in a spontaneously immortalized aneuploid human keratinocyte cell line, *J Cell Biol*, **106,** 761-71.

Boutros M, Paricio N, Strutt DI and Mlodzik M. (1998). Dishevelled activates JNK and discriminates between JNK pathways in planar polarity and wingless signaling, *Cell*, **94,** 109-18.

Boutwell RK. (1974). The function and mechanism of promoters of carcinogenesis, *CRC Crit Rev Toxicol*, **2,** 419-43.

Boveri T. (2008). Concerning the origin of malignant tumours by Theodor Boveri. Translated and annotated by Henry Harris, *J Cell Sci*, **121 Suppl 1,** 1-84.

Bowles J, Schepers G and Koopman P. (2000). Phylogeny of the SOX family of developmental transcription factors based on sequence and structural indicators, *Dev Biol*, **227,** 239-55.

Boyce ST and Ham RG. (1983). Calcium-regulated differentiation of normal human epidermal keratinocytes in chemically defined clonal culture and serum-free serial culture, *J Invest Dermatol*, **81,** 33s-40s.

Boyer LA, Lee TI, Cole MF, Johnstone SE, Levine SS, Zucker JP, Guenther MG, Kumar RM, Murray HL, Jenner RG, Gifford DK, Melton DA, Jaenisch R and Young RA. (2005). Core transcriptional regulatory circuitry in human embryonic stem cells, *Cell*, **122,** 947-56.

Brabletz T, Jung A, Dag S, Hlubek F and Kirchner T. (1999). beta-catenin regulates the expression of the matrix metalloproteinase-7 in human colorectal cancer, *Am J Pathol*, **155,** 1033-8.

Brakebusch C, Grose R, Quondamatteo F, Ramirez A, Jorcano JL, Pirro A, Svensson M, Herken R, Sasaki T, Timpl R, Werner S and Fassler R. (2000). Skin and hair follicle integrity is crucially dependent on beta 1 integrin expression on keratinocytes, *Embo J*, **19,** 3990-4003.

Brakebusch C, Hirsch E, Potocnik A and Fassler R. (1997). Genetic analysis of beta1 integrin function: confirmed, new and revised roles for a crucial family of cell adhesion molecules, *J Cell Sci*, **110 (Pt 23),** 2895-904.

Brash DE and Haseltine WA. (1982). UV-induced mutation hotspots occur at DNA damage hotspots, *Nature*, **298,** 189-92.

Brash DE and Ponten J. (1998). Skin precancer, *Cancer Surv*, **32,** 69-113.

Brembeck FH, Rosario M and Birchmeier W. (2006). Balancing cell adhesion and Wnt signaling, the key role of beta-catenin, *Curr Opin Genet Dev*, **16,** 51-9.

Brewster R, Mullor JL and Ruiz i Altaba A. (2000). Gli2 functions in FGF signaling during antero-posterior patterning, *Development*, **127,** 4395-405.

Brinkley BR. (2001). Managing the centrosome numbers game: from chaos to stability in cancer cell division, *Trends Cell Biol*, **11,** 18-21.

Brown CI and Perry AE. (2000). Incidence of perineural invasion in histologically aggressive types of basal cell carcinoma, *Am J Dermatopathol*, **22,** 123-5.

Brown JM and Attardi LD. (2005). The role of apoptosis in cancer development and treatment response, *Nat Rev Cancer*, **5,** 231-7.

Brown K, Strathdee D, Bryson S, Lambie W and Balmain A. (1998). The malignant capacity of skin tumours induced by expression of a mutant H-ras transgene depends on the cell type targeted, *Curr Biol*, **8,** 516-24.

Brown KW and Parkinson EK. (1983). Glycoproteins and glycosaminoglycans of cultured normal human epidermal keratinocytes, *J Cell Sci*, **61,** 325-38.

Brugarolas J, Chandrasekaran C, Gordon JI, Beach D, Jacks T and Hannon GJ. (1995). Radiation-induced cell cycle arrest compromised by p21 deficiency, *Nature*, **377,** 552-7.

Buchner T, Hiddemann W, Wormann B, Kleinemeier B, Schumann J, Gohde W, Ritter J, Muller KM, von Bassewitz DB, Roessner A and et al. (1985). Differential pattern of DNA-aneuploidy in human malignancies, *Pathol Res Pract*, **179,** 310-7.

Bull JJ, Muller-Rover S, Patel SV, Chronnell CM, McKay IA and Philpott MP. (2001). Contrasting localization of c-Myc with other Myc superfamily transcription factors in the human hair follicle and during the hair growth cycle, *J Invest Dermatol*, **116,** 617-22.

Bunz F, Dutriaux A, Lengauer C, Waldman T, Zhou S, Brown JP, Sedivy JM, Kinzler KW and Vogelstein B. (1998). Requirement for p53 and p21 to sustain G2 arrest after DNA damage, *Science*, **282,** 1497-501.

Bunz F, Fauth C, Speicher MR, Dutriaux A, Sedivy JM, Kinzler KW, Vogelstein B and Lengauer C. (2002). Targeted inactivation of p53 in human cells does not result in aneuploidy, *Cancer Res*, **62,** 1129-33.

Buttitta L, Mo R, Hui CC and Fan CM. (2003). Interplays of Gli2 and Gli3 and their requirement in mediating Shh-dependent sclerotome induction, *Development*, **130,** 6233-43.

Cabrera CV, Alonso MC, Johnston P, Phillips RG and Lawrence PA. (1987). Phenocopies induced with antisense RNA identify the wingless gene, *Cell*, **50,** 659-63.

Cadigan KM. (2008). Wnt-beta-catenin signaling, *Curr Biol*, **18,** R943-7.

Cadigan KM and Nusse R. (1997). Wnt signaling: a common theme in animal development, *Genes Dev*, **11,** 3286-305.

Cahill DP, Kinzler KW, Vogelstein B and Lengauer C. (1999). Genetic instability and darwinian selection in tumours, *Trends Cell Biol*, **9,** M57-60.

Cairns J. (1975). Mutation selection and the natural history of cancer, *Nature*, **255,** 197-200.

Caldwell CM, Green RA and Kaplan KB. (2007). APC mutations lead to cytokinetic failures in vitro and tetraploid genotypes in Min mice, *J Cell Biol*, **178,** 1109-20.

Callahan CA and Oro AE. (2001). Monstrous attempts at adnexogenesis: regulating hair follicle progenitors through Sonic hedgehog signaling, *Curr Opin Genet Dev*, **11,** 541-6.

Candi E, Schmidt R and Melino G. (2005). The cornified envelope: a model of cell death in the skin, *Nat Rev Mol Cell Biol*, **6,** 328-40.

Cano A, Perez-Moreno MA, Rodrigo I, Locascio A, Blanco MJ, del Barrio MG, Portillo F and Nieto MA. (2000). The transcription factor snail controls epithelial-mesenchymal transitions by repressing E-cadherin expression, *Nat Cell Biol*, **2,** 76-83.

Cardoso J, Molenaar L, de Menezes RX, van Leerdam M, Rosenberg C, Moslein G, Sampson J, Morreau H, Boer JM and Fodde R. (2006). Chromosomal instability in MYH- and APC-mutant adenomatous polyps, *Cancer Res*, **66,** 2514-9.

Carless MA, Ashton KJ and Griffiths LR. (2006). *Cytogenetics of Basal Cell Carcinoma and Squamous Cell Carcinomas. In:Jorg Reichrath (ed.).Molecular Mechanisms of Basal Cell and Squamous Cell Carcinomas, pp 49-57.United States: Landes Bioscience*.

Carmon KS and Loose DS. (2008). Secreted frizzled-related protein 4 regulates two Wnt7a signaling pathways and inhibits proliferation in endometrial cancer cells, *Mol Cancer Res*, **6,** 1017-28.

Carpenter D, Stone DM, Brush J, Ryan A, Armanini M, Frantz G, Rosenthal A and de Sauvage FJ. (1998). Characterization of two patched receptors for the vertebrate hedgehog protein family, *Proc Natl Acad Sci U S A*, **95,** 13630-4.

Carroll JM, Romero MR and Watt FM. (1995). Suprabasal integrin expression in the epidermis of transgenic mice results in developmental defects and a phenotype resembling psoriasis, *Cell*, **83,** 957-68.

Carter BZ, Mak DH, Shi Y, Schober WD, Wang RY, Konopleva M, Koller E, Dean NM and Andreeff M. (2006). Regulation and targeting of Eg5, a mitotic motor protein in blast crisis CML: overcoming imatinib resistance, *Cell Cycle*, **5,** 2223-9.

Carter WG, Wayner EA, Bouchard TS and Kaur P. (1990). The role of integrins alpha 2 beta 1 and alpha 3 beta 1 in cell-cell and cell-substrate adhesion of human epidermal cells, *J Cell Biol*, **110,** 1387-404.

Castedo M, Coquelle A, Vivet S, Vitale I, Kauffmann A, Dessen P, Pequignot MO, Casares N, Valent A, Mouhamad S, Schmitt E, Modjtahedi N, Vainchenker W, Zitvogel L, Lazar V, Garrido C and Kroemer G. (2006). Apoptosis regulation in tetraploid cancer cells, *Embo J*, **25,** 2584-95.

Castillo A, Morse HC, 3rd, Godfrey VL, Naeem R and Justice MJ. (2007). Overexpression of Eg5 causes genomic instability and tumor formation in mice, *Cancer Res*, **67,** 10138-47.

Cavallaro U and Christofori G. (2004). Cell adhesion and signalling by cadherins and Ig-CAMs in cancer, *Nat Rev Cancer*, **4,** 118-32.

Cavallo RA, Cox RT, Moline MM, Roose J, Polevoy GA, Clevers H, Peifer M and Bejsovec A. (1998). Drosophila Tcf and Groucho interact to repress Wingless signalling activity, *Nature*, **395,** 604-8.

Cereijido M and Anderson J. (2001). *Tight junctions. 2nd ed. CRC press LLC.*

Chalfie M, Tu Y, Euskirchen G, Ward WW and Prasher DC. (1994). Green fluorescent protein as a marker for gene expression, *Science*, **263,** 802-5.

Chan EF, Gat U, McNiff JM and Fuchs E. (1999a). A common human skin tumour is caused by activating mutations in beta-catenin, *Nat Genet*, **21,** 410-3.

Chan TA, Hermeking H, Lengauer C, Kinzler KW and Vogelstein B. (1999b). 14-3-3Sigma is required to prevent mitotic catastrophe after DNA damage, *Nature*, **401,** 616-20.

Chang YW, Jakobi R, McGinty A, Foschi M, Dunn MJ and Sorokin A. (2000). Cyclooxygenase 2 promotes cell survival by stimulation of dynein light chain expression and inhibition of neuronal nitric oxide synthase activity, *Mol Cell Biol*, **20,** 8571-9.

Chehab NH, Malikzay A, Stavridi ES and Halazonetis TD. (1999). Phosphorylation of Ser-20 mediates stabilization of human p53 in response to DNA damage, *Proc Natl Acad Sci U S A*, **96,** 13777-82.

Chen CH, von Kessler DP, Park W, Wang B, Ma Y and Beachy PA. (1999a). Nuclear trafficking of Cubitus interruptus in the transcriptional regulation of Hedgehog target gene expression, *Cell*, **98,** 305-16.

Chen G, Fernandez J, Mische S and Courey AJ. (1999b). A functional interaction between the histone deacetylase Rpd3 and the corepressor groucho in Drosophila development, *Genes Dev*, **13,** 2218-30.

Chen J, Willingham T, Shuford M, Bruce D, Rushing E, Smith Y and Nisen PD. (1996). Effects of ectopic overexpression of p21(WAF1/CIP1) on aneuploidy and the malignant phenotype of human brain tumor cells, *Oncogene*, **13,** 1395-403.

Chen JG, Yang CP, Cammer M and Horwitz SB. (2003). Gene expression and mitotic exit induced by microtubule-stabilizing drugs, *Cancer Res*, **63,** 7891-9.

Chen MH, Gao N, Kawakami T and Chuang PT. (2005). Mice deficient in the fused homolog do not exhibit phenotypes indicative of perturbed hedgehog signaling during embryonic development, *Mol Cell Biol*, **25,** 7042-53.

Chen Y, Shi L, Zhang L, Li R, Liang J, Yu W, Sun L, Yang X, Wang Y, Zhang Y and Shang Y. (2008). The molecular mechanism governing the oncogenic potential of SOX2 in breast cancer, *J Biol Chem*, **283,** 17969-78.

Chen Y and Struhl G. (1996). Dual roles for patched in sequestering and transducing Hedgehog, *Cell*, **87,** 553-63.

Cheng SY and Bishop JM. (2002). Suppressor of Fused represses Gli-mediated transcription by recruiting the SAP18-mSin3 corepressor complex, *Proc Natl Acad Sci U S A*, **99,** 5442-7.

Cheng T, Xu CY, Wang YB, Chen M, Wu T, Zhang J and Xia NS. (2004). A rapid and efficient method to express target genes in mammalian cells by baculovirus, *World J Gastroenterol*, **10,** 1612-8.

Chi TY, Chen GG, Ho LK and Lai PB. (2005). Establishment of a doxycycline-regulated cell line with inducible, doubly-stable expression of the wild-type p53 gene from p53-deleted hepatocellular carcinoma cells, *Cancer Cell Int*, **5,** 27.

Chiang C, Litingtung Y, Lee E, Young KE, Corden JL, Westphal H and Beachy PA. (1996). Cyclopia and defective axial patterning in mice lacking Sonic hedgehog gene function, *Nature*, **383,** 407-13.

Chiang C, Swan RZ, Grachtchouk M, Bolinger M, Litingtung Y, Robertson EK, Cooper MK, Gaffield W, Westphal H, Beachy PA and Dlugosz AA. (1999). Essential role for Sonic hedgehog during hair follicle morphogenesis, *Dev Biol*, **205,** 1-9.

Christenson LJ, Borrowman TA, Vachon CM, Tollefson MM, Otley CC, Weaver AL and Roenigk RK. (2005). Incidence of basal cell and squamous cell carcinomas in a population younger than 40 years, *Jama*, **294,** 681-90.

Chuang PT and McMahon AP. (1999). Vertebrate Hedgehog signalling modulated by induction of a Hedgehog-binding protein, *Nature*, **397,** 617-21.

Clarke MF, Dick JE, Dirks PB, Eaves CJ, Jamieson CH, Jones DL, Visvader J, Weissman IL and Wahl GM. (2006). Cancer stem cells--perspectives on current status and future directions: AACR Workshop on cancer stem cells, *Cancer Res*, **66,** 9339-44.

Claudinot S, Nicolas M, Oshima H, Rochat A and Barrandon Y. (2005). Long-term renewal of hair follicles from clonogenic multipotent stem cells, *Proc Natl Acad Sci U S A*, **102,** 14677-82.

Clausen OP, Kirkhus B, Thorud E, Schjolberg A, Moen E and Cromarty A. (1986). Evidence of mouse epidermal subpopulations with different cell cycle times, *J Invest Dermatol*, **86,** 266-70.

Clausen OP and Potten CS. (1990). Heterogeneity of keratinocytes in the epidermal basal cell layer, *J Cutan Pathol*, **17,** 129-43.

Clayton E, Doupe DP, Klein AM, Winton DJ, Simons BD and Jones PH. (2007). A single type of progenitor cell maintains normal epidermis, *Nature*, **446,** 185-9.

Clement V, Sanchez P, de Tribolet N, Radovanovic I and Ruiz i Altaba A. (2007). HEDGEHOG-GLI1 signaling regulates human glioma growth, cancer stem cell self-renewal, and tumorigenicity, *Curr Biol*, **17,** 165-72.

Clevers H. (2006). Wnt/beta-catenin signaling in development and disease, *Cell*, **127,** 469-80.
Cohen MM, Jr. (2003). The hedgehog signaling network, *Am J Med Genet A*, **123,** 5-28.
Conboy MJ, Karasov AO and Rando TA. (2007). High incidence of non-random template strand segregation and asymmetric fate determination in dividing stem cells and their progeny, *PLoS Biol*, **5,** e102.
Contard P, Bartel RL, Jacobs L, 2nd, Perlish JS, MacDonald ED, 2nd, Handler L, Cone D and Fleischmajer R. (1993). Culturing keratinocytes and fibroblasts in a three-dimensional mesh results in epidermal differentiation and formation of a basal lamina-anchoring zone, *J Invest Dermatol*, **100,** 35-9.
Cooper M and Pinkus H. (1977). Intrauterine transplantation of rat basal cell carcinoma as a model for reconversion of malignant to benign growth, *Cancer Res*, **37,** 2544-52.
Cormier P, Pyronnet S, Salaun P, Mulner-Lorillon O and Sonenberg N. (2003). Cap-dependent translation and control of the cell cycle, *Prog Cell Cycle Res*, **5,** 469-75.
Cory S and Adams JM. (2002). The Bcl2 family: regulators of the cellular life-or-death switch, *Nat Rev Cancer*, **2,** 647-56.
Cotsarelis G, Sun TT and Lavker RM. (1990). Label-retaining cells reside in the bulge area of pilosebaceous unit: implications for follicular stem cells, hair cycle, and skin carcinogenesis, *Cell*, **61,** 1329-37.
Coulombe PA, Kopan R and Fuchs E. (1989). Expression of keratin K14 in the epidermis and hair follicle: insights into complex programs of differentiation, *J Cell Biol*, **109,** 2295-312.
Couve-Privat S, Bouadjar B, Avril MF, Sarasin A and Daya-Grosjean L. (2002). Significantly high levels of ultraviolet-specific mutations in the smoothened gene in basal cell carcinomas from DNA repair-deficient xeroderma pigmentosum patients, *Cancer Res*, **62,** 7186-9.
Couve-Privat S, Le Bret M, Traiffort E, Queille S, Coulombe J, Bouadjar B, Avril MF, Ruat M, Sarasin A and Daya-Grosjean L. (2004). Functional analysis of novel sonic hedgehog gene mutations identified in basal cell carcinomas from xeroderma pigmentosum patients, *Cancer Res*, **64,** 3559-65.
Cowan JM. (1992). Cytogenetics in head and neck cancer, *Otolaryngol Clin North Am*, **25,** 1073-87.
Cowell JK. (1982). Double minutes and homogeneously staining regions: gene amplification in mammalian cells, *Annu Rev Genet*, **16,** 21-59.
Cowell JK and Wigley CB. (1980). Changes in DNA content during in vitro transformation of mouse salivary gland epithelium, *J Natl Cancer Inst*, **64,** 1443-9.
Cox LS and Lane DP. (1995). Tumour suppressors, kinases and clamps: how p53 regulates the cell cycle in response to DNA damage, *Bioessays*, **17,** 501-8.
Crabtree GR and Olson EN. (2002). NFAT signaling: choreographing the social lives of cells, *Cell*, **109 Suppl,** S67-79.
Cross SM, Sanchez CA, Morgan CA, Schimke MK, Ramel S, Idzerda RL, Raskind WH and Reid BJ. (1995). A p53-dependent mouse spindle checkpoint, *Science*, **267,** 1353-6.
Crowson AN. (2006). Basal cell carcinoma: biology, morphology and clinical implications, *Mod Pathol*, **19 Suppl 2,** S127-47.

Cui C, Elsam T, Tian Q, Seykora JT, Grachtchouk M, Dlugosz A and Tseng H. (2004). Gli proteins up-regulate the expression of basonuclin in Basal cell carcinoma, *Cancer Res*, **64,** 5651-8.

Curran S and Murray GI. (2000). Matrix metalloproteinases: molecular aspects of their roles in tumour invasion and metastasis, *Eur J Cancer*, **36,** 1621-30.

Cuzin F and Jacob F. (1965). [Existence in Escherichia coli of a segregation genetic unit formed from different replicons], *C R Acad Sci Hebd Seances Acad Sci D*, **260,** 5411-4.

D'Assoro AB, Lingle WL and Salisbury JL. (2002). Centrosome amplification and the development of cancer, *Oncogene*, **21,** 6146-53.

D'Errico M, Calcagnile A, Canzona F, Didona B, Posteraro P, Cavalieri R, Corona R, Vorechovsky I, Nardo T, Stefanini M and Dogliotti E. (2000). UV mutation signature in tumor suppressor genes involved in skin carcinogenesis in xeroderma pigmentosum patients, *Oncogene*, **19,** 463-7.

Dahmane N, Lee J, Robins P, Heller P and Ruiz i Altaba A. (1997). Activation of the transcription factor Gli1 and the Sonic hedgehog signalling pathway in skin tumours, *Nature*, **389,** 876-81.

Dahmane N, Sanchez P, Gitton Y, Palma V, Sun T, Beyna M, Weiner H and Ruiz i Altaba A. (2001). The Sonic Hedgehog-Gli pathway regulates dorsal brain growth and tumorigenesis, *Development*, **128,** 5201-12.

Dai P, Akimaru H, Tanaka Y, Maekawa T, Nakafuku M and Ishii S. (1999). Sonic Hedgehog-induced activation of the Gli1 promoter is mediated by GLI3, *J Biol Chem*, **274,** 8143-52.

Dale TC. (1998). Signal transduction by the Wnt family of ligands, *Biochem J*, **329 (Pt 2),** 209-23.

Daniels DL and Weis WI. (2005). Beta-catenin directly displaces Groucho/TLE repressors from Tcf/Lef in Wnt-mediated transcription activation, *Nat Struct Mol Biol*, **12,** 364-71.

Daniels MJ, Wang Y, Lee M and Venkitaraman AR. (2004). Abnormal cytokinesis in cells deficient in the breast cancer susceptibility protein BRCA2, *Science*, **306,** 876-9.

Darzynkiewicz Z, Evenson D, Staiano-Coico L, Sharpless T and Melamed MR. (1979). Relationship between RNA content and progression of lymphocytes through S phase of cell cycle, *Proc Natl Acad Sci U S A*, **76,** 358-62.

Darzynkiewicz Z, Traganos F, Sharpless TK and Melamed MR. (1977). Cell cycle-related changes in nuclear chromatin of stimulated lymphocytes as measured by flow cytometry, *Cancer Res*, **37,** 4635-40.

Dasgupta P, Kinkade R, Joshi B, Decook C, Haura E and Chellappan S. (2006). Nicotine inhibits apoptosis induced by chemotherapeutic drugs by up-regulating XIAP and survivin, *Proc Natl Acad Sci U S A*, **103,** 6332-7.

DasGupta R and Fuchs E. (1999). Multiple roles for activated LEF/TCF transcription complexes during hair follicle development and differentiation, *Development*, **126,** 4557-68.

Davis MA, Ireton RC and Reynolds AB. (2003). A core function for p120-catenin in cadherin turnover, *J Cell Biol*, **163,** 525-34.

Davis MG and Huang ES. (1988). Transfer and expression of plasmids containing human cytomegalovirus immediate-early gene 1 promoter-enhancer sequences in eukaryotic and prokaryotic cells, *Biotechnol Appl Biochem*, **10,** 6-12.

Daya-Grosjean L and Couve-Privat S. (2005). Sonic hedgehog signaling in basal cell carcinomas, *Cancer Lett*, **225,** 181-92.

de Gruijl FR, van Kranen HJ and Mullenders LH. (2001). UV-induced DNA damage, repair, mutations and oncogenic pathways in skin cancer, *J Photochem Photobiol B*, **63,** 19-27.

De Strooper B, Van der Schueren B, Jaspers M, Saison M, Spaepen M, Van Leuven F, Van den Berghe H and Cassiman JJ. (1989). Distribution of the beta 1 subgroup of the integrins in human cells and tissues, *J Histochem Cytochem*, **37,** 299-307.

de Vries E, Louwman M, Bastiaens M, de Gruijl F and Coebergh JW. (2004). Rapid and continuous increases in incidence rates of basal cell carcinoma in the southeast Netherlands since 1973, *J Invest Dermatol*, **123,** 634-8.

Delehedde M, Cho SH, Sarkiss M, Brisbay S, Davies M, El-Naggar AK and McDonnell TJ. (1999). Altered expression of bcl-2 family member proteins in nonmelanoma skin cancer, *Cancer*, **85,** 1514-22.

Delfino S, Innocenzi D, Di Lorenzo G, Scalvenzi M, Montesarchio V, Feroce F, Baldi A and Persichetti P. (2006). An increase in basal cell carcinoma among the young: an epidemiological study in a middle-south Italian population, *Anticancer Res*, **26,** 4979-83.

Dellambra E, Golisano O, Bondanza S, Siviero E, Lacal P, Molinari M, D'Atri S and De Luca M. (2000). Downregulation of 14-3-3sigma prevents clonal evolution and leads to immortalization of primary human keratinocytes, *J Cell Biol*, **149,** 1117-30.

Demirkan NC, Colakoglu N and Duzcan E. (2000). Value of p53 protein in biological behavior of basal cell carcinoma and in normal epithelia adjacent to carcinomas, *Pathol Oncol Res*, **6,** 272-4.

Denef N, Neubuser D, Perez L and Cohen SM. (2000). Hedgehog induces opposite changes in turnover and subcellular localization of patched and smoothened, *Cell*, **102,** 521-31.

Deng H, Lin Q and Khavari PA. (1997). Sustainable cutaneous gene delivery, *Nat Biotechnol*, **15,** 1388-91.

DePinho RA, Schreiber-Agus N and Alt FW. (1991). myc family oncogenes in the development of normal and neoplastic cells, *Adv Cancer Res*, **57,** 1-46.

Dhar S, Squire JA, Hande MP, Wellinger RJ and Pandita TK. (2000). Inactivation of 14-3-3sigma influences telomere behavior and ionizing radiation-induced chromosomal instability, *Mol Cell Biol*, **20,** 7764-72.

Di Croce L and Pelicci PG. (2003). Tumour-associated hypermethylation: silencing E-cadherin expression enhances invasion and metastasis, *Eur J Cancer*, **39,** 413-4.

Di Cunto F, Topley G, Calautti E, Hsiao J, Ong L, Seth PK and Dotto GP. (1998). Inhibitory function of p21Cip1/WAF1 in differentiation of primary mouse keratinocytes independent of cell cycle control, *Science*, **280,** 1069-72.

Di Micco R, Fumagalli M, Cicalese A, Piccinin S, Gasparini P, Luise C, Schurra C, Garre M, Nuciforo PG, Bensimon A, Maestro R, Pelicci PG and d'Adda di Fagagna F. (2006). Oncogene-induced senescence is a DNA damage response triggered by DNA hyper-replication, *Nature*, **444,** 638-42.

Dicker T, Siller G and Saunders N. (2002). Molecular and cellular biology of basal cell carcinoma, *Australas J Dermatol*, **43,** 241-6.

Dickson MA, Hahn WC, Ino Y, Ronfard V, Wu JY, Weinberg RA, Louis DN, Li FP and Rheinwald JG. (2000). Human keratinocytes that express hTERT and also bypass a p16(INK4a)-enforced mechanism that limits life span become immortal yet retain normal growth and differentiation characteristics, *Mol Cell Biol*, **20,** 1436-47.

Diepgen TL and Mahler V. (2002). The epidemiology of skin cancer, *Br J Dermatol*, **146 Suppl 61,** 1-6.

Ding Q, Fukami S, Meng X, Nishizaki Y, Zhang X, Sasaki H, Dlugosz A, Nakafuku M and Hui C. (1999). Mouse suppressor of fused is a negative regulator of sonic hedgehog signaling and alters the subcellular distribution of Gli1, *Curr Biol*, **9,** 1119-22.

Ding Q, Motoyama J, Gasca S, Mo R, Sasaki H, Rossant J and Hui CC. (1998). Diminished Sonic hedgehog signaling and lack of floor plate differentiation in Gli2 mutant mice, *Development*, **125,** 2533-43.

DiPersio CM, van der Neut R, Georges-Labouesse E, Kreidberg JA, Sonnenberg A and Hynes RO. (2000). alpha3beta1 and alpha6beta4 integrin receptors for laminin-5 are not essential for epidermal morphogenesis and homeostasis during skin development, *J Cell Sci*, **113 (Pt 17),** 3051-62.

Doak SH, Jenkins GJ, Parry EM, Griffiths AP, Baxter JN and Parry JM. (2004). Differential expression of the MAD2, BUB1 and HSP27 genes in Barrett's oesophagus-their association with aneuploidy and neoplastic progression, *Mutat Res*, **547,** 133-44.

Dollar G and Sokol S. (2007). *Wnt signaling and the establishment of cell polarity. In: Sergei Y Sokol (ed.). Wnt signaling in embryonic development (Advances in Developmental Biology)*. Elsevier.

Dong C, Wilhelm D and Koopman P. (2004). Sox genes and cancer, *Cytogenet Genome Res*, **105,** 442-7.

Dooley TP, Mattern VL, Moore CM, Porter PA, Robinson ES and VandeBerg JL. (1993). Cell lines derived from ultraviolet radiation-induced benign melanocytic nevi in Monodelphis domestica exhibit cytogenetic aneuploidy, *Cancer Genet Cytogenet*, **71,** 55-66.

Dotto GP. (2000). p21(WAF1/Cip1): more than a break to the cell cycle?, *Biochim Biophys Acta*, **1471,** M43-56.

Dover R and Potten CS. (1983). Cell cycle kinetics of cultured human epidermal keratinocytes, *J Invest Dermatol*, **80,** 423-9.

Dowling J, Yu QC and Fuchs E. (1996). Beta4 integrin is required for hemidesmosome formation, cell adhesion and cell survival, *J Cell Biol*, **134,** 559-72.

Downer CS, Watt FM and Speight PM. (1993). Loss of alpha 6 and beta 4 integrin subunits coincides with loss of basement membrane components in oral squamous cell carcinomas, *J Pathol*, **171,** 183-90.

Doxsey S. (2001). Re-evaluating centrosome function, *Nat Rev Mol Cell Biol*, **2,** 688-98.

Duelli D and Lazebnik Y. (2007). Cell-to-cell fusion as a link between viruses and cancer, *Nat Rev Cancer*, **7,** 968-76.

Duelli DM, Padilla-Nash HM, Berman D, Murphy KM, Ried T and Lazebnik Y. (2007). A virus causes cancer by inducing massive chromosomal instability through cell fusion, *Curr Biol*, **17,** 431-7.

Duensing A, Ghanem L, Steinman RA, Liu Y and Duensing S. (2006). p21(Waf1/Cip1) deficiency stimulates centriole overduplication, *Cell Cycle*, **5,** 2899-902.

Duensing S, Duensing A, Crum CP and Munger K. (2001). Human papillomavirus type 16 E7 oncoprotein-induced abnormal centrosome synthesis is an early event in the evolving malignant phenotype, *Cancer Res*, **61,** 2356-60.

Duensing S, Lee LY, Duensing A, Basile J, Piboonniyom S, Gonzalez S, Crum CP and Munger K. (2000). The human papillomavirus type 16 E6 and E7 oncoproteins cooperate to induce mitotic defects and genomic instability by uncoupling

centrosome duplication from the cell division cycle, *Proc Natl Acad Sci U S A*, **97,** 10002-7.
Duensing S and Munger K. (2001). Centrosome abnormalities, genomic instability and carcinogenic progression, *Biochim Biophys Acta*, **1471,** M81-8.
Duensing S and Munger K. (2002). The human papillomavirus type 16 E6 and E7 oncoproteins independently induce numerical and structural chromosome instability, *Cancer Res*, **62,** 7075-82.
Duensing S and Munger K. (2003). Centrosomes, genomic instability, and cervical carcinogenesis, *Crit Rev Eukaryot Gene Expr*, **13,** 9-23.
Duensing S and Munger K. (2004). Mechanisms of genomic instability in human cancer: insights from studies with human papillomavirus oncoproteins, *Int J Cancer*, **109,** 157-62.
Duesberg P and Rasnick D. (2000). Aneuploidy, the somatic mutation that makes cancer a species of its own, *Cell Motil Cytoskeleton*, **47,** 81-107.
Duesberg P, Rausch C, Rasnick D and Hehlmann R. (1998). Genetic instability of cancer cells is proportional to their degree of aneuploidy, *Proc Natl Acad Sci U S A*, **95,** 13692-7.
Duman-Scheel M, Weng L, Xin S and Du W. (2002). Hedgehog regulates cell growth and proliferation by inducing Cyclin D and Cyclin E, *Nature*, **417,** 299-304.
Echelard Y, Epstein DJ, St-Jacques B, Shen L, Mohler J, McMahon JA and McMahon AP. (1993). Sonic hedgehog, a member of a family of putative signaling molecules, is implicated in the regulation of CNS polarity, *Cell*, **75,** 1417-30.
Ehrhart JC, Gosselet FP, Culerrier RM and Sarasin A. (2003). UVB-induced mutations in human key gatekeeper genes governing signalling pathways and consequences for skin tumourigenesis, *Photochem Photobiol Sci*, **2,** 825-34.
Eichberger T, Regl G, Ikram MS, Neill GW, Philpott MP, Aberger F and Frischauf AM. (2004). FOXE1, a new transcriptional target of GLI2 is expressed in human epidermis and basal cell carcinoma, *J Invest Dermatol*, **122,** 1180-7.
Eichberger T, Sander V, Schnidar H, Regl G, Kasper M, Schmid C, Plamberger S, Kaser A, Aberger F and Frischauf AM. (2006). Overlapping and distinct transcriptional regulator properties of the GLI1 and GLI2 oncogenes, *Genomics*, **87,** 616-32.
Eichenmuller M, Gruner I, Hagl B, Haberle B, Muller-Hocker J, von Schweinitz D and Kappler R. (2009). Blocking the hedgehog pathway inhibits hepatoblastoma growth, *Hepatology*, **49,** 482-90.
Eisinger M, Lee JS, Hefton JM, Darzynkiewicz Z, Chiao JW and de Harven E. (1979). Human epidermal cell cultures: growth and differentiation in the absence of differentiation in the absence of dermal components or medium supplements, *Proc Natl Acad Sci U S A*, **76,** 5340-4.
El-Bahrawy M, El-Masry N, Alison M, Poulsom R and Fallowfield M. (2003). Expression of beta-catenin in basal cell carcinoma, *Br J Dermatol*, **148,** 964-70.
el-Deiry WS, Harper JW, O'Connor PM, Velculescu VE, Canman CE, Jackman J, Pietenpol JA, Burrell M, Hill DE, Wang Y and et al. (1994). WAF1/CIP1 is induced in p53-mediated G1 arrest and apoptosis, *Cancer Res*, **54,** 1169-74.
Elledge SJ. (1996). Cell cycle checkpoints: preventing an identity crisis, *Science*, **274,** 1664-72.
Ellis T, Smyth I, Riley E, Bowles J, Adolphe C, Rothnagel JA, Wicking C and Wainwright BJ. (2003). Overexpression of Sonic Hedgehog suppresses embryonic hair follicle morphogenesis, *Dev Biol*, **263,** 203-15.

Epstein EH. (2008). Basal cell carcinomas: attack of the hedgehog, *Nat Rev Cancer*, **8,** 743-54.
Erb P, Ji J, Kump E, Mielgo A and Wernli M. (2008). Apoptosis and pathogenesis of melanoma and nonmelanoma skin cancer, *Adv Exp Med Biol*, **624,** 283-95.
Erb P, Ji J, Wernli M, Kump E, Glaser A and Buchner SA. (2005). Role of apoptosis in basal cell and squamous cell carcinoma formation, *Immunol Lett*, **100,** 68-72.
Fan H and Khavari PA. (1999). Sonic hedgehog opposes epithelial cell cycle arrest, *J Cell Biol*, **147,** 71-6.
Fan H, Oro AE, Scott MP and Khavari PA. (1997). Induction of basal cell carcinoma features in transgenic human skin expressing Sonic Hedgehog, *Nat Med*, **3,** 788-92.
Fantes J, Ragge NK, Lynch SA, McGill NI, Collin JR, Howard-Peebles PN, Hayward C, Vivian AJ, Williamson K, van Heyningen V and FitzPatrick DR. (2003). Mutations in SOX2 cause anophthalmia, *Nat Genet*, **33,** 461-3.
Ferguson AT, Evron E, Umbricht CB, Pandita TK, Chan TA, Hermeking H, Marks JR, Lambers AR, Futreal PA, Stampfer MR and Sukumar S. (2000). High frequency of hypermethylation at the 14-3-3 sigma locus leads to gene silencing in breast cancer, *Proc Natl Acad Sci U S A*, **97,** 6049-54.
Fields RD and Lancaster MV. (1993). Dual-attribute continuous monitoring of cell proliferation/cytotoxicity, *Am Biotechnol Lab*, **11,** 48-50.
Finch PW, He X, Kelley MJ, Uren A, Schaudies RP, Popescu NC, Rudikoff S, Aaronson SA, Varmus HE and Rubin JS. (1997). Purification and molecular cloning of a secreted, Frizzled-related antagonist of Wnt action, *Proc Natl Acad Sci U S A*, **94,** 6770-5.
Flaxman BA. (1972). Growth in vitro and induction of differentiation in cells of basal cell cancer, *Cancer Res*, **32,** 462-9.
Flaxman BA and Van Scott EJ. (1968). Keratinization in vitro of cells from a basal cell carcinoma, *J Natl Cancer Inst*, **40,** 411-22.
Fodde R, Smits R and Clevers H. (2001). APC, signal transduction and genetic instability in colorectal cancer, *Nat Rev Cancer*, **1,** 55-67.
Fong H, Hohenstein KA and Donovan PJ. (2008). Regulation of self-renewal and pluripotency by Sox2 in human embryonic stem cells, *Stem Cells*, **26,** 1931-8.
Fortier-Beaulieu M, Laquerriere A, Thomine E, Lauret P and Hemet J. (1994). DNA flow-cytometric analysis of basal cell carcinomas and its relevance to their morphological differentiation: a retrospective study, *Dermatology*, **188,** 94-9.
Fortunel NO, Hatzfeld JA, Rosemary PA, Ferraris C, Monier MN, Haydont V, Longuet J, Brethon B, Lim B, Castiel I, Schmidt R and Hatzfeld A. (2003). Long-term expansion of human functional epidermal precursor cells: promotion of extensive amplification by low TGF-beta1 concentrations, *J Cell Sci*, **116,** 4043-52.
Freinkel RK and Woodley DT. (2001). *Biology of the skin*. Parthenon publishing group.
Frentz G and Moller U. (1983). Clonal heterogeneity in curetted human epidermal cancers and precancers analysed by flow cytometry and compared with histology, *Br J Dermatol*, **109,** 173-81.
Frentz G, Moller U and Larsen JK. (1985). DNA flow cytometry of human epidermal tumours. Intra- and intertumour variability in ploidy and proliferative characteristics, *Virchows Arch B Cell Pathol Incl Mol Pathol*, **48,** 175-83.
Fuchs E. (1990). Epidermal differentiation: the bare essentials, *J Cell Biol*, **111,** 2807-14.

Fuchs E. (1993). Epidermal differentiation and keratin gene expression, *J Cell Sci Suppl*, **17,** 197-208.
Fuchs E. (2008). Skin stem cells: rising to the surface, *J Cell Biol*, **180,** 273-84.
Fuerer C, Nusse R and Ten Berge D. (2008). Wnt signalling in development and disease. Max Delbruck Center for Molecular Medicine meeting on Wnt signaling in Development and Disease, *EMBO Rep*, **9,** 134-8.
Fujita Y, Krause G, Scheffner M, Zechner D, Leddy HE, Behrens J, Sommer T and Birchmeier W. (2002). Hakai, a c-Cbl-like protein, ubiquitinates and induces endocytosis of the E-cadherin complex, *Nat Cell Biol*, **4,** 222-31.
Fujiwara T, Bandi M, Nitta M, Ivanova EV, Bronson RT and Pellman D. (2005). Cytokinesis failure generating tetraploids promotes tumorigenesis in p53-null cells, *Nature*, **437,** 1043-7.
Fukasawa K. (2005). Centrosome amplification, chromosome instability and cancer development, *Cancer Lett*, **230,** 6-19.
Fukasawa K. (2007). Oncogenes and tumour suppressors take on centrosomes, *Nat Rev Cancer*, **7,** 911-24.
Fukasawa K, Choi T, Kuriyama R, Rulong S and Vande Woude GF. (1996). Abnormal centrosome amplification in the absence of p53, *Science*, **271,** 1744-7.
Fukumoto T, Watanabe-Fukunaga R, Fujisawa K, Nagata S and Fukunaga R. (2001). The fused protein kinase regulates Hedgehog-stimulated transcriptional activation in Drosophila Schneider 2 cells, *J Biol Chem*, **276,** 38441-8.
Fuller LC, Allen MH, Montesu M, Barker JN and Macdonald DM. (1996). Expression of E-cadherin in human epidermal non-melanoma cutaneous tumours, *Br J Dermatol*, **134,** 28-32.
Futreal PA, Coin L, Marshall M, Down T, Hubbard T, Wooster R, Rahman N and Stratton MR. (2004). A census of human cancer genes, *Nat Rev Cancer*, **4,** 177-83.
Gafter-Gvili A, Sredni B, Gal R, Gafter U and Kalechman Y. (2003). Cyclosporin A-induced hair growth in mice is associated with inhibition of calcineurin-dependent activation of NFAT in follicular keratinocytes, *Am J Physiol Cell Physiol*, **284,** C1593-603.
Gailani MR and Bale AE. (1997). Developmental genes and cancer: role of patched in basal cell carcinoma of the skin, *J Natl Cancer Inst*, **89,** 1103-9.
Gailani MR, Bale SJ, Leffell DJ, DiGiovanna JJ, Peck GL, Poliak S, Drum MA, Pastakia B, McBride OW, Kase R and et al. (1992). Developmental defects in Gorlin syndrome related to a putative tumor suppressor gene on chromosome 9, *Cell*, **69,** 111-7.
Gailani MR, Stahle-Backdahl M, Leffell DJ, Glynn M, Zaphiropoulos PG, Pressman C, Unden AB, Dean M, Brash DE, Bale AE and Toftgard R. (1996). The role of the human homologue of Drosophila patched in sporadic basal cell carcinomas, *Nat Genet*, **14,** 78-81.
Galipeau PC, Cowan DS, Sanchez CA, Barrett MT, Emond MJ, Levine DS, Rabinovitch PS and Reid BJ. (1996). 17p (p53) allelic losses, 4N (G2/tetraploid) populations, and progression to aneuploidy in Barrett's esophagus, *Proc Natl Acad Sci U S A*, **93,** 7081-4.
Gallico GG, 3rd, O'Connor NE, Compton CC, Kehinde O and Green H. (1984). Permanent coverage of large burn wounds with autologous cultured human epithelium, *N Engl J Med*, **311,** 448-51.

Galloway SM and Buckton KE. (1978). Aneuploidy and ageing: chromosome studies on a random sample of the population using G-banding, *Cytogenet Cell Genet*, **20,** 78-95.
Gandarillas A and Watt FM. (1995). Changes in expression of members of the fos and jun families and myc network during terminal differentiation of human keratinocytes, *Oncogene*, **11,** 1403-7.
Gandarillas A and Watt FM. (1997). c-Myc promotes differentiation of human epidermal stem cells, *Genes Dev*, **11,** 2869-82.
Ganem NJ, Storchova Z and Pellman D. (2007). Tetraploidy, aneuploidy and cancer, *Curr Opin Genet Dev*, **17,** 157-62.
Garrod DR. (1993). Desmosomes and hemidesmosomes, *Curr Opin Cell Biol*, **5,** 30-40.
Gat U, DasGupta R, Degenstein L and Fuchs E. (1998). De Novo hair follicle morphogenesis and hair tumors in mice expressing a truncated beta-catenin in skin, *Cell*, **95,** 605-14.
Gebhart E. (2005). Double minutes, cytogenetic equivalents of gene amplification, in human neoplasia - a review, *Clin Transl Oncol*, **7,** 477-85.
Gemenetzidis E, Bose A, Riaz AM, Chaplin T, Young BD, Ali M, Sugden D, Thurlow JK, Cheong SC, Teo SH, Wan H, Waseem A, Parkinson EK, Fortune F and Teh MT. (2009). FOXM1 upregulation is an early event in human squamous cell carcinoma and it is enhanced by nicotine during malignant transformation, *PLoS One*, **4,** e4849.
Georges-Labouesse E, Messaddeq N, Yehia G, Cadalbert L, Dierich A and Le Meur M. (1996). Absence of integrin alpha 6 leads to epidermolysis bullosa and neonatal death in mice, *Nat Genet*, **13,** 370-3.
Ghali L, Wong ST, Green J, Tidman N and Quinn AG. (1999). Gli1 protein is expressed in basal cell carcinomas, outer root sheath keratinocytes and a subpopulation of mesenchymal cells in normal human skin, *J Invest Dermatol*, **113,** 595-9.
Gilbertson RJ. (2004). Medulloblastoma: signalling a change in treatment, *Lancet Oncol*, **5,** 209-18.
Giles RH, van Es JH and Clevers H. (2003). Caught up in a Wnt storm: Wnt signaling in cancer, *Biochim Biophys Acta*, **1653,** 1-24.
Gisselsson D, Hakanson U, Stoller P, Marti D, Jin Y, Rosengren AH, Stewenius Y, Kahl F and Panagopoulos I. (2008). When the genome plays dice: circumvention of the spindle assembly checkpoint and near-random chromosome segregation in multipolar cancer cell mitoses, *PLoS One*, **3,** e1871.
Glinka A, Wu W, Delius H, Monaghan AP, Blumenstock C and Niehrs C. (1998). Dickkopf-1 is a member of a new family of secreted proteins and functions in head induction, *Nature*, **391,** 357-62.
Goldsmith LA. (2005a). *Physiology, Biochemistry, and molecular biology of the skin*. Oxford University Press.
Goodrich LV, Johnson RL, Milenkovic L, McMahon JA and Scott MP. (1996). Conservation of the hedgehog/patched signaling pathway from flies to mice: induction of a mouse patched gene by Hedgehog, *Genes Dev*, **10,** 301-12.
Goodrich LV, Milenkovic L, Higgins KM and Scott MP. (1997). Altered neural cell fates and medulloblastoma in mouse patched mutants, *Science*, **277,** 1109-13.
Gorbsky GJ. (1997). Cell cycle checkpoints: arresting progress in mitosis, *Bioessays*, **19,** 193-7.
Gordon MD and Nusse R. (2006). Wnt signaling: multiple pathways, multiple receptors, and multiple transcription factors, *J Biol Chem*, **281,** 22429-33.

Gore SD, Jones C and Kirkpatrick P. (2006). Decitabine, *Nat Rev Drug Discov*, **5,** 891-2.
Gorgoulis VG, Vassiliou LV, Karakaidos P, Zacharatos P, Kotsinas A, Liloglou T, Venere M, Ditullio RA, Jr., Kastrinakis NG, Levy B, Kletsas D, Yoneta A, Herlyn M, Kittas C and Halazonetis TD. (2005). Activation of the DNA damage checkpoint and genomic instability in human precancerous lesions, *Nature*, **434,** 907-13.
Gorlin RJ. (1987). Nevoid basal-cell carcinoma syndrome, *Medicine (Baltimore)*, **66,** 98-113.
Gorlin RJ. (1995). Nevoid basal cell carcinoma syndrome, *Dermatol Clin*, **13,** 113-25.
Gottardi CJ and Gumbiner BM. (2004). Distinct molecular forms of beta-catenin are targeted to adhesive or transcriptional complexes, *J Cell Biol*, **167,** 339-49.
Grachtchouk M, Mo R, Yu S, Zhang X, Sasaki H, Hui CC and Dlugosz AA. (2000). Basal cell carcinomas in mice overexpressing Gli2 in skin, *Nat Genet*, **24,** 216-7.
Grachtchouk V, Grachtchouk M, Lowe L, Johnson T, Wei L, Wang A, de Sauvage F and Dlugosz AA. (2003). The magnitude of hedgehog signaling activity defines skin tumor phenotype, *Embo J*, **22,** 2741-51.
Graham V, Khudyakov J, Ellis P and Pevny L. (2003). SOX2 functions to maintain neural progenitor identity, *Neuron*, **39,** 749-65.
Greaves MF and Wiemels J. (2003). Origins of chromosome translocations in childhood leukaemia, *Nat Rev Cancer*, **3,** 639-49.
Green DR. (2005). Apoptotic pathways: ten minutes to dead, *Cell*, **121,** 671-4.
Green DR and Kroemer G. (2004). The pathophysiology of mitochondrial cell death, *Science*, **305,** 626-9.
Green H. (1977). Terminal differentiation of cultured human epidermal cells, *Cell*, **11,** 405-16.
Greenhalgh DA, Rothnagel JA, Quintanilla MI, Orengo CC, Gagne TA, Bundman DS, Longley MA and Roop DR. (1993). Induction of epidermal hyperplasia, hyperkeratosis, and papillomas in transgenic mice by a targeted v-Ha-ras oncogene, *Mol Carcinog*, **7,** 99-110.
Groden J, Thliveris A, Samowitz W, Carlson M, Gelbert L, Albertsen H, Joslyn G, Stevens J, Spirio L, Robertson M and et al. (1991). Identification and characterization of the familial adenomatous polyposis coli gene, *Cell*, **66,** 589-600.
Grose R, Hutter C, Bloch W, Thorey I, Watt FM, Fassler R, Brakebusch C and Werner S. (2002). A crucial role of beta 1 integrins for keratinocyte migration in vitro and during cutaneous wound repair, *Development*, **129,** 2303-15.
Grosschedl R, Giese K and Pagel J. (1994). HMG domain proteins: architectural elements in the assembly of nucleoprotein structures, *Trends Genet*, **10,** 94-100.
Grossman D and Leffell DJ. (1997). The molecular basis of nonmelanoma skin cancer: new understanding, *Arch Dermatol*, **133,** 1263-70.
Gu Y, Turck CW and Morgan DO. (1993). Inhibition of CDK2 activity in vivo by an associated 20K regulatory subunit, *Nature*, **366,** 707-10.
Gubbay J, Collignon J, Koopman P, Capel B, Economou A, Munsterberg A, Vivian N, Goodfellow P and Lovell-Badge R. (1990). A gene mapping to the sex-determining region of the mouse Y chromosome is a member of a novel family of embryonically expressed genes, *Nature*, **346,** 245-50.
Gumbiner BM. (1996). Cell adhesion: the molecular basis of tissue architecture and morphogenesis, *Cell*, **84,** 345-57.

Gumbiner BM. (2000). Regulation of cadherin adhesive activity, *J Cell Biol*, **148,** 399-404.
Gumbiner BM. (2005). Regulation of cadherin-mediated adhesion in morphogenesis, *Nat Rev Mol Cell Biol*, **6,** 622-34.
Gure AO, Stockert E, Scanlan MJ, Keresztes RS, Jager D, Altorki NK, Old LJ and Chen YT. (2000). Serological identification of embryonic neural proteins as highly immunogenic tumor antigens in small cell lung cancer, *Proc Natl Acad Sci U S A*, **97,** 4198-203.
Habas R, Dawid IB and He X. (2003). Coactivation of Rac and Rho by Wnt/Frizzled signaling is required for vertebrate gastrulation, *Genes Dev*, **17,** 295-309.
Hahn H, Christiansen J, Wicking C, Zaphiropoulos PG, Chidambaram A, Gerrard B, Vorechovsky I, Bale AE, Toftgard R, Dean M and Wainwright B. (1996a). A mammalian patched homolog is expressed in target tissues of sonic hedgehog and maps to a region associated with developmental abnormalities, *J Biol Chem*, **271,** 12125-8.
Hahn H, Wicking C, Zaphiropoulous PG, Gailani MR, Shanley S, Chidambaram A, Vorechovsky I, Holmberg E, Unden AB, Gillies S, Negus K, Smyth I, Pressman C, Leffell DJ, Gerrard B, Goldstein AM, Dean M, Toftgard R, Chenevix-Trench G, Wainwright B and Bale AE. (1996b). Mutations of the human homolog of Drosophila patched in the nevoid basal cell carcinoma syndrome, *Cell*, **85,** 841-51.
Hahn H, Wojnowski L, Zimmer AM, Hall J, Miller G and Zimmer A. (1998). Rhabdomyosarcomas and radiation hypersensitivity in a mouse model of Gorlin syndrome, *Nat Med*, **4,** 619-22.
Hahn WC, Counter CM, Lundberg AS, Beijersbergen RL, Brooks MW and Weinberg RA. (1999). Creation of human tumour cells with defined genetic elements, *Nature*, **400,** 464-8.
Hahn WC and Weinberg RA. (2002). Rules for making human tumor cells, *N Engl J Med*, **347,** 1593-603.
Hahne M, Rimoldi D, Schroter M, Romero P, Schreier M, French LE, Schneider P, Bornand T, Fontana A, Lienard D, Cerottini J and Tschopp J. (1996). Melanoma cell expression of Fas(Apo-1/CD95) ligand: implications for tumor immune escape, *Science*, **274,** 1363-6.
Hajra KM, Chen DY and Fearon ER. (2002). The SLUG zinc-finger protein represses E-cadherin in breast cancer, *Cancer Res*, **62,** 1613-8.
Halazonetis TD, Gorgoulis VG and Bartek J. (2008). An oncogene-induced DNA damage model for cancer development, *Science*, **319,** 1352-5.
Hall A. (1998). Rho GTPases and the actin cytoskeleton, *Science*, **279,** 509-14.
Hamburger AW and Salmon SE. (1977). Primary bioassay of human tumor stem cells, *Science*, **197,** 461-3.
Hamilton SR, Liu B, Parsons RE, Papadopoulos N, Jen J, Powell SM, Krush AJ, Berk T, Cohen Z, Tetu B and et al. (1995). The molecular basis of Turcot's syndrome, *N Engl J Med*, **332,** 839-47.
Hanahan D and Weinberg RA. (2000). The hallmarks of cancer, *Cell*, **100,** 57-70.
Happle R. (1999). Loss of heterozygosity in human skin, *J Am Acad Dermatol*, **41,** 143-64.
Hardcastle Z, Mo R, Hui CC and Sharpe PT. (1998). The Shh signalling pathway in tooth development: defects in Gli2 and Gli3 mutants, *Development*, **125,** 2803-11.

Hardman MJ, Liu K, Avilion AA, Merritt A, Brennan K, Garrod DR and Byrne C. (2005). Desmosomal cadherin misexpression alters beta-catenin stability and epidermal differentiation, *Mol Cell Biol*, **25,** 969-78.

Hardy PA and Zacharias H. (2005). Reappraisal of the Hansemann-Boveri hypothesis on the origin of tumors, *Cell Biol Int*, **29,** 983-92.

Harnden DG, Benn PA, Oxford JM, Taylor AM and Webb TP. (1976). Cytogenetically marked clones in human fibroblasts cultured from normal subjects, *Somatic Cell Genet*, **2,** 55-62.

Harper JW, Adami GR, Wei N, Keyomarsi K and Elledge SJ. (1993). The p21 Cdk-interacting protein Cip1 is a potent inhibitor of G1 cyclin-dependent kinases, *Cell*, **75,** 805-16.

Harper LJ, Piper K, Common J, Fortune F and Mackenzie IC. (2007). Stem cell patterns in cell lines derived from head and neck squamous cell carcinoma, *J Oral Pathol Med*, **36,** 594-603.

Harris H. (2008a). Concerning the origin of malignant tumours by Theodor Boveri. Translated and annotated by Henry Harris. Preface, *J Cell Sci*, **121 Suppl 1,** v-vi.

Harris H. (2008b). Standing on Boveri's shoulders., *J. Cell Sci.*, **121(1),** 3-3.

Hartwell LH and Weinert TA. (1989). Checkpoints: controls that ensure the order of cell cycle events, *Science*, **246,** 629-34.

Hau PM, Siu WY, Wong N, Lai PB and Poon RY. (2006). Polyploidization increases the sensitivity to DNA-damaging agents in mammalian cells, *FEBS Lett*, **580,** 4727-36.

Hausmann G, Banziger C and Basler K. (2007). Helping Wingless take flight: how WNT proteins are secreted, *Nat Rev Mol Cell Biol*, **8,** 331-6.

Hawley-Nelson P, Stanley JR, Schmidt J, Gullino M and Yuspa SH. (1982). The tumor promoter, 12-O-tetradecanoylphorbol-13-acetate accelerates keratinocyte differentiation and stimulates growth of an unidentified cell type in cultured human epidermis, *Exp Cell Res*, **137,** 155-67.

Hawley-Nelson P, Sullivan JE, Kung M, Hennings H and Yuspa SH. (1980). Optimized conditions for the growth of human epidermal cells in culture, *J Invest Dermatol*, **75,** 176-82.

He TC, Chan TA, Vogelstein B and Kinzler KW. (1999). PPARdelta is an APC-regulated target of nonsteroidal anti-inflammatory drugs, *Cell*, **99,** 335-45.

He TC, Sparks AB, Rago C, Hermeking H, Zawel L, da Costa LT, Morin PJ, Vogelstein B and Kinzler KW. (1998). Identification of c-MYC as a target of the APC pathway, *Science*, **281,** 1509-12.

He X, Saint-Jeannet JP, Wang Y, Nathans J, Dawid I and Varmus H. (1997). A member of the Frizzled protein family mediating axis induction by Wnt-5A, *Science*, **275,** 1652-4.

He X, Semenov M, Tamai K and Zeng X. (2004). LDL receptor-related proteins 5 and 6 in Wnt/beta-catenin signaling: arrows point the way, *Development*, **131,** 1663-77.

Hecht A, Vleminckx K, Stemmler MP, van Roy F and Kemler R. (2000). The p300/CBP acetyltransferases function as transcriptional coactivators of beta-catenin in vertebrates, *Embo J*, **19,** 1839-50.

Heim S, Mandahl N and Mitelman F. (1988). Genetic convergence and divergence in tumor progression, *Cancer Res*, **48,** 5911-6.

Hendzel MJ, Wei Y, Mancini MA, Van Hooser A, Ranalli T, Brinkley BR, Bazett-Jones DP and Allis CD. (1997). Mitosis-specific phosphorylation of histone H3

initiates primarily within pericentromeric heterochromatin during G2 and spreads in an ordered fashion coincident with mitotic chromosome condensation, *Chromosoma*, **106,** 348-60.
Hengartner MO. (2000). The biochemistry of apoptosis, *Nature*, **407,** 770-6.
Hennings H, Michael D, Cheng C, Steinert P, Holbrook K and Yuspa SH. (1980). Calcium regulation of growth and differentiation of mouse epidermal cells in culture, *Cell*, **19,** 245-54.
Hermeking H. (2003). The 14-3-3 cancer connection, *Nat Rev Cancer*, **3,** 931-43.
Hermeking H, Lengauer C, Polyak K, He TC, Zhang L, Thiagalingam S, Kinzler KW and Vogelstein B. (1997). 14-3-3 sigma is a p53-regulated inhibitor of G2/M progression, *Mol Cell*, **1,** 3-11.
Hernandez AD, Hibbs MS and Postlethwaite AE. (1985). Establishment of basal cell carcinoma in culture: evidence for a basal cell carcinoma-derived factor(s) which stimulates fibroblasts to proliferate and release collagenase, *J Invest Dermatol*, **85,** 470-5.
Hernando E, Nahle Z, Juan G, Diaz-Rodriguez E, Alaminos M, Hemann M, Michel L, Mittal V, Gerald W, Benezra R, Lowe SW and Cordon-Cardo C. (2004). Rb inactivation promotes genomic instability by uncoupling cell cycle progression from mitotic control, *Nature*, **430,** 797-802.
Hertle MD, Kubler MD, Leigh IM and Watt FM. (1992). Aberrant integrin expression during epidermal wound healing and in psoriatic epidermis, *J Clin Invest*, **89,** 1892-901.
Herzberg AJ, Garcia JA, Kerns BJ, Jordan PA, Pence JC, Rotter SM and Dzubow LM. (1993). DNA ploidy of basal cell carcinoma determined by image cytometry of fresh smears, *J Cutan Pathol*, **20,** 216-22.
Hidalgo M and Maitra A. (2009). The hedgehog pathway and pancreatic cancer, *N Engl J Med*, **361,** 2094-6.
Hinchcliffe EH and Sluder G. (2001). "It takes two to tango": understanding how centrosome duplication is regulated throughout the cell cycle, *Genes Dev*, **15,** 1167-81.
Hirohashi S. (1998). Inactivation of the E-cadherin-mediated cell adhesion system in human cancers, *Am J Pathol*, **153,** 333-9.
Hirohashi S and Kanai Y. (2003). Cell adhesion system and human cancer morphogenesis, *Cancer Sci*, **94,** 575-81.
Hirotsu M, Setoguchi T, Sasaki H, Matsunoshita Y, Gao H, Nagao H, Kunigou O and Komiya S. (2010). Smoothened as a new therapeutic target for human osteosarcoma, *Mol Cancer*, **9,** 5.
Hoban PR, Lear JT and Strange RC. (2006). Basal cell carcinoma: genetic homogeneity in a tumour type displaying phenotypic diversity, *Eur J Hum Genet*, **14,** 977-8.
Hockenbery D, Nunez G, Milliman C, Schreiber RD and Korsmeyer SJ. (1990). Bcl-2 is an inner mitochondrial membrane protein that blocks programmed cell death, *Nature*, **348,** 334-6.
Hockenbery DM. (1995). bcl-2, a novel regulator of cell death, *Bioessays*, **17,** 631-8.
Holcik M and Sonenberg N. (2005). Translational control in stress and apoptosis, *Nat Rev Mol Cell Biol*, **6,** 318-27.
Holland AJ and Cleveland DW. (2009). Boveri revisited: chromosomal instability, aneuploidy and tumorigenesis, *Nat Rev Mol Cell Biol*, **10,** 478-87.
Holland EC, Celestino J, Dai C, Schaefer L, Sawaya RE and Fuller GN. (2000). Combined activation of Ras and Akt in neural progenitors induces glioblastoma formation in mice, *Nat Genet*, **25,** 55-7.

Hollingsworth MA and Swanson BJ. (2004). Mucins in cancer: protection and control of the cell surface, *Nat Rev Cancer*, **4,** 45-60.

Holmen SL, Salic A, Zylstra CR, Kirschner MW and Williams BO. (2002). A novel set of Wnt-Frizzled fusion proteins identifies receptor components that activate beta -catenin-dependent signaling, *J Biol Chem*, **277,** 34727-35.

Hooper JE and Scott MP. (1989). The Drosophila patched gene encodes a putative membrane protein required for segmental patterning, *Cell*, **59,** 751-65.

Hooper JE and Scott MP. (2005). Communicating with Hedgehogs, *Nat Rev Mol Cell Biol*, **6,** 306-17.

Hotchin NA, Gandarillas A and Watt FM. (1995). Regulation of cell surface beta 1 integrin levels during keratinocyte terminal differentiation, *J Cell Biol*, **128,** 1209-19.

Hotchin NA, Kovach NL and Watt FM. (1993). Functional down-regulation of alpha 5 beta 1 integrin in keratinocytes is reversible but commitment to terminal differentiation is not, *J Cell Sci*, **106 (Pt 4),** 1131-8.

Hotchin NA and Watt FM. (1992). Transcriptional and post-translational regulation of beta 1 integrin expression during keratinocyte terminal differentiation, *J Biol Chem*, **267,** 14852-8.

Hsieh JC, Kodjabachian L, Rebbert ML, Rattner A, Smallwood PM, Samos CH, Nusse R, Dawid IB and Nathans J. (1999). A new secreted protein that binds to Wnt proteins and inhibits their activities, *Nature*, **398,** 431-6.

Hu D, Valentine M, Kidd VJ and Lahti JM. (2007). CDK11(p58) is required for the maintenance of sister chromatid cohesion, *J Cell Sci*, **120,** 2424-34.

Huang H, Mahler-Araujo BM, Sankila A, Chimelli L, Yonekawa Y, Kleihues P and Ohgaki H. (2000). APC mutations in sporadic medulloblastomas, *Am J Pathol*, **156,** 433-7.

Huang S, He J, Zhang X, Bian Y, Yang L, Xie G, Zhang K, Tang W, Stelter AA, Wang Q, Zhang H and Xie J. (2006). Activation of the hedgehog pathway in human hepatocellular carcinomas, *Carcinogenesis*, **27,** 1334-40.

Huelsken J and Behrens J. (2002). The Wnt signalling pathway, *J Cell Sci*, **115,** 3977-8.

Huelsken J, Vogel R, Erdmann B, Cotsarelis G and Birchmeier W. (2001). beta-Catenin controls hair follicle morphogenesis and stem cell differentiation in the skin, *Cell*, **105,** 533-45.

Hugh TJ, Dillon SA, O'Dowd G, Getty B, Pignatelli M, Poston GJ and Kinsella AR. (1999). beta-catenin expression in primary and metastatic colorectal carcinoma, *Int J Cancer*, **82,** 504-11.

Hugo H, Ackland ML, Blick T, Lawrence MG, Clements JA, Williams ED and Thompson EW. (2007). Epithelial--mesenchymal and mesenchymal--epithelial transitions in carcinoma progression, *J Cell Physiol*, **213,** 374-83.

Hui CC, Slusarski D, Platt KA, Holmgren R and Joyner AL. (1994). Expression of three mouse homologs of the Drosophila segment polarity gene cubitus interruptus, Gli, Gli-2, and Gli-3, in ectoderm- and mesoderm-derived tissues suggests multiple roles during postimplantation development, *Dev Biol*, **162,** 402-13.

Huntzicker EG, Estay IS, Zhen H, Lokteva LA, Jackson PK and Oro AE. (2006). Dual degradation signals control Gli protein stability and tumor formation, *Genes Dev*, **20,** 276-81.

Hurlin PJ, Foley KP, Ayer DE, Eisenman RN, Hanahan D and Arbeit JM. (1995). Regulation of Myc and Mad during epidermal differentiation and HPV-associated tumorigenesis, *Oncogene*, **11,** 2487-501.

Hutchin ME, Kariapper MS, Grachtchouk M, Wang A, Wei L, Cummings D, Liu J, Michael LE, Glick A and Dlugosz AA. (2005). Sustained Hedgehog signaling is required for basal cell carcinoma proliferation and survival: conditional skin tumorigenesis recapitulates the hair growth cycle, *Genes Dev*, **19,** 214-23.

Hynes RO. (1992). Integrins: versatility, modulation, and signaling in cell adhesion, *Cell*, **69,** 11-25.

Igney FH and Krammer PH. (2002). Death and anti-death: tumour resistance to apoptosis, *Nat Rev Cancer*, **2,** 277-88.

Ikram MS, Neill GW, Regl G, Eichberger T, Frischauf AM, Aberger F, Quinn A and Philpott M. (2004). GLI2 is expressed in normal human epidermis and BCC and induces GLI1 expression by binding to its promoter, *J Invest Dermatol*, **122,** 1503-9.

Ingham PW and McMahon AP. (2001). Hedgehog signaling in animal development: paradigms and principles, *Genes Dev*, **15,** 3059-87.

Irmler M, Thome M, Hahne M, Schneider P, Hofmann K, Steiner V, Bodmer JL, Schroter M, Burns K, Mattmann C, Rimoldi D, French LE and Tschopp J. (1997). Inhibition of death receptor signals by cellular FLIP, *Nature*, **388,** 190-5.

Ishitani T, Kishida S, Hyodo-Miura J, Ueno N, Yasuda J, Waterman M, Shibuya H, Moon RT, Ninomiya-Tsuji J and Matsumoto K. (2003). The TAK1-NLK mitogen-activated protein kinase cascade functions in the Wnt-5a/Ca(2+) pathway to antagonize Wnt/beta-catenin signaling, *Mol Cell Biol*, **23,** 131-9.

Ishitani T, Ninomiya-Tsuji J, Nagai S, Nishita M, Meneghini M, Barker N, Waterman M, Bowerman B, Clevers H, Shibuya H and Matsumoto K. (1999). The TAK1-NLK-MAPK-related pathway antagonizes signalling between beta-catenin and transcription factor TCF, *Nature*, **399,** 798-802.

Issa JP and Kantarjian H. (2005). Azacitidine, *Nat Rev Drug Discov*, **Suppl,** S6-7.

Ito M, Liu Y, Yang Z, Nguyen J, Liang F, Morris RJ and Cotsarelis G. (2005). Stem cells in the hair follicle bulge contribute to wound repair but not to homeostasis of the epidermis, *Nat Med*, **11,** 1351-4.

Ito M, Yang Z, Andl T, Cui C, Kim N, Millar SE and Cotsarelis G. (2007). Wnt-dependent de novo hair follicle regeneration in adult mouse skin after wounding, *Nature*, **447,** 316-20.

Jacob A. (1827). Observations respecting an ulcer of peculiar character. which attacks the eyelids and other parts of the face., *Dublin Hospital Rep Commun Med Surg*, **4,** 232-239.

Jaenisch R and Bird A. (2003). Epigenetic regulation of gene expression: how the genome integrates intrinsic and environmental signals, *Nat Genet*, **33 Suppl,** 245-54.

Jaks V, Barker N, Kasper M, van Es JH, Snippert HJ, Clevers H and Toftgard R. (2008). Lgr5 marks cycling, yet long-lived, hair follicle stem cells, *Nat Genet*, **40,** 1291-9.

Jamora C, DasGupta R, Kocieniewski P and Fuchs E. (2003). Links between signal transduction, transcription and adhesion in epithelial bud development, *Nature*, **422,** 317-22.

Jamora C and Fuchs E. (2002). Intercellular adhesion, signalling and the cytoskeleton, *Nat Cell Biol*, **4,** E101-8.

Janisson-Dargaud D, Durlach A, Lorenzato M, Grange F, Bernard P and Birembaut P. (2008). Aneuploidy, but not Ki-67 or EGFR expression, is associated with recurrences in basal cell carcinoma, *J Cutan Pathol*, **35,** 916-21.

Jannink G, Duplantier B and Sikorav JL. (1996). Forces on chromosomal DNA during anaphase, *Biophys J*, **71,** 451-65.
Jefford CE and Irminger-Finger I. (2006). Mechanisms of chromosome instability in cancers, *Crit Rev Oncol Hematol*, **59,** 1-14.
Jensen KB and Watt FM. (2006). Single-cell expression profiling of human epidermal stem and transit-amplifying cells: Lrig1 is a regulator of stem cell quiescence, *Proc Natl Acad Sci U S A*, **103,** 11958-63.
Jensen UB, Lowell S and Watt FM. (1999). The spatial relationship between stem cells and their progeny in the basal layer of human epidermis: a new view based on whole-mount labelling and lineage analysis, *Development*, **126,** 2409-18.
Ji J, Kump E, Wernli M and Erb P. (2008). Gene silencing of transcription factor Gli2 inhibits basal cell carcinomalike tumor growth in vivo, *Int J Cancer*, **122,** 50-6.
Jia J, Tong C and Jiang J. (2003). Smoothened transduces Hedgehog signal by physically interacting with Costal2/Fused complex through its C-terminal tail, *Genes Dev*, **17,** 2709-20.
Jiang H, Lin J, Su ZZ, Collart FR, Huberman E and Fisher PB. (1994). Induction of differentiation in human promyelocytic HL-60 leukemia cells activates p21, WAF1/CIP1, expression in the absence of p53, *Oncogene*, **9,** 3397-406.
Jiang J. (2006). Regulation of Hh/Gli signaling by dual ubiquitin pathways, *Cell Cycle*, **5,** 2457-63.
Jiang J and Struhl G. (1998). Regulation of the Hedgehog and Wingless signalling pathways by the F-box/WD40-repeat protein Slimb, *Nature*, **391,** 493-6.
Jiang M and Milner J. (2003). Bcl-2 constitutively suppresses p53-dependent apoptosis in colorectal cancer cells, *Genes Dev*, **17,** 832-7.
Jiang SB and Szyfelbein K. (2009). Pathology - Basal Cell Carcinoma. eMedicine from web MD.
Jiang W, Ananthaswamy HN, Muller HK and Kripke ML. (1999). p53 protects against skin cancer induction by UV-B radiation, *Oncogene*, **18,** 4247-53.
Jih DM, Shapiro M, James WD, Levin M, Gelfand J, Williams PT, Oakey RJ, Fakharzadeh S and Seykora JT. (2003). Familial basaloid follicular hamartoma: lesional characterization and review of the literature, *Am J Dermatopathol*, **25,** 130-7.
Jin Y, Martins C, Salemark L, Persson B, Jin C, Miranda J, Fonseca I and Jonsson N. (2001). Nonrandom karyotypic features in basal cell carcinomas of the skin, *Cancer Genet Cytogenet*, **131,** 109-19.
Johnson RL, Rothman AL, Xie J, Goodrich LV, Bare JW, Bonifas JM, Quinn AG, Myers RM, Cox DR, Epstein EH, Jr. and Scott MP. (1996). Human homolog of patched, a candidate gene for the basal cell nevus syndrome, *Science*, **272,** 1668-71.
Jonason AS, Kunala S, Price GJ, Restifo RJ, Spinelli HM, Persing JA, Leffell DJ, Tarone RE and Brash DE. (1996). Frequent clones of p53-mutated keratinocytes in normal human skin, *Proc Natl Acad Sci U S A*, **93,** 14025-9.
Jones DL, Alani RM and Munger K. (1997). The human papillomavirus E7 oncoprotein can uncouple cellular differentiation and proliferation in human keratinocytes by abrogating p21Cip1-mediated inhibition of cdk2, *Genes Dev*, **11,** 2101-11.
Jones PH, Harper S and Watt FM. (1995). Stem cell patterning and fate in human epidermis, *Cell*, **80,** 83-93.
Jones PH, Simons BD and Watt FM. (2007). Sic transit gloria: farewell to the epidermal transit amplifying cell?, *Cell Stem Cell*, **1,** 371-81.

Jones PH and Watt FM. (1993). Separation of human epidermal stem cells from transit amplifying cells on the basis of differences in integrin function and expression, *Cell*, **73,** 713-24.

Kain SR, Adams M, Kondepudi A, Yang TT, Ward WW and Kitts P. (1995). Green fluorescent protein as a reporter of gene expression and protein localization, *Biotechniques*, **19,** 650-5.

Kajino Y, Yamaguchi A, Hashimoto N, Matsuura A, Sato N and Kikuchi K. (2001). beta-Catenin gene mutation in human hair follicle-related tumors, *Pathol Int*, **51,** 543-8.

Kalderon D. (2000). Transducing the hedgehog signal, *Cell*, **103,** 371-4.

Kallassy M, Toftgard R, Ueda M, Nakazawa K, Vorechovsky I, Yamasaki H and Nakazawa H. (1997). Patched (ptch)-associated preferential expression of smoothened (smoh) in human basal cell carcinoma of the skin, *Cancer Res*, **57,** 4731-5.

Kamachi Y, Cheah KS and Kondoh H. (1999). Mechanism of regulatory target selection by the SOX high-mobility-group domain proteins as revealed by comparison of SOX1/2/3 and SOX9, *Mol Cell Biol*, **19,** 107-20.

Kamachi Y, Uchikawa M and Kondoh H. (2000). Pairing SOX off: with partners in the regulation of embryonic development, *Trends Genet*, **16,** 182-7.

Kameda C, Tanaka H, Yamasaki A, Nakamura M, Koga K, Sato N, Kubo M, Kuroki S, Tanaka M and Katano M. (2009). The Hedgehog pathway is a possible therapeutic target for patients with estrogen receptor-negative breast cancer, *Anticancer Res*, **29,** 871-9.

Kameda T, Hatakeyama S, Terada K and Sugiyama T. (2001). Acceleration of the formation of cultured epithelium using the sonic hedgehog expressing feeder cells, *Tissue Eng*, **7,** 545-55.

Kaneko Y and Knudson AG. (2000). Mechanism and relevance of ploidy in neuroblastoma, *Genes Chromosomes Cancer*, **29,** 89-95.

Karagas MR, Stannard VA, Mott LA, Slattery MJ, Spencer SK and Weinstock MA. (2002). Use of tanning devices and risk of basal cell and squamous cell skin cancers, *J Natl Cancer Inst*, **94,** 224-6.

Karhadkar SS, Bova GS, Abdallah N, Dhara S, Gardner D, Maitra A, Isaacs JT, Berman DM and Beachy PA. (2004). Hedgehog signalling in prostate regeneration, neoplasia and metastasis, *Nature*, **431,** 707-12.

Karpowicz P, Morshead C, Kam A, Jervis E, Ramunas J, Cheng V and van der Kooy D. (2005). Support for the immortal strand hypothesis: neural stem cells partition DNA asymmetrically in vitro, *J Cell Biol*, **170,** 721-32.

Kasper M, Regl G, Frischauf AM and Aberger F. (2006a). GLI transcription factors: mediators of oncogenic Hedgehog signalling, *Eur J Cancer*, **42,** 437-45.

Kasper M, Schnidar H, Neill GW, Hanneder M, Klingler S, Blaas L, Schmid C, Hauser-Kronberger C, Regl G, Philpott MP and Aberger F. (2006b). Selective modulation of Hedgehog/GLI target gene expression by epidermal growth factor signaling in human keratinocytes, *Mol Cell Biol*, **26,** 6283-98.

Kastan MB, Zhan Q, el-Deiry WS, Carrier F, Jacks T, Walsh WV, Plunkett BS, Vogelstein B and Fornace AJ, Jr. (1992). A mammalian cell cycle checkpoint pathway utilizing p53 and GADD45 is defective in ataxia-telangiectasia, *Cell*, **71,** 587-97.

Katanaev VL, Ponzielli R, Semeriva M and Tomlinson A. (2005). Trimeric G protein-dependent frizzled signaling in Drosophila, *Cell*, **120,** 111-22.

Kelly PN, Dakic A, Adams JM, Nutt SL and Strasser A. (2007). Tumor growth need not be driven by rare cancer stem cells, *Science*, **317,** 337.

Kemler R. (1993). From cadherins to catenins: cytoplasmic protein interactions and regulation of cell adhesion, *Trends Genet*, **9,** 317-21.

Kenney AM and Rowitch DH. (2000). Sonic hedgehog promotes G(1) cyclin expression and sustained cell cycle progression in mammalian neuronal precursors, *Mol Cell Biol*, **20,** 9055-67.

Khan SH and Wahl GM. (1998). p53 and pRb prevent rereplication in response to microtubule inhibitors by mediating a reversible G1 arrest, *Cancer Res*, **58,** 396-401.

Khanna KK and Jackson SP. (2001). DNA double-strand breaks: signaling, repair and the cancer connection, *Nat Genet*, **27,** 247-54.

Khavari PA. (2006). Modelling cancer in human skin tissue, *Nat Rev Cancer*, **6,** 270-80.

Kiernan AE, Pelling AL, Leung KK, Tang AS, Bell DM, Tease C, Lovell-Badge R, Steel KP and Cheah KS. (2005). Sox2 is required for sensory organ development in the mammalian inner ear, *Nature*, **434,** 1031-5.

Kimonis VE, Goldstein AM, Pastakia B, Yang ML, Kase R, DiGiovanna JJ, Bale AE and Bale SJ. (1997). Clinical manifestations in 105 persons with nevoid basal cell carcinoma syndrome, *Am J Med Genet*, **69,** 299-308.

Kinzler KW, Bigner SH, Bigner DD, Trent JM, Law ML, O'Brien SJ, Wong AJ and Vogelstein B. (1987). Identification of an amplified, highly expressed gene in a human glioma, *Science*, **236,** 70-3.

Kinzler KW, Nilbert MC, Su LK, Vogelstein B, Bryan TM, Levy DB, Smith KJ, Preisinger AC, Hedge P, McKechnie D and et al. (1991). Identification of FAP locus genes from chromosome 5q21, *Science*, **253,** 661-5.

Kinzler KW, Ruppert JM, Bigner SH and Vogelstein B. (1988). The GLI gene is a member of the Kruppel family of zinc finger proteins, *Nature*, **332,** 371-4.

Kinzler KW and Vogelstein B. (1990). The GLI gene encodes a nuclear protein which binds specific sequences in the human genome, *Mol Cell Biol*, **10,** 634-42.

Kirkhus B and Clausen OP. (1990). Cell kinetics in mouse epidermis studied by bivariate DNA/bromodeoxyuridine and DNA/keratin flow cytometry, *Cytometry*, **11,** 253-60.

Klaus A and Birchmeier W. (2008). Wnt signalling and its impact on development and cancer, *Nat Rev Cancer*, **8,** 387-98.

Klipp E and Liebermeister W. (2006). Mathematical modeling of intracellular signaling pathways, *BMC Neurosci*, **7 Suppl 1,** S10.

Knoblich JA, Sauer K, Jones L, Richardson H, Saint R and Lehner CF. (1994). Cyclin E controls S phase progression and its down-regulation during Drosophila embryogenesis is required for the arrest of cell proliferation, *Cell*, **77,** 107-20.

Kobayashi K, Rochat A and Barrandon Y. (1993). Segregation of keratinocyte colony-forming cells in the bulge of the rat vibrissa, *Proc Natl Acad Sci U S A*, **90,** 7391-5.

Kogerman P, Grimm T, Kogerman L, Krause D, Unden AB, Sandstedt B, Toftgard R and Zaphiropoulos PG. (1999). Mammalian suppressor-of-fused modulates nuclear-cytoplasmic shuttling of Gli-1, *Nat Cell Biol*, **1,** 312-9.

Kohn AD and Moon RT. (2005). Wnt and calcium signaling: beta-catenin-independent pathways, *Cell Calcium*, **38,** 439-46.

Kolligs FT, Hu G, Dang CV and Fearon ER. (1999). Neoplastic transformation of RK3E by mutant beta-catenin requires deregulation of Tcf/Lef transcription but not activation of c-myc expression, *Mol Cell Biol*, **19,** 5696-706.

Kolodka TM, Garlick JA and Taichman LB. (1998). Evidence for keratinocyte stem cells in vitro: long term engraftment and persistence of transgene expression from retrovirus-transduced keratinocytes, *Proc Natl Acad Sci U S A*, **95,** 4356-61.

Kondo T, Johnson SA, Yoder MC, Romand R and Hashino E. (2005). Sonic hedgehog and retinoic acid synergistically promote sensory fate specification from bone marrow-derived pluripotent stem cells, *Proc Natl Acad Sci U S A*, **102,** 4789-94.

Kondo T and Raff M. (2004). Chromatin remodeling and histone modification in the conversion of oligodendrocyte precursors to neural stem cells, *Genes Dev*, **18,** 2963-72.

Koopman G, Reutelingsperger CP, Kuijten GA, Keehnen RM, Pals ST and van Oers MH. (1994). Annexin V for flow cytometric detection of phosphatidylserine expression on B cells undergoing apoptosis, *Blood*, **84,** 1415-20.

Kooy AJ, Tank B, de Jong AA, Vuzevski VD, van der Kwast TH and van Joost T. (1999). Expression of E-cadherin, alpha- & beta-catenin, and CD44V6 and the subcellular localization of E-cadherin and CD44V6 in normal epidermis and basal cell carcinoma, *Hum Pathol*, **30,** 1328-35.

Korinek V, Barker N, Moerer P, van Donselaar E, Huls G, Peters PJ and Clevers H. (1998). Depletion of epithelial stem-cell compartments in the small intestine of mice lacking Tcf-4, *Nat Genet*, **19,** 379-83.

Korinek V, Barker N, Morin PJ, van Wichen D, de Weger R, Kinzler KW, Vogelstein B and Clevers H. (1997). Constitutive transcriptional activation by a beta-catenin-Tcf complex in APC-/- colon carcinoma, *Science*, **275,** 1784-7.

Krahn G, Leiter U, Kaskel P, Udart M, Utikal J, Bezold G and Peter RU. (2001). Coexpression patterns of EGFR, HER2, HER3 and HER4 in non-melanoma skin cancer, *Eur J Cancer*, **37,** 251-9.

Kriegl L, Horst D, Kirchner T and Jung A. (2009). LEF-1 expression in basal cell carcinomas, *Br J Dermatol*, **160,** 1353-6.

Krishan A. (1990). Rapid DNA content analysis by the propidium iodide-hypotonic citrate method, *Methods Cell Biol*, **33,** 121-5.

Kruger K, Blume-Peytavi U and Orfanos CE. (1999). Basal cell carcinoma possibly originates from the outer root sheath and/or the bulge region of the vellus hair follicle, *Arch Dermatol Res*, **291,** 253-9.

Kubista M, Akerman B and Norden B. (1987). Characterization of interaction between DNA and 4',6-diamidino-2-phenylindole by optical spectroscopy, *Biochemistry*, **26,** 4545-53.

Kubo M, Nakamura M, Tasaki A, Yamanaka N, Nakashima H, Nomura M, Kuroki S and Katano M. (2004). Hedgehog signaling pathway is a new therapeutic target for patients with breast cancer, *Cancer Res*, **64,** 6071-4.

Kubo M, Norris DA, Howell SE, Ryan SR and Clark RA. (1984). Human keratinocytes synthesize, secrete, and deposit fibronectin in the pericellular matrix, *J Invest Dermatol*, **82,** 580-6.

Kuerbitz SJ, Plunkett BS, Walsh WV and Kastan MB. (1992). Wild-type p53 is a cell cycle checkpoint determinant following irradiation, *Proc Natl Acad Sci U S A*, **89,** 7491-5.

Kuhl M, Geis K, Sheldahl LC, Pukrop T, Moon RT and Wedlich D. (2001). Antagonistic regulation of convergent extension movements in Xenopus by Wnt/beta-catenin and Wnt/Ca2+ signaling, *Mech Dev*, **106,** 61-76.

Kuhl M, Sheldahl LC, Malbon CC and Moon RT. (2000a). Ca(2+)/calmodulin-dependent protein kinase II is stimulated by Wnt and Frizzled homologs and promotes ventral cell fates in Xenopus, *J Biol Chem*, **275,** 12701-11.

Kuhl M, Sheldahl LC, Park M, Miller JR and Moon RT. (2000b). The Wnt/Ca2+ pathway: a new vertebrate Wnt signaling pathway takes shape, *Trends Genet*, **16,** 279-83.

Kump E, Ji J, Wernli M, Hausermann P and Erb P. (2008). Gli2 upregulates cFlip and renders basal cell carcinoma cells resistant to death ligand-mediated apoptosis, *Oncogene*, **27,** 3856-64.

Kwon M, Godinho SA, Chandhok NS, Ganem NJ, Azioune A, Thery M and Pellman D. (2008). Mechanisms to suppress multipolar divisions in cancer cells with extra centrosomes, *Genes Dev*, **22,** 2189-203.

Lacour JP. (2002). Carcinogenesis of basal cell carcinomas: genetics and molecular mechanisms, *Br J Dermatol*, **146 Suppl 61,** 17-9.

Lajtha LG. (1963). On the Concept of the Cell Cycle, *J Cell Physiol*, **62,** SUPPL1:143-5.

Lajtha LG. (1979). Stem cell concepts, *Differentiation*, **14,** 23-34.

Lane DP. (1992). Cancer. p53, guardian of the genome, *Nature*, **358,** 15-6.

Lane EB, Wilson CA, Hughes BR and Leigh IM. (1991). Stem cells in hair follicles. Cytoskeletal studies, *Ann N Y Acad Sci*, **642,** 197-213.

Laner-Plamberger S, Kaser A, Paulischta M, Hauser-Kronberger C, Eichberger T and Frischauf AM. (2009). Cooperation between GLI and JUN enhances transcription of JUN and selected GLI target genes, *Oncogene*, **28,** 1639-51.

Lanni JS and Jacks T. (1998). Characterization of the p53-dependent postmitotic checkpoint following spindle disruption, *Mol Cell Biol*, **18,** 1055-64.

Lansdorp PM. (2007). Immortal strands? Give me a break, *Cell*, **129,** 1244-7.

Larjava H, Peltonen J, Akiyama SK, Yamada SS, Gralnick HR, Uitto J and Yamada KM. (1990). Novel function for beta 1 integrins in keratinocyte cell-cell interactions, *J Cell Biol*, **110,** 803-15.

Lark KG. (1967). Nonrandom segregation of sister chromatids in Vicia faba and Triticum boeoticum, *Proc Natl Acad Sci U S A*, **58,** 352-9.

Lark KG, Consigli RA and Minocha HC. (1966). Segregation of sister chromatids in mammalian cells, *Science*, **154,** 1202-5.

Laronga C, Yang HY, Neal C and Lee MH. (2000). Association of the cyclin-dependent kinases and 14-3-3 sigma negatively regulates cell cycle progression, *J Biol Chem*, **275,** 23106-12.

Latres E, Chiaur DS and Pagano M. (1999). The human F box protein beta-Trcp associates with the Cul1/Skp1 complex and regulates the stability of beta-catenin, *Oncogene*, **18,** 849-54.

Lavker RM and Sun TT. (2000). Epidermal stem cells: properties, markers, and location, *Proc Natl Acad Sci U S A*, **97,** 13473-5.

Lee HY, Kleber M, Hari L, Brault V, Suter U, Taketo MM, Kemler R and Sommer L. (2004). Instructive role of Wnt/beta-catenin in sensory fate specification in neural crest stem cells, *Science*, **303,** 1020-3.

Lee JM, Dedhar S, Kalluri R and Thompson EW. (2006). The epithelial-mesenchymal transition: new insights in signaling, development, and disease, *J Cell Biol*, **172,** 973-81.

Lehman TA, Modali R, Boukamp P, Stanek J, Bennett WP, Welsh JA, Metcalf RA, Stampfer MR, Fusenig N, Rogan EM and et al. (1993). p53 mutations in human immortalized epithelial cell lines, *Carcinogenesis*, **14,** 833-9.

Lehmann AR. (2003). DNA repair-deficient diseases, xeroderma pigmentosum, Cockayne syndrome and trichothiodystrophy, *Biochimie*, **85,** 1101-11.
Lengauer C, Kinzler KW and Vogelstein B. (1997). Genetic instability in colorectal cancers, *Nature*, **386,** 623-7.
Lengauer C, Kinzler KW and Vogelstein B. (1998). Genetic instabilities in human cancers, *Nature*, **396,** 643-9.
Lessene G, Czabotar PE and Colman PM. (2008). BCL-2 family antagonists for cancer therapy, *Nat Rev Drug Discov*, **7,** 989-1000.
Levanon D, Goldstein RE, Bernstein Y, Tang H, Goldenberg D, Stifani S, Paroush Z and Groner Y. (1998). Transcriptional repression by AML1 and LEF-1 is mediated by the TLE/Groucho corepressors, *Proc Natl Acad Sci U S A*, **95,** 11590-5.
Levine AJ. (1997). p53, the cellular gatekeeper for growth and division, *Cell*, **88,** 323-31.
Levine AJ, Momand J and Finlay CA. (1991a). The p53 tumour suppressor gene, *Nature*, **351,** 453-6.
Levine DS, Sanchez CA, Rabinovitch PS and Reid BJ. (1991b). Formation of the tetraploid intermediate is associated with the development of cells with more than four centrioles in the elastase-simian virus 40 tumor antigen transgenic mouse model of pancreatic cancer, *Proc Natl Acad Sci U S A*, **88,** 6427-31.
Levy L, Broad S, Diekmann D, Evans RD and Watt FM. (2000). beta1 integrins regulate keratinocyte adhesion and differentiation by distinct mechanisms, *Mol Biol Cell*, **11,** 453-66.
Levy V, Lindon C, Harfe BD and Morgan BA. (2005). Distinct stem cell populations regenerate the follicle and interfollicular epidermis, *Dev Cell*, **9,** 855-61.
Levy V, Lindon C, Zheng Y, Harfe BD and Morgan BA. (2007). Epidermal stem cells arise from the hair follicle after wounding, *Faseb J*, **21,** 1358-66.
Li A, Simmons PJ and Kaur P. (1998). Identification and isolation of candidate human keratinocyte stem cells based on cell surface phenotype, *Proc Natl Acad Sci U S A*, **95,** 3902-7.
Li H, Chen X, Calhoun-Davis T, Claypool K and Tang DG. (2008). PC3 human prostate carcinoma cell holoclones contain self-renewing tumor-initiating cells, *Cancer Res*, **68,** 1820-5.
Li L, Tucker RW, Hennings H and Yuspa SH. (1995). Inhibitors of the intracellular Ca(2+)-ATPase in cultured mouse keratinocytes reveal components of terminal differentiation that are regulated by distinct intracellular Ca2+ compartments, *Cell Growth Differ*, **6,** 1171-84.
Li L, Yuan H, Xie W, Mao J, Caruso AM, McMahon A, Sussman DJ and Wu D. (1999). Dishevelled proteins lead to two signaling pathways. Regulation of LEF-1 and c-Jun N-terminal kinase in mammalian cells, *J Biol Chem*, **274,** 129-34.
Li R, Sonik A, Stindl R, Rasnick D and Duesberg P. (2000). Aneuploidy vs. gene mutation hypothesis of cancer: recent study claims mutation but is found to support aneuploidy, *Proc Natl Acad Sci U S A*, **97,** 3236-41.
Li X, Deng W, Lobo-Ruppert SM and Ruppert JM. (2007). Gli1 acts through Snail and E-cadherin to promote nuclear signaling by beta-catenin, *Oncogene*, **26,** 4489-98.
Li X, Deng W, Nail CD, Bailey SK, Kraus MH, Ruppert JM and Lobo-Ruppert SM. (2006). Snail induction is an early response to Gli1 that determines the efficiency of epithelial transformation, *Oncogene*, **25,** 609-21.

Lickert H, Bauer A, Kemler R and Stappert J. (2000). Casein kinase II phosphorylation of E-cadherin increases E-cadherin/beta-catenin interaction and strengthens cell-cell adhesion, *J Biol Chem*, **275,** 5090-5.

Liisberg MF. (1968). Rhodamine B as an extremely specific stain for cornification, *Acta Anat (Basel)*, **69,** 52-7.

Lilien J, Balsamo J, Arregui C and Xu G. (2002). Turn-off, drop-out: functional state switching of cadherins, *Dev Dyn*, **224,** 18-29.

Limbourg-Bouchon B, Busson D and Lamour-Isnard C. (1991). Interactions between fused, a segment-polarity gene in Drosophila, and other segmentation genes, *Development*, **112,** 417-29.

Lin YM, Ono K, Satoh S, Ishiguro H, Fujita M, Miwa N, Tanaka T, Tsunoda T, Yang KC, Nakamura Y and Furukawa Y. (2001). Identification of AF17 as a downstream gene of the beta-catenin/T-cell factor pathway and its involvement in colorectal carcinogenesis, *Cancer Res*, **61,** 6345-9.

Ling G, Ahmadian A, Persson A, Unden AB, Afink G, Williams C, Uhlen M, Toftgard R, Lundeberg J and Ponten F. (2001). PATCHED and p53 gene alterations in sporadic and hereditary basal cell cancer, *Oncogene*, **20,** 7770-8.

Lingle WL, Barrett SL, Negron VC, D'Assoro AB, Boeneman K, Liu W, Whitehead CM, Reynolds C and Salisbury JL. (2002). Centrosome amplification drives chromosomal instability in breast tumor development, *Proc Natl Acad Sci U S A*, **99,** 1978-83.

Lingle WL, Lutz WH, Ingle JN, Maihle NJ and Salisbury JL. (1998). Centrosome hypertrophy in human breast tumors: implications for genomic stability and cell polarity, *Proc Natl Acad Sci U S A*, **95,** 2950-5.

Litingtung Y and Chiang C. (2000). Specification of ventral neuron types is mediated by an antagonistic interaction between Shh and Gli3, *Nat Neurosci*, **3,** 979-85.

Liu C, Kato Y, Zhang Z, Do VM, Yankner BA and He X. (1999). beta-Trcp couples beta-catenin phosphorylation-degradation and regulates Xenopus axis formation, *Proc Natl Acad Sci U S A*, **96,** 6273-8.

Liu C, Li Y, Semenov M, Han C, Baeg GH, Tan Y, Zhang Z, Lin X and He X. (2002). Control of beta-catenin phosphorylation/degradation by a dual-kinase mechanism, *Cell*, **108,** 837-47.

Liu G, Bafico A and Aaronson SA. (2005). The mechanism of endogenous receptor activation functionally distinguishes prototype canonical and noncanonical Wnts, *Mol Cell Biol*, **25,** 3475-82.

Liu G, Bafico A, Harris VK and Aaronson SA. (2003). A novel mechanism for Wnt activation of canonical signaling through the LRP6 receptor, *Mol Cell Biol*, **23,** 5825-35.

Liu G, Parant JM, Lang G, Chau P, Chavez-Reyes A, El-Naggar AK, Multani A, Chang S and Lozano G. (2004a). Chromosome stability, in the absence of apoptosis, is critical for suppression of tumorigenesis in Trp53 mutant mice, *Nat Genet*, **36,** 63-8.

Liu W, Dong X, Mai M, Seelan RS, Taniguchi K, Krishnadath KK, Halling KC, Cunningham JM, Boardman LA, Qian C, Christensen E, Schmidt SS, Roche PC, Smith DI and Thibodeau SN. (2000). Mutations in AXIN2 cause colorectal cancer with defective mismatch repair by activating beta-catenin/TCF signalling, *Nat Genet*, **26,** 146-7.

Liu X, Zhou T, Kuriyama R and Erikson RL. (2004b). Molecular interactions of Polo-like-kinase 1 with the mitotic kinesin-like protein CHO1/MKLP-1, *J Cell Sci*, **117,** 3233-46.

Lo Celso C, Berta MA, Braun KM, Frye M, Lyle S, Zouboulis CC and Watt FM. (2008). Characterization of bipotential epidermal progenitors derived from human sebaceous gland: contrasting roles of c-Myc and beta-catenin, *Stem Cells*, **26,** 1241-52.

Lo Celso C, Prowse DM and Watt FM. (2004). Transient activation of beta-catenin signalling in adult mouse epidermis is sufficient to induce new hair follicles but continuous activation is required to maintain hair follicle tumours, *Development*, **131,** 1787-99.

Lobjois V, Benazeraf B, Bertrand N, Medevielle F and Pituello F. (2004). Specific regulation of cyclins D1 and D2 by FGF and Shh signaling coordinates cell cycle progression, patterning, and differentiation during early steps of spinal cord development, *Dev Biol*, **273,** 195-209.

Lobo NA, Shimono Y, Qian D and Clarke MF. (2007). The biology of cancer stem cells, *Annu Rev Cell Dev Biol*, **23,** 675-99.

Lobrich M and Jeggo PA. (2007). The impact of a negligent G2/M checkpoint on genomic instability and cancer induction, *Nat Rev Cancer*, **7,** 861-9.

Locke M, Heywood M, Fawell S and Mackenzie IC. (2005). Retention of intrinsic stem cell hierarchies in carcinoma-derived cell lines, *Cancer Res*, **65,** 8944-50.

Locker M, Agathocleous M, Amato MA, Parain K, Harris WA and Perron M. (2006). Hedgehog signaling and the retina: insights into the mechanisms controlling the proliferative properties of neural precursors, *Genes Dev*, **20,** 3036-48.

Lodish H, Berk A, Zipursky S, Matsudaira P, Baltimore D and Darnell J. (1999a). *DNA Replication, Repair, and Recombination. Molecular Cell Biology, pp 472. 4th ed.* WH Freeman: New York, NY.

Lodish H, Berk A, Zipursky S, Matsudaira P, Baltimore D and Darnell J. (1999b). *Regulation of the Eukaryotic Cell Cycle. Molecular Cell Biology, pp 496. 4th ed.* WH Freeman: New York, NY.

Lodygin D, Diebold J and Hermeking H. (2004). Prostate cancer is characterized by epigenetic silencing of 14-3-3sigma expression, *Oncogene*, **23,** 9034-41.

Lodygin D and Hermeking H. (2005). The role of epigenetic inactivation of 14-3-3sigma in human cancer, *Cell Res*, **15,** 237-46.

Lodygin D and Hermeking H. (2006). Epigenetic silencing of 14-3-3sigma in cancer, *Semin Cancer Biol*, **16,** 214-24.

Lodygin D, Yazdi AS, Sander CA, Herzinger T and Hermeking H. (2003). Analysis of 14-3-3sigma expression in hyperproliferative skin diseases reveals selective loss associated with CpG-methylation in basal cell carcinoma, *Oncogene*, **22,** 5519-24.

Loeffler M, Potten CS and Wichmann HE. (1987). Epidermal cell proliferation. II. A comprehensive mathematical model of cell proliferation and migration in the basal layer predicts some unusual properties of epidermal stem cells, *Virchows Arch B Cell Pathol Incl Mol Pathol*, **53,** 286-300.

Logan CY and Nusse R. (2004). The Wnt signaling pathway in development and disease, *Annu Rev Cell Dev Biol*, **20,** 781-810.

Louro ID, Bailey EC, Li X, South LS, McKie-Bell PR, Yoder BK, Huang CC, Johnson MR, Hill AE, Johnson RL and Ruppert JM. (2002). Comparative gene expression profile analysis of GLI and c-MYC in an epithelial model of malignant transformation, *Cancer Res*, **62,** 5867-73.

Lowry WE, Blanpain C, Nowak JA, Guasch G, Lewis L and Fuchs E. (2005). Defining the impact of beta-catenin/Tcf transactivation on epithelial stem cells, *Genes Dev*, **19,** 1596-611.

Lum L and Beachy PA. (2004). The Hedgehog response network: sensors, switches, and routers, *Science*, **304,** 1755-9.

Lum L, Zhang C, Oh S, Mann RK, von Kessler DP, Taipale J, Weis-Garcia F, Gong R, Wang B and Beachy PA. (2003). Hedgehog signal transduction via Smoothened association with a cytoplasmic complex scaffolded by the atypical kinesin, Costal-2, *Mol Cell*, **12,** 1261-74.

Lyle S, Christofidou-Solomidou M, Liu Y, Elder DE, Albelda S and Cotsarelis G. (1998). The C8/144B monoclonal antibody recognizes cytokeratin 15 and defines the location of human hair follicle stem cells, *J Cell Sci*, **111 (Pt 21),** 3179-88.

Lyle S, Christofidou-Solomidou M, Liu Y, Elder DE, Albelda S and Cotsarelis G. (1999). Human hair follicle bulge cells are biochemically distinct and possess an epithelial stem cell phenotype, *J Investig Dermatol Symp Proc*, **4,** 296-301.

Maccubbin AE, Przybyszewski J, Evans MS, Budzinski EE, Patrzyc HB, Kulesz-Martin M and Box HC. (1995). DNA damage in UVB-irradiated keratinocytes, *Carcinogenesis*, **16,** 1659-60.

MacDonald BT, Tamai K and He X. (2009). Wnt/beta-catenin signaling: components, mechanisms, and diseases, *Dev Cell*, **17,** 9-26.

Mackenzie IC. (1970). Relationship between mitosis and the ordered structure of the stratum corneum in mouse epidermis, *Nature*, **226,** 653-5.

Mackenzie IC. (1997). Retroviral transduction of murine epidermal stem cells demonstrates clonal units of epidermal structure, *J Invest Dermatol*, **109,** 377-83.

Mackenzie IC, Zimmerman K and Peterson L. (1981). The pattern of cellular organization of human epidermis, *J Invest Dermatol*, **76,** 459-61.

Mackenzie JC. (1969). Ordered structure of the stratum corneum of mammalian skin, *Nature*, **222,** 881-2.

Malanchi I, Peinado H, Kassen D, Hussenet T, Metzger D, Chambon P, Huber M, Hohl D, Cano A, Birchmeier W and Huelsken J. (2008). Cutaneous cancer stem cell maintenance is dependent on beta-catenin signalling, *Nature*, **452,** 650-3.

Malbon CC, Wang H and Moon RT. (2001). Wnt signaling and heterotrimeric G-proteins: strange bedfellows or a classic romance?, *Biochem Biophys Res Commun*, **287,** 589-93.

Maley CC. (2007). Multistage carcinogenesis in Barrett's esophagus, *Cancer Lett*, **245,** 22-32.

Maley CC, Galipeau PC, Li X, Sanchez CA, Paulson TG, Blount PL and Reid BJ. (2004). The combination of genetic instability and clonal expansion predicts progression to esophageal adenocarcinoma, *Cancer Res*, **64,** 7629-33.

Maltzman W and Czyzyk L. (1984). UV irradiation stimulates levels of p53 cellular tumor antigen in nontransformed mouse cells, *Mol Cell Biol*, **4,** 1689-94.

Mancuso M, Leonardi S, Tanori M, Pasquali E, Pierdomenico M, Rebessi S, Di Majo V, Covelli V, Pazzaglia S and Saran A. (2006). Hair cycle-dependent basal cell carcinoma tumorigenesis in Ptc1neo67/+ mice exposed to radiation, *Cancer Res*, **66,** 6606-14.

Mantel C, Braun SE, Reid S, Henegariu O, Liu L, Hangoc G and Broxmeyer HE. (1999). p21(cip-1/waf-1) deficiency causes deformed nuclear architecture, centriole overduplication, polyploidy, and relaxed microtubule damage checkpoints in human hematopoietic cells, *Blood*, **93,** 1390-8.

Mao B, Wu W, Davidson G, Marhold J, Li M, Mechler BM, Delius H, Hoppe D, Stannek P, Walter C, Glinka A and Niehrs C. (2002). Kremen proteins are

Dickkopf receptors that regulate Wnt/beta-catenin signalling, *Nature*, **417,** 664-7.

Mao X, Young BD, Chaplin T, Shipley J and Lu YJ. (2008). Subtle genomic alterations and genomic instability revealed in diploid cancer cell lines, *Cancer Lett*, **267,** 49-54.

Marchenko GN, Marchenko ND, Leng J and Strongin AY. (2002). Promoter characterization of the novel human matrix metalloproteinase-26 gene: regulation by the T-cell factor-4 implies specific expression of the gene in cancer cells of epithelial origin, *Biochem J*, **363,** 253-62.

Margolis RL. (2005). Tetraploidy and tumor development, *Cancer Cell*, **8,** 353-4.

Margolis RL, Lohez OD and Andreassen PR. (2003). G1 tetraploidy checkpoint and the suppression of tumorigenesis, *J Cell Biochem*, **88,** 673-83.

Marigo V and Tabin CJ. (1996). Regulation of patched by sonic hedgehog in the developing neural tube, *Proc Natl Acad Sci U S A*, **93,** 9346-51.

Marks R, Staples M and Giles GG. (1993). Trends in non-melanocytic skin cancer treated in Australia: the second national survey, *Int J Cancer*, **53,** 585-90.

Marlow F, Topczewski J, Sepich D and Solnica-Krezel L. (2002). Zebrafish Rho kinase 2 acts downstream of Wnt11 to mediate cell polarity and effective convergence and extension movements, *Curr Biol*, **12,** 876-84.

Martin BM. (1994). *Tissue Culture Techniques: An introduction*. Birkhauser Boston.

Martin SJ, Reutelingsperger CP, McGahon AJ, Rader JA, van Schie RC, LaFace DM and Green DR. (1995). Early redistribution of plasma membrane phosphatidylserine is a general feature of apoptosis regardless of the initiating stimulus: inhibition by overexpression of Bcl-2 and Abl, *J Exp Med*, **182,** 1545-56.

Massague J. (2004). G1 cell-cycle control and cancer, *Nature*, **432,** 298-306.

Masui S, Nakatake Y, Toyooka Y, Shimosato D, Yagi R, Takahashi K, Okochi H, Okuda A, Matoba R, Sharov AA, Ko MS and Niwa H. (2007). Pluripotency governed by Sox2 via regulation of Oct3/4 expression in mouse embryonic stem cells, *Nat Cell Biol*, **9,** 625-35.

Matise MP, Epstein DJ, Park HL, Platt KA and Joyner AL. (1998). Gli2 is required for induction of floor plate and adjacent cells, but not most ventral neurons in the mouse central nervous system, *Development*, **125,** 2759-70.

Matise MP and Joyner AL. (1999). Gli genes in development and cancer, *Oncogene*, **18,** 7852-9.

Matsumoto N, Fujimoto M, Kato R and Niikawa N. (1996). Assignment of the human GLI2 gene to 2q14 by fluorescence in situ hybridization, *Genomics*, **36,** 220-1.

Matsumoto Y, Hayashi K and Nishida E. (1999). Cyclin-dependent kinase 2 (Cdk2) is required for centrosome duplication in mammalian cells, *Curr Biol*, **9,** 429-32.

Mayer VW and Aguilera A. (1990). High levels of chromosome instability in polyploids of Saccharomyces cerevisiae, *Mutat Res*, **231,** 177-86.

Mazumdar M, Lee JH, Sengupta K, Ried T, Rane S and Misteli T. (2006). Tumor formation via loss of a molecular motor protein, *Curr Biol*, **16,** 1559-64.

McArdle JP, Roff BT, Muller HK and Murphy WH. (1984). The basal lamina in basal cell carcinoma, Bowen's disease, squamous cell carcinoma and keratoacanthoma: an immunoperoxidase study using an antibody to type IV collagen, *Pathology*, **16,** 67-72.

McCabe MT, Davis JN and Day ML. (2005). Regulation of DNA methyltransferase 1 by the pRb/E2F1 pathway, *Cancer Res*, **65,** 3624-32.

McCrea PD and Gumbiner BM. (1991). Purification of a 92-kDa cytoplasmic protein tightly associated with the cell-cell adhesion molecule E-cadherin (uvomorulin). Characterization and extractability of the protein complex from the cell cytostructure, *J Biol Chem*, **266,** 4514-20.

McCrea PD, Turck CW and Gumbiner B. (1991). A homolog of the armadillo protein in Drosophila (plakoglobin) associated with E-cadherin, *Science*, **254,** 1359-61.

McEwen DG and Peifer M. (2000). Wnt signaling: Moving in a new direction, *Curr Biol*, **10,** R562-4.

McNeil N and Ried T. (2000). Novel molecular cytogenetic techniques for identifying complex chromosomal rearrangements: technology and applications in molecular medicine, *Expert Rev Mol Med*, **2000,** 1-14.

Medina D. (2002). Biological and molecular characteristics of the premalignant mouse mammary gland, *Biochim Biophys Acta*, **1603,** 1-9.

Mendoza M and Barral Y. (2008). Co-ordination of cytokinesis with chromosome segregation, *Biochem Soc Trans*, **36,** 387-90.

Meng X, Poon R, Zhang X, Cheah A, Ding Q, Hui CC and Alman B. (2001). Suppressor of fused negatively regulates beta-catenin signaling, *J Biol Chem*, **276,** 40113-9.

Menon GK, Grayson S and Elias PM. (1985). Ionic calcium reservoirs in mammalian epidermis: ultrastructural localization by ion-capture cytochemistry, *J Invest Dermatol*, **84,** 508-12.

Meraldi P, Honda R and Nigg EA. (2002). Aurora-A overexpression reveals tetraploidization as a major route to centrosome amplification in p53-/- cells, *Embo J*, **21,** 483-92.

Meraldi P, Honda R and Nigg EA. (2004). Aurora kinases link chromosome segregation and cell division to cancer susceptibility, *Curr Opin Genet Dev*, **14,** 29-36.

Merchant M, Evangelista M, Luoh SM, Frantz GD, Chalasani S, Carano RA, van Hoy M, Ramirez J, Ogasawara AK, McFarland LM, Filvaroff EH, French DM and de Sauvage FJ. (2005). Loss of the serine/threonine kinase fused results in postnatal growth defects and lethality due to progressive hydrocephalus, *Mol Cell Biol*, **25,** 7054-68.

Merchant M, Vajdos FF, Ultsch M, Maun HR, Wendt U, Cannon J, Desmarais W, Lazarus RA, de Vos AM and de Sauvage FJ. (2004). Suppressor of fused regulates Gli activity through a dual binding mechanism, *Mol Cell Biol*, **24,** 8627-41.

Merok JR, Lansita JA, Tunstead JR and Sherley JL. (2002). Cosegregation of chromosomes containing immortal DNA strands in cells that cycle with asymmetric stem cell kinetics, *Cancer Res*, **62,** 6791-5.

Methot N and Basler K. (1999). Hedgehog controls limb development by regulating the activities of distinct transcriptional activator and repressor forms of Cubitus interruptus, *Cell*, **96,** 819-31.

Methot N and Basler K. (2000). Suppressor of fused opposes hedgehog signal transduction by impeding nuclear accumulation of the activator form of Cubitus interruptus, *Development*, **127,** 4001-10.

Methot N and Basler K. (2001). An absolute requirement for Cubitus interruptus in Hedgehog signaling, *Development*, **128,** 733-42.

Mhawech P, Benz A, Cerato C, Greloz V, Assaly M, Desmond JC, Koeffler HP, Lodygin D, Hermeking H, Herrmann F and Schwaller J. (2005). Downregulation of 14-3-3sigma in ovary, prostate and endometrial carcinomas is associated with CpG island methylation, *Mod Pathol*, **18,** 340-8.

Mikels AJ and Nusse R. (2006a). Purified Wnt5a protein activates or inhibits beta-catenin-TCF signaling depending on receptor context, *PLoS Biol*, **4,** e115.
Mikels AJ and Nusse R. (2006b). Wnts as ligands: processing, secretion and reception, *Oncogene*, **25,** 7461-8.
Mill P, Mo R, Fu H, Grachtchouk M, Kim PC, Dlugosz AA and Hui CC. (2003). Sonic hedgehog-dependent activation of Gli2 is essential for embryonic hair follicle development, *Genes Dev*, **17,** 282-94.
Millar SE. (2002). Molecular mechanisms regulating hair follicle development, *J Invest Dermatol*, **118,** 216-25.
Miller AD and Chen F. (1996). Retrovirus packaging cells based on 10A1 murine leukemia virus for production of vectors that use multiple receptors for cell entry, *J Virol*, **70,** 5564-71.
Miller DL and Weinstock MA. (1994). Nonmelanoma skin cancer in the United States: incidence, *J Am Acad Dermatol*, **30,** 774-8.
Miller JR, Hocking AM, Brown JD and Moon RT. (1999). Mechanism and function of signal transduction by the Wnt/beta-catenin and Wnt/Ca2+ pathways, *Oncogene*, **18,** 7860-72.
Miller SJ. (1991a). Biology of basal cell carcinoma (Part I), *J Am Acad Dermatol*, **24,** 1-13.
Miller SJ. (1991b). Biology of basal cell carcinoma (Part II), *J Am Acad Dermatol*, **24,** 161-75.
Ming JE, Roessler E and Muenke M. (1998). Human developmental disorders and the Sonic hedgehog pathway, *Mol Med Today*, **4,** 343-9.
Minn AJ, Boise LH and Thompson CB. (1996). Expression of Bcl-xL and loss of p53 can cooperate to overcome a cell cycle checkpoint induced by mitotic spindle damage, *Genes Dev*, **10,** 2621-31.
Missero C, Calautti E, Eckner R, Chin J, Tsai LH, Livingston DM and Dotto GP. (1995). Involvement of the cell-cycle inhibitor Cip1/WAF1 and the E1A-associated p300 protein in terminal differentiation, *Proc Natl Acad Sci U S A*, **92,** 5451-5.
Missero C, Di Cunto F, Kiyokawa H, Koff A and Dotto GP. (1996). The absence of p21Cip1/WAF1 alters keratinocyte growth and differentiation and promotes ras-tumor progression, *Genes Dev*, **10,** 3065-75.
Mitelman F, Johansson B and Mertens F. (2003). Mitelman Database of Chromosomes Aberrations in Cancer. http://cgap.nci.gov/Chromosomes/Mitelman.
Mitelman F, Johansson B and Mertens F. (2007). The impact of translocations and gene fusions on cancer causation, *Nat Rev Cancer*, **7,** 233-45.
Mizejewski GJ. (1999). Role of integrins in cancer: survey of expression patterns, *Proc Soc Exp Biol Med*, **222,** 124-38.
Mo R, Freer AM, Zinyk DL, Crackower MA, Michaud J, Heng HH, Chik KW, Shi XM, Tsui LC, Cheng SH, Joyner AL and Hui C. (1997). Specific and redundant functions of Gli2 and Gli3 zinc finger genes in skeletal patterning and development, *Development*, **124,** 113-23.
Molenaar M, van de Wetering M, Oosterwegel M, Peterson-Maduro J, Godsave S, Korinek V, Roose J, Destree O and Clevers H. (1996). XTcf-3 transcription factor mediates beta-catenin-induced axis formation in Xenopus embryos, *Cell*, **86,** 391-9.
Monnier V, Dussillol F, Alves G, Lamour-Isnard C and Plessis A. (1998). Suppressor of fused links fused and Cubitus interruptus on the hedgehog signalling pathway, *Curr Biol*, **8,** 583-6.

Monzo M, Moreno I, Artells R, Ibeas R, Navarro A, Moreno J, Hernandez R, Granell M and Pie J. (2006). Sonic hedgehog mRNA expression by real-time quantitative PCR in normal and tumor tissues from colorectal cancer patients, *Cancer Lett*, **233,** 117-23.

Moreno-Bueno G, Gamallo C, Perez-Gallego L, Contreras F and Palacios J. (2001). beta-catenin expression in pilomatrixomas. Relationship with beta-catenin gene mutations and comparison with beta-catenin expression in normal hair follicles, *Br J Dermatol*, **145,** 576-81.

Morin PJ, Sparks AB, Korinek V, Barker N, Clevers H, Vogelstein B and Kinzler KW. (1997). Activation of beta-catenin-Tcf signaling in colon cancer by mutations in beta-catenin or APC, *Science*, **275,** 1787-90.

Morris RJ. (2000). Keratinocyte stem cells: targets for cutaneous carcinogens, *J Clin Invest*, **106,** 3-8.

Morris RJ, Coulter K, Tryson K and Steinberg SR. (1997). Evidence that cutaneous carcinogen-initiated epithelial cells from mice are quiescent rather than actively cycling, *Cancer Res*, **57,** 3436-43.

Morris RJ, Fischer SM, Klein-Szanto AJ and Slaga TJ. (1990). Subpopulations of primary adult murine epidermal basal cells sedimented on density gradients, *Cell Tissue Kinet*, **23,** 587-602.

Morris RJ, Fischer SM and Slaga TJ. (1986). Evidence that a slowly cycling subpopulation of adult murine epidermal cells retains carcinogen, *Cancer Res*, **46,** 3061-6.

Morris RJ, Liu Y, Marles L, Yang Z, Trempus C, Li S, Lin JS, Sawicki JA and Cotsarelis G. (2004). Capturing and profiling adult hair follicle stem cells, *Nat Biotechnol*, **22,** 411-7.

Morris RJ and Potten CS. (1994). Slowly cycling (label-retaining) epidermal cells behave like clonogenic stem cells in vitro, *Cell Prolif*, **27,** 279-89.

Morris RJ and Potten CS. (1999). Highly persistent label-retaining cells in the hair follicles of mice and their fate following induction of anagen, *J Invest Dermatol*, **112,** 470-5.

Morris RJ, Tryson KA and Wu KQ. (2000). Evidence that the epidermal targets of carcinogen action are found in the interfollicular epidermis of infundibulum as well as in the hair follicles, *Cancer Res*, **60,** 226-9.

Mosmann T. (1983). Rapid colorimetric assay for cellular growth and survival: application to proliferation and cytotoxicity assays, *J Immunol Methods*, **65,** 55-63.

Motoyama J, Heng H, Crackower MA, Takabatake T, Takeshima K, Tsui LC and Hui C. (1998a). Overlapping and non-overlapping Ptch2 expression with Shh during mouse embryogenesis, *Mech Dev*, **78,** 81-4.

Motoyama J, Liu J, Mo R, Ding Q, Post M and Hui CC. (1998b). Essential function of Gli2 and Gli3 in the formation of lung, trachea and oesophagus, *Nat Genet*, **20,** 54-7.

Muffler S, Stark HJ, Amoros M, Falkowska-Hansen B, Boehnke K, Buhring HJ, Marme A, Bickenbach JR and Boukamp P. (2008). A stable niche supports long-term maintenance of human epidermal stem cells in organotypic cultures, *Stem Cells*, **26,** 2506-15.

Mufson RA, Steinberg ML and Defendi V. (1982). Effects of 12-O-tetradecanoylphorbol-13-acetate on the differentiation of simian virus 40-infected human keratinocytes, *Cancer Res*, **42,** 4600-5.

Mullor JL, Dahmane N, Sun T and Ruiz i Altaba A. (2001). Wnt signals are targets and mediators of Gli function, *Curr Biol*, **11,** 769-73.
Mullor JL, Sanchez P and Altaba AR. (2002). Pathways and consequences: Hedgehog signaling in human disease, *Trends Cell Biol*, **12,** 562-9.
Murone M, Luoh SM, Stone D, Li W, Gurney A, Armanini M, Grey C, Rosenthal A and de Sauvage FJ. (2000). Gli regulation by the opposing activities of fused and suppressor of fused, *Nat Cell Biol*, **2,** 310-2.
Murphy GF, Flynn TC, Rice RH and Pinkus GS. (1984). Involucrin expression in normal and neoplastic human skin: a marker for keratinocyte differentiation, *J Invest Dermatol*, **82,** 453-7.
Murray AW. (1992). Creative blocks: cell-cycle checkpoints and feedback controls, *Nature*, **359,** 599-604.
Musacchio A and Hardwick KG. (2002). The spindle checkpoint: structural insights into dynamic signalling, *Nat Rev Mol Cell Biol*, **3,** 731-41.
Nagase H and Woessner JF, Jr. (1999). Matrix metalloproteinases, *J Biol Chem*, **274,** 21491-4.
Nahabedian MY. (2008). Skin malignancies, Basal Cell Carcinoma. eMedicine from webMD.
Nakano Y, Guerrero I, Hidalgo A, Taylor A, Whittle JR and Ingham PW. (1989). A protein with several possible membrane-spanning domains encoded by the Drosophila segment polarity gene patched, *Nature*, **341,** 508-13.
Nambiar M, Kari V and Raghavan SC. (2008). Chromosomal translocations in cancer, *Biochim Biophys Acta*, **1786,** 139-52.
Nazmi MN, Dykes PJ and Marks R. (1990). Epidermal growth factor receptors in human epidermal tumours, *Br J Dermatol*, **123,** 153-61.
Neef R, Preisinger C, Sutcliffe J, Kopajtich R, Nigg EA, Mayer TU and Barr FA. (2003). Phosphorylation of mitotic kinesin-like protein 2 by polo-like kinase 1 is required for cytokinesis, *J Cell Biol*, **162,** 863-75.
Negrini S, Gorgoulis VG and Halazonetis TD. (2010). Genomic instability - an evolving hallmark of cancer, *Nat Rev Mol Cell Biol*, **11,** 220-8.
Neill GW, Harrison WJ, Ikram MS, Williams TD, Bianchi LS, Nadendla SK, Green JL, Ghali L, Frischauf AM, O'Toole EA, Aberger F and Philpott MP. (2008). GLI1 repression of ERK activity correlates with colony formation and impaired migration in human epidermal keratinocytes, *Carcinogenesis*, **29,** 738-46.
Nelson DA, Tan TT, Rabson AB, Anderson D, Degenhardt K and White E. (2004). Hypoxia and defective apoptosis drive genomic instability and tumorigenesis, *Genes Dev*, **18,** 2095-107.
Nelson WJ and Nusse R. (2004). Convergence of Wnt, beta-catenin, and cadherin pathways, *Science*, **303,** 1483-7.
Nicholson LJ and Watt FM. (1991). Decreased expression of fibronectin and the alpha 5 beta 1 integrin during terminal differentiation of human keratinocytes, *J Cell Sci*, **98 (Pt 2),** 225-32.
Nicolas M, Wolfer A, Raj K, Kummer JA, Mill P, van Noort M, Hui CC, Clevers H, Dotto GP and Radtke F. (2003). Notch1 functions as a tumor suppressor in mouse skin, *Nat Genet*, **33,** 416-21.
Niemann C, Owens DM, Hulsken J, Birchmeier W and Watt FM. (2002). Expression of DeltaNLef1 in mouse epidermis results in differentiation of hair follicles into squamous epidermal cysts and formation of skin tumours, *Development*, **129,** 95-109.

Niemann C, Unden AB, Lyle S, Zouboulis Ch C, Toftgard R and Watt FM. (2003). Indian hedgehog and beta-catenin signaling: role in the sebaceous lineage of normal and neoplastic mammalian epidermis, *Proc Natl Acad Sci U S A*, **100 Suppl 1,** 11873-80.

Niemann C and Watt FM. (2002). Designer skin: lineage commitment in postnatal epidermis, *Trends Cell Biol*, **12,** 185-92.

Nieto MA. (2002). The snail superfamily of zinc-finger transcription factors, *Nat Rev Mol Cell Biol*, **3,** 155-66.

Nievers MG, Schaapveld RQ and Sonnenberg A. (1999). Biology and function of hemidesmosomes, *Matrix Biol*, **18,** 5-17.

Nigg EA. (2002). Centrosome aberrations: cause or consequence of cancer progression?, *Nat Rev Cancer*, **2,** 815-25.

Nikaido M, Tada M, Takeda H, Kuroiwa A and Ueno N. (1999). In vivo analysis using variants of zebrafish BMPR-IA: range of action and involvement of BMP in ectoderm patterning, *Development*, **126,** 181-90.

Nilsson M, Unden AB, Krause D, Malmqwist U, Raza K, Zaphiropoulos PG and Toftgard R. (2000). Induction of basal cell carcinomas and trichoepitheliomas in mice overexpressing GLI-1, *Proc Natl Acad Sci U S A*, **97,** 3438-43.

Nishisho I, Nakamura Y, Miyoshi Y, Miki Y, Ando H, Horii A, Koyama K, Utsunomiya J, Baba S and Hedge P. (1991). Mutations of chromosome 5q21 genes in FAP and colorectal cancer patients, *Science*, **253,** 665-9.

Niwa H. (2007). How is pluripotency determined and maintained?, *Development*, **134,** 635-46.

Noordermeer J, Klingensmith J, Perrimon N and Nusse R. (1994). dishevelled and armadillo act in the wingless signalling pathway in Drosophila, *Nature*, **367,** 80-3.

Noselli S and Agnes F. (1999). Roles of the JNK signaling pathway in Drosophila morphogenesis, *Curr Opin Genet Dev*, **9,** 466-72.

Nowak MA, Komarova NL, Sengupta A, Jallepalli PV, Shih Ie M, Vogelstein B and Lengauer C. (2002). The role of chromosomal instability in tumor initiation, *Proc Natl Acad Sci U S A*, **99,** 16226-31.

Nowell PC. (1976). The clonal evolution of tumor cell populations, *Science*, **194,** 23-8.

Nusse R. (2005). Wnt signaling in disease and in development, *Cell Res*, **15,** 28-32.

Nusse R, Fuerer C, Ching W, Harnish K, Logan C, Zeng A, ten Berge D and Kalani Y. (2008). Wnt signaling and stem cell control, *Cold Spring Harb Symp Quant Biol*, **73,** 59-66.

Nusse R and Varmus HE. (1982). Many tumors induced by the mouse mammary tumor virus contain a provirus integrated in the same region of the host genome, *Cell*, **31,** 99-109.

Nusslein-Volhard C and Wieschaus E. (1980). Mutations affecting segment number and polarity in Drosophila, *Nature*, **287,** 795-801.

O'Driscoll L, McMorrow J, Doolan P, McKiernan E, Mehta JP, Ryan E, Gammell P, Joyce H, O'Donovan N, Walsh N and Clynes M. (2006). Investigation of the molecular profile of basal cell carcinoma using whole genome microarrays, *Mol Cancer*, **5,** 74.

O'Keefe EJ, Woodley D, Castillo G, Russell N and Payne RE, Jr. (1984). Production of soluble and cell-associated fibronectin by cultured keratinocytes, *J Invest Dermatol*, **82,** 150-5.

Oguchi M, Kobayasi T and Asboe-Hansen G. (1985). Secretion of type IV collagen by keratinocytes of human adult, *J Invest Dermatol*, **85,** 79-81.

Ohlmeyer JT and Kalderon D. (1998). Hedgehog stimulates maturation of Cubitus interruptus into a labile transcriptional activator, *Nature*, **396,** 749-53.

Ohta M, Tateishi K, Kanai F, Watabe H, Kondo S, Guleng B, Tanaka Y, Asaoka Y, Jazag A, Imamura J, Ijichi H, Ikenoue T, Sata M, Miyagishi M, Taira K, Tada M, Kawabe T and Omata M. (2005). p53-Independent negative regulation of p21/cyclin-dependent kinase-interacting protein 1 by the sonic hedgehog-glioma-associated oncogene 1 pathway in gastric carcinoma cells, *Cancer Res*, **65,** 10822-9.

Ojeh NO, Frame JD and Navsaria HA. (2001). In vitro characterization of an artificial dermal scaffold, *Tissue Eng*, **7,** 457-72.

Okamoto E and Kitano Y. (1993). Expression of basement membrane components in skin equivalents--influence of dermal fibroblasts, *J Dermatol Sci*, **5,** 81-8.

Okubo T, Pevny LH and Hogan BL. (2006). Sox2 is required for development of taste bud sensory cells, *Genes Dev*, **20,** 2654-9.

Olaharski AJ, Sotelo R, Solorza-Luna G, Gonsebatt ME, Guzman P, Mohar A and Eastmond DA. (2006). Tetraploidy and chromosomal instability are early events during cervical carcinogenesis, *Carcinogenesis*, **27,** 337-43.

Olive PL, Banath JP and Durand RE. (1996). Development of apoptosis and polyploidy in human lymphoblast cells as a function of position in the cell cycle at the time of irradiation, *Radiat Res*, **146,** 595-602.

Olmeda D, Castel S, Vilaro S and Cano A. (2003). Beta-catenin regulation during the cell cycle: implications in G2/M and apoptosis, *Mol Biol Cell*, **14,** 2844-60.

Oniscu A, James RM, Morris RG, Bader S, Malcomson RD and Harrison DJ. (2004). Expression of Sonic hedgehog pathway genes is altered in colonic neoplasia, *J Pathol*, **203,** 909-17.

Opferman JT. (2008). Apoptosis in the development of the immune system, *Cell Death Differ*, **15,** 234-42.

Orenic TV, Slusarski DC, Kroll KL and Holmgren RA. (1990). Cloning and characterization of the segment polarity gene cubitus interruptus Dominant of Drosophila, *Genes Dev*, **4,** 1053-67.

Ornitz DM, Hammer RE, Messing A, Palmiter RD and Brinster RL. (1987). Pancreatic neoplasia induced by SV40 T-antigen expression in acinar cells of transgenic mice, *Science*, **238,** 188-93.

Oro AE and Higgins K. (2003). Hair cycle regulation of Hedgehog signal reception, *Dev Biol*, **255,** 238-48.

Oro AE, Higgins KM, Hu Z, Bonifas JM, Epstein EH, Jr. and Scott MP. (1997). Basal cell carcinomas in mice overexpressing sonic hedgehog, *Science*, **276,** 817-21.

Oshima H, Rochat A, Kedzia C, Kobayashi K and Barrandon Y. (2001). Morphogenesis and renewal of hair follicles from adult multipotent stem cells, *Cell*, **104,** 233-45.

Oskarsson T, Essers MA, Dubois N, Offner S, Dubey C, Roger C, Metzger D, Chambon P, Hummler E, Beard P and Trumpp A. (2006). Skin epidermis lacking the c-Myc gene is resistant to Ras-driven tumorigenesis but can reacquire sensitivity upon additional loss of the p21Cip1 gene, *Genes Dev*, **20,** 2024-9.

Owens DM and Watt FM. (2003). Contribution of stem cells and differentiated cells to epidermal tumours, *Nat Rev Cancer*, **3,** 444-51.

Page-McCaw A, Ewald AJ and Werb Z. (2007). Matrix metalloproteinases and the regulation of tissue remodelling, *Nat Rev Mol Cell Biol*, **8,** 221-33.

Palma V and Ruiz i Altaba A. (2004). Hedgehog-GLI signaling regulates the behavior of cells with stem cell properties in the developing neocortex, *Development*, **131,** 337-45.
Pan Y, Bai CB, Joyner AL and Wang B. (2006). Sonic hedgehog signaling regulates Gli2 transcriptional activity by suppressing its processing and degradation, *Mol Cell Biol*, **26,** 3365-77.
Pan Y and Wang B. (2007). A novel protein-processing domain in Gli2 and Gli3 differentially blocks complete protein degradation by the proteasome, *J Biol Chem*, **282,** 10846-52.
Paquin C and Adams J. (1983). Frequency of fixation of adaptive mutations is higher in evolving diploid than haploid yeast populations, *Nature*, **302,** 495-500.
Parisi MJ and Lin H. (1998). The role of the hedgehog/patched signaling pathway in epithelial stem cell proliferation: from fly to human, *Cell Res*, **8,** 15-21.
Park HL, Bai C, Platt KA, Matise MP, Beeghly A, Hui CC, Nakashima M and Joyner AL. (2000). Mouse Gli1 mutants are viable but have defects in SHH signaling in combination with a Gli2 mutation, *Development*, **127,** 1593-605.
Park JI, Venteicher AS, Hong JY, Choi J, Jun S, Shkreli M, Chang W, Meng Z, Cheung P, Ji H, McLaughlin M, Veenstra TD, Nusse R, McCrea PD and Artandi SE. (2009). Telomerase modulates Wnt signalling by association with target gene chromatin, *Nature*, **460,** 66-72.
Parkinson EK, Al-Yaman FM and Appleby MW. (1987). The effect of donor age on the proliferative response of human and mouse keratinocytes to phorbol, 12-myristate, 13-acetate, *Carcinogenesis*, **8,** 907-12.
Parkinson EK and Emmerson A. (1982). The effects of tumour promoters on the multiplication and morphology of cultured human epidermal keratinocytes, *Carcinogenesis*, **3,** 525-31.
Parkinson EK, Grabham P and Emmerson A. (1983). A subpopulation of cultured human keratinocytes which is resistant to the induction of terminal differentiation-related changes by phorbol, 12-myristate, 13-acetate: evidence for an increase in the resistant population following transformation, *Carcinogenesis*, **4,** 857-61.
Pasca di Magliano M and Hebrok M. (2003). Hedgehog signalling in cancer formation and maintenance, *Nat Rev Cancer*, **3,** 903-11.
Patel D, Incassati A, Wang N and McCance DJ. (2004). Human papillomavirus type 16 E6 and E7 cause polyploidy in human keratinocytes and up-regulation of G2-M-phase proteins, *Cancer Res*, **64,** 1299-306.
Pathi S, Pagan-Westphal S, Baker DP, Garber EA, Rayhorn P, Bumcrot D, Tabin CJ, Blake Pepinsky R and Williams KP. (2001). Comparative biological responses to human Sonic, Indian, and Desert hedgehog, *Mech Dev*, **106,** 107-17.
Paulovich AG, Toczyski DP and Hartwell LH. (1997). When checkpoints fail, *Cell*, **88,** 315-21.
Pavletich NP and Pabo CO. (1993). Crystal structure of a five-finger GLI-DNA complex: new perspectives on zinc fingers, *Science*, **261,** 1701-7.
Pearse RV, 2nd, Collier LS, Scott MP and Tabin CJ. (1999). Vertebrate homologs of Drosophila suppressor of fused interact with the gli family of transcriptional regulators, *Dev Biol*, **212,** 323-36.
Pecina-Slaus N. (2003). Tumor suppressor gene E-cadherin and its role in normal and malignant cells, *Cancer Cell Int*, **3,** 17.
Peifer M, McCrea PD, Green KJ, Wieschaus E and Gumbiner BM. (1992). The vertebrate adhesive junction proteins beta-catenin and plakoglobin and the

Drosophila segment polarity gene armadillo form a multigene family with similar properties, *J Cell Biol*, **118,** 681-91.
Peifer M and McEwen DG. (2002). The ballet of morphogenesis: unveiling the hidden choreographers, *Cell*, **109,** 271-4.
Pelengaris S, Littlewood T, Khan M, Elia G and Evan G. (1999). Reversible activation of c-Myc in skin: induction of a complex neoplastic phenotype by a single oncogenic lesion, *Mol Cell*, **3,** 565-77.
Pellman D. (2007). Cell biology: aneuploidy and cancer, *Nature*, **446,** 38-9.
Peltonen J, Larjava H, Jaakkola S, Gralnick H, Akiyama SK, Yamada SS, Yamada KM and Uitto J. (1989). Localization of integrin receptors for fibronectin, collagen, and laminin in human skin. Variable expression in basal and squamous cell carcinomas, *J Clin Invest*, **84,** 1916-23.
Pentel M, Helm KF and Maloney MM. (1995). Cell surface molecules in basal cell carcinomas, *Dermatol Surg*, **21,** 858-61.
Perez-Losada J and Balmain A. (2003). Stem-cell hierarchy in skin cancer, *Nat Rev Cancer*, **3,** 434-43.
Perez-Ordonez B, Beauchemin M and Jordan RC. (2006). Molecular biology of squamous cell carcinoma of the head and neck, *J Clin Pathol*, **59,** 445-53.
Perrimon N, Engstrom L and Mahowald AP. (1989). Zygotic lethals with specific maternal effect phenotypes in Drosophila melanogaster. I. Loci on the X chromosome, *Genetics*, **121,** 333-52.
Perrone L, Pasca di Magliano M, Zannini M and Di Lauro R. (2000). The thyroid transcription factor 2 (TTF-2) is a promoter-specific DNA-binding independent transcriptional repressor, *Biochem Biophys Res Commun*, **275,** 203-8.
Petretti C, Savoian M, Montembault E, Glover DM, Prigent C and Giet R. (2006). The PITSLRE/CDK11p58 protein kinase promotes centrosome maturation and bipolar spindle formation, *EMBO Rep*, **7,** 418-24.
Pevny LH and Lovell-Badge R. (1997). Sox genes find their feet, *Curr Opin Genet Dev*, **7,** 338-44.
Philipp J, Vo K, Gurley KE, Seidel K and Kemp CJ. (1999). Tumor suppression by p27Kip1 and p21Cip1 during chemically induced skin carcinogenesis, *Oncogene*, **18,** 4689-98.
Piepenburg O, Vorbruggen G and Jackle H. (2000). Drosophila segment borders result from unilateral repression of hedgehog activity by wingless signaling, *Mol Cell*, **6,** 203-9.
Pihan GA, Purohit A, Wallace J, Knecht H, Woda B, Quesenberry P and Doxsey SJ. (1998). Centrosome defects and genetic instability in malignant tumors, *Cancer Res*, **58,** 3974-85.
Pihan GA, Purohit A, Wallace J, Malhotra R, Liotta L and Doxsey SJ. (2001). Centrosome defects can account for cellular and genetic changes that characterize prostate cancer progression, *Cancer Res*, **61,** 2212-9.
Pihan GA, Wallace J, Zhou Y and Doxsey SJ. (2003). Centrosome abnormalities and chromosome instability occur together in pre-invasive carcinomas, *Cancer Res*, **63,** 1398-404.
Pillai S, Bikle DD, Mancianti ML, Cline P and Hincenbergs M. (1990). Calcium regulation of growth and differentiation of normal human keratinocytes: modulation of differentiation competence by stages of growth and extracellular calcium, *J Cell Physiol*, **143,** 294-302.
Pizarro A. (2000). E-cadherin expression in basal cell carcinoma: association with local invasiveness but not with metastatic inefficiency, *J Cutan Pathol*, **27,** 479-80.

Pizarro A, Benito N, Navarro P, Palacios J, Cano A, Quintanilla M, Contreras F and Gamallo C. (1994). E-cadherin expression in basal cell carcinoma, *Br J Cancer*, **69,** 157-62.

Pizarro A, Gamallo C, Benito N, Palacios J, Quintanilla M, Cano A and Contreras F. (1995). Differential patterns of placental and epithelial cadherin expression in basal cell carcinoma and in the epidermis overlying tumours, *Br J Cancer*, **72,** 327-32.

Pokutta S, Herrenknecht K, Kemler R and Engel J. (1994). Conformational changes of the recombinant extracellular domain of E-cadherin upon calcium binding, *Eur J Biochem*, **223,** 1019-26.

Polakis P. (1999). The oncogenic activation of beta-catenin, *Curr Opin Genet Dev*, **9,** 15-21.

Polakis P. (2000). Wnt signaling and cancer, *Genes Dev*, **14,** 1837-51.

Polakis P. (2007). The many ways of Wnt in cancer, *Curr Opin Genet Dev*, **17,** 45-51.

Ponten F, Berg C, Ahmadian A, Ren ZP, Nister M, Lundeberg J, Uhlen M and Ponten J. (1997). Molecular pathology in basal cell cancer with p53 as a genetic marker, *Oncogene*, **15,** 1059-67.

Potten CS. (1974). The epidermal proliferative unit: the possible role of the central basal cell, *Cell Tissue Kinet*, **7,** 77-88.

Potten CS and Booth C. (2002). Keratinocyte stem cells: a commentary, *J Invest Dermatol*, **119,** 888-99.

Potten CS and Hendry JH. (1973). Letter: Clonogenic cells and stem cells in epidermis, *Int J Radiat Biol Relat Stud Phys Chem Med*, **24,** 537-40.

Potten CS, Hume WJ, Reid P and Cairns J. (1978). The segregation of DNA in epithelial stem cells, *Cell*, **15,** 899-906.

Potten CS and Morris RJ. (1988). Epithelial stem cells in vivo, *J Cell Sci Suppl*, **10,** 45-62.

Potten CS, Owen G and Booth D. (2002). Intestinal stem cells protect their genome by selective segregation of template DNA strands, *J Cell Sci*, **115,** 2381-8.

Potten CS, Wichmann HE, Loeffler M, Dobek K and Major D. (1982). Evidence for discrete cell kinetic subpopulations in mouse epidermis based on mathematical analysis, *Cell Tissue Kinet*, **15,** 305-29.

Preat T. (1992). Characterization of Suppressor of fused, a complete suppressor of the fused segment polarity gene of Drosophila melanogaster, *Genetics*, **132,** 725-36.

Preat T, Therond P, Lamour-Isnard C, Limbourg-Bouchon B, Tricoire H, Erk I, Mariol MC and Busson D. (1990). A putative serine/threonine protein kinase encoded by the segment-polarity fused gene of Drosophila, *Nature*, **347,** 87-9.

Pyronnet S, Dostie J and Sonenberg N. (2001). Suppression of cap-dependent translation in mitosis, *Genes Dev*, **15,** 2083-93.

Qualtrough D, Buda A, Gaffield W, Williams AC and Paraskeva C. (2004). Hedgehog signalling in colorectal tumour cells: induction of apoptosis with cyclopamine treatment, *Int J Cancer*, **110,** 831-7.

Que J, Okubo T, Goldenring JR, Nam KT, Kurotani R, Morrisey EE, Taranova O, Pevny LH and Hogan BL. (2007). Multiple dose-dependent roles for Sox2 in the patterning and differentiation of anterior foregut endoderm, *Development*, **134,** 2521-31.

Quignon F, Rozier L, Lachages AM, Bieth A, Simili M and Debatisse M. (2007). Sustained mitotic block elicits DNA breaks: one-step alteration of ploidy and chromosome integrity in mammalian cells, *Oncogene*, **26,** 165-72.

Quintana E, Shackleton M, Sabel MS, Fullen DR, Johnson TM and Morrison SJ. (2008). Efficient tumour formation by single human melanoma cells, *Nature*, **456,** 593-8.

Quintyne NJ, Reing JE, Hoffelder DR, Gollin SM and Saunders WS. (2005). Spindle multipolarity is prevented by centrosomal clustering, *Science*, **307,** 127-9.

Radisky DC. (2005). Epithelial-mesenchymal transition, *J Cell Sci*, **118,** 4325-6.

Raffel C, Jenkins RB, Frederick L, Hebrink D, Alderete B, Fults DW and James CD. (1997). Sporadic medulloblastomas contain PTCH mutations, *Cancer Res*, **57,** 842-5.

Raghavan S, Bauer C, Mundschau G, Li Q and Fuchs E. (2000). Conditional ablation of beta1 integrin in skin. Severe defects in epidermal proliferation, basement membrane formation, and hair follicle invagination, *J Cell Biol*, **150,** 1149-60.

Rajagopalan H and Lengauer C. (2004). Aneuploidy and cancer, *Nature*, **432,** 338-41.

Ramsey ML. (2009). Basal Cell Carcinoma. eMedicine from web MD.

Rando TA. (2007). The immortal strand hypothesis: segregation and reconstruction, *Cell*, **129,** 1239-43.

Rattner A, Hsieh JC, Smallwood PM, Gilbert DJ, Copeland NG, Jenkins NA and Nathans J. (1997). A family of secreted proteins contains homology to the cysteine-rich ligand-binding domain of frizzled receptors, *Proc Natl Acad Sci U S A*, **94,** 2859-63.

Ravid K, Lu J, Zimmet JM and Jones MR. (2002). Roads to polyploidy: the megakaryocyte example, *J Cell Physiol*, **190,** 7-20.

Raynal P and Pollard HB. (1994). Annexins: the problem of assessing the biological role for a gene family of multifunctional calcium- and phospholipid-binding proteins, *Biochim Biophys Acta*, **1197,** 63-93.

Reddy S, Andl T, Bagasra A, Lu MM, Epstein DJ, Morrisey EE and Millar SE. (2001). Characterization of Wnt gene expression in developing and postnatal hair follicles and identification of Wnt5a as a target of Sonic hedgehog in hair follicle morphogenesis, *Mech Dev*, **107,** 69-82.

Regl G, Kasper M, Schnidar H, Eichberger T, Neill GW, Ikram MS, Quinn AG, Philpott MP, Frischauf AM and Aberger F. (2004a). The zinc-finger transcription factor GLI2 antagonizes contact inhibition and differentiation of human epidermal cells, *Oncogene*, **23,** 1263-74.

Regl G, Kasper M, Schnidar H, Eichberger T, Neill GW, Philpott MP, Esterbauer H, Hauser-Kronberger C, Frischauf AM and Aberger F. (2004b). Activation of the BCL2 promoter in response to Hedgehog/GLI signal transduction is predominantly mediated by GLI2, *Cancer Res*, **64,** 7724-31.

Regl G, Neill GW, Eichberger T, Kasper M, Ikram MS, Koller J, Hintner H, Quinn AG, Frischauf AM and Aberger F. (2002). Human GLI2 and GLI1 are part of a positive feedback mechanism in Basal Cell Carcinoma, *Oncogene*, **21,** 5529-39.

Reid BJ, Barrett MT, Galipeau PC, Sanchez CA, Neshat K, Cowan DS and Levine DS. (1996). Barrett's esophagus: ordering the events that lead to cancer, *Eur J Cancer Prev*, **5 Suppl 2,** 57-65.

Reifenberger G, Ichimura K, Reifenberger J, Elkahloun AG, Meltzer PS and Collins VP. (1996). Refined mapping of 12q13-q15 amplicons in human malignant gliomas suggests CDK4/SAS and MDM2 as independent amplification targets, *Cancer Res*, **56,** 5141-5.

Reifenberger J, Wolter M, Knobbe CB, Kohler B, Schonicke A, Scharwachter C, Kumar K, Blaschke B, Ruzicka T and Reifenberger G. (2005). Somatic

mutations in the PTCH, SMOH, SUFUH and TP53 genes in sporadic basal cell carcinomas, *Br J Dermatol*, **152,** 43-51.

Reifenberger J, Wolter M, Weber RG, Megahed M, Ruzicka T, Lichter P and Reifenberger G. (1998). Missense mutations in SMOH in sporadic basal cell carcinomas of the skin and primitive neuroectodermal tumors of the central nervous system, *Cancer Res*, **58,** 1798-803.

Reya T and Clevers H. (2005). Wnt signalling in stem cells and cancer, *Nature*, **434,** 843-50.

Reya T, Duncan AW, Ailles L, Domen J, Scherer DC, Willert K, Hintz L, Nusse R and Weissman IL. (2003). A role for Wnt signalling in self-renewal of haematopoietic stem cells, *Nature*, **423,** 409-14.

Reya T, Morrison SJ, Clarke MF and Weissman IL. (2001). Stem cells, cancer, and cancer stem cells, *Nature*, **414,** 105-11.

Rheinwald JG and Beckett MA. (1980). Defective terminal differentiation in culture as a consistent and selectable character of malignant human keratinocytes, *Cell*, **22,** 629-32.

Rheinwald JG, Hahn WC, Ramsey MR, Wu JY, Guo Z, Tsao H, De Luca M, Catricala C and O'Toole KM. (2002). A two-stage, p16(INK4A)- and p53-dependent keratinocyte senescence mechanism that limits replicative potential independent of telomere status, *Mol Cell Biol*, **22,** 5157-72.

Riccardi C and Nicoletti I. (2006). Analysis of apoptosis by propidium iodide staining and flow cytometry, *Nat Protoc*, **1,** 1458-61.

Rice RH and Green H. (1977). The cornified envelope of terminally differentiated human epidermal keratinocytes consists of cross-linked protein, *Cell*, **11,** 417-22.

Rice RH and Green H. (1979). Presence in human epidermal cells of a soluble protein precursor of the cross-linked envelope: activation of the cross-linking by calcium ions, *Cell*, **18,** 681-94.

Richardson C and Jasin M. (2000). Frequent chromosomal translocations induced by DNA double-strand breaks, *Nature*, **405,** 697-700.

Ried T, Heselmeyer-Haddad K, Blegen H, Schrock E and Auer G. (1999). Genomic changes defining the genesis, progression, and malignancy potential in solid human tumors: a phenotype/genotype correlation, *Genes Chromosomes Cancer*, **25,** 195-204.

Rieder CL and Palazzo RE. (1992). Colcemid and the mitotic cycle, *J Cell Sci*, **102 (Pt 3),** 387-92.

Rieder CL, Schultz A, Cole R and Sluder G. (1994). Anaphase onset in vertebrate somatic cells is controlled by a checkpoint that monitors sister kinetochore attachment to the spindle, *J Cell Biol*, **127,** 1301-10.

Riedl SJ and Shi Y. (2004). Molecular mechanisms of caspase regulation during apoptosis, *Nat Rev Mol Cell Biol*, **5,** 897-907.

Riggleman B, Schedl P and Wieschaus E. (1990). Spatial expression of the Drosophila segment polarity gene armadillo is posttranscriptionally regulated by wingless, *Cell*, **63,** 549-60.

Rijsewijk F, Schuermann M, Wagenaar E, Parren P, Weigel D and Nusse R. (1987). The Drosophila homolog of the mouse mammary oncogene int-1 is identical to the segment polarity gene wingless, *Cell*, **50,** 649-57.

Riobo NA, Lu K, Ai X, Haines GM and Emerson CP, Jr. (2006). Phosphoinositide 3-kinase and Akt are essential for Sonic Hedgehog signaling, *Proc Natl Acad Sci U S A*, **103,** 4505-10.

Risinger JI, Berchuck A, Kohler MF and Boyd J. (1994). Mutations of the E-cadherin gene in human gynecologic cancers, *Nat Genet*, **7,** 98-102.

Rittie L, Kansra S, Stoll SW, Li Y, Gudjonsson JE, Shao Y, Michael LE, Fisher GJ, Johnson TM and Elder JT. (2007). Differential ErbB1 signaling in squamous cell versus basal cell carcinoma of the skin, *Am J Pathol*, **170,** 2089-99.

Robbins DJ, Nybakken KE, Kobayashi R, Sisson JC, Bishop JM and Therond PP. (1997). Hedgehog elicits signal transduction by means of a large complex containing the kinesin-related protein costal2, *Cell*, **90,** 225-34.

Roberts WM, Douglass EC, Peiper SC, Houghton PJ and Look AT. (1989). Amplification of the gli gene in childhood sarcomas, *Cancer Res*, **49,** 5407-13.

Robertson KD, Uzvolgyi E, Liang G, Talmadge C, Sumegi J, Gonzales FA and Jones PA. (1999). The human DNA methyltransferases (DNMTs) 1, 3a and 3b: coordinate mRNA expression in normal tissues and overexpression in tumors, *Nucleic Acids Res*, **27,** 2291-8.

Rochat A, Kobayashi K and Barrandon Y. (1994). Location of stem cells of human hair follicles by clonal analysis, *Cell*, **76,** 1063-73.

Rodriguez-Villanueva J, Colome MI, Brisbay S and McDonnell TJ. (1995). The expression and localization of bcl-2 protein in normal skin and in non-melanoma skin cancers, *Pathol Res Pract*, **191,** 391-8.

Rodriguez-Villanueva J, Greenhalgh D, Wang XJ, Bundman D, Cho S, Delehedde M, Roop D and McDonnell TJ. (1998). Human keratin-1.bcl-2 transgenic mice aberrantly express keratin 6, exhibit reduced sensitivity to keratinocyte cell death induction, and are susceptible to skin tumor formation, *Oncogene*, **16,** 853-63.

Roessler E, Belloni E, Gaudenz K, Jay P, Berta P, Scherer SW, Tsui LC and Muenke M. (1996). Mutations in the human Sonic Hedgehog gene cause holoprosencephaly, *Nat Genet*, **14,** 357-60.

Roessler E, Du YZ, Mullor JL, Casas E, Allen WP, Gillessen-Kaesbach G, Roeder ER, Ming JE, Ruiz i Altaba A and Muenke M. (2003). Loss-of-function mutations in the human GLI2 gene are associated with pituitary anomalies and holoprosencephaly-like features, *Proc Natl Acad Sci U S A*, **100,** 13424-9.

Roessler E, Ermilov AN, Grange DK, Wang A, Grachtchouk M, Dlugosz AA and Muenke M. (2005). A previously unidentified amino-terminal domain regulates transcriptional activity of wild-type and disease-associated human GLI2, *Hum Mol Genet*, **14,** 2181-8.

Rohatgi R and Scott MP. (2007). Patching the gaps in Hedgehog signalling, *Nat Cell Biol*, **9,** 1005-9.

Roop D and Toftgard R. (2008). Hedgehog in wnterland, *Nat Genet*, **40,** 1040-1.

Roose J and Clevers H. (1999). TCF transcription factors: molecular switches in carcinogenesis, *Biochim Biophys Acta*, **1424,** M23-37.

Roura S, Miravet S, Piedra J, Garcia de Herreros A and Dunach M. (1999). Regulation of E-cadherin/Catenin association by tyrosine phosphorylation, *J Biol Chem*, **274,** 36734-40.

Rowley JD. (2001). Chromosome translocations: dangerous liaisons revisited, *Nat Rev Cancer*, **1,** 245-50.

Rubin AI, Chen EH and Ratner D. (2005). Basal-cell carcinoma, *N Engl J Med*, **353,** 2262-9.

Rubin LL and de Sauvage FJ. (2006). Targeting the Hedgehog pathway in cancer, *Nat Rev Drug Discov*, **5,** 1026-33.

Rubinfeld B, Souza B, Albert I, Muller O, Chamberlain SH, Masiarz FR, Munemitsu S and Polakis P. (1993). Association of the APC gene product with beta-catenin, *Science*, **262,** 1731-4.

Rudner AD and Murray AW. (1996). The spindle assembly checkpoint, *Curr Opin Cell Biol*, **8,** 773-80.

Ruiz-Gomez A, Molnar C, Holguin H, Mayor F, Jr. and de Celis JF. (2007). The cell biology of Smo signalling and its relationships with GPCRs, *Biochim Biophys Acta*, **1768,** 901-12.

Ruiz i Altaba A. (1999a). Gli proteins encode context-dependent positive and negative functions: implications for development and disease, *Development*, **126,** 3205-16.

Ruiz i Altaba A. (1999b). The works of GLI and the power of hedgehog, *Nat Cell Biol*, **1,** E147-8.

Ruiz i Altaba A, Nguyen V and Palma V. (2003). The emergent design of the neural tube: prepattern, SHH morphogen and GLI code, *Curr Opin Genet Dev*, **13,** 513-21.

Ruiz i Altaba A, Palma V and Dahmane N. (2002a). Hedgehog-Gli signalling and the growth of the brain, *Nat Rev Neurosci*, **3,** 24-33.

Ruiz i Altaba A, Sanchez P and Dahmane N. (2002b). Gli and hedgehog in cancer: tumours, embryos and stem cells, *Nat Rev Cancer*, **2,** 361-72.

Ruppert JM, Kinzler KW, Wong AJ, Bigner SH, Kao FT, Law ML, Seuanez HN, O'Brien SJ and Vogelstein B. (1988). The GLI-Kruppel family of human genes, *Mol Cell Biol*, **8,** 3104-13.

Ruppert JM, Vogelstein B, Arheden K and Kinzler KW. (1990). GLI3 encodes a 190-kilodalton protein with multiple regions of GLI similarity, *Mol Cell Biol*, **10,** 5408-15.

Ruppert JM, Vogelstein B and Kinzler KW. (1991). The zinc finger protein GLI transforms primary cells in cooperation with adenovirus E1A, *Mol Cell Biol*, **11,** 1724-8.

Said JW, Sassoon AF, Shintaku IP and Banks-Schlegel S. (1984). Involucrin in squamous and basal cell carcinomas of the skin: an immunohistochemical study, *J Invest Dermatol*, **82,** 449-52.

Saijo T, Ishii G, Ochiai A, Yoh K, Goto K, Nagai K, Kato H, Nishiwaki Y and Saijo N. (2006). Eg5 expression is closely correlated with the response of advanced non-small cell lung cancer to antimitotic agents combined with platinum chemotherapy, *Lung Cancer*, **54,** 217-25.

Saldanha G, Ghura V, Potter L and Fletcher A. (2004). Nuclear beta-catenin in basal cell carcinoma correlates with increased proliferation, *Br J Dermatol*, **151,** 157-64.

Sanchez P, Hernandez AM, Stecca B, Kahler AJ, DeGueme AM, Barrett A, Beyna M, Datta MW, Datta S and Ruiz i Altaba A. (2004). Inhibition of prostate cancer proliferation by interference with SONIC HEDGEHOG-GLI1 signaling, *Proc Natl Acad Sci U S A*, **101,** 12561-6.

Saneyoshi T, Kume S, Amasaki Y and Mikoshiba K. (2002). The Wnt/calcium pathway activates NF-AT and promotes ventral cell fate in Xenopus embryos, *Nature*, **417,** 295-9.

Santini MP, Talora C, Seki T, Bolgan L and Dotto GP. (2001). Cross talk among calcineurin, Sp1/Sp3, and NFAT in control of p21(WAF1/CIP1) expression in keratinocyte differentiation, *Proc Natl Acad Sci U S A*, **98,** 9575-80.

Sarkisian CJ, Keister BA, Stairs DB, Boxer RB, Moody SE and Chodosh LA. (2007). Dose-dependent oncogene-induced senescence in vivo and its evasion during mammary tumorigenesis, *Nat Cell Biol*, **9,** 493-505.

Sasaki H, Nishizaki Y, Hui C, Nakafuku M and Kondoh H. (1999). Regulation of Gli2 and Gli3 activities by an amino-terminal repression domain: implication of Gli2 and Gli3 as primary mediators of Shh signaling, *Development*, **126,** 3915-24.

Satoh S, Daigo Y, Furukawa Y, Kato T, Miwa N, Nishiwaki T, Kawasoe T, Ishiguro H, Fujita M, Tokino T, Sasaki Y, Imaoka S, Murata M, Shimano T, Yamaoka Y and Nakamura Y. (2000). AXIN1 mutations in hepatocellular carcinomas, and growth suppression in cancer cells by virus-mediated transfer of AXIN1, *Nat Genet*, **24,** 245-50.

Sattler HP, Lensch R, Rohde V, Zimmer E, Meese E, Bonkhoff H, Retz M, Zwergel T, Bex A, Stoeckle M and Wullich B. (2000). Novel amplification unit at chromosome 3q25-q27 in human prostate cancer, *Prostate*, **45,** 207-15.

Saunders W. (2005). Centrosomal amplification and spindle multipolarity in cancer cells, *Semin Cancer Biol*, **15,** 25-32.

Saunders WS, Shuster M, Huang X, Gharaibeh B, Enyenihi AH, Petersen I and Gollin SM. (2000). Chromosomal instability and cytoskeletal defects in oral cancer cells, *Proc Natl Acad Sci U S A*, **97,** 303-8.

Savelyeva L and Schwab M. (2001). Amplification of oncogenes revisited: from expression profiling to clinical application, *Cancer Lett*, **167,** 115-23.

Schmidt-Ullrich R and Paus R. (2005). Molecular principles of hair follicle induction and morphogenesis, *Bioessays*, **27,** 247-61.

Schneider TE, Barland C, Alex AM, Mancianti ML, Lu Y, Cleaver JE, Lawrence HJ and Ghadially R. (2003). Measuring stem cell frequency in epidermis: a quantitative in vivo functional assay for long-term repopulating cells, *Proc Natl Acad Sci U S A*, **100,** 11412-7.

Schrock E, du Manoir S, Veldman T, Schoell B, Wienberg J, Ferguson-Smith MA, Ning Y, Ledbetter DH, Bar-Am I, Soenksen D, Garini Y and Ried T. (1996). Multicolor spectral karyotyping of human chromosomes, *Science*, **273,** 494-7.

Scribner JD and Suss R. (1978). Tumor initiation and promotion, *Int Rev Exp Pathol*, **18,** 137-98.

Seeger RC, Brodeur GM, Sather H, Dalton A, Siegel SE, Wong KY and Hammond D. (1985). Association of multiple copies of the N-myc oncogene with rapid progression of neuroblastomas, *N Engl J Med*, **313,** 1111-6.

Seifert JR and Mlodzik M. (2007). Frizzled/PCP signalling: a conserved mechanism regulating cell polarity and directed motility, *Nat Rev Genet*, **8,** 126-38.

Seoane J, Le HV, Shen L, Anderson SA and Massague J. (2004). Integration of Smad and forkhead pathways in the control of neuroepithelial and glioblastoma cell proliferation, *Cell*, **117,** 211-23.

Serre G, Mils V, Haftek M, Vincent C, Croute F, Reano A, Ouhayoun JP, Bettinger S and Soleilhavoup JP. (1991). Identification of late differentiation antigens of human cornified epithelia, expressed in re-organized desmosomes and bound to cross-linked envelope, *J Invest Dermatol*, **97,** 1061-72.

Sexton M, Jones DB and Maloney ME. (1990). Histologic pattern analysis of basal cell carcinoma. Study of a series of 1039 consecutive neoplasms, *J Am Acad Dermatol*, **23,** 1118-26.

Shackney SE, Smith CA, Miller BW, Burholt DR, Murtha K, Giles HR, Ketterer DM and Pollice AA. (1989). Model for the genetic evolution of human solid tumors, *Cancer Res*, **49,** 3344-54.

Shain KH, Landowski TH and Dalton WS. (2002). Adhesion-mediated intracellular redistribution of c-Fas-associated death domain-like IL-1-converting enzyme-like inhibitory protein-long confers resistance to CD95-induced apoptosis in hematopoietic cancer cell lines, *J Immunol*, **168,** 2544-53.

Shapiro HM. (1981a). Flow cytometric estimation of DNA and RNA content in intact cells stained with Hoechst 33342 and pyronin Y, *Cytometry*, **2,** 143-50.

Shapiro HM. (1981b). Flow cytometric probes of early events in cell activation, *Cytometry*, **1,** 301-12.

Shapiro JR, Yung WK and Shapiro WR. (1981). Isolation, karyotype, and clonal growth of heterogeneous subpopulations of human malignant gliomas, *Cancer Res*, **41,** 2349-59.

Shea CR, McNutt NS, Volkenandt M, Lugo J, Prioleau PG and Albino AP. (1992). Overexpression of p53 protein in basal cell carcinomas of human skin, *Am J Pathol*, **141,** 25-9.

Sheldahl LC, Park M, Malbon CC and Moon RT. (1999). Protein kinase C is differentially stimulated by Wnt and Frizzled homologs in a G-protein-dependent manner, *Curr Biol*, **9,** 695-8.

Sheldahl LC, Slusarski DC, Pandur P, Miller JR, Kuhl M and Moon RT. (2003). Dishevelled activates Ca2+ flux, PKC, and CamKII in vertebrate embryos, *J Cell Biol*, **161,** 769-77.

Shen KC, Heng H, Wang Y, Lu S, Liu G, Deng CX, Brooks SC and Wang YA. (2005). ATM and p21 cooperate to suppress aneuploidy and subsequent tumor development, *Cancer Res*, **65,** 8747-53.

Sheng H, Goich S, Wang A, Grachtchouk M, Lowe L, Mo R, Lin K, de Sauvage FJ, Sasaki H, Hui CC and Dlugosz AA. (2002). Dissecting the oncogenic potential of Gli2: deletion of an NH(2)-terminal fragment alters skin tumor phenotype, *Cancer Res*, **62,** 5308-16.

Sheng T, Li C, Zhang X, Chi S, He N, Chen K, McCormick F, Gatalica Z and Xie J. (2004). Activation of the hedgehog pathway in advanced prostate cancer, *Mol Cancer*, **3,** 29.

Sherley JL, Stadler PB and Johnson DR. (1995). Expression of the wild-type p53 antioncogene induces guanine nucleotide-dependent stem cell division kinetics, *Proc Natl Acad Sci U S A*, **92,** 136-40.

Sherr CJ. (1996). Cancer cell cycles, *Science*, **274,** 1672-7.

Sherr CJ. (2004). Principles of tumor suppression, *Cell*, **116,** 235-46.

Sherr CJ and McCormick F. (2002). The RB and p53 pathways in cancer, *Cancer Cell*, **2,** 103-12.

Sherr CJ and Roberts JM. (1995). Inhibitors of mammalian G1 cyclin-dependent kinases, *Genes Dev*, **9,** 1149-63.

Shi Q and King RW. (2005). Chromosome nondisjunction yields tetraploid rather than aneuploid cells in human cell lines, *Nature*, **437,** 1038-42.

Shih IM, Yu J, He TC, Vogelstein B and Kinzler KW. (2000). The beta-catenin binding domain of adenomatous polyposis coli is sufficient for tumor suppression, *Cancer Res*, **60,** 1671-6.

Shin SH, Kogerman P, Lindstrom E, Toftgard R and Biesecker LG. (1999). GLI3 mutations in human disorders mimic Drosophila cubitus interruptus protein functions and localization, *Proc Natl Acad Sci U S A*, **96,** 2880-4.

Shinin V, Gayraud-Morel B, Gomes D and Tajbakhsh S. (2006). Asymmetric division and cosegregation of template DNA strands in adult muscle satellite cells, *Nat Cell Biol*, **8,** 677-87.

Shirahama S, Furukawa F, Wakita H and Takigawa M. (1996). E- and P-cadherin expression in tumor tissues and soluble E-cadherin levels in sera of patients with skin cancer, *J Dermatol Sci*, **13,** 30-6.

Shono M, Sato N, Mizumoto K, Maehara N, Nakamura M, Nagai E and Tanaka M. (2001). Stepwise progression of centrosome defects associated with local tumor growth and metastatic process of human pancreatic carcinoma cells transplanted orthotopically into nude mice, *Lab Invest*, **81,** 945-52.

Shtutman M, Zhurinsky J, Simcha I, Albanese C, D'Amico M, Pestell R and Ben-Ze'ev A. (1999). The cyclin D1 gene is a target of the beta-catenin/LEF-1 pathway, *Proc Natl Acad Sci U S A*, **96,** 5522-7.

Siegfried E, Wilder EL and Perrimon N. (1994). Components of wingless signalling in Drosophila, *Nature*, **367,** 76-80.

Silva-Vargas V, Lo Celso C, Giangreco A, Ofstad T, Prowse DM, Braun KM and Watt FM. (2005). Beta-catenin and Hedgehog signal strength can specify number and location of hair follicles in adult epidermis without recruitment of bulge stem cells, *Dev Cell*, **9,** 121-31.

Sinclair AH, Berta P, Palmer MS, Hawkins JR, Griffiths BL, Smith MJ, Foster JW, Frischauf AM, Lovell-Badge R and Goodfellow PN. (1990). A gene from the human sex-determining region encodes a protein with homology to a conserved DNA-binding motif, *Nature*, **346,** 240-4.

Singer MJ, Mesner LD, Friedman CL, Trask BJ and Hamlin JL. (2000). Amplification of the human dihydrofolate reductase gene via double minutes is initiated by chromosome breaks, *Proc Natl Acad Sci U S A*, **97,** 7921-6.

Sisson JC, Ho KS, Suyama K and Scott MP. (1997). Costal2, a novel kinesin-related protein in the Hedgehog signaling pathway, *Cell*, **90,** 235-45.

Sjoblom T, Jones S, Wood LD, Parsons DW, Lin J, Barber TD, Mandelker D, Leary RJ, Ptak J, Silliman N, Szabo S, Buckhaults P, Farrell C, Meeh P, Markowitz SD, Willis J, Dawson D, Willson JK, Gazdar AF, Hartigan J, Wu L, Liu C, Parmigiani G, Park BH, Bachman KE, Papadopoulos N, Vogelstein B, Kinzler KW and Velculescu VE. (2006). The consensus coding sequences of human breast and colorectal cancers, *Science*, **314,** 268-74.

Sluder G. (1991). *The practical use of colchicine and colcemid to reversibly block microtubule assembly in living cells. In: K.W. Adolph (ed.). Advanced Techniques in Chromosome Research, pp. 427-447.* New York: Marcel Dckker.

Slusarski DC, Corces VG and Moon RT. (1997). Interaction of Wnt and a Frizzled homologue triggers G-protein-linked phosphatidylinositol signalling, *Nature*, **390,** 410-3.

Smith GH. (2005). Label-retaining epithelial cells in mouse mammary gland divide asymmetrically and retain their template DNA strands, *Development*, **132,** 681-7.

Smyth I, Narang MA, Evans T, Heimann C, Nakamura Y, Chenevix-Trench G, Pietsch T, Wicking C and Wainwright BJ. (1999). Isolation and characterization of human patched 2 (PTCH2), a putative tumour suppressor gene inbasal cell carcinoma and medulloblastoma on chromosome 1p32, *Hum Mol Genet*, **8,** 291-7.

Snijders AM, Huey B, Connelly ST, Roy R, Jordan RC, Schmidt BL and Albertson DG. (2008). Stromal control of oncogenic traits expressed in response to the overexpression of GLI2, a pleiotropic oncogene, *Oncogene*.

Snippert HJ, Haegebarth A, Kasper M, Jaks V, van Es JH, Barker N, van de Wetering M, van den Born M, Begthel H, Vries RG, Stange DE, Toftgard R and Clevers

H. (2010). Lgr6 marks stem cells in the hair follicle that generate all cell lineages of the skin, *Science*, **327,** 1385-9.
Soehnge H, Ouhtit A and Ananthaswamy ON. (1997). Mechanisms of induction of skin cancer by UV radiation, *Front Biosci*, **2,** d538-51.
Sokol S. (2000). A role for Wnts in morpho-genesis and tissue polarity, *Nat Cell Biol*, **2,** E124-5.
Solomon E, Borrow J and Goddard AD. (1991). Chromosome aberrations and cancer, *Science*, **254,** 1153-60.
Sotillo R, Hernando E, Diaz-Rodriguez E, Teruya-Feldstein J, Cordon-Cardo C, Lowe SW and Benezra R. (2007). Mad2 overexpression promotes aneuploidy and tumorigenesis in mice, *Cancer Cell*, **11,** 9-23.
Southern SA, Evans MF and Herrington CS. (1997). Basal cell tetrasomy in low-grade cervical squamous intraepithelial lesions infected with high-risk human papillomaviruses, *Cancer Res*, **57,** 4210-3.
Speek M, Njunkova O, Pata I, Valdre E and Kogerman P. (2006). A potential role of alternative splicing in the regulation of the transcriptional activity of human GLI2 in gonadal tissues, *BMC Mol Biol*, **7,** 13.
Speicher MR, Gwyn Ballard S and Ward DC. (1996). Karyotyping human chromosomes by combinatorial multi-fluor FISH, *Nat Genet*, **12,** 368-75.
Speicher MR and Ward DC. (1996). The coloring of cytogenetics, *Nat Med*, **2,** 1046-8.
Srsen V, Gnadt N, Dammermann A and Merdes A. (2006). Inhibition of centrosome protein assembly leads to p53-dependent exit from the cell cycle, *J Cell Biol*, **174,** 625-30.
St-Jacques B, Dassule HR, Karavanova I, Botchkarev VA, Li J, Danielian PS, McMahon JA, Lewis PM, Paus R and McMahon AP. (1998). Sonic hedgehog signaling is essential for hair development, *Curr Biol*, **8,** 1058-68.
Staiano-Coico L, Higgins PJ, Darzynkiewicz Z, Kimmel M, Gottlieb AB, Pagan-Charry I, Madden MR, Finkelstein JL and Hefton JM. (1986). Human keratinocyte culture. Identification and staging of epidermal cell subpopulations, *J Clin Invest*, **77,** 396-404.
Staibano S, Lo Muzio L, Pannone G, Mezza E, Argenziano G, Vetrani A, Lucariello A, Franco R, Errico ME and De Rosa G. (2001). DNA ploidy and cyclin D1 expression in basal cell carcinoma of the head and neck, *Am J Clin Pathol*, **115,** 805-13.
Stamenkovic I. (2000). Matrix metalloproteinases in tumor invasion and metastasis, *Semin Cancer Biol*, **10,** 415-33.
Stanley JR, Woodley DT, Katz SI and Martin GR. (1982). Structure and function of basement membrane, *J Invest Dermatol*, **79 Suppl 1,** 69s-72s.
Stary A and Sarasin A. (2002). The genetics of the hereditary xeroderma pigmentosum syndrome, *Biochimie*, **84,** 49-60.
Stein U, Arlt F, Walther W, Smith J, Waldman T, Harris ED, Mertins SD, Heizmann CW, Allard D, Birchmeier W, Schlag PM and Shoemaker RH. (2006). The metastasis-associated gene S100A4 is a novel target of beta-catenin/T-cell factor signaling in colon cancer, *Gastroenterology*, **131,** 1486-500.
Steinman RA, Hoffman B, Iro A, Guillouf C, Liebermann DA and el-Houseini ME. (1994). Induction of p21 (WAF-1/CIP1) during differentiation, *Oncogene*, **9,** 3389-96.
Stemmer V, de Craene B, Berx G and Behrens J. (2008). Snail promotes Wnt target gene expression and interacts with beta-catenin, *Oncogene*, **27,** 5075-80.

Sterling JA, Oyajobi BO, Grubbs B, Padalecki SS, Munoz SA, Gupta A, Story B, Zhao M and Mundy GR. (2006). The hedgehog signaling molecule Gli2 induces parathyroid hormone-related peptide expression and osteolysis in metastatic human breast cancer cells, *Cancer Res*, **66,** 7548-53.

Steven AC and Steinert PM. (1994). Protein composition of cornified cell envelopes of epidermal keratinocytes, *J Cell Sci*, **107 (Pt 2),** 693-700.

Steven AF. (2007). *Dynamics of Cancer: Incidence, Inheritance, and Evolution, pp 251-270. Princeton University Press: United Kingdom, UK.*

Stewart ZA, Leach SD and Pietenpol JA. (1999). p21(Waf1/Cip1) inhibition of cyclin E/Cdk2 activity prevents endoreduplication after mitotic spindle disruption, *Mol Cell Biol*, **19,** 205-15.

Stoler A, Kopan R, Duvic M and Fuchs E. (1988). Use of monospecific antisera and cRNA probes to localize the major changes in keratin expression during normal and abnormal epidermal differentiation, *J Cell Biol*, **107,** 427-46.

Stone DM, Hynes M, Armanini M, Swanson TA, Gu Q, Johnson RL, Scott MP, Pennica D, Goddard A, Phillips H, Noll M, Hooper JE, de Sauvage F and Rosenthal A. (1996). The tumour-suppressor gene patched encodes a candidate receptor for Sonic hedgehog, *Nature*, **384,** 129-34.

Stone DM, Murone M, Luoh S, Ye W, Armanini MP, Gurney A, Phillips H, Brush J, Goddard A, de Sauvage FJ and Rosenthal A. (1999). Characterization of the human suppressor of fused, a negative regulator of the zinc-finger transcription factor Gli, *J Cell Sci*, **112 (Pt 23),** 4437-48.

Storchova Z, Breneman A, Cande J, Dunn J, Burbank K, O'Toole E and Pellman D. (2006). Genome-wide genetic analysis of polyploidy in yeast, *Nature*, **443,** 541-7.

Storchova Z and Kuffer C. (2008). The consequences of tetraploidy and aneuploidy, *J Cell Sci*, **121,** 3859-66.

Storchova Z and Pellman D. (2004). From polyploidy to aneuploidy, genome instability and cancer, *Nat Rev Mol Cell Biol*, **5,** 45-54.

Strachan T and Read A. (2004a). *Cromosome structure and function. Human Molecular Genetics, pp 41. 3rd ed.* Garland Science: New York, NY.

Strachan T and Read A. (2004b). *Cromosome structure and function. Human Molecular Genetics, pp 49. 3rd ed.* Garland Science: New York, NY.

Strathdee G. (2002). Epigenetic versus genetic alterations in the inactivation of E-cadherin, *Semin Cancer Biol*, **12,** 373-9.

Strefford JC, Lillington DM, Young BD and Oliver RT. (2001). The use of multicolor fluorescence technologies in the characterization of prostate carcinoma cell lines: a comparison of multiplex fluorescence in situ hybridization and spectral karyotyping data, *Cancer Genet Cytogenet*, **124,** 112-21.

Strutt D. (2003). Frizzled signalling and cell polarisation in Drosophila and vertebrates, *Development*, **130,** 4501-13.

Strutt DI, Weber U and Mlodzik M. (1997). The role of RhoA in tissue polarity and Frizzled signalling, *Nature*, **387,** 292-5.

Sumitomo S, Kumasa S, Iwai Y and Mori M. (1986). Involucrin expression in epithelial tumors of oral and pharyngeal mucosa and skin, *Oral Surg Oral Med Oral Pathol*, **62,** 155-63.

Svard J, Heby-Henricson K, Persson-Lek M, Rozell B, Lauth M, Bergstrom A, Ericson J, Toftgard R and Teglund S. (2006). Genetic elimination of Suppressor of fused reveals an essential repressor function in the mammalian Hedgehog signaling pathway, *Dev Cell*, **10,** 187-97.

Tada H, Hatoko M, Muramatsu T and Shirai T. (1996). Expression of E-cadherin in skin carcinomas, *J Dermatol*, **23,** 104-10.
Tada H, Hatoko M, Tanaka A, Kuwahara M and Muramatsu T. (2000). Expression of desmoglein I and plakoglobin in skin carcinomas, *J Cutan Pathol*, **27,** 24-9.
Taipale J and Beachy PA. (2001). The Hedgehog and Wnt signalling pathways in cancer, *Nature*, **411,** 349-54.
Taipale J, Chen JK, Cooper MK, Wang B, Mann RK, Milenkovic L, Scott MP and Beachy PA. (2000). Effects of oncogenic mutations in Smoothened and Patched can be reversed by cyclopamine, *Nature*, **406,** 1005-9.
Taipale J, Cooper MK, Maiti T and Beachy PA. (2002). Patched acts catalytically to suppress the activity of Smoothened, *Nature*, **418,** 892-7.
Takahashi K, Tanabe K, Ohnuki M, Narita M, Ichisaka T, Tomoda K and Yamanaka S. (2007). Induction of pluripotent stem cells from adult human fibroblasts by defined factors, *Cell*, **131,** 861-72.
Takanaga H, Tsuchida-Straeten N, Nishide K, Watanabe A, Aburatani H and Kondo T. (2009). Gli2 is a novel regulator of sox2 expression in telencephalic neuroepithelial cells, *Stem Cells*, **27,** 165-74.
Takeda H, Lyle S, Lazar AJ, Zouboulis CC, Smyth I and Watt FM. (2006). Human sebaceous tumors harbor inactivating mutations in LEF1, *Nat Med*, **12,** 395-7.
Tamai K, Semenov M, Kato Y, Spokony R, Liu C, Katsuyama Y, Hess F, Saint-Jeannet JP and He X. (2000). LDL-receptor-related proteins in Wnt signal transduction, *Nature*, **407,** 530-5.
Tamai K, Zeng X, Liu C, Zhang X, Harada Y, Chang Z and He X. (2004). A mechanism for Wnt coreceptor activation, *Mol Cell*, **13,** 149-56.
Tamura G, Yin J, Wang S, Fleisher AS, Zou T, Abraham JM, Kong D, Smolinski KN, Wilson KT, James SP, Silverberg SG, Nishizuka S, Terashima M, Motoyama T and Meltzer SJ. (2000). E-Cadherin gene promoter hypermethylation in primary human gastric carcinomas, *J Natl Cancer Inst*, **92,** 569-73.
Tani H, Morris RJ and Kaur P. (2000). Enrichment for murine keratinocyte stem cells based on cell surface phenotype, *Proc Natl Acad Sci U S A*, **97,** 10960-5.
Tanimura A, Dan S and Yoshida M. (1998). Cloning of novel isoforms of the human Gli2 oncogene and their activities to enhance tax-dependent transcription of the human T-cell leukemia virus type 1 genome, *J Virol*, **72,** 3958-64.
Tao Q, Yokota C, Puck H, Kofron M, Birsoy B, Yan D, Asashima M, Wylie CC, Lin X and Heasman J. (2005). Maternal wnt11 activates the canonical wnt signaling pathway required for axis formation in Xenopus embryos, *Cell*, **120,** 857-71.
Taranova OV, Magness ST, Fagan BM, Wu Y, Surzenko N, Hutton SR and Pevny LH. (2006). SOX2 is a dose-dependent regulator of retinal neural progenitor competence, *Genes Dev*, **20,** 1187-202.
Tarapore P, Horn HF, Tokuyama Y and Fukasawa K. (2001). Direct regulation of the centrosome duplication cycle by the p53-p21Waf1/Cip1 pathway, *Oncogene*, **20,** 3173-84.
Taylor EW. (1965). The Mechanism of Colchicine Inhibition of Mitosis. I. Kinetics of Inhibition and the Binding of H3-Colchicine, *J Cell Biol*, **25,** SUPPL:145-60.
Taylor G, Lehrer MS, Jensen PJ, Sun TT and Lavker RM. (2000). Involvement of follicular stem cells in forming not only the follicle but also the epidermis, *Cell*, **102,** 451-61.
Taylor MD, Liu L, Raffel C, Hui CC, Mainprize TG, Zhang X, Agatep R, Chiappa S, Gao L, Lowrance A, Hao A, Goldstein AM, Stavrou T, Scherer SW, Dura WT,

Wainwright B, Squire JA, Rutka JT and Hogg D. (2002). Mutations in SUFU predispose to medulloblastoma, *Nat Genet*, **31,** 306-10.
Taylor MV. (2002). Muscle differentiation: how two cells become one, *Curr Biol*, **12,** R224-8.
Taylor RC, Cullen SP and Martin SJ. (2008). Apoptosis: controlled demolition at the cellular level, *Nat Rev Mol Cell Biol*, **9,** 231-41.
Taylor WR and Stark GR. (2001). Regulation of the G2/M transition by p53, *Oncogene*, **20,** 1803-15.
Teh MT, Blaydon D, Chaplin T, Foot NJ, Skoulakis S, Raghavan M, Harwood CA, Proby CM, Philpott MP, Young BD and Kelsell DP. (2005). Genomewide single nucleotide polymorphism microarray mapping in basal cell carcinomas unveils uniparental disomy as a key somatic event, *Cancer Res*, **65,** 8597-603.
Teh MT, Wong ST, Neill GW, Ghali LR, Philpott MP and Quinn AG. (2002). FOXM1 is a downstream target of Gli1 in basal cell carcinomas, *Cancer Res*, **62,** 4773-80.
Telfer NR, Colver GB and Morton CA. (2008). Guidelines for the management of basal cell carcinoma, *Br J Dermatol*, **159,** 35-48.
Temin HM and Mizutani S. (1970). RNA-dependent DNA polymerase in virions of Rous sarcoma virus, *Nature*, **226,** 1211-3.
Tenchini ML, Adams JC, Gilberty C, Steel J, Hudson DL, Malcovati M and Watt FM. (1993). Evidence against a major role for integrins in calcium-dependent intercellular adhesion of epidermal keratinocytes, *Cell Adhes Commun*, **1,** 55-66.
Thayer SP, di Magliano MP, Heiser PW, Nielsen CM, Roberts DJ, Lauwers GY, Qi YP, Gysin S, Fernandez-del Castillo C, Yajnik V, Antoniu B, McMahon M, Warshaw AL and Hebrok M. (2003). Hedgehog is an early and late mediator of pancreatic cancer tumorigenesis, *Nature*, **425,** 851-6.
Theisen H, Syed A, Nguyen BT, Lukacsovich T, Purcell J, Srivastava GP, Iron D, Gaudenz K, Nie Q, Wan FY, Waterman ML and Marsh JL. (2007). Wingless directly represses DPP morphogen expression via an armadillo/TCF/Brinker complex, *PLoS One*, **2,** e142.
Thiery JP. (2002). Epithelial-mesenchymal transitions in tumour progression, *Nat Rev Cancer*, **2,** 442-54.
Thiyagarajan S, Bhatia N, Reagan-Shaw S, Cozma D, Thomas-Tikhonenko A, Ahmad N and Spiegelman VS. (2007). Role of GLI2 transcription factor in growth and tumorigenicity of prostate cells, *Cancer Res*, **67,** 10642-6.
Thomas JT and Laimins LA. (1998). Human papillomavirus oncoproteins E6 and E7 independently abrogate the mitotic spindle checkpoint, *J Virol*, **72,** 1131-7.
Thomas RK, Kallenborn A, Wickenhauser C, Schultze JL, Draube A, Vockerodt M, Re D, Diehl V and Wolf J. (2002). Constitutive expression of c-FLIP in Hodgkin and Reed-Sternberg cells, *Am J Pathol*, **160,** 1521-8.
Thompson B, Townsley F, Rosin-Arbesfeld R, Musisi H and Bienz M. (2002). A new nuclear component of the Wnt signalling pathway, *Nat Cell Biol*, **4,** 367-73.
Thompson DA, Desai MM and Murray AW. (2006). Ploidy controls the success of mutators and nature of mutations during budding yeast evolution, *Curr Biol*, **16,** 1581-90.
Thompson SL and Compton DA. (2008). Examining the link between chromosomal instability and aneuploidy in human cells, *J Cell Biol*, **180,** 665-72.
Todd C and Reynolds NJ. (1998). Up-regulation of p21WAF1 by phorbol ester and calcium in human keratinocytes through a protein kinase C-dependent pathway, *Am J Pathol*, **153,** 39-45.

Toftgard R. (2000). Hedgehog signalling in cancer, *Cell Mol Life Sci*, **57,** 1720-31.
Tojo M, Kiyosawa H, Iwatsuki K and Kaneko F. (2002). Expression of a sonic hedgehog signal transducer, hedgehog-interacting protein, by human basal cell carcinoma, *Br J Dermatol*, **146,** 69-73.
Tojo M, Kiyosawa H, Iwatsuki K, Nakamura K and Kaneko F. (2003). Expression of the GLI2 oncogene and its isoforms in human basal cell carcinoma, *Br J Dermatol*, **148,** 892-7.
Tojo M, Mori T, Kiyosawa H, Honma Y, Tanno Y, Kanazawa KY, Yokoya S, Kaneko F and Wanaka A. (1999). Expression of sonic hedgehog signal transducers, patched and smoothened, in human basal cell carcinoma, *Pathol Int*, **49,** 687-94.
Topley GI, Okuyama R, Gonzales JG, Conti C and Dotto GP. (1999). p21(WAF1/Cip1) functions as a suppressor of malignant skin tumor formation and a determinant of keratinocyte stem-cell potential, *Proc Natl Acad Sci U S A*, **96,** 9089-94.
Topol L, Jiang X, Choi H, Garrett-Beal L, Carolan PJ and Yang Y. (2003). Wnt-5a inhibits the canonical Wnt pathway by promoting GSK-3-independent beta-catenin degradation, *J Cell Biol*, **162,** 899-908.
Torres EM, Williams BR and Amon A. (2008). Aneuploidy: cells losing their balance, *Genetics*, **179,** 737-46.
Tortora GJ and Grabowski SR. (2003). *Principles of Anatomy and Physiology*. John Wiley and Sons, Inc.
Tostar U, Malm CJ, Meis-Kindblom JM, Kindblom LG, Toftgard R and Unden AB. (2006). Deregulation of the hedgehog signalling pathway: a possible role for the PTCH and SUFU genes in human rhabdomyoma and rhabdomyosarcoma development, *J Pathol*, **208,** 17-25.
Trask BJ. (2002). Human cytogenetics: 46 chromosomes, 46 years and counting, *Nat Rev Genet*, **3,** 769-78.
Traul KA, Kachevsky V and Wolff JS. (1979). A rapid in vitro assay for carcinogenicity of chemical substances in mammalian cells utilizing an attachment-independence endpoint, *Int J Cancer*, **23,** 193-6.
Traul KA, Takayama K, Kachevsky V, Hink RJ and Wolff JS. (1981). A rapid in vitro assay for carcinogenicity of chemical substances in mammalian cells utilizing an attachment-independence endpoint. 2 - Assay validation, *J Appl Toxicol*, **1,** 190-5.
Travis A, Amsterdam A, Belanger C and Grosschedl R. (1991). LEF-1, a gene encoding a lymphoid-specific protein with an HMG domain, regulates T-cell receptor alpha enhancer function [corrected], *Genes Dev*, **5,** 880-94.
Tron VA, Tang L, Yong WP and Trotter MJ. (1996). Differentiation-associated overexpression of the cyclin-dependent kinase inhibitor p21waf-1 in human cutaneous squamous cell carcinoma, *Am J Pathol*, **149,** 1139-46.
Tschopp J, Irmler M and Thome M. (1998). Inhibition of fas death signals by FLIPs, *Curr Opin Immunol*, **10,** 552-8.
Tumbar T, Guasch G, Greco V, Blanpain C, Lowry WE, Rendl M and Fuchs E. (2004). Defining the epithelial stem cell niche in skin, *Science*, **303,** 359-63.
Uetake Y and Sluder G. (2004). Cell cycle progression after cleavage failure: mammalian somatic cells do not possess a "tetraploidy checkpoint", *J Cell Biol*, **165,** 609-15.
Ulloa F, Itasaki N and Briscoe J. (2007). Inhibitory Gli3 activity negatively regulates Wnt/beta-catenin signaling, *Curr Biol*, **17,** 545-50.

Umbhauer M, Djiane A, Goisset C, Penzo-Mendez A, Riou JF, Boucaut JC and Shi DL. (2000). The C-terminal cytoplasmic Lys-thr-X-X-X-Trp motif in frizzled receptors mediates Wnt/beta-catenin signalling, *Embo J*, **19,** 4944-54.

Umbricht CB, Evron E, Gabrielson E, Ferguson A, Marks J and Sukumar S. (2001). Hypermethylation of 14-3-3 sigma (stratifin) is an early event in breast cancer, *Oncogene*, **20,** 3348-53.

Unden AB, Holmberg E, Lundh-Rozell B, Stahle-Backdahl M, Zaphiropoulos PG, Toftgard R and Vorechovsky I. (1996). Mutations in the human homologue of Drosophila patched (PTCH) in basal cell carcinomas and the Gorlin syndrome: different in vivo mechanisms of PTCH inactivation, *Cancer Res*, **56,** 4562-5.

Unden AB, Zaphiropoulos PG, Bruce K, Toftgard R and Stahle-Backdahl M. (1997). Human patched (PTCH) mRNA is overexpressed consistently in tumor cells of both familial and sporadic basal cell carcinoma, *Cancer Res*, **57,** 2336-40.

Upender MB, Habermann JK, McShane LM, Korn EL, Barrett JC, Difilippantonio MJ and Ried T. (2004). Chromosome transfer induced aneuploidy results in complex dysregulation of the cellular transcriptome in immortalized and cancer cells, *Cancer Res*, **64,** 6941-9.

Vallin J, Thuret R, Giacomello E, Faraldo MM, Thiery JP and Broders F. (2001). Cloning and characterization of three Xenopus slug promoters reveal direct regulation by Lef/beta-catenin signaling, *J Biol Chem*, **276,** 30350-8.

van Amerongen R, Mikels A and Nusse R. (2008). Alternative wnt signaling is initiated by distinct receptors, *Sci Signal*, **1,** re9.

van de Wetering M, Oosterwegel M, Dooijes D and Clevers H. (1991). Identification and cloning of TCF-1, a T lymphocyte-specific transcription factor containing a sequence-specific HMG box, *Embo J*, **10,** 123-32.

van den Brink GR, Bleuming SA, Hardwick JC, Schepman BL, Offerhaus GJ, Keller JJ, Nielsen C, Gaffield W, van Deventer SJ, Roberts DJ and Peppelenbosch MP. (2004). Indian Hedgehog is an antagonist of Wnt signaling in colonic epithelial cell differentiation, *Nat Genet*, **36,** 277-82.

van den Heuvel M and Ingham PW. (1996). smoothened encodes a receptor-like serpentine protein required for hedgehog signalling, *Nature*, **382,** 547-51.

van der Flier A and Sonnenberg A. (2001). Function and interactions of integrins, *Cell Tissue Res*, **305,** 285-98.

van der Neut R, Krimpenfort P, Calafat J, Niessen CM and Sonnenberg A. (1996). Epithelial detachment due to absence of hemidesmosomes in integrin beta 4 null mice, *Nat Genet*, **13,** 366-9.

van Es JH, Barker N and Clevers H. (2003). You Wnt some, you lose some: oncogenes in the Wnt signaling pathway, *Curr Opin Genet Dev*, **13,** 28-33.

Van Mater D, Kolligs FT, Dlugosz AA and Fearon ER. (2003). Transient activation of beta -catenin signaling in cutaneous keratinocytes is sufficient to trigger the active growth phase of the hair cycle in mice, *Genes Dev*, **17,** 1219-24.

van Ooyen A and Nusse R. (1984). Structure and nucleotide sequence of the putative mammary oncogene int-1; proviral insertions leave the protein-encoding domain intact, *Cell*, **39,** 233-40.

Van Scott EJ and Reinertson RP. (1961). The modulating influence of stromal environment on epithelial cells studied in human autotransplants, *J Invest Dermatol*, **36,** 109-31.

Vandesompele J, De Preter K, Pattyn F, Poppe B, Van Roy N, De Paepe A and Speleman F. (2002). Accurate normalization of real-time quantitative RT-PCR

data by geometric averaging of multiple internal control genes, *Genome Biol*, **3,** RESEARCH0034.
Varjosalo M, Li SP and Taipale J. (2006). Divergence of hedgehog signal transduction mechanism between Drosophila and mammals, *Dev Cell*, **10,** 177-86.
Varjosalo M and Taipale J. (2007). Hedgehog signaling, *J Cell Sci*, **120,** 3-6.
Vaux DL, Cory S and Adams JM. (1988). Bcl-2 gene promotes haemopoietic cell survival and cooperates with c-myc to immortalize pre-B cells, *Nature*, **335,** 440-2.
Veeman MT, Axelrod JD and Moon RT. (2003). A second canon. Functions and mechanisms of beta-catenin-independent Wnt signaling, *Dev Cell*, **5,** 367-77.
Veitch NC. (2004). Horseradish peroxidase: a modern view of a classic enzyme, *Phytochemistry*, **65,** 249-59.
Vermes I, Haanen C, Steffens-Nakken H and Reutelingsperger C. (1995). A novel assay for apoptosis. Flow cytometric detection of phosphatidylserine expression on early apoptotic cells using fluorescein labelled Annexin V, *J Immunol Methods*, **184,** 39-51.
Vidal VP, Chaboissier MC, Lutzkendorf S, Cotsarelis G, Mill P, Hui CC, Ortonne N, Ortonne JP and Schedl A. (2005). Sox9 is essential for outer root sheath differentiation and the formation of the hair stem cell compartment, *Curr Biol*, **15,** 1340-51.
Vidal VP, Ortonne N and Schedl A. (2008). SOX9 expression is a general marker of basal cell carcinoma and adnexal-related neoplasms, *J Cutan Pathol*, **35,** 373-9.
Vignery A. (2000). Osteoclasts and giant cells: macrophage-macrophage fusion mechanism, *Int J Exp Pathol*, **81,** 291-304.
Villavicencio EH, Walterhouse DO and Iannaccone PM. (2000). The sonic hedgehog-patched-gli pathway in human development and disease, *Am J Hum Genet*, **67,** 1047-54.
Vlad A, Rohrs S, Klein-Hitpass L and Muller O. (2008). The first five years of the Wnt targetome, *Cell Signal*, **20,** 795-802.
Vogelstein B and Kinzler KW. (2004). Cancer genes and the pathways they control, *Nat Med*, **10,** 789-99.
Vogt N, Lefevre SH, Apiou F, Dutrillaux AM, Cor A, Leuraud P, Poupon MF, Dutrillaux B, Debatisse M and Malfoy B. (2004). Molecular structure of double-minute chromosomes bearing amplified copies of the epidermal growth factor receptor gene in gliomas, *Proc Natl Acad Sci U S A*, **101,** 11368-73.
Von Ohlen T, Lessing D, Nusse R and Hooper JE. (1997). Hedgehog signaling regulates transcription through cubitus interruptus, a sequence-specific DNA binding protein, *Proc Natl Acad Sci U S A*, **94,** 2404-9.
Vortkamp A, Gessler M and Grzeschik KH. (1991). GLI3 zinc-finger gene interrupted by translocations in Greig syndrome families, *Nature*, **352,** 539-40.
Vortkamp A, Gessler M and Grzeschik KH. (1995). Identification of optimized target sequences for the GLI3 zinc finger protein, *DNA Cell Biol*, **14,** 629-34.
Vousden KH. (1994). Interactions between papillomavirus proteins and tumor suppressor gene products, *Adv Cancer Res*, **64,** 1-24.
Vousden KH and Lu X. (2002). Live or let die: the cell's response to p53, *Nat Rev Cancer*, **2,** 594-604.
Waikel RL, Kawachi Y, Waikel PA, Wang XJ and Roop DR. (2001). Deregulated expression of c-Myc depletes epidermal stem cells, *Nat Genet*, **28,** 165-8.

Waldman T, Lengauer C, Kinzler KW and Vogelstein B. (1996). Uncoupling of S phase and mitosis induced by anticancer agents in cells lacking p21, *Nature*, **381,** 713-6.

Walling HW, Fosko SW, Geraminejad PA, Whitaker DC and Arpey CJ. (2004). Aggressive basal cell carcinoma: presentation, pathogenesis, and management, *Cancer Metastasis Rev*, **23,** 389-402.

Wang B, Fallon JF and Beachy PA. (2000a). Hedgehog-regulated processing of Gli3 produces an anterior/posterior repressor gradient in the developing vertebrate limb, *Cell*, **100,** 423-34.

Wang B and Li Y. (2006). Evidence for the direct involvement of {beta}TrCP in Gli3 protein processing, *Proc Natl Acad Sci U S A*, **103,** 33-8.

Wang HY and Malbon CC. (2004). Wnt-frizzled signaling to G-protein-coupled effectors, *Cell Mol Life Sci*, **61,** 69-75.

Wang LC, Liu ZY, Gambardella L, Delacour A, Shapiro R, Yang J, Sizing I, Rayhorn P, Garber EA, Benjamin CD, Williams KP, Taylor FR, Barrandon Y, Ling L and Burkly LC. (2000b). Regular articles: conditional disruption of hedgehog signaling pathway defines its critical role in hair development and regeneration, *J Invest Dermatol*, **114,** 901-8.

Wang S, Krinks M, Lin K, Luyten FP and Moos M, Jr. (1997). Frzb, a secreted protein expressed in the Spemann organizer, binds and inhibits Wnt-8, *Cell*, **88,** 757-66.

Wang X, Zhou YX, Qiao W, Tominaga Y, Ouchi M, Ouchi T and Deng CX. (2006). Overexpression of aurora kinase A in mouse mammary epithelium induces genetic instability preceding mammary tumor formation, *Oncogene*, **25,** 7148-58.

Wang Y, McMahon AP and Allen BL. (2007). Shifting paradigms in Hedgehog signaling, *Curr Opin Cell Biol*, **19,** 159-65.

Wang Y and Nathans J. (2007). Tissue/planar cell polarity in vertebrates: new insights and new questions, *Development*, **134,** 647-58.

Wang Y, Rosenstein B, Goldwyn S, Zhang X, Lebwohl M and Wei H. (1998). Differential regulation of P53 and Bcl-2 expression by ultraviolet A and B, *J Invest Dermatol*, **111,** 380-4.

Watkins DN, Berman DM, Burkholder SG, Wang B, Beachy PA and Baylin SB. (2003). Hedgehog signalling within airway epithelial progenitors and in small-cell lung cancer, *Nature*, **422,** 313-7.

Watt FM. (1983). Involucrin and other markers of keratinocyte terminal differentiation, *J Invest Dermatol*, **81,** 100s-3s.

Watt FM. (1998). Epidermal stem cells: markers, patterning and the control of stem cell fate, *Philos Trans R Soc Lond B Biol Sci*, **353,** 831-7.

Watt FM. (2001). Stem cell fate and patterning in mammalian epidermis, *Curr Opin Genet Dev*, **11,** 410-7.

Watt FM. (2002). Role of integrins in regulating epidermal adhesion, growth and differentiation, *Embo J*, **21,** 3919-26.

Watt FM and Collins CA. (2008). Role of beta-catenin in epidermal stem cell expansion, lineage selection, and cancer, *Cold Spring Harb Symp Quant Biol*, **73,** 503-12.

Watt FM, Frye M and Benitah SA. (2008). MYC in mammalian epidermis: how can an oncogene stimulate differentiation?, *Nat Rev Cancer*, **8,** 234-42.

Watt FM and Hertle MD. (1994). *Keratinocyte integrins. In: Leigh IM, Lane EB, Watt FM (ed.). The Keratinocyte Handbook.* Cambridge University Press.

Watt FM, Kubler MD, Hotchin NA, Nicholson LJ and Adams JC. (1993). Regulation of keratinocyte terminal differentiation by integrin-extracellular matrix interactions, *J Cell Sci*, **106 (Pt 1),** 175-82.

Watt FM, Lo Celso C and Silva-Vargas V. (2006). Epidermal stem cells: an update, *Curr Opin Genet Dev*, **16,** 518-24.

Weaver BA and Cleveland DW. (2006). Does aneuploidy cause cancer?, *Curr Opin Cell Biol*, **18,** 658-67.

Weaver BA, Silk AD, Montagna C, Verdier-Pinard P and Cleveland DW. (2007). Aneuploidy acts both oncogenically and as a tumor suppressor, *Cancer Cell*, **11,** 25-36.

Wegner M. (1999). From head to toes: the multiple facets of Sox proteins, *Nucleic Acids Res*, **27,** 1409-20.

Wehrli M, Dougan ST, Caldwell K, O'Keefe L, Schwartz S, Vaizel-Ohayon D, Schejter E, Tomlinson A and DiNardo S. (2000). arrow encodes an LDL-receptor-related protein essential for Wingless signalling, *Nature*, **407,** 527-30.

Weinberg RA. (1995). The retinoblastoma protein and cell cycle control, *Cell*, **81,** 323-30.

Weinberg WC and Denning MF. (2002). P21Waf1 control of epithelial cell cycle and cell fate, *Crit Rev Oral Biol Med*, **13,** 453-64.

Weinberg WC, Fernandez-Salas E, Morgan DL, Shalizi A, Mirosh E, Stanulis E, Deng C, Hennings H and Yuspa SH. (1999). Genetic deletion of p21WAF1 enhances papilloma formation but not malignant conversion in experimental mouse skin carcinogenesis, *Cancer Res*, **59,** 2050-4.

Weiner HL, Bakst R, Hurlbert MS, Ruggiero J, Ahn E, Lee WS, Stephen D, Zagzag D, Joyner AL and Turnbull DH. (2002). Induction of medulloblastomas in mice by sonic hedgehog, independent of Gli1, *Cancer Res*, **62,** 6385-9.

Weiss L. (2000). Cancer cell heterogeneity, *Cancer Metastasis Rev*, **19,** 345-50.

Werner CA, Dohner H, Joos S, Trumper LH, Baudis M, Barth TF, Ott G, Moller P, Lichter P and Bentz M. (1997). High-level DNA amplifications are common genetic aberrations in B-cell neoplasms, *Am J Pathol*, **151,** 335-42.

Werner MH and Burley SK. (1997). Architectural transcription factors: proteins that remodel DNA, *Cell*, **88,** 733-6.

Werner MH, Huth JR, Gronenborn AM and Clore GM. (1995). Molecular basis of human 46X,Y sex reversal revealed from the three-dimensional solution structure of the human SRY-DNA complex, *Cell*, **81,** 705-14.

Westermarck J and Kahari VM. (1999). Regulation of matrix metalloproteinase expression in tumor invasion, *Faseb J*, **13,** 781-92.

Wetmore C. (2003). Sonic hedgehog in normal and neoplastic proliferation: insight gained from human tumors and animal models, *Curr Opin Genet Dev*, **13,** 34-42.

Wetmore C, Eberhart DE and Curran T. (2001). Loss of p53 but not ARF accelerates medulloblastoma in mice heterozygous for patched, *Cancer Res*, **61,** 513-6.

Wicking C, Smyth I and Bale A. (1999). The hedgehog signalling pathway in tumorigenesis and development, *Oncogene*, **18,** 7844-51.

Wieschaus E and Riggleman R. (1987). Autonomous requirements for the segment polarity gene armadillo during Drosophila embryogenesis, *Cell*, **49,** 177-84.

Wilker EW, van Vugt MA, Artim SA, Huang PH, Petersen CP, Reinhardt HC, Feng Y, Sharp PA, Sonenberg N, White FM and Yaffe MB. (2007). 14-3-3sigma controls mitotic translation to facilitate cytokinesis, *Nature*, **446,** 329-32.

Willert K, Brown JD, Danenberg E, Duncan AW, Weissman IL, Reya T, Yates JR, 3rd and Nusse R. (2003). Wnt proteins are lipid-modified and can act as stem cell growth factors, *Nature*, **423,** 448-52.

Williamson KA, Hever AM, Rainger J, Rogers RC, Magee A, Fiedler Z, Keng WT, Sharkey FH, McGill N, Hill CJ, Schneider A, Messina M, Turnpenny PD, Fantes JA, van Heyningen V and FitzPatrick DR. (2006). Mutations in SOX2 cause anophthalmia-esophageal-genital (AEG) syndrome, *Hum Mol Genet*, **15,** 1413-22.

Willis RC. (2004). Sorting out the mess, *Modern Drug Discovery*, **7,** 29-32.

Wilson M and Koopman P. (2002). Matching SOX: partner proteins and co-factors of the SOX family of transcriptional regulators, *Curr Opin Genet Dev*, **12,** 441-6.

Winklbauer R, Medina A, Swain RK and Steinbeisser H. (2001). Frizzled-7 signalling controls tissue separation during Xenopus gastrulation, *Nature*, **413,** 856-60.

Withers HR. (1967). Recovery and repopulation in vivo by mouse skin epithelial cells during fractionated irradiation, *Radiat Res*, **32,** 227-39.

Wodarz A and Nusse R. (1998). Mechanisms of Wnt signaling in development, *Annu Rev Cell Dev Biol*, **14,** 59-88.

Wolf D, Rodova M, Miska EA, Calvet JP and Kouzarides T. (2002). Acetylation of beta-catenin by CREB-binding protein (CBP), *J Biol Chem*, **277,** 25562-7.

Wong C and Stearns T. (2005). Mammalian cells lack checkpoints for tetraploidy, aberrant centrosome number, and cytokinesis failure, *BMC Cell Biol*, **6,** 6.

Wong CS, Strange RC and Lear JT. (2003). Basal cell carcinoma, *Bmj*, **327,** 794-8.

Wu R, Zhai Y, Fearon ER and Cho KR. (2001). Diverse mechanisms of beta-catenin deregulation in ovarian endometrioid adenocarcinomas, *Cancer Res*, **61,** 8247-55.

Wynshaw-Boris A. (2007). Cell biology: lost in mitotic translation, *Nature*, **446,** 274-5.

Xia J, Urabe K, Moroi Y, Koga T, Duan H, Li Y and Furue M. (2006). beta-Catenin mutation and its nuclear localization are confirmed to be frequent causes of Wnt signaling pathway activation in pilomatricomas, *J Dermatol Sci*, **41,** 67-75.

Xia X, Qian S, Soriano S, Wu Y, Fletcher AM, Wang XJ, Koo EH, Wu X and Zheng H. (2001). Loss of presenilin 1 is associated with enhanced beta-catenin signaling and skin tumorigenesis, *Proc Natl Acad Sci U S A*, **98,** 10863-8.

Xia Y, Papalopulu N, Vogt PK and Li J. (2000). The oncogenic potential of the high mobility group box protein Sox3, *Cancer Res*, **60,** 6303-6.

Xie J, Aszterbaum M, Zhang X, Bonifas JM, Zachary C, Epstein E and McCormick F. (2001). A role of PDGFRalpha in basal cell carcinoma proliferation, *Proc Natl Acad Sci U S A*, **98,** 9255-9.

Xie J, Murone M, Luoh SM, Ryan A, Gu Q, Zhang C, Bonifas JM, Lam CW, Hynes M, Goddard A, Rosenthal A, Epstein EH, Jr. and de Sauvage FJ. (1998). Activating Smoothened mutations in sporadic basal-cell carcinoma, *Nature*, **391,** 90-2.

Xie Z, Singleton PA, Bourguignon LY and Bikle DD. (2005). Calcium-induced human keratinocyte differentiation requires src- and fyn-mediated phosphatidylinositol 3-kinase-dependent activation of phospholipase C-gamma1, *Mol Biol Cell*, **16,** 3236-46.

Xiong Y, Hannon GJ, Zhang H, Casso D, Kobayashi R and Beach D. (1993). p21 is a universal inhibitor of cyclin kinases, *Nature*, **366,** 701-4.

Yaffe MB. (2002). How do 14-3-3 proteins work?-- Gatekeeper phosphorylation and the molecular anvil hypothesis, *FEBS Lett*, **513,** 53-7.

Yamazaki F, Aragane Y, Kawada A and Tezuka T. (2001). Immunohistochemical detection for nuclear beta-catenin in sporadic basal cell carcinoma, *Br J Dermatol*, **145,** 771-7.

Yang L, Yamasaki K, Shirakata Y, Dai X, Tokumaru S, Yahata Y, Tohyama M, Hanakawa Y, Sayama K and Hashimoto K. (2006). Bone morphogenetic protein-2 modulates Wnt and frizzled expression and enhances the canonical pathway of Wnt signaling in normal keratinocytes, *J Dermatol Sci*, **42,** 111-9.

Yang SH, Andl T, Grachtchouk V, Wang A, Liu J, Syu LJ, Ferris J, Wang TS, Glick AB, Millar SE and Dlugosz AA. (2008a). Pathological responses to oncogenic Hedgehog signaling in skin are dependent on canonical Wnt/beta3-catenin signaling, *Nat Genet*, **40,** 1130-5.

Yang X, Yu K, Hao Y, Li DM, Stewart R, Insogna KL and Xu T. (2004). LATS1 tumour suppressor affects cytokinesis by inhibiting LIMK1, *Nat Cell Biol*, **6,** 609-17.

Yang Z, Loncarek J, Khodjakov A and Rieder CL. (2008b). Extra centrosomes and/or chromosomes prolong mitosis in human cells, *Nat Cell Biol*, **10,** 748-51.

Yook JI, Li XY, Ota I, Hu C, Kim HS, Kim NH, Cha SY, Ryu JK, Choi YJ, Kim J, Fearon ER and Weiss SJ. (2006). A Wnt-Axin2-GSK3beta cascade regulates Snail1 activity in breast cancer cells, *Nat Cell Biol*, **8,** 1398-406.

Yoon JW, Kita Y, Frank DJ, Majewski RR, Konicek BA, Nobrega MA, Jacob H, Walterhouse D and Iannaccone P. (2002). Gene expression profiling leads to identification of GLI1-binding elements in target genes and a role for multiple downstream pathways in GLI1-induced cell transformation, *J Biol Chem*, **277,** 5548-55.

Yoshiura K, Kanai Y, Ochiai A, Shimoyama Y, Sugimura T and Hirohashi S. (1995). Silencing of the E-cadherin invasion-suppressor gene by CpG methylation in human carcinomas, *Proc Natl Acad Sci U S A*, **92,** 7416-9.

Youle RJ and Strasser A. (2008). The BCL-2 protein family: opposing activities that mediate cell death, *Nat Rev Mol Cell Biol*, **9,** 47-59.

Youssef KK, Van Keymeulen A, Lapouge G, Beck B, Michaux C, Achouri Y, Sotiropoulou PA and Blanpain C. (2010). Identification of the cell lineage at the origin of basal cell carcinoma, *Nat Cell Biol*, **12,** 299-305.

Yu J, Vodyanik MA, Smuga-Otto K, Antosiewicz-Bourget J, Frane JL, Tian S, Nie J, Jonsdottir GA, Ruotti V, Stewart R, Slukvin, II and Thomson JA. (2007). Induced pluripotent stem cell lines derived from human somatic cells, *Science*, **318,** 1917-20.

Yu M, Zloty D, Cowan B, Shapiro J, Haegert A, Bell RH, Warshawski L, Carr N and McElwee KJ. (2008). Superficial, nodular, and morpheiform basal-cell carcinomas exhibit distinct gene expression profiles, *J Invest Dermatol*, **128,** 1797-805.

Yuspa SH, Ben T, Hennings H and Lichti U. (1980). Phorbol ester tumor promoters induce epidermal transglutaminase activity, *Biochem Biophys Res Commun*, **97,** 700-8.

Yuspa SH, Ben T, Hennings H and Lichti U. (1982). Divergent responses in epidermal basal cells exposed to the tumor promoter 12-O-tetradecanoylphorbol-13-acetate, *Cancer Res*, **42,** 2344-9.

Yuspa SH, Hennings H and Saffiotti U. (1976). Cutaneous chemical carcinogenesis: past, present, and future, *J Invest Dermatol*, **67,** 199-208.

Yuspa SH, Viguera C and Nims R. (1979). Maintenance of human skin on nude mice for studies of chemical carcinogenesis, *Cancer Lett*, **6,** 301-10.

Zanet J, Pibre S, Jacquet C, Ramirez A, de Alboran IM and Gandarillas A. (2005). Endogenous Myc controls mammalian epidermal cell size, hyperproliferation, endoreplication and stem cell amplification, *J Cell Sci*, **118,** 1693-704.

Zannini M, Avantaggiato V, Biffali E, Arnone MI, Sato K, Pischetola M, Taylor BA, Phillips SJ, Simeone A and Di Lauro R. (1997). TTF-2, a new forkhead protein, shows a temporal expression in the developing thyroid which is consistent with a role in controlling the onset of differentiation, *Embo J*, **16,** 3185-97.

Zaphiropoulos PG, Unden AB, Rahnama F, Hollingsworth RE and Toftgard R. (1999). PTCH2, a novel human patched gene, undergoing alternative splicing and up-regulated in basal cell carcinomas, *Cancer Res*, **59,** 787-92.

Zappone MV, Galli R, Catena R, Meani N, De Biasi S, Mattei E, Tiveron C, Vescovi AL, Lovell-Badge R, Ottolenghi S and Nicolis SK. (2000). Sox2 regulatory sequences direct expression of a (beta)-geo transgene to telencephalic neural stem cells and precursors of the mouse embryo, revealing regionalization of gene expression in CNS stem cells, *Development*, **127,** 2367-82.

Zechner D, Muller T, Wende H, Walther I, Taketo MM, Crenshaw EB, 3rd, Treier M, Birchmeier W and Birchmeier C. (2007). Bmp and Wnt/beta-catenin signals control expression of the transcription factor Olig3 and the specification of spinal cord neurons, *Dev Biol*, **303,** 181-90.

Zeng X, Huang H, Tamai K, Zhang X, Harada Y, Yokota C, Almeida K, Wang J, Doble B, Woodgett J, Wynshaw-Boris A, Hsieh JC and He X. (2008). Initiation of Wnt signaling: control of Wnt coreceptor Lrp6 phosphorylation/activation via frizzled, dishevelled and axin functions, *Development*, **135,** 367-75.

Zhang D, Hirota T, Marumoto T, Shimizu M, Kunitoku N, Sasayama T, Arima Y, Feng L, Suzuki M, Takeya M and Saya H. (2004). Cre-loxP-controlled periodic Aurora-A overexpression induces mitotic abnormalities and hyperplasia in mammary glands of mouse models, *Oncogene*, **23,** 8720-30.

Zhang W, Zhao Y, Tong C, Wang G, Wang B, Jia J and Jiang J. (2005). Hedgehog-regulated Costal2-kinase complexes control phosphorylation and proteolytic processing of Cubitus interruptus, *Dev Cell*, **8,** 267-78.

Zhang Y and Kalderon D. (2001). Hedgehog acts as a somatic stem cell factor in the Drosophila ovary, *Nature*, **410,** 599-604.

Zhivotovsky B and Kroemer G. (2004). Apoptosis and genomic instability, *Nat Rev Mol Cell Biol*, **5,** 752-62.

Zhou JX, Jia LW, Liu WM, Miao CL, Liu S, Cao YJ and Duan EK. (2006). Role of sonic hedgehog in maintaining a pool of proliferating stem cells in the human fetal epidermis, *Hum Reprod*, **21,** 1698-704.

Zhou JX, Jia LW, Yang YJ, Peng S, Cao YJ and Duan EK. (2004). Enrichment and characterization of mouse putative epidermal stem cells, *Cell Biol Int*, **28,** 523-9.

Zhou W, Lin L, Majumdar A, Li X, Zhang X, Liu W, Etheridge L, Shi Y, Martin J, Van de Ven W, Kaartinen V, Wynshaw-Boris A, McMahon AP, Rosenfeld MG and Evans SM. (2007). Modulation of morphogenesis by noncanonical Wnt signaling requires ATF/CREB family-mediated transcriptional activation of TGFbeta2, *Nat Genet*, **39,** 1225-34.

Zhou ZH, Ping YF, Yu SC, Yi L, Yao XH, Chen JH, Cui YH and Bian XW. (2009). A novel approach to the identification and enrichment of cancer stem cells from a cultured human glioma cell line, *Cancer Lett*, **281,** 92-9.

Zhu AJ, Haase I and Watt FM. (1999). Signaling via beta1 integrins and mitogen-activated protein kinase determines human epidermal stem cell fate in vitro, *Proc Natl Acad Sci U S A*, **96,** 6728-33.

Zhu AJ and Scott MP. (2004). Incredible journey: how do developmental signals travel through tissue?, *Genes Dev*, **18,** 2985-97.

Zhu AJ and Watt FM. (1999). beta-catenin signalling modulates proliferative potential of human epidermal keratinocytes independently of intercellular adhesion, *Development*, **126,** 2285-98.

Zhu C and Jiang W. (2005). Cell cycle-dependent translocation of PRC1 on the spindle by Kif4 is essential for midzone formation and cytokinesis, *Proc Natl Acad Sci U S A*, **102,** 343-8.

Zimonjic D, Brooks MW, Popescu N, Weinberg RA and Hahn WC. (2001). Derivation of human tumor cells in vitro without widespread genomic instability, *Cancer Res*, **61,** 8838-44.

Zufferey R, Dull T, Mandel RJ, Bukovsky A, Quiroz D, Naldini L and Trono D. (1998). Self-inactivating lentivirus vector for safe and efficient in vivo gene delivery, *J Virol*, **72,** 9873-80.

Zurawel RH, Chiappa SA, Allen C and Raffel C. (1998). Sporadic medulloblastomas contain oncogenic beta-catenin mutations, *Cancer Res*, **58,** 896-9.

Appendices

Appendix I. Standard reagents, buffers and cell culture supplements

Cell culture

1x RM+ supplements (various mitogens) in 500 ml media

Supplement	Final Concentration
Hydrocortisone	0.4 μg/ml
Insulin	5 μg/ml
Epidermal Growth Factor	10 ng/ml
Cholera Toxin	0.1 nM
Transferrin	5 μg/ml
Liothyronine	20 pM

Making up the stock vials for addition to the 200 ml 100x RM+ supplements

Epidermal growth factor (EGF)

Final media concentration = 10 ng/ml

Thus in 200 ml of 100x RM+ = 1 μg/ml

In order to prepare 200 ml of 100x RM+ = 1 μg/ml, dissolve 1 mg in 10 ml ddH_2O (double distilled water) = 100 μg/ml stock concentration and aliquot in 2 ml and store at -20^{o}C.

This EGF stock concentration is later diluted in 1:100, 2 ml EGF (100 μg/ml stock) in 200 ml of 100x RM+ to give a final concentration of 1 μg/ml.

Hydrocortisone

Final media concentration = 0.4 μg/ml

Thus in 200 ml of 100x RM+ = 40 μg/ml

In order to prepare 200 ml of 100x RM+ = 40 μg/ml, dissolve 100 mg in 25 ml ddH_2O (double distilled water) = 4 mg/ml stock concentration and aliquot in 2 ml and store at -20^{o}C.

This hydrocortisone stock concentration is later diluted in 1:100, 2 ml hydrocortisone (4 mg/ml stock) in 200 ml of 100x RM+ to give a final concentration of 40 μg/ml.

Insulin

Final media concentration = 5 μg/ml

Thus in 200 ml of 100x RM+ = 500 μg/ml

In order to prepare 200 ml of 100x RM+ = 500 μg/ml, dissolve 500 mg in 10 ml 0.05 M HCl = 50 mg/ml stock concentration and aliquot in 2 ml and store at -20^{o}C.

This insulin stock concentration is later diluted in 1:100, 2 ml insulin (50 mg/ml stock) in 200 ml of 100x RM+ to give a final concentration of 500 μg/ml.

To prepare 10 ml 0.05 M HCl, take 500 μl from 1 M HCl in 9.5 ml ddH_2O (double distilled water).

Cholera toxin

Final media concentration = 0.1 nM or 10^{-10} M

Thus in 200 ml of 100x RM+ = 10 nM or 10^{-8} M

Molecular weight = 84,000

In order to prepare 200 ml of 100x RM+ = 1 μM or 10^{-6} M, dissolve 1 mg (the actual amount is 0.84 mg but for ease of use 1 mg is dissolved instead) in 10 ml ddH_2O (double distilled water) = 1 μM or 10^{-6} M stock concentration and aliquot in 2 ml and store at -20^{o}C.

This cholera toxin stock concentration is later diluted in 1:100, 2 ml cholera toxin (1 μM or 10^{-6} M mg/ml stock) in 200 ml of 100x RM+ to give a final concentration of 10 nM or 10^{-8} M or 1 μg/ml.

Liothyronine

Final media concentration = 20 pM or $2x10^{-11}$ M

Thus in 200 ml of 100x RM+ = ~ 20 nM or $2x10^{-9}$ M

Molecular weight = 651

In order to prepare 200 ml of 100x RM+ = ~ 20 nM or $2x10^{-9}$ M, dissolve 6 mg in 200 μl 1 N NaOH (for NaOH 1 N (Normality = 1 M), swirl and add 9.8 ml ddH_2O (double

distilled water) = 0.92 mM or $9.2x10^{-4}$ M stock concentration **(L1)** and aliquot in 0.5 ml and store at -20°C.

Then a dilution series is prepared as follows:

L2 (1:26 dilution): Take 0.5 ml **L1** and add 12.5 ml ddH_2O (double distilled water) = 35 µM or $3.5x10^{-5}$ M concentration **(L2)** and aliquot in 1 ml and store at -20°C.

L3 (1:10 dilution): Take 1 ml **L2** and add 9 ml ddH_2O (double distilled water) = 3.5 µM or $3.5x10^{-6}$ M concentration **(L3)** and aliquot in 1 ml and store at -20°C.

Then take one of the 1 ml **L3**, 3.5 µM or $3.5x10^{-6}$ M concentration vials and aliquot it in 100 µl/vial **(L4)** and store at -20°C.

This **L4** vial is later diluted in 1:2000, 100 µl liothyronine (3.5 µM or $3.5x10^{-6}$ M concentration) in 200 ml of 100x RM+ to give a final concentration of 2 nM or ~ $2x10^{-9}$ M.

Making up 200 ml 100x RM+ supplements

Chemical	Volume of stock in 200 ml of 100x RM+	Final Concentration in 200 ml 100x RM+
Hydrocortisone	2 ml	40 µg/ml
Insulin	2 ml	500 µg/ml
Epidermal Growth Factor	2 ml	1 µg/ml
Cholera Toxin	2 ml	~ 10^{-8} M (1 µg/ml)
Transferrin	2 ml	500 µg/ml
Liothyronine	100 µl	2 nM

The indicated quantities of each stock chemicals described in the above table were added in a sterile measuring cylinder and were mixed with 100 ml of sterile ddH_20 until they are completely dissolved, following the subsequent procedure: The first step was the re-suspension of insulin solution, which was performed as follows. The 2 ml of

insulin solution were pipetted along with 5 ml of ddH_2O against a measuring cylinder very slowly. Then, 5 ml of ddH_2O were used to wash the insulin vial in order to acquire any drops of insulin that may have been left in the vial. The same procedure was then followed for all other chemicals. Next, the cylinder was filled with ddH_2O up to 100 ml. The 100 ml solution was then filter-sterilised through a 500 ml vaccum filter unit stericup with a pore size 0.22 μm filter (Fisher, Leicestershire, UK) into the sterile 500 ml receiver (Fisher, Leicestershire, UK). Next, another 100 ml of DMEM/F12 were added to the cylinder and were also filtered as described above. The entire sterile filtered solution of 200 ml 100x RM+ was finally aliquoted in sterile bijoux tubes as 5 ml/tube and was stored at -20^{o}C.

Each 5 ml aliquot of 100x RM+ was used for each 500 ml bottle of cell culture medium (1:100 dilution), giving the final media concentration for each supplement (1x RM+ supplements in 500 ml media).

Doxycycline (Dox)

Stock solution (1 mg/ml) (45 ml)

Doxycycline (stored at 4^{o}C in the dark)	45 mg
dH_2O sterile	45 ml

Solution was filter-sterilised, aliquoted in 1 ml eppendorf tubes and stored at 4^{o}C for short-term and at -20^{o}C for long-term, wrapped in foil due to light sensitivity.

Stock solution (10 μg/ml) (6 ml); (1:100 dilution of 1 mg/ml stock solution)

Doxycycline (1 mg/ml)	60 μl
dH_2O sterile	6 ml (5940 μl)

Solution was filter-sterilised, aliquoted in 1 ml eppendorf tubes and stored at 4^{o}C for short-term and at -20^{o}C for long-term, wrapped in foil due to light sensitivity.

- For cell culture Dox (1 mg/ml) was diluted 1:100 in RM+ growth medium to achieve a final concentration of 10 μg/ml (100 μl Dox from 1 mg/ml stock solution in 10 ml RM+ growth medium).

- For cell culture Dox (10 μg/ml) was diluted 1:250 in RM+ growth medium to achieve a final concentration of 40 ng/ml (40 μl Dox from 10 μg/ml stock solution in 10 ml RM+ growth medium).

Geneticin (G418)

Stock solution (50 mg/ml) (2 ml)

G418 (stored at 4°C)	100 mg
PBS (1x) sterile	2 ml

Solution was filter-sterilised, aliquoted in 1 ml eppendorf tubes and stored at -20°C.

- For cell selection G418 was diluted 1:100 in RM+ growth medium to achieve a final concentration of 500 μg/ml (100 μl G418 from 50 mg/ml stock solution in 10 ml RM+ growth medium).

- For cell maintenance G418 was diluted 1:200 in RM+ growth medium to achieve a final concentration of 250 μg/ml (50 μl G418 from 50 mg/ml stock solution in 10 ml RM+ growth medium).

Hygromycin B (Hygro B)

Stock solution (50 mg/ml) (20 ml)

Already supplied as a solution from Clontech, Palo Alto, CA and stored at 4°C.

- For cell selection Hygro B was diluted 1:500 in RM+ growth medium to achieve a final concentration of 100 μg/ml (20 μl Hygro B from 50 mg/ml stock solution in 10 ml RM+ growth medium).

- For cell maintenance Hygro B was diluted 1:1000 in RM+ growth medium to achieve a final concentration of 50 μg/ml (10 μl G418 from 50 mg/ml stock solution in 10 ml RM+ growth medium).

Staining and Proliferation assays

4% (v/v) Formaldehyde/Formalin (200 ml)

		Final Concentration
PBS 100x Tablets (Oxoid, Hampshire, UK)	2 tablets	1x
37% (v/v) Formaldehyde/Formalin	21 ml	4% v/v
dH_2O	179 ml	

Stored at 4°C, wrapped in foil due to light sensitivity.

MTT solution

Stock solution (5 mg/ml) (10 ml)

MTT	50 mg
PBS (1x) sterile	10 ml

Stored at 4°C, wrapped in foil due to light sensitivity.

A final solution of MTT 500 µg/ml was prepared by diluting the working stock solution 1:10 in growth medium (1 ml of stock solution (5 mg/ml) in 9 ml of growth medium) prior to adding to the target cells.

Staining and Cell cycle analysis

Hoechst-33342

Stock solution (20 mg/ml) (2 ml)

Hoechst-33342	100 mg
dH_2O sterile	2 ml

Stored at 4°C, wrapped in foil due to light sensitivity.

Working stock solution (10 mg/ml) (1 ml)

Hoechst-33342 Stock solution (20 mg/ml)	500 µl
dH_2O sterile	500 µl

Stored at 4°C, wrapped in foil due to light sensitivity.

To stain cells for flow cytometry analysis a final solution of Hoechst-33342 10 µg/ml was prepared by diluting the working stock solution 1:1000 in 1x sterile PBS (1 µl of working stock solution (10 mg/ml) for each ml of 1x sterile PBS).

70% Ethanol (200 ml)

Ethanol (99.8% v/v)	60 ml
dH_2O	40 ml

Kept at -20°C.

NaCitrate (100 mM; 200 ml)

		Final Concetration
NaCitrate	25.8 g	100 mM

Made up to 200 ml with dH_2O (distilled water) and kept at RT.

Propidium Iodide/RNaseA solution mix (1 ml)

		Final Concentration
Propidium Iodide (1 mg/ml)	50 µl	50 µg/ml
RNase A (5 mg/ml)	25 µl	125 µg/ml
NaCitrate (100 mM)	380 µl	38 mM
PBS (1x) sterile	545 µl	

Kept on ice, wrapped in foil due to light sensitivity.

RNase A solution (5 mg/ml; 2 ml)

		Final Concentration
RNase A (lyophilised powder)	10 mg	5 mg/ml
dH_2O	2 ml	

The RNAse A stock solution was aliquoted in 200 µl and was stored at -20°C.

DAPI solution

Stock solution (20 mg/ml) (0.5 ml)	
DAPI	10 mg
dH_2O	0.5 ml

Stored at -20°C, wrapped in foil due to light sensitivity.

Working stock solution (20 µg/ml) (1 ml)	
DAPI Stock solution (20 mg/ml)	1 µl
dH_2O	999 µl

Stored at -20°C, wrapped in foil due to light sensitivity.

To stain cells a final solution of DAPI 200 ng/ml was prepared by diluting the working stock solution 1:100 in 1x Annexin V Binding Buffer or in 1x sterile PBS (1 µl of working stock solution (20 µg/ml) for each 100 µl of 1x Annexin V Binding Buffer or 1x sterile PBS).

Agarose gel electrophoresis

DNA Loading Dye Buffer (2x; 10 ml)

		Final Concentration
Glycerol	7.5 ml	75% v/v
Bromophenol Blue	0.5 ml from 1.5% (w/v) stock	0.075% v/v
Xylene Cyanol	0.5 ml from 1.5% (w/v) stock	0.075% v/v
dH_2O	1.5 ml	

Whole, cytoplasmic and nuclear extraction buffers

RIPA Buffer (1x; 250 ml)

		Final Concentration
Tris-base 1 M, pH 7.3	12.5 ml	50 mM
NaCl	2.19 g	150 mM
SDS 20% (w/v)	1.25 ml	0.1% v/v
Nonidet P-40	2.5 ml	1% v/v
Na_3VO_4 1 M (sodium orthovanadate)	2.5 ml	10 mM

Made up to 250 ml with dH_2O (distilled water) and kept on ice or stored at 4^oC.

SDS 20% (w/v) (100 ml)

SDS 20 g

Made up to 100 ml with dH_2O (distilled water) and stored at room temperature (RT).

Complete mini (CM) EDTA-free protease inhibitor cocktail tablets

One tablet from 10x Complete mini EDTA-free protease inhibitor cocktail tablets is dissolved in 1 ml dH2O (10x stock of CM EDTA-free protease inhibitor cocktail) (vortex very well and wait 5-10 minutes until completely dissolved) and aliquoted in 100 µl per eppendorf tube and stored at -20^oC.

To prepare either 1x RIPA Buffer containing 1x CM EDTA-free protease inhibitor cocktail, or 1x Reporter lysis buffer containing 1x CM EDTA-free protease inhibitor cocktail, the 10x stock of CM EDTA-free protease inhibitor cocktail was diluted 1:10 in 1x RIPA or 1x Reporter lysis buffer, vortexed very well and kept in ice.

1x PBS/PMSF (10 ml)

10x PBS	1 ml
(Imgenex, San Diego, CA)	
Deionized water	8.9 ml
PMSF (100 mM)	100 µl
(Imgenex, San Diego, CA)	

Kept on ice.

1x Hypotonic Buffer (1 ml)

10x Hypotonic buffer	100 µl
(Imgenex, San Diego, CA)	
Deionized water	900 µl

Kept on ice.

Nuclear Lysis Buffer (100 µl)

10 mM DTT	5 µl
(Imgenex, San Diego, CA)	
Nuclear extraction buffer	94 µl
(Imgenex, San Diego, CA)	
PIC (100x) (protease inhibitor cocktail)	1 µl
(Imgenex, San Diego, CA)	

Kept on ice.

Western Blot Buffers

10% (v/v) polyacrylamide gel (30 ml)

30% (w/v) acrylamide	10 ml
(Protogel, National Diagnostics, Atlanta,USA)	
1.5 M Tris-HCl, pH 8.8	7.5 ml
10% (w/v) SDS	0.3 ml
dH_2O	11.88 ml
TEMED (tetramethylethylenediamine)	20 µl
10% (w/v) APS (ammonium persulfate)	300 µl

8% (v/v) polyacrylamide gel (30 ml)

30% (w/v) acrylamide	8 ml
(Protogel, National Diagnostics, Atlanta,USA)	
1.5 M Tris-HCl, pH 8.8	7.5 ml
10% (w/v) SDS	0.3 ml
dH_2O	11.88 ml
TEMED (tetramethylethylenediamine)	20 µl
10% (w/v) APS (ammonium persulfate)	300 µl

5% (v/v) stacking gel (10 ml)

30% (w/v) acrylamide	1.67 ml
(Protogel, National Diagnostics, Atlanta,USA)	
1 M Tris-HCl, pH 6.8	1.25 ml
10% (w/v) SDS	0.1 ml
dH_2O	6.87 ml
TEMED (tetramethylethylenediamine)	10 µl
10% (w/v) APS (ammonium persulfate)	100 µl

SDS 10% (w/v) (100 ml)

SDS 10 g

Made up to 100 ml with dH_2O (distilled water) and stored at room temperature (RT).

APS (ammonium persulfate) 10% (w/v) (3 ml)

APS	0.3 g
dH_2O	2.7 ml

Kept on ice and for longer-term storage at 4°C.

Tris-HCl (pH 8.8; 1 L)

		Final Concentration
Tris-HCl	181.5 g	1.5 M
dH_2O	500 ml	

The pH of the solution was adjusted to 8.8 with 1 M HCl and 1 M NaOH and was finally brought to a final volume of 1 L with dH_2O (distilled water) and stored at RT.

Tris-HCl (pH 6.8; 1 L)

		Final Concentration
Tris-HCl	121 g	1 M

The pH of the solution was adjusted to 6.8 with 1 M HCl and 1 M NaOH and was finally brought to a final volume of 1 L with dH_2O (distilled water) and stored at RT.

Running Buffer (10x; 1 L)

		Final Concentration
Tris-Base	30 g	0.25 M
Glycine	144 g	192 mM
SDS	10 g	10% w/v

Made up to 1 L with dH_2O (distilled water) and stored at room temperature (RT).

Transfer Buffer (10x; 1 L)

		Final Concentration
Tris-Base	60.4 g	0.5 M
Glycine	288 g	384 mM

Made up to 1 L with dH_2O (distilled water) and stored at room temperature (RT).

To make 1 L of 1x Protein transfer buffer, 100 ml of 10x Protein Transfer Buffer were mixed with 700 ml dH_2O and 200 ml Methanol (20% (v/v) Methanol final concentration).

Protein SDS Sample Buffer (5x; 10 ml)

		Final Concetration
Tris-HCl	3.13 ml of 1 M Tris-HCl, pH 6.8	0.31 M
Dithiothreitol (DTT)	1.25 ml of 2 M DTT	0.25 M
Bromophenol Blue	0.67 ml of 1.5% (w/v) stock	0.1% v/v
Glycerol	5 ml	50% v/v
SDS	1 g	10% w/v

Aliquot 200 µl in eppendorf tubes and store at -20^{o}C.

Tris Buffered Saline (TBS) (pH 7.6) (10x; 1 L)

		Final Concentration
NaCl	86 g	150 mM
Tris-Base	30 g	25 mM
dH_2O	500 ml	

The pH of the solution was adjusted to 7.6 with 1 M HCl and 1 M NaOH and was finally brought to a final volume of 1 L with dH_2O (distilled water) and stored at RT.

Phosphate Buffered Saline (PBS) (pH 7.3 ± 0.2) (1x; 1 L)

One tablet of 100x PBS (Oxoid, Hampshire, UK) is diluted in 100 ml dH_2O (1x). To prepare 1 L of 1x PBS solution, 10 tablets of 100x PBS (Oxoid, Hampshire, UK) are diluted in 1 L dH_2O (1x) which contains the following:

		Final Concentration
NaCl	8.0 g	137 mM
KCl	0.2 g	2.7 mM
Na_2HPO_4 (di-sodium hydrogen phosphate)	1.15 g	10 mM
KH_2HPO_4 (potassium di-hydrogen phosphate)	0.2 g	1.76 mM

Made up to 1 L with dH_2O (distilled water) and stored at room temperature (RT).

HCl (100 ml)

		Final Concentration
HCl (37%)	8.4 ml	1 M
dH_2O	91.6 ml	

NaOH (100 ml)

		Final Concentration
NaOH	4 g	1 M

Made up to 100 ml with dH_2O (distilled water) and stored at room temperature (RT).

Tris-base (pH 7.3; 1 L)

		Final Concentration
Tris-base	121 g	1 M
dH_2O	500 ml	

The pH of the solution was adjusted to 7.3 with 1 M HCl and 1 M NaOH and was finally brought to a final volume of 1 L with dH_2O (distilled water) and stored at RT.

5% (w/v) milk TBS/T or PBS/T (200 ml)

Non-fat dry milk 10 g

Made up to 200 ml with dH_2O (distilled water) and kept at 4^oC.

3% (w/v) milk TBS/T or PBS/T (200 ml)

Non-fat dry milk 6 g

Made up to 200 ml with dH_2O (distilled water) and kept at 4^oC.

M-FISH

KCl (0.075 M; 200 ml)

		Final Concetration
KCl	1.1 g	0.075 M

Made up to 200 ml with dH_2O (distilled water) and kept at RT.

Fix solution (100% methanol : 100% acetic acid = 3 : 1) (72ml)

Methanol (99.9+%)	52 ml
Acetic acid (99+%)	18 ml

Kept at RT.

20x Saline Sodium Citrate (SSC) (pH 7.0 - 7.5) (500 ml)

20x SSC	132 g
ddH_2O	400 ml

The pH of the solution was adjusted to 7.0 - 7.5 with 1 M HCl and 1 M NaOH and was finally brought to a final volume of 500 ml with ddH_2O (double distilled water) and stored at RT.

2x Saline Sodium Citrate (SSC) (pH 7.0 - 7.4) (500 ml)

20x SSC	50 ml
ddH_2O	400 ml

The pH of the solution was adjusted to 7.0 - 7.4 with 1 M HCl and 1 M NaOH and was finally brought to a final volume of 500 ml with ddH_2O (double distilled water) and stored at RT.

0.4x Saline Sodium Citrate (SSC)/0.3% (v/v) NP-40 Wash solution (pH 7.0 - 7.5) (500 ml)

20x SSC	10 ml
ddH_2O	470 ml
NP-40	1.5 ml

The pH of the solution was adjusted to 7.0 - 7.5 with 1 M HCl and 1 M NaOH and was finally brought to a final volume of 500 ml with ddH_2O (double distilled water) and stored at RT.

2x Saline Sodium Citrate (SSC)/0.1% (v/v) NP-40 Wash solution (pH 7.0 ± 0.2) (500 ml)

20x SSC	50 ml
ddH_2O	420 ml
NP-40	0.5 ml

The pH of the solution was adjusted to 7.0 ± 0.2 with 1 M HCl and 1 M NaOH and was finally brought to a final volume of 500 ml with ddH_2O (double distilled water) and stored at RT.

RNase A Stock (10 mg/ml; 1 ml) and Working (0.1 mg/ml; 1 ml) Solution

Stock solution (10 mg/ml) (1 ml)

RNase A (lyophilised powder)	10 mg
2x Saline Sodium Citrate (SSC)	1 ml

The RNAse A stock solution was aliquoted in 10 µl and was stored at -20^{o}C.

Working solution (0.1 mg/ml) (1 ml)

RNase A stock solution (10 mg/ml)	10 µl
2x Saline Sodium Citrate (SSC)	990 µl

At time of use, the RNAse A stock solution (10 mg/ml; 10 µl) was defrosted and was diluted 1:100 in 2x SSC by adding 990 µl of 2x SSC in 10 µl RNAse A stock solution (vortexed to mix), giving a working solution with a concentration of 0.1 mg/ml (0.1 mg/ml; 1 ml).

Pepsin Stock (10% (w/v); 1 ml) and Working (0.005% (v/v); 70 ml) Solution

Stock solution (10% (w/v)) (1 ml)

Pepsin	0.1 g
ddH_2O (pre-warmed to 37 ^{o}C in a water bath)	1 ml

The Pepsin stock solution was aliquoted in 40 µl and was stored at -20^{o}C.

Working solution (0.005% (v/v)) (70 ml)

Pepsin stock solution (10% (w/v))	35 µl
ddH_2O (pre-warmed to 37 ^{o}C in a water bath)	69.3 ml
1 M HCl (pre-warmed to 37 ^{o}C in a water bath)	0.7 ml

At time of use, the Pepsin stock solution (10% (w/v); 40 µl) was defrosted and was diluted 1:2000, in pre-warmed 69.3 ml ddH_2O and 0.7 ml 1 M HCl giving a 0.005% (v/v) working solution. A beaker containing 69.3 ml of ddH_2O and 0.7 ml 1 M HCl, and a glass Coplin jar were all pre-warmed to 37 ^{o}C using a water bath. Then 35 µl from the 40 µl defrosted Pepsin stock solution (10% (w/v); 40 µl) were mixed into the solution of the beaker and then were all transferred to the pre-warmed glass Coplin jar.

Formaldehyde Fixation Solution (70 ml)

		Final Concetration
ddH_2O	57.7 ml	
1 M $MgCl_2$	3.5 ml	0.05 M
10x PBS	7 ml	1x
37% formaldehyde	1.89 ml	1%

Prepared in a fume hood and kept at RT.

Phosphate Buffered Saline (PBS) (10x; 100 ml)

One tablet of 100x PBS (Oxoid, Hampshire, UK) is diluted in 10 ml dH_2O (10x). To prepare 100 ml of 10x PBS solution, 10 tablets of 100x PBS (Oxoid, Hampshire, UK) are diluted in 100 ml dH_2O (10x) and stored at room temperature (RT).

$MgCl_2$ (1 M) (50 ml)

		Final Concetration
$MgCl_2 . 6\ H_2O$	10.16 g	1 M

Made up to 50 ml with dH_2O (distilled water) and kept at RT.

Denaturation Solution (70% Formamide/2x SSC) (pH 7.0 - 8.0) (60 ml)

		Final Concetration
Formamide (100%)	42 ml	70%
20x Saline Sodium Citrate (SSC)	6 ml	2x
ddH_2O	10 ml	

The pH of the solution was measured using pH indicator strips to verify pH is 7.0 - 8.0. and was finally brought to a final volume of 60 ml with ddH_2O (double distilled water). The solution was prepared in a fume hood and kept at 4^oC.

Appendix II. Involucrin

RNA was harvested from N/TERT, SINCE, and SINEG2 cells to examine the levels of involucrin mRNA expression using specific primers. Quantitative RT-PCR analysis of involucrin showed a decrease in SINEG2 cells compared to N/TERT and SINCE control cells. Each bar represents mean fold suppression relative to N/TERT (arbitary value of 1) ± s.e.m of triplicate samples. *** *P≤0.001*.

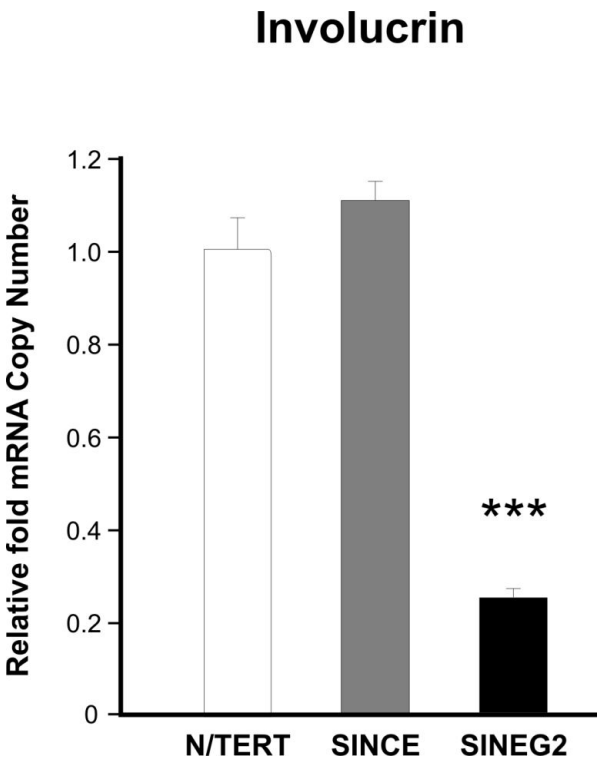

Appendix III. 10K SNP Microarray Mapping Assay of human N/TERT keratinocytes

The ploidy status of N/TERT keratinocytes was examined by means of 10K SNP Microarray Mapping Assay. Genomic DNA from N/TERT (top panel) and SINCE (bottom panel) keratinocytes was analysed against reference genomic DNA of primary keratinocytes derived form three separate healthy donors. The average ploidy status of all the SNPs located on each chromosome after Affymetrix GTYPE analysis was plotted. Both N/TERT and SINCE keratinocytes show a normal genotype apart from the fact that chromosome 20 (trisomy) was consistently gained in all samples tested. Note that that the large error bar for chromosome X is due to the sexual variability of primary keratinocyte reference samples. Bars represent the average ploidy status of all SNPs per chromosome ± s.e.m of three individual reference primary keratinocyte samples. Experiment and analysis was performed by Dr Muy-Teck Teh, Clinical and Diagnostic Oral Sciences, Institute of Dentistry, Barts and the London School of Medicine and Dentistry, London, UK.

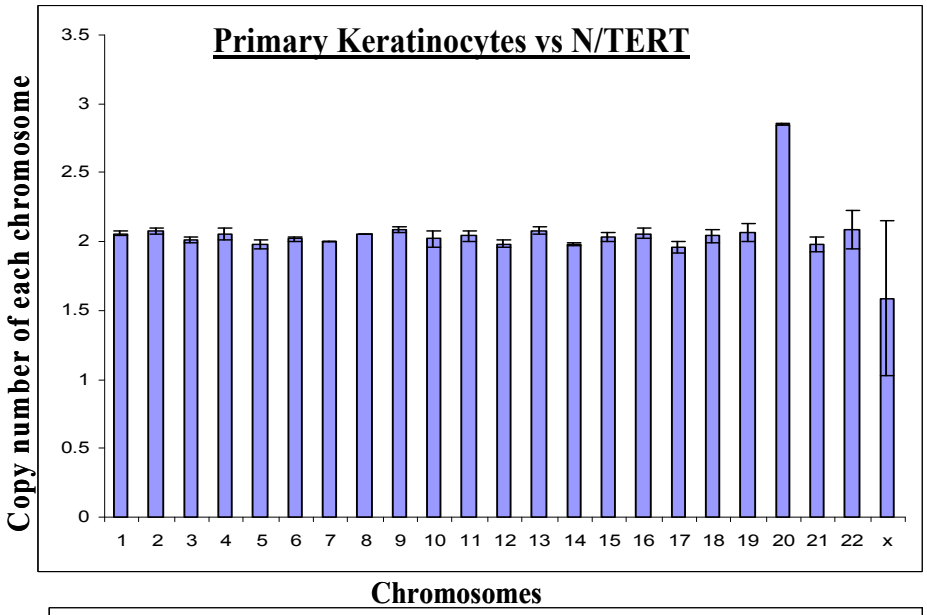
Primary Keratinocytes vs N/TERT
Copy number of each chromosome
3.5
3
2.5
2
1.5
1
0.5
0
1 2 3 4 5 6 7 8 9 10 11 12 13 14 15 16 17 18 19 20 21 22 x
Chromosomes

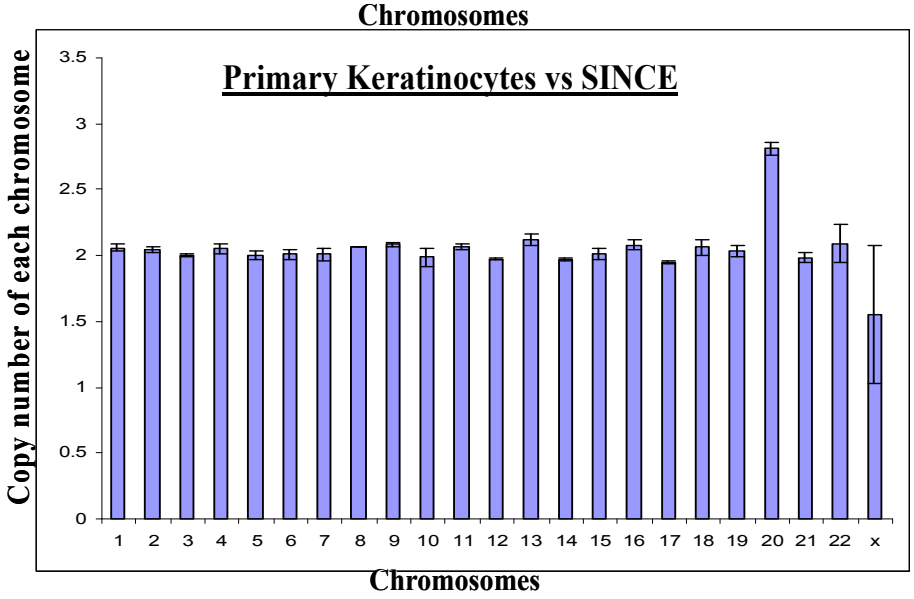
Primary Keratinocytes vs SINCE
Copy number of each chromosome
3.5
3
2.5
2
1.5
1
0.5
0
1 2 3 4 5 6 7 8 9 10 11 12 13 14 15 16 17 18 19 20 21 22 x
Chromosomes